A Physical-Organic Approach to Asymmetric Catalysis: Design and Synthesis of Chiral Ligands using Multivariate Modelling

Alexandre Brethomé

Wolfson College

University of Oxford

A thesis presented in partial fulfilment of

the requirements for the award of the degree of

Doctor of Philosophy

Michaelmas 2019

Author's Declaration

This thesis describes work carried out in the Chemistry Research Laboratory, Oxford, between October 2015 and August 2019 under the supervision of Prof. Stephen Fletcher and Prof. Robert Paton. The thesis is a result of my own work, except when clearly stated otherwise, and has not been submitted for any other degree at this or any other university.

Alexandre Brethomé

October 2019

Abstract

Discovery of new asymmetric metal-catalyzed transformations is closely related to the development of efficient and robust chiral ligands, such that ligand optimisation is a crucial step in reaction development but its success is highly uncertain. Mostly based on trial-and-error, such a daunting task can be intellectually frustrating and exhausting, wherein the use of any predictive tool is much appreciated. The limited mechanistic knowledge in asymmetric catalysis is unfortunately prohibitive to the use of many computational techniques. As a result, we turn our attention toward multivariate modelling, a data-driven statistical approach which is believed to be a promising platform to rationally drive the successful identification of a highly enantioselective ligand.

In this work, we introduce the importance of ligands in asymmetric catalysis and detail the notion of ligand design, and more particularly, we fully report the multivariate modelling approach (**Chapter 1**). We then apply such a strategy on systems developed in our group where the ligand design previously failed using traditional approaches. For instance, **Chapter 2** fully uses multivariate modelling to reoptimize a copper-catalysed asymmetric conjugate addition of alkylzirconium species that failed on sterically challenging *linear* substrates. While modelling this asymmetric transformation, we realized that conformational flexibility of ligands could produce large amplitudes of underestimated uncertainty in predictions. Thus, conformational effects on physical-organic descriptors are explored in **Chapter 3** with the specific case of steric Sterimol parameters, from which new descriptors called wSterimol ("weighted Sterimol") were developed. Inspired by the success of our approach in **Chapter 2**, the ligand design workflow is applied to the

development of a copper-catalysed asymmetric conjugate addition to *exocyclic* enones (**Chapter 4**). Finally, we examine the remaining challenges for the data-driven approach to become a go-to method and we envision the future of ligand design in asymmetric catalysis (**Chapter 5**).

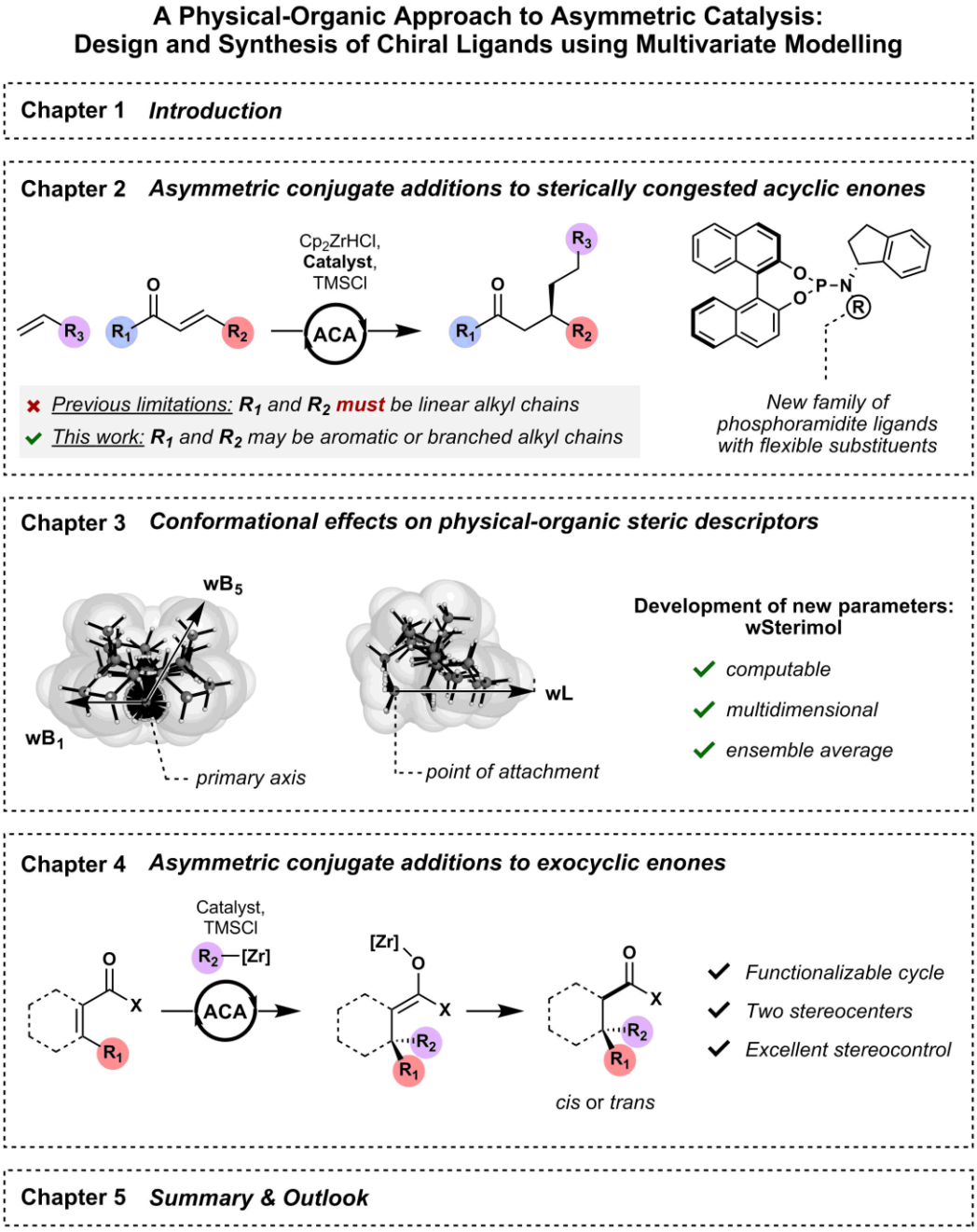

Acknowledgement

First and foremost, I would like to thank my DPhil supervisors, Prof. Stephen Fletcher and Prof. Robert Paton, for giving me this exciting opportunity of working on an interdisciplinary project. I could not have achieved this work without your guidance, vision, and commitment. More particularly, you have always supported and encouraged me in all my interests and I am deeply grateful to have been mentored by such excellent supervisors.

This DPhil would not have been so enjoyable without the fantastic members of the Paton and Fletcher Group, past and present. You always have been of great help and available for scientific discussions about computational or organic chemistry. More particularly, the atmosphere in the lab has always been joyful, to which I need to thank my great labmates for their jokes and stories! A special mention goes to Dr. (now Prof.!) Fernanda Duarte and Dr. Ruchuta Ardkhean for your support at the beginning of my PhD and for your long-lasting kindness.

This DPhil has been an exceptional experience in my life, particularly in Oxford, but it has also been an emotionally challenging journey. Fortunately, I am blessed with an incredibly supportive family. More particularly, my soon-to-be wife was the best support I could have hoped for. Despite frustrating days or weeks (as all organic chemists experience), you have always been here for me with your love, kindness and laughter. You also came to Oxford with me to start a new life and sacrificed opportunities dear to you, for which I will never thank you and love you enough.

Table of Contents

Glossary of Abbreviations

ACA	asymmetric conjugate addition
AD	applicability domain or domain of applicability
AIC	Akaike information criterion
aq.	aqueous
BINAP	2,2'-bis(diphenylphosphino)-1,1'-binaphthyl
BINOL	1,1'-bi-2-napthol
ca	approximately, from the latin *circa*
CC	coupled-cluster
CCSD(T)	coupled-cluster method including perturbative single, double and triple excitations
cf.	see, from the latin *confer*
CPK	Corey-Pauling-Koltun
DFT	density functional theory
DoE	design of experiment
dr	diastereomeric ratio
e.g.	for example, from the latin *exempli gratia*
ee	enantiomeric excess
eq.	equivalents
et al.	and others, from the latin *et alia*
etc.	and other similar things, from the latin *et cetera*
EXSY	exchange spectroscopy
HOMO	highest occupied molecular orbital
HPLC	high performance liquid chromatography
HTS	high throughput screening
i.e.	in other words, from the latin *id est*
in situ	on site, from latin
IR	infra-red
LFER	linear free energy relationship
LKB	ligand knowledge base
LPNO	local pair natural orbital
LS	ligand space
MLR	multivariate linear regression
MM	molecular mechanics
NBO	natural bond orbital
NCI	non-covalent interaction
NHC	*N*-heterocyclic carbene
NMR	nuclear magnetic resonance
o/n	overnight
OLS	ordinary least squares regression
PC	principal component
PES	potential energy surface
PLS	partial least squares regression
Q2MM	quantum guided molecular mechanics
QM	quantum mechanic

QSAR	quantitative structure-activity relationship
QSSR	quantitative structure-selectivity relationship
rt	room temperature
sat.	saturated
SFC	supercritical fluid chromatography
SMD	solvation model based on density
SUMM	systemic unbounded multiple minimum
TL	transfer learning
TMS	trimethylsilyl
TS	transition state
TSFF	fitted transition state force field
WFT	wave function theory

1

Introduction

Ligand design in asymmetric catalysis

1 Asymmetric catalysis

1.1 Enantiopure materials and their preparation

In 1883, Lord Kelvin introduced the word "chirality" to describe a class of compounds that are non-superimposable on their mirror image and he chose a left-handed helix and its right-handed mirror image to illustrate what would later be called enantiomers.[1] By definition, physical and chemical properties of enantiomers are identical but diastereomeric interactions arise when they are placed in a chiral environment whereby each enantiomer has a different behaviour. This is of tremendous importance because amino acids and sugars, the building blocks of life, are homochiral. Beyond the scientific curiosity arising from this observation,[2] it suggests that right- and left-handed chiral compounds behave differently in living systems such that the properties of only one enantiomer might be of interest.

Implications for modern chemical industries such as pharmaceuticals, agrochemicals and fine chemicals are immense, as enantiopure compounds play a role in solving tomorrow's challenges. For instance, the increased demand for environmentally-friendly agrochemicals such as herbicides, pesticides and fungicides paves the way to highly selective active ingredients that are synthesized from chiral chemicals. Coupled with an increasing population and the need for better crop yields, the demand for chiral compounds is forecast to increase significantly.[3] Likewise, the cosmetic industry generates a high demand for fragrances. Depending on their application, enantiopure fragrances were found to enjoy greater biodegradability[4] or a more intense scent[5,6] that is of great promise in the industry. Last but not least, development of safer and more effective drugs with

better therapeutic values in the pharma industry continues to drive the chiral molecules' market on its own, through the demand for chiral building blocks.[7]

To date, the major end-use industries of chiral compounds are therefore the pharmaceutical, agrochemical and fragrance manufacturers. Their substantial appetite requires a constant supply of materials and there are several approaches to produce large quantities of chiral molecules (**Scheme 1.1**).

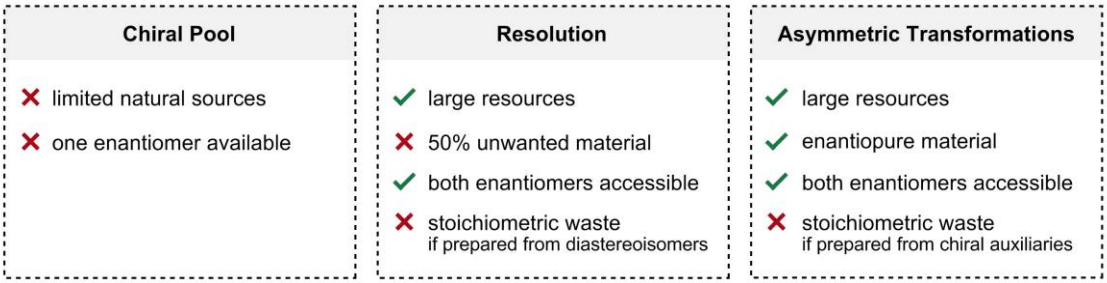

Scheme 1.1. Several approaches to access enantioenriched materials.

The first one consists of extracting chiral compounds directly from natural sources, commonly referred to as the "chiral pool", but this approach has considerable downsides such as high manufacturing costs and the availability of only one enantiomer.[8] Alternatively, the separation of racemic mixture is a very popular strategy that represented >50% of the chiral market in 2015.[7] The traditional methods convert racemates into diastereoisomers followed by their separation using either analytical techniques or crystallisation, while more recent techniques include enzymatic resolution, where substrate selectively reacts with only one enantiomer. Nevertheless, resolution entails the necessary production of 50% unwanted material that is poorly valorised.

The manufacturing cost drives the need for more eco-friendly chemistry where atom-[9] and redox-economies[10] are fundamental principles. Thus, asymmetric

synthesis methods were developed to directly produce highly enantioenriched compounds with excellent yields, a strategy that represented ~30% of the global chiral market in 2015.[7] Among these asymmetric transformations, chiral auxiliaries were initially popular but those still required the introduction of the chiral auxiliary and its removal, which generated stoichiometric waste. In that regard, asymmetric catalysis is another method that has the advantage of yielding a high quantity of enantiopure materials using sub-stoichiometric quantities of active compounds. More particularly, the impact of metal-catalyzed asymmetric catalysis was recognised by the 2001 Nobel Prize in chemistry, where K. B. Sharpless, W. S. Knowles and R. Noyori were recipients for their work on catalytic asymmetric hydrogenation and oxidation.[11]

1.2 Privileged ligands

Asymmetric catalysis is a fruitful and active research area that has implications across a wide variety of real-world applications and the discovery of new asymmetric transformations is closely related to the development of efficient and robust chiral catalysts. Thus, a wide diversity of chiral ligands and metal complexes has been uncovered for the last thirty years to carry out numerous asymmetric transformations. As Knowles explained in his Nobel lecture,[12] all these chiral systems were initially expected to be highly substrate-specific like enzymes, but surprisingly, a subset of catalysts showed excellent results over a wide range of substrates. From a synthetic chemist's point of view, the substrate tolerance of these ligands made them superior to enzymes thanks mainly to the predictable behaviour of these catalysts when planning new syntheses.[13] Additionally, a derivatized core scaffold was enough to create an effective chiral environment for numerous

mechanistically unrelated reactions such that Jacobson *et al.* decided in 2003 to call classes of particularly useful catalysts "privileged structures".[13] Although a universal catalyst may exist for a specific reaction,[14] a universal asymmetric catalyst that works for all asymmetric transformations is highly unlikely. However, we can imagine a collection of such privileged catalysts in a catalyst toolbox that spans most asymmetric catalyzed methods.

The features required for chiral catalysts to be considered as "privileged" have evolved over time[13,15,16] but there are nevertheless commonly agreed criteria. A privileged structure achieves good enantioselectivity over a wide range of substrates, is enantioselective with mechanistically unrelated reactions, is made in few steps from readily available starting materials, and is synthetically easily modified (**Scheme 1.2**).

The first generation presented by Jacobson *et al.* consisted of phospholane derivatives (*e.g.* DuPhos), BINAP derivatives, BINOL derivatives, Brintzinger's complexes, Salen complexes, bis(oxazolines) (BOX) and Cinchona alkaloids.[13] To this list was added in 2011 ferrocenyl-based ligands (*e.g.* Josiphos), phosphinooxazolines (PHOX), spiro-based ligands, tartrate derivatives (*e.g.* TADDOL), biphenylphosphines (BIPHEP, *e.g.* Tunephos) and proline derivatives.[16]

In 2010, Feringa *et al.* noted that monodentate phosphoramidites should also be treated like privileged ligands because they achieve impressive results over a large number of reactions.[15] Phosphites,[17–19] which are structurally close to phosphoramidites, unsurprisingly present similar behaviour and both ligands may be grouped in a family called monodentate P-donor ligands.[20,21] In view of the last decade, we argue that the list of privileged structures may be updated with

quaternary ammonium ions,[22,23] *N*-heterocyclic carbenes (NHC),[24] and phosphoric acids.[25,26]

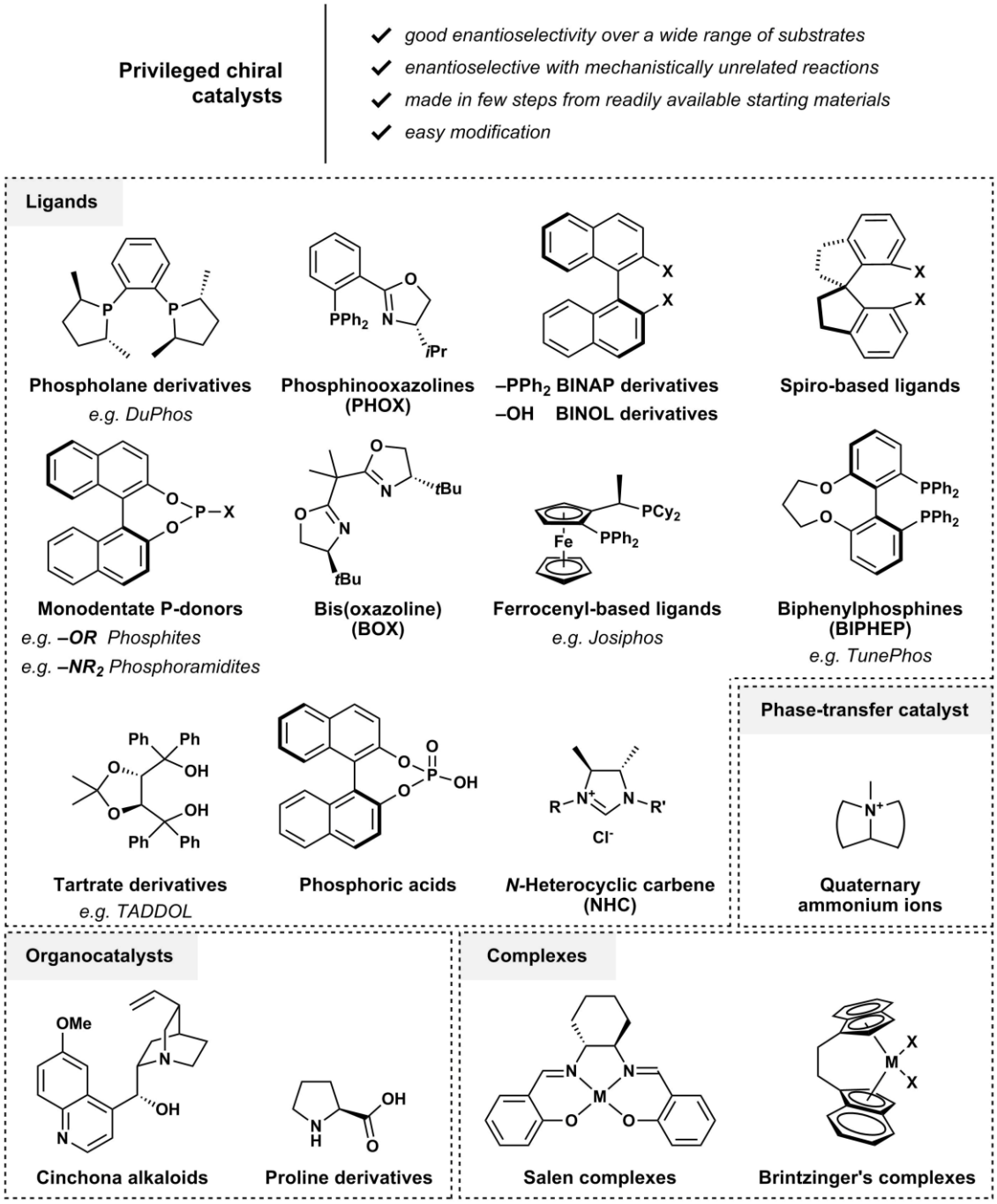

Scheme 1.2. List of privileged chiral catalysts.

2 Ligand design

The development of new asymmetric metal-catalyzed transformations to target new reactivities or substrates requires the optimisation of chiral ligands, which are usually chosen among privileged structures. Such ligand optimisation remains a challenge due to the absence of recipes to achieve high reactivity and enantioselectivity. The traditional approach involves the use of chemical intuition, from which a trained chemist derivatizes a core scaffold until satisfactory results are obtained. Accordingly, a lot of guesswork is needed which is heavily based on trial-and-error and systematic screening, a process that is often resource intensive and intellectually frustrating. As a result, other approaches to ligand optimisation have emerged that rely less on chance to save time, efforts and resources.

In this work, we are only interested in ligand design (or quantitative ligand optimisation). It is the rational derivatization of a ligand structure that is intended to improve the yield or the selectivity of the reaction under consideration.

Examples of ligand optimisation without ligand design are accelerated serendipitous discovery[27,28] and high-throughput screening (HTS).[29–31] Although these techniques are undeniably powerful, the notion of design lies in the protocol which examines numerous structures in a limited amount of time, but the derivatization of the ligand structure itself is not based on rational thinking. Conversely, mechanistically-driven ligand discovery is a robust way to rationally optimise a ligand[32–34] but its optimisation is a consequence of a deeper mechanistic understanding and is not the primary aim. In a mechanistic study, one is not examining conditions to improve enantioselectivity or reactivity, but the experiments are primarily intended to reveal

mechanistic insights. Although all these optimisation approaches are extremely promising, we will only focus on the quantitative ligand optimisation in this work.

Ligand design is possible if the modifications are somehow supported by quantitative predictions of enantioselectivity and not by qualitative guessworks. Its goal is therefore to quantify the impact of substituent modifications by correlating geometrical and chemical differences with *ee* values. However, this has been a longstanding challenge for those designing and studying asymmetric catalysis. Nobel laureate William Knowles explained this challenge when he was still working for Monsanto: "Since achieving 95% [enantiomeric excess] only involves energy differences of about 2 kcal [per mol], which is no more than the barrier encountered in a simple rotation of ethane, it is unlikely that […] one can predict what kind of ligand structures will be effective".[35] He points out here that the energy difference of high enantiomeric excess (>90% *ee*) is relatively small compared to a conformational change like the eclipsed-anti conformation of butane (16 kJ/mol, **Scheme 1.3**).

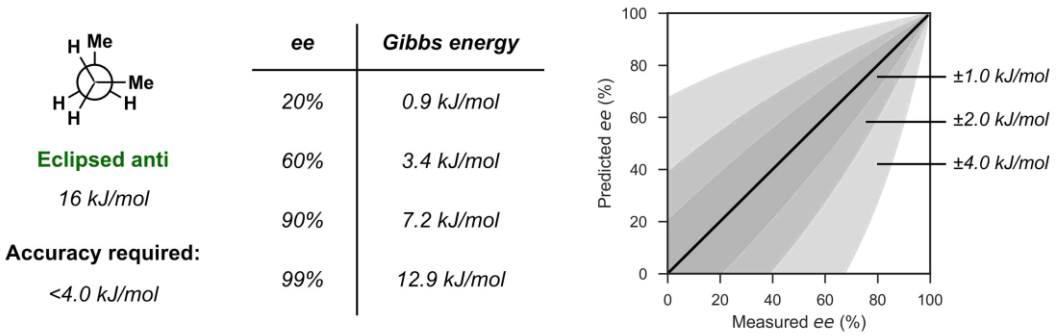

Scheme 1.3. To make useful enantioselectivity predictions, an accuracy of minimum 4.0 kJ/mol is required. The free energy calculations are realized at 293K.

For instance 90% *ee* represents a Gibbs energy difference of only 7 kJ/mol and 99% *ee* is 13 kJ/mol. An error in calculations of only 4 kJ/mol (1 kcal/mol) translates to predicting a racemic product or a selectivity of 60% *ee* at room temperature (**Scheme 1.3**). However, predictions at higher levels of enantioselectivity (>90% *ee*) are more robust to inaccuracies due to the exponential dependence to convert free energies into *ee's.* At 95% *ee*, 4 kJ/mol indeed represents a smaller error interval of 77% and 99% *ee*. Nevertheless, this remains a large amplitude of *ee* values and to achieve useful quantitative predictions, calculations must possess even tighter error margins (<4 kJ/mol). Such levels of accuracy are nowadays still testing the limits of most state-of-the-art computation tools which explain why Knowles expressed doubt at reliably predicting *ee* in 1982.

To generate predictive power, it is therefore crucial to probe the subtle energy differences between diastereomeric transition states, to which Knowles made reference. Based on the concepts of transition state (TS) and activation barrier, schematic energy profiles can be drawn to represent a catalyzed asymmetric transformation (**Scheme 1.4**).

Since enantiomers are isoenergetic, thermodynamic control obviously produces racemates and therefore asymmetric transformations are necessarily limited to reactions under kinetic control. Stereoselectivity is then determined by the relative rates of formation of each product and the measured *ee* is directly correlated to the difference in the rate of irreversible stereodetermining steps ($\Delta\Delta G^{\ddagger}$) of the two competing diastereomeric transition states (Equation **1.1** and **1.2**). *R* in equation **1.2** corresponds to the Gas constant and *T* the temperature. The major enantiomeric product is the one possessing the lowest TS.

$$ee = \frac{|R - S|}{R + S} \tag{1.1}$$

hence

$$ee = \frac{1 - e^{\frac{-\Delta\Delta G^{\ddagger}}{RT}}}{e^{\frac{-\Delta\Delta G^{\ddagger}}{RT}} + 1} \tag{1.2}$$

Most synthetic transformations, however, involve a multistep sequence such that the kinetic control scheme depicted in **Scheme 1.4** may be oversimplistic. In practice, several species likely equilibrate in asymmetric catalysis and if the interconversion is fast compared to the forward reaction, then the Curtin-Hammett scenario is met. In that case, $\mathbf{R_R}$ and $\mathbf{R_S}$ can be adducts of the prochiral substrate or conformations that are essential for the irreversible forward reaction to occur.

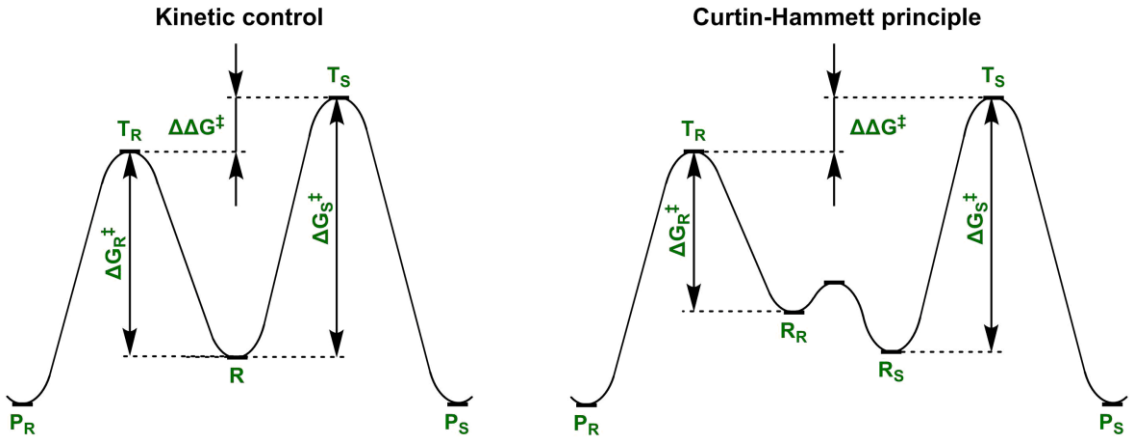

Scheme 1.4. Schematic energy profiles of a reaction under kinetic control or the likely more realistic Curtin-Hammett scenario.

The mathematical relationship between measured enantiomeric excess and computed ΔΔG‡ lays the foundation for the quantitative prediction of enantioselectivity. If the catalysts proceed via the same pathway, structural derivatization of ligands induces changes in the stereodetermining step that

translate into the empirical observations (*ee's*). The next sections showcase two approaches used to generate quantitative predictions of selectivity based on computation that probes the effect of ligand substitution. The first goes through the transition-state driven designs and the second is about data-driven models.

2.1 Transition-state based design

Transition-state driven ligand design computes both stereodetermining transition states $\mathbf{T_S}$ and $\mathbf{T_R}$, from which subtraction of the Gibbs free energies produces the $\Delta\Delta G^{\ddagger}$ value. This strategy requires a well-defined reaction mechanism to build a plausible transition state. Additionally, the level of theory should provide accurate $\Delta\Delta G^{\ddagger}$ values that are validated with experimental data and are converted into *ee's* within a useful interval.

Summarized by Houk *et al.*, this popular approach starts from a mechanistic hypothesis, from which a TS can be imagined (**Scheme 1.5**).[36] Using Molecular Mechanics (MM), conformational sampling of several ligands allows for the generation of initial geometries that are then used to optimise TSs with Quantum Mechanical (QM) methods. Once the computed $\Delta\Delta G^{\ddagger}$ values are in agreement with experimental data, a measured/predicted quantitative model is established. TSs are then scrutinized to identify the interactions responsible for enantioinduction but these are difficult to grasp using visual inspection alone and alternative tools such as non-covalent interaction (NCI) analysis are therefore useful at this stage.[37] The *in-silico* prediction of ligands is finally realised and allow for the synthesis of promising new ligands that will hopefully achieve higher selectivities.

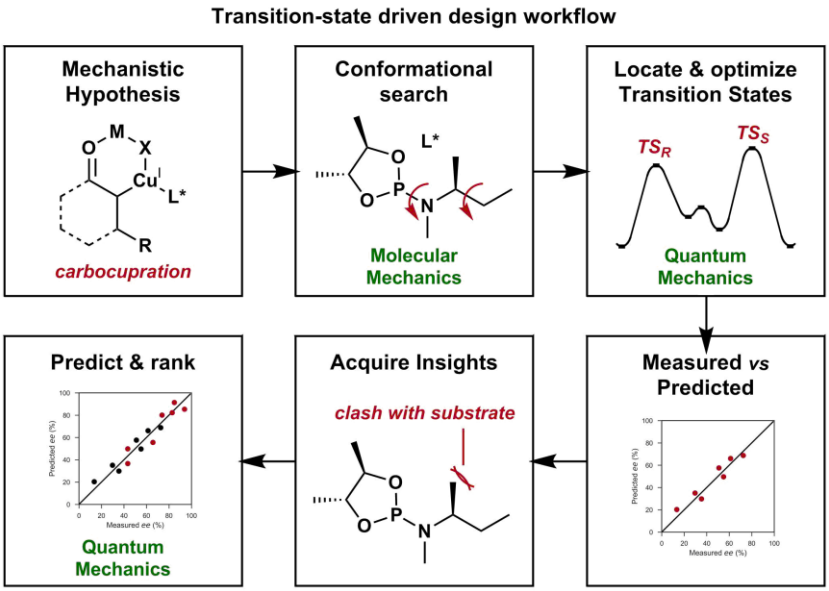

Scheme 1.5. General summary of workflow commonly used in the transition state-driven design of chiral ligands.

In 2017, Wheeler *et al.* alleviated much of the pain involved in this workflow by automating the quantum mechanical predictions of enantioselectivity for metal-catalyzed asymmetric reactions.[38]

QM calculations are usually limited by the computational power required to compute large and flexible systems. Geometries with hundreds of atoms can currently be used with the very popular density functional theory (DFT) methods but most TS optimisations are nevertheless carried out on truncated geometries, sometimes to their most simple forms with only key functional groups remaining. Such simplifications require further validation to confirm that the resulting model still sufficiently grasps the substituent effect to produce accurate quantitative predictions.

Although DFT is very popular, its accuracy remains challenging for quantitative selectivity predictions (~4 kJ/mol)[37] and can even be unreliable for the computation

of transition-state barriers, certain types of electronically excited states, or dispersion-dominated interactions.[39] Achieving accurate prediction is the Holy Grail in chiral ligand design and the hierarchy of functionals according to their simplicity against accuracy has already been established.[40] Among the different QM methods, correlated wave function theory (WFT) such as coupled-cluster (CC) represents the state-of-the-art in accuracy but the computational price to pay is high, even considering hardware amelioration over the years.[41] Geometry optimisation with such methods also remains out of reach and slower convergence is observed compared to DFT,[42] although these limitations have been mitigated through simplification schemes such as linear scaling (linear scaling CCSD(T))[39] or LPNO approximation.[43] Nevertheless, there is a trade-off between accuracy and computational power that leads to a low throughput of *in-silico* ligand calculations.

Aware of these limitations, quantum-guided molecular mechanics (Q2MM) have been developed by Norrby *et al.* to overcome the computational cost-accuracy intractability.[44] As shown in **Scheme 1.6-A**, once the stereodetermining transition states of a reaction have been identified using QM calculations, the workflow uses them to parameterize an inexpensive arbitrary force field to generate accurate reaction-specific fitted transition state force field (TSFF). Such process can take months.[44] Once the TSFF is validated with unseen ligands, the method reaches the production stage where it can be used on a large quantity of data at low computational cost. Thus, the accuracy of electronic structure calculations and the rapidity of a classical method are achieved. Such an approach has successfully been applied to a range of transition metal-catalyzed reactions, such as a Rh-catalyzed hydrogenation of ketones (**Scheme 1.6-B**).[44] Comparison of Q2MM-derived force

field and experimental results showed an impressive correlation of determination (R^2 = 79%), illustrating the predictive power of such an approach. Development of the force field, however, remains a daunting task that needs to be performed for each new reaction and requires a thorough mechanistic understanding.[44,45]

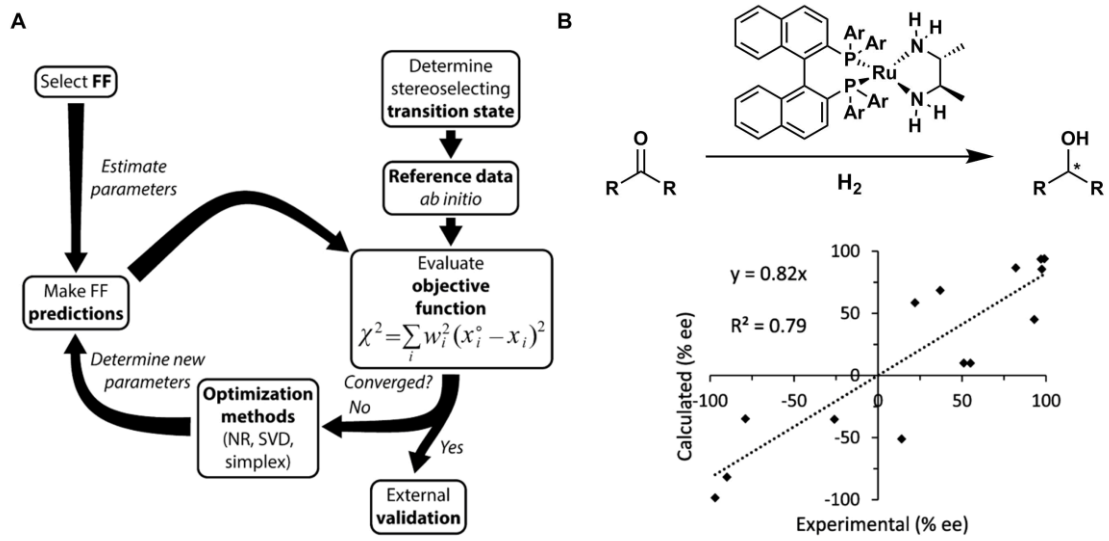

Scheme 1.6. A) Flowchart of the Quantum-Guided Molecular Mechanics (Q2MM) method developed by Norrby *et al.* and **B)** selectivity comparison of Q2MM-derived force field and experimental results for Rh-catalyzed hydrogenation of ketones. Reprinted with permission.[44]

Transition-state driven ligand design is undeniably one of the most powerful strategies for the rational optimisation of chiral ligands, but beyond the practical issue of computational cost and accuracy, the fundamental drawback remains that a well-understood mechanism is crucial to build plausible transition states. Unfortunately, there is usually a very poor mechanistic understanding in asymmetric catalysis, to say the least,[46] and guessworks involving much computational efforts are therefore required to fill the gap. Additionally, ligand optimisation is in practice needed during reaction development, at which point a

mechanistic study can not be realistically carried out. Further modification of experimental conditions, such as additives, can indeed profoundly modify the mechanistic pathway. Thus, insights about the mechanism remain limited during reaction development, which makes even more difficult the construction of plausible transition states for ligand design. Accordingly, the strong dependence on mechanistic hypotheses has led the scientific community toward finding alternatives to TS-based design.

2.2 Data-driven design

Statistical modelling methods fundamentally assume a relationship between chemical structure and selectivity, such that one or several independent variables (*e.g.* molecular descriptors) will describe the potency of a response (or dependent variable, *e.g. ee's*). Identification of a mathematical relationship provides insights into the interactions responsible for high enantioinduction, where molecular descriptors can be viewed as probes used to analyse the effect of catalyst modifications on stereodetermining TSs, without the actual need to calculate any TSs. Accordingly, no prior mechanistic knowledge is required[47] which makes such approaches particularly attractive in asymmetric catalysis.

Statistical model construction is inexpensive and the computational cost mainly lies with the generation of molecular descriptors. This is particularly true when working with physically meaningful descriptors where DFT level of theory is the norm. For instance, the Sigman laboratory has used infra-red molecular vibrations to describe key steric and electronic interactions in catalysis.[48] They first optimized each catalyst ground state using QM level of theory, then computed vibrations and selected the most interesting ones based on mechanistic hypotheses.

Nevertheless, the computational cost to compute ground states remains much lower than what can be found in TS optimisations, and it allows for an accuracy of ~2 kJ/mol[49,50] which should be viewed favourably compared to TS-based methods (~4 kJ/mol).[40,44] There is therefore a much better computational cost/accuracy ratio.

Statistical methods have limitations, and one of the most important appears when no satisfactory correlations between molecular descriptors and *ee* values can be found. This usually happens due to a need for different molecular descriptors that still have to be found. Another rare possibility is the presence of interactions that involve complex processes difficult to describe, in which case a statistically valid correlation might be laborious to achieve.

The first use of a quantitative structure-activity relationship (QSAR) can be traced back in 1962 when Hansch *et al.* correlated the biological activity of phenoxyacetic acids.[51] Since then, this approach has been heavily used in medicinal chemistry[52] and it is only in the new millennium that statistical tools started to be used on catalysts. Noteworthily, the Fey group played a major role in the development of ligand knowledge base (LKB),[20,21,53–59] which allowed for the development of comprehensive descriptor databases. In particular, the LKB introduced different "types" of descriptors such as electronic, steric and energetic. LKB also permits the comprehensive sampling of ligand space and help visualizing clustering of ligands in chemically meaningful subsets.[21] We must wait until 2003 for the Kozlowski group to realise the first quantitative structure-enantioselectivity relationship (QSSR) in asymmetric catalysis,[60,61] swiftly followed by the Hoogenraad group in 2005.[62] A few years later, the Sigman group accomplished several resounding works[26,48,52,63,64] that

played a fundamental role at igniting a great deal of interest in the use of QSSR in catalysis. More particularly, the Sigman group employed state-of-the-art multivariate modelling to predict reaction enantioselectivity of an asymmetric C–N dehydrogenative coupling (**Scheme 1.7**).

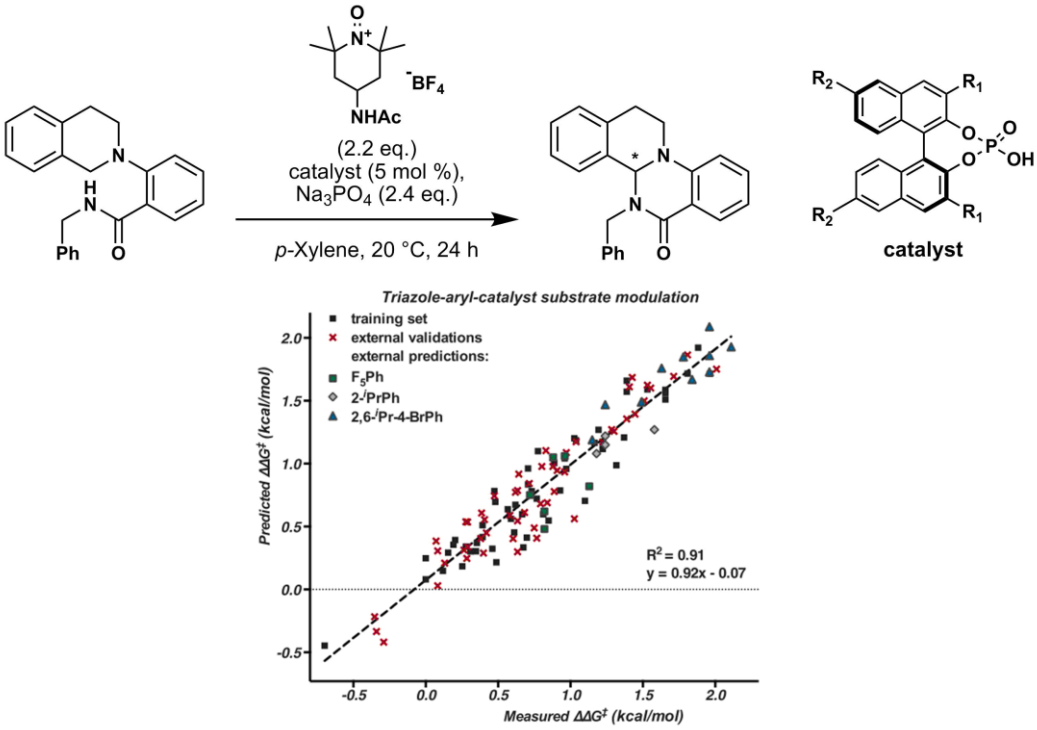

Scheme 1.7. Sigman's use of multivariate modelling to predict reaction enantioselectivity of an asymmetric C–N dehydrogenative coupling. Reprinted with permission.[26]

Using a BINOL-based phosphoric acid catalyst and different substrates, they successfully predicted the enantioselective outcome by describing both the substrates and catalysts with molecular and vibrational descriptors. It resulted in a model equation with eleven different parameters, describing a correlation with an excellent goodness-of-fit (R^2 = 91%) and externally validated with unseen values.

A plethora of statistical regression methods have been explored in asymmetric catalysis, among which one of the most popular is the ordinary least squares regression (OLS). Its simplest form is the univariate linear regression which is often called linear free energy relationship (LFER). LFERs in asymmetric catalysis are usually depicted with the activation free energy ($\Delta\Delta G^{\ddagger}$) on the y-axis and a molecular descriptor (*e.g.* Charton) on the x-axis.[63,65] In most cases, univariate correlations are however insufficient to explain selectivity and describing complex interactions requires the use of multiple molecular descriptors where α is the intercept and β_j the regression coefficients of the molecular descriptor x_j (Equation **1.3**).

$$\Delta\Delta G^{\ddagger} = \alpha + \beta_1 x_1 + \beta_2 x_2 + \cdots + \beta_n x_n \qquad (\mathbf{1.3})$$

This corresponds to a multivariate least squares linear regression that is commonly referred to as multivariate linear regression (MLR).[66] It is a very popular approach in asymmetric catalysis[67,68] that uses datasets of moderate size.[37] The tremendous successes of LFER and MLR resulted in the linearity approach remaining unchallenged until 2011 with the first nonlinear multivariate least squares regression in asymmetric catalysis.[64] However, the loss of linear relationships also signaled the end of models that are easily explained: a feature that played a substantial role in the adoption of QSSR by the scientific community.

Another regression method used in asymmetric catalysis is partial least squares regression (PLS).[62] This is useful when working with a large set of molecular descriptors (*e.g.* $>10^2$ descriptors for a unique *ee* response), wherein the use of a dimensionality reduction algorithm (principal component analysis, PCA)[69] is highly recommended due to the fact that a large number of interrelated variables likely

exist. The objective of PLS is to create linear combinations of the original molecular descriptors to explain most of the variation observed in both descriptors and response (unlike Principal Component Regression, PCR, which only takes into account descriptors). Such combinations of descriptors are called latent variables, which are then used in the least squares regression, hence *partial* least squares regression. Accordingly, the dimensionality reduction improves the modelling efficiency and solves the descriptor colinearity issues but complicates the model interpretation. Such regression method is common in grid-based QSSR.[70–73]

More recently, support vector machine (SVM) and neural networks (NN) regression methods have been investigated for the first time in asymmetric catalysis by the Denmark's group (**Scheme 1.8**).[50] Their workflow started by constructing an *in silico* library of synthetically accessible catalysts within four well-established synthetic steps and then computed molecular descriptors generated from optimized 3D geometries for both substrates and catalysts. The catalyst space was then mapped using the first two principal components and the authors selected only a representative subset of the catalyst space with a Kennard-Stone algorithm, the so-called Universal Training Set (UTS, **Scheme 1.8-A**). With Denmark's approach, the catalyst space was thoroughly explored and allowed for *intrapolated* design of new catalysts, which they claimed helped building more robust predictive models. Such mapping approach however requires that the optimum ligand is *within the chosen feature space*, and that all the features being explored are *worth the resources* in terms of synthesis (time, labour).

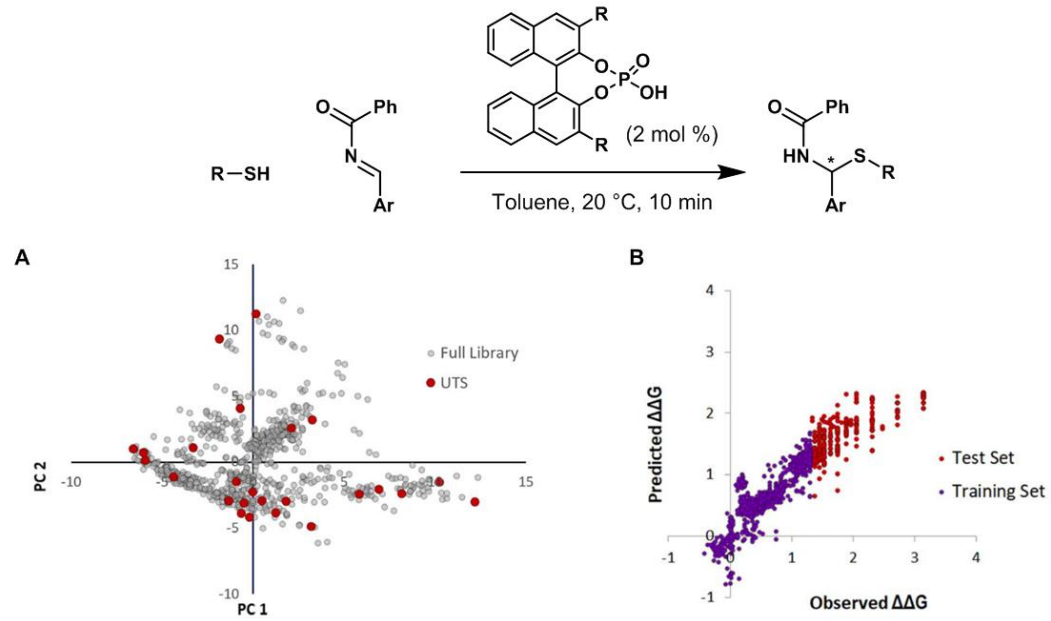

Scheme 1.8. Denmark's use of machine learning to predict reaction enantioselectivity of *N,S*-acetals formation. **A)** 2D chemical space of catalysts and **B)** prediction of enantioselectivity of *N,S*-acetals formation using a deep feed-forward neural network. Reprinted with permission.[50]

A deep feed-forward neural network was finally created by only using the data giving outputs below 80% *ee* in the training set (substrates & catalysts), and the remaining data in the test set, thus simulating an actual reaction optimization where no highly enantioselective catalyst has been found yet (**Scheme 1.8-B**). An impressive correlation was obtained, where the model successfully predicted the reaction outcomes with *ee*'s above 80%, which the author claimed showcased the capability of their approach to predict selectivity of higher-performing catalysts. However, based on the supporting information, it seems that some of the catalysts did not satisfactorily worked with few substrates (*ee* < 80%), while being selective with others (*ee* > 80%). Thus, most catalysts were actually found in both training and test sets due to the choice of data splitting based on the *ee* threshold only (80%),

and not on the combination of catalysts and substrates. As most of the catalysts chemical information was already described in the training set, the successful predictions in the high-performing regime are somewhat less impressive and less representative of an actual reaction optimization where the best catalysts have not been synthesized yet.

To our knowledge, K nearest neighbors (kNN), random forest (RF) and generalized linear model (GLM) have not been employed in enantioselectivity prediction yet. Although not based on an asymmetric reaction, a noteworthy contribution from the Doyle's group successfully employs such algorithms to predict the reaction performance of a C–N cross-coupled reaction (**Scheme 1.9**).[74] The raw data was obtained from high-throughput experimentation and they computed atomic, molecular and vibrational descriptors to correlate the observed reactivity. Using these descriptors as inputs and yield as output, they explored several regression algorithms, among which random forest showed the best predictive power on out-of-sample predictions. However, they did not demonstrate accurate predictions beyond the bound of the training data, whereas such predictive power is essential for the usefulness of predictive modelling in catalysis. More importantly, Keiser *et al.* consecutively showed that Doyle's models trained on chemical features, random features or one-hot encoding gave similar levels of goodness of fit,[75] suggesting that the observed correlation was not based on any chemical information. This also drastically reduced the impact of the discovery and reminded us the importance of internal and external validations even with machine learning algorithms.

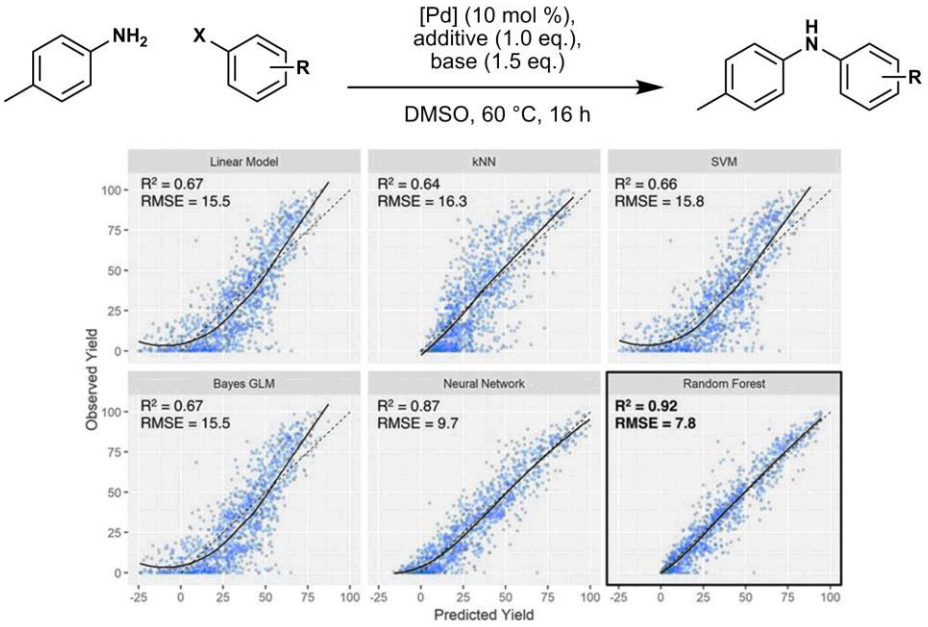

Scheme 1.9. Doyle's use of machine learning to predict reaction performance of a C–N cross-coupled reaction. Reprinted with permission.[74]

Developed in the 60s,[76] these machine learning regression methods shows remarkable promise in identifying patterns in large datasets (*e.g.* >500 entries in ligand design) but the mathematical relationship between chemical structure and selectivity is now a complete black box.[77] These "black box" methods tend to be more data-hungry than the more interpretable ones, such that there is a fundamental tension between methods and data availability. For instance, the utility of modelling databases of large size is arguable as one would expect to already have a workable system after so much screening effort, particularly in catalysis. The crucial need of large datasets in a field where data are usually scarce therefore contributes to its limited applicability in enantioselectivity prediction, as yet.

The choice of regression method also depends on the primary objective of the study. Accuracy and generalizability are compulsory for predictions in ligand design while model interpretability can be put aside. Conversely, modelling for mechanistic

insights requires meaningful descriptors and linear interpretable models, albeit diminished predictive power. Although the algorithms are fundamentally different, their general workflow of ligand design remains similar.

A common way to introduce this workflow to a non-expert audience employs the cartographic metaphor (**Scheme 1.10-A**). Supposing that the altitude corresponds to the enantioselectivity and the map to the catalyst chemical space, then the objective of ligand design is to identify the highest mountain in Western Europe as efficiently as possible. In that scenario, the ocean and the seas could be all the catalysts that are theoretically accessible but in practice unfeasible. Since finding a mountain in the Netherlands for instance would be counterproductive as the highest mountain is a hill, the first step usually involves the exploration of the map to identify a promising "lead", an area around which high mountains (*i.e ee's*) are likely to be found and thorough examination is promising. There exist many different approaches. It usually starts with a pragmatic exploration of the major cities (location marker) because they have the benefit of being well-served by transport links. In this metaphor, this corresponds to the easy synthesis of ligands (**Scheme 1.10-B**). Unfortunately, we might also miss important areas and if visiting major cities was unsuccessful, we can still establish a grid and systematically transit to each intersection. However, this should be a case of last resort as such specific places may sometimes be hard to reach. In our case, we directly find the city of Zurich to be an excellent lead candidate and start the second step which is the iterative model construction. At the beginning, we do not have any information about the topography around the city and we therefore start with small modifications of our coordinates (black dots).

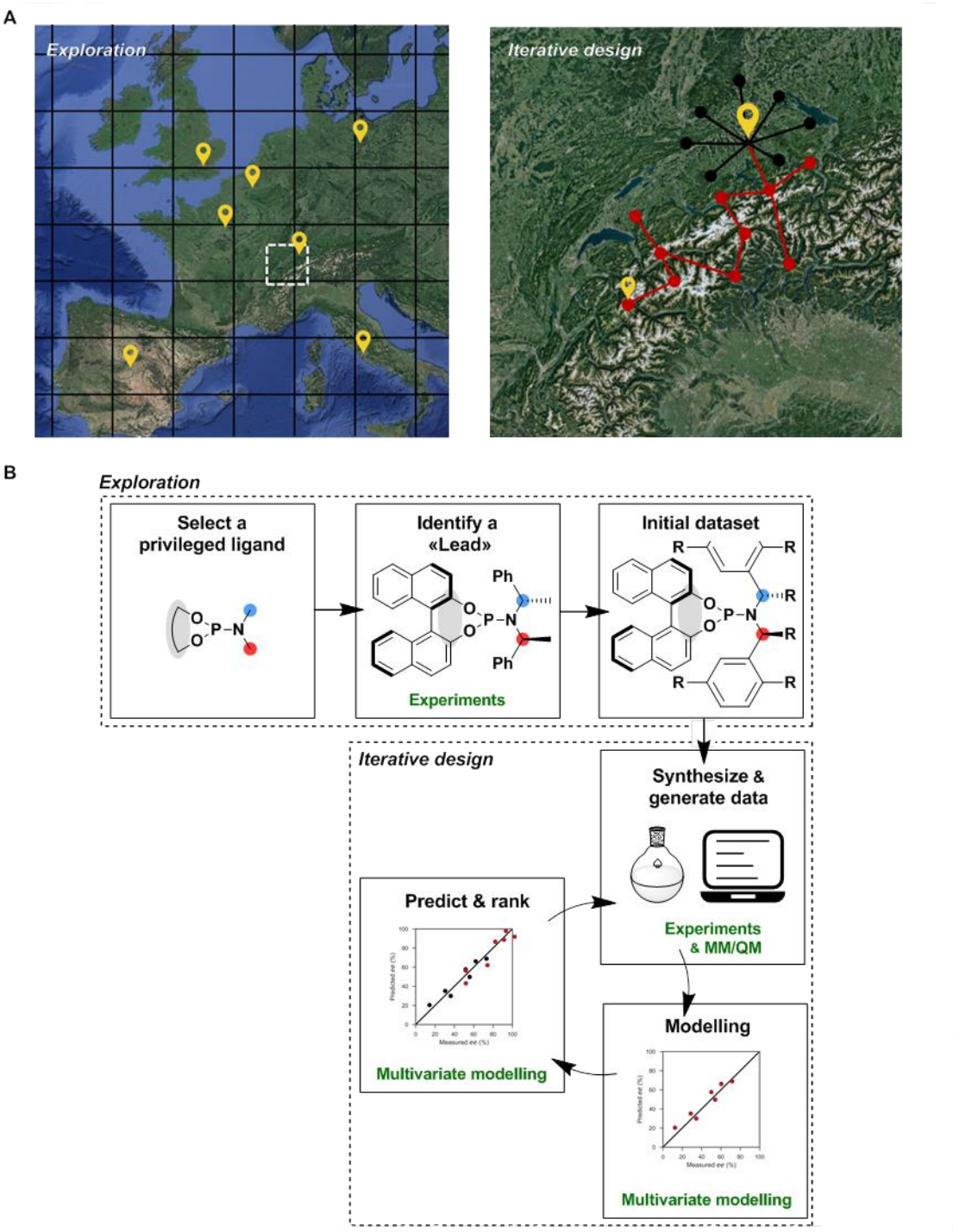

Scheme 1.10. A) Cartographic metaphor explaining the philosophy of statistical modelling. **B)** General summary of workflow commonly used in the data-driven design of chiral ligands.

This enables the creation of our initial dataset and modelling of the altitude allows us to reach our first mountain pass (red dot). The altitude of the new coordinates

can then be included in the model in an iterative way, such that the predictive power of the model gradually gets stronger. After ten iterations (red dots), we fortunately find the highest mountain in Western Europe. As shown in **Scheme 1.10-B**, the commonly used workflow in the data-driven design of chiral ligands is similar. The catalyst chemical space is huge and the first step therefore involves exploration of structurally different ligands, from which ligand synthesis is usually the rate limiting step. A promising core scaffold is then identified ("lead") and iterative design allows for improving the enantioinduction of the ligands.

3 Multivariate modelling workflow in details

In this work, multivariate modelling (MLR) is the most suited regression algorithm due to the use of datasets of moderate size (~20 datapoints) and the ease at interpreting the models to gain mechanistic insights.[66] This section describes in details the workflow of model construction which will be used throughout the chapters, and underpins the essential statistical steps (**Scheme 1.11**).

3.1 Exploration

Building a statistical model requires that a ligand achieves at least a sufficient range of activation free energy ($\Delta\Delta G^{\ddagger}$, *ee*) to describe trends in the data. Here, we propose >2 kJ/mol (>40% *ee* at room temperature), which is the common accuracy achieved with statistical modelling of metal-catalyzed asymmetric transformations.[67,68] Traditionally, a ligand scaffold is directly selected based on literature precedence, such that the core scaffold is implicitly supposed to have been found without any exploration.[64,65]

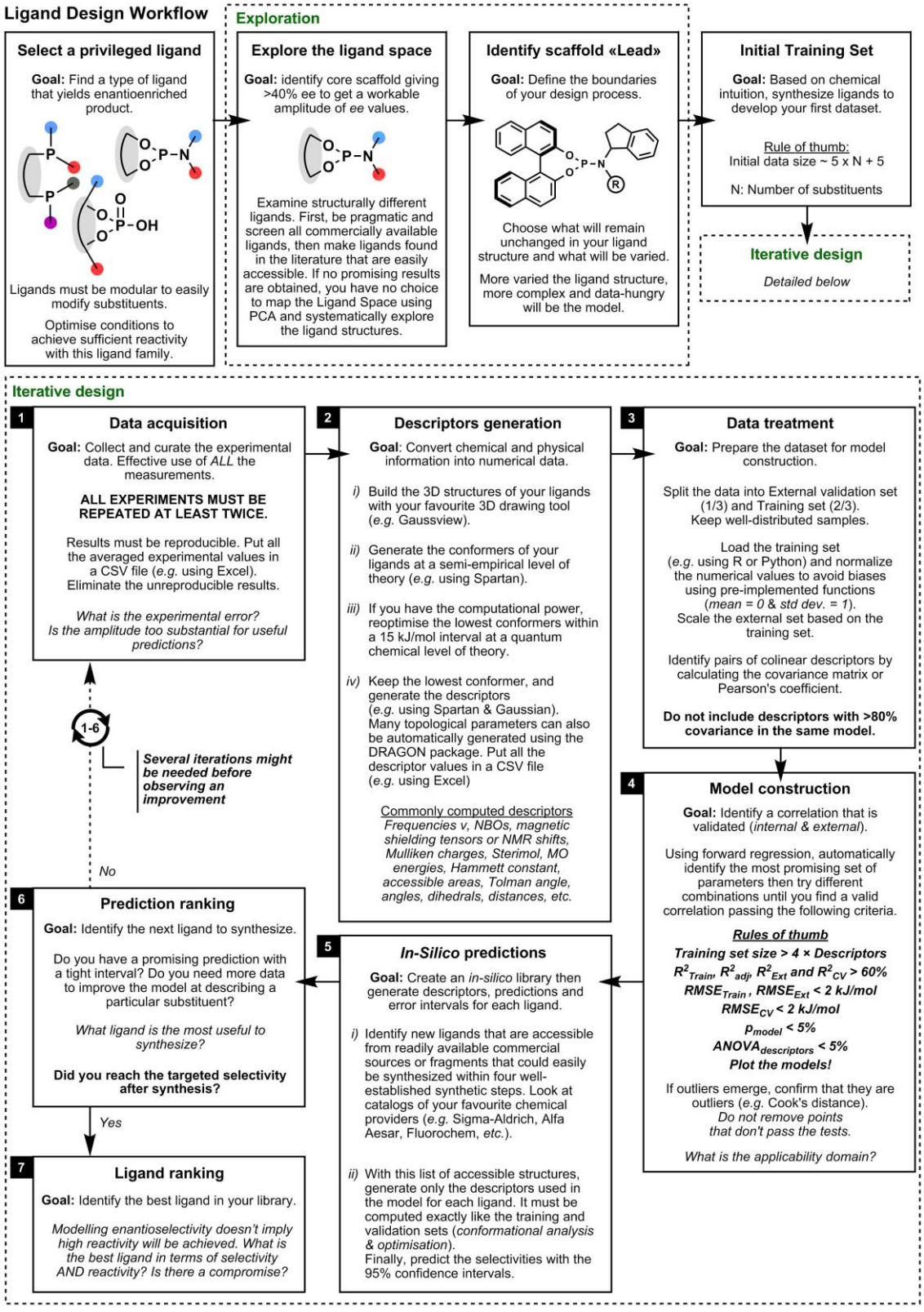

Scheme 1.11. Detailed ligand design workflow used in this work.

However, development of novel reactions or expanding the scope of a reaction on substrates known to be incompatible with a catalyst often requires completely revisiting a ligand core scaffold.

In such case, exploring the Ligand Space (LS) plays a crucial role, which consists of finding a ligand achieving high enantioinduction as effectively as possible. Here, a LS relates all the possible ligands within chosen boundaries that are described by a set of features. Each feature represents an axis and their combination forms a multidimensional space which can be huge (10^{60} compounds in pharmaceutics).[78] Accordingly, the LS is (usually implicitly) limited to a specific family of ligand (*e.g.* phosphoramidites). Such a statistical approach is well-suited to the study of "privileged" catalysts and/or ligands, since these provide a tunable platform on which to optimize catalytic performance. There exist two common strategies to efficiently explore the LS.

First, the pragmatic approach enables a severe reduction of the LS to easily accessible ligands.[67,79] For instance, laboratories often possess ligand databases and the initial search may be limited to what is available to the chemists. Selection of ligands can also be based on their commercial availability or the easy preparation of their precursors. The selected compounds are then categorized (often by chemical intuition) and only the most structurally different ligands are examined. Hopefully, a ligand lead (>40% *ee*) is then identified. The pragmatic approach should always be realised first as it seems unnecessary to further explore the LS if easily accessible ligands are suitable candidates. However, such a strategy is sometimes not sufficient, and a systematic exploration is then required.

The second approach maps the ligands according to chosen molecular descriptors and rationally categorizes the corresponding LS.[50,53,80] The representative ligands of each group are then examined and fortunately one of them usually shows promise. Because there are too many dimensions in the LS to be interpreted, dimensionality reduction algorithms (*e.g.* principal component analysis) are a prerequisite before clustering (*e.g. k*-means or Kennard-Stone methods). Note that in this approach, molecular descriptors are chosen to differentiate between different ligand structures but the relative importance of a given feature descriptor is *a priori* unknown. Therefore it can lead to the exploration of unimportant feature space while substantial efforts have been invested into the synthesis of ligands. Ligand synthesis is usually the limiting factor in the design process and there is little appeal to invest the considerable resources (time, money) needed to prepare many ligands prior to identification of a lead. Arguably, the ligands can be reused during the development of other reactions and they constitute the so-called universal training set,[50] such that the synthetic investment might be beneficial in the long run. Nevertheless, this mapping approach remains the best to rationally explore the LS, particularly if the optimum ligand is *within the chosen feature space*.

3.2 Iterative design

3.2.1 Data acquisition

Data collection plays a crucial role in the construction of a statistically valid model. Compounds present in the dataset should be homogeneous, where homogeneity in the case of ligand design designates a diverse class of compounds that are all related with an identical mechanistic pathway.[81] Additionally, we found that there is an absolute requirement to repeat all the response variables (*ee's*) at least twice using

identical reaction settings. This allows for the detection of irreproducible results that inherently damage the predictive quality of a model due to the presence of substantial statistical noise. A highly irreproducible value should be removed from the dataset or repeated until the source of uncertainty is resolved. Additionally, the analysis of the repeats quantifies the experimental error and we propose that this error should be within <3% *ee* on average in the case of chiral ligand design. We also found it difficult to know how much data are needed before starting to model. Here, we propose to correlate the size of the initial dataset with the number of substituents *N* being varied (Equation **1.4**).

$$size\ of\ initial\ dataset \approx 5 \times N + 5 \qquad (\mathbf{1.4})$$

After acquisition of the experimental data, statistical modelling requires the generation of molecular descriptors for each catalyst to convert chemical and physical information into numerical data. Historically, those are derived from experiments and published in tables, with a famous example being the Charton descriptor.[82] However, numerous substituents are absent from these datasets and measurement of the missing data requires synthesizing the compounds of interests and using identical experimental settings. This is an expensive and time-consuming process such that there is little appeal to complete the datasets. Accordingly, computable descriptors are nowadays much preferred over experiment-based tabulated values. Some computed molecular descriptors are, however, purely theoretical and not based on any physically meaningful properties, which lead to models that are hard to interpret.[83,84] Accordingly, the use of newly developed[85] or unearthed[52] physically meaningful descriptors is highly recommended.[86]

These molecular descriptors can be classified as either electronic or steric although these two categories are not absolute.[87] On one hand, electronic descriptors describe any variation related to the electronic density, which engulfs covalent (*e.g.* NBO,[88] HOMO energy,[89] IR,[88] NMR[90]) or non-covalent interactions (*e.g.* π-interactions[85,91]).[47] On the other hand, steric descriptors refer to the 3D shape of the molecule and the changes caused by the substituents (repulsion, volume, surface and distance).[47] A "steric effect" is a somewhat intuitive yet controversial notion that has no uniform definition such that several steric descriptors have been developed to describe similar interactions (*e.g.* interference,[92] Taft,[93] Charton,[94] A values,[95] B values,[96] Sterimol,[97] Tolman's angle[90,98]). The steric and electronic descriptors that have been implemented in asymmetric catalysis are summarized in **Table 1.1**. Diversity of the descriptor nature usually aids with describing the complex interations involved in enantioinduction.

3.2.2 Data treatment

After acquisition, the data must be reordered randomly to remove any systematic variation in the dataset and avoid patterns from the experimental screening. Then, the dataset is split into training and external validation sets, whereby the model is built on the training set and its predictive power is validated with the unseen values saved in the external validation set. We empirically found that a working ratio used in model construction is ⅔ for the training and ⅓ for the external validation. It is important to preserve a good statistical distribution of the sample and some chemical similarities in both sets, to the extent that the splitting is quasi-random. Molecular descriptors also possess numerical values that describe different orders of magnitude (*e.g.* ^{1}H NMR between 0-10 ppm and ν_{IR} between 800-2500 cm^{-1}) such

that the relative importance of each descriptor might be biased in the mathematical relationship. To avoid such issue, the values are normalized to obtain a null dimension (Equation **1.5**), where the sample (x) is substracted to the mean ($\bar{x}$) and the resulting value divided by the standard deviation (σ).

$$x_{norm} = \frac{x - \bar{x}}{\sigma} \qquad (\mathbf{1.5})$$

Normalisation of the data is realised on the training set while the validation set is converted accordingly, but it must not be realised on the entire dataset as this would output a training set that is not normalized ($\bar{x} \neq 0$ and $\sigma \neq 1$).

In multivariate modelling (unlike PLS regression), highly intercorrelated descriptors must also be avoided in the same model,[66] called colinear or confounded descriptors. They cause the redundant description of an interaction in a model such that the corresponding regression coefficient estimates can be erroneous, thus deteriorating the model reliability. Study of the covariance matrix helps identifying such confounded descriptors, whereby pairs of descriptors with a covariance above 80% must not be used simultaneously.[99] A popular alternative is the correlation coefficient (r) also called Pearson's coefficient, which is the covariance of two variables divided by the product of their standard deviations and is usually depicted as a colourful correlation heatmap.[100] It is used to measure the linear correlation between two descriptors.

Table 1.1. List of descriptors used in asymmetric catalysis and selected examples.

Descriptors	Description	Sources	Examples
Taft	Steric descriptor describing the relative rates of hydrolysis in methyl esters. Experimentally based.	seminal work & tabulated values[93]	101
Charton	Taft-based steric descriptor that approximate substituents as sphere-like. Experimentally based.	seminal work & tabulated values[82,102]	101,103
Sterimol	3D structure steric descriptor made of three subparameters: two width parameters (B_1 and B_5) and a length parameter (L). Computationally based.	seminal work[104] Python code[87]	88,89,101,105
Tolman	Steric descriptor using cone angles (originally used on phosphines). Computationally based.	seminal work[106] Python code[87]	101
Hammett	Electronic descriptor for aromatic substituents. Derived from the pKa of benzoic acid derivatives. Experimentally based, but can be computationally approximated.	seminal work[107] comp. approx.[108]	88,103
NCI	Electronic descriptor for non-covalent interaction. Computationally based.	seminal work[85]	85
NBO	Electronic descriptor describing atomic electron density. Computationally based.	*ND*	88,105
MO	Electronic descriptor describing electron density using molecule orbitals. Computationally based.	*ND*	89
IR	Electronic descriptor describing electronic density affecting bond frequencies. Computationally based and experimentally based.	seminal work[48]	88,101,105

3.2.3 Fitting

Once the set of descriptors has been curated, fitting molecular descriptors to a response variable entails selecting a combination of molecular descriptors. There exist algorithms (usually pre-implemented) to automatically identify the descriptor linear combination that best correlates the response variable. The most popular methods are forward and backward selections. Forward selection starts from an empty formula (null) and incrementally adds descriptors until no further improvement is observed based on Akaike information criterion (AIC). AIC estimates the quality of each model, relative to each other models and the number of descriptors involved to avoid overfitting.[109]

Conversely, backward selection uses all the descriptors at the beginning then discards stepwise the descriptor with the lowest contribution. Forward selection is less prone to overfitting and is usually preferred, although forward followed by backward selection is also utilized. Both selection algorithms are, however, limited to linear combinations of descriptors and do not assess the relevance of cross-terms (*e.g.* NBO × Charton), which could be describing a synergy between terms. A common issue is also the selection of descriptors that have the best contribution in the training set but fail to account for generalizability in the external validation set. As a result, there is a trade-off between the goodness-of-fit and the predictive ability of a model. Testing different combinations of descriptors that achieve lower fit on the training set, but better generalizability of the entire dataset, is often essential to identify a predictive model.

Overfitting is the use of too many descriptors in the model equation compared to the amount of datapoints and must be avoided.[110] This causes the model to describe the

statistical noise as if it was relevant to the enantioselectivity response. A rule of thumb is to have at least four times more datapoints in the training set than descriptors (**Scheme 1.11**).[111]

Once a promising combination of molecular descriptors is found, the fitting outputs a coefficient of determination (R^2). It represents the variance explained by the model divided by the total variance, such that 90% R^2 means that the model explains 90% of the variance in the training set. It is an indicator of the goodness-of-fit but is not sufficient. R^2 has many caveats famously depicted by the Anscombe's quartet[112] and it is highly recommended to always plot the associated data. A R^2 greater than 60% is usually acceptable.[111] Alternatively, the adjusted coefficient of determination (R^2_{adj}) is popular because it penalises the use of additional descriptors in the model, thus reducing the impact of overfitting.

Finally, outliers can emerge at this stage of model construction, which is why plotting the models is important. A satisfactory R^2 can hide a regression possessing isolated outliers or break of linearity and simply plotting the models allows for their immediate detection. Isolated outliers usually appear due to measurement errors or irreproducible results, but break of linearity tends to be due to mechanistic change with different activation barriers.[66] The most popular tools to identify outliers from the sample are the boxplot visualization technique, the Cook's distance or the leverage point,[113,114] and it is important to keep datapoints that do not pass such tests.

3.2.4 Statistical significance

Correlation does not imply causation. For instance, a relationship between *ee* and molecular descriptors can be obtained by chance, originate from flaws in the

measurements and the model construction, be indirect with a third (unknown) variable, or finally be a direct correlation with causality.[81] Thus, several tests (significance, internal and external validations) are used to confirm that the correlation truly describes a relationship between chemical structure and selectivity.

The significance test (called F-test) tries to estimate the probability (p-value) that the correlation occurred by chance, which is the null hypothesis. In this hypothesis, our model fits the response as equally as an intercept-only model (no molecular descriptors). If the probability of the null hypothesis is less than 5%, then the model is significant. However, 5% is a thin threshold and it is always better to obtain substantially lower p-values (*e.g.* 0.05%). Such tests are usually pre-implemented in statistical softwares.

Descriptors can jointly achieve a significant model compared to the null hypothesis, but they can still individually contribute to the response by chance. Thus, it is crucial to carry out an analysis of variance (called ANOVA test) to calculate the probability (p-value) that a descriptor truly relates a chemical interaction. Accordingly, each descriptor must also possess a p-value below 5% for the model to be significant.

3.2.5 Internal validation

Internal validation demonstrates that a model provides accurate predictions regardless of the sampling distribution in the training set. For instance, some models can be sensitive to inclusion or exclusion of datapoints in the sample, particularly with the use of small datasets (<30 variables). Such a test can be viewed as a measure of robustness and generalizability. There are several internal validation methods, but the most popular are bootstrapping and leave-many-out cross-

validation (n×k-CV). In this work, only cross-validation has been used. The method randomly divides all the datapoints from the training set into subsets of a fixed number (k), then removes one subset at a time and retrains the same model formula based on the remaining data. Average of the coefficient of determination of the predictions of each hold-out subset allows quantifying the effect of the sample distribution on the statistics of the model. Data splitting with $k > 1$ leads to a variety of combinations such that the k-fold cross validation is repeated n times to avoid biases, hence n×k-CV.

As our datasets are of moderate size (~20 entries), we only use leave-one-out cross validation in this work (LOOCV *i.e.* 1-CV). The goodness-of-prediction can be estimated with R^2_{CV}, where 60% is generally acceptable.[111] Note that R^2_{CV} is also called Q^2, but this terminology is equally used in internal or external validation such that it can be ambiguous and we prefer to avoid it. Indeed, Q^2 is implemented in popular packages to be applied by default on the external validation set but if no data is provided, then the predictive power is calculated using a cross-validation.

3.2.6 External validation

Since a model is truly useful in ligand design only if it can reliably predict the enantioselectivity of new ligands, the external validation is an important prerequisite.[115] Using the external validation set previously hold out, the predictions obtained with the model are compared to the unseen experimental values. Thus, the predictive power is estimated using R^2_{ext}, where 50% is usually acceptable.[116]

Note that the terms external validation or test sets are used interchangeably, although the subtle difference between both is that the test set usually involves the predictions to happen before the experimental results.[66]

3.2.7 Domain of applicability

Models are useful but also inherently incorrect because they only capture parts of reality provided by the training set. Although a model is significant, robust and validated, it would not be infinitely linear and applicable on any chemical structure. The domain of applicability is therefore used to define a chemical space (based on descriptors) in which the model makes reliable predictions at a given accuracy. There is no singular definition of the domain of applicability and it mostly depends on the objectives of the model.

However, ligand design entails predicting *ee* values greater than those already achieved so far, such that prediction using a *linear* regression *necessarily* involves extrapolation to a previously unexplored region of descriptor space. Defining the domain of applicability is therefore unhelpful in the specific case of identifying better ligands with linear regressions. Additionally, the iterative nature of the ligand design workflow allows for learning from exploring less reliable regions.[99] Finally, the change in predictive reliability is usually gradual, so that extrapolated predictions can remain useful although deviating from reality.

In that regard, an (implicit) domain of applicability is recommended to identify predicted values that might be overly optimistic as they are far away from the training set, but it should be seen more like an advisory measure to be substantiated by an expert judgment.

3.2.8 Prediction errors

The final step of our workflow involves the construction of an *in-silico* library based on chemical intuition and limited to structures that are readily available commercial

sources or easily-synthesized fragments (**Scheme 1.11**). Once the descriptors are acquired, they are normalized based on the training set.

Feeding the model with this *in-silico* library produces predictions that can be used to select the most promising ligands to synthesize in the next round. It is interesting at this stage to measure the prediction error to take the best decisions, as values predicted with the highest enantioselectivity might also possess the largest amplitudes of error. Ideally, error estimation should provide an average error of no more than 2 kJ/mol. There exist three possible sources of error in a model: the experimental measurement, the descriptor acquisition, and the statistical model. The experimental error is already estimated during data acquisition, but it is worth noting that the model can not be more accurate than the noise brought by the experimental error. Descriptor acquisition is, however, a source of error that is often underestimated. It is hardly quantifiable as this can be as broad as the level of theory utilized to compute the descriptors or the use of proper conformational sampling. Inadequate acquisition can even lead to the appearance of outliers.[110] The final source of error comes from the statistical model and it can be quantified with the 95% confidence interval. This measure is useful because among 100 ligands that are synthesized, 95 of them should statistically be within the boundaries of the interval. As these errors are cumulative, note that the overall prediction uncertainty is often underestimated.

4 Project aims

Discovery of new asymmetric metal-catalyzed transformations is closely related to the development of efficient and robust chiral ligands, such that ligand optimisation is a crucial step in reaction development but its success is highly uncertain. Such a daunting task can be intellectually frustrating and exhausting, wherein the use of any predictive tool is much appreciated. The limited mechanistic knowledge in asymmetric catalysis is unfortunately prohibitive to the use of many computational techniques. As a result, we turn our attention toward multivariate modelling, which is believed to be a promising platform to rationally drive the successful identification of a highly enantioselective ligand. In this work, we aim to apply such a strategy to metal-catalyzed asymmetric transformations developed in our group where the ligand design previously failed using traditional approaches. Additionally, we hope that the computational workflow presented in these projects will be sufficiently accessible to organic chemists to be reused, as this general approach is theoretically applicable to any asymmetric transformation with the use of any privileged ligand. **Chapter 2** fully uses multivariate modelling to reoptimize a copper-catalysed asymmetric conjugate addition of alkylzirconium species that failed on sterically challenging substrates (**Scheme 1.12**). While modelling, we realized that conformational sampling could yield large amplitudes of underestimated uncertainty in predictions. Thus, conformational effects on physical-organic descriptors are explored in **Chapter 3** with the specific case of Sterimol parameters, from which new parameters called wSterimol ("weighted Sterimol") were developed. Finally, the ligand design workflow is applied on the development

of a copper-catalysed asymmetric conjugate addition to exocyclic enones that is developed in **Chapter 4**.

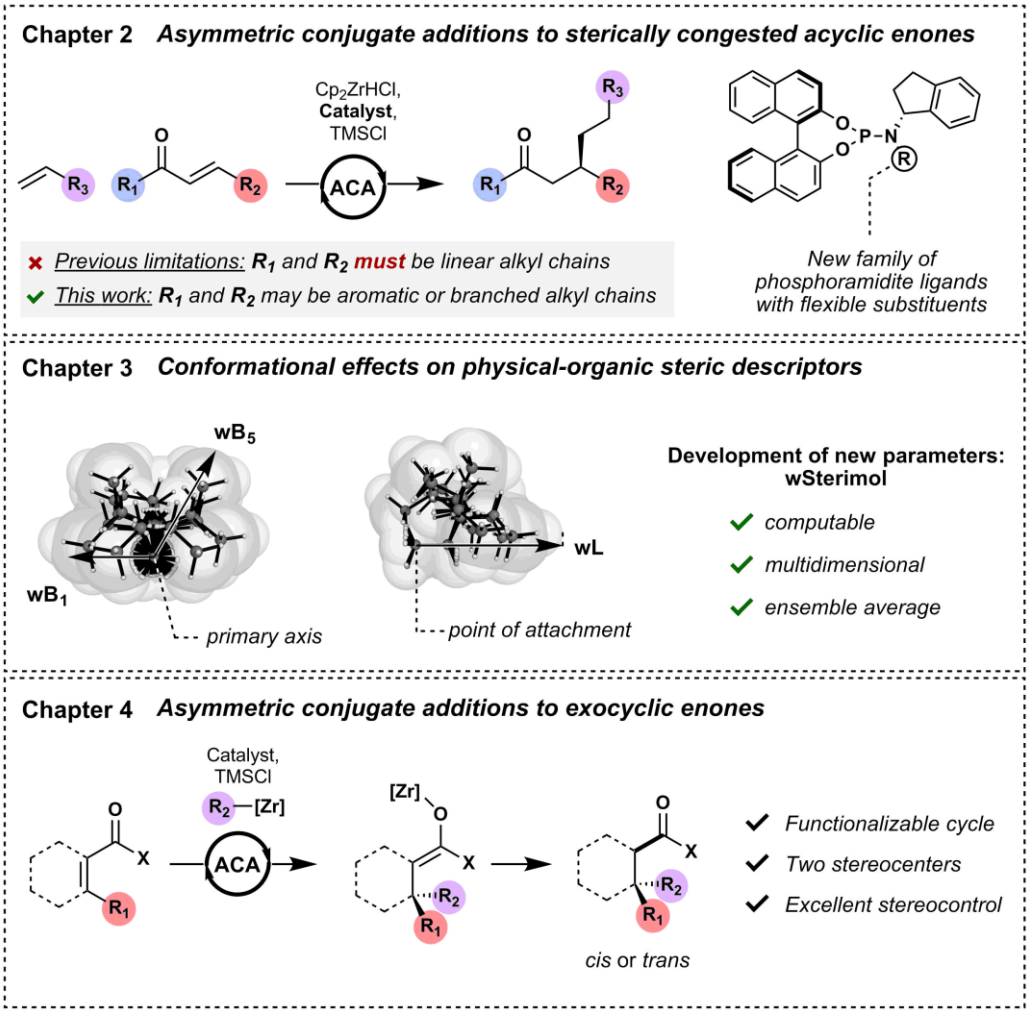

Scheme 1.12. Chapters studied throughout this work.

5 References

1 L. D. Barron, *Chirality and Life*, Springer US, Boston, 2008.

2 S. P. Fletcher, *Nat. Chem.*, 2009, **1**, 692–693.

3 P. M. Donate and D. Frederico, *Sustainable Agrochemistry*, Springer International Publishing, Cham, 2019.

4 S. Baldermann, M. Kato, A. Fujita, P. Fleischmann, P. Winterhalter and N. Watanabe, in *Carotenoid Cleavage Products*, eds. P. Winterhalter and S. E. Ebeler, American Chemical Society, Washington, 2013, pp. 65–72.

5 C. Geithe and D. Krautwurst, in *Importance of Chirality to Flavor Compounds*, eds. K.-H. Engel and G. Takeoka, American Chemical Society, Washington, 2015, pp. 161–181.

6 S. Schoenauer, J. Polster and P. Schieberle, in *Importance of Chirality to Flavor Compounds*, eds. K.-H. Engel and G. Takeoka, American Chemical Society, Washington, 2015, pp. 135–146.

7 *Chiral Chemicals Market Analysis By Technology, By Application And Segment Forecasts To 2024*, 2016.

8 K. C. Nicolaou, D. Pappo, K. Y. Tsang, R. Gibe and D. Y.-K. Chen, *Angew. Chem. Int. Ed.*, 2008, **47**, 944–946.

9 B. M. Trost, *Angew. Chemie Int. Ed. English*, 1995, **34**, 259–281.

10 N. Z. Burns, P. S. Baran and R. W. Hoffmann, *Angew. Chem. Int. Ed.*, 2009, **48**, 2854–2867.

11 A. Ault, *J. Chem. Educ.*, 2002, **79**, 572.

12 W. S. Knowles, *Angew. Chem. Int. Ed.*, 2002, **41**, 1998–2007.

13 T. P. Yoon and E. N. Jacobsen, *Science*, 2003, **299**, 1691–1693.

14 S. D. Walker, T. E. Barder, J. R. Martinelli and S. L. Buchwald, *Angew. Chem. Int. Ed.*, 2004, **43**, 1871–1876.

15 J. F. Teichert and B. L. Feringa, *Angew. Chem. Int. Ed. Engl.*, 2010, **49**, 2486–2528.

16 Q.-L. Zhou, *Privileged Chiral Ligands and Catalysts*, Wiley-VCH, Weinheim, Germany, 2011.

17 M. T. Reetz, A. Meiswinkel, G. Mehler, K. Angermund, M. Graf, W. Thiel, R. Mynott and D. G. Blackmond, *J. Am. Chem. Soc.*, 2005, **127**, 10305–10313.

18 V. M. Shoba, N. C. Thacker, A. J. Bochat and J. M. Takacs, *Angew. Chem. Int. Ed.*, 2016, **55**, 1465–1469.

19 A. Alexakis, J. E. Bäckvall, N. Krause, O. Pàmies and M. Diéguez, *Chem. Rev.*, 2008, **108**, 2796–2823.

20 J. Jover, N. Fey, J. N. Harvey, G. C. Lloyd-Jones, A. G. Orpen, G. J. J. Owen-Smith, P. Murray, D. R. J. Hose, R. Osborne and M. Purdie, *Organometallics*, 2010, **29**, 6245–6258.

21 D. J. Durand and N. Fey, *Chem. Rev.*, 2019, **119**, 6561–6594.

22 S. E. Denmark, N. D. Gould and L. M. Wolf, *J. Org. Chem.*, 2011, **76**, 4260–4336.

23 B. Lygo and B. I. Andrews, *Acc. Chem. Res.*, 2004, **37**, 518–525.

24 C. Fliedel, A. Labande, E. Manoury and R. Poli, *Coord. Chem. Rev.*, 2019, **394**, 65–103.

25 J. P. Reid and J. M. Goodman, *J. Am. Chem. Soc.*, 2016, **138**, 7910–7917.

26 A. Milo, A. J. Neel, F. D. Toste and M. S. Sigman, *Science*, 2015, **347**, 737–743.

27 A. McNally, C. K. Prier and D. W. C. MacMillan, *Science*, 2011, **334**, 1114–1117.

28 K. D. Collins, T. Gensch and F. Glorius, *Nat. Chem.*, 2014, **6**, 859–871.

29 J. G. De Vries and L. Lefort, *Oil Gas Sci. Technol. – Rev. d'IFP Energies Nouv.*, 2013, **68**, 519–528.

30 C. Jäkel and R. Paciello, *Chem. Rev.*, 2006, **106**, 2912–2942.

31 S. H. Shabbir, C. J. Regan and E. V Anslyn, *Proc. Natl. Acad. Sci.*, 2009, **106**, 10487–10492.

32 G. J. Cheng, X. Zhang, L. W. Chung, L. Xu and Y. D. Wu, *J. Am. Chem. Soc.*, 2015, **137**, 1706–1725.

33 M. Żyła-Karwowska, L. Moshniaha, H. Zhylitskaya and M. Stępień, *J. Org. Chem.*,

2018, **83**, 5199–5209.

34 Q. Zhang, Y. Liu, T. Wang, X. Zhang, C. Long, Y. D. Wu and M. X. Wang, *J. Am. Chem. Soc.*, 2018, **140**, 5579–5587.

35 W. S. Knowles, *Acc. Chem. Res.*, 1983, **16**, 106–112.

36 Y. Lam, M. N. Grayson, M. C. Holland, A. Simon and K. N. Houk, *Acc. Chem. Res.*, 2016, **49**, 750–762.

37 J. P. Reid and M. S. Sigman, *Nat. Rev. Chem.*, 2018, **2**, 290–305.

38 Y. Guan and S. E. Wheeler, *Angew. Chem. Int. Ed.*, 2017, **56**, 9101–9105.

39 Z. Rolik, L. Szegedy, I. Ladjánszki, B. Ladóczki and M. Kállay, *J. Chem. Phys.*, 2013, **139**, 094105.

40 Q. Peng, F. Duarte and R. S. Paton, *Chem. Soc. Rev.*, 2016, **45**, 6093–6107.

41 S. Grimme and P. R. Schreiner, *Angew. Chem. Int. Ed.*, 2018, **57**, 4170–4176.

42 L. E. Rush, P. G. Pringle and J. N. Harvey, *Angew. Chem. Int. Ed.*, 2014, **53**, 8672–8676.

43 A. Anoop, W. Thiel and F. Neese, *J. Chem. Theory Comput.*, 2010, **6**, 3137–3144.

44 E. Hansen, A. R. Rosales, B. Tutkowski, P.-O. O. Norrby and O. Wiest, *Acc. Chem. Res.*, 2016, **49**, 996–1005.

45 A. R. Rosales, J. Wahlers, E. Limé, R. E. Meadows, K. W. Leslie, R. Savin, F. Bell, E. Hansen, P. Helquist, R. H. Munday, O. Wiest and P.-O. Norrby, *Nat. Catal.*, 2019, **2**, 41–45.

46 P.-F. Larsson, P.-O. Norrby and S. Woodward, in *Copper-catalyzed asymmetric synthesis*, eds. A. Alexakis, N. Krause and S. Woodward, 2014, pp. 325–351.

47 K. C. Harper and M. S. Sigman, *Science*, 2011, **333**, 1875–1878.

48 A. Milo, E. N. Bess and M. S. Sigman, *Nature*, 2014, **507**, 210–214.

49 J. P. Reid and M. S. Sigman, *Nature*, 2019, **571**, 343–348.

50 A. F. Zahrt, J. J. Henle, B. T. Rose, Y. Wang, W. T. Darrow and S. E. Denmark, *Science*, 2019, **363**, eaau5631.

51 C. Hansch, P. P. Maloney, T. Fujita and R. M. Muir, *Nature*, 1962, **194**, 178–180.

52 K. C. Harper, E. N. Bess and M. S. Sigman, *Nat. Chem.*, 2012, **4**, 366–374.

53 A. Lai, J. Clifton, P. L. Diaconescu and N. Fey, *Chem. Commun.*, 2019, **55**, 7021–7024.

54 N. Fey, A. C. Tsipis, S. E. Harris, J. N. Harvey, A. G. Orpen and R. A. Mansson, *Chem. - A Eur. J.*, 2006, **12**, 291–302.

55 J. Jover and N. Fey, *Chem. - An Asian J.*, 2014, **9**, 1714–1723.

56 J. Jover, N. Fey, M. Purdie, G. C. Lloyd-Jones and J. N. Harvey, *J. Mol. Catal. A Chem.*, 2010, **324**, 39–47.

57 N. Fey, M. F. Haddow, J. N. Harvey, C. L. McMullin and A. G. Orpen, *Dalt. Trans.*, 2009, 8183.

58 R. A. Mansson, A. H. Welsh, N. Fey and A. G. Orpen, *J. Chem. Inf. Model.*, 2006, **46**, 2591–2600.

59 J. Jover, N. Fey, J. N. Harvey, G. C. Lloyd-Jones, A. G. Orpen, G. J. J. Owen-Smith, P. Murray, D. R. J. Hose, R. Osborne and M. Purdie, *Organometallics*, 2012, **31**, 5302–5306.

60 M. C. Kozlowski, S. L. Dixon, M. Panda and G. Lauri, *J. Am. Chem. Soc.*, 2003, **125**, 6614–6615.

61 K. B. Lipkowitz and M. C. Kozlowski, *Synlett*, 2003, **10**, 1547–1565.

62 J. B. van der Linden, E.-J. Ras, S. M. Hooijschuur, G. M. Klaus, N. T. Luchters, P. Dani, G. Verspui, A. A. Smith, E. W. P. Damen, B. McKay and M. Hoogenraad, *QSAR Comb. Sci.*, 2005, **24**, 94–98.

63 J. J. Miller and M. S. Sigman, *Angew. Chem. Int. Ed.*, 2008, **47**, 771–774.

64 K. C. Harper and M. S. Sigman, *Proc. Natl. Acad. Sci.*, 2011, **108**, 2179–2183.

65 M. S. Sigman and J. J. Miller, *J. Org. Chem.*, 2009, **74**, 7633–7643.

66 C. B. Santiago, J. Y. Guo and M. S. Sigman, *Chem. Sci.*, 2018, **9**, 2398–2412.

67 R. Ardkhean, M. Mortimore, R. S. Paton and S. P. Fletcher, *Chem. Sci.*, 2018, **9**, 2628–2632.

68 R. Ardkhean, P. M. C. Roth, R. M. Maksymowicz, A. Curran, Q. Peng, R. S. Paton

and S. P. Fletcher, *ACS Catal.*, 2017, **7**, 6729–6737.

69 W. Wu, D. L. Massart and S. de Jong, *Chemom. Intell. Lab. Syst.*, 1997, **36**, 165–172.

70 M. C. Kozlowski, S. L. Dixon, M. Panda and G. Lauri, *J. Am. Chem. Soc.*, 2003, **125**, 6614–6615.

71 P.-W. Phuan, J. C. Ianni and M. C. Kozlowski, *J. Am. Chem. Soc.*, 2004, **126**, 15473–15479.

72 J. C. Ianni, V. Annamalai, P.-W. Phuan, M. Panda and M. C. Kozlowski, *Angew. Chem. Int. Ed.*, 2006, **45**, 5502–5505.

73 S. Sciabola, A. Alex, P. D. Higginson, J. C. Mitchell, M. J. Snowden and I. Morao, *J. Org. Chem.*, 2005, **70**, 9025–9027.

74 D. T. Ahneman, J. G. Estrada, S. Lin, S. D. Dreher and A. G. Doyle, *Science*, 2018, **360**, 186–190.

75 K. V. Chuang and M. J. Keiser, *Science*, 2018, **362**, eaat8603.

76 A. L. Samuel, *IBM J. Res. Dev.*, 1959, **3**, 210–229.

77 M. T. Ribeiro, S. Singh and C. Guestrin, in *Proceedings of the 22nd ACM SIGKDD International Conference on Knowledge Discovery and Data Mining - KDD '16*, ACM Press, New York, 2016, pp. 1135–1144.

78 J.-L. Reymond and M. Awale, *ACS Chem. Neurosci.*, 2012, **3**, 649–657.

79 A. V Brethomé, R. S. Paton and S. P. Fletcher, *ACS Catal.*, 2019, **9**, 7179–7187.

80 P. S. Gromski, A. B. Henson, J. M. Granda and L. Cronin, *Nat. Rev. Chem.*, 2019, **3**, 119–128.

81 R. Kiralj and M. M. C. Ferreira, *J. Chemom.*, 2010, **24**, 681–693.

82 M. Charton, *J. Am. Chem. Soc.*, 1975, **97**, 1552–1556.

83 R. Todeschini and V. Consonni, *Handbook of Molecular Descriptors*, Wiley-VCH, Weinheim, Germany, 2000.

84 W. Beker, E. P. Gajewska, T. Badowski and B. A. Grzybowski, *Angew. Chem. Int. Ed.*, 2019, **58**, 4515–4519.

85 A. J. Neel, M. J. Hilton, M. S. Sigman and F. D. Toste, *Nature*, 2017, **543**, 637–646.

86 R. Kiralj and M. M. C. Ferreira, *J. Chemom.*, 2010, **24**, 681–693.

87 T. Piou, F. Romanov-Michailidis, M. Romanova-Michaelides, K. E. Jackson, N. Semakul, T. D. Taggart, B. S. Newell, C. D. Rithner, R. S. Paton and T. Rovis, *J. Am. Chem. Soc.*, 2017, **139**, 1296–1310.

88 C. B. Santiago, A. Milo and M. S. Sigman, *J. Am. Chem. Soc.*, 2016, **138**, 13424–13430.

89 R. Ardkhean, P. M. C. Roth, R. M. Maksymowicz, A. Curran, Q. Peng, R. S. Paton and S. P. Fletcher, *ACS Catal.*, 2017, **7**, 6729–6737.

90 T. Piou, F. Romanov-Michailidis, M. Romanova-Michaelides, K. E. Jackson, N. Semakul, T. D. Taggart, B. S. Newell, C. D. Rithner, R. S. Paton and T. Rovis, *J. Am. Chem. Soc.*, 2017, **139**, 1296–1310.

91 M. Orlandi, J. A. S. Coelho, M. J. Hilton, F. D. Toste and M. S. Sigman, *J. Am. Chem. Soc.*, 2017, **139**, 6803–6806.

92 J. C. Ianni, V. Annamalai, P. W. Phuan, M. Panda and M. C. Kozlowski, *Angew. Chem. Int. Ed.*, 2006, **45**, 5502–5505.

93 R. W. Taft, *J. Am. Chem. Soc.*, 1952, **74**, 2729–2732.

94 M. Charton, *J. Org. Chem.*, 1976, **41**, 2217–2220.

95 S. Winstein and N. J. Holness, *J. Am. Chem. Soc.*, 1955, **77**, 5562–5578.

96 R. Ruzziconi, S. Spizzichino, L. Lunazzi, A. Mazzanti and M. Schlosser, *Chem. – A Eur. J.*, 2009, **15**, 2645–2652.

97 K. C. Harper, E. N. Bess and M. S. Sigman, *Nat. Chem.*, 2012, **4**, 366–374.

98 C. A. Tolman, *Chem. Rev.*, 1977, **77**, 313–348.

99 J. C. Dearden, M. T. D. Cronin and K. L. E. Kaiser, *SAR QSAR Environ. Res.*, 2009, **20**, 241–266.

100 J.-Y. Guo, Y. Minko, C. B. Santiago and M. S. Sigman, *ACS Catal.*, 2017, **7**, 4144–4151.

101 M. S. Sigman, K. C. Harper, E. N. Bess and A. Milo, *Acc. Chem. Res.*, 2016, **49**, 1292–1301.

102 M. Charton, *J. Org. Chem.*, 1976, **41**, 2217–2220.

103 K. C. Harper and M. S. Sigman, *J. Org. Chem.*, 2013, **78**, 2813–2818.

104 A. Verloop, *Drug Design Vol. III*, Academic Press, New York, 1976.

105 J.-Y. Y. Guo, Y. Minko, C. B. Santiago and M. S. Sigman, *ACS Catal.*, 2017, **7**, 4144–4151.

106 C. A. Tolman, *Chem. Rev.*, 1977, **77**, 313–348.

107 L. P. Hammett, *Chem. Rev.*, 1935, **17**, 125–136.

108 C. B. Santiago, A. Milo and M. S. Sigman, *J. Am. Chem. Soc.*, 2016, **138**, 13424–13430.

109 H. Akaike, *IEEE Trans. Automat. Contr.*, 1974, **19**, 716–723.

110 A. Tropsha, *Mol. Inform.*, 2010, **29**, 476–488.

111 A. Tropsha, P. Gramatica and V. K. Gombar, *QSAR Comb. Sci.*, 2003, **22**, 69–77.

112 F. J. Anscombe, *Am. Stat.*, 1973, **27**, 17–21.

113 K. S. Kannan and K. Manoj, *Appl. Math. Sci.*, 2015, **9**, 2317–2324.

114 R. L. Lipnick, *Sci. Total Environ.*, 1991, **109**–**110**, 131–153.

115 A. Golbraikh and A. Tropsha, *J. Mol. Graph. Model.*, 2002, **20**, 269–276.

116 A. Tropsha, P. Gramatica and V. K. Gombar, *Qsar Comb. Sci.*, 2003, **22**, 69–77.

2

Asymmetric conjugate additions to sterically congested acyclic enones

Part of this work was published in *ACS Catalysis* in 2019.[1]

The section discussing the mechanistic study was inspired from Dr Emeline Rideau's work, but the results are my own work, except where clearly stated otherwise.

1 Introduction

Copper-catalyzed asymmetric conjugate addition (ACA) of organometallic species on acyclic enones was first investigated by the van Koten group in 1991[2,3] and has received considerable attention for the last three decades. It is now one of the most useful asymmetric transformations available to synthetic chemists, such that numerous natural product syntheses use it as a strategy to control the formation of stereocenters with control of absolute configuration (**Scheme 2.1**).[4–6]

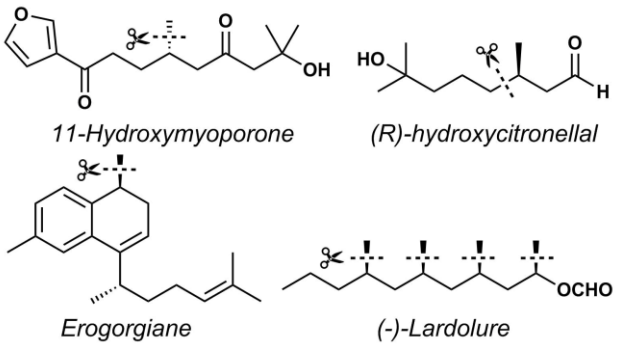

Scheme 2.1. Examples of natural products or fragrances prepared from ACA on acyclic enones.

The success of ACA comes from its ability to create new C–C bonds from simple and readily available substrates such as linear α,β-unsaturated carbonyl compounds,[7–14] but also thanks to its intuitive disconnections that make it a powerful tool. Efforts from a broad scientific community have enabled α,β-unsaturated carbonyl acyclic compounds to undergo ACAs with preformed reactive organometallics such as Grignard,[2,3,15–19] organoaluminium,[20,21] organoboron[22] and organozinc[23–26] species in high yield and high selectivity (**Scheme 2.2**). However, highly reactive alkylmetal reagents present practical and safety issues, while the incompatibility of functional groups considerably limits the scope of these reactions.

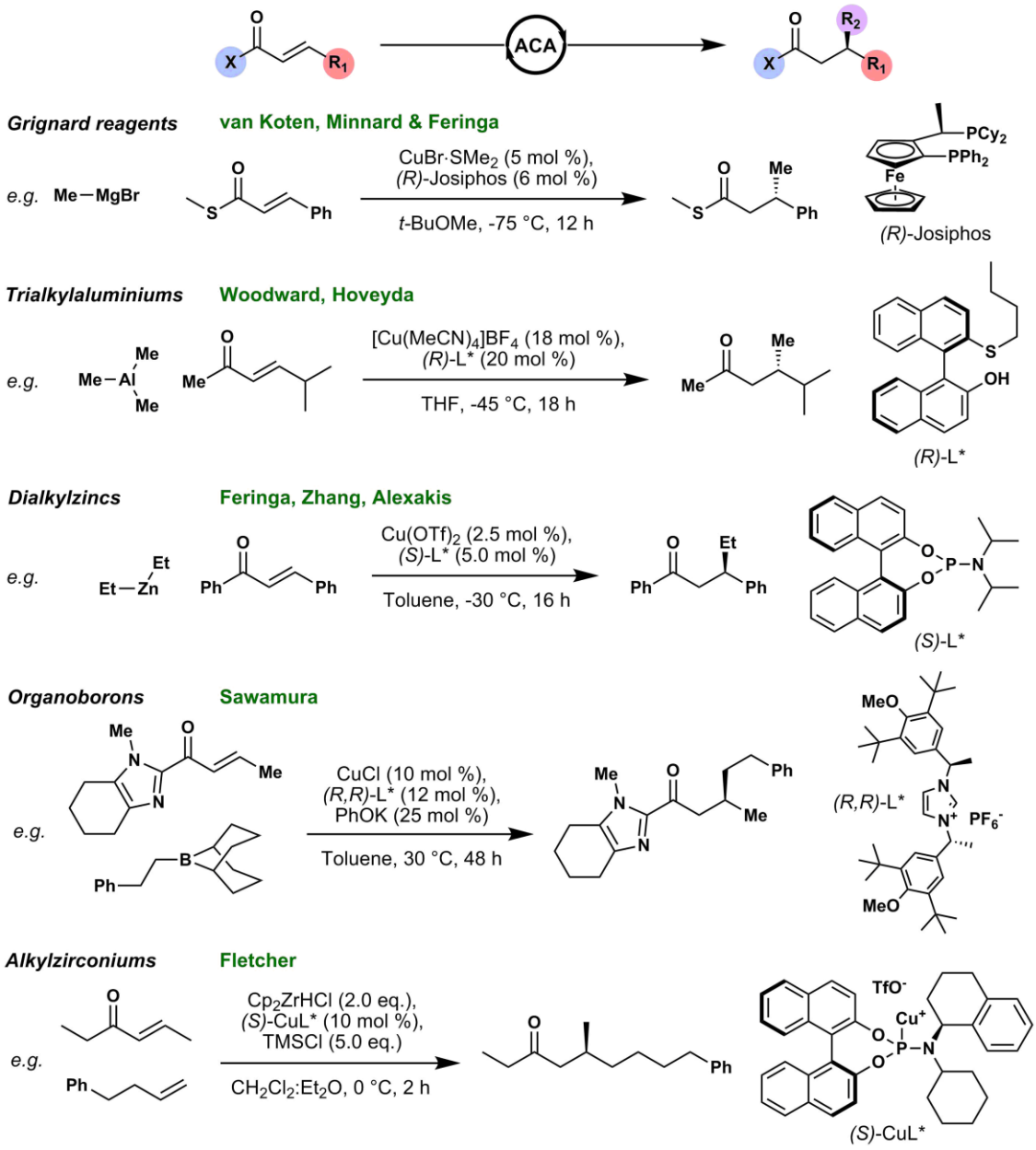

Scheme 2.2. Copper-catalyzed ACAs of organometallics on acyclic substrates.

Cryogenic temperatures required to obtain high levels of selectivity can also be difficult to achieve in industrial settings and, more importantly, all these organometallic reagents must be premade. Alternatively, the Fletcher group reported a copper-catalyzed asymmetric addition of alkylzirconium species generated *in situ* by simply mixing the Schwartz reagent (zirconocene hydrochloride) with terminal olefins (**Scheme 2.2**).[4,27–30] Alkenes are particularly

abundant and commonly used as feedstock in industrial processes (~10^4 terminal olefins according to Reaxys®) while functional group compatibility of alkylzirconiums enables the use of a broader choice of nucleophiles[31] to form tertiary[32] and quaternary stereocenters.[30]

However, the development of all these catalytic asymmetric methods started from the investigation of a simple, readily available and prototypical substrate.[33] This approach permits the validation of a new reaction concept without the daunting need of a multistep and gramscale substrate synthesis. Although this strategy is undoubtedly effective, it also often leads to a reaction protocol that is not widely applicable beyond the simple starting scaffold. More highly-substituted reaction partners either do not display the desired reactivity or fail to reach suitable levels of enantioselectivity.[19,34]

Accordingly, there is a significant gap in the scope of products theoretically accessible through the ACA methods and those that can be produced in practice. This lack of reliability has led to the underutilization of ACAs in mainstream synthetic strategies of medicinal chemistry[35,36] and this continues to be a difficult challenge to address. To use ACA's full potential and to become a "go-to methodology",[35] the method should still tolerate a wider variety of substrates.

Extending the scope of a method to more decorated reaction partners remains a formidable task that is often driven by empirical trial-and-error screening, a process that relies on chance and intuition. We argue that a more rational approach grounded in statistical analyses of the data collected would be more time-effective. This would then facilitate the reoptimisation (*i.e.* fine-tuning) of a ligand to tolerate electronically and/or sterically more challenging substrates. Our particular focus

has been on phosphoramidite privileged ligands because they are modular, air-stable, cheap, scalable, good yielding, available in few steps from commercial starting materials and known to achieve high enantioinduction in copper catalysis.

During the initial work on copper-catalyzed ACA of alkylzirconium species, Dr Philippe Roth found that acyclic enones possessing linear alkyl substituents work well (>90% ee),[32] but additions to sterically demanding enones produced results below 50% *ee* (**Scheme 2.3**). This behaviour is not unusual in ACA chemistry.[34,37] Substrate limitations include the presence of large groups, aromatic moieties, electron-rich or –withdrawing functional groups. The origins of these limitations may come from steric hindrance of the substrate preventing the addition to occur or undesirable interactions of organometallic reagents with functional groups that disrupt the catalytic cycle. Also well-known is that acyclic substrates are more challenging than cyclic counterparts, likely due to *s-cis/s-trans* interconversion.[34,38]

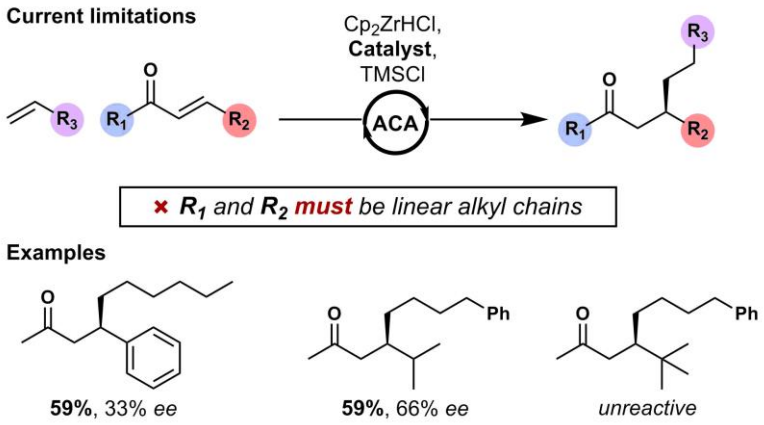

Scheme 2.3. Examples of ACAs on acyclic enones that restrict its wide use.

In this chapter, the reoptimization of a copper-catalysed ACA of alkylzirconium species motivated us to explore rational approaches to expand the scope to acyclic enones bearing branched substituents or conjugated aromatic rings. This

longstanding challenge was addressed by the use of multivariate modelling, which allowed the development of new phosphoramidite ligands.[14,39,40] Selection of the best ligand from this series achieved high selectivity and reactivity with linear α,β-unsaturated ketones bearing β-substituents as bulky as *tert*-butyl groups. Initial mechanistic study revealed intricate catalytic cycles, where our best ligand possesses kinetics about an order of magnitude faster than the original catalyst, with the reaction now typically complete within 30 min.

2 Condition reoptimisation

Although structurally simple, the acyclic enone benzylideneacetone **2.1a** proved to be a particularly challenging substrate for the copper-catalyzed ACA (59% yield, 33% ee)[32] and we reasoned that it would be a good candidate to extend this method to bulkier substituents. Previous conditions were first reoptimized by examining equivalents, solvent, temperature and copper sources (**Scheme 2.4**).

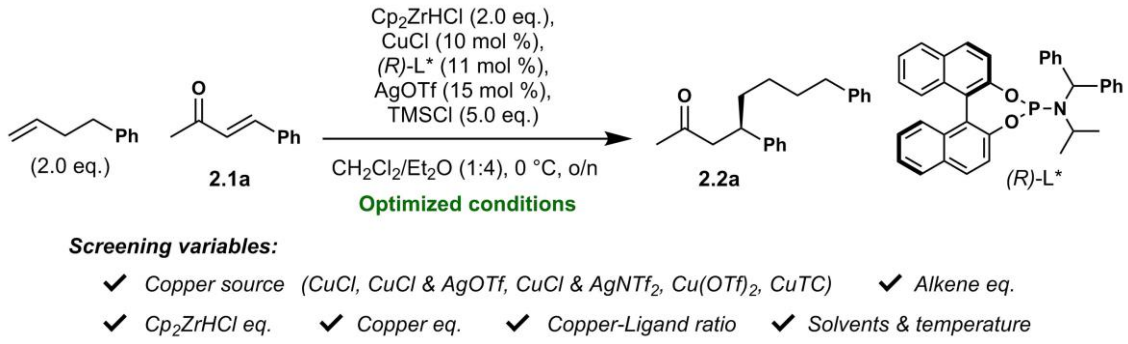

Scheme 2.4. Six key reaction variables were examined to reoptimized ACA's conditions on benzylideneacetone.

We found that the use of copper(I) triflate and phosphoramidite ligand in the presence of TMSCl were critical to achieve high reactivity (>80% yield). The

combination of CH_2Cl_2 and Et_2O in a 1:4 mixture at 0 °C also proved to be the optimum for selectivity, consistent with previously published work.[30]

3 Structure-enantioselectivity relationships

As always, it is unnecessary to design new ligands if the use of known compounds improves the reaction. Accordingly, we started our exploration of a better chiral phosphoramidite ligand by selecting structurally diverse ligands found in our database (**Scheme 2.5**). Such selection was based on the structural diversity of compounds according to chemical intuition, and not from scoring functions. Our objective was to probe the phosphoramidite Ligand Space (LS) to identify a promising ligand "lead" that would be further improved.

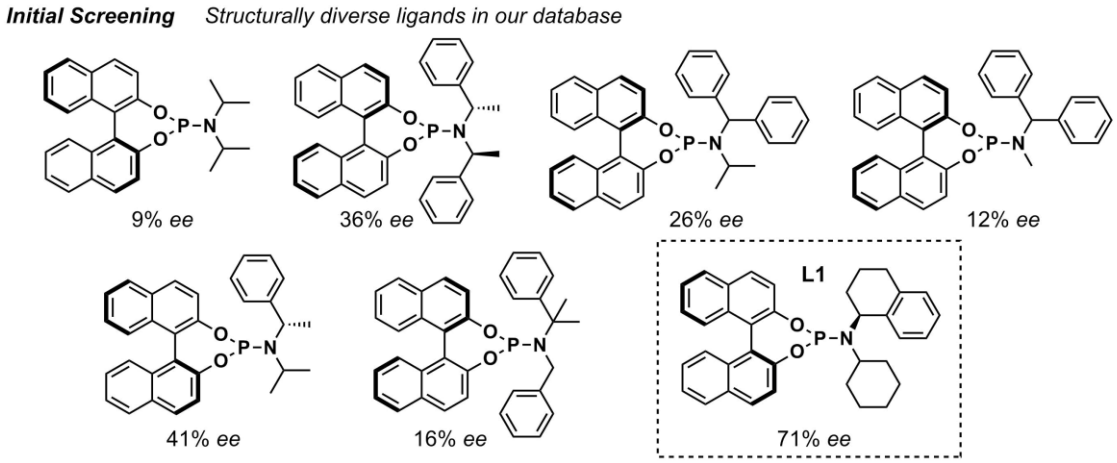

Scheme 2.5. Seven structurally diverse phosphoramidite ligands from the ligand database that were used to initially explore the phosphoramidite Ligand Space known to be relevant in the copper-catalysed conjugate addition. *Ee*'s are reported for the asymmetric addition to form **2.2a**, and are averaged from at least two reaction repeats.

These preliminary experiments uncovered an initially promising ligand **L1** giving 90% yield and 71% *ee*. We synthesized ligands derived from **L1** and identified several important features as part of a *qualitative* structure-enantioselectivity relationship (**Scheme 2.6**). First, the aminoindane ring size does not dramatically affect enantioselectivity (*cf.* **L1-L2**), however, the use of acyclic alternatives is detrimental to selectivity. Additionally, the BINOL configuration dictates the formation of the major enantiomer, while the stereocenter on the indane represents a *matched-mismatched* effect (*cf.* **L3-L4**). Finally, enantioselectivity can be improved by modification of the alkyl group with results ranging from 67% to 92% *ee* (*cf.* **L2**, **L4-L6**). The yields were obtained using calibrated ^{1}H NMR (see **Chapter 6** for details).

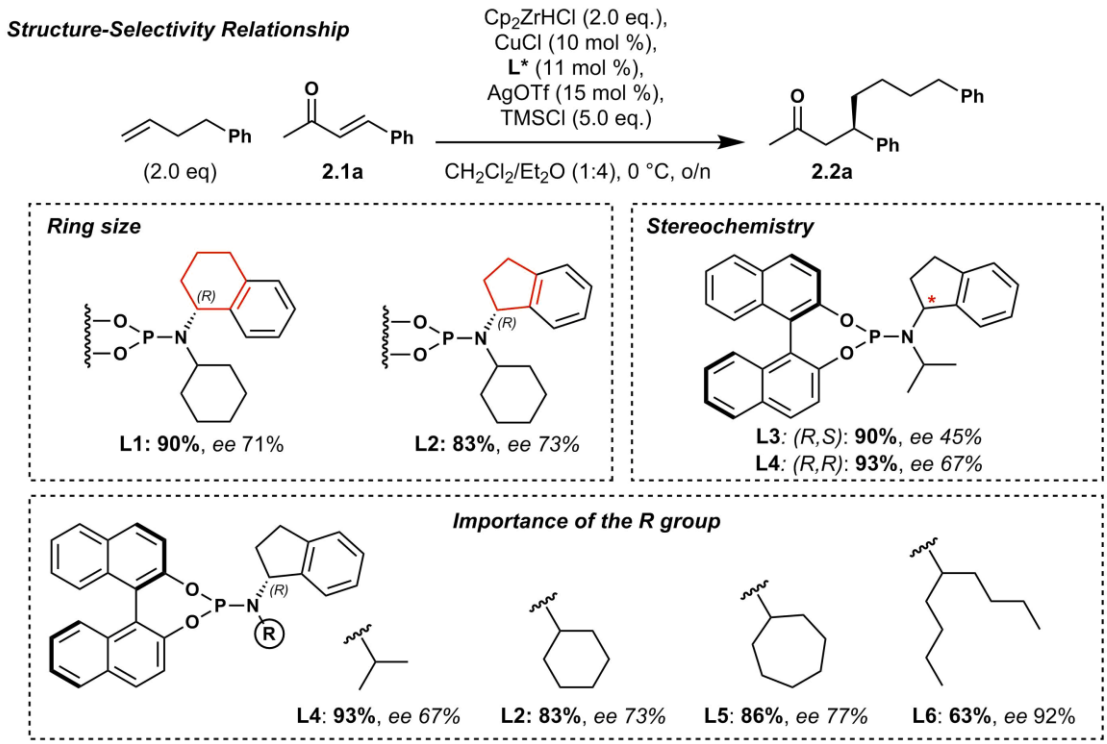

Scheme 2.6. Analysis of the structure-selectivity relationship from the initial ligand derivatization.

Marked differences in enantioselectivity obtained from rather small modifications of the alkyl substituent were unforeseen. Applying the Curtin-Hammett principle[41] and calculating from the measured enantiomeric excess, the macroscopic Gibbs energy difference between competing diastereomeric transition states ($\Delta\Delta G^{\ddagger}$) for ligand **L4** with an isopropyl moiety is of 3.8 kJ/mol at 0 °C, whereas replacement of isopropyl to isononyl (**L6**) more than doubles this value to 7.7 kJ/mol. These non-intuitive effects are common in asymmetric catalysis using transition metal catalysis,[29] usually due to the complexity of interactions involved, and they expose our incomplete understanding of mechanism.

Qualitative conclusions can be drawn from a structure-selectivity relationship such as the intuitive lengthening of the alkyl chain, but it does not provide much more guidance in terms of shape or properties. While human brains are formidable at recognising trends, accurately quantifying the influence of a structural modification on enantioselectivity is a much more difficult task. To reduce the importance of chance and intuition in the design process, we would prefer to make decisions based on predicted *ee* values before investing efforts in the synthesis of new ligands, or for example, deciding when to stop optimizing.

4 Iterative data-driven design

The insufficient mechanistic understanding of complex multi-component catalytic reactions involving transiently-formed reactive species meant that transition state calculations with electronic structure theory were not well-suited to our aims. Instead we turned our attention toward the use of multivariate modeling. Our objective was to achieve high enantioinduction of **1a** by conducting rounds of

statistical model construction and ligand synthesis in parallel, an iterative process resulting in progressive refinement. Guided by the qualitative structure-selectivity relationship, we decided to maintain the BINOL backbone and indanyl group in a *matched* configuration, where ligand modification was restricted to the alkyl substituent. We reasoned that this reduced search space for ligand optimization could be explored more efficiently, while still providing sufficient amplitude in selectivity values from which to uncover promising ligands. Following these criteria, nine data points were initially used for model construction out of sixteen ligands examined in the initial screening. The descriptors were first generated either from the ligand or the copper-complex 3D coordinates, such as NBO coefficient of key atoms, logP, Sterimol parameters, angles, distances and dihedrals (see **Chapter 7** for details). The first round of ligand design unveiled a statistically significant and validated correlation between enantioselectivity and the lipophilicity parameter logP (**Scheme 2.7**). This topological descriptor represents the logarithm of *n*-octanol/water partition coefficient generated with the ALOGPS algorithm.[42] **Model I** passed all the statistical tests: the training set possesses a satisfactory 6:1 ratio between the amount of datapoints (6 ligands) and descriptors (logP only), which produced a good fit (R^2) of 89% and a RMSE of 0.66 kJ/mol. Internal validation with leave-one-out cross validation (LOOCV) also proved the model to be fairly robust, particularly in consideration of the limited amount of data in the training set (R^2_{CV} = 78% & RMSE = 0.96 kJ/mol). ANOVA test confirmed the statistical significance of the only parameter ($p < 0.05$) and external validation formed from a hold-out subset of three ligands also afforded a good R^2 (87%) and an RMSE of 1.93 kJ/mol.

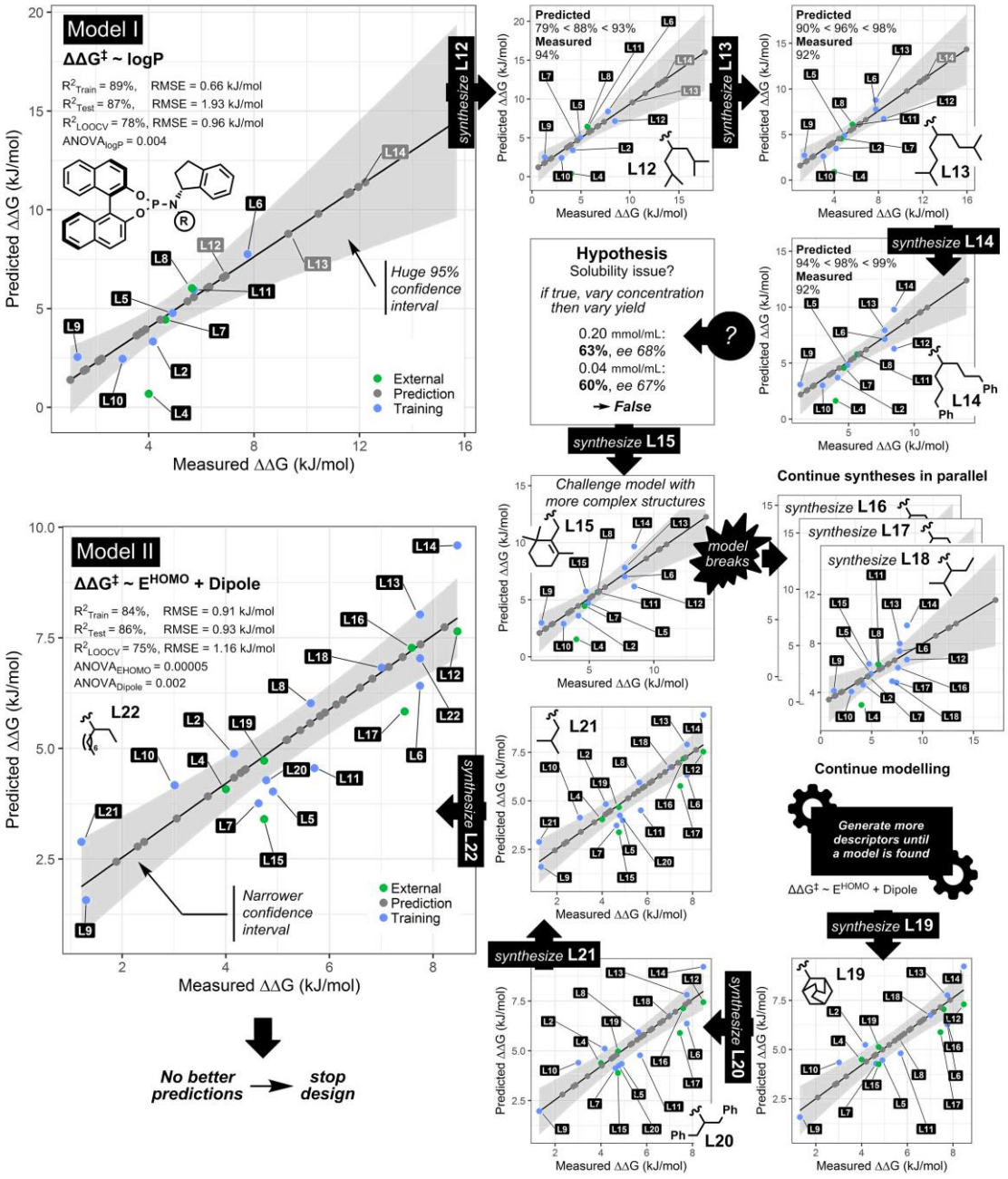

Scheme 2.7. Iterative data-driven design led to models that correlated experimentally measured enantioselectivity and predicted enantioselectivity. The gray area represents the standard error at 95% confidence interval. *Ee*'s are reported for the asymmetric addition to form **2.2a**, and are averaged from at least two reaction repeats. The full list of ligand structures can be found in the computational section with the predicted values.

It is important to note that all measured values are an average of at least two reaction repeats that were determined by HPLC on a chiral non-racemic stationary phase. Experimental reproducibility was found to be within ±3% for yields and within ±1% for *ee* values, which accordingly limited the statistical model accuracy to 1% *ee* at best.

An *in silico* library was then pragmatically created based on the synthetic accessibility of ligands (see computational section for the full list of ligands). Compared to model construction, ligand synthesis indeed represents the bottleneck of our workflow even if phosphoramidite synthesis is trivial. Additional steps in the preparation of precursors considerably lengthen the ligand design process; so much that we limited the amine fragment to readily available commercial sources or four well-established synthetic steps. Additionally, we only envisaged potential *in silico* ligands possessing aliphatic *R* groups due to the applicability domain of our model (AD). Although the utility of this concept is contested,[43] AD is an area of feature space in which the model can make reliable predictions. Absent from the training set, the influence of heteroelements on the lipophilicity values was therefore ignored.

Molecular descriptors were computed for each of the twenty-five *in-silico* ligands, from which the model predicted *ee* values represented as grey dots in **Scheme 2.7**. Note that the full list of ligand structures can be found in **Chapter 7** alongside predicted values. We focused our efforts in the region above 6.0 kJ/mol (>85% *ee*) and selected evenly spaced values along the range of predicted selectivities (grey labels). Our reasoning was to improve stepwise the predictive power of our model while also targeting higher enantioselectivities.

According to Model I, **L12** was expected to produce a level of enantioselectivity between 79-93% *ee* (95% confidence interval) and we satisfactorily obtained 94% *ee*. Retraining the model by incorporating this new data point led to almost identical statistical performance, but with slightly narrower error intervals. The *in silico* ligand library was then predicted again and **L13** emerged as a promising ligand for the next round of ligand synthesis. Predicted to give between 90-98% *ee*, **L13** was synthesized and afforded 92% *ee*. Model construction with **L13** achieved again slightly narrower confidence intervals with similar statistical quality, and the *in silico* library was fed into the new model. Synthesis and testing of **L14** resulted in 92% *ee*, within 0.7 kJ/mol of the predicted range of 94-99% *ee*.

We searched a mechanistic interpretation behind the observed correlation of enantioselectivity and lipophilicity, and we reasoned that lipophilic alkyl substituents could help to either solubilize the active catalyst or disperse inactive aggregates. To challenge this hypothesis, concentration of active catalyst was varied by an order of magnitude but both reactivity and selectivity remained unchanged, forcing us to abandon this assumption.

The predictions so far allowed for a slight improvement of enantioselectivity (92% to 94% *ee*), which can be viewed as a rather small *ee* difference but is actually a significant ~1 kJ/mol increase that our approach successfully predicted. In the meantime, we started to envisage that the applicability domain of the model was overly narrow and decided to prepare phosphoramidite ligands with unsymmetrical and more branched alkyl groups. Thus, more predictive models with tighter confidence intervals should be obtained through a more widely-distributed and uniform sample of data points.

Although the next ligand **L15** possessed an unusual alkyl substituent derived from a β-cyclocitral precursor, it satisfactorily afforded 75% *ee* that is within the predicted range of 75% and 88% *ee*. **L16**, **L17** and **L18**, however, performed unexpectedly well and the correlation broke. In particular, small structural changes in **L17** led to a striking difference between predicted and measured enantioselectivity. Such sudden changes of enantioselectivity are unpredictable by nature and can be viewed as large "cliffs" in terms of enantioselectivity, similar to the so-called "magic methyl effect" encountered in drug discovery.[44]

Although our ligand design workflow only considers enantioselectivity, we always aimed to achieve good selectivity *and* reactivity with ACA. In that regard, **L17** was remarkable as it produced a level of enantioselectivity similar to our best ligands (92% *ee*) but with far better reactivity (99% *versus* 63% isolated yield with **L6**). As shown in **Scheme 2.8**, reactivity and selectivity jumped going from **L4** (93%, 67% *ee*) to **L17** (99%, 92% *ee*).

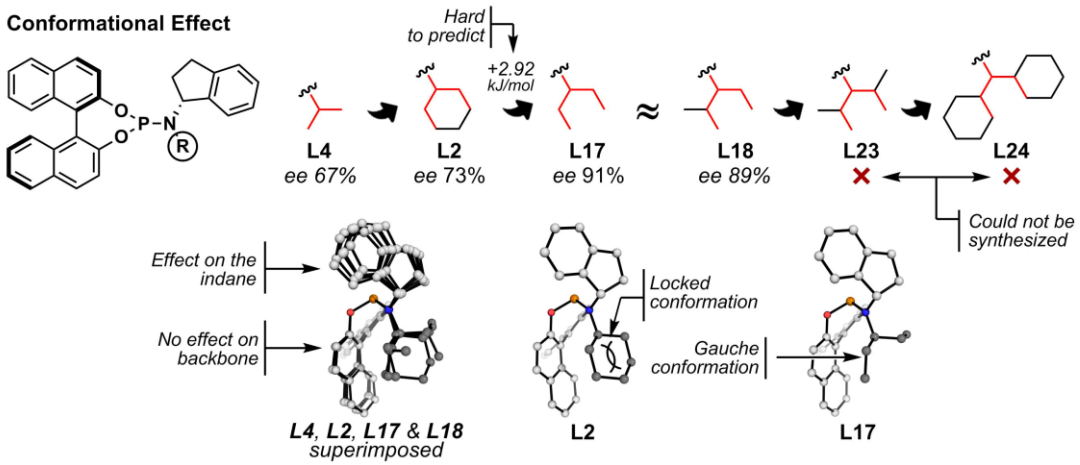

Scheme 2.8. Substitution of isopropyl with methyl groups leads to an important selectivity jump, likely due to a conformational change. Global minimum conformers were optimized at the ωB97X-D/6-31G(d) level of theory.

Reaction completion time was also about an order of magnitude faster, with the reaction now typically complete in 30 min instead of overnight. Our mechanistic interpretation lies in the preferred conformation adopted by the alkyl substituent that somehow affects the $\Delta\Delta G^{\ddagger}$ by +2.92 kJ/mol between **L17** and **L2**. A gauche conformation is indeed favoured by the acyclic 3-pentyl group that might cause a long-distance change in the active catalyst and produce better enantioselectivity. Superimposition of **L4** and **L2** proved analogous whereas **L17** and **L18** both had similar gauche conformations that avoid destabilizing *syn*-pentane interactions. This observation was consistent with the classification of the observed enantioselectivities for these four ligands.

Without any predictive modelling insights, and using our chemical intuition, we then decided to further substitute **L18** to produce ligands **L23** and **L24** in the hope of observing another jump in selectivity that previous models might not have comprehended (**Scheme 2.8**). Preparation of both amine precursors by reductive amination was however difficult and required harsh conditions (reflux in toluene for 4 days, see experimental section). Unlike previous syntheses, these secondary amines also eluted faster on TLC than their ketone starting material, which suggested a poor interaction of the nitrogen lone pair with silica likely due to steric hindrance. Unfortunately, the bulky secondary amines remained unreactive and phosphoramidites **L23** and **L24** could never be isolated.

As the substituent effect was not correctly captured by changes in lipophilicity values, we generated additional descriptors to examine whether better correlation could be obtained. Guided by our mechanistic hypothesis that conformations play an important role, we realised that most steric parameters likely fail to grasp the

important features responsible for enantioinduction since flexible chains are often treated statically in a single conformation. For instance, Sterimol steric parameters describe a particular geometry and do not automatically take into account effects of a conformational ensemble.[45] In contrast to this, weighted Sterimol (wSterimol)[46] parameters are based on a Boltzmann average along with minimum and maximum values across the ensemble (see **Chapter 3**). However, the use of wSterimol parameters led to no meaningful correlation even if it confirmed the anticipated impact of conformation on the uncertainty of predicted values (on average ±6 kJ/mol for flexible substituents).

Inspired by Doyle's use of electronic structure calculations to generate molecular descriptors as described in **Chapter 1**,[47] we used the *Spartan* package[48] to generate parameters from which the highest occupied molecular orbital (HOMO) energy and dipole moment were found to correlate with enantioselectivity (**Scheme 2.7**). To further validate this model with unseen values, **L19** predicted at 78% *ee* was synthesized and actually afforded 75% *ee*. The descriptors of our *in silico* library (which was updated with new ligands at that point) were computed again and were fed to the newly generated model. **L20** followed by **L21** and **L22** were thus accurately predicted and then synthesized.

The final model called **Model II** possessed fourteen ligands in the training set for only two descriptors in the model equation, which produced a good fit (R^2 = 84%, RMSE = 0.91 kJ/mol). Additionally, LOOCV (R^2_{CV} = 75%, RMSE = 1.16 kJ/mol) and the external test set (six ligands, R^2_{ext} = 86%, RMSE = 0.93 kJ/mol)) remained satisfactory. Finally, the ANOVA test confirmed the statistical significance of the descriptors ($p < 0.05$).

On one hand, we assumed that the ligand HOMO energy represents a more electron-rich σ-donating ligand that produces a stronger metal-ligand bond. A positive coefficient in the model equation indicates that higher HOMO energies lead to higher levels of selectivity. On the other hand, the definition of dipole moment suggests that it describes the overall charge distribution in the ligand. But as the classification of molecular descriptors as either electronic or steric is not absolute,[49] the dipole moment could also capture the gross molecular shape of ligands. For instance, 2.26 D was obtained with **L4** but only 2.09 D with **L17**, which was an 8% relative difference arising due to a small change in the length of the alkyl chain. This parameter therefore indirectly reflects steric as well as electronic differences between ligands, and is very sensitive to the length and branching of the *N*-alkyl substituent. Its equation coefficient is negative meaning that smaller dipole moments afford higher levels of selectivity.

The final model was fed with an *in silico* library of twenty-four ligands but none of the predictions were greater than the previous experimental *ee* values (see computational section). This suggested that a maximum in selectivity had been reached across the structural diversification of the alkyl substituents and that further ligand syntheses would only produce, at best, equally selective ligands. Accordingly, ligand optimization was halted at this stage.

5 Importance of multivariate modelling

Retrospectively, the role of multivariate modelling in ligand design is not necessarily obvious when analysing the sequence of events that happened during the iterative data-driven process. For example, the best performing ligand may intuitively be

"obvious" to a trained chemist, especially in retrospect. If we compare our statistical approach against chemical intuition, two major advantages emerge. The first involves the use of descriptors to provide structural suggestions that are not discernible based purely on chemical intuition, and the second is that potential candidates can be ranked based on their quantitative predictions.

It is crucial to understand that generating new ideas of ligand diversification are *not* the rate limiting step, but the time required to test all these ideas substantially limits the design process. Since there are many logical modifications of a ligand in principle, there is value in prioritizing synthetic effort to ensure that structural and electronic variations are done as efficiently as possible.

The value in developing a multivariate model therefore lies in all the discarded potential candidates that were not synthesized. Even for cases where structures could be developed using chemical intuition alone, the overall reduction in non-value added ligand syntheses is a critical component in the acceleration of the ligand design process. This approach allowed us to systematically discard unpromising ideas and to rationally prioritize the synthesis of the most useful ligands, from both practical and statistical points of view.

6 Multiobjective ranking

As always, catalyst development aims to achieve high reactivity *and* enantioselectivity, which is why selection of the best ligand should focus on both criteria. To identify the best overall performance, we plotted our synthesized ligands according to their yield and enantioselectivity (**Scheme 2.9**).

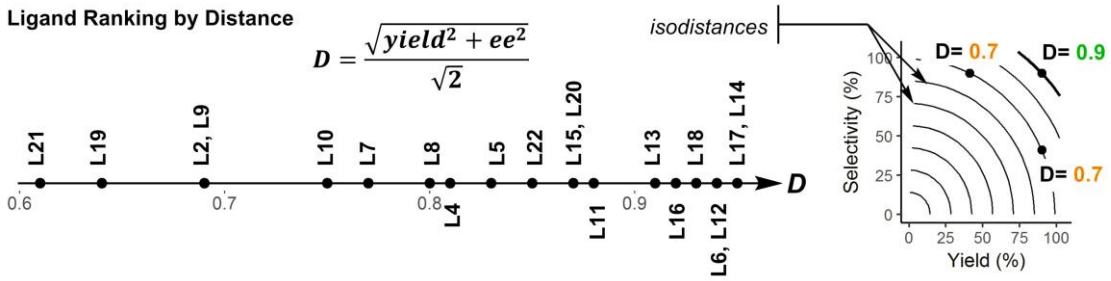

Scheme 2.9. Synthesized ligands ranked following their distance from the origin in a *yield versus selectivity* plot. Distances further from the origin indicate superior performance.

If we compute the normalized distance of each point to the origin (described by the equation in **Scheme 2.9**), that allows for the simultaneous ranking of more than one objective function (in this case yield and selectivity, but we could add ligand cost for instance). The equation produces sets of equally good, *non-dominated* solutions (also called the Pareto optimal set[50]) rather than a singular value.[51] In practice, we identified **L17** as the best ligand of this optimization campaign, placed equal first with **L14**. However, **L14** was not selected due to the tedious synthesis of its precursor in three steps with mediocre yields and we decided to continue with **L17** (derived from a commercially available ketone) as the best ligand in our library that gives the largest yield of the product major enantiomer. Interestingly, the development of **L17** also turned out to be useful outside this work, giving higher levels of reactivity in the desymmetrization of meso-bisphosphates.[52]

7 Scope

We investigated the impact of our new ligand **L17** on the scope of the reaction and synthesized substrates possessing substituents in various positions that were not

previously tolerated. The Horner-Wadsworth-Emmons reaction was used to prepare all the α,β-unsaturated carbonyl compounds and only the *trans* isomers were isolated. Analysis of the scope revealed that the use of ligand **L17** significantly improved the copper-catalyzed ACA to acyclic enones (**Scheme 2.10**).

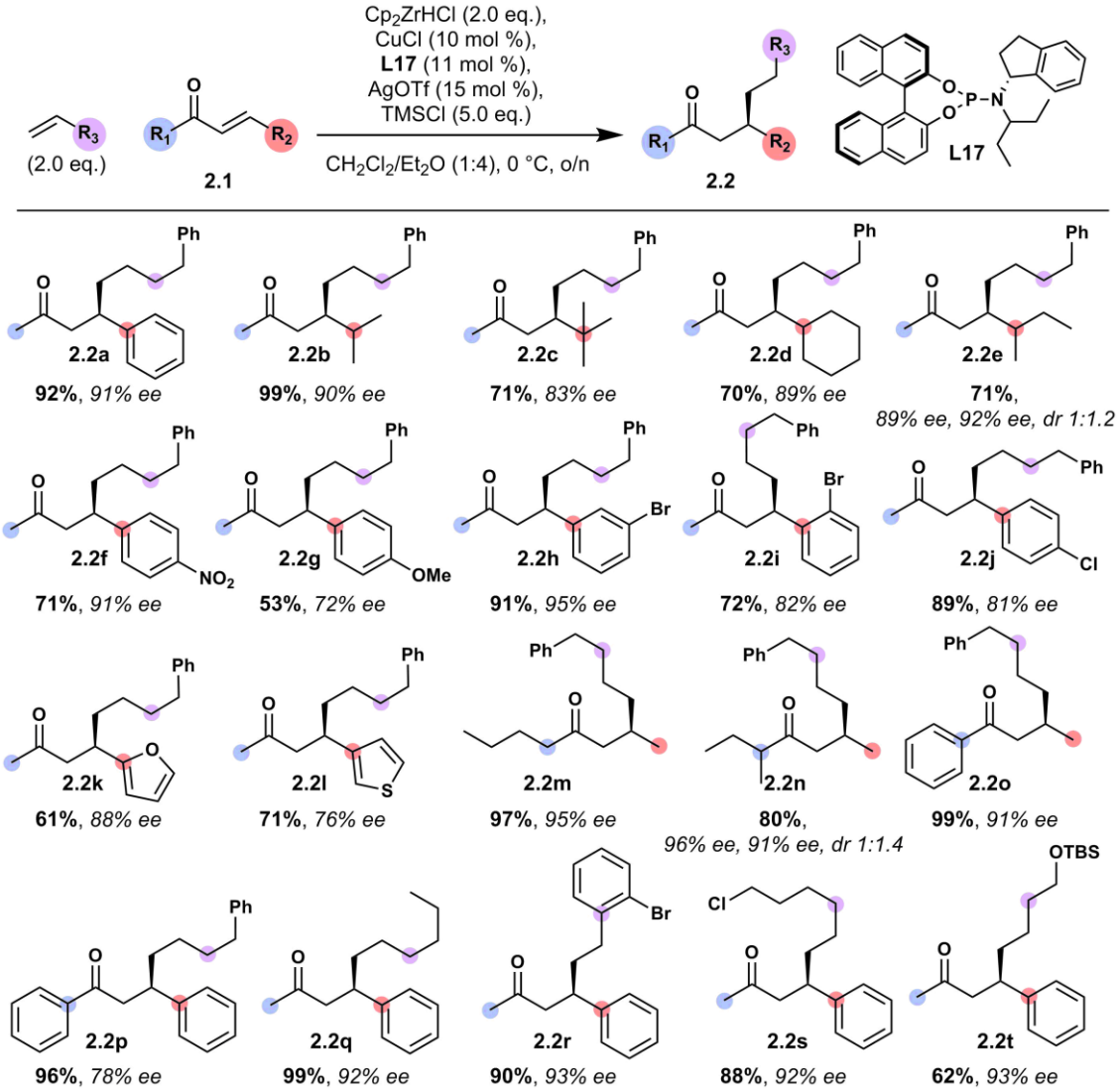

Scheme 2.10. Optimized conditions and substrate scope of the ACA on linear α,β-unsaturated ketone bearing branched or aromatic moieties, using newly developed ligand **L17**.

While a phenyl ring and an isopropyl group at the R_2 position (**2.2a** and **2.2b**, respectively) were previously detrimental features, they afforded yields and

selectivities above 90% (**Scheme 2.10**). Well known to be unsuitably reactive, even a *tert*-butyl group in **2.2c** gave satisfactory yield (71%) and 82% *ee*. Other branched and hindered electrophiles at the 4-position provided product with high *ee* (**2.2d** and **2.2e**). Substitution of R_2 phenyl ring was also tolerated with a nitro group (**2.2f**, 91% *ee*) and with halogen substituents at different positions (**2.2h**, **2.2i** & **2.2j**), but an electron donating methoxy group gave poor results (**2.2g**, 72% *ee*). Medicinally relevant, heteroaromatic rings (**2.2k** & **2.2l**) gave moderate selectivity maybe due to unfavourable interactions with the copper catalyst. In contrast, substitution on R_1 was widely tolerated with high *ee* and excellent reactivity in the case of branched aliphatic or aromatic substituents (**2.2m**, **2.2n** & **2.2o**). Even chalcone, to give **2.2p**, was very reactive although a somewhat lower selectivity was obtained (96% yield, 78% *ee*). Finally, we varied the nucleophiles to showcase the diversity of functional groups that is tolerated in our chemistry. For instance, **2.2q** was obtained with 99% yield and 92% *ee* (59% yield and 33% *ee* achieved in previous work).[32] Functionalized alkenes such as bromostyrene afforded 90% yield of **2.2r** with 93% *ee* and 6-chlorohexene gave **2.2s** in high yield (88%) and high *ee* (91%). Use of protected alcohol (**2.2t**) is also accepted (62%, 93% *ee*), with lower yield due to competitive slow *in-situ* TBS deprotection that disrupts the reaction. In that case, freshly distilled TMSCl stored in a Schlenk flask with CaH_2 under an argon atmosphere is crucial to keep protected the hydroxyl group.

8 Mechanistic study

The main benefit of using multivariate modelling to improve enantioselectivity is that the reaction under investigation can be treated as a black box while mechanistic

hypotheses can be deduced from the statistical model. This is a powerful approach in methodology development but our mechanistic understanding remained limited to the role of the alkyl substituents in the ligand geometry. As the copper-catalyzed ACA now achieves high reactivity and selectivity for a large scope of linear enones, we were keen on further investigating the mechanism.

8.1 Copper precatalyst

For both the reactivity and enantioselectivity, the optimal copper source depends on the organometallic species and ligands used to carry out the reaction.[33] In the case of alkylzirconocenes with phosphoramidite ligands, the nature of the counterion has a profound effect on enantioselectivity and electron-deficient copper salts provide better selectivity results.[53] For instance, the ACA performed remarkably well with copper triflate (CuOTf, 89% yield, 36% *ee* during condition optimisation) while copper triflamide ($CuNTf_2$) gave satisfactory results (83% yield, 12% *ee*), but other copper salts such as copper chloride (CuCl) behaved poorly (<40% yield).

In practice, copper chloride was mixed with ligand **L17** for one hour followed by addition of silver triflate and by filtration of the silver chloride precipitate, thus only retaining copper triflate complex (**Scheme 2.11-A**). One hour of premixing is required likely due to the slow process of breaking oligonuclear aggregates of insoluble copper chloride[54] to form a Cu-L* complex. The structure of this Cu-L* complex is difficult to identify. Indeed, the aggregation and reactivity of organocopper complexes depend on ligand-metal ratio, solvent chelation, ligand stereo-electronic properties, counterion effect, as well as a multitude of other parameters such as temperature and concentration.[55] Nevertheless, analogous complexes to Cu-L* suggest the presence of a binuclear precatalytic complex with a

mixture of trigonal and tetrahedral geometries (**Scheme 2.11-A**).[55] Likewise, precisely fifteen minutes of stirring copper chloride with the silver triflate is crucial for high reproducibility, likely due to the formation (or solubilisation) of different aggregates when a longer stirring time is used. We assumed here that only traces of silver would remain after filtration of AgCl, simply due to the slight excess of AgOTf compared to CuCl. As AgOTf is hygroscopic and difficult to weight, such a slight excess was found to be necessary to avoid the presence of copper chloride, which is known to catalyze the reaction with poor enantioinduction, thus eroding the overall enantioselectivity of product. On the contrary, the slight excess of AgOTf and the *in situ* preparation of the copper triflate complex were found to produce analogous results to the use of the CuOTf·½C_6H_6 precatalyst.[32] However, the presence of silver can sometimes lead to the so-called "silver effect", as found in gold-catalysis.[56] As the preparation and isolation of CuOTf·½C_6H_6 precatalyst (without silver salts) afforded similar levels of enantioselectivity and reactivity, and no obvious difference was observed with the *in situ* preparation of copper triflate complex from AgOTf salt (*i.e.* no silver effect), we assumed that the remaining excess of AgOTf in solution was not involved in the mechanism.

We started our mechanistic study by investigating the ligand-copper catalyst precursor. NMR spectroscopy was our technique of choice due to its non-invasive and non-destructive qualities that enables the study of catalytically active complexes directly in solution. This is more pertinent than the study of aggregates in the solid state due to the possible isolation of inactive complexes.[57,58]

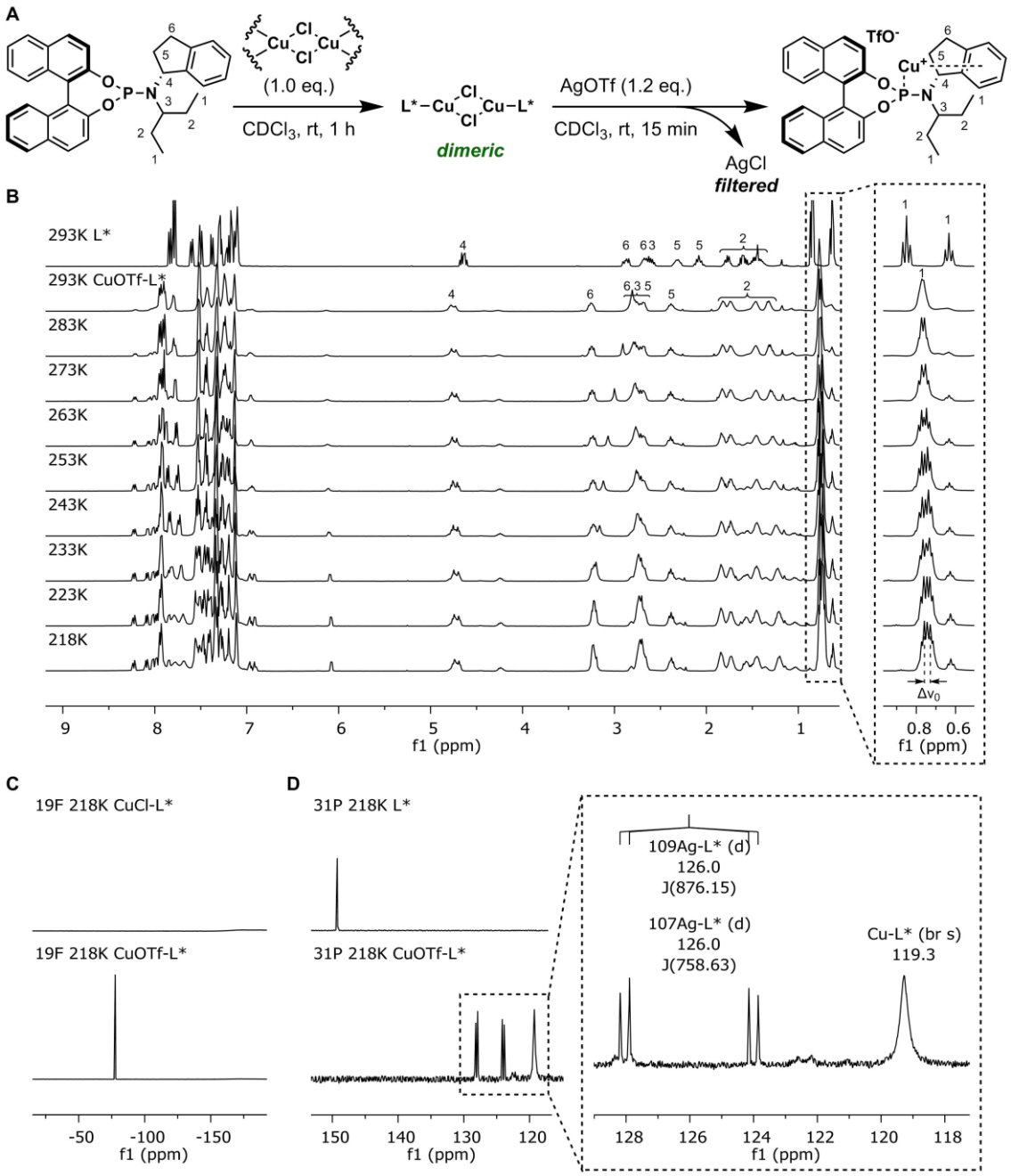

Scheme 2.11. NMR study shows the chiral ligand-copper triflate complex in $CDCl_3$ solution. **A)** Preparation of the ligand-copper complex. **B)** ^{1}H VT-NMR experiment shows complexation. **C)** ^{19}F NMR experiment shows the presence of non-coordinating triflate. **D)** ^{31}P NMR experiment displays the presence of copper complex with a minor silver species.

Our ACA reaction is carried out in a 1:4 mixture of CH_2Cl_2 and Et_2O solvents but such a combination is problematic in NMR experiments. We found that $CHCl_3$ and CH_2Cl_2 produce similar results within the reproducibility error, but removal of Et_2O is detrimental to reactivity. As Et_2O-d_{10} is incredibly expensive (£140/g), we nevertheless limited our study to the use of $CDCl_3$, bearing in mind that solvent might change the aggregate state of the active catalyst.

As ligand conformation plays an important role, we examined the copper triflate complex at 293 K then slowly decreased the temperature down to 218 K, without going further down due to the melting point of $CHCl_3$ (210 K). As shown in **Scheme 2.11-B**, an important deshielding of ^{1}H atoms *5* and *6* was observed upon copper complexation at 293 K, which is consistent with the presence of the copper species next to the indanyl group and not in close proximity of the isopentyl substituent. Additionally, the free ligand possesses two diastereotopic methyl groups that have two different magnetic environments. In the copper triflate complex, the signals coalesce to form a broad singlet, which suggests a drastic conformational change where the two methyl groups now rotate faster. Cooling the system down to 218 K, the two signals reappear at the NMR time scale. At the coalescence temperature (T_c=298K), an approximate exchange rate (k) of 30 Hz was computed using the Equation **2.1**, where $\Delta\nu_0$ represents the differential frequency of the two rotamers at slow exchange (**Scheme 2.11-B)**.[59]

$$k(Tc) = \frac{\pi\,\Delta\nu_0}{\sqrt{2}} \qquad (\mathbf{2.1})$$

^{19}F experiment before and after the addition of silver triflate followed by filtration showed the expected presence of a sharp signal at -77.7 ppm, a chemical shift corresponding to the noncoordinating triflate counterion (**Scheme 2.11-C**).[60] The

counterion is therefore present in the outer shell of the catalyst and not directly involved in a dimeric species as could be found with copper halide salts.[54] Further investigation led us to study the effect of complexation using ^{31}P nucleus (**Scheme 2.11-D**). The sharp singlet at 149.3 ppm corresponding to the free ligand was replaced by a broad singlet at 119.3 ppm consistent with the formation of the copper complex. Interestingly, the experiment also showed the presence of a silver complex, as expected by the addition in slight excess of silver triflate. Silver indeed possesses two isotopes with natural abundances of 52% for ^{107}Ag and 48% for ^{109}Ag, both with a nuclear spin of ½. Thus, two distinct doublets are present due to both silver isotopes coupling to the adjacent ^{31}P nucleus: $^{1}J(^{31}P\text{-}^{109}Ag)$ = 876.15 Hz and $^{1}J(^{31}P\text{-}^{107}Ag)$ = 758.63 Hz. The observed $^{1}J(^{107}Ag)/^{1}J(^{109}Ag)$ coupling ratio (86.6%) is in good agreement with the gyromagnetic ratio of Ag nuclei $\gamma(^{107}Ag)/\gamma(^{109}Ag)$ (86.9%).[61]

Finally, DFT calculations published by Dr Ruchuta Ardkhean suggest the presence of a monomeric copper triflate species, where copper strongly binds to phosphorus while it also interacts with the aromatic ring of the indanyl group by extrapolation in the specific case of ligand **L17**.[29]

8.2 Alkylzirconocenes

While the copper triflate complex is being prepared, the Schwarz reagent is mixed with the alkene in another flask to form *in situ* the corresponding alkylzirconocene. In 1974, Schwartz's laboratory described for the first time how zirconocene hydrochloride could readily hydrometallate alkenes[62] and it was only in 1991 that the Wipf group applied alkylzirconocenes in racemic conjugate additions.[63] The polarization of the C–Zr bond is comparable to Grignard reagents, but only small

electrophiles can be attacked due to the steric hindrance around the zirconium atom, hence the wide functional group tolerance observed.[31] These seminal works showed that alkylzirconocenes can rapidly rearrange internally at room temperature *via* Zr–H elimination and readdition. The reduction of carbonyl compounds such as α,β-unsaturated ketones was observed only once due to the retro-hydrometallation regenerating residual Schwartz reagent. This occured in the specific case of electron-rich allylsilane in combination with slowly reacting electrophiles.[53] Such behaviour was however never observed in this work, which suggests that the rate of Zr–H elimination and dissociation followed by ketone reduction is negligible compared to the rate of ACA. Upon mixing with the copper precursor, only alkylzirconocenes are likely present in solution.

8.3 Transmetallation

Interestingly, the Feringa group has shown that partial transmetallation occurs when copper bromide is mixed with Grignard reagents, thus forming a binuclear Cu/Mg complex as shown in **Scheme 2.12-A**.[16] Likewise, dialkylzinc species with copper halide salts form an intricate multinuclear complex, where only one alkyl substituent is partially transmetallated (**Scheme 2.12-B**).[64]

Inspired by these mechanistic studies, Dr Emeline Rideau extensively studied the transmetallation of copper triflate precatalyst with organozirconium species using NMR techniques. Her work demonstrated that the Cu–L* complex interacts with the alkylzirconocenes within the NMR time scale, but chemical shifts in ^{1}H NMR also suggested that only a partial transmetallation of the alkyl substituent to copper occurred. A bimetallic Zr/Cu complex is therefore highly likely as drawn in **Scheme 2.12-C**.

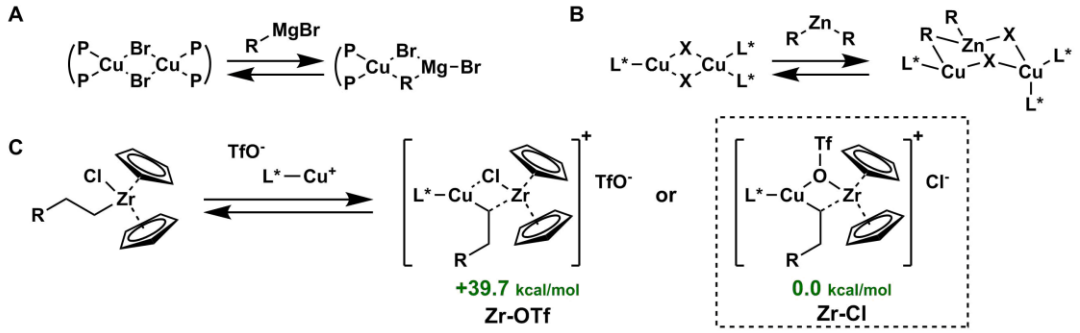

Scheme 2.12. Proposed primary catalytic species of copper salts with **A)** Grignard reagents, **B)** organozinc and **C)** organozirconium species. Free energies (ΔG) of the two bimetallic species were computed at the (SMD Et_2O) ωB97XD/def2tzvpp//ωB97XD/6-31G(d)/LANL2DZ(Zr/Cu) level of theory.

To our knowledge, it has not been shown that the triflate counterion is non-coordinating in presence of both copper and zirconium species and there are therefore two possible bimetallic species (**Zr-OTf** and **Zr-Cl**). Our calculations of both ground states revealed that the **Zr-OTf** complex was actually the most favoured geometry by a large 39.7 kcal/mol energy difference (50.8 kcal/mol without ligand). Although more stable species are not necessarily more reactive in subsequent steps in a catalytic cycle, such a difference in relative stabilities suggests that the formation of a **Zr-Cl** bimetallic complex can be disregarded.

8.4 Asymmetric conjugate addition

Once the bimetallic Zr/Cu complex is formed, the α,β-unsaturated carbonyl substrate is added, immediately followed by a large excess of TMSCl additive. At this step, the NMR analysis of the reaction mixture becomes excessively complicated due to intricate interactions. According to Dr Emeline Rideau's unpublished work, deconvoluting the role of each reagent proved impossible by NMR and we therefore turned our attention to kinetic experiments instead.

The role of the TMSCl additive was crucial in achieving higher enantioselectivities. The effect was only of ±5% *ee* in the case of ligand **L17** (**Scheme 2.13-A**) but substantial differences have already been observed going from 80% yield with the additive to low reactivity (9% yield) without it.[30] We monitored the crude reaction mixture by HPLC on a chiral non-racemic stationary phase (**Scheme 2.13-B**). An absence of TMSCl additive led to slower **2.2q** formation, but satisfactorily, its addition afforded an impressive rate acceleration. More importantly, we discovered that the reaction is nearly racemic for the first five minutes, and then becomes enantioselective over time (**Scheme 2.13-B**). Such a dynamic effect was unanticipated.[65] This discovery is of importance because it suggests that the bimetallic complex characterized so far is a poorly selective complex, from which an (unknown) enantioselective catalyst is formed after about 10% conversion. We also observed a small *ee* erosion over time without TMSCl.

To prove that such behavior was not unique to the linear ACA, we decided to realize an identical kinetic study using 4,4-diphenyl-2-cyclohexen-1-one **2.3** with Feringa's ligand, a system which was extensively studied by Dr Emeline Rideau using NMR technique (**Scheme 2.13-C**).[66] Likewise, we found that the reaction starts at low *ee*'s and then quickly increases upon *in-situ* formation of the active catalyst. Absence of the TMSCl additive has even a greater impact on enantioselectivity with cyclic substrates. Any NMR study should therefore be done at a precise time because the enantioselective catalyst only fully takes over after 10 min. Below that time, the slow and poorly enantioselective catalyst is likely to be the most predominant species in solution. This is also consistent with previous observations by Dr Emeline Rideau that stoichiometric copper catalyst leads to poor reactivity and enantioselectivity.[66]

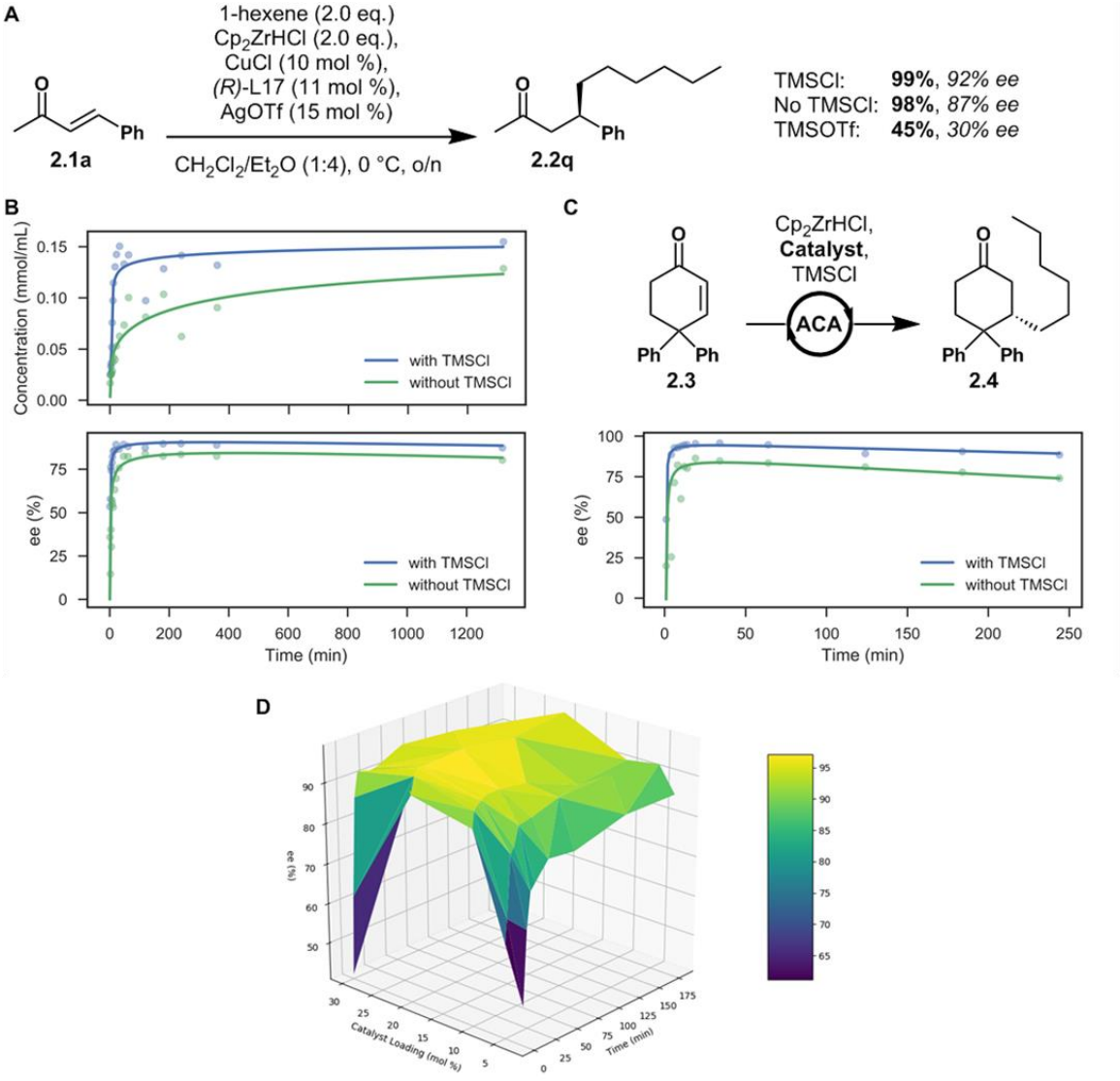

Scheme 2.13. Effect of TMSCl on reactivity and enantioselectivity. **A)** Effect of additives on isolated linear product. **B)** Concentration and enantioselectivity of linear product over time with and without TMSCl. **C)** Enantioselectivity of cyclic product over time with and without TMSCl. **D)** 3D plot representing the enantioselectivity of cyclic product over time as a function of catalyst loading with TMSCl.

In both cyclic and linear systems, we observed that the active catalyst really takes over after 10% conversion that roughly corresponds to one turnover. Therefore, we varied the catalyst loading and monitored the product enantioselectivity, which

correlates the formation of the enantioselective complex (**Scheme 2.13-C**). At low catalyst loading, the background reaction competes with the active catalyst and the product enantioselectivity increases up to 85% *ee* after 40 min. At 20% catalyst loading, an optimum is reached with *ee* achieving 95% in less than 2 min. Above that value, the copper salt crashes out of the reaction mixture thus slowing down the formation of active catalyst. Dilution to solubilize all the 30 mol % catalyst still triggered a slower formation of enantiopure product due to dilution effects.

Such data strongly indicate that active highly-enantioselective catalyst formation requires one turnover, and not simply time to break or solubilize aggregates.

8.5 Pre-generation of the active catalyst

The discovery that the active catalyst is formed *during the course of the reaction* led us to reconsider all the insights from prior studies, particularly about the copper triflate pre-catalyst. As the active catalyst was formed after one turnover, we reasoned that it might involve a copper enolate complex (**Scheme 2.14-A**).

Attempts to preform a copper enolate complex **2.6** starting from ketone **2.5** however led to racemic product. We then decided to take a different approach and used a sacrificial enone instead. *(E)*-tetradec-3-en-2-one **2.7** was chosen due to its easy separation and non-UV active properties. Satisfactorily, the use of 10 mol % of the sacrificial enone enabled the formation of enantiopure product even during the first minutes of the reaction (**Scheme 2.14-B**). Note that the differences in enantioselectivity are likely due to the poor signal/noise ratio.

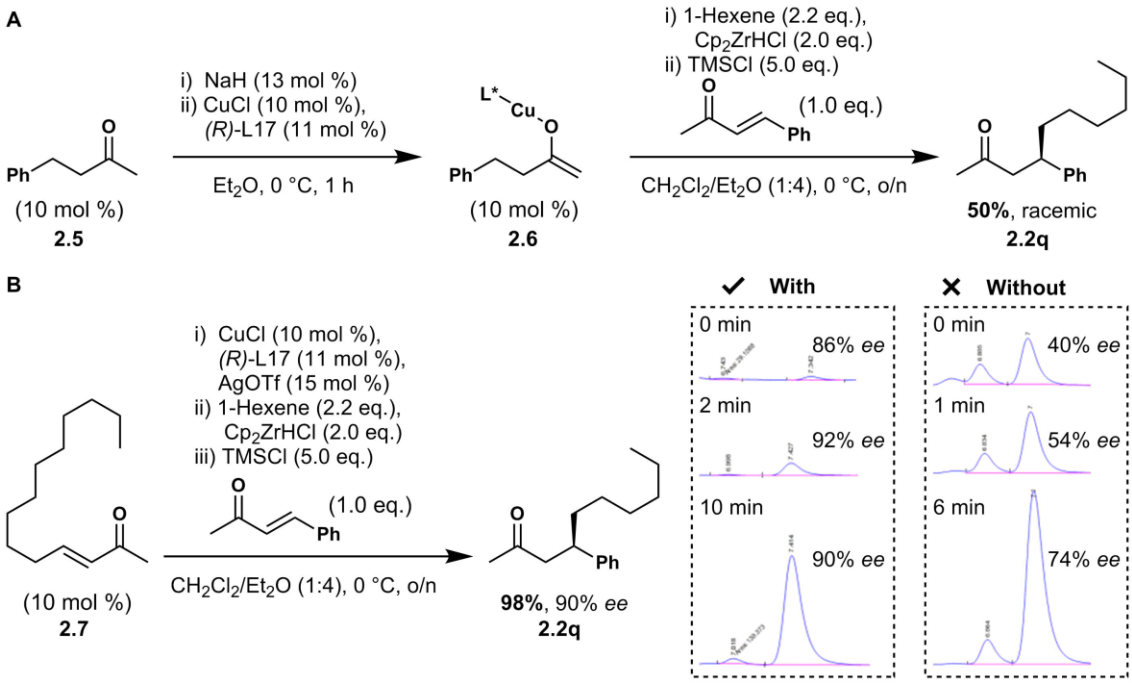

Scheme 2.14. ACA of linear enones with a preformed catalyst. **A)** Copper enolate complex and **B)** sacrificial enone. HPLC traces with and without the sacrificial enone.

8.6 Reformation of the active catalyst

The ACA of alkylzirconocenes to α,β-unsaturated carbonyl substrates is a heterogeneous reaction due to the slow formation of dark grey precipitates over time that are likely Zr salts. NMR study of such complexes, however, proved unfruitful. In theory, the Zr or Cu enolate product produced from the 1,4-addition likely reacts with the excess of TMSCl, driving the formation of Cp_2ZrCl_2 and CuOTf *or* CuCl and $Cp_2ZrClOTf$. Accordingly, we computed the ground states of CuOTf, Cp_2ZrCl_2 and TMSCl then compared them to the ground states of other possible salts (**Scheme 2.15-A**). We found that CuOTf (+5.9 kcal/mol) is not reformed under thermodynamic control but CuCl is, a copper salt that is known to be poorly selective in experiments. Noteworthily, the aggregation state and solubility of regenerated copper chloride are, however, likely very different. Zr metal also prefers the triflate

counterion over chloride as shown previously, which also suggests that regeneration of copper triflate is unlikely. The importance of the chloride counterion is consistent with the poor reactivity and enantioselectivity obtained when using TMSOTf as an additive (**Scheme 2.13-A**). However, the Gibbs energy difference is not large enough to make a clear conclusion.

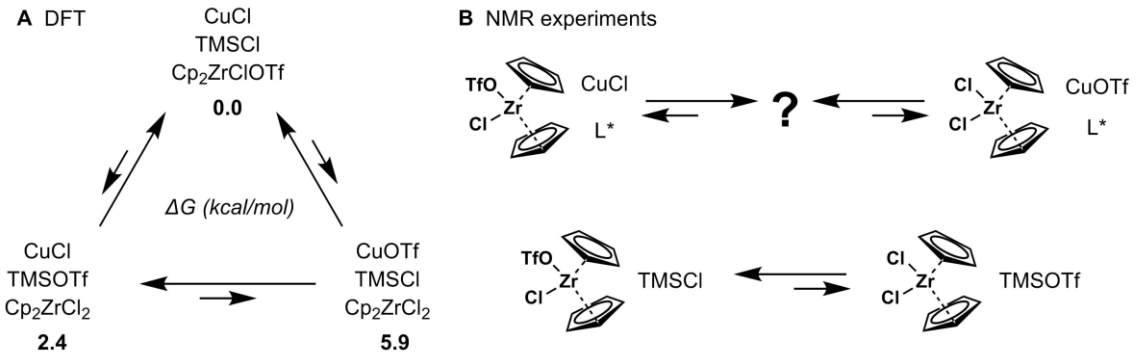

Scheme 2.15. A) Free energies of CuOTf, Cp_2ZrCl_2 and TMSCl mixed together at the (SMD Et_2O) ωB97XD/def2tzvpp//ωB97XD/6-31G(d)/LANL2DZ(Zr/Cu) level of theory and **B)** NMR experiments mixing: $Cp_2ZrClOTf$, CuCl and **L17** ; Cp_2ZrCl_2, CuOTf and **L17**; $Cp_2ZrClOTf$ and TMSCl.

To support the hypothesis of a **Zr-OTf** species, we synthesized $Cp_2ZrClOTf$ and mixed it with CuCl and **L17** (**Scheme 2.15-B**). ^1H NMR spectroscopy showed the formation of a new species, likely bimetallic, that was also produced upon mixing Cp_2ZrCl_2 and premade copper triflate complex with **L17**. Additionally, $Cp_2ZrClOTf$ was unreactive with TMSCl.

8.7 DFT calculations

Asymmetric conjugate addition has been thoroughly studied and two consensual mechanisms have emerged from the organic community.[33] On one hand, the *d* orbital of copper(I) can interact with the alkene π^* of α,β-unsaturated carbonyl

substrates to form a π-complex that undergo carbocupration (**Scheme 2.16**). The metal salt produced after transmetallation such as MgX_2 or ZnRX can act as a Lewis acid to activate the carbonyl moiety in large aggregates with the enone.[16,64] On the other hand, oxidative addition of copper(I) can form the copper(III) intermediate, which possesses a σ-bond at the 4 position while coordinating the enolate olefin.[16,67] The metal salt acts again as a Lewis acid to activate the carbonyl moiety.

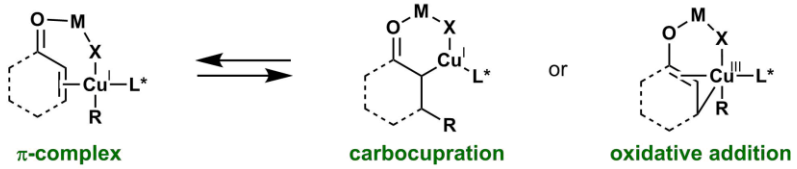

Scheme 2.16. Two mechanistic proposals involve copper at different oxidation states.

In order to distinguish both possible mechanistic pathways, a DFT mechanistic study was carried out. Several modelling simplifications were considered to obtain a workable system. Thus, the alkylzirconocene was truncated to only two alkyl carbons while **L17** ligand (isopentyl) was replaced by **L2** (cyclohexyl) to reduce the amount of conformers to examine. The counterion of TMS was also considered in the outer shell of the catalyst and was computed at an infinite distance from copper. We chose the B97D pure functional due to the possibility to accelerate the calculations with density fitting and also because it proved well-suited in similar work.[27]

Unfortunately, no transition states involving copper(III) were found due to the lack of geometry convergence such that the optimisation often directly went to the product. We therefore focused on the formation of a π-complex and examined an aggregate involving the zirconium acting as a Lewis acid on the enone. A very large amount of conformers is however possible and we found it difficult to study them

all. Additionally, several negative frequencies were sometimes obtained which further complicated the identification of transition states. Inspired by literature precedence,[29] we found that using TMSCl as a Lewis acid directly in the diastereoselective transition state proved successful (**Scheme 2.17**).

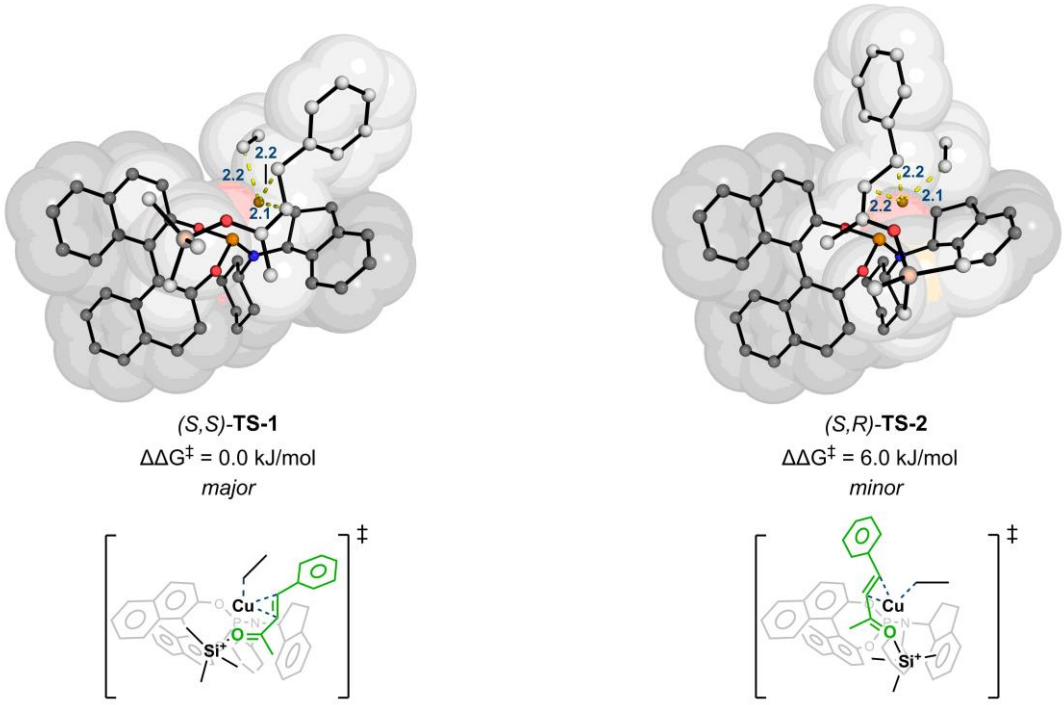

Scheme 2.17. Lowest competing diastereoselective transition structures computed at the B97D/def2tzvpp//B97D/def2SVP/def2SVP level of theory. Distances of Cu-C shown in blue (Å).

We identified two TS leading to the (*S*) and (*R*) products, **TS-1** and **TS-2** respectively. Interestingly, the *cis* conformation of the starting material is preferred to avoid steric clashes with the ligand, and complexation of the carbonyl group helps discriminating both diastereotopic transition states. According to literature precedence and DFT calculations, the formation of a π-complex from copper(I) is therefore the most likely favoured pathway, although copper(III) mechanism can not be discarded.

8.8 Proposed mechanism

Combining all the results obtained so far, we propose the formation of a dimeric complex upon mixing copper chloride salt **$CuCl_{(s)}$** with the chiral ligand **L*** (**Scheme 2.18**). Addition of silver triflate affords the copper triflate precatalyst that is monomeric with a non-coordinating triflate counterion.

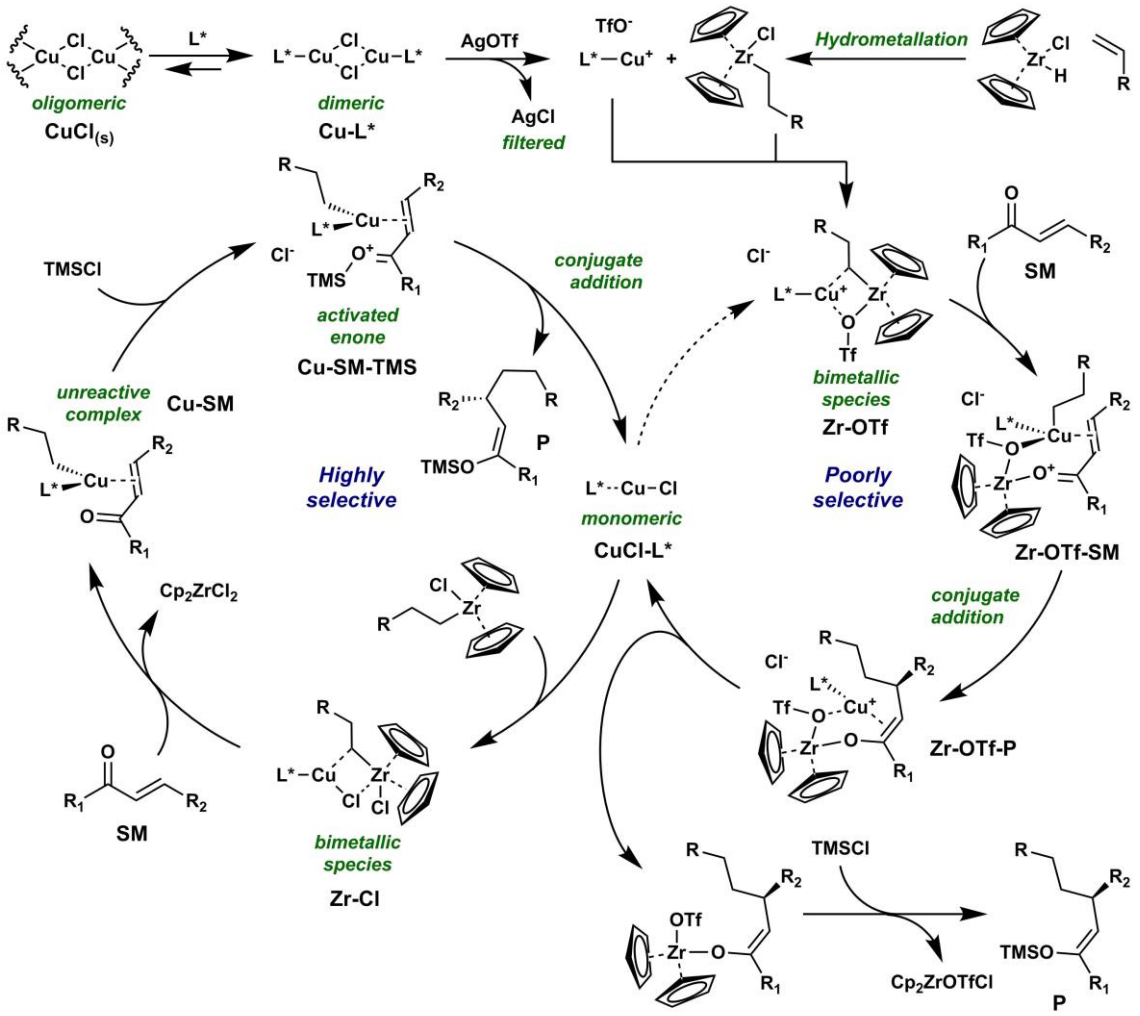

Scheme 2.18. Proposed mechanism for the asymmetric conjugate addition of alkylzirconocenes to linear enones.

Hydrometallation of a terminal olefin with the Schwartz reagent produces an alkylzirconocene, which partially transmetallates with copper and creates a

bimetallic species **Zr-OTf**. Coordination of the enone substrate breaks the aggregate and forms a copper π-complex where the carbonyl moiety is activated by a bridged Zr species, called **Zr-OTf-SM**. The resulting conjugate addition is then poorly selective (**Zr-OTf-P**), followed by trapping of the Zr-enolate with TMSCl releasing $Cp_2ZrOTfCl$. Dissociation of the product **P** frees the monomeric form of copper chloride **CuCl-L***, hence the enantioselective catalyst. We reason here that the commercial oligomeric copper chloride salt $\mathbf{CuCl_{(s)}}$ likely does not disaggregate to its single unit under the reaction condition, yielding a poorly enantioenriched product. The role of copper triflate is therefore to produce a monomeric species from the copper chloride salt, which will be a monomeric copper chloride complex **CuCl-L*** after one turnover. Monomeric copper chloride **CuCl-L*** is in catalytic amount and formed over time. Accordingly, it is unlikely to reform a dimeric copper chloride species **Cu-L*** but more probably reacts immediately with the two equivalents of alkylzirconocenes (kinetic control). Partial transmetallation of monomeric copper chloride **CuCl-L*** affords a new bimetallic species **Zr-Cl** that collapses upon enone complexation to form **Cu-SM**. The resulting species **Cu-SM** is unreactive and a large excess of TMSCl (5 eq.) is crucial to push the activation of the enone by trimethylsilyl to produce **Cu-SM-TMS**. Zr salt could also act as a Lewis acid but the marked impact of the TMSCl additive on *ee* values in the case of cyclic enones suggest a key role of the additive in the diastereoselective TSs. This time, the conjugated addition is highly stereoselective and produces enantiopure product **P**. Its release finally regenerates the active catalyst **CuCl-L***.

9 Conclusion and future work

In conclusion, sterically hindered α,β-unsaturated ketones that initially behaved poorly in copper-catalyzed asymmetric conjugate additions now achieve high reactivity and enantioselectivity thanks to the development of a new ligand (**L17**).

The ligand design was guided by an iterative data-driven approach which successfully predicted enantioselectivities. However, a selectivity cliff was identified when challenging the model with structures dissimilar from the training set. Generation of ligands on a broader spectrum of enantioselectivity (from 30% *ee* to 80% *ee*) and computing of new molecular descriptors helped design a more robust model. Interestingly, predictive modelling allowed us to identify a maximum in selectivity based on the structural diversification of the alkyl substituents. Such information is valuable to stop working on the expensive process of ligand development and put a clear end to ligand design. This is a clear advantage compared to the traditional approach using chemical intuition and extensive screening. Additionally, the core strength of the data-led strategy resides in identifying unpromising potential ligand structures that were not synthesized, as synthesis remains the bottleneck of the design process. However, it is worth noting that the development of models based on a challenging but unique substrate **2.1a** might have led to an optimized ligand **L17** that is too specific, thus yielding high enantioselectivy only for structurally-related substrates. Fortuitously, we found that the method now achieves up to 99% yield and 95% *ee* on a broader range of substrates (cf. scope). To decrease the impact of chance in ligand design, a healthier approach might be to generate data for multiple substrates possessing different steric and electronic features, as employed by the Sigman group.[68] Obviously, such

consideration entails the generation of new molecular descriptors to describe the chemical features of theses substrates, which are then included in the model.

Once ligand design is halted, it is also straightforward to neglect the importance of achieving both high reactivity and enantioselectivity by simply taking the best ligand according to the model.[29] Inspired by the Nobel laureate in economy Pareto and his work on multiobjective optimisation,[50] we proposed an independant multiobjective ranking of the synthesized ligands to select the best ligands according to their overall experimental results, which produced **L17** as the best trade-off.

Finally, mechanistic study of the optimized reaction revealed the formation of the active enantioselective catalyst during the course of the reaction and showcased the rate acceleration observed with the use of ligand **L17**. Although intensive work was carried out to deconvolute the importance of each reagent and its impact on the mechanistic pathway, the observed complexity of interactions only allowed us to propose a mechanism. The lack of mechanistic understanding even after thorough examination demonstrates the superiority of data-led approaches compared to TS-based strategies in the case of metal-catalyzed asymmetric transformations.

10 References

1 A. V Brethomé, R. S. Paton and S. P. Fletcher, *ACS Catal.*, 2019, **9**, 7179–7187.

2 M. van Klaveren, F. Lambert, D. J. F. M. Eijkelkamp, D. M. Grove and G. van Koten, *Tetrahedron Lett.*, 1994, **35**, 6135–6138.

3 F. Lambert, D. M. Knotter, M. D. Janssen, M. van Klaveren, J. Boersma and G. van Koten, *Tetrahedron: Asymmetry*, 1991, **2**, 1097–1100.

4 Z. Gao and S. P. Fletcher, *Chem. Commun.*, 2017, **53**, 10216–10219.

5 D. Zaleta-Pinet, A. McCluskey, S. Hall, J. Brophy, C. Ashhurst-Smith, J. Sakoff and I. van Altena, *Aust. J. Chem.*, 2016, **69**, 161.

6 B. C. Calvo, J. Buter and A. J. Minnaard, in *Copper-catalyzed asymmetric synthesis*, eds. A. Alexakis, N. Krause and S. Woodward, 2014, pp. 373–447.

7 C. Wu, X. Qin, A. M. P. Moeljadi, H. Hirao and J. S. Zhou, *Angew. Chem. Int. Ed.*, 2019, **58**, 2705–2709.

8 O. Reiser, *Angew. Chem. Int. Ed.*, 2001, **40**, 3255–3255.

9 C. Wu, G. Yue, C. D.-T. Nielsen, K. Xu, H. Hirao and J. Zhou, *J. Am. Chem. Soc.*, 2016, **138**, 742–745.

10 D. L. J. Pinheiro, P. P. de Castro and G. W. Amarante, *Euro. J. Org. Chem.*, 2018, **2018**, 4828–4844.

11 M. P. Sibi and S. Manyem, *Tetrahedron*, 2000, **56**, 8033–8061.

12 A. Alexakis, N. Krause and S. Woodward, *Copper-catalyzed asymmetric synthesis*, 2014.

13 S. R. Harutyunyan, T. den Hartog, K. Geurts, A. J. Minnaard and B. L. Feringa, *Chem. Rev.*, 2008, **108**, 2824–2852.

14 T. Jerphagnon, M. G. Pizzuti, A. J. Minnaard and B. L. Feringa, *Chem. Soc. Rev.*, 2009, **38**, 1039–1075.

15 B. Maciá Ruiz, K. Geurts, M. Á. Fernández-Ibáñez, B. ter Horst, A. J. Minnaard and B. L. Feringa, *Org. Lett.*, 2007, **9**, 5123–5126.

16 S. R. Harutyunyan, F. López, W. R. Browne, A. Correa, D. Peña, R. Badorrey, A. Meetsma, A. J. Minnaard and B. L. Feringa, *J. Am. Chem. Soc.*, 2006, **128**, 9103–9118.

17 F. López, S. R. Harutyunyan, A. Meetsma, A. J. Minnaard and B. L. Feringa, *Angew. Chem. Int. Ed.*, 2005, **44**, 2752–2756.

18 R. Des Mazery, M. Pullez, F. López, S. R. Harutyunyan, A. J. Minnaard and B. L. Feringa, *J. Am. Chem. Soc.*, 2005, **127**, 9966–9967.

19 F. López, S. R. Harutyunyan, A. J. Minnaard and B. L. Feringa, *J. Am. Chem. Soc.*, 2004, **126**, 12784–12785.

20 K. P. McGrath and A. H. Hoveyda, *Angew. Chem. Int. Ed.*, 2014, **53**, 1910–1914.

21 P. K. Fraser and S. Woodward, *Chem. - A Eur. J.*, 2003, **9**, 776–783.

22 M. Yoshida, H. Ohmiya and M. Sawamura, *J. Am. Chem. Soc.*, 2012, **134**, 11896–11899.

23 L. A. Arnold, R. Imbos, A. Mandoli, A. H. . de Vries, R. Naasz and B. L. Feringa, *Tetrahedron*, 2000, **56**, 2865–2878.

24 A. Alexakis, D. Polet, C. Benhaim and S. Rosset, *Tetrahedron: Asymmetry*, 2004, **15**, 2199–2203.

25 X. Hu, H. Chen and X. Zhang, *Angew. Chem. Int. Ed.*, 1999, **38**, 3518–3521.

26 A. Alexakis and C. Benhaim, *Org. Lett.*, 2000, **2**, 2579–2581.

27 R. Ardkhean, P. M. C. Roth, R. M. Maksymowicz, A. Curran, Q. Peng, R. S. Paton and S. P. Fletcher, *ACS Catal.*, 2017, **7**, 6729–6737.

28 M. Sidera, P. M. C. Roth, R. M. Maksymowicz and S. P. Fletcher, *Angew. Chem. Int. Ed.*, 2013, **52**, 7995–7999.

29 R. Ardkhean, M. Mortimore, R. S. Paton and S. P. Fletcher, *Chem. Sci.*, 2018, **9**,

2628–2632.

30 Z. Gao and S. P. Fletcher, *Chem. Sci.*, 2017, **8**, 641–646.

31 P. Wipf and H. Jahn, *Tetrahedron*, 1996, **52**, 12853–12910.

32 P. M. C. Roth and S. P. Fletcher, *Org. Lett.*, 2015, **17**, 912–915.

33 A. Alexakis, N. Krause and S. Woodward, in *Copper-catalyzed asymmetric synthesis*, eds. A. Alexakis, N. Krause and S. Woodward, 2014, pp. 33–68.

34 A. Alexakis and C. Benhaim, *Euro. J. Org. Chem.*, 2002, **2002**, 3221–3236.

35 J. Boström, D. G. Brown, R. J. Young and G. M. Keserü, *Nat. Rev. Drug Discov.*, 2018, **17**, 709–727.

36 G. P. Howell, *Org. Process Res. Dev.*, 2012, **16**, 1258–1272.

37 I. Némethová, S. Bilka and R. Šebesta, *J. Organomet. Chem.*, 2018, **856**, 100–108.

38 A. Alexakis, J. E. Bäckvall, N. Krause, O. Pàmies and M. Diéguez, *Chem. Rev.*, 2008, **108**, 2796–2823.

39 B. L. Feringa, *Acc. Chem. Res.*, 2000, **33**, 346–353.

40 W. Fu and W. Tang, *ACS Catal.*, 2016, **6**, 4814–4858.

41 Q. Peng, F. Duarte and R. S. Paton, *Chem. Soc. Rev.*, 2016, **45**, 6093–6107.

42 I. V. Tetko and V. Y. Tanchuk, *J. Chem. Inf. Comput. Sci.*, 2002, **42**, 1136–1145.

43 J. C. Dearden, M. T. D. Cronin and K. L. E. Kaiser, *SAR QSAR Environ. Res.*, 2009, **20**, 241–266.

44 H. Schönherr and T. Cernak, *Angew. Chem. Int. Ed.*, 2013, **52**, 12256–12267.

45 K. C. Harper, E. N. Bess and M. S. Sigman, *Nat. Chem.*, 2012, **4**, 366–374.

46 A. V. Brethomé, S. P. Fletcher and R. S. Paton, *ACS Catal.*, 2019, **9**, 2313–2323.

47 D. T. Ahneman, J. G. Estrada, S. Lin, S. D. Dreher and A. G. Doyle, *Science*, 2018,

360, 186–190.

48 *Spartan'16*, Wavefunction, Inc., Irvine, CA, 2016.

49 T. Piou, F. Romanov-Michailidis, M. Romanova-Michaelides, K. E. Jackson, N. Semakul, T. D. Taggart, B. S. Newell, C. D. Rithner, R. S. Paton and T. Rovis, *J. Am. Chem. Soc.*, 2017, **139**, 1296–1310.

50 C. A. Nicolaou, N. Brown and C. S. Pattichis, *Curr. Opin. Drug Discov. Devel.*, 2007, **10**, 316–324.

51 V. Bhaskar, S. K. Gupta and A. K. Ray, *Rev. Chem. Eng.*, 2000, **16**, 1–54.

52 R. Jacques, R. D. C. Pullin and S. P. Fletcher, *Nat. Commun.*, 2019, **10**, 21.

53 R. M. Maksymowicz, P. M. C. Roth and S. P. Fletcher, *Nat. Chem.*, 2012, **4**, 649–654.

54 C. Floriani, D. Jacoby, A. Chiesi-Villa and C. Guastini, *Angew. Chemie Int. Ed. English*, 1989, **28**, 1376–1377.

55 F. von Rekowski and R. M. Gschwind, *Organometallics*, 2014, **33**, 6259–6262.

56 A. Zhdanko and M. E. Maier, *ACS Catal.*, 2015, **5**, 5994–6004.

57 B. L. Feringa, *Angew. Chem. Int. Ed.*, 1996, **35**, 2374–2376.

58 R. M. Gschwind, *Chem. Rev.*, 2008, **108**, 3029–3053.

59 F. P. Gasparro and N. H. Kolodny, *J. Chem. Educ.*, 1977, **54**, 258.

60 J. F. Modder, J. M. Ernsting, K. Vrieze, M. De Wit, C. H. Stam and G. Van Koten, *Inorg. Chem.*, 1991, **30**, 1208–1214.

61 A. Cingolani, Effendy, M. Pellei, C. Pettinari, C. Santini, B. W. Skelton and A. H. White, *Inorg. Chem.*, 2002, **41**, 6633–6645.

62 D. W. Hart and J. Schwartz, *J. Am. Chem. Soc.*, 1974, **96**, 8115–8116.

63 P. Wipf and J. H. Smitrovich, *J. Org. Chem.*, 1991, **56**, 6494–6496.

64 H. Zhang and R. M. Gschwind, *Chem. - A Eur. J.*, 2007, **13**, 6691–6700.

65 K. P. Bryliakov, *ACS Catal.*, 2019, **9**, 5418–5438.

66 E. Rideau, *Organozirconocene nucleophiles in cu-catalysed asymmetric transformations : methodologies, applications to total synthesis and NMR mechanistic studies*, Thesis, University of Oxford, 2016.

67 N. Yoshikai and E. Nakamura, *Chem. Rev.*, 2012, **112**, 2339–2372.

68 A. Milo, A. J. Neel, F. D. Toste and M. S. Sigman, *Science*, 2015, **347**, 737–743.

3

Conformational effects on physical-organic steric descriptors

Part of this work was published in *ACS Catalysis* in 2019.[1]

wSterimol program is my own work but it uses Verloop's Sterimol program, which was entirely recoded by Dr K. Jackson in Python,[2] as clearly stated in the text.

1 Introduction

Steric effects are among the most important nonbonding interactions that impact molecular conformation, reactivity and selectivity. Each atom in a molecule occupies a certain amount of space resulting in repulsive interatomic interactions when neighboring electron clouds overlap, which leads to an increase in the quantum mechanical exchange energy (Pauli repulsion).[3] Traditionally derived from empirical relationships, development of physical-organic parameters such as interference values,[4] A-values,[5] Charton,[6] and Taft parameters[7] resulted from efforts to evaluate steric influence across different substituents. More recent work has also been published such as the topographic steric maps.[8,9]

We observed that substituent flexibility was originally described in experimentally-derived steric physical-organic descriptors, which inherently capture an ensemble average. For instance, the Taft parameters were measured from the relative rates of hydrolysis in methyl esters and changes due to the adjacent substituent were therefore necessarily describing the steric bulk of all its conformers.[10] But the main problem of experimentally-derived descriptors is that they require the synthesis of all the considered derivatives and carrying out the experiments in identical settings to avoid discrepancy in the data. In comparison, computable descriptors are superior and were preferentially adopted by the scientific community due to the fact that catalyst modifications can be tested *in silico* without requiring any synthetic efforts and descriptor values are easily reproducible.

Examining flexibility in computable descriptors, however, requires the identification of all the conformers using conformational sampling of each catalyst followed by their further optimisation. Back in 1960, with the first use of quantitative structure–

activity relationships (QSAR) in chemistry,[11] this was a tedious and computationally expensive process and, to our knowledge, all the descriptors were computed from rigid structures while ignoring conformers. This simplification was not an issue at that time as most considered substituents did not have any significant amount of rotatable dihedrals. Charton for instance, who developed the eponymous parameter from a correction of Taft values, tabulated a lot of commonly used substituents such as *i*-Pr, *t*-Bu, Me, OMe, *c*-C_3H_5 and *c*-C_5H_9.[6,12] Rigidity was also highly desirable because it was thought that flexibility added degrees of freedom, thus leading to more unproductive conformations. This was for instance the classic 'lock and key' hypothesis in enzyme catalysis[13] and has guided medicinal chemistry development for a long time.[14]

The previously mentioned steric descriptors (Taft, Charton, *etc.*) were also capturing the steric effects of potentially unsymmetrical functional groups using a single parameter. This was not suited to describe different steric demands along several axes, which is crucial in asymmetric catalysis. In this context, Verloop developed the multidimensional Sterimol parameters in 1976 to capture the steric interactions of a substituent along different directions.[15] The original Sterimol program was developed in Fortran by Verloop and Hoogenstraaten, working at Duphar (Netherlands)[9] and they first applied it in QSAR studies in medicinal chemistry.[10] Using the Corey-Pauling-Koltun (CPK) molecular model,[16] the principal axes B_1, B_5 and L can be defined about the point of attachment of a given substituent (**Figure 3.1**). In brief, B_1 and B_5 represent respectively the shortest and the longest distance perpendicular to the primary axis of attachment. These two subparameters can be viewed as the minimum and maximum widths of a substituent and as such,

define its extent of branching. The final subparameter *L* is the total distance along the primary axis of attachment and describes the length of the substituent.

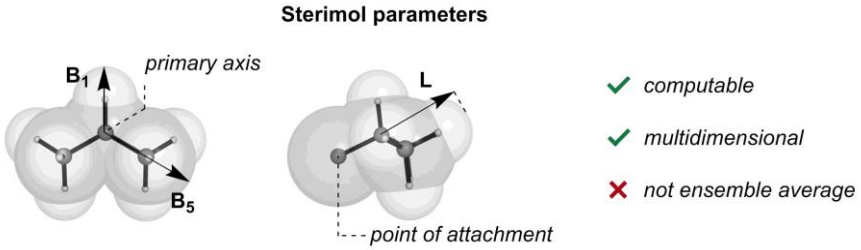

Figure 3.1. Sterimol parameters B_1, B_5 and L with front and lateral profiles of an *i*-propyl moiety calculated using the CPK molecular model.

Although they were developed in the 1970s, Sterimol parameters remained underused by the organic community until more recently, likely due to their existence being largely unknown. The Sigman laboratory reintroduced them in 2012, where they showed that Sterimol parameters could be used to quantitatively correlate the shape of a substituent and enantioselectivity in cases where unidimensional steric parameters failed.[10] This discovery was of great importance in the use of multivariate relationships in catalysis,[17] and it has also led to the adoption of Sterimol parameters much more widely in describing and predicting functional group effects on stereoselectivity.

In 2017, our work with phosphoramidite ligands containing long and flexible linear substituents (**Chapter 2**) forced us to quantify the role of conformations in physical-organic descriptors such as Sterimol parameters. Around the same time, Sigman realised that flexibility had been overlooked and could actually be a constructive feature.[18] The inclusion of conformationally flexible groups (but which were treated as rigid) can also be observed in more recent studies in asymmetric catalysis.[10,15,16]

While Sterimol parameters are well-suited to describe the steric demands along different axes, they were not created to capture substituent flexibility. An important question immediately arises regarding which sets of 3D coordinates should be used to define these parameters: is it chemically more meaningful to use the most stable conformation, a catalytically-relevant conformation such as a transition state, or an ensemble average? For instance, *n*-pentyl group has recently been used in a QSAR model[16] but such linear substituents are often challenging because of their flat potential energy surface (PES). They indeed tend to possess conformers, which are very close in energy but sometimes have completely different 3D shape, and hence Sterimol values. The use of only a single conformer (even the most stable) may therefore give rise to potentially misleading steric parameters. For instance, the all-*anti* conformer of *n*-pentyl is characterized by large L and small B_5 values, but L drops and B_5 increases when just one dihedral adopts a *gauche* conformation. There is a consensus to take the most stable conformer and assume it describes the main steric interactions, but different sets (maximum and minimum values for instance) have also been used in order to explore a range of Sterimol values.[18,22] Acknowledging the issue of conformation, outliers in multivariate models using Sterimol parameters may emerge more often for flexible groups even as simple as *n*-butyl. Parameters computed for flexible functional groups should therefore be treated with caution. This observation can of course be extrapolated to any parameter that is structure-dependent such as the Tolman's cone angle.[19] It is therefore essential to understand that the approach chosen to tackle the issue of conformational sampling may introduce variations in steric parameters greater than the inherent noise of a statistical model. Given the relatively small error-bar which can be tolerated to generate useful predictions of stereoselectivity (<1 kcal/mol),

great care should be given to conformational sampling in the computation of physical-organic descriptors that are intended to statistically model catalytic enantioselective reactions.

In this chapter, we turn our attention to the uncertainty of Sterimol parameters due to substituent conformer flexibility. We have developed an automated and easy-to-use approach to monitor and Boltzmann-weight conformational effects for flexible groups that we hope will be useful to the wider organic community. Named *weighted Sterimol* (wSterimol for short), it can be used within a graphical user interface and with open-source programs on several platforms.[24] We will give an overview of the algorithm, describe the benchmarking realized to get reproducible wSterimol values and finally apply our approach on three case studies found in the literature.

2 Methodology

B_1, B_5 and L Sterimol parameters are well-suited to describe the multidimensionality of steric interactions but they were not created to capture substituent flexibility. To improve these commonly used descriptors, we envisaged that each parameter could be defined as an ensemble value such that the effect of different conformers could be weighted according to a Boltzmann distribution. Similar to the state-of-the-art in computational NMR prediction,[25] our strategy involves the automatic conformer generation, geometry optimization, filtering and the computation of Sterimol values (**Figure 3.2**).

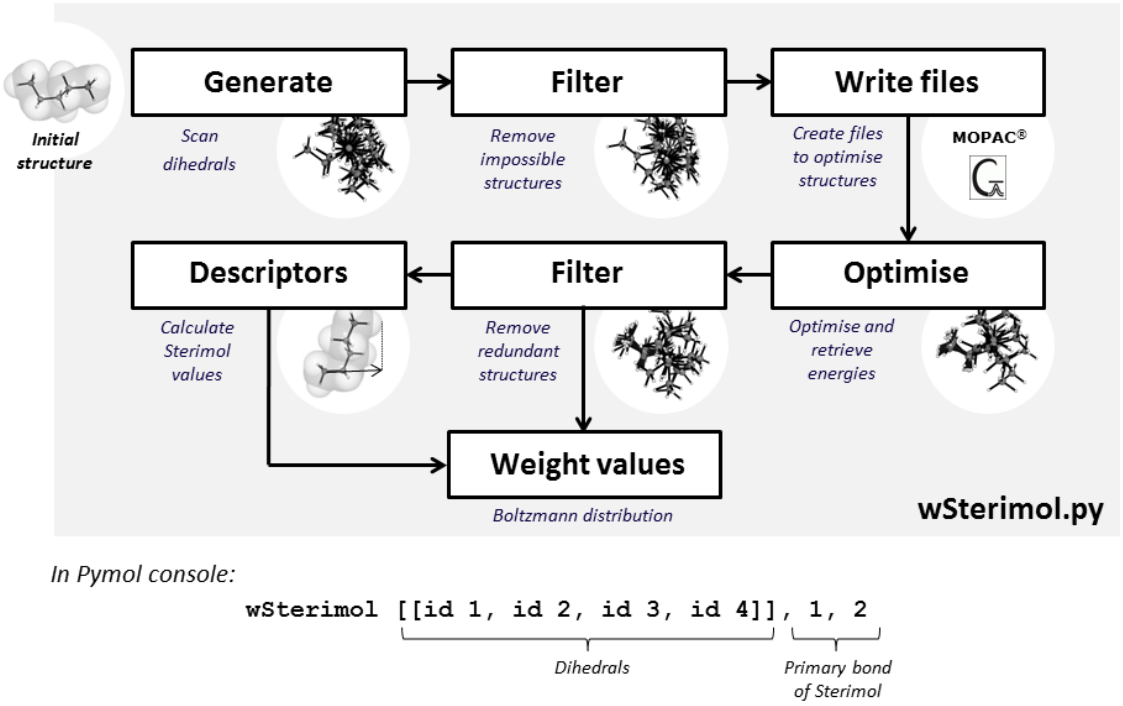

Figure 3.2. Workflow utilized in wSterimol algorithm that is started by a single command in *Pymol* console.

Coded in Python, we implemented an automated modular workflow that can be executed using a single command within the *Pymol* graphical interface. We chose this implementation to allow the end-user to visualize the different conformers at the different stages of the algorithm with the same molecular model used to calculate Sterimol parameters. We envisaged that this could be an important feature to help understanding of the mechanistic justification behind a potential correlation in multivariate modelling.[24] The first argument of the command represents a list of dihedrals to be explored and the last arguments are the atoms to define the primary axis of attachment in Sterimol calculation. The wSterimol package is released under an open-source MIT license and is also freely available.

In more detail, the first step of our workflow consists of generating all the potential conformers using a conformational sampling method. Conformer sampling has been

extensively studied,[27] with a recurring theme being the thorough exploration of all the possible conformers while limiting the computational cost associated to the search. Most approaches can be grouped into two categories.[27] The *systematic* search explores all the different conformers by incremental rotation of dihedrals, such as the SUMM approach (Systemic Unbounded Multiple Minimum).[28] The *stochastic* approach randomly explores new conformers and usually stops when two (or more) similar structures are found, for instance Molecular Dynamics[29] or the Monte-Carlo search.[30] In our case, we decided to code the conformational sampling due to our need to explore only substituent conformations based on their 3D coordinates, and no open-source package met our needs at that time. The code is built to use a SUMM-like approach, where a small number of rotatable bonds is explored by systematic torsional exploration. Simultaneous rotation of different dihedrals may lead to large interatomic clashes and the next step consists of filtering out these impossible geometries. The remaining structures are then optimized using either semi-empirical calculations (with *Mopac*[31]) or density functional theory (DFT, with *Gaussia*n[32] or *ORCA*[33]).

Unless necessary, the electronic energy is usually taken for the Boltzmann distribution, and not the Gibbs energy, since the entropy is approximately equal for every conformer. Solvent effects could also be included at this stage. After geometry optimization, many structures have usually converged toward the same conformer and structural alignment allows us to merge in the same group those structures that have a standard deviation value below an empirically-chosen threshold. In each group, only the lowest in energy conformation is kept to be the representative structure of its group, also called a conformer. Sterimol parameters are finally

computed for each conformer using a script developed by Dr K. Jackson[2] and the Boltzmann distribution produces three final values: wB_1, wB_5 and wL.

3 Benchmarking

Many default options are used during wSterimol calculation that may have an important impact on the output values. As always, benchmarking is a prerequisite to identify the limits of a program and six key variables are explored in this section. First, we compare Sterimol seminal code with the Python implementation, then we analyse the influence of the clustering cut-off on the conformer generation. Additionally, two different molecular models are studied and we investigate the effect of the dihedral division number on wSterimol reproducibility. Finally, we scrutinize the impact of the level of theory to describe different types of substituents.

3.1 Comparison to Sterimol seminal code

The original Fortran code of Verloop's Sterimol program[35,36] was entirely recoded by Dr K. Jackson in Python.[2] The wSterimol script reuses this Python implementation to compute the different Sterimol parameters for each generated conformer because it has the advantage of being able to process the commonly used Cartesian coordinates as well as including the Bondi molecular model. Professor R. Paton compared the Sterimol descriptors between the original Fortran and the Python programs using identical structures of twenty-two common substituents. Most values agreed to two decimal points and the largest difference was only of 0.01 Å.

3.2 Clustering cut-off

A conformer is a local energy minimum on a PES but geometry optimization on a smooth curvature can produce several structures located around the minimum without being exactly identical. This usual result requires the use of a cut-off to decide if two structures are members of the same conformational local minimum cluster or two distinct potential conformers. This is a common challenge in conformational sampling that has already been extensively explored.[27]

In our program, pair-alignment of the structures returns the corresponding standard deviation that is compared to the clustering cut-off (**Figure 3.3-A**). If the value is below the threshold, then the two structures are placed in the same conformational cluster, otherwise they are arranged in two distinct conformational groups.

In each cluster, the lowest in energy geometry is selected to represent the local minimum, in other words a conformer. The clustering cut-off is therefore a key variable that will define the amount of conformers to be used by the wSterimol parameters. To quantify the impact on the final values, five different substituents were selected due to their potentially flat PES that would render the clustering cut-off very sensitive (**Figure 3.3-B**). PM6-DH2 semi-empirical level of theory was chosen because of its good description of aliphatic chains and its low computational cost.

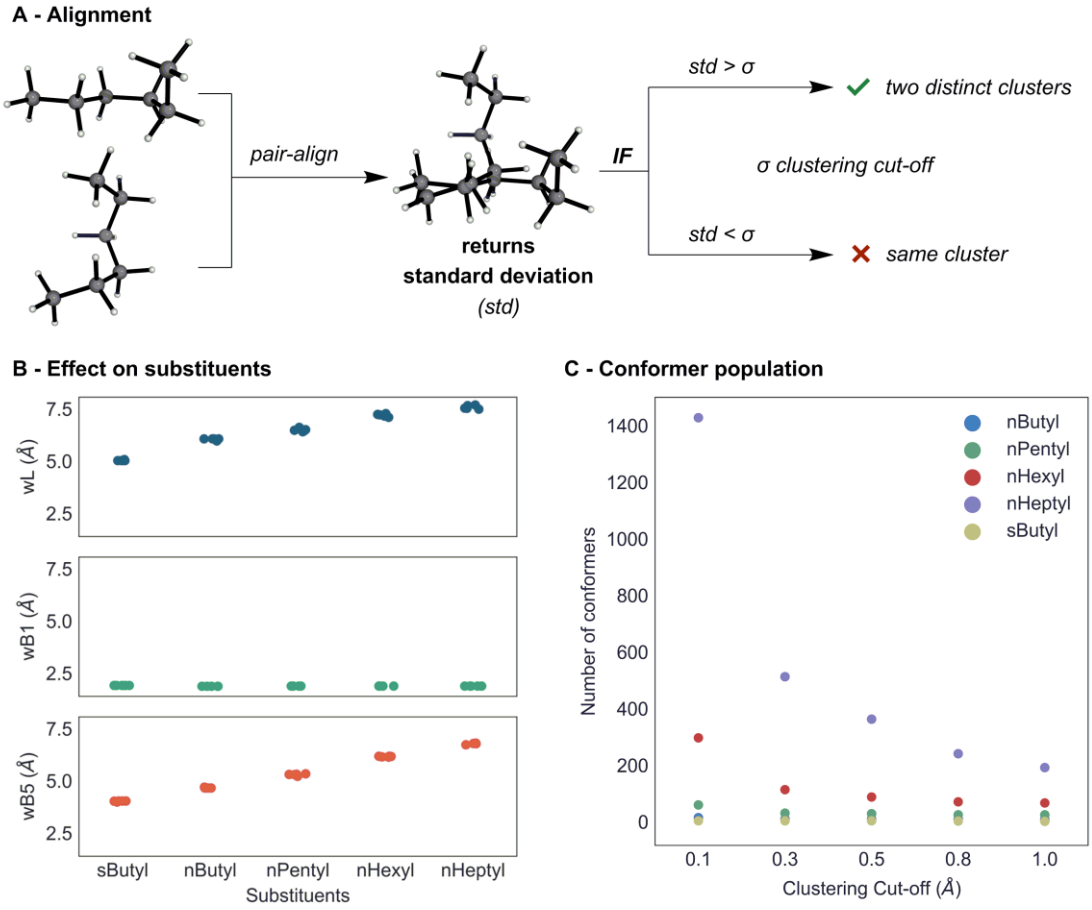

Figure 3.3. Graphic represents **A)** the workflow used to compare two geometries, **B)** the effect of the clustering cut-off on *wL*, wB_1 and wB_5 wSterimol values for different substituents (namely *n*-butyl, *n*-pentyl, *n*-hexyl, *n*-heptyl and *s*-butyl) using PM6-DH2 semi-empirical level of theory and **C)** the number of considered "conformers" compared to the clustering cut-off used.

Unexpectedly, the cut-offs spanning a wide range of 0.1 to 1.0 Å were indistinguishable or had a rather small influence on the wSterimol values, although the number of conformers used in the Boltzmann distribution was completely different (**Figure 3.3-C**). This exponential increase of conformers when lowering the clustering cut-off has a computational cost and likely does not represent the reality, while a higher cut-off (> 1.0 Å) should be limited to avoid merging theoretically

different conformers. A cut-off between 0.3 and 0.5 Å was empirically found to be the optimum range, the default in the script being 0.3 Å.

3.3 Molecular models

Original tabulated values of Sterimol parameters were generated more than forty years ago from 3D structures constructed according to CPK definitions of bond lengths and atomic radii. Since then, quantum mechanical optimization of molecular structures routinely generates 3D coordinates, from which Sterimol parameters can be computed. However, this still requires a subjective molecular model to be chosen where CPK values remain faithful to the original Sterimol implementation and take factors such as hybridization into account.

As used in Verloop's original program, the CPK molecular model uses connectivity information to segregate "types" of the same atom. For instance, a carbon atom could possess an atomic radius ranging from 1.5 to 1.7 Å depending on formal hybridization, aromaticity and ring-size. The space-filling model, however, limits itself to organic molecules containing the elements H, C, N, O, F, P, S, Cl, Br, and I. In contrast, we found that Bondii radius values are unique for each element, span a better fraction of the periodic table and derive directly from crystallographic data (**Figure 3.4-A**).[35,36] Introduction of a new molecular model inherently changes the shape of a substituent, and we therefore investigated its influence on wSterimol values. As the original CPK model takes into account hybridization patterns unlike Bondi radii, we considered five saturated substituents and four alkenes (**Figure 3.4-B**).

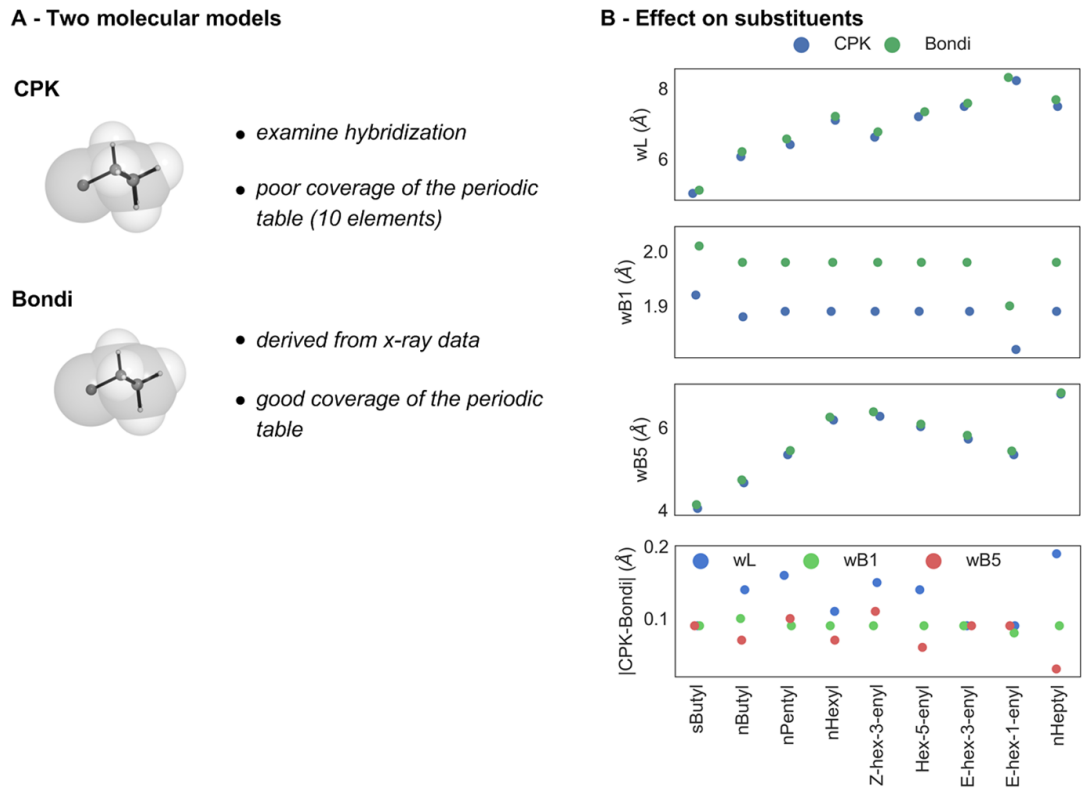

Figure 3.4. Graph charts represent **A)** the *i*-propyl group using CPK and Bondi molecular model and **B)** the influence of CPK and Bondi molecular models on wSterimol values for nine substituents at the PM6-DH2 semi-empirical level of theory.

Satisfactorily, we only observed a small difference between the two molecular models (<0.2 Å) that will become negligible when linear regression is applied during model construction. Additionally, the actual variation is rather small compared to the effect of other key variables such as the level of theory (see the levels of theory section). Both molecular models can therefore be equally employed, although the CPK model slightly remains computationally more expensive due to the need to categorize different "types" of the same atom.

3.4 Dihedral division number

A straightforward strategy to generate conformers consists in exploring the torsional angles using a systematic angle increment (**Figure 3.5-A**). This angle increment results from the division of a circle (2π) by an integer *n*, called the dihedral division number that describes how accurately the torsional exploration is realized (Equation **3.1**).

$$angle = \frac{2\pi}{n} \qquad (\mathbf{3.1})$$

In theory, a complete search of the PES is carried out when *n* is tending to ∞, but in practice, one digit is statistically enough to reach the curvature of all local minima that the optimization will later follow. Since the number of generated structures follows n^k with *k* the amount of explored dihedrals, the computational cost will drastically increase with the dihedral division number. This suggests that a compromise between cost and accuracy is reachable.

To evaluate the impact of the dihedral division number on wSterimol values, three linear substituents (namely *n*-butyl, *n*-pentyl and *n*-hexyl) were considered. The structures generated by dihedral exploration were also highly dependent on the initial geometry, such that we analysed nine different initial conformations to identify the threshold from which reproducible results can be obtained. We showed that the dihedral division number starts to output consistent wSterimol values from *n* = 5 while remaining computationally inexpensive (**Figure 3.5-B**).

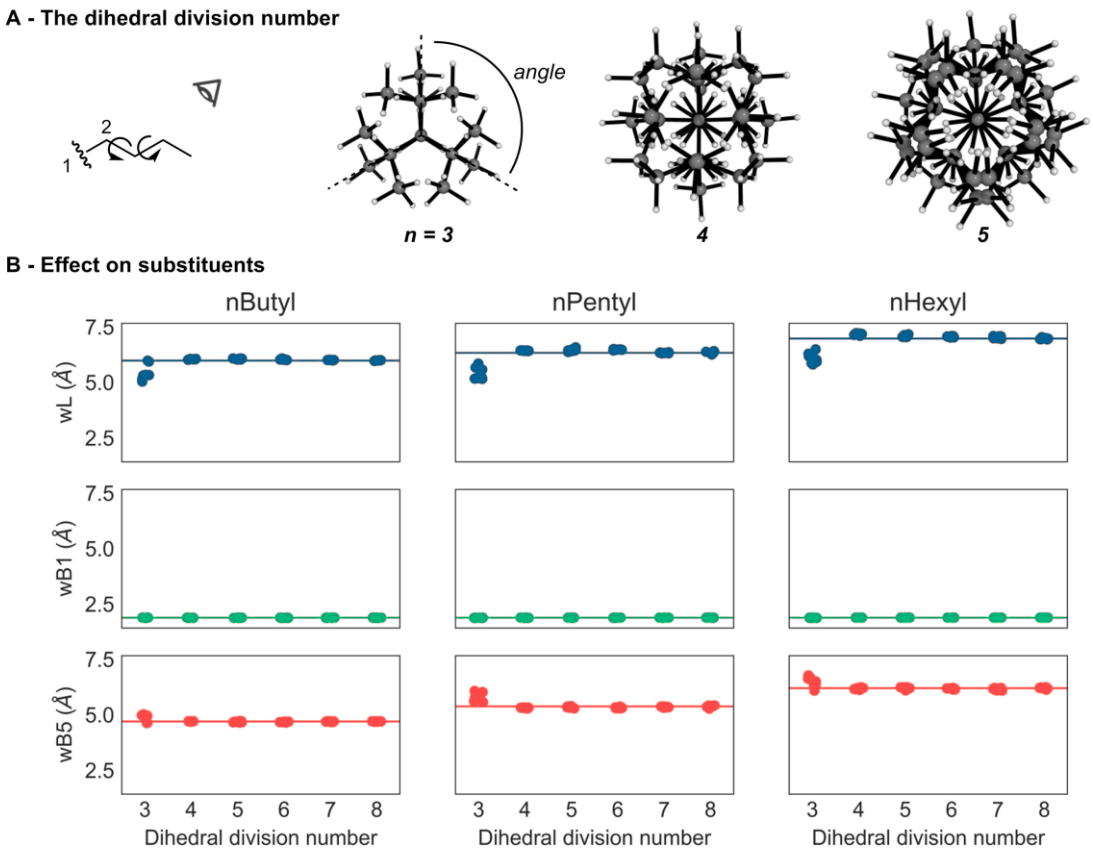

Figure 3.5. Graphic represents **A)** the aligned conformers of *n*-butyl using dihedral division number ranging from 3 to 5 and **B)** the wSterimol values for *n*-butyl, *n*-pentyl and *n*-*h*exyl at dihedral division number ranging from 3 to 8 starting from nine different initial structures. The asymptotes are represented by a horizontal line in each graph.

3.5 Levels of theory

wSterimol parameters are computed from the Sterimol values of each conformer that are weighted following the Boltzmann equation, where N_i is the population of the state i and N_T the total population of all the states (Equation **3.2**).

$$\frac{N_i}{N_T} = \frac{e^{-\frac{E_i}{kT}}}{\sum_j e^{-\frac{E_j}{kT}}} \qquad (\mathbf{3.2})$$

Therefore, the Boltzmann distribution depends on the computed energies and we previously showed that clustering uses the coordinates of the optimized geometry to define conformers. As optimization criteria and computed energies are controlled by the level of theory, it was thought to have the greatest influence on wSterimol values and we considered four compounds possessing prototypical functional groups to test this key variable. The first substituent contains an alcohol and a carbonyl functional group that possibly form a hydrogen bond, while the second is a linear organic molecule with van der Waals interactions only. The next substituent is a sub-unit of a phosphoramidite ligand to determine the effect of the level of theory on the entire scaffold and we finally chose two adjacent aromatic rings that are involved in a dispersion-dominated interaction.

Looking at the level of theory itself, we tried to monitor popular DFT functionals such as B3LYP, M06-2X and ωB97xD and two semi-empirical methods PM6-DH2 and PM7.[37] Given the computational cost required to optimize a large number of conformers, we preferred M06-2X/6-31G(d) level of theory as a reference in this work. As expected, the influence of the level of theory depends on the intramolecular interactions which need to be accurately computed (**Figure 3.6**). Starting from the aliphatic moiety, we observed a rather negligible effect possibly due to the ease of semi-empirical method to describe van der Waals interactions. However, the clustering population generated from semi-empirical level of theory starts to differ from DFT-derived distribution of conformers in cases where hydrogen bonding and dispersion-dominated interactions are involved. Although apparent wSterimol values remain similar (black ticks are close), we realized that twice as many conformers continuously scattered along the y-axis were generated when PM6-DH2

and PM7 were used compared to the DFT functionals. This is likely due to both the underlying differences of the PES and the convergence criteria that are significantly different between Mopac and Gaussian programs. To test this hypothesis, we optimized our four compounds at the PM7 level of theory with a convergence criterion that was a hundred times more precise (called PM7 P in **Figure 3.6**).

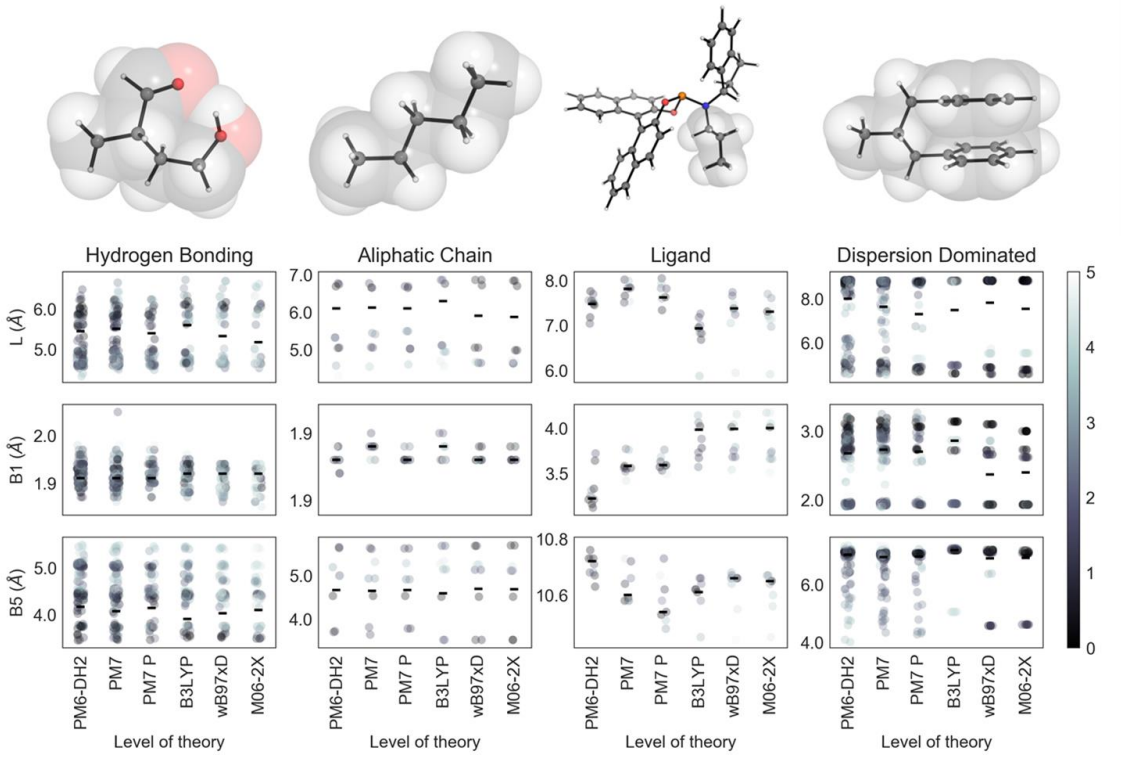

Figure 3.6. Charts represent the effect of different levels of theory (PM6-DH2, PM7, PM7 P, B3LYP, ωB97xD and M06-2X) on Sterimol values (L, B_1, B_5) of all the conformers (coloured dots) used to calculate wSterimol values (black ticks) for a substituent which contains hydrogen bonding interaction, for an aliphatic molecule, for a prototypical ligand and finally for a dispersion-dominated functional group. Sterimol values of all the conformers are coloured according to their relative energies going from 0.0 to 5.0 kcal/mol. A cut-off of 5.0 kcal/mol was used to remove energetically disfavoured conformers.

Satisfactorily, PM7 P improved the conformer distribution to levels between PM7 and B3LYP but it still failed with more complex and dispersion-dominated functional groups. Such substituents necessitated the optimization of their conformers at the DFT level of theory.

We believe that descriptors should remain easily computable[20] and there is therefore a trade-off between affordable and sufficiently accurate DFT levels of theory, from which ωB97xD and M06-2X likely represent the best candidates. An exception occurs in cases that only involve aliphatic susbtituents where semi-emprical methods should be preferred. Although we are currently limited by the computational cost, it might change in the near future as algorithms and computational power are continually improving.[39]

3.6 Point of attachment

A substituent is defined as an atom or a group of atoms connected to a parent structure from a point of attachment. Since quantum mechanical or semi-empirical optimisation of a compound does not tolerate a truncated geometry, computing physical-organic descriptors of substituents requires defining the point of attachment with either the entire molecule or with a simplified moiety as usually found in tabulated values.

In the case of conformational sampling, we reasoned that various descriptions of the point of attachment may lead to distinct steric clashes with the parent structure, such that the ensemble average could be influenced, and hence wSterimol parameters as well.

We computed wSterimol parameters using three different definitions of the point of attachment at the PM6-DH2 semi-empirical level of theory. First, the anchored atom was replaced by a hydrogen, then a methyl group and finally the full structure of the molecule under study, here a tertiary amine (**Scheme 2.1**). It is important to note that the dihedral angle involving the primary bond is always fixed and that methyl rotamers are neglected. Additionally, the bond length of the primary bond, which can vary depending on C–H, C–C or C–N bonds, does not affect the *L* subparameter because the distance is calculated from the first atom of the substituent (numbered atom 2 in **Scheme 2.1**).

We found that systematic differences between substituents were obtained, likely due to the same steric environment that is created by the parent structure, such that the effect on model regression is negligible. However, the wSterimol values substantially differ depending on the point of attachment, although smaller effects are observed with the DFT level of theory. For instance, wB_1 subparameter of *n*-butyl substituent gave 17% relative difference from –H to $–CH_3$ and 37% from –H to the full compound. Therefore, a consistent use of the same point of attachment along substituents does not impact model construction, but great care must be taken when tabulated values are used to avoid associating uncompatible data.

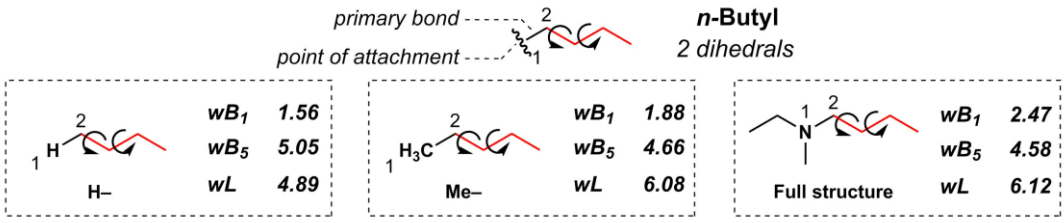

Scheme 2.1. Using the *n*-butyl substituent, various descriptions of the point of attachment lead to different wSterimol values at the PM6-DH2 level of theory.

4 Applications

In order to identify how flexible substituents were utilised in the literature, a list of papers using Sterimol were identified starting from 2000. Using Google Scholar, all the papers found by searching "sterimol" were considered (search realised in November 2017). A rough selection was primarily done according to the journals, the language (only English was considered) and the relevance of the paper for this work. We went through about 900 entries, mostly irrelevant medicinal papers. Each paper was then quickly read to identify the domain of application, and kept if the latter was related to asymmetric catalysis. Each remaining model was examined in greater details and those containing only Sterimol parameters were eventually considered as a case study. Looking at the SI of each paper, we determined if the model seemed interesting to try on wSterimol. The rigid and flexible substituents were counted at this stage (**Table 3.1**). To our surprise, Sterimol was mainly used on "rigid" substituents. In this work, rigid substituents are moieties possessing no rotatable dihedrals when neglecting hydrogens. A moderate rigidity will have a maximum of two rotatable dihedrals which usually lead to a very small deviation of Sterimol values (empirically observed), and all the remaining substituents are considered flexible. The results are shown in **Table 3.1**, where rigid and moderately rigid substituents account for more than 80% of the substituents on average. In this section, we apply our new approach on three interesting case studies found in the literature and evaluate the importance of conformational effects in the application of quantitative structure selectivity relationship (QSSR). Selection of case studies was limited to asymmetric catalysis, from which a multivariate model was constructed using Sterimol parameters *alone*.

Table 3.1. List of papers selected when searching "sterimol" in Google Scholar. The medicinal papers were not considered in this study.

References	*Theme*	*Sterimol only?*	*Rigid*	*Moderate*	*Flexible*	*Conformation Sampling?*	*Case-Study?*
*Nature Chemistry, **2012,** 4, 366*	*Asym. cat.*	*Yes*	*55%*	*45%*	*0%*	*Yes*	*Yes*
	Asym. cat.	*Yes*				*Yes*	*Yes – in the computational section*
*J. Org. Chem., **2012**, 77, 10427*	*Asym. cat.*	*Yes*	*63%*	*13%*	*25%*	*Not said*	*Yes*
*J. Org. Chem., **2014**, 79, 9455*	*Asym. cat.*	*Yes*	*38%*	*50%*	*13%*	*Optimisation only (MM2)*	*Yes*
*J. Am. Chem. Soc., **2013**, 135, 2482*	*Asym. cat.*	*Yes*	*50%*	*33%*	*17%*	*Optimisation only (MM2)*	*Yes – in the computational section*
*Angew.Chem. Int. Ed., **2016**, 55,6506*	*Asym. cat.*	*Yes*	*67%*	*22%*	*11%*	*Opt only*	*Yes – But almost only rigid substituents – Not interesting*
*Chem. Eur.J., **2017**, 23,5488*	*Asym. cat.*	*Yes*	*78%*	*11%*	*11%*	*Not said*	*Yes – But almost only rigid substituents – Not interesting*
*J. Am. Chem. Soc., **2016**, 138, 8045*	*Analytical*	*Yes*	*44%*	*44%*	*11%*	*No*	*No – Not asymmetric catalysis*
*J. Am. Chem. Soc., **2016**, 138, 13424*	*Asym. cat.*	*No*	-	-	-	*Yes*	*No – We want Sterimol only models*
*Nature Chemistry, **2016**, 8, 610*	*Asym. cat.*	*No*	-	-	-	*Yes*	*No – We want Sterimol only models*
*Carbohydrate Research, **2000**, 328, 635*	*Analytical*	*No*	-	-	-	*Optimisation only*	*No – We want Sterimol only models*
*Chem. Sci., **2015**, 6, 1355*	*Asym. cat.*	*No*	-	-	-	*Not said*	*No – We want Sterimol only models*
*PNAS, **2014**, 111, 14698*	*Asym. cat.*	*No*	-	-	-	*Not said*	*No – We want Sterimol only models*
*ACS Catal., **2017**, 7, 3973*	*Asym. cat.*	*No*	-	-	-	*Yes*	*No – We want Sterimol only models*
*J. Am. Chem. Soc., **2016**, 138, 13424*	*Asym. cat.*	*No*	-	-	-	*Not said*	*No – We want Sterimol only models*
*ACS Catal., **2017**, 7, 6729*	*Asym. cat.*	*No*	-	-	-	*Not said*	*No – We want Sterimol only models*
*J. Am. Chem. Soc., **2015**, 137, 15668*	*Asym. cat.*	*No*	-	-	-	*Not said*	*No – We want Sterimol only models*
*J. Am. Chem. Soc., **2017**, 139, 1296*	*Catalysis*	*No*	-	-	-	*Not said*	*No – We want Sterimol only models*
*J. Am. Chem. Soc., **2016**, 138, 3863*	*Asym. cat.*	*No*	-	-	-	*Not said*	*No – We want Sterimol only models*

Thereby, we managed to avoid complex and intractable models where steric interactions do not provide the main contribution. In the last decade, efforts were realised to improve statistical standards in model construction, such that some prior works do not necessarily possess a validated multivariate model. Therefore, we tried to reproduce these models as precisely as possible and challenged them with state-of-the-art rigour. Since the predictive and interpretative powers of these models were already discussed in the original papers, our attention will mainly be on the additional information provided by wSterimol and the effect of flexibility on model uncertainty.

In the first case, we demonstrate that equivalent performance to Sterimol parameters can be achieved thanks to its design which encompasses both flexible and rigid substituents. The second example shows improved correlation and confirms that the range of conformer values can be far greater than the statistical model error. In the final case study, wSterimol helps to identify the region of the model where conformational sampling could have an impact on statistical performance and predictivity. Other case studies are only discussed in the computational section, since they showed similar behavior compared to aforementioned examples.

4.1 Case study One

Sigman and Miller found in 2010 that steric interactions on the bisphenol substrates **3.1** play a crucial role in their organocatalysed desymmetrization[10,40] and that enantioselectivity was quantitatively correlated to B_1 and L subparameters (**Figure 3.7**).

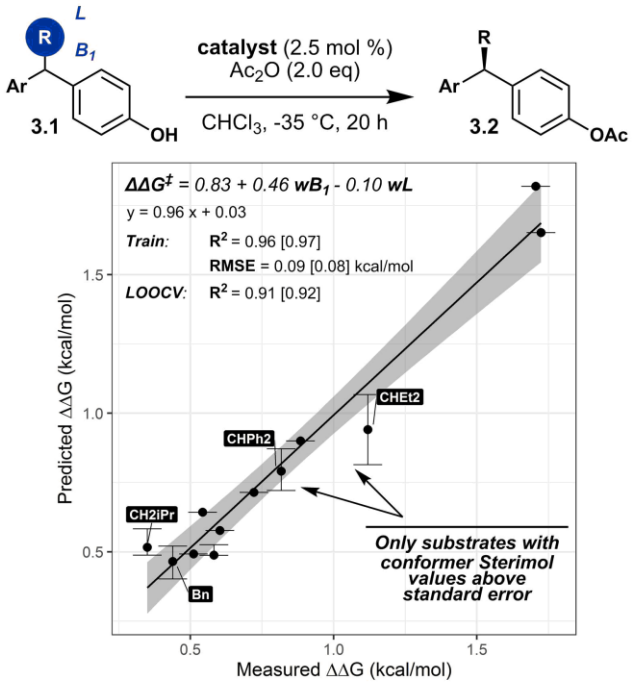

Figure 3.7. Multivariate model of the desymmetrization of bisphenol substrates correlates wSterimol values with enantioselectivity. Error bars represent the range of Sterimol values of the conformers within 3.0 kcal/mol window while the gray area represents the standard error of the model at 95% confidence interval. Only the substituents with a range of Sterimol values greater than 0.05 kcal/mol were labelled. Original model values were put in bracket for comparison. wSterimol model (this work): ΔΔG‡ = 0.83 + 0.46 wB_1 - 0.10 wL, Training [R^2=0.96, RMSE=0.09 kcal/mol], LOOCV [R^2=0.91, RMSE=0.14 kcal/mol], ANOVA [$wB_1 = 2.1e^{-07}$, $wL = 1.4e^{-02}$]. Sterimol model (original work): ΔΔG‡ = 0.83 + 0.47 B_1 - 0.10 L, Training [R^2=0.97, RMSE=0.08 kcal/mol], LOOCV [R^2=0.92, RMSE=0.13 kcal/mol], ANOVA [$B_1 = 6.9e^{-08}$, $L = 7.3e^{-03}$].

This discovery suggested that an optimal substrate would have a large minimum width (B_1) and a short length (L), likely due to a propeller-like twist of the aryl rings in the reaction mechanism. As the authors noted, the use of static multidimensional parameters such as Sterimol is consistent with substituents exhibiting limited flexibility through a strong conformational preference.

We believe that challenging wSterimol is a healthy approach to define the limit of its applicability and we aimed to ensure that its use on rigid substituents found in the bisphenol substrates would not lead to any degradation of the linear relationship. As expected, the model obtained with wSterimol parameters showed negligible differences in terms of correlation (R^2), uncertainty (RMSE, standard error) and significance (ANOVA, p-value). More interestingly, we also observed that the standard error of the model at 95% confidence interval (grey band) is greater than the range of Sterimol values of all the conformers (error bars). The inherent uncertainty of the statistical model is therefore more relevant than the error attributable to different conformations and this is particularly true for isotropic functional groups such as Me, *t*-Bu and Ad. Dynamics of the substituents do not play a major role in model construction and performance, which is in agreement with the hypothesised mechanistic explanation previously observed. This case study demonstrates that wSterimol approach of including weighted parameters is resilient and overlaps the domain of applicability of the conventional Sterimol parameters. Model construction is therefore unified by the use of wSterimol regardless of the substituent dynamic. Similar conclusion was drawn from the Nozaki-Hiyama-Kishi (NHK) propargylation of acetophenone (see computational section).[10]

4.2 Case study Two

The Song laboratory studied the asymmetric addition of diethylzinc on benzaldehyde **3.3** using chiral phosphoramide ligands and discovered a relationship between the shape of these *N*-substituted ligands and the observed enantioselectivity (**Figure 3.8**).[19] Interestingly, their first strategy was to describe steric interactions of the entire amine using Sterimol parameters but the authors only obtained a poor correlation. However, they found that the construction of a robust model was achieved by dividing their amino substituents into two subgroups, such that the alkyl chains could be treated as rigid while doubling the steric terms in the model equation.

A larger proximal steric bulk (B_1) of R_2 increased the enantioselectivity although the minimal width (B_1) of R_1 was detrimental, likely explained by the mechanistic hypothesis that the carbonyl group is pushed away from the zinc centre. Complexation of the zinc metal to the amine substituent was claimed to lock the ligand structure and to explain the need of rigidifying the full amine substitutent (which failed) by only considering the R_1 and R_2 subgroups.

Noting that static Sterimol parameters are recorded from the primary axis defined in this case by the point of attachement to the nitrogen atom, we reasoned that the dihedral rotation of the amine is not explored even for the full substituent. Therefore, their unsuccessful first attempt to correlate enantioselectivity with the full amine was unlikely due to a lack of rigidity. On the contrary, we hypothesized that the conformational effect here played a fundamental role to correctly describe the full system, which possesses many degrees of freedom, and the separate treatment of R_1 and R_2 subgroups somehow helped to solve this issue.

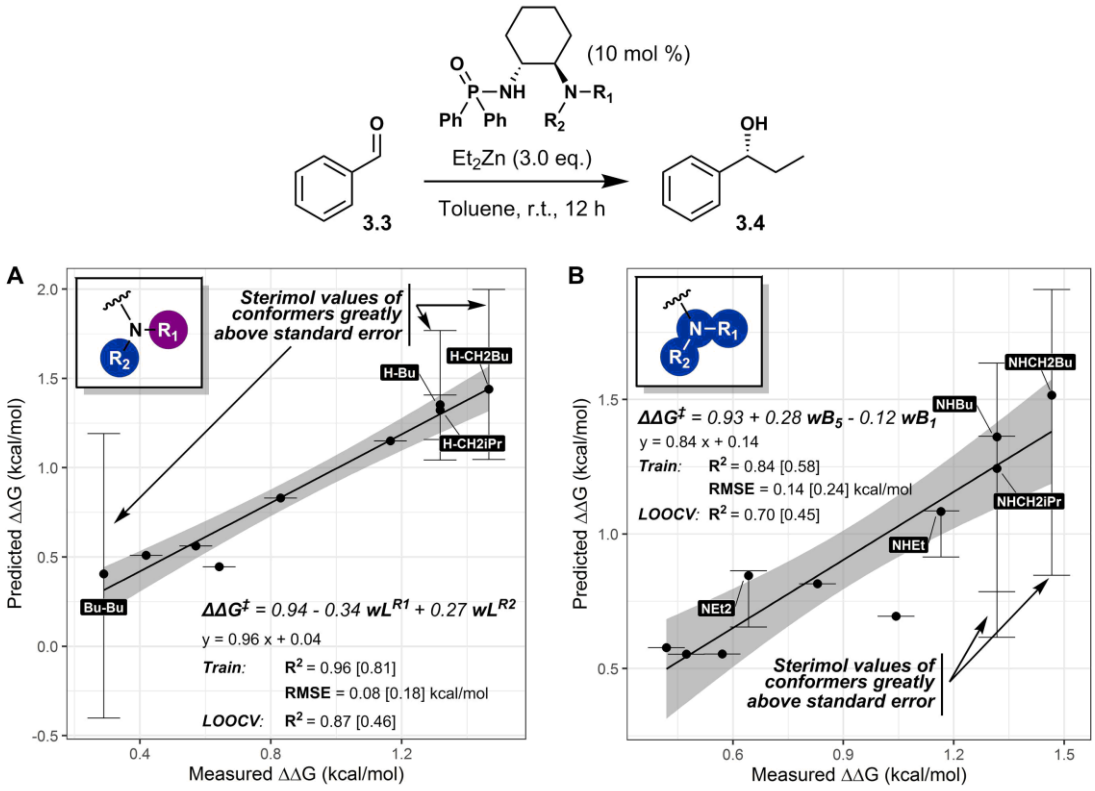

Figure 3.8. Graphs represent the QSSR analysis of the asymmetric addition of diethylzinc on benzaldehyde using chiral phosphoramide ligands. Grey area shows the standard error of the model at 95% confidence interval and error bars represent the range of Sterimol values of the conformers within 3.0 kcal/mol window. Only the substituents with a range of Sterimol values greater than 0.05 kcal/mol were labelled. Original model values were put in bracket for comparison. **A)** Model using wSterimol on R_1 and R_2 subgroups, with two outliers removed. wSterimol model (this work): $\Delta\Delta G^{\ddagger}$ = 0.94 - 0.34 wL^{R1} + 0.27 wL^{R2}, Training [R^2=0.96, RMSE=0.08 kcal/mol], LOOCV [R^2=0.87, RMSE=0.15 kcal/mol], ANOVA [wL^{R1} = $1.4e^{-04}$, wL^{R2} = $1.7e^{-04}$]. Sterimol model (original work): $\Delta\Delta G^{\ddagger}$ = 1.04 - 0.36 B_1^{R1} + 0.29 B_1^{R2}, Training [R^2=0.80, RMSE=0.18 kcal/mol], LOOCV [R^2=0.46, RMSE=0.32 kcal/mol], ANOVA [B_1^{R1} = $5.7e^{-03}$, B_1^{R2}= $3.8e^{-02}$]. **B)** Model using wSterimol on the full amine of the ligand, with two outliers removed. wSterimol model (this work): $\Delta\Delta G^{\ddagger}$ = 0.93 + 0.28 wB_5 - 0.12 wB_1, Training [R^2=0.84,

RMSE=0.14 kcal/mol], LOOCV [R^2=0.70, RMSE=0.20 kcal/mol], ANOVA [$wB_5 = 7.6e^{-04}$, $wB_1 = 5.1e^{-02}$]. Sterimol model (original work): $\Delta\Delta G^{\ddagger} = 0.95 + 0.27\ B_5$, Training [$R^2$=0.58, RMSE=0.24 kcal/mol], LOOCV [R^2=0.45, RMSE=0.28 kcal/mol], ANOVA [$B_5 = 1.0e^{-2}$].

We started our investigation by using wSterimol parameters on the R_1 and R_2 moeities. As found by Song laboratory, two outliers were identified using the boxplot visualization technique and the correlation in **Figure 3.8-A** was obtained. Compared to the original model, a much improved fit was achieved with wSterimol values (R^2=96% with wSterimol and 81% with Sterimol). More importantly, the amplitude in Sterimol values at the extremities of the model leads to predicted enantioselectivity greater than the model standard error, which further reinforces that the predictive power of the model in these regions may be weaker. Conformational effect is therefore a greater source of uncertainty than the statistical model itself and great care should be given to conformational sampling for the construction of a successful predictive multivariate model.

Realising the importance of the conformers in this work, we decided to apply wSterimol parameters on the entire amino-group of the chiral phosphoramide ligands that was initially unsuccessful with static Sterimol parameters (**Figure 3.8-B**). Remarkably, our approach allowed the identification of the same outliers and afforded again much improved correlation compared to Sterimol values (R^2=84% with wSterimol and 58% with Sterimol) but a weaker correlation than the sub-systems as previously shown (R^2=84% with NR_1R_2 and 96% with R_1 & R_2). We were pleased to observe an improved consistency in model construction regardless

of the fragmentation of the ligand used to describe its functional group (both NR_1R_2 full substituent and R_1 & R_2 subgroups gave satisfying models).

As the conformational uncertainty included in Sterimol values is greater than the statistical error of the model, it is likely that this was the original reason behind the lack of correlation for the full amine and not its rigidity. In this example, the amplitude of conformational uncertainty was substantial enough to mislead the authors to hypothesize a problem of rigidity that was initially supported by a poor correlation obtained with the full amine. Additionally, we observed that the magnitude of the range of conformer values at the higher end of the predicted values is particularly marked, which is crucial to realize since the predictive power of the model was deteriorated in this region. This showcases the importance of conformational sampling and the superiority of wSterimol parameters in terms of model performance and consistency, particularly when working with flexible substituents.

4.3 Case study Three

In 2014, the Song laboratory applied their chiral 1,2-amino phosphonamide ligands to the zinc-catalysed asymmetric Henry reaction as shown in **Figure 3.9**.[20] They successfully established a QSSR model that correlates enantioselectivity with Sterimol parameters of the ligands' *N*-substituents. Likely inspired by their work shown previously, they used R_1 and R_2 subgroups to describe their amino group. A smaller proximal steric bulk (B_1) of R_1 and a larger maximal width (B_5) of R_2 increased the enantioselectivity as found in their model.

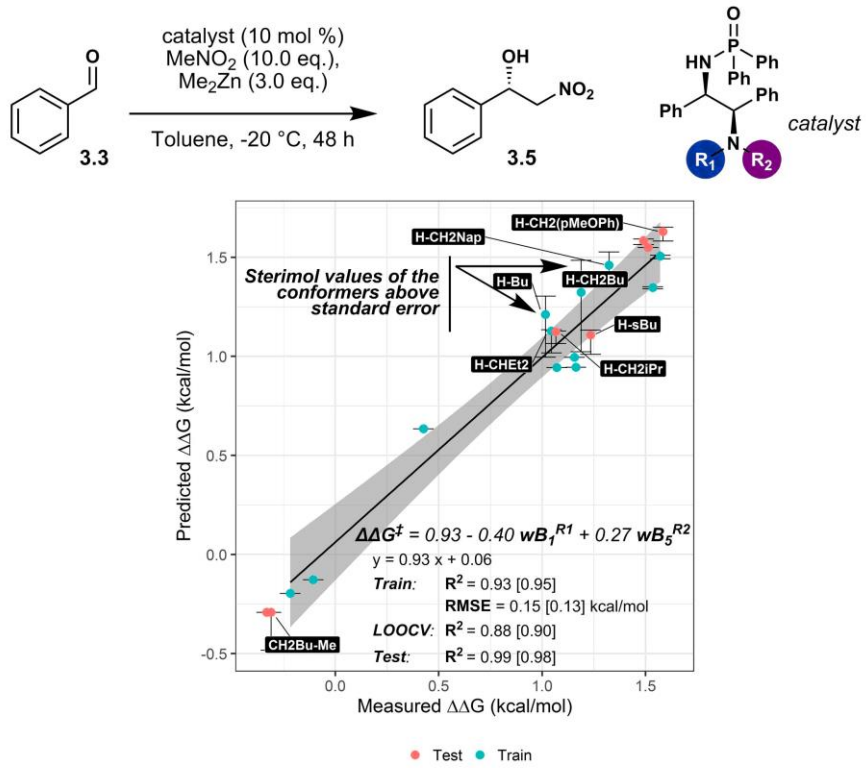

Figure 3.9. QSSR analysis of asymmetric Henry reaction using wSterimol values from chiral 1,2-amino phosphoramide ligands. Gray area represents the standard error of the model at 95% confidence interval while error bars represent the range of Sterimol values of the conformers within 3.0 kcal/mol window. Only the substituents with a range of Sterimol values greater than 0.05 kcal/mol were labelled. Original model values were put in bracket for comparison. wSterimol model (this work): ΔΔG‡ = 0.93 - 0.40 wB_1^{R1} + 0.27 wB_5^{R2}, Training [R^2=0.93, RMSE=0.15 kcal/mol], LOOCV [R^2=0.88, RMSE=0.20 kcal/mol], Test [R^2=0.99, RMSE=0.07 kcal/mol], ANOVA [wB_1^{R1}= $3.5e^{-06}$, wB_5^{R2}= $8.2e^{-04}$]. Sterimol model (original work): ΔΔG‡ = 0.93 - 0.40 B_1^{R1} + 0.28 B_5^{R2}, Training [R^2=0.95, RMSE=0.13 kcal/mol], LOOCV [R^2=0.90, RMSE=0.18 kcal/mol], Test [R^2=0.98, RMSE=0.11 kcal/mol], ANOVA [B_1^{R1}= $1.2e^{-06}$, B_5^{R2}= $2.9e^{-04}$].

We applied wSterimol in this system and achieved a slightly lower correlation than previously, where singular Sterimol values were used (R^2=93% with wSterimol and 95% with Sterimol). In the case of two phosphoramide ligands, we found that the amplitude of Sterimol values for the low-energy conformers within 3.0 kcal/mol is greater than the error of the model. Additionally, four other ligands located in the same region possessed an amplitude of Sterimol values lower than the error of the model but noticeably above 0.05 kcal/mol, which suggests a weaker predictive power around these datapoints.

This case study demonstrates that wSterimol values give at least as good correlations as when using the static Sterimol values, and also provide additional information regarding regions of the model which may be weaker.

5 Conclusion and Future work

Conformational analysis is well-known in the organic scientific community but its use with electronic structure calculations to compute ensemble-averaged properties remains a daunting effort. Additionally, synthetically-relevant functional groups may either have tabulated values without conformational consideration or simply be absent from the literature. The wSterimol computational workflow aims to fill this gap by allowing the computation of Sterimol parameters for a conformational ensemble from a graphical user interface. It was designed to be used by non-experts with open-source softwares that are triggered from a single command.

We have demonstrated the importance of our approach with three case studies that showed improved results where flexible substituents were present, while rigid substituents gave equal performance. Notably, uncertainty due to the range of

conformer values was sometimes found to exceed the standard deviation of models up to a difference of 1 kcal/mol, above the accuracy required for accurate predictions in enantioselective catalysis.

Therefore, this tool is hoped to develop the awareness of the scientific community about conformer uncertainty in physical-organic descriptors such as Sterimol parameters, and to enable the use of a broader scope that includes flexible substituents.

The current version of wSterimol implements automatic conformer generation, geometry optimization, filtering and Sterimol computation of an *acyclic* conformational ensemble. Ring conformer sampling remains a delicate task that is not carried out in this implementation but could be in the future by using distance-geometry methods or molecular dynamics. Nevertheless, the modular aspect of wSterimol scripts allows a third-party program to generate the missing conformers that can easily be reintroduced in the workflow. Rotatable dihedrals are also not automatically detected, although this feature allows the exclusion of selected torsions if desired. Additionally, more physical organic descriptors such as Tolman's cone angle[23] could easily be included, thanks to the modular nature of our program. Finally, solvent effects play a fundamental role in many reactions and wSterimol allows through the use of third-party programs to consider such effect during geometry optimization.

6 References

1 A. V. Brethomé, S. P. Fletcher and R. S. Paton, *ACS Catal.*, 2019, **9**, 2313–2323.

2 T. Piou, F. Romanov-Michailidis, M. Romanova-Michaelides, K. E. Jackson, N. Semakul, T. D. Taggart, B. S. Newell, C. D. Rithner, R. S. Paton and T. Rovis, *J. Am. Chem. Soc.*, 2017, **139**, 1296–1310.

3 I. V. Alabugin, *Stereoelectronic Effects*, John Wiley & Sons, Ltd, Chichester, UK, 2016.

4 G. Bott, L. D. Field and S. Sternhell, *J. Am. Chem. Soc.*, 1980, **102**, 5618–5626.

5 S. Winstein and N. J. Holness, *J. Am. Chem. Soc.*, 1955, **77**, 5562–5578.

6 M. Charton, *J. Am. Chem. Soc.*, 1975, **97**, 1552–1556.

7 R. W. Taft, *J. Am. Chem. Soc.*, 1952, **74**, 2729–2732.

8 J. P. Reid and J. M. Goodman, *J. Am. Chem. Soc.*, 2016, **138**, 7910–7917.

9 L. Falivene, R. Credendino, A. Poater, A. Petta, L. Serra, R. Oliva, V. Scarano and L. Cavallo, *Organometallics*, 2016, **35**, 2286–2293.

10 K. C. Harper, E. N. Bess and M. S. Sigman, *Nat. Chem.*, 2012, **4**, 366–374.

11 C. Hansch, P. P. Maloney, T. Fujita and R. M. Muir, *Nature*, 1962, **194**, 178–180.

12 M. Charton, *J. Org. Chem.*, 1976, **41**, 2217–2220.

13 E. Fischer, *Berichte der deutschen chemischen Gesellschaft*, 1894, **27**, 2985–2993.

14 A. D. G. Lawson, M. MacCoss and J. P. Heer, *J. Med. Chem.*, 2018, **61**, 4283–4289.

15 A. Verloop, *Drug Design Vol. III*, Academic Press, New York, 1976.

16 L. Pauling and R. Corey, *Proc. Natl. Acad. Sci.*, 1951, **37**, 235–240.

17 M. S. Sigman, K. C. Harper, E. N. Bess and A. Milo, *Acc. Chem. Res.*, 2016, **49**, 1292–1301.

18 J. Crawford and M. Sigman, *Synthesis*, 2019, **51**, 1021–1036.

19 H. Huang, H. Zong, G. Bian and L. Song, *J. Org. Chem.*, 2012, **77**, 10427–10434.

20 H. Huang, H. Zong, G. Bian, H. Yue and L. Song, *J. Org. Chem.*, 2014, **79**, 9455–9464.

21 Z. L. Niemeyer, A. Milo, D. P. Hickey and M. S. Sigman, *Nat. Chem.*, 2016, **8**, 610–617.

22 S. Zhao, T. Gensch, B. Murray, Z. L. Niemeyer, M. S. Sigman and M. R. Biscoe, *Science*, 2018, **362**, 670–674.

23 C. A. Tolman, *Chem. Rev.*, 1977, **77**, 313–348.

24 V. H. Masand and V. Rastija, *Chemom. Intell. Lab. Syst.*, 2017, **169**, 12–18.

25 Q. N. N. Nguyen and D. J. Tantillo, *The Journal of Antibiotics*, 2016, **69**, 534–540.

26 A. C. Brueckner, O. M. Ogba, K. M. Snyder, H. C. Richardson and P. H.-Y. Cheong, in *Applied Theoretical Organic Chemistry*, ed. D. J. Tantillo, World Scientific, 2018, pp. 147–164.

27 P. C. D. Hawkins, *J. Chem. Inf. Model.*, 2017, **57**, 1747–1756.

28 J. M. Goodman and W. C. Still, *J. Comput. Chem.*, 1991, **12**, 1110–1117.

29 D. Hamelberg, J. Mongan and J. A. McCammon, *J. Chem. Phys.*, 2004, **120**, 11919–11929.

30 G. Chang, W. C. Guida and W. C. Still, *J. Am. Chem. Soc.*, 1989, **111**, 4379–4386.

31 J. J. P. Stewart, *MOPAC2016*, Stewart Computational Chemistry, Colorado Springs, 2016.

32 M. J. Frisch, G. W. Trucks, H. B. Schlegel, G. E. Scuseria, M. A. Robb, J. R. Cheeseman, G. Scalmani, V. Barone, B. Mennucci, G. A. Petersson, H. Nakatsuji, M. Caricato, X. Li, H. P. Hratchian, A. F. Izmaylov, J. Bloino, G. Zheng, J. L. Sonnenberg, M. Hada, M. Ehara, K. Toyota, R. Fukuda, J. Hasegawa, M. Ishida, T.

Nakajima, Y. Honda, O. Kitao, H. Nakai, T. Vreven, J. Montgomery, J. A., J. E. Peralta, F. Ogliaro, M. Bearpark, J. J. Heyd, E. Brothers, K. N. Kudin, V. N. Staroverov, R. Kobayashi, J. Normand, K. Raghavachari, A. Rendell, J. C. Burant, S. S. Iyengar, J. Tomasi, M. Cossi, N. Rega, J. M. Millam, M. Klene, J. E. Knox, J. B. Cross, V. Bakken, C. Adamo, J. Jaramillo, R. Gomperts, R. E. Stratmann, O. Yazyev, A. J. Austin, R. Cammi, C. Pomelli, J. W. Ochterski, R. L. Martin, K. Morokuma, V. G. Zakrzewski, G. A. Voth, P. Salvador, J. J. Dannenberg, S. Dapprich, A. D. Daniels, Ö. Farkas, J. B. Foresman, J. V. Ortiz, J. Cioslowski and D. J. Fox, *Gaussian 09, Revision D.01*, Gaussian Inc., Wallingford, 2009.

33 F. Neese, *Wiley Interdiscip. Rev. Comput. Mol. Sci.*, 2012, **2**, 73–78.

34 T. Piou, F. Romanov-Michailidis, M. A. Ashley, M. Romanova-Michaelides and T. Rovis, *J. Am. Chem. Soc.*, 2018, **140**, 9587–9593.

35 A. Bondi, *J. Phys. Chem.*, 1964, **68**, 441–451.

36 R. S. Rowland and R. Taylor, *J. Phys. Chem.*, 1996, **100**, 7384–7391.

37 L. Goerigk and S. Grimme, *Phys. Chem. Chem. Phys.*, 2011, **13**, 6670–6688.

38 C. B. Santiago, J. Y. Guo and M. S. Sigman, *Chem. Sci.*, 2018, **9**, 2398–2412.

39 S. Grimme and P. R. Schreiner, *Angew. Chem. Int. Ed.*, 2018, **57**, 4170–4176.

40 J. L. Gustafson, M. S. Sigman and S. J. Miller, *Org. Lett.*, 2010, **12**, 2794–2797.

4

Asymmetric conjugate additions to exocyclic enones

1 Introduction

Copper-catalyzed asymmetric conjugate addition (ACA) of organometallic species to cyclic α,β-unsaturated carbonyl compounds has been, and remains, a fruitful research area. Like its linear counterpart, it has been used as a strategy to control the formation of stereocenters in the synthesis of numerous natural products[1–6] and examples of ACAs yielding >50 g of product[7,8] have recently been reported (**Scheme 4.1**).

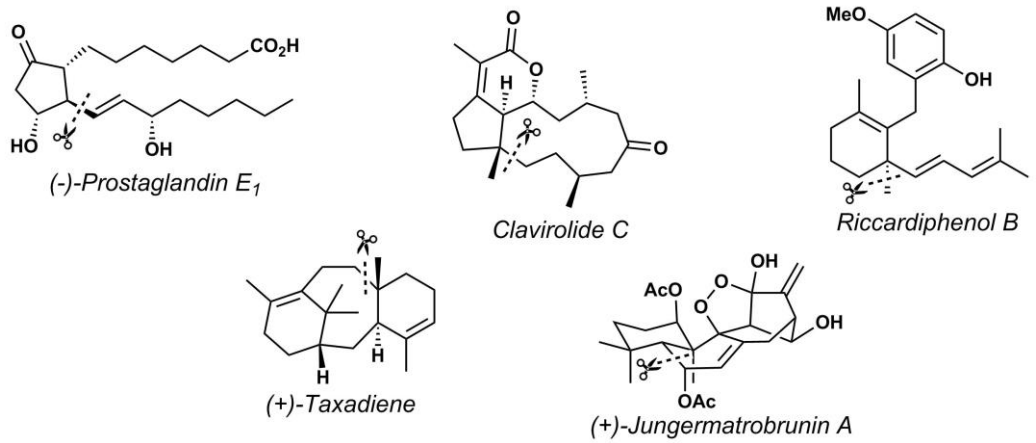

Scheme 4.1. Examples of natural products prepared from ACA on cyclic enones.

In the reaction "toolkit" accessible to synthetic chemists, ACA remains one of the most powerful reactions for stereoselective C–C bond formation involving cyclic compounds. In the last three decades, great advances have been achieved in the further development of ACA, such that cyclic α,β-unsaturated carbonyl substrates now undergo ACAs with Grignard,[9] organoaluminium[9–11] and organozinc[9,10,12–14] species in high yield and high selectivity (**Scheme 4.2**). For the same reasons outlined in **Chapter 1**, the Fletcher group developed a robust copper-catalyzed ACA of alkylzirconocenes on a wide variety of cyclic substrates with a tremendous

functional group tolerance (**Scheme 4.2**).[15–22] Interestingly, tertiary[15] and quaternary[21,22] stereocenters are equally accessible through this methodology.

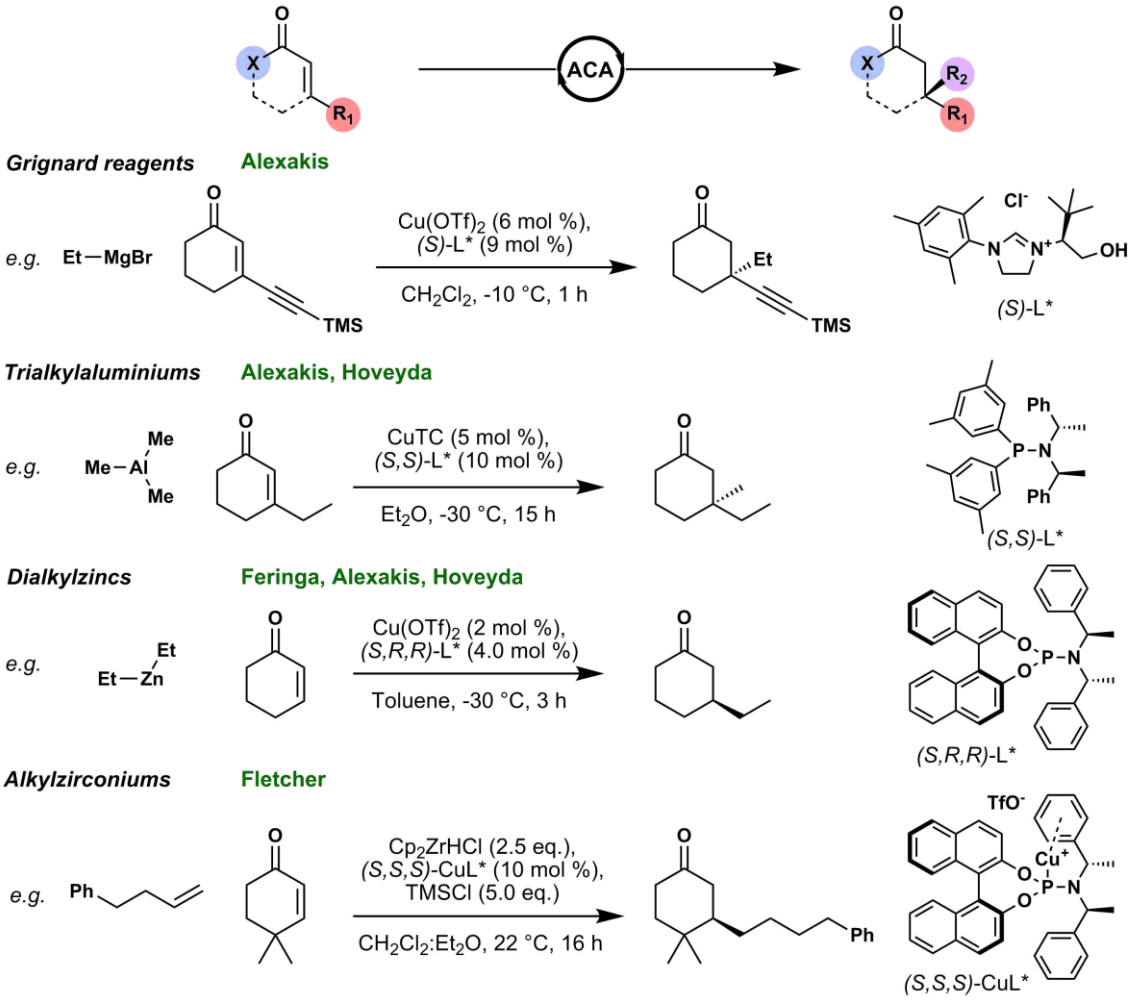

Scheme 4.2. Copper-catalyzed ACAs of organometallics on cyclic substrates.

The copper-catalyzed ACA of organometallic species also becomes extremely attractive when its enolate intermediate can be sequentially trapped with an electrophile (**Scheme 4.3**). This tandem ACA/trapping strategy produces multiple bonds and stereocenters such that higher levels of structural complexity can be obtained in a single step. It is particularly powerful in natural product synthesis and many different electrophiles have already been explored with Grignard, organoaluminum, and organozinc reagents.[23–32,33]

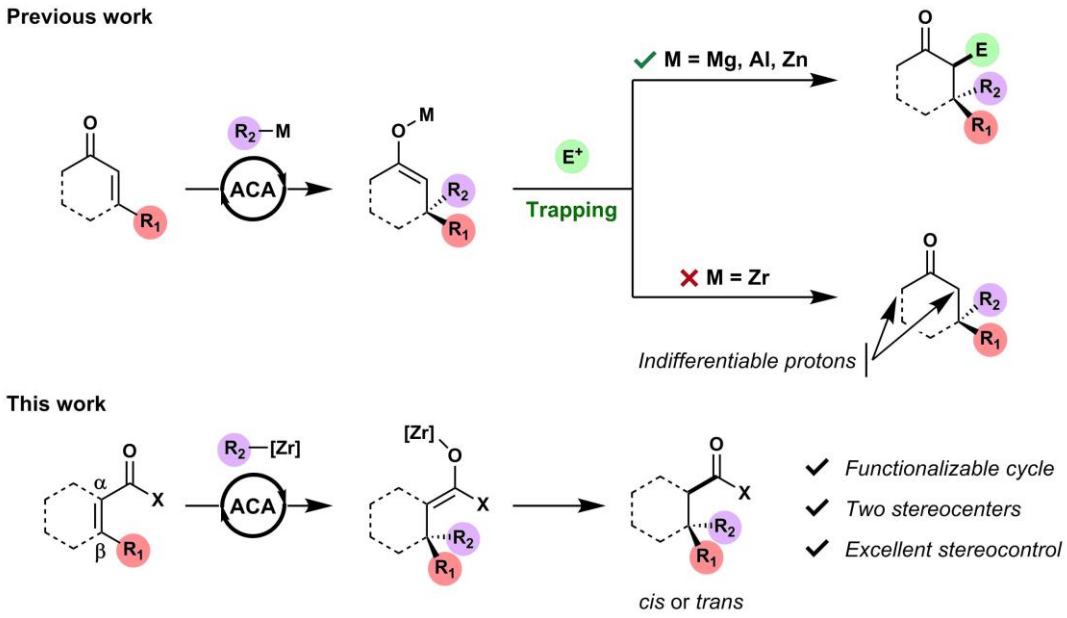

Scheme 4.3. Previous tandem ACA/trapping strategy used with alkylmetals and our work to reach similar structural complexity with alkylzirconiums.

Likewise, trapping of alkylzirconocenes has been thoroughly explored in our group inspired by a variety of approaches applied to other alkylmetals, but it proved extremely difficult and the likely zirconium enolate was much less reactive than anticipated (<10% yield). We reasoned that the strength of the Zr–O bond in the intermediate enolate renders most electrophiles unreactive, while the crucial need of using TMSCl as an additive in numerous substrates further complicates attempts to use the tandem strategy.

Remarkably, the Sebesta group showed that the trapping of zirconium enolates was feasible with carbenium ions but unfortunately the reaction proved very low yielding (<20%).[34,35] Additionally, our group recently disclosed the formation of β-chloroaldehydes in moderate yields (~50%) upon trapping of zirconium enolates with the Vilsmeier–Haack reagent.[36] This reaction was highly substrate dependent which is not unusual in ACA/trapping chemistry.[25,32]

Without electrophilic trapping, quenching of the zirconium enolate intermediate leads to the formation of cyclohexanone derivatives that possess indifferentiable protons (**Scheme 4.3**). Accordingly, further functionalization becomes extremely complicated due to poor regioselectivity and a mixture of compounds is often recovered.

In summary, there is a clear lack of reactivity from zirconium enolate intermediates and the crucial TMSCl additive is incompatible with the ACA/trapping strategy. This forced us to reconsider our strategy to obtain multiply substituted products, with similar levels of structural complexity than those accessed after trapping. We realized that ACAs of alkylzirconocenes to *exocyclic* α,β-unsaturated carbonyls would afford products possessing two adjacent stereocenters and a ring that would be much more amenable to further functionalization (**Scheme 4.3**). To our knowledge, copper-catalyzed conjugate additions of alkylmetals on exocyclic α,β-unsaturated carbonyls have already been reported[37–40] but their asymmetric versions have only been described once. In 2007, the Alexakis laboratory indeed disclosed the ACA of alkylaluminiums to exocyclic enones but high yield and high enantioselectivity (>90% yield, >80 *ee*) were limited to the use of trimethylaluminium (**Scheme 4.4**).[41]

Although not copper-catalyzed, a noteworthy contribution from the Tomioka group showed in 1997 the ACA of organolithiums to BHA (2,6-di-*tert*-butyl-4-methoxyphenyl) enoate (**Scheme 4.4**).[42] High yields and enantioselectivities were, however, limited to phenyllithium and *n*-butyllithium reagents (>80% yield, >90% *ee*).

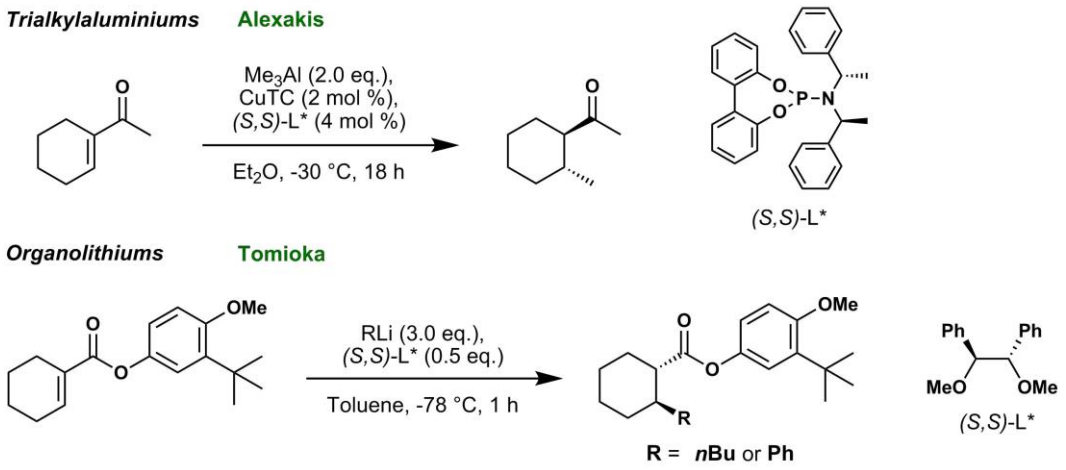

Scheme 4.4. Asymmetric conjugate additions of alkylmetals to exocyclic α,β-unsaturated carbonyls.

Additionally, in asymmetric addition to α,β-unsaturated carbonyl compounds, α-substitution is detrimental in terms of both yield and enantioselectivity, to the extent that this substitution pattern is almost always absent from the scope of reported reactions. Since exocyclic substrates are likely very similar in steric hindrance, we expected that previously optimized conditions for cyclic enones would behave poorly when applied to exocyclic substrates such that the design of new ligands would be necessary to achieve high enantioselectivity. The need of new ligands for different types of substrates is indeed a commonly found behavior in asymmetric catalysis.[43] Additionally, as addition to exocyclic enones produces two new stereogenic centers, the reaction may possibly form four diastereoisomers, making analysis difficult.

In this chapter, we aimed to produce only a single isomer through development of an enantio- and diastereoselective copper-catalyzed ACA to exocyclic enones. Multivariate modelling was hoped to allow for the time-efficient design of new phosphoramidite ligands that induce high enantioselectivity to exocyclic products.

We started by attempting classic optimization of the asymmetric reaction conditions, then applied a statistical approach which builds on the work previously discussed in the thesis. The statistical approach was planned to involve two steps. The first step consisted of exploring the available chemical space (in this case, the phosphoramidite Ligand Space) to identify the best core scaffold. The second phase involved constructing a rational statistical model to guide ligand optimization. Fortuitously, exploration of the phosphoramidite Ligand Space (LS) proved sufficient in identifying a ligand achieving high selectivity (>90%) and reactivity (>80%). Remarkably, we also found that the protocol used to quench the enolate intermediate allows selection of the major stereoisomers (either *cis* or *trans*). In the near future, we hope that statistical model construction from our data will help further improving the ligand efficiency such that this ACA will be tested on a varied scope of exocyclic substrates.

2 Condition optimisation

We started by examining different exocyclic substrates such as α,β-unsaturated thioesters, esters, ketones and aldehydes (**Scheme 4.5**). Copper-catalyzed ACA using conditions developed for the linear system described in **Chapter 1** led to no formation of ester **4.1** and thioester **4.2**, but did afford a small amout of product using aldehyde **4.3** (10% yield) and ketone **4.4** (23% yield). Unfortunately, the α,β-unsaturated aldehyde and the corresponding conjugate addition product **4.3** decomposed upon isolation and under reaction conditions (~70%), such that the enantiomeric excess could never be reliably determined.

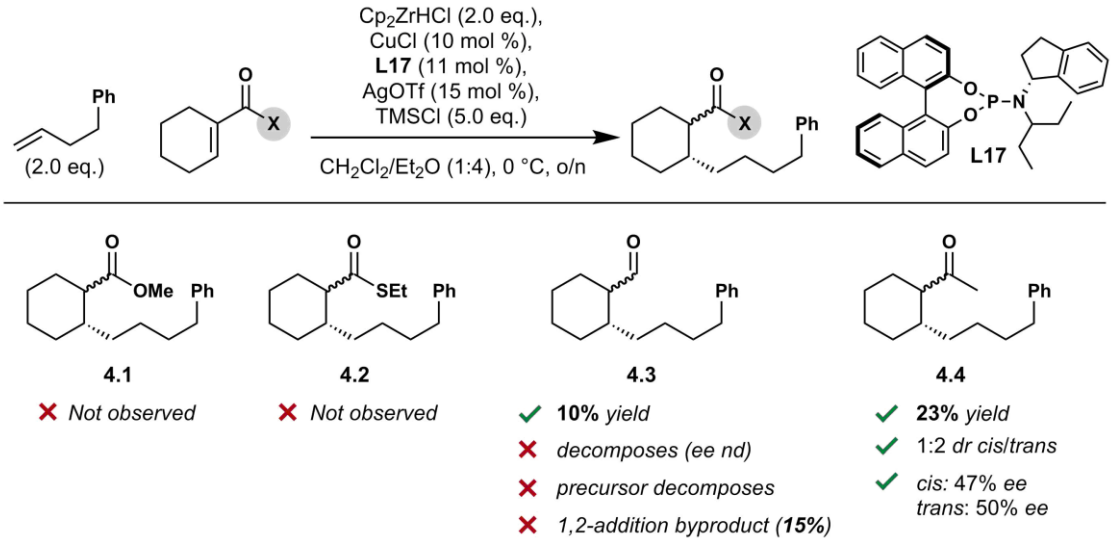

Scheme 4.5. Substrate exploration for ACAs on exocyclic α,β-unsaturated carbonyls, including an ester, thioester, aldehyde and ketone.

Aldehydes are also excellent electrophiles and a significant amount of the 1,2-addition byproduct was always obtained (15%). Screening of copper salts, Schwartz and copper equivalents, concentrations and copper/ligand ratios did not allow for the identification of better results (not shown). Accordingly, we decided to turn our attention to the α,β-unsaturated ketone instead.

Initial experiments on the ketone showed a promising 50% *ee* with 23% yield and 1:2 *dr* with ligand **L17** (**Scheme 4.5**). To improve the yield, several copper sources were examined as shown in **Table 4.1**. Among the five salts, "$CuNTf_2$" (prepared by mixing CuCl and $AgNTf_2$) gave a satisfactory 74% yield and was used for further optimisation. Noteworthily, "CuOTf" (prepared by mixing CuCl and AgOTf) however gave the best *ee's*. Note that the *ee's* are low also due to the use of a cheaper ligand for screening.

Table 4.1. Screening of different copper salts to improve yield. "CuOTf" salt was prepared by mixing CuCl (0.1 eq.) and AgOTf (0.15 eq.). "$CuNTf_2$" salt was prepared by mixing CuCl (0.1 eq.) and $AgNTf_2$ (0.15 eq.). Yield determined by calibrated ^1H NMR spectroscopy.

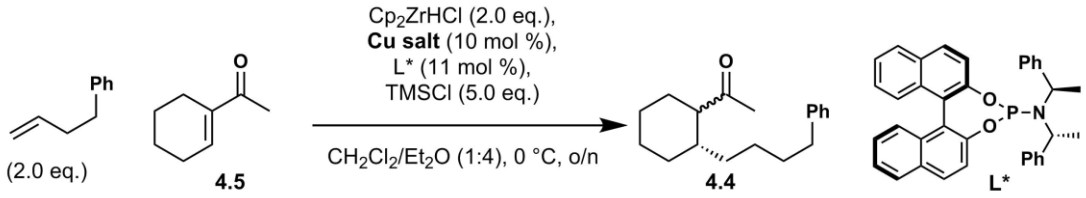

	"CuOTf"	CuCl	"$CuNTf_2$"	$Cu(OTf)_2$	CuTC
Yield	21%	32%	74%	9%	12%
Unreacted SM	28%	27%	0%	48%	47%
$dr_{cis/trans}$	1:2.2	1:1.5	1:0.5	1:2.6	1:7.9
ee_{cis}	11%	5%	1%	8%	6%
ee_{trans}	12%	1%	5%	9%	1%

A design of experiments (DoE, see the experimental section for detailed description)[44] was realised and several continuous reaction factors were examined such as equivalents and reagent ratios (**Scheme 4.6**). We found that the Schwartz and TMSCl equivalents afforded better yields at a high level while the alkene/Schwartz ratio, copper equivalent and $AgNTf_2$/copper ratio were preferred at a low level.

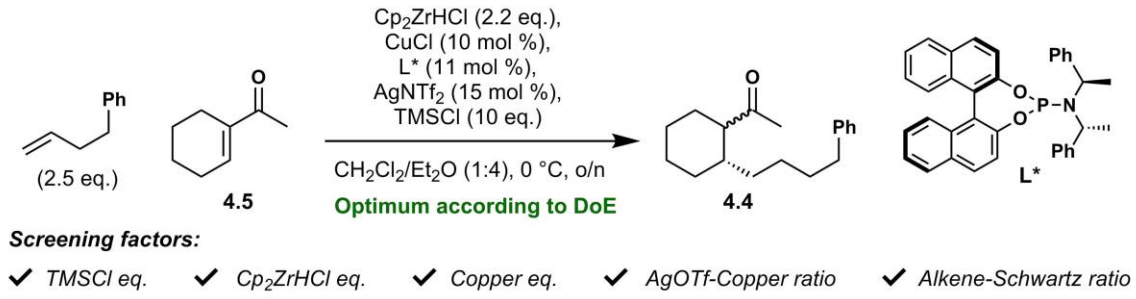

Scheme 4.6. Design of experiment to optimize yield of ACA to exocyclic α,β-unsaturated ketones. A regular two-level fractional factorial design was utilized.

However, the levels of enantioselectivity did not improve after condition optimization and remained low (~10% *ee*). Use of the optimized conditions in the presence of **L17** confirmed the improved yield but poor enantioinduction with copper(I) triflamide (**Table 4.2**) while copper(I) triflate showed a good trade-off between yield and enantioselectivity (50% yield, ~50% *ee*). Accordingly, we decided to realise the ligand optimisation with copper(I) triflate, with which a large excess of TMSCl (10 eq.) was critical to achieve satisfactory reactivity (50% yield). The combination of CH_2Cl_2 and Et_2O in a 1:4 mixture at 0 °C proved again to be the optimum for selectivity (~50% *ee*).

Table 4.2. Screening of different silver salts for *ee* optimisation. Yield determined by calibrated ^{1}H NMR spectroscopy.

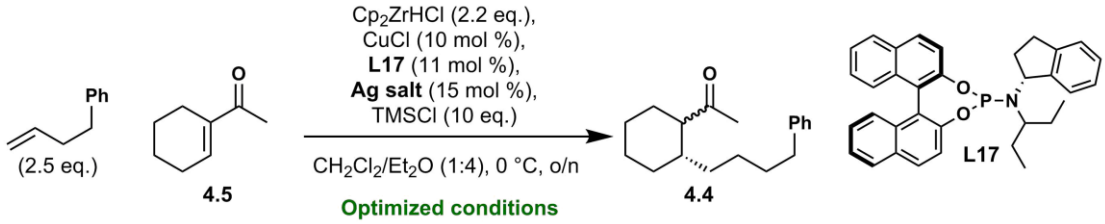

	AgOTf	$AgNTf_2$
Yield	50%	90%
$dr_{cis/trans}$	1:1.4	1:1.5
ee_{cis}	52%	10%
ee_{trans}	49%	11%

3 Lead identification

After the initial optimisation of condition described above began the ligand design campaign. It started with examining structurally diverse ligands found in our database, as it is unnecessary to design new ligands if already known compounds could improve the reaction. Here, our strategy was to explore the phosphoramidite

LS to identify a promising ligand lead from which structural modification and model construction could improve results. As expected, this initial screening confirmed the poor reactivity and selectivity of most ligands that had been previously structurally optimized for other reactions (**Scheme 4.7**). Note that the yields and enantioselectivities are an average from at least two repeat reactions for reproducibility purposes.

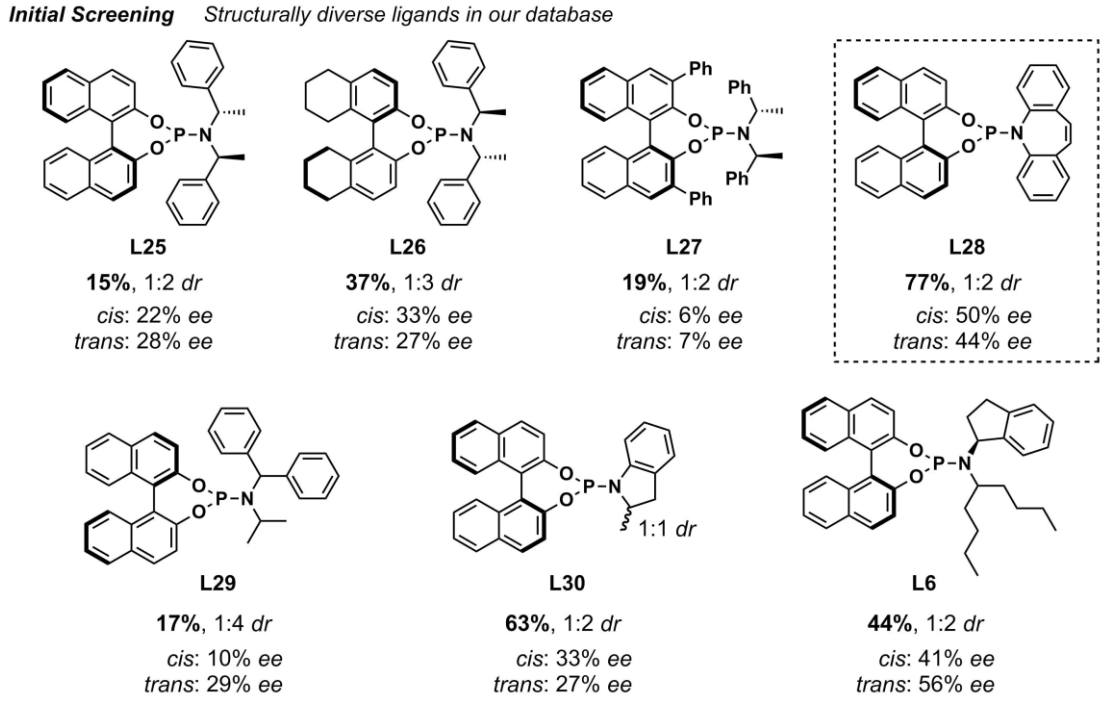

Scheme 4.7. Seven structurally diverse phosphoramidite ligands from the ligand database that were used to initially explore the phosphoramidite ligand space. The yields and enantioselectivities are an average from at least two repeat reactions.

For instance, ligand **L25** developed by the Feringa group[13,27,45] provided poor enantioinduction and reactivity as well as related BINOL-derived backbone containing ligands (**L26** and **L27**). Ligand **L28** developed by the Carreira group[46,47] however provided a promising 77% yield and moderate enantioselectivity (50% *ee* and 44% *ee*, for *cis* and *trans* products respectively). Developed by Dr Philippe Roth

for ACA on cyclic α,β-unsaturated ketones,[17,18] **L29** also behaved poorly. **L30**, a surrogate ligand to tetrahydroquinoline-derived ligand,[48] provided 63% yield but only ~30% *ee*. **L6**, developed by Dr Zhenbo Gao for ACA on linear enones,[49] gave 44% yield and 56% *ee* of the *trans* product which was promising. In terms of combining both reactivity and enantioselectivity, **L28** ligand clearly stood out from all the results and we decided to continue with **L28** as our lead structure. However, repeating the key experiments showed an irreproducibility in the observed diastereomeric ratios, which ranged from 1:1 to 1:4 under seemingly identical conditions. Worse, some reaction repeats led to the opposite major diastereoisomer being favoured (*trans* then *cis*). We had chosen to ignore this unexplained behaviour during lead identification and decided to tackle this diastereomeric ratio issue separately (see improving the diastereomeric ratio section). Once a lead is identified, its structural diversification enables refinement of the core scaffold that will be used in model construction, where the newly synthesized ligands will constitute the initial training set. **L28** is actually a flawed lead, because modification of its amine unit via the preparation of azepine precursors requires much more than four well-established synthetic steps. Only the Pd-catalyzed condensation of 2-bromostyrene and 2-chloroaniline derivatives developed by Buchwald *et al.* allowed the formation of azepine derivatives in one step (see experimental section).[50] These derivatives were however either not commercially available or were prohibitively expensive. Accordingly, we envisaged that six amines in total could be reasonably made, of which four of these were successfully synthesized and led to the corresponding ligands **L31**, **L32**, **L33** and **L34** (**Scheme 4.8-A**). Attempted syntheses using nitro- and iodo-substituted anilines failed because they decomposed under the reaction conditions.

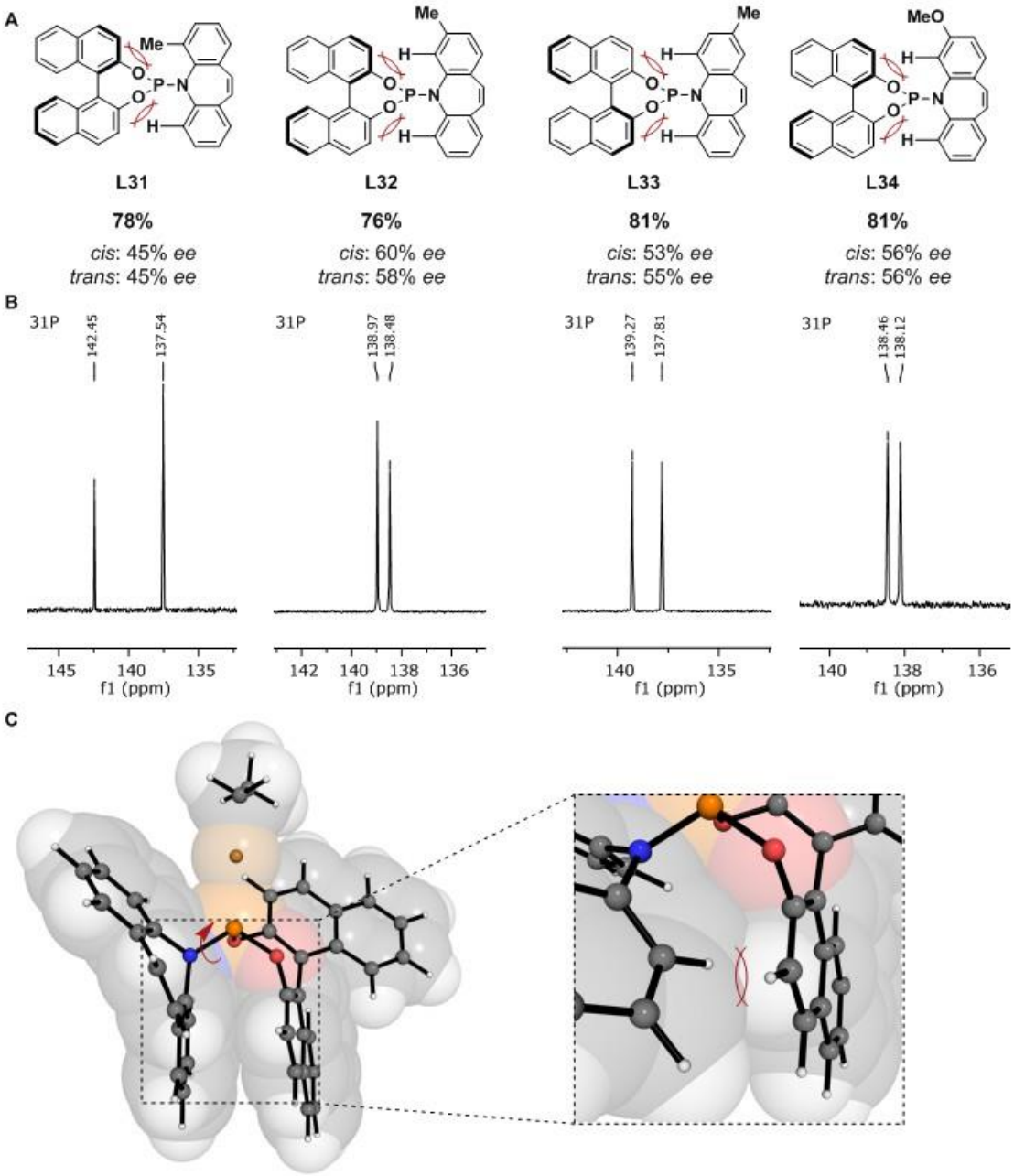

Scheme 4.8. A) Structural diversification of ligand **L28** based on modifying the ligand's amine. Yields and enantioselectivities are reported for the asymmetric addition producing **4.4**, and are averaged from at least two reaction repeats. **B)** ^{31}P NMR spectra of ligands demonstrating the presence of two diastereoisomers due to atropisomerism. **C)** Ligand **L28** with CuEt complex optimised at the ωB97XD/6-31G(d)/LANL2DZ(Cu) level of theory. Rotation around the P–N bond leads to an important steric clash between the backbone and the amine moiety.

Unexpectedly, monosubstitution of the ligand amino group produced two diastereoisomers and 3D modelling of the geometry confirmed that a steric clash occurs between the BINOL backbone and the amine group (**Scheme 4.8-C**). Thus, no rotation around the P–N bond is allowed at the experimental temperature and the different stereoisomers do not interconvert, hence resulting in atropisomerism. This forms two diastereoisomers visible in ^{31}P NMR (**Scheme 4.8-B**). An overlooked technique to differentiate diastereoisomers from rotamers is the NOE (or EXSY) NMR experiment.[51] For instance, 1D NOE consists in irradiating a targeted peak such that if the corresponding proton is under significant chemical exchange with another proton on the NMR time scale, then the second proton will also appear. This technique further confirmed the presence of diastereoisomers (see experimental section). Unfortunately, the use of diastereoisomers in ligand design is extremely troublesome because diastereoisomers likely do not achieve similar levels of enantioselectivity and this adds a layer of complexity in model construction. Unfortunately, we could not achieve the separation of the diastereoisomers via column chromatography or recrystallization and synthesis of C_2 symmetric amines appeared lengthy.

Looking at the ACA results (**Scheme 4.8**), 2-methyl substitution resulted in unchanged enantioselectivity (**L31**, 45% ee) but a small improvement was observed with 3-methyl and 4-methyl substituents (58% and 55% *ee*, **L32** and **L33** respectively). Additionally, adding an electron donating group such as a methoxy group did not lead to any improvement (**L34**). Overall, all the ligands gave satisfactory yields but enantioselectivities were insignificantly improved to justify pursuing more synthetically challenging azepine derivatives.

Accordingly, we abandoned the **L28** derivatization strategy. Instead, we decided to identify the key features responsible for high enantioinduction and we reasoned that this might enable the construction of a mimic lead ligand, whereby similar reactivity and selectivity are achieved with an amine precursor that is synthetically modular and derived from well-established chemistry.

As shown in **Scheme 4.9**, removal of the bridging alkene was extremely detrimental for selectivity (**L35**, 9% *ee*) while alkene reduction significantly reduced reactivity but not enantioselectivity (**L36**, 30% yield, 57% *ee*). Conversely, retaining the double bond while opening the azepine ring decreased both yield and enantioselectivity (**L37**, 30% yield & 17% *ee*). *Ortho*-styrene substituted **L38**'s olefin was designed to act like the alkene in **L28** but poor enantioselectivity was obtained even though a noteworthy reactivity was observed (**L38**, 91% yield).

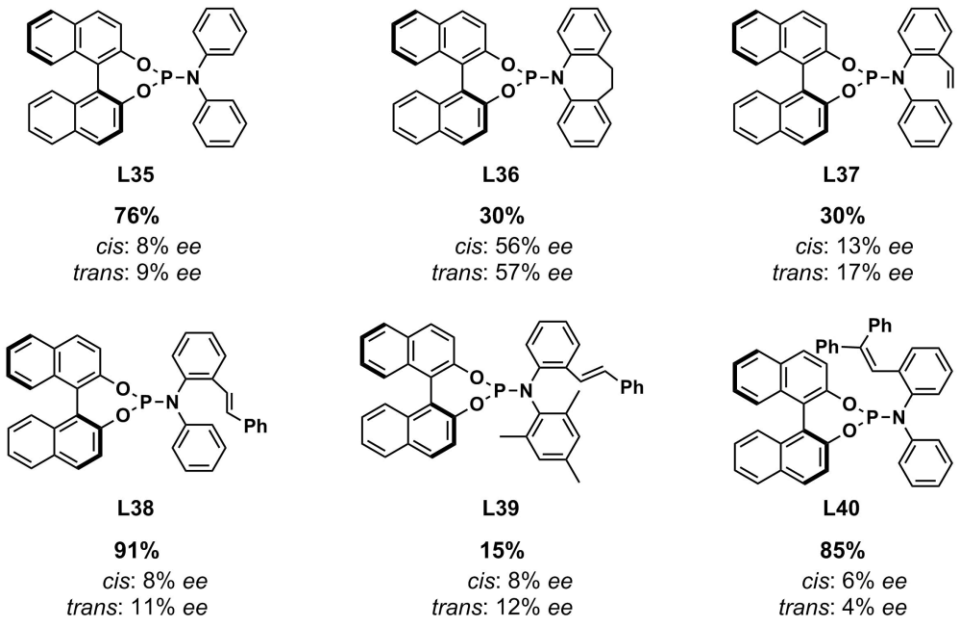

Scheme 4.9. Modification of **L28**'s amine to identify the key features inducing high enantioselectivity and reactivity. Yields and enantioselectivities are averaged from at least two reaction repeats.

The azepine group is locked in fewer conformations compared to the ring opened ligand **L38** and tri-substituted **L39** was hoped to trigger a constructive conformational change. Unfortunately, both reactivity and selectivity dropped. Finally, we decided to disubstitute the terminal alkene as a surrogate of **L38** *cis* isomer but 85% yield of a virtually racemic product was obtained (**L40**). These experiments suggested that the double bond played a crucial role in achieving high reactivity, likely to form a semi-labile ligand.[52] Unfortunately it also demonstrated that the synthetically unattractive azepine ring was essential in getting high enantioinduction.

We decided to completely abandon the **L28** scaffold and turned our attention to **L6**, which was also a promising ligand giving 50% *ee* and 44% yield. This ligand however possesses a core scaffold similar to **L17**, a ligand used during the optimization of reaction conditions where it achieved a promising 52% *ee* and 50% yield. **L17** was developed in **Chapter 1** and represents the best of the aliphatic series. Accordingly, we decided to explore a structurally different amine precursor, from which a new optimum might be obtained. Inspired by the previous ligands, we synthesized **L41** with an aromatic substituent to imitate **L38** reactivity but the ACA product was racemic (**Scheme 4.10**). Locking the structure by tri-methyl substitution of the phenyl ring however led to a sharp increase in enantioselectivity from nearly racemic (**L41**) to 45% *ee* (**L42**). This seemed to be a promising lead but replacement of methyl groups by isopropyl substituents only gave a disappointing 50% *ee* (+5% *ee*) and a drop to 31% yield (**L43**). Additionally, replacement of the phenyl ring by a naphthalene moiety afforded nearly racemic product (**L44**).

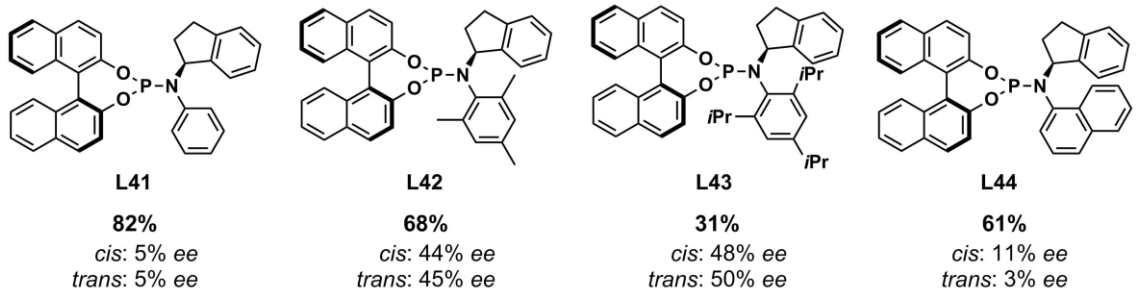

Scheme 4.10. Structural diversification of the amine of ligand **L6**. Yields and enantioselectivities are averaged from at least two reaction repeats.

On one hand, a lead should be sufficiently selective to work with good magnitudes of *ee* values during model construction (>40% *ee*) and on the other hand, it should be synthetically accessible and modular for its easy derivatization. In our case, a compromise between both aspects seemed impossible such that we decided to continue exploring the phosphoramidite LS. This ligand space is huge and we previously limited ourselves to ligands found in our database. Here, we pragmatically decided to firstly limit our search to phosphoramidite scaffolds already synthesized in the literature. Extensive review of the literature allowed us to establish an exhaustive list of the phosphoramidite backbones and amine groups (**Scheme 4.11**).

For instance, diol backbone **C7** with amine **D3** forms ligand **L25** and **C7** with **D14** is **L28**. Each combination of a diol with an amine forms the core scaffold of a family of phosphoramidite ligands. As diol backbones have the main effect on selectivity and tend to impose the absolute stereochemistry,[53] they are unsurprisingly very diverse in structure. Most rely on a C_2 symmetric diol with the most popular being based on tartrate, TADDOL, BINOL or bisphenols. In comparison, the amine group tends to be more highly derivatized but involves more subtle structural changes, such that the

core scaffold is often retained. Only a few unclassifiable phosphoramidites were found (*cf.* **E1**-**E3**).

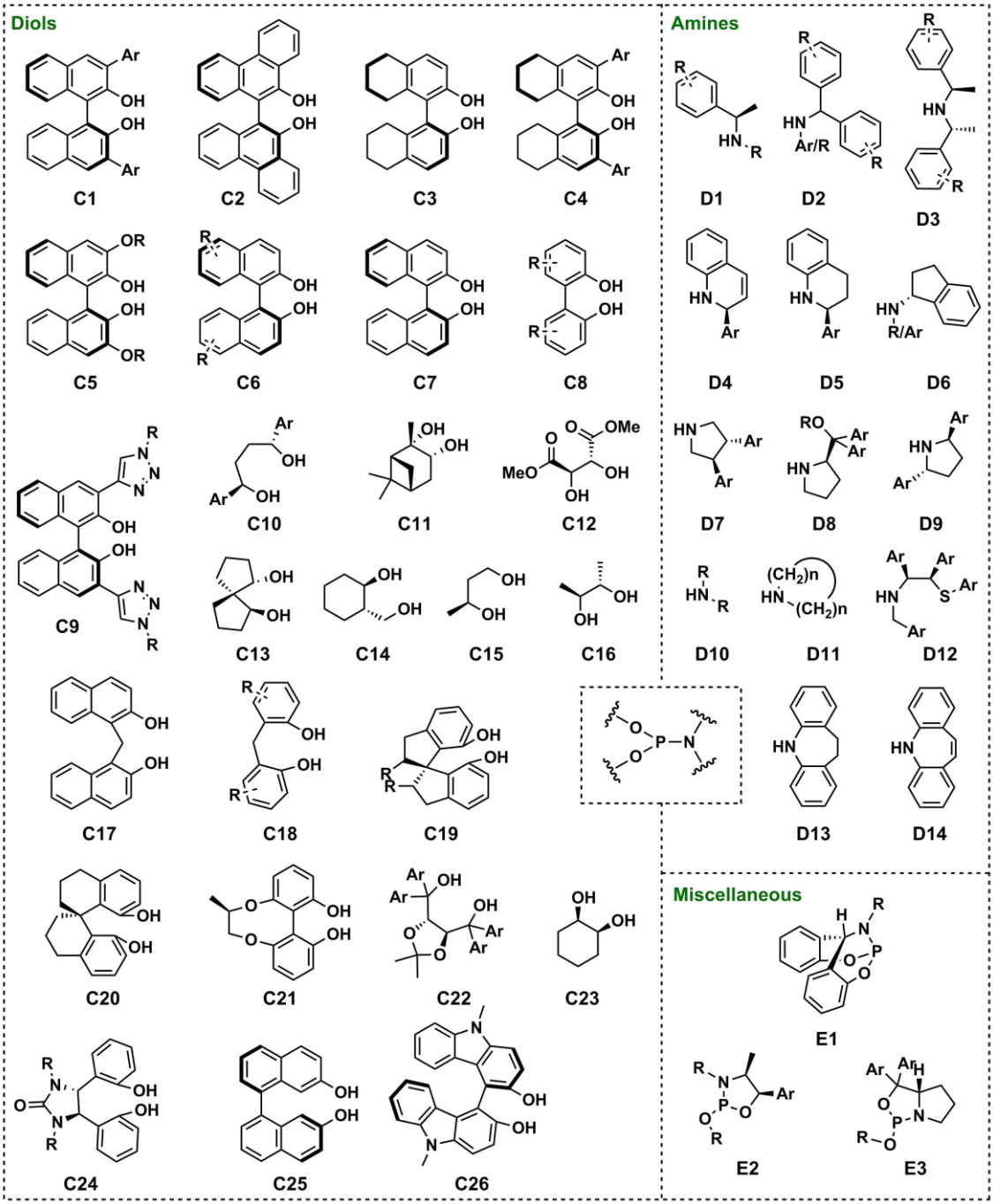

Scheme 4.11. Exhaustive list of diols and amines used to synthesize phosphoramidite ligands.

We decided to explore one of the most popular BINOL-derived backbones (**C1**) in combination with amine **D14**, but unfortunately 3,3'-disubstitution of the backbone with phenyl groups (**L45**) gave a drastic drop in yield and enantioselectivity compared to **L28** (**Scheme 4.12-A**). Dibromination of BINOL to prepare **C1** afforded large quantities of the monobrominated byproduct such that the monosubstituted version of **L45** was easily synthesized.[54] In 2005, the Reetz laboratory prepared similarly mono-substituted phosphoramidite ligands that were used in rhodium-catalyzed olefin hydrogenation.[55] To our delight, when **L46** was tested in the asymmetric 1,4-addition 83% yield of highly enantioenriched product was isolated (93% *ee*). Based on this striking result, we chose **L46** to be our new ligand lead and exploration of the phosphoramidite LS was therefore halted at this stage.

Like ligands **L31-L34**, it could be deduced from ^{31}P NMR spectroscopy that ligand **L46** was composed of diastereoisomers. Based on previous observations from Dr Nisha Mistry,[56] we hypothesized that a stereogenic centre is present on the phosphorus atom upon breaking the C_2 symmetry of the BINOL backbone. The resulting monosubstituted ligand has its amine group in either an "equatorial" or "axial" configuration and diastereoisomer interconversion likely does not occur at room temperature (**Scheme 4.12-A**).[56] Two diastereoisomers are formed[55] and those are unlikely to achieve similar levels of enantioselectivity, which, as previously explained, is troublesome in statistical modelling. The reactivity and enantioselectivity were however remarkably promising and we aimed to separate the diastereoisomeric mixture by HPLC on a preparative chiral non-racemic stationary phase. Analytical conditions were easily found and efforts to purify about 300 mg of **L46** are currently on-going through a collaboration with Vertex

Pharmaceuticals. Alternatively, Reetz *et al.* have shown that diastereomerically pure ligands can be obtained when the phenyl group is replaced by trialkylsilyl substituents (**Scheme 4.12-B**).[55]

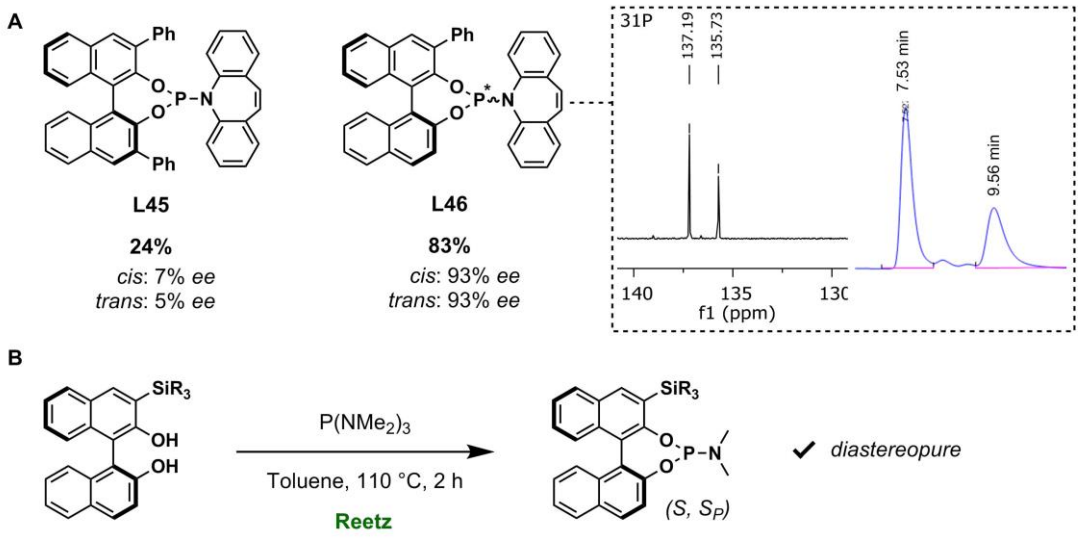

Scheme 4.12. A) First syntheses of new diol backbones and their corresponding phosphoramidites led to the identification of an excellent ligand **L46**, which is a mixture of two diastereoisomers. ^{31}P NMR spectrum of the ligand mixture and its separation by HPLC on a chiral non-racemic stationary phase (Chiralpak© ID 99:1 Hexane:IPA 1.0 mL/min). **B)** Reetz's protocol used to prepare diastereopure phosphoramidites. The trialkylsylil group is crucial for high diastereoselectivity.

4 Improving the diastereomeric ratio

ACA of alkylzirconocenes on exocyclic enones creates two adjacent stereocenters in one step but the stereocenter α to the carbonyl group is only formed after collapse of the trimethylsilyl enol intermediate, upon which the chiral ligand has no control. Accordingly, the diastereomeric ratio of *cis* and *trans* products was always poor with the average ratio being *ca.* 1:2. However, the results were highly unpredictable and

obtaining the *cis*-product as the major epimer was seemingly as likely as its *trans* counterpart.

We started by examining different sets of conditions to catalyze the epimerization of an isolated product possessing 1:1.4 *dr* (**Scheme 4.13-A**). After screening several bases and solvents at different temperatures, a satisfactory 1:15 *dr* in favour of the *trans*-isomer with preserved *ee* values was achieved by treating the product with a large excess of sodium hydroxide in a protic solvent at 50 °C. However, the need for a second step to reach high *dr* was unattractive and we decided to investigate the lack of reproducibility observed with the *cis* and *trans* ratio.

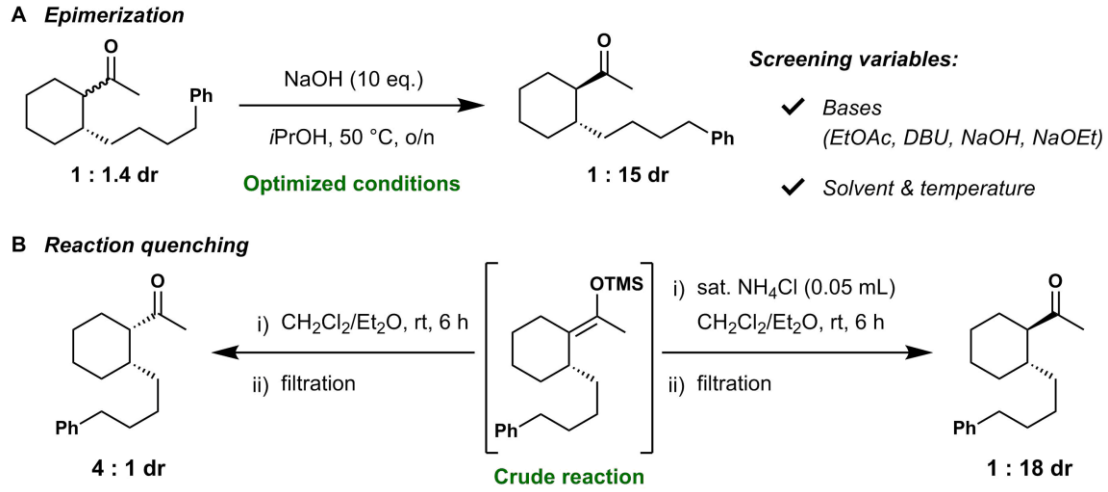

Scheme 4.13. Improvement of the diastereomeric ratio by epimerization of the α-stereocenter. **A)** Use of base after isolation of product. **B)** Reaction quenching protocol controls which major epimer is formed.

Interestingly, *dr* values started to change based on the stirring time after addition of a saturated solution of NH_4Cl so that stirring the quenched crude reaction mixture for a longer time (6 h instead of 10 min) achieved an impressive 1:18 *dr* in favour of the *trans*-product (**Scheme 4.13-B**). We assume that hydrochloric acid is created

upon addition of NH_4Cl solution as TMSCl is present in excess and this HCl catalyzes the epimerization of the α-stereocenter to the thermodynamic product. Unexpectedly, we also found during optimization of the quenching protocol that stirring at room temperature without addition of NH_4Cl favoured the *cis* isomer in a 4:1 *dr*. This suggests that the major isomer (*cis* or *trans*) obtained after ACA of alkylzirconocenes on exocyclic enones can directly be controlled by the quenching protocol.

5 Conclusion and future work

In this work, exploration of the phosphoramidite ligand space allowed the discovery of promising ligands (>40% *ee*) to asymmetric conjugate addition to *exocyclic* α,β-unsaturated ketones, but identification of a ligand lead proved difficult due to limitations in preparing the amine precursors. This showcases the difference between a promising ligand and a ligand lead. Ideally, modification of the core scaffold should indeed be accessible in few well-established synthetic steps while providing a large range of *ee* values for quantitative model construction. In practice, the synthetic difficulty to derive the promising ligand scaffolds unfortunately limited the corresponding ligand space within which design could take place. Thus, there was limited incentive to build a model as the amount of synthetically accessible ligands to predict would be of one digit or, conversely, a large number of predicted ligands would be infeasible. We therefore tried to identify an equivalent but modular amine precursor, from which the corresponding ligand would afford satisfactory yields and enantioselectivities, but it proved unsuccessful.

Data-led ligand optimisation is therefore only viable if the initial data span a workable range of *ee* values and if the corresponding synthetically accessible ligand space is large enough to justify modelling it to prioritise ligands for synthesis. Similarly, we found that data homogeneity was extremely important. As the amount of datapoints is scarce in asymmetric catalysis, structural variation of ligands should remain limited in order to obtain a statistically significant model possessing a tight margin of error. In our case, substantial structural variation of scaffolds prevented us from building a predictive model with interesting insights using all the synthesized ligands.

We therefore abandoned the ligand structures synthesized so far and decided to further explore the phosphoramidite LS by first exhaustively listing diols and amines used to synthesize phosphoramidite ligands. Trying the synthetically accessible and modular scaffolds, we fortuitously identified ligand **L46** whereby high reactivity (>80%) and enantioselectivity (>90%) were achieved. In the near future, it is hoped that derivatization of **L46** diol backbone can further improve selectivity, and statistical model construction from the generated data might help determine an optimum ligand. Finally, examination of the substrate scope will evaluate the robustness of the ACA and few potential candidates are proposed in **Scheme 4.14**. It is also possible that a procedure to add *sp2*-hybridized nucleophiles, for example using the combination of Rh-catalysts and boronic nucleophiles, may be developed by building on the proof of concept chemistry demonstrated here.

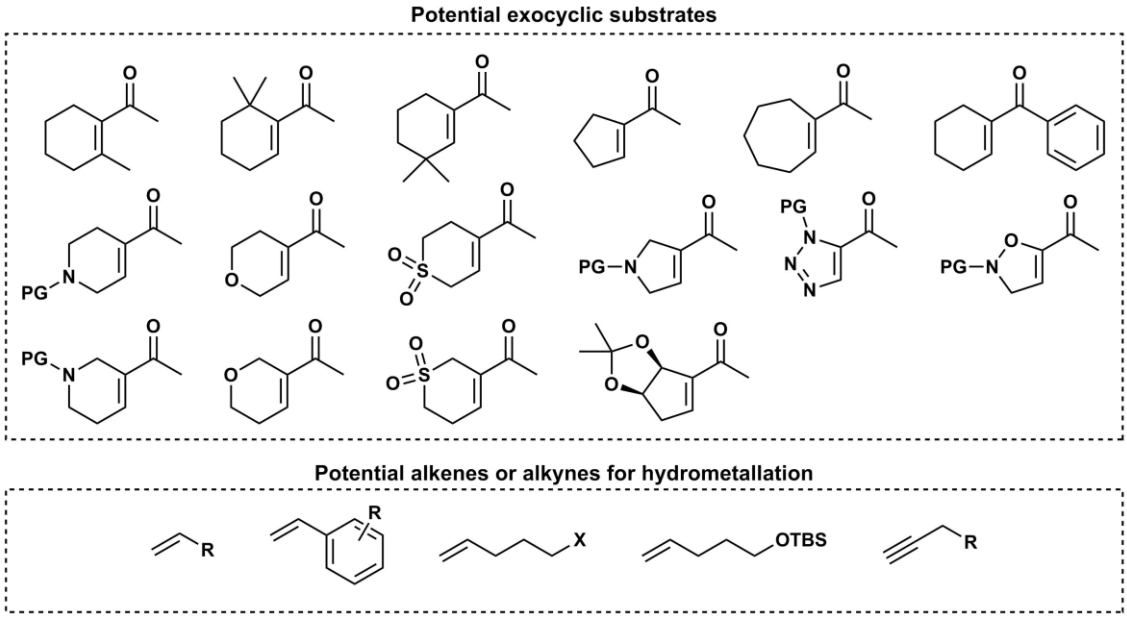

Scheme 4.14. Proposed potentially interesting exocyclic substrates and the associated alkene reaction partners.

6 References

1 B. C. Calvo, J. Buter and A. J. Minnaard, in *Copper-catalyzed asymmetric synthesis*, eds. A. Alexakis, N. Krause and S. Woodward, 2014, pp. 373–447.

2 M. Zeng, S. K. Murphy and S. B. Herzon, *J. Am. Chem. Soc.*, 2017, **139**, 16377–16388.

3 L. A. Arnold, R. Naasz, A. J. Minnaard and B. L. Feringa, *J. Org. Chem.*, 2002, **67**, 7244–7254.

4 A. Mendoza, Y. Ishihara and P. S. Baran, *Nat. Chem.*, 2012, **4**, 21–25.

5 M. K. Brown and A. H. Hoveyda, *J. Am. Chem. Soc.*, 2008, **130**, 12904–12906.

6 X. Yu, F. Su, C. Liu, H. Yuan, S. Zhao, Z. Zhou, T. Quan and T. Luo, *J. Am. Chem. Soc.*, 2016, **138**, 6261–6270.

7 S. G. Krasutsky, S. H. Jacobo, S. R. Tweedie, R. Krishnamoorthy and A. S. Filatov, *Org. Process Res. Dev.*, 2015, **19**, 284–289.

8 J. Wu, Y. Kadonaga, B. Hong, J. Wang and X. Lei, *Angew. Chem. Int. Ed.*, 2019, **58**, 10879–10883.

9 M. Tissot, D. Poggiali, H. Hénon, D. Müller, L. Guénée, M. Mauduit and A. Alexakis, *Chem. - A Eur. J.*, 2012, **18**, 8731–8747.

10 C. Hawner and A. Alexakis, *Chem. Commun.*, 2010, **46**, 7295–7306.

11 T. L. May, M. K. Brown and A. H. Hoveyda, *Angew. Chem. Int. Ed.*, 2008, **47**, 7358–7362.

12 K. S. Lee, M. K. Brown, A. W. Hird and A. H. Hoveyda, *J. Am. Chem. Soc.*, 2006, **128**, 7182–7184.

13 B. L. Feringa, M. Pineschi, L. A. Arnold, R. Imbos and A. H. M. De Vries, *Angew. Chem. Int. Ed.*, 1997, **36**, 2620–2623.

14 A. Alexakis, J. Burton, J. Vastra, C. Benhaim, X. Fournioux, A. van den Heuvel, J.-M. Levêque, F. Mazé and S. Rosset, *Euro. J. Org. Chem.*, 2000, **2000**, 4011–4027.

15 R. M. Maksymowicz, P. M. C. Roth and S. P. Fletcher, *Nat. Chem.*, 2012, **4**, 649–654.

16 L. Mola, M. Sidera and S. P. Fletcher, *Aust. J. Chem.*, 2015, **68**, 401–403.

17 R. Ardkhean, P. M. C. Roth, R. M. Maksymowicz, A. Curran, Q. Peng, R. S. Paton and S. P. Fletcher, *ACS Catal.*, 2017, **7**, 6729–6737.

18 E. E. Maciver, R. M. Maksymowicz, N. Wilkinson, P. M. C. Roth and S. P. Fletcher, *Org. Lett.*, 2014, **16**, 3288–3291.

19 R. M. Maksymowicz, P. M. C. Roth, A. L. Thompson and S. P. Fletcher, *Chem. Commun.*, 2013, **49**, 4211–4213.

20 R. Ardkhean, M. Mortimore, R. S. Paton and S. P. Fletcher, *Chem. Sci.*, 2018, **9**, 2628–2632.

21 M. Sidera, P. M. C. Roth, R. M. Maksymowicz and S. P. Fletcher, *Angew. Chem. Int. Ed.*, 2013, **52**, 7995–7999.

22 P. M. C. Roth, M. Sidera, R. M. Maksymowicz and S. P. Fletcher, *Nat. Protoc.*, 2013, **9**, 104–111.

23 G. K. Jarugumilli, C. Zhu and S. P. Cook, *Euro. J. Org. Chem.*, 2012, **2012**, 1712–1715.

24 Y.-M. Hung, C.-H. Tseng and B.-J. Uang, *Tetrahedron: Asymmetry*, 2015, **26**, 1369–1374.

25 S. K. Murphy, M. Zeng and S. B. Herzon, *Org. Lett.*, 2016, **18**, 4880–4883.

26 S. K. Murphy, M. Zeng and S. B. Herzon, *Org. Lett.*, 2017, **19**, 4980–4983.

27 T. Jerphagnon, M. G. Pizzuti, A. J. Minnaard and B. L. Feringa, *Chem. Soc. Rev.*, 2009, **38**, 1039–1075.

28 M. Drusan, E. Rakovský, J. Marek and R. Šebesta, *Adv. Synth. Catal.*, 2015, **357**, 1493–1498.

29 Z. Galeštoková and R. Šebesta, *Euro. J. Org. Chem.*, 2012, **2012**, 6688–6695.

30 H.-C. Guo and J.-A. Ma, *Angew. Chem. Int. Ed.*, 2006, **45**, 354–366.

31 C. Bleschke, M. Tissot, D. Müller and A. Alexakis, *Org. Lett.*, 2013, **15**, 2152–2155.

32 N. Germain, D. Schlaefli, M. Chellat, S. Rosset and A. Alexakis, *Org. Lett.*, 2014, **16**, 2006–2009.

33 D. Vargová, I. Némethová, K. Plevová and R. Šebesta, *ACS Catal.*, 2019, **9**, 3104–3143.

34 I. Némethová, Z. Sorádová and R. Šebesta, *Synthesis*, 2017, **49**, 2461–2469.

35 I. Némethová, S. Bilka and R. Šebesta, *J. Organomet. Chem.*, 2018, **856**, 100–108.

36 J. Y. J. Wang, T. Palacin and S. P. Fletcher, *Org. Lett.*, 2019, **21**, 378–381.

37 J. Kabbara, S. Flemming, K. Nickisch, H. Neh and J. Westermann, *Tetrahedron*, 1995, **51**, 743–754.

38 S. Marquais, M. Alami and G. Cahiez, *Org. Synth.*, 1995, **72**, 135.

39 J. G. Rodríguez, A. Urrutia, J. Eugenio de Diego, M. Paz Martínez-Alcazar and I. Fonseca, *J. Org. Chem.*, 1998, **63**, 4332–4337.

40 J.-L. Zhu and Y.-P. Wu, *Synlett*, 2017, **28**, 1467–1472.

41 M. Vuagnoux-d'Augustin and A. Alexakis, *Chem. - A Eur. J.*, 2007, **13**, 9647–9662.

42 Y. Asano, A. Iida and K. Tomioka, *Tetrahedron Lett.*, 1997, **38**, 8973–8976.

43 X.-H. Yang, R. T. Davison, S.-Z. Nie, F. A. Cruz, T. M. McGinnis and V. M. Dong, *J. Am. Chem. Soc.*, 2019, **141**, 3006–3013.

44 S. A. Weissman and N. G. Anderson, *Org. Process Res. Dev.*, 2015, **19**, 1605–1633.

45 B. L. Feringa, *Acc. Chem. Res.*, 2000, **33**, 346–353.

46 T. M. Beck and B. Breit, *Angew. Chem. Int. Ed.*, 2017, **56**, 1903–1907.

47 S. Panda and J. M. Ready, *J. Am. Chem. Soc.*, 2018, **140**, 13242–13252.

48 W.-B. Liu, C. Zheng, C.-X. Zhuo, L.-X. Dai and S.-L. You, *J. Am. Chem. Soc.*, 2012, **134**, 4812–4821.

49 Z. Gao and S. P. Fletcher, *Chem. Sci.*, 2017, **8**, 641–646.

50 D. Tsvelikhovsky and S. L. Buchwald, *J. Am. Chem. Soc.*, 2010, **132**, 14048–14051.

51 D. X. Hu, P. Grice and S. V Ley, *J. Org. Chem.*, 2012, **77**, 5198–5202.

52 S. L. Rössler, S. Krautwald and E. M. Carreira, *J. Am. Chem. Soc.*, 2017, **139**, 3603–3606.

53 A. Alexakis, N. Krause and S. Woodward, *Copper-catalyzed asymmetric synthesis*, 2014.

54 Y. Kobayashi, *Org. Synth.*, 2019, **96**, 312–332.

55 M. T. Reetz, J.-A. Ma and R. Goddard, *Angew. Chem. Int. Ed.*, 2005, **44**, 412–415.

56 N. Mistry and S. P. Fletcher, *Adv. Synth. Catal.*, 2016, **358**, 2489–2496.

5

Summary & Outlook

The future of ligand design

in asymmetric catalysis

1 Summary

Optimisation of new chiral ligands is a crucial step in reaction development to achieve high levels of enantioselectivity but this process remains a daunting challenge mainly due to the absence of a structured and systematic way to afford better results. In this work, we have coupled the traditional experimental screening approach with multivariate modelling in order to accelerate the ligand design.

In **Chapter 2**, this has been applied to the reoptimization of a copper-catalysed ACA of alkylzirconium species that failed on sterically challenging substrates, which now achieves high reactivity and enantioselectivity thanks to the development of ligand **L17**. Interestingly, predictive modelling allowed us to identify a maximum in selectivity based on the structural diversification of the alkyl substituents. Such information is valuable to stop working on the expensive process of ligand development and put a clear end to ligand design. This is a clear advantage compared to the traditional approach using chemical intuition and extensive screening. Additionally, we proposed an independant multiobjective ranking of the synthesized ligands to select the best ones according to their overall experimental results (yield *and* *ee*), which produced **L17** as the best trade-off. Mechanistic study also confirmed the complexity of interactions involved in metal-catalyzed asymmetric transformations, and showcased the superiority of data-led approaches compared to TS-based strategies in cases where there is a clear lack of mechanistic understanding.

During model construction, the use of ligands with flexible substituents prompted us to investigate the impact of conformer ensembles on physical-organic descriptors such as Sterimol parameters. We realised that substituent flexibility could result in

large amplitudes of underestimated uncertainty in model construction. More importantly, uncertainty due to the range of conformer values was sometimes found to exceed the standard deviation of models up to a difference of 1 kcal/mol, above the accuracy required for accurate predictions in enantioselective catalysis. As a result, wSterimol was developed to improve the famous steric Sterimol parameters on flexible catalysts and the use of wSterimol was applied in several case studies (**Chapter 3**).

Finally, further application of the ligand design workflow to the development of a new copper-catalysed ACA to exocyclic enones assisted us in identifying a promising new ligand (**L46**) that is currently under further investigation (**Chapter 4**). Ligand **L46** was discovered by exploring the phosphoramidite ligand space, which proved to be of paramount importance in the ligand design process. Inspired by the Denmark's group,[1] rational exploration of the phosphoramidite ligand space might lead us in a near future to compute the Universal Training Set (UTS) for phosphoramidite ligands.

Although the data-led approach proved successful and superior to a traditional experimental screening, several limitations were identified in this work. In **Chapter 2**, an unpredicted selectivity cliff was for instance identified, that is, measured *ee* of new ligands were significantly different from their predicted values and outside their error intervals. Such misleading effect is always a possibility in predictive modelling, even in TS-based approaches, and usually occurs if molecular features do not satisfactorily describe key interactions in diastereoselective TSs. Here, it showcased that even a statistically significant and validated model can fail

grasping subtle interactions, which was solved with additional data and a better diversity of molecular descriptors.

Additionally, **Chapter 2** was dedicated to the development of a new ligand affording high *ee* to a broader scope of α,β-unsaturated ketones. Our data-led approach successfully used a challenging but unique substrate **2.1a** to design a new ligand (**L17**), but it is worth noting that it might have led to an optimized ligand **L17** that is too specific, thus yielding high enantioselectivity only for substrates that are structurally-related to **2.1a**. Fortuitously, we found that the method achieved up to 99% yield and 95% *ee* on a broad range of substrates. To decrease the impact of chance in ligand design, a healthier approach might be to generate data for multiple substrates possessing different steric and electronic features, as employed by the Sigman group.[2] Obviously, such consideration entails the generation of new molecular descriptors to describe the chemical features of theses substrates to be included in the model.

In **Chapter 4**, identification of a ligand, which possess a modular and synthetically accessible scaffold while providing a large range of *ee* values for quantitative model construction, proved challenging. There was indeed limited incentive to build a model, as the amount of synthetically accessible ligands to predict would be of one digit or, conversely, a large number of predicted ligands would be infeasible. This is a clear limitation of the data-led approach, because it is only viable if the initial data span a workable range of *ee* values (0–40% *ee*) and if the corresponding synthetically accessible ligand space is large enough to justify modelling it to prioritise ligands for synthesis. Similarly, we found that structural variation of ligands should remain limited in order to obtain a statistically significant model

possessing a tight margin of error, mainly due to the scarcity of data that easily lead to overfitted models. Indeed, substantial structural variation requires more molecular descriptors, a number that is limited by the amount of datapoints to avoid overfitting. Such conundrum would necessarily require the use of better algorithms or the easy generation of data of large sizes in metal-catalyzed asymmetric transformations (>500 datapoints), and hence high-throughput synthesis and purification of ligands.

2 The future of ligand design

Although all models are inherently wrong and limited, QSSR has much added value compared to others ways of tackling ligand optimisation. But there remain many challenges for the data-driven approach to become a go-to method.

First, the design of chiral ligands generally aims to develop catalysts which afford high enantioselectivity with a wide variety of substrates, whereas the model is usually constructed on a unique prototypical substrate.[3] To avoid grasping specific substrate features, and limiting the scope of newly developed catalysts, several starting materials that are sterically and electronically dissimilar should be included in future models as developed by the Sigman group.[4]

Second, ligand synthesis is prioritized based on the predicted *ee* of a model, and its corresponding uncertainty. However, a better selection process should take into account the complexity of synthesis of ligands as it is the bottleneck of the process. For instance, synthetically lengthy ligands should be of lower priority than an easy-to-synthesize ligand even if they both provide valuable information to the model. Likewise, the tolerated uncertainty for synthesis of a ligand should be proportional

to its synthesis complexity. For example, a 10-step ligand predicted at 95% *ee* (±5% *ee*) should be of lower priority than a 2-step ligand predicted at 90% *ee* (±10% *ee*), because both are likely to be excellent ligands (>90% ee) but one requires a lot of resources that might not be worth the predicted uncertainty.

Third, initial structural exploration of ligands is of critical importance, but it is often limited due to the synthetic effort associated to it. In the future, laboratories will likely possess sets of catalysts that contain representative ligand structures rationally mapping most of the ligand space.

Fourth, one of the main current problems in asymmetric catalysis is the scarcity of data. This may be explained by two factors. On one hand, the need to reproduce each reaction at least twice doubles the amount of laboratory work. As a result, the use of screening equipment (*e.g.* 48 well-plates) is attractive although it is worth noting that robots also have reproducibility issues.[5,6] On the other hand, the synthesis of new ligands *in high purity* within a few steps remains the bottleneck of the design process. For instance, the high-throughput synthesis of phosphoramidites using robots has been attempted, but the results were mitigated due to the absence of purification.[7] An option could be to streamline purification of phosphoramidites using automatic mass-directed purification technologies.[8] The high-throughput screening setup needed for acquiring large amount of data, however, remains out of reach of organic laboratories and most small to medium-sized companies, such that the need for robotic infrastructure, and expertise in running the robots, is likely prohibitive in making the QSSR approach a go-to methodology in ligand design. Automation nevertheless remains an active research area particularly in drug discovery,[9] from which ligand design could benefit.

Finally, new algorithms should be created to take into account the scarcity of data as found in metal-catalyzed asymmetric transformations. For instance, the data generated for each ligand design is utilized only once during the data-driven approach, which does not seem effective. This is particularly true considering that it is common for laboratories to develop a series of closely related reactions. A rising regression approach is the use of Transfer Learning (TL),[10] which uses the knowledge acquired in previous datasets and tweaks the resulting model with a smaller but specialized dataset. Thus, large datasets initially required for machine learning algorithms, such as those used by the Doyle's group,[11] now can be reduced to moderate size datasets (~50 datapoints), which looks like it might be a particularly promising approach to use in asymmetric catalysis.

3 References

1 A. F. Zahrt, J. J. Henle, B. T. Rose, Y. Wang, W. T. Darrow and S. E. Denmark, *Science*, 2019, **363**, eaau5631.

2 A. Milo, A. J. Neel, F. D. Toste and M. S. Sigman, *Science*, 2015, **347**, 737–743.

3 R. Ardkhean, M. Mortimore, R. S. Paton and S. P. Fletcher, *Chem. Sci.*, 2018, **9**, 2628–2632.

4 E. N. Bess, A. J. Bischoff and M. S. Sigman, *Proc. Natl. Acad. Sci.*, 2014, **111**, 14698–14703.

5 J. G. de Vries and L. Lefort, *Oil Gas Sci. Technol. – Rev. d'IFP Energies Nouv.*, 2013, **68**, 519–528.

6 K. P. Bryliakov, *ACS Catal.*, 2019, **9**, 5418–5438.

7 L. Lefort, J. A. F. Boogers, A. H. M. De Vries and J. G. De Vries, *Org. Lett.*, 2004, **6**, 1733–1735.

8 J. Boström, D. G. Brown, R. J. Young and G. M. Keserü, *Nat. Rev. Drug Discov.*, 2018, **17**, 709–727.

9 G. Schneider and D. E. Clark, *Angew. Chem. Int. Ed.*, 2019, **58**, 10792–10803.

10 J. S. Smith, B. T. Nebgen, R. Zubatyuk, N. Lubbers, C. Devereux, K. Barros, S. Tretiak, O. Isayev and A. E. Roitberg, *Nat. Commun.*, 2019, **10**, 2903.

11 D. T. Ahneman, J. G. Estrada, S. Lin, S. D. Dreher and A. G. Doyle, *Science*, 2018, **360**, 186–190.

6

Experimental section

1 General information

Procedures were all carried out in flame-dried flasks with anhydrous solvents under argon atmosphere, except where stated otherwise. Analytical thin-layer chromatography (TLC) was conducted on silica gel coated aluminium-backed plates (Silica Gel 60 F254, Merck). Visualization was performed by UV light (254 nm), *p*-anisaldehyde, ceric ammonium molybdate (CAN) and aqueous basic potassium permanganate ($KMnO_4$) stains as stated in the general methods. Flash column chromatography was carried out using VWR (40-63 μm) silica gel or Sigma Aldrich silica gel. SCX column chromatography was carried out using Isolute® flash SCX-2 columns from Biotage.

Reaction temperature at 0 °C was achieved using an ice-water bath. The reactions were regularly topped up with ice and wrapped with cotton in order to keep the reaction at 0 °C if stirred overnight. Light sensitive reactions were processed under aluminium foil protection. Preformed ligand-copper complexes were filtered under argon atmosphere through polytetrafluorethane (PTFE) syringe filter (13 mm, 0.2 μm) from Camlab.

All NMR spectra were recorded at room temperature. ^{1}H, ^{13}C, ^{19}F and ^{31}P nuclear magnetic resonance (NMR) experiments were carried out using “AVG-400” (Bruker AVIIIHD 400 nanobay 400/100 MHz), “AVH-400” (Bruker AVIIIHD 400 nanobay 400/100 MHz) or “AVC-500” (Bruker AVII 500 with 13C cryoprobe 500/125 MHz) spectrometers. Quantitative ^{1}H NMR experiments were carried out using “AV700” (Bruker AVIII 700 with He cryoprobe). Chemical shifts (δ) were reported in part per million (ppm), referenced to the residual solvent peak. Scalar coupling patterns were described as singlet (s), doublet (d), triplet (t), quartet (q), quintet (p) or

multiplet (m). Broad peaks are indicated as broad (br). Coupling constants (J) were quoted to one decimal place in hertz (Hz). Chemical shifts were quoted to two decimal places in ^{1}H NMR and one decimal place in ^{13}C NMR, ^{19}F and ^{31}P NMR. HSQC, COSY and HMBC based experiments were performed to aid the assignment of spectra.

Chiral HPLC separations were achieved using an Agilent 1260 Infinity series normal phase HPLC unit and HP Chemstation software. Retention times (t_R) are given in min. Chiralpak® columns (250×4.6 mm), fitted with matching Chiralpak® Guard Cartridges (10×4 mm), were used as specified in the text. Chiral SFC (supercritical fluid chromatography) separations were conducted on a Waters Acquity UPC2 system using Waters Empower software. Chiralpak® columns (150 × 3 mm, particle size 3 μm) were used. Solvents used were of HPLC grade (Fisher Scientific, Sigma Aldrich or Rathburn). All eluent systems were isocratic, except where stated otherwise.

Infra-red spectra were recorded on a Bruker Tensor 27 FTIR spectrometer equipped with a PIKE Miracle Attenuated Total Reflectance sampling accessory using a solid sample or thin film for liquid compounds ($CHCl_3$). IR data was reported in wavenumbers (cm^{-1}).

High Resolution Mass spectra were carried out by internal service at the University of Oxford. Electron spray ionisation (ESI^+) was recorded on a Fisons Platform II. Electron ionisation (EI)/Chemical ionisation (CI) was performed on an Agilent 7200 quadrupole time of flight (Q-ToF) instrument equipped with a direct insertion probe supplied by Scientific instrument Manufacturer (SIM) GmbH. Instrument control and data processing were performed using Agilent MassHunter software. The system

was calibrated on the day of the analysis and its mass accuracy with external calibration (as used for these experiments) is better than 5 ppm for 24 h following calibration. Source conditions for both EI and CI were adjusted to maximise sensitivity, the reagent gas used in CI was either methane or ammonia. Atmospheric pressure chemical ionisation ($APCI^+$) was performed using a Thermo Exactive mass spectrometer equipped with Waters Acquity liquid chromatography system. Instrument control and data processing were performed using Thermo Xcalibur Software. The system was calibrated on the day of the analysis and its mass accuracy with external calibration (as used for these experiments) is better than 5 ppm for 24 h following calibration. The mass spectrometry was operated using the APCI probe and resolution was set to 50,000. APCI source conditions were adjusted to maximise sensitivity. A mixture of 10% water, 89.9% methanol and 0.1% formic acid was used to transport samples to the mass spectrometer at a flow rate of 0.2 mL/min.

Chemical names were generated from CambridgeSoft ChemBioDraw Ultra programme (version 17.1.0.105). Optical rotations ($[\alpha]^{T}_{D}$) were recorded from a Perkin Elmer 241 Polarimeter and are reported in degree·ml(·g·dm)$^{-1}$. Samples were prepared at concentration (c) measured in g·100 ml^{-1}.

2 Chemicals

Unless stated otherwise, commercially available reagents were purchased from Sigma-Aldrich, Fisher Scientific, Apollo Scientific, Acros Organics, Strem Chemicals, Alfa Aesar, Fluorochem or TCI UK and were used without further purification. Deuterated solvents were purchased from Sigma-Aldrich ($CDCl_3$). The 99.99% purity

CuCl was from Sigma-Aldrich and was used without any further purification. Dry Trimethylsilyl chloride (TMSCl) under inert atmosphere was used without further purification from Sigma-Aldrich, and was distilled fresh and stored in a Schlenk flask with CaH_2(s) under an argon atmosphere when stated differently in the text. PCl_3 from Sigma-Aldrich was freshly distilled every time before use. Anhydrous Et_2O, CH_2Cl_2, THF, pentane, toluene, DMF, TBME and 1,4-dioxane were obtained from mBraun SPS-800 solvent purification system equipped with anhydrous alumina columns. Anhydrous THF was further dried onto 4 Å molecular sieves and degassed with argon when used with very water-sensitive reagents such as reactive metal alkyls. Anhydrous MeOH and other solvents were used as purchased. Anhydrous EtOH was dried onto 4 Å molecular sieves.

$AgNTf_2$ was prepared according to a procedure developed by Huber and Rolling.[1]

3 General procedures

3.1 Preparation of copper-catalysed conjugate addition products

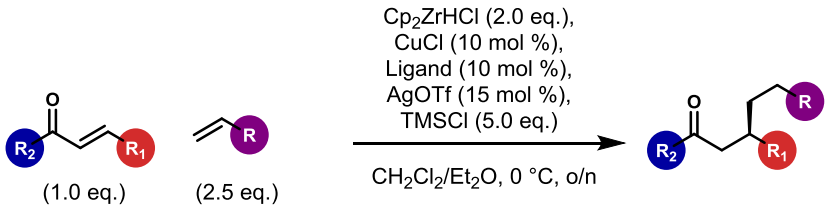

General Procedure A (racemic product):

In a flamed dried round bottom flask was added CuCl (0.1 eq.), (*R,R*) ligand **L17** (0.055 eq.) and (*S,S*) ligand **L6** (0.055 eq.). The flask was purged (3 × argon/vacuum), covered with aluminium foil to protect it from the light and dry

Et_2O (2 mL) was then added under an argon atmosphere. The resulting colourless clear solution was stirred for 1 h at rt.

In the meantime, Cp_2ZrHCl (2.0 eq.) was added to a second flame dried round bottom flask, purged (3 × argon/vacuum), and covered with aluminium foil to protect it from the light. Addition of dry CH_2Cl_2 (0.5 mL) under an argon atmosphere forms a milky solution. Alkene (2.5 eq.) was rapidly added during the next minute as the Schwartz reagent is unstable with CH_2Cl_2 after about 10 min. After stirring for 15 min, the resulting yellow clear solution was manually agitated to remove the traces of Schwartz reagent on the sides of the flask and stirring was continued.

After stirring the foiled flask containing CuCl for 1 h, AgOTf (0.15 eq.) was added, and the grey-brown cloudy solution was stirred for precisely 15 min (results become less reproducible if stirring continues for over 20 min). The mixture was then transferred over about 30 sec via syringe using a syringe filter to the yellow clear Zr-containing solution. The resulting black mixture was then cooled with an ice bath and stirred for a further 5 min before the enone (1.0 eq.) and then TMSCl (5.0 eq.) were added dropwise via syringe. Stirring at 0 °C was continued overnight for about 15 h. The reaction was then quenched by the addition of NH_4Cl (1 M aq., *ca* 0.1 mL) and stirring was continued for 30 min. The mixture was concentrated under reduced pressure then diluted with hexane (*ca* 1mL). The crude mixture was purified by flash column chromatography.

Note: These reactions require ligand to give product, as (S,S) ***L17*** *was not available we used (S,S) ligand* ***L6*** *as a pseudoenantiomer* for *(R,R)* ***L17****. Using this procedure generally gives products with ee's between 0% (rac) and ~30% ee.*

General Procedure B (asymmetric product):

In a flame-dried round bottom flask was added CuCl (0.1 eq.) and (*R,R*) Ligand **L17** (0.11 eq.). The flask was purged (3 × argon/vacuum), covered with aluminium foil to protect it from the light and dry Et_2O (2 mL) was then added under an argon atmosphere. The resulting colourless clear solution was stirred for 1 h at rt.

In the meantime, Cp_2ZrHCl (2.0 eq.) was added to a second flame dried round bottom flask, purged (3 × argon/vacuum), and covered with aluminium foil to protect it from the light. Addition of dry CH_2Cl_2 (0.5 mL) under an argon atmosphere forms a milky solution. Alkene (2.5 eq.) was rapidly added during the next minute as the Schwartz reagent is unstable with CH_2Cl_2 after about 10 min. After stirring for 15 min, the resulting yellow clear solution was manually swirled in order to remove the traces of Schwartz reagent on the sides of the flask and stirring was continued.

After stirring the foiled flask containing CuCl for 1 h, AgOTf (0.15 eq.) was added, and the grey-brown cloudy solution was stirred for precisely 15 min. The mixture was then transferred over about 30 sec via syringe using a syringe filter to the yellow clear solution. The resulting black mixture was then cooled with an ice bath and stirred for a further 5 min before the enone (1.0 eq.) and then TMSCl (5.0 eq.) were added dropwise via syringe. Stirring at 0 °C was continued overnight for about 15 h. The reaction was then quenched by the addition of NH_4Cl (1 M aq., *ca* 0.1 mL) and stirring was continued for 30 min. The mixture was concentrated under reduced pressure then diluted with hexane (1 mL). The crude mixture was purified by flash column chromatography.

3.2 Preparation of enones

General Procedure C:

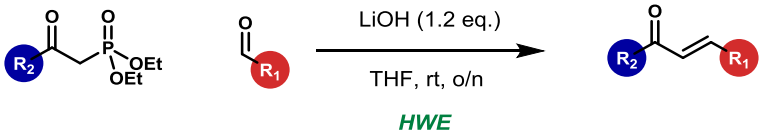

According to a procedure reported by Jacobson *et al.*,[2] lithium hydroxide (1.2 eq.) and the diethyl phosphonate (1.05 eq.) were added sequentially to a solution of the aldehyde (1.0 eq.) in THF (0.2 mmol·mL^{-1}). The reaction was stirred for 15 h, and then concentrated under reduced pressure. The residue was dissolved in Et_2O, and washed with aqueous hydrochloric acid (1 M, 2 × *ca* 20 mL) then with saturated aqueous sodium bicarbonate solution (2 × *ca* 20 mL). The combined organic phase was dried over $MgSO_4$, filtered and concentrated under reduced pressure. The (*E*)-enone was isolated after flash column chromatography.

3.3 Preparation of amines

General Procedure D:

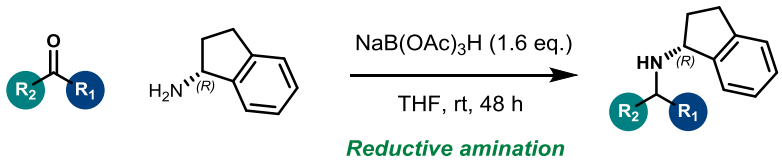

According to a modified procedure reported by Abdel-Magid *et al.*,[3] *(R)*-2,3-dihydro-1H-inden-1-aminium chloride (1.0 eq.) was mixed with aq. NaOH (2 M) until pH paper indicated 12-14. The aqueous phase was extracted with CH_2Cl_2 (3 × 20 mL). The combined organic phases were dried over $MgSO_4$, filtered and concentrated under reduced pressure. Then the ketone (1.0 eq.) was immediately added to a stirring solution of concentrated amine in dry THF (0.25 mmol·mL^{-1}) at rt. After 5 min, $NaB(OAc)_3H$ (1.6 eq.) was added into the reaction mixture at rt and the

suspension was stirred for 48 h. The mixture was diluted with Et_2O (*ca* 20 mL) and $NaHCO_3$ (aq. sat., *ca* 20 mL) was added. After 30 min, the organic and aqueous layers were partitioned and the aqueous phase was extracted with Et_2O (3 × 20 mL).

Acid-base purification: To protonate the secondary amine, HCl (aq. 2.0 M) was added dropwise into the organic phase until pH paper indicated 1. The mixture was partitioned between the aqueous and organic phases, and the organic phase was extracted with HCl (aq. 2.0 M). Then CH_2Cl_2 was added to the combined aqueous phases and NaOH (4 M) was added to deprotonate the secondary amine (until pH = 12-14). The mixture was partitioned between aqueous and organic phases. CH_2Cl_2 was used to extract residual product from the aqueous layer (3 × 20 mL). The combined organic phases were dried over $MgSO_4$, filtered and concentrated under reduced pressure to give the desired product.

Although pure enough in practice to carry out the phosphoramidite synthesis, most amines remained impure after acid-base workup for characterisation. We therefore tried to purify the amines through crystallization with various acids but not all attempts were successful. Therefore, pure amines were usually obtained after flash column chromatography unless otherwise stated.

In cases, even the flash column chromatography was unsuccessful and the amine was filtered through a strong cation exchange column ISOLUTE® SCX-2 (propylsulfonic acid) with MeOH to wash off non-basic component followed by ammonia solution in MeOH (2 M), which releases the pure product. Final column chromatography is usually required to remove ammonia contaminant that would interfere with phosphoramidite synthesis.

General Procedure E:

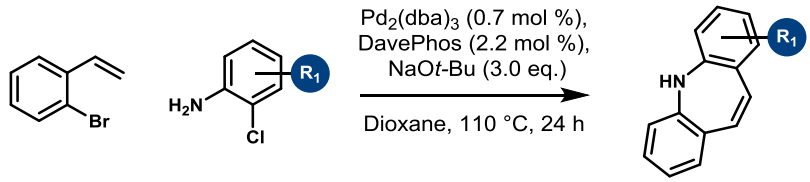

According to a modified procedure,[4] $Pd_2(dba)_3$ (0.75 mol %), DavePhos (2.3 mol %), sodium *tert*-butoxide (3.0 eq.) were added into a flame dried flask and purged (3 × argon/vacuum). 1,4-Dioxane (1.0 mmol/mL), 2-chloroaniline derivative (1.2 eq.) and 2-bromostyrene (1.0 eq.) were added and the resulting mixture was stirred for 24 h at reflux. After completion, hexane (*ca.* 10 mL) was added then the reaction was filtered and concentrated under reduced pressure. The product was isolated after flash column chromatography.

General Procedure F:

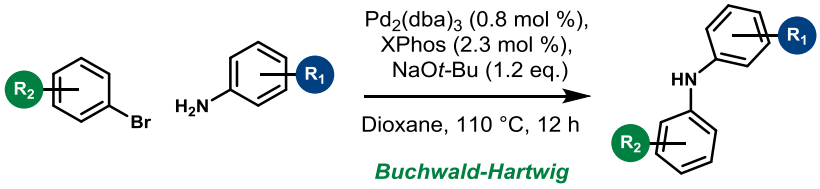

According to a modified procedure,[5] $Pd_2(dba)_3$ (0.8 mol %), XPhos (2.3 mol %), sodium *tert*-butoxide (1.2 eq.) were added into a flame dried flask and purged (3 × argon/vacuum). 1,4-Dioxane (1.0 mmol/mL), aniline (1.2 eq.) and 2-bromostyrene (1.0 eq.) were added and the resulting mixture was stirred overnight at reflux. After completion, Et_2O (*ca.* 10 mL) was added then the reaction was filtered and concentrated under reduced pressure. The product was isolated after flash column chromatography.

3.4 Preparation of phosphoramidite ligands

Important comment about phosphoramidite purification*. Mixing of phosphoramidite with silica (e.g. solid deposit) usually leads to the desctruction of the material, which is why Et_3N is commonly used during column chromatography. The base quenches the acidity of silica, thus preventing the oxidation to occur. However, we have found that Et_3N contaminant was impossible to remove (even in high vaccum, traces remain), and batches with various amount of Et_3N led to irreproducible results in our copper-catalyzed ACA. Accordingly, column chromatography should be carried out <u>without</u> Et_3N, eluting the phosphoramidite compound as fast as possible without interruption with a large amount of solvent and under nitrogen pressure.*

<u>General Procedure G:</u>

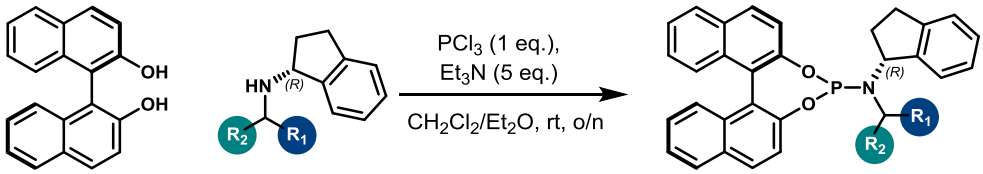

According to a procedure reported by Fletcher *et al.*,[6] triethylamine (5.0 eq.) was added dropwise to a stirred solution of freshly distilled PCl_3 (1.0 eq.) in CH_2Cl_2 (20 mL) at 0 °C. The ice bath was removed and the solution left to warm up to rt before the *(R)*-amine (1.0 eq.) was added. After 5 hours, *(R)*-binaphthol (1.0 eq.) was added to the suspension and the resultant mixture was left to stir for an additional 18 h. Hexane (*ca.* 20 mL) was poured into the flask and most of the white precipitate was filtered through a small pad of celite® and rinsed with a 1:2 mixture of CH_2Cl_2 and hexane (*ca.* 20 mL). The resulting solution was concentrated under reduced pressure to afford a yellow viscuous oil. The phosphoramidite was obtained as a foamy white solid after flash column chromatography.

General Procedure H:

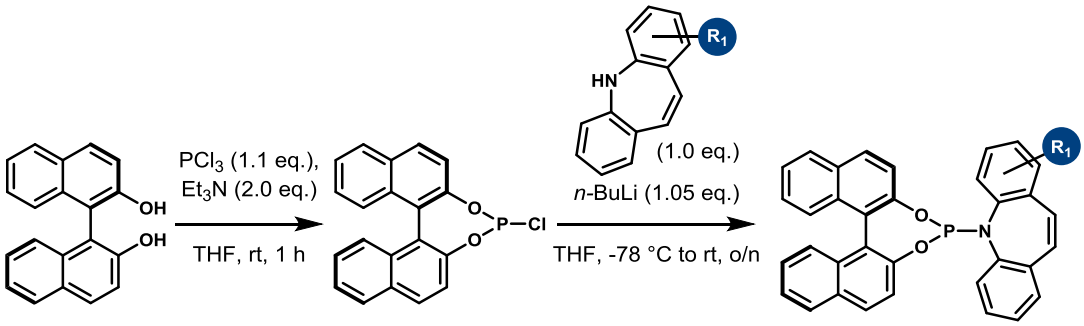

According to a modified procedure reported by Breit *et al.*,[7] PCl_3 (1.1 eq.) and THF (20 mL) were added to a flame dried flask and cooled to 0 °C. Et_3N (2.0 eq.) in THF (10 mL) was added dropwise followed by the dropwise addition of *(R)*-binaphthol (1.0 eq.) in THF (10 mL) over 20 min. The reaction was stirred at 0 °C for 10 min, then for 1 h at rt. The resulting reaction mixture was filtered over celite® under inert atmosphere and washed with THF (30 mL). Solvent was removed under reduced pressure and the resulting foamy white solid was dried under high vacuum before being redissolved in THF (10 mL).

Additionally, *n*-BuLi (2.5 M in hexanes, 1.05 eq.) was added dropwise over 25 min into a solution of the amine (1.0 eq.) in THF (15 ml) at -78 °C and the resulting solution was stirred at this temperature for 1 h. The previously prepared solution of chlorodioxaphosphenine in THF was added dropwise over 20 min. The reaction was then allowed to warm up at rt and stirred overnight. The resulting mixture was concentrated under reduced pressure to afford a pale yellow viscuous oil. The phosphoramidite was obtained as a foamy white solid after flash column chromatography.

4 Characterization of compounds

4.1 Acyclic copper-catalysed ACA products

***(R)*-4-phenyldecan-2-one**

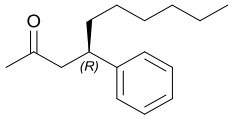

General Procedure B: CuCl (4.0 mg, 0.040 mmol, 0.1 eq.), Ligand **L17** (23.2 mg, 0.040 mmol, 0.1 eq.), Et_2O (2.0 mL), Cp_2ZrHCl (208 mg, 0.807 mmol, 2.0 eq.), CH_2Cl_2 (0.5 mL), hex-1-ene (0.12 mL, 1.010 mmol, 2.5 eq.), AgOTf (15.6 mg, 0.061 mmol, 0.15 eq.), *(E)*-4-phenylbut-3-en-2-one (59 mg, 0.404 mmol, 1.0 eq.), TMSCl (0.26 mL, 2.018 mmol, 5.0 eq.).

The crude mixture was treated as described above and was purified by flash column chromatography (EtOAc/Hexane 5:100, SiO_2) to afford (*R*)-4-phenyldecan-2-one (93 mg, 0.400 mmol, 99%) as a slightly yellow oil.

HPLC analysis indicated an enantiomeric excess of 92% [Chiralpak® IB; flow: 0.8 mL/min; hexane/*i*-PrOH: 99:1; λ = 210 nm; minor enantiomer, t_R = 7.9 min; major enantiomer, t_R = 8.3 min]. Racemic product was realised using *General Procedure A*.

Absolute configuration was assigned by comparison to literature data.[8]

^{1}H NMR (400 MHz, Chloroform-*d*) δ 7.26 – 7.17 (m, 2H, 2 × Ar-H), 7.16 – 7.06 (m, 3H, 3 × Ar-H), 3.03 (dtd, *J* = 9.3, 7.2, 5.5 Hz, 1H, CH), 2.64 (d, *J* = 9.3 Hz, 1H, ½ × CH_2), 2.64 (d, *J* = 5.5 Hz, 1H, ½ × CH_2), 1.94 (s, 3H, CH_3), 1.59 – 1.43 (m, 2H, CH_2), 1.25 – 0.95 (m, 8H, 4 × CH_2), 0.77 (t, *J* = 7.0 Hz, 3H, CH_3).

^{13}C NMR (101 MHz, Chloroform-*d*) δ 208.1, 144.6, 128.4 (2 C), 127.5 (2 C), 126.3, 51.0, 41.3, 36.5, 31.7, 30.7, 29.2, 27.4, 22.6, 14.1.

IR υ_{max} (film): 2926, 2855, 1717, 1453, 1356, 1159.

HRMS (GCMS Methane Cl) *m/z* calcd for $C_{16}H_{25}O$ $[M+H]^+$: 233.1900, found 233.1907.

$[\alpha]^{25}_{589}$ = +10.3 (*c* 1.2, $CHCl_3$) for 92% ee.

Analytical data are in agreement with the literature.[8]

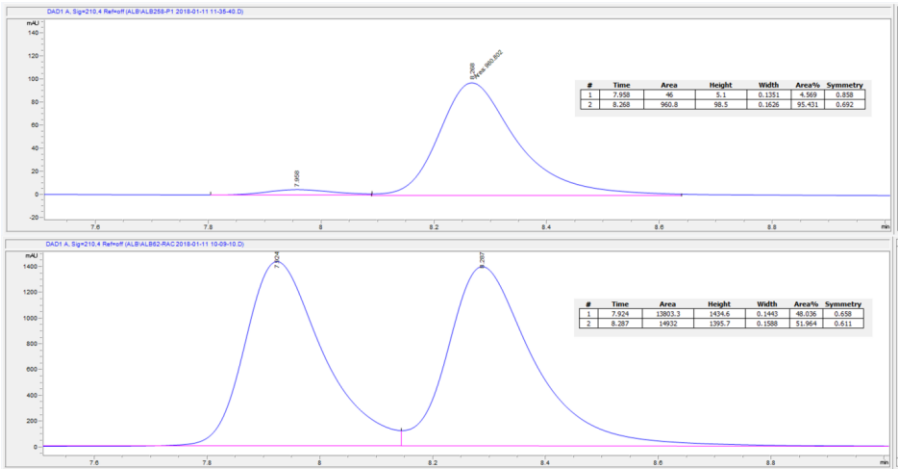

***(R)*-4,8-diphenyloctan-2-one**

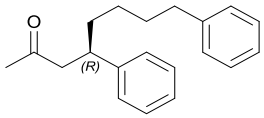

General Procedure B: CuCl (4.0 mg, 0.040 mmol, 0.1 eq.), Ligand **L17** (23.2 mg, 0.040 mmol, 0.1 eq.), Et_2O (2.0 mL), Cp_2ZrHCl (208 mg, 0.807 mmol, 2.0 eq.), CH_2Cl_2 (0.5 mL), 4-phenyl-1-butene (0.15 mL, 1.010 mmol, 2.5 eq.), AgOTf (15.6 mg, 0.061 mmol, 0.15 eq.), (*E*)-4-phenylbut-3-en-2-one (59 mg, 0.404 mmol, 1.0 eq.), TMSCl (0.26 mL, 2.018 mmol, 5.0 eq.).

The crude mixture was treated as described above and was purified by flash column chromatography (EtOAc/Hexane 5:100, SiO_2) to afford (*R*)-4,8-diphenyloctan-2-one (105 mg, 0.372 mmol, 92%) as a slightly yellow oil.

HPLC analysis indicated an enantiomeric excess of 91% [Chiralpak® IB; flow: 0.8 mL/min; hexane/*i*-PrOH: 99:1; λ = 210 nm; minor enantiomer, t_R = 10.3 min; major enantiomer, t_R = 10.9 min]. Racemic product was realised using *General Procedure A*.

Absolute configuration was assigned by comparison to literature data.[8]

^{1}H NMR (400 MHz, Chloroform-*d*) δ 7.36 – 7.10 (m, 10H, 10 × Ar-H), 3.20 – 3.08 (m, 1H, CH), 2.74 (d, J = 10.4 Hz, 1H, ½ × CH_2), 2.74 (d, J = 4.1 Hz, 1H, ½ × CH_2), 2.64 – 2.46 (m, 2H, CH_2), 2.04 (s, 3H, CH_3), 1.75 – 1.50 (m, 4H, 2 × CH_2), 1.33 – 1.15 (m, 2H, CH_2).

^{13}C NMR (126 MHz, Chloroform-*d*) δ 208.0, 144.6, 142.8, 128.6 (2 C), 128.5 (2 C), 128.4 (2 C), 127.6 (2 C), 126.5, 125.7, 51.0, 41.3, 36.4, 35.9, 31.5, 30.8, 27.2.

IR υ_{max} (film): 3026, 2929, 2361, 1716, 1494, 1453, 1356, 1160.

HRMS (APCI$^+$) *m/z* calcd for C_{20} H_{25} O $[M+H]^+$: 281.1900, found 281.1898.

$[\alpha]^{25}_{589}$ = -4.8 (*c* 1.0, $CHCl_3$) for 91% ee.

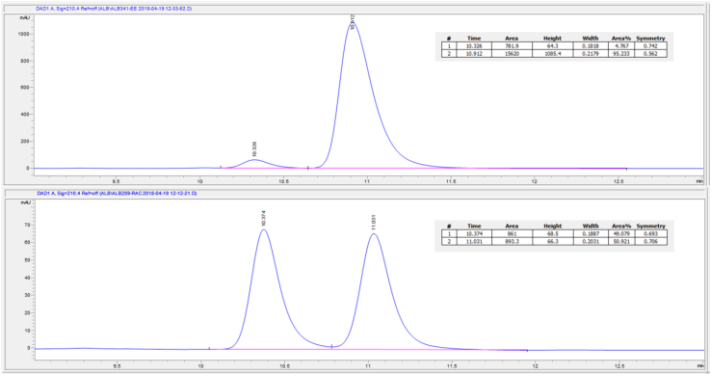

***(R)*-4-isopropyl-8-phenyloctan-2-one**

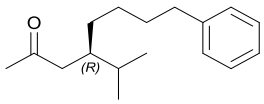

General Procedure B: CuCl (4.0 mg, 0.040 mmol, 0.1 eq.), Ligand **L17** (23.2 mg, 0.040 mmol, 0.1 eq.), Et_2O (2.0 mL), Cp_2ZrHCl (208 mg, 0.807 mmol, 2.0 eq.), CH_2Cl_2 (0.5 mL), 4-phenyl-1-butene (0.15 mL, 1.010 mmol, 2.5 eq.), AgOTf (15.6 mg, 0.061 mmol, 0.15 eq.), (*E*)-5-methylhex-3-en-2-one 75% from Aldrich (53 µL, 0.404 mmol, 1.0 eq.), TMSCl (0.26 mL, 2.018 mmol, 5.0 eq.).

The crude mixture was treated as described above and was purified by flash column chromatography (EtOAc/Hexane 5:100, SiO_2) to afford (*R*)-4-isopropyl-8-phenyloctan-2-one (98.7 mg, 0.402 mmol, >99%) as a slightly yellow oil.

Note: Commercially available starting material was bought from Aldrich but was not pure. As the obtained yield is higher than the purity of commercial reagent, the impurity most likely isomerizes to the starting material in-situ in the presence of copper species. See ^{1}H-NMR below.

SFC analysis indicated an enantiomeric excess of 90% [Chiralpak® ID-3; 1500 psi, 30 °C, flow: 2.0 mL/min; 0.1% to 0.7% MeOH in 5 min; λ = 218 nm; major enantiomer, t_R = 4.20 min; minor enantiomer, t_R = 4.76 min]. Racemic product was realised using *General Procedure A*.

Absolute configuration was assigned by comparison to literature data.[8]

^{1}H NMR (400 MHz, Chloroform-*d*) δ 7.34 – 7.25 (m, 2H, 2 × Ar-H), 7.24 – 7.15 (m, 3H, 3 × Ar-H), 2.62 (t, J=7.5 Hz, 2H, CH_2), 2.39 (dd, *J* = 16.2, 5.6 Hz, 1H, ½ × CH_2), 2.25 (dd, *J* = 16.2, 7.4 Hz, 1H, ½ × CH_2), 2.15 (s, 3H, CH_3), 1.87 (ttd, *J* = 7.4, 5.6, 4.0 Hz, 1H, CH), 1.78 – 1.65 (m, 1H, CH), 1.69 – 1.56 (m, 2H, CH_2), 1.42 – 1.25 (m, 3H, CH_2 & ½ ×

CH_2), 1.19 (ddd, J = 14.2, 7.8, 4.0 Hz, 1H, ½ × CH_2), 0.87 (d, J = 6.8 Hz, 3H, CH_3), 0.84 (d, J = 6.8 Hz, 3H, CH_3).

^{13}C NMR (101 MHz, Chloroform-*d*) δ 209.6, 142.8, 128.5 (2 C), 128.4 (2 C), 125.7, 45.60, 39.5, 36.0, 31.8, 31.3, 30.5, 29.8, 27.1, 19.6, 18.6.

IR υ_{max} (film): 2980, 1715, 1462, 1383, 1251, 1154, 1072.

HRMS (APCI) *m/z* calcd for C_{17} H_{27} O $[M+H]^+$: 247.2056, found 247.2058.

$[\alpha]^{25}_{589}$ = -0.9 (*c* 1.0, $CHCl_3$) for 90% ee.

Analytical data are in agreement with the literature.[8]

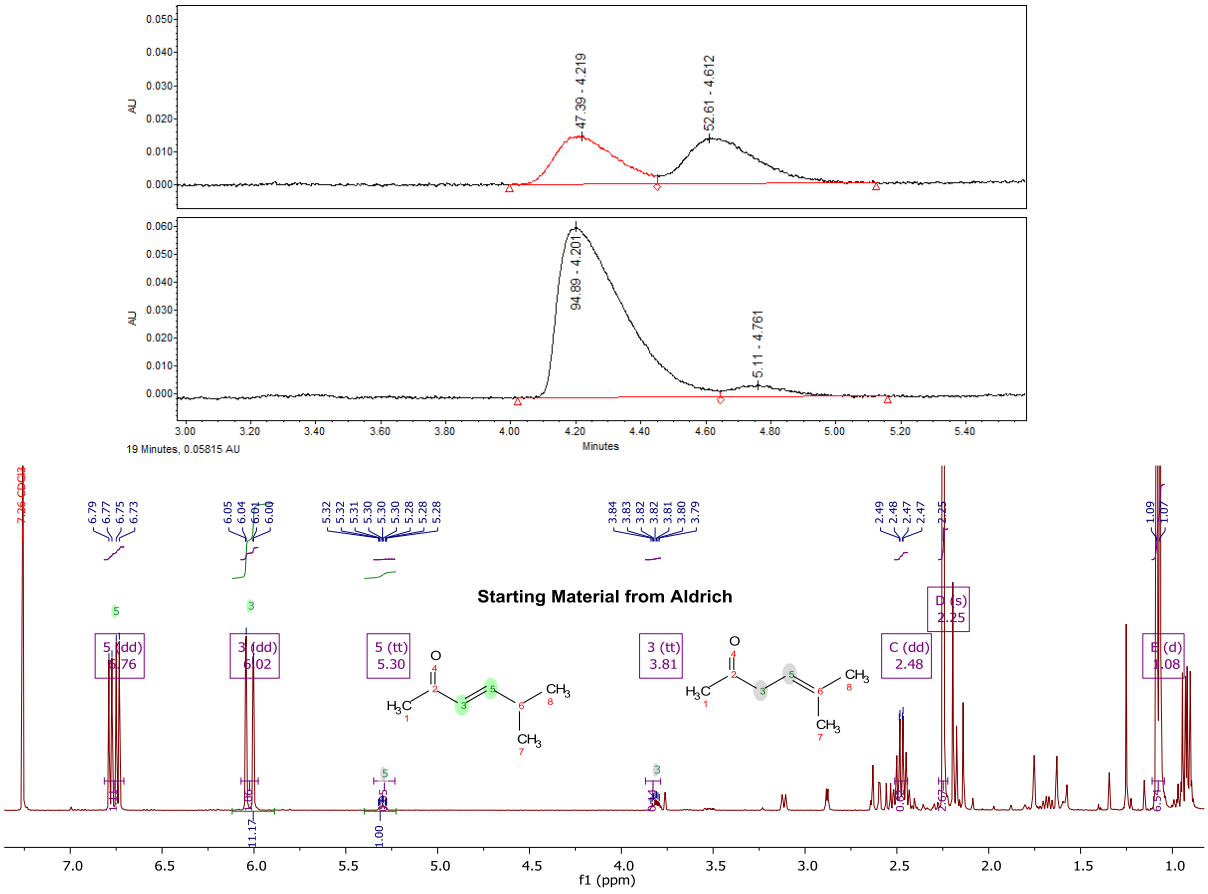

***(R)*-4-(4-chlorophenyl)-8-phenyloctan-2-one**

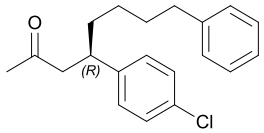

General Procedure B: CuCl (4.0 mg, 0.040 mmol, 0.1 eq.), Ligand **L17** (23.2 mg, 0.040 mmol, 0.1 eq.), Et_2O (2.0 mL), Cp_2ZrHCl (208 mg, 0.807 mmol, 2.0 eq.), CH_2Cl_2 (0.5 mL), 4-phenyl-1-butene (0.15 mL, 1.010 mmol, 2.5 eq.), AgOTf (15.6 mg, 0.061 mmol, 0.15 eq.), (*E*)-4-(4-chlorophenyl)but-3-en-2-one (73 mg, 0.404 mmol, 1.0 eq.), TMSCl (0.26 mL, 2.018 mmol, 5.0 eq.).

The crude mixture was treated as described above and was purified by flash column chromatography (EtOAc/Hexane 5:100, SiO_2) to afford (*R*)-4-(4-chlorophenyl)-8-phenyloctan-2-one (113.8 mg, 0.372 mmol, 89%) as a slightly yellow oil.

HPLC analysis indicated an enantiomeric excess of 81% [Chiralpak® ID; flow: 0.8 mL/min; hexane/*i*-PrOH: 99:1; λ = 210 nm; minor enantiomer, t_R = 12.5 min; major enantiomer, t_R = 13.0 min]. Racemic product was realised using *General Procedure A*.

Absolute configuration was assigned by comparison to literature data.[8]

^{1}H NMR (400 MHz, Chloroform-*d*) δ 7.22 – 7.13 (m, 4H, 4 × Ar-H), 7.12 – 6.98 (m, 5H, 5 × Ar-H), 3.02 (dtd, *J* = 9.6, 7.1, 5.3 Hz, 1H, CH), 2.61 (d, *J* = 7.1 Hz, 2H, CH_2), 2.53 – 2.36 (m, 2H, CH_2), 1.94 (s, 3H, CH_3), 1.63 – 1.37 (m, 4H, 2 × CH_2), 1.23 – 0.98 (m, 2H, CH_2).

^{13}C NMR (101 MHz, Chloroform-*d*) δ 207.5, 143.1, 142.6, 132.1, 129.0 (2 C), 128.7 (2 C), 128.5 (2 C), 128.4 (2 C), 125.8, 50.8, 40.5, 36.3, 35.8, 31.4, 30.8, 27.0.

IR υ_{max} (film): 2980, 1716, 1492, 1382, 1251, 1155, 1089, 954.

HRMS (APCI$^+$) *m/z* calcd for $C_{20}H_{24}OCl$ $[M+H]^+$: 315.1510, found 315.1511.

$[\alpha]^{25}_{589}$ = -1.0 (*c* 1.0, $CHCl_3$) for 81% ee.

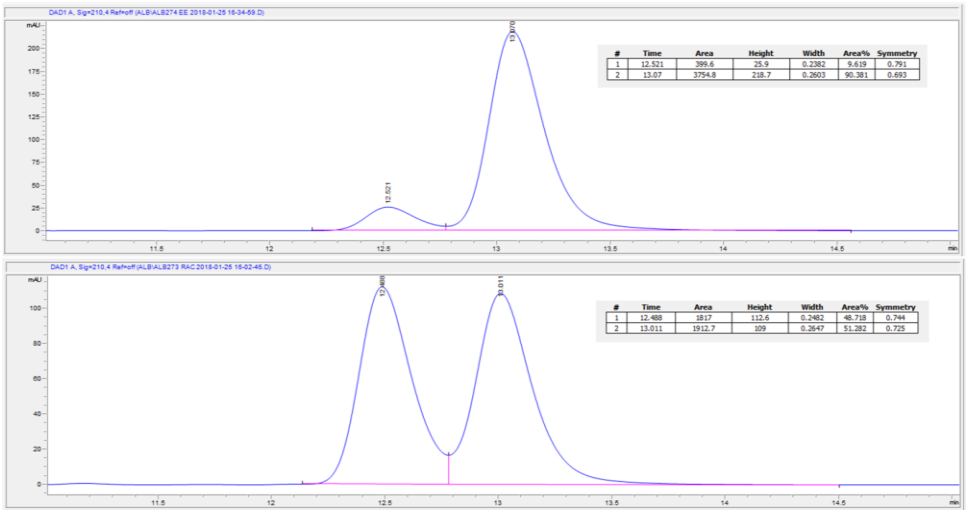

***(R)*-4-(4-methoxyphenyl)-8-phenyloctan-2-one**

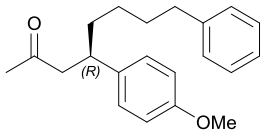

General Procedure B: CuCl (4.0 mg, 0.040 mmol, 0.1 eq.), Ligand **L17** (23.2 mg, 0.040 mmol, 0.1 eq.), Et_2O (2.0 mL), Cp_2ZrHCl (208 mg, 0.807 mmol, 2.0 eq.), CH_2Cl_2 (0.5 mL), 4-phenyl-1-butene (0.15 mL, 1.010 mmol, 2.5 eq.), AgOTf (15.6 mg, 0.061 mmol, 0.15 eq.), (*E*)-4-(4-methoxyphenyl)but-3-en-2-one (71 mg, 0.404 mmol, 1.0 eq.), TMSCl (0.26 mL, 2.018 mmol, 5.0 eq.).

The crude mixture was treated as described above and was purified by flash column chromatography (EtOAc/Hexane 5:100, SiO_2) to afford (*R*)-4-(4-methoxyphenyl)-8-phenyloctan-2-one (69.1 mg, 0.214 mmol, 53%) as a slightly yellow oil.

HPLC analysis indicated an enantiomeric excess of 72% [Chiralpak® ID; flow: 1.0 mL/min; hexane/*i*-PrOH: 99:1; λ = 210 nm; minor enantiomer, t_R = 19.4 min;

major enantiomer, t_R = 22.1 min]. Racemic product was realised using *General Procedure A*.

Absolute configuration was assigned by comparison to literature data.[8]

^{1}H NMR (400 MHz, Chloroform-*d*) δ 7.32 – 7.23 (m, 3H, 3 × Ar-H), 7.21 – 7.07 (m, 4H, 4 × Ar-H), 6.90 – 6.82 (m, 2H, 2 × Ar-H), 3.81 (s, 3H, CH_3), 3.09 (dtd, *J* = 9.4, 7.2, 5.3 Hz, 1H, CH), 2.77 – 2.62 (m, 2H, CH_2), 2.64 – 2.46 (m, 2H, CH_2), 2.03 (s, 3H, CH_3), 1.72 – 1.50 (m, 4H, 2 × CH_2), 1.34 – 1.13 (m, 2H, CH_2).

^{13}C NMR (101 MHz, Chloroform-*d*) δ 208.3, 158.2, 142.8, 136.6, 128.5 (4 C), 128.3 (2 C), 125.7, 114.0 (2 C), 55.3, 51.2, 40.6, 36.6, 35.9, 31.5, 30.8, 27.2.

IR υ_{max} (film): 2980, 1714, 1610, 1512, 1382, 1249, 1155, 1072, 954.

HRMS (APCI$^+$) *m/z* calcd for $C_{21}H_{26}O_2Na$ $[M+Na]^+$: 333.1825, found 333.1826.

$[\alpha]^{25}_{589}$ = -3.4 (*c* 1.0, $CHCl_3$) for 72% ee.

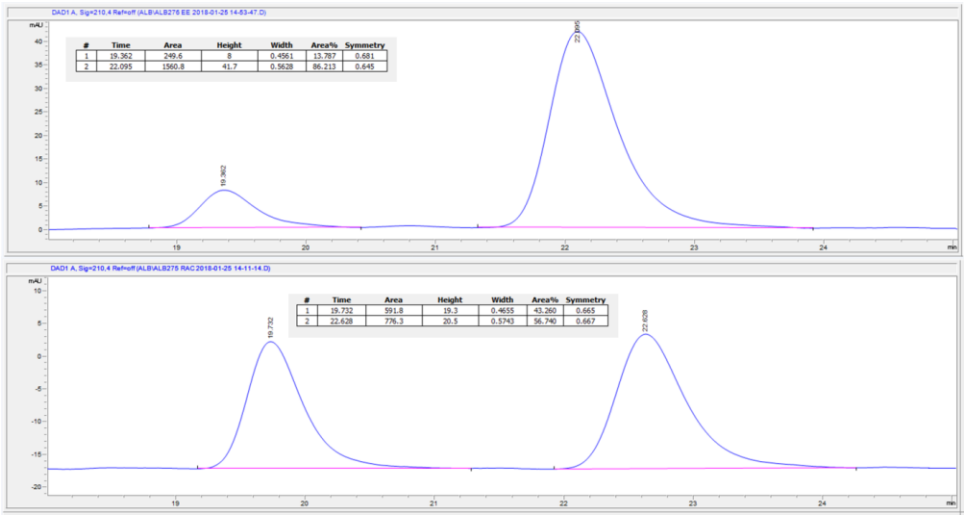

***(R)*-4-(furan-2-yl)-8-phenyloctan-2-one**

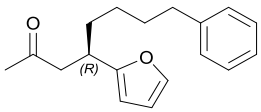

General Procedure B: CuCl (4.0 mg, 0.040 mmol, 0.1 eq.), Ligand **L17** (23.2 mg, 0.040 mmol, 0.1 eq.), Et_2O (2.0 mL), Cp_2ZrHCl (208 mg, 0.807 mmol, 2.0 eq.), CH_2Cl_2 (0.5 mL), 4-phenyl-1-butene (0.15 mL, 1.010 mmol, 2.5 eq.), AgOTf (15.6 mg, 0.061 mmol, 0.15 eq.), (*E*)-4-(furan-2-yl)but-3-en-2-one (55 mg, 0.404 mmol, 1.0 eq.), TMSCl (0.26 mL, 2.018 mmol, 5.0 eq.).

Note: Commercially available (E)-4-(furan-2-yl)but-3-en-2-one was bought from Acros. Prior to use, the enone was dissolved in CH_2Cl_2, filtered to remove an unknown precipitate, and concentrated.^{1}H and ^{13}C NMR confirmed the structure of the enone.

The crude mixture was treated as described above and was purified by flash column chromatography (EtOAc/Hexane 5:100, SiO_2) to afford (*R*)-4-(furan-2-yl)-8-phenyloctan-2-one (66.6 mg, 0.246 mmol, 61%) as a slightly yellow oil.

HPLC analysis indicated an enantiomeric excess of 88% [Chiralpak® IB; flow: 0.8 mL/min; hexane/*i*-PrOH: 99:1; λ = 210 nm; minor enantiomer, t_R = 10.2 min; major enantiomer, t_R = 10.6 min]. Racemic product was realised using *General Procedure A*.

Absolute configuration was assigned by comparison to literature data.[8]

^{1}H NMR (400 MHz, Chloroform-*d*) δ 7.25 – 7.14 (m, 3H, 3 × Ar-H), 7.14 – 7.02 (m, 3H, 3 × Ar-H), 6.19 (dd, *J* = 3.2, 1.8 Hz, 1H, Ar-H), 5.91 (dt, *J* = 3.2, 0.7 Hz, 1H, Ar-H), 3.19 (dtd, *J* = 8.7, 7.0, 5.6 Hz, 1H, CH), 2.75 – 2.44 (m, 4H, 2 × CH_2), 1.99 (s, 3H, CH_3), 1.65 – 1.41 (m, 4H, 2 × CH_2), 1.29 – 1.11 (m, 2H, CH_2).

^{13}C NMR (101 MHz, Chloroform-*d*) δ 207.4, 157.4, 142.6, 141.0, 128.4 (2 C), 128.2 (2 C), 125.6, 110.0, 105.2, 47.9, 35.7, 34.4, 33.8, 31.2, 30.4, 26.8.

IR υ_{max} (film): 2980, 1717, 1461, 1382, 1251, 1151, 1073, 1009.

HRMS (APCI$^+$) *m/z* calcd for $C_{18}H_{23}O_2$ $[M+H]^+$: 271.1693, found 271.1695.

$[\alpha]^{25}_{589}$ = +3.6 (*c* 1.0, $CHCl_3$) for 88% ee.

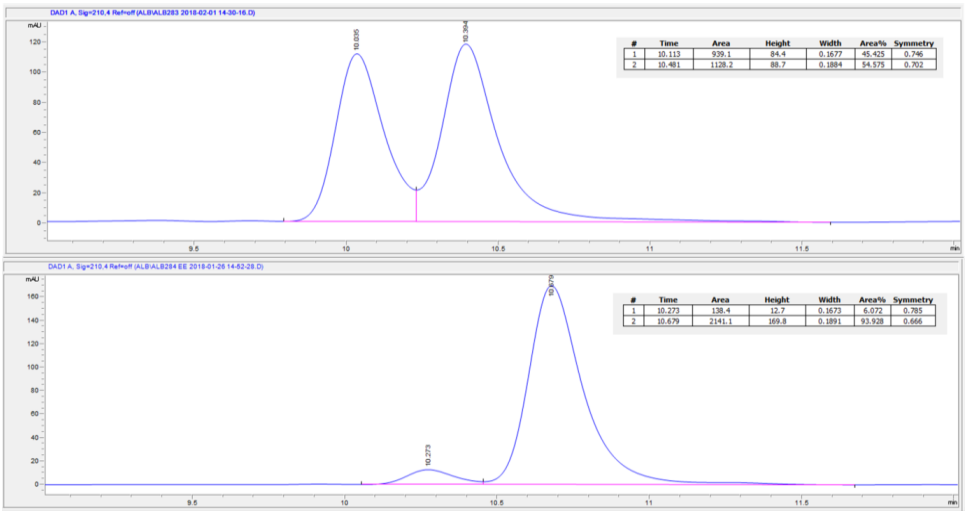

***(R)*-8-phenyl-4-(thiophen-3-yl)octan-2-one**

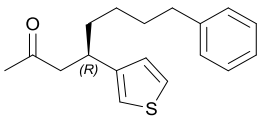

General Procedure B: CuCl (4.0 mg, 0.040 mmol, 0.1 eq.), Ligand **L17** (23.2 mg, 0.040 mmol, 0.1 eq.), Et_2O (2.0 mL), Cp_2ZrHCl (208 mg, 0.807 mmol, 2.0 eq.), CH_2Cl_2 (0.5 mL), 4-phenyl-1-butene (0.15 mL, 1.010 mmol, 2.5 eq.), AgOTf (15.6 mg, 0.061 mmol, 0.15 eq.), (*E*)-4-(thiophen-3-yl)but-3-en-2-one (61 mg, 0.404 mmol, 1.0 eq.), TMSCl (0.26 mL, 2.018 mmol, 5.0 eq.).

The crude mixture was treated as described above and was purified by flash column chromatography (EtOAc/Hexane 5:100, SiO_2) to afford (*R*)-8-phenyl-4-(thiophen-3-yl)octan-2-one (82.0 mg, 0.286 mmol, 71%) as a slightly yellow oil.

HPLC analysis indicated an enantiomeric excess of 76% [Chiralpak® IB; flow: 0.8 mL/min; hexane/*i*-PrOH: 99:1; λ = 210 nm; minor enantiomer, t_R = 12.9 min; major enantiomer, t_R = 13.7 min]. Racemic product was realised using *General Procedure A*.

Absolute configuration was assigned by comparison to literature data.[8]

^{1}H NMR (400 MHz, Chloroform-*d*) δ 7.34 – 7.25 (m, 2H, 2 × Ar-H), 7.24 – 7.13 (m, 4H, 4 × Ar-H), 6.97 – 6.90 (m, 1H, Ar-H), 6.85 – 6.79 (m, 1H, Ar-H), 3.57 – 3.45 (m, 1H, CH), 2.86 – 2.68 (m, 2H, CH_2), 2.67 – 2.50 (m, 2H, CH_2), 2.09 (s, 3H, CH_3), 1.81 – 1.54 (m, 4H, 2 × CH_2), 1.41 – 1.26 (m, 2H, CH_2).

^{13}C NMR (126 MHz, Chloroform-*d*) δ 207.3, 148.5, 142.6, 128.4 (2 C), 128.3 (2 C), 126.6, 125.6, 124.0, 123.0, 51.6, 37.3, 36.4, 35.7, 31.2, 30.7, 26.9.

IR υ_{max} (film): 2930, 1716, 1495, 1453, 1357, 1158.

HRMS (APCI$^+$) *m/z* calcd for $C_{18}H_{23}OS$ $[M+H]^+$: 287.1464, found 287.1461.

$[\alpha]^{25}_{589}$ = -4.6 (*c* 1.0, $CHCl_3$) for 76% ee.

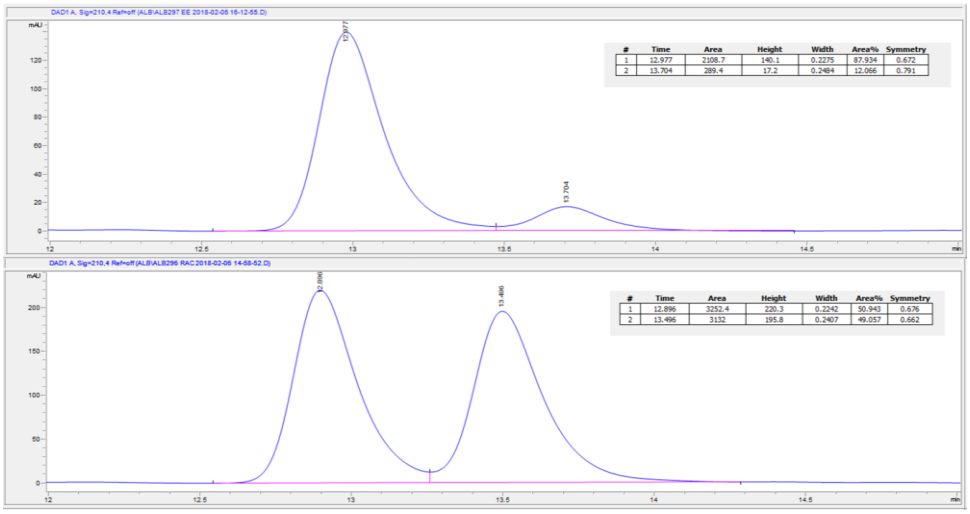

***(R)*-4-(3-bromophenyl)-8-phenyloctan-2-one**

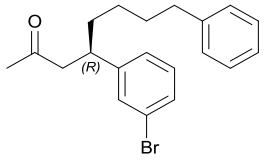

General Procedure B: CuCl (4.0 mg, 0.040 mmol, 0.1 eq.), Ligand **L17** (23.2 mg, 0.040 mmol, 0.1 eq.), Et_2O (2.0 mL), Cp_2ZrHCl (208 mg, 0.807 mmol, 2.0 eq.), CH_2Cl_2 (0.5 mL), 4-phenyl-1-butene (0.15 mL, 1.010 mmol, 2.5 eq.), AgOTf (15.6 mg, 0.061 mmol, 0.15 eq.), (*E*)-4-(3-bromophenyl)but-3-en-2-one (91 mg, 0.404 mmol, 1.0 eq.), TMSCl (0.26 mL, 2.018 mmol, 5.0 eq.).

The crude mixture was treated as described above and was purified by flash column chromatography (EtOAc/Hexane 5:100, SiO_2) to afford (*R*)-4-(3-bromophenyl)-8-phenyloctan-2-one (132.4 mg, 0.367 mmol, 91%) as a slightly yellow oil.

HPLC analysis indicated an enantiomeric excess of 95% [Chiralpak® ID; flow: 0.8 mL/min; hexane/*i*-PrOH: 99:1; λ = 210 nm; minor enantiomer, t_R = 11.7 min; major enantiomer, t_R = 12.3 min]. Racemic product was realised using *General Procedure A*.

Absolute configuration was assigned by comparison to literature data.[8]

^{1}H NMR (400 MHz, Chloroform-*d*) δ 7.39 – 7.25 (m, 4H, 4 × Ar-H), 7.23 – 7.08 (m, 5H, 5 × Ar-H), 3.12 (dtd, *J* = 9.4, 7.1, 5.3 Hz, 1H, CH), 2.72 (d, *J* = 7.1 Hz, 2H, CH_2), 2.64 – 2.47 (m, 2H, CH_2), 2.06 (s, 3H, CH_3), 1.73 – 1.50 (m, 4H, 2 × CH_2), 1.33 – 1.11 (m, 2H, CH_2).

^{13}C NMR (101 MHz, Chloroform-*d*) δ 207.2, 147.1, 142.5, 130.4, 130.1, 129.5, 128.3 (2 C), 128.3 (2 C), 126.4, 125.6, 122.6, 50.5, 40.7, 36.1, 35.7, 31.2, 30.7, 26.9.

IR υ_{max} (film): 2930, 1716, 1593, 1566, 1427, 1358, 1161.

HRMS (APCI$^+$) *m/z* calcd for C_{20} H_{24} O Br $[M+H]^+$: 359.1005, found 359.1000.

$[\alpha]^{25}_{589}$ = -0.3 (*c* 1.0, $CHCl_3$) for 95% ee.

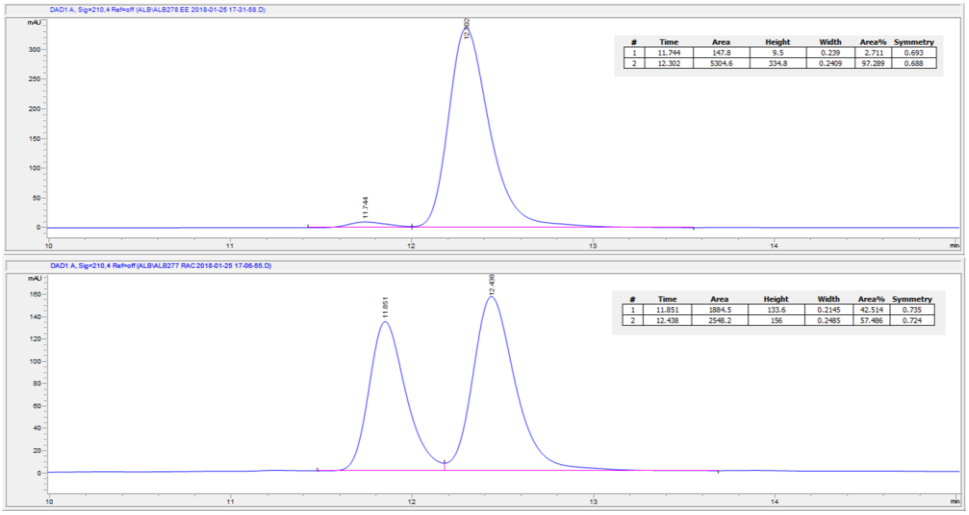

***(R)*-4-(2-bromophenyl)-8-phenyloctan-2-one**

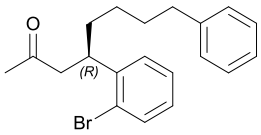

General Procedure B: CuCl (4.0 mg, 0.040 mmol, 0.1 eq.), Ligand **L17** (23.2 mg, 0.040 mmol, 0.1 eq.), Et_2O (2.0 mL), Cp_2ZrHCl (208 mg, 0.807 mmol, 2.0 eq.), CH_2Cl_2 (0.5 mL), 4-phenyl-1-butene (0.15 mL, 1.010 mmol, 2.5 eq.), AgOTf (15.6 mg, 0.061 mmol, 0.15 eq.), (*E*)-4-(2-bromophenyl)but-3-en-2-one (91 mg, 0.404 mmol, 1.0 eq.), TMSCl (0.26 mL, 2.018 mmol, 5.0 eq.).

The crude mixture was treated as described above and was purified by flash column chromatography (EtOAc/Hexane 5:100, SiO_2) to afford (*R*)-4-(2-bromophenyl)-8-phenyloctan-2-one (104.5 mg, 0.291 mmol, 72%) as a slightly yellow oil.

HPLC analysis indicated an enantiomeric excess of 82% [Chiralpak® IB; flow: 0.8 mL/min; hexane/*i*-PrOH: 99:1; λ = 210 nm; minor enantiomer, t_R = 14.4 min;

major enantiomer, t_R = 16.6 min]. Racemic product was realised using *General Procedure A*.

Absolute configuration was assigned by comparison to literature data.[8]

^{1}H NMR (400 MHz, Chloroform-*d*) δ 7.58 (dd, *J* = 8.0, 1.3 Hz, 1H, Ar-H), 7.34 – 7.04 (m, 8H, 8 × Ar-H), 3.77 (p, *J* = 7.2 Hz, 1H, CH), 2.80 – 2.64 (m, 2H, CH_2), 2.57 (ddd, *J* = 8.5, 7.2, 1.7 Hz, 2H, CH_2), 2.11 (s, 3H, CH_3), 1.76 – 1.50 (m, 4H, 2 × CH_2), 1.41 – 1.15 (m, 2H, CH_2).

^{13}C NMR (126 MHz, Chloroform-*d*) δ 207.3, 143.3, 142.6, 133.1, 128.4 (2 C), 128.2 (2 C), 127.8, 127.7, 125.6, 125.1, 50.0, 39.3, 35.7, 35.3, 31.4, 30.1, 26.7.

IR υ_{max} (film): 2930, 1715, 1470, 1356, 1161, 1021.

HRMS (APCI$^+$) *m/z* calcd for C_{20} H_{24} O Br $[M+H]^+$: 359.1005, found 359.1000.

$[\alpha]^{25}_{589}$ = -3.5 (*c* 1.0, $CHCl_3$) for 82% ee.

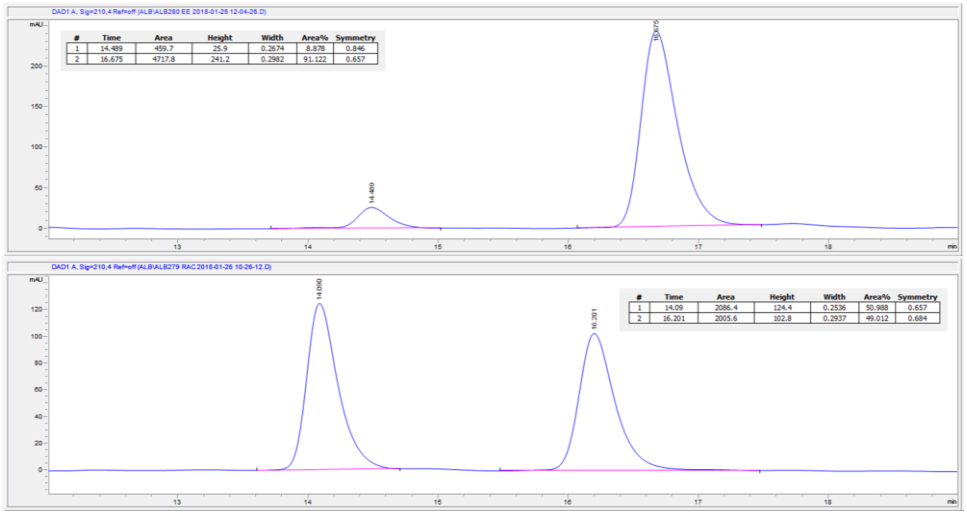

(R)-4-(4-nitrophenyl)-8-phenyloctan-2-one

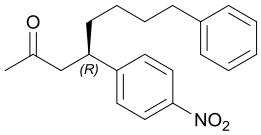

General Procedure B: CuCl (4.0 mg, 0.040 mmol, 0.1 eq.), Ligand **L17** (23.2 mg, 0.040 mmol, 0.1 eq.), Et_2O (2.0 mL), Cp_2ZrHCl (208 mg, 0.807 mmol, 2.0 eq.), CH_2Cl_2 (0.5 mL), 4-phenyl-1-butene (0.15 mL, 1.010 mmol, 2.5 eq.), AgOTf (15.6 mg, 0.061 mmol, 0.15 eq.), (*E*)-4-(4-nitrophenyl)but-3-en-2-one (77 mg, 0.404 mmol, 1.0 eq.), TMSCl (0.26 mL, 2.018 mmol, 5.0 eq.).

The crude mixture was treated as described above and was purified by flash column chromatography (EtOAc/Hexane 5:100, SiO_2) to afford (*R*)-4-(4-nitrophenyl)-8-phenyloctan-2-one (93.3 mg, 0.286 mmol, 71%) as a slightly yellow oil.

SFC analysis indicated an enantiomeric excess of 91% [Chiralpak® ID-3; 1500 psi, 30 °C, flow: 1.5 mL/min; 1.0% to 30.0% MeOH in 5 min; λ = 218 nm; major enantiomer, t_R = 3.57 min; minor enantiomer, t_R = 3.83 min]. Racemic product was realised using *General Procedure A*.

Absolute configuration was assigned by comparison to literature data.[8]

^{1}H NMR (500 MHz, Chloroform-*d*) δ 8.10 – 8.03 (m, 2H, 2 × Ar-H), 7.28 – 6.99 (m, 7H, 7 × Ar-H), 3.19 (ddt, *J* = 12.4, 9.4, 6.2 Hz, 1H, CH), 2.72 – 2.65 (m, 2H, CH_2), 2.54 – 2.36 (m, 2H, CH_2), 1.98 (s, 3H, CH_3), 1.68 – 1.42 (m, 4H, 2 × CH_2), 1.22 – 0.97 (m, 2H, CH_2).

^{13}C NMR (126 MHz, Chloroform-*d*) δ 206.5, 152.6, 146.6, 142.2, 128.4 (2 C), 128.3 (4 C), 125.7, 123.8 (2 C), 50.1, 40.6, 35.9, 35.6, 31.1, 30.6, 26.8.

IR υ_{max} (film): 2931, 1716, 1603, 1517, 1345, 856, 699.

HRMS (APCI$^+$) *m/z* calcd for $C_{20}H_{24}O_3N$ $[M+H]^+$: 326.1751, found 326.1754.

$[\alpha]^{25}_{589}$ = +5.9 (*c* 1.0, $CHCl_3$) for 91% ee.

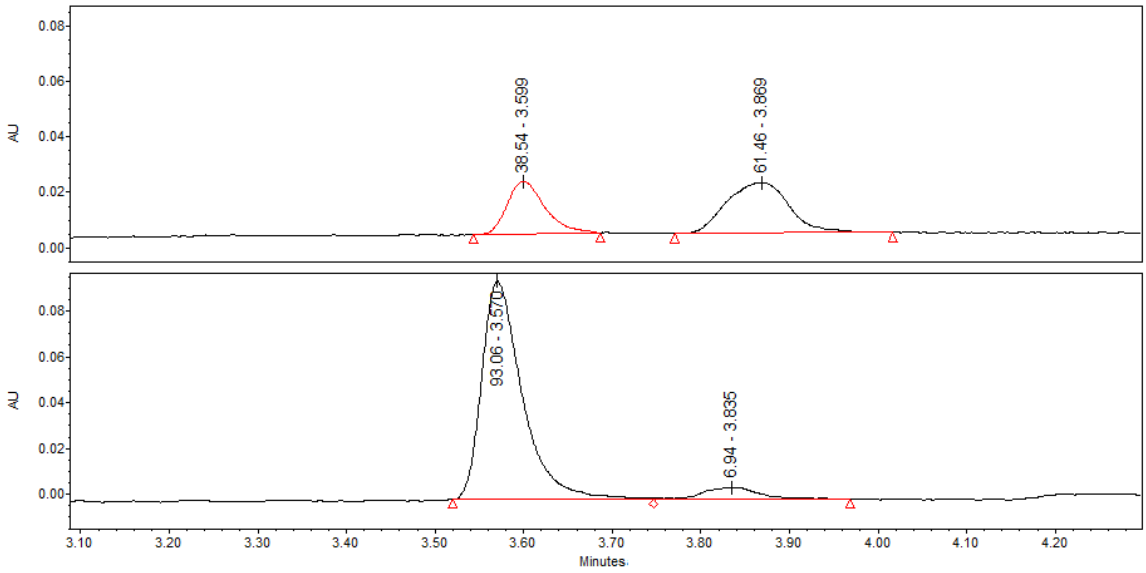

***(R)*-1,3,7-triphenylheptan-1-one**

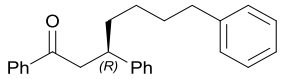

General Procedure B: CuCl (4.0 mg, 0.040 mmol, 0.1 eq.), Ligand **L17** (23.2 mg, 0.040 mmol, 0.1 eq.), Et_2O (2.0 mL), Cp_2ZrHCl (208 mg, 0.807 mmol, 2.0 eq.), CH_2Cl_2 (0.5 mL), 4-phenyl-1-butene (0.15 mL, 1.010 mmol, 2.5 eq.), AgOTf (15.6 mg, 0.061 mmol, 0.15 eq.), (*E*)-chalcone (84 mg, 0.404 mmol, 1.0 eq.), TMSCl (0.26 mL, 2.018 mmol, 5.0 eq.).

The crude mixture was treated as described above and was purified by flash column chromatography (EtOAc/Hexane 5:100, SiO_2) to afford (*R*)-1,3,7-triphenylheptan-1-one (132.8 mg, 0.388 mmol, 96%) as a slightly yellow oil.

HPLC analysis indicated an enantiomeric excess of 78% [Chiralpak® ID; flow: 0.8 mL/min; hexane/*i*-PrOH: 99:1; λ = 210 nm; minor enantiomer, t_R = 13.5 min;

major enantiomer, t_R = 15.6 min]. Racemic product was realised using *General Procedure A*.

Absolute configuration was assigned by comparison to literature data.[8]

^{1}H NMR (400 MHz, Chloroform-*d*) δ 7.85 – 7.78 (m, 2H, 2 × Ar-H), 7.50 – 7.41 (m, 1H, Ar-H), 7.39 – 7.30 (m, 2H, 2 × Ar-H), 7.25 – 6.99 (m, 10H, 10 × Ar-H), 3.30 – 3.09 (m, 3H, CH & CH_2), 2.44 (hept, *J* = 7.1 Hz, 2H, CH_2), 1.76 – 1.39 (m, 4H, 2 × CH_2), 1.28 – 1.06 (m, 2H, CH_2).

^{13}C NMR (126 MHz, Chloroform-*d*) δ 199.1, 144.9, 142.7, 137.2, 132.9, 128.5 (2 C), 128.5 (2 C), 128.3 (2 C), 128.2 (2 C), 128.1 (2 C), 127.6 (2 C), 126.3, 125.6, 46.0, 41.2, 36.1, 35.7, 31.4, 27.2.

IR υ_{max} (film): 2980, 1685, 1494, 1382, 1251, 1153, 1073.

HRMS (APCI$^+$) *m/z* calcd for C_{25} H_{27} O $[M+H]^+$: 343.2056, found 343.2057.

$[\alpha]^{25}_{589}$ = +4.2 (*c* 1.0, $CHCl_3$) for 78% ee.

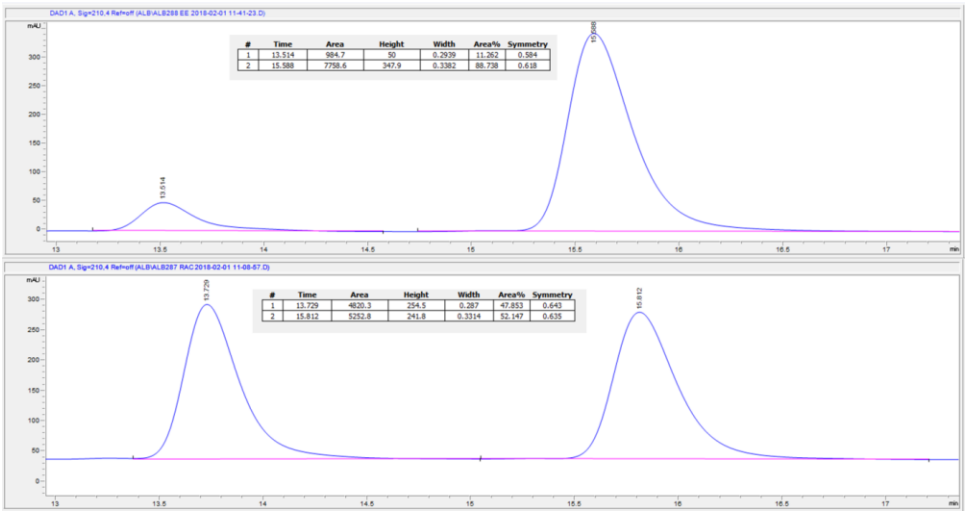

(R)-3-methyl-1,7-diphenylheptan-1-one

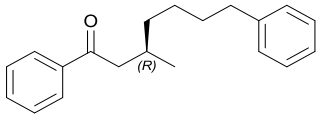

General Procedure B: CuCl (4.0 mg, 0.040 mmol, 0.1 eq.), Ligand **L17** (23.2 mg, 0.040 mmol, 0.1 eq.), Et_2O (2.0 mL), Cp_2ZrHCl (208 mg, 0.807 mmol, 2.0 eq.), CH_2Cl_2 (0.5 mL), 4-phenyl-1-butene (0.15 mL, 1.010 mmol, 2.5 eq.), AgOTf (15.6 mg, 0.061 mmol, 0.15 eq.), (*E*)-1-phenylbut-2-en-1-one (58 µL, 0.404 mmol, 1.0 eq.), TMSCl (0.26 mL, 2.018 mmol, 5.0 eq.).

The crude mixture was treated as described above and was purified by flash column chromatography (EtOAc/Hexane 5:100, SiO_2) to afford (*R*)-3-methyl-1,7-diphenylheptan-1-one (112.5 mg, 0.401 mmol, >99%) as a slightly yellow oil.

HPLC analysis indicated an enantiomeric excess of 91% [Chiralpak® IB; flow: 0.8 mL/min; hexane/*i*-PrOH: 99:1; λ = 210 nm; minor enantiomer, t_R = 9.6 min; major enantiomer, t_R = 10.5 min]. Racemic product was realised using *General Procedure A*.

Absolute configuration was assigned by comparison to literature data.[8]

^{1}H NMR (400 MHz, Chloroform-*d*) δ 8.02 – 7.93 (m, 2H, 2 × Ar-H), 7.61 – 7.55 (m, 1H, Ar-H), 7.52 – 7.46 (m, 2H, 2 × Ar-H), 7.33 – 7.26 (m, 2H, 2 × Ar-H), 7.22 – 7.16 (m, 3H, 3 × Ar-H), 2.96 (dd, *J* = 15.8, 5.7 Hz, 1H, ½ × CH_2), 2.78 (dd, *J* = 15.8, 7.9 Hz, 1H, ½ × CH_2), 2.63 (t, *J* = 7.7 Hz, 2H, CH_2), 2.27 – 2.13 (m, 1H, CH), 1.71 – 1.56 (m, 2H, CH_2), 1.51 – 1.21 (m, 4H, 2 × CH_2), 0.98 (d, *J* = 6.7 Hz, 3H, CH_3).

^{13}C NMR (126 MHz, Chloroform-*d*) δ 200.4, 142.7, 137.5, 132.8, 128.5 (2 C), 128.4 (2 C), 128.2 (2 C), 128.1 (2 C), 125.6, 46.0, 36.9, 35.9, 31.6, 29.7, 26.7, 20.0.

IR υ_{max} (film): 2980, 1685, 1449, 1379, 1252, 1155.

HRMS (APCI$^+$) *m/z* calcd for $C_{20}H_{25}O$ $[M+H]^+$: 281.1899, found 281.1900.

$[\alpha]^{25}_{589}$ = -0.5 (*c* 1.0, $CHCl_3$) for 91% ee.

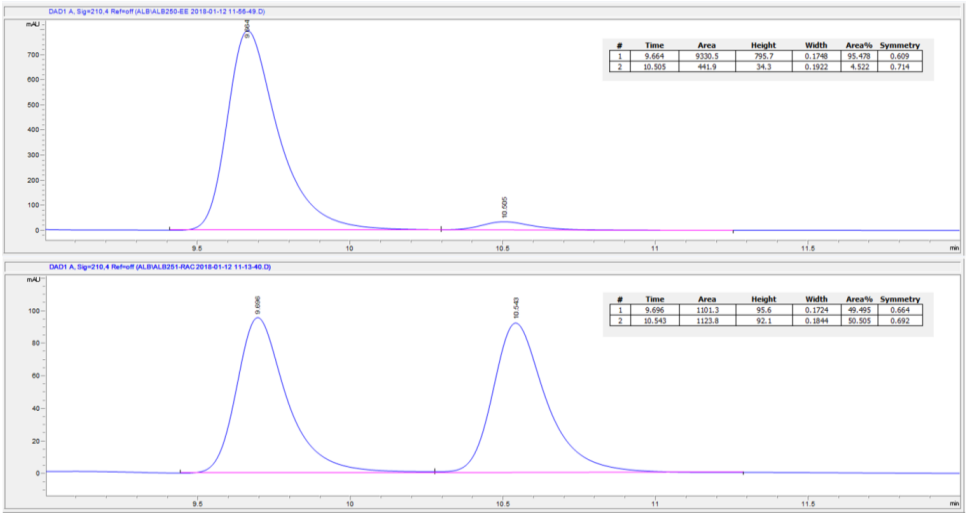

***(R)*-7-methyl-11-phenylundecan-5-one**

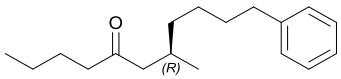

General Procedure B: CuCl (4.0 mg, 0.040 mmol, 0.1 eq.), Ligand **L17** (23.2 mg, 0.040 mmol, 0.1 eq.), Et_2O (2.0 mL), Cp_2ZrHCl (208 mg, 0.807 mmol, 2.0 eq.), CH_2Cl_2 (0.5 mL), 4-phenyl-1-butene (0.15 mL, 1.010 mmol, 2.5 eq.), AgOTf (15.6 mg, 0.061 mmol, 0.15 eq.), (*E*)-oct-2-en-4-one (60 µL, 0.404 mmol, 1.0 eq.), TMSCl (0.26 mL, 2.018 mmol, 5.0 eq.).

The crude mixture was treated as described above and was purified by flash column chromatography (EtOAc/Hexane 5:100, SiO_2) to afford (*R*)-7-methyl-11-phenylundecan-5-one (102.1 mg, 0.392 mmol, 97%) as a slightly yellow oil.

HPLC analysis indicated an enantiomeric excess of 95% [Chiralpak® IC; flow: 1.0 mL/min; hexane/*i*-PrOH: 99:1; λ = 210 nm; minor enantiomer, t_R = 6.9 min;

major enantiomer, t_R = 7.3 min]. Racemic product was realised using *General Procedure A*.

Absolute configuration was assigned by comparison to literature data.[8]

^{1}H NMR (400 MHz, Chloroform-*d*) δ 7.34 – 7.26 (m, 2H, 2 × Ar-H), 7.24 – 7.15 (m, 3H, 3 × Ar-H), 2.63 (t, *J* = 7.7 Hz, 2H, CH_2), 2.43 – 2.33 (m, 3H, CH_2 & ½ × CH_2), 2.22 (dd, *J* = 15.8, 8.0 Hz, 1H, ½ × CH_2), 2.02 (hept, *J* = 6.6, 6.1 Hz, 1H, CH), 1.71 – 1.51 (m, 4H, 2 × CH_2), 1.46 – 1.14 (m, 6H, 3 × CH_2), 0.98 – 0.86 (m, 6H, 2 × CH_3).

^{13}C NMR (126 MHz, Chloroform-*d*) δ 211.4, 142.7, 128.4 (2 C), 128.2 (2 C), 125.6, 50.3, 43.1, 36.8, 35.9, 31.6, 29.2, 26.6, 25.9, 22.4, 19.9, 13.9.

IR υ_{max} (film): 2930, 1712, 1454, 1377.

HRMS (APCI$^+$) *m/z* calcd for $C_{18}H_{29}O$ $[M+H]^+$: 261.2212, found 261.2212.

$[\alpha]^{25}_{589}$ = +6.5 (*c* 1.0, $CHCl_3$) for 95% ee.

Analytical data are in agreement with the literature.[8]

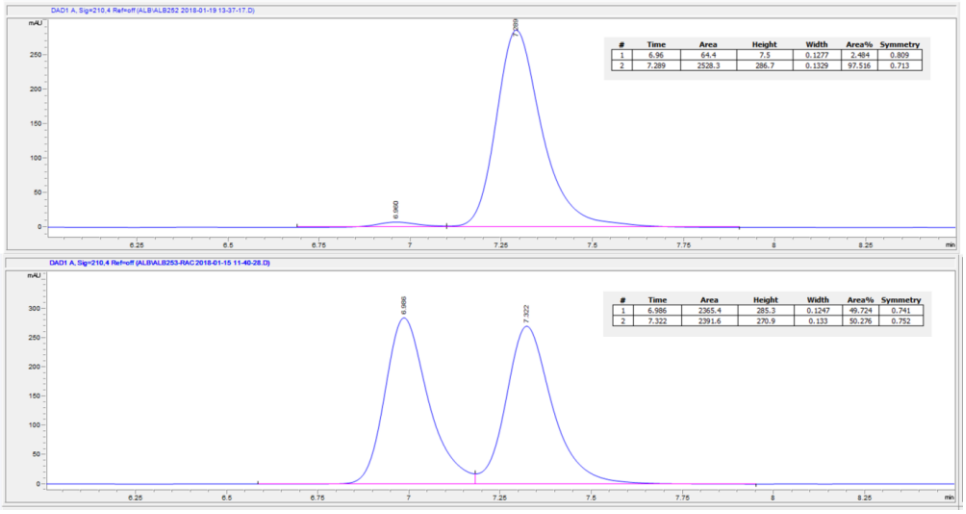

***(6R)*-3,6-dimethyl-10-phenyldecan-4-one**

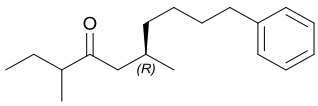

General Procedure B: CuCl (4.0 mg, 0.040 mmol, 0.1 eq.), Ligand **L17** (23.2 mg, 0.040 mmol, 0.1 eq.), Et_2O (2.0 mL), Cp_2ZrHCl (208 mg, 0.807 mmol, 2.0 eq.), CH_2Cl_2 (0.5 mL), 4-phenyl-1-butene (0.15 mL, 1.010 mmol, 2.5 eq.), AgOTf (15.6 mg, 0.061 mmol, 0.15 eq.), (*E*)-5-methylhept-2-en-4-one (60 µL, 0.404 mmol, 1.0 eq.), TMSCl (0.26 mL, 2.018 mmol, 5.0 eq.).

The crude mixture was treated as described above and was purified by flash column chromatography (EtOAc/Hexane 5:100, SiO_2) to afford a mixture of inseparable diastereoisomers (6*R*)-3,6-dimethyl-10-phenyldecan-4-one (83.4 mg, 0.322 mmol, 80%) as a slightly yellow oil.

Quantitative ^{1}H NMR experiment analysis indicated a diastereomeric ratio of 1:1.4.

Diastereoisomer 1: SFC analysis indicated an enantiomeric excess of 96% [Chiralpak® IF-3; 1500 psi, 30 °C, flow: 1.5 mL/min; 1.0% to 30.0% MeOH in 5 min; λ = 218 nm; major enantiomer, t_R = 2.02 min; minor enantiomer, t_R = 2.28 min].

Diastereoisomer 2: SFC analysis indicated an enantiomeric excess of 91% [Chiralpak® IF-3; 1500 psi, 30 °C, flow: 1.5 mL/min; 1.0% to 30.0% MeOH in 5 min; λ = 218 nm; major enantiomer, t_R = 2.02 min; minor enantiomer, t_R = 2.36 min].

Racemic product was realised using *General Procedure A*. Absolute configuration was assigned by comparison to literature data.[8]

Mixture of diastereoisomers:

^{1}H NMR (400 MHz, Chloroform-*d*) δ 7.29 – 7.19 (m, 2H, 2 × Ar-H), 7.19 – 7.09 (m, 3H, 3 × Ar-H), 2.57 (t, *J* = 7.7 Hz, 2H, CH_2), 2.45 – 2.29 (m, 2H, CH & ½ × CH_2), 2.22 (ddd, *J* = 16.5, 7.8, 6.4 Hz, 1H, ½ × CH_2), 2.06 – 1.92 (m, 1H, CH), 1.73 – 1.49 (m, 3H, CH_2 & ½ × CH_2), 1.41 – 1.22 (m, 4H, CH_2 & ½ × CH_2 & ½ × CH_2), 1.21 – 1.09 (m, 1H, ½ × CH_2), 1.01 (dd, *J* = 6.9, 1.2 Hz, 3H, CH_3), 0.88 – 0.81 (m, 6H, 2 × CH_3).

Diastereoisomer 1:

^{13}C NMR (101 MHz, Chloroform-*d*) δ 214.7, 142.8, 128.5 (2 C), 128.4 (2 C), 125.7, 48.9, 48.3, 36.9, 36.0, 31.7, 28.9, 26.8, 26.0, 20.1, 16.0, 11.9.

Diastereoisomer 2:

^{13}C NMR (101 MHz, Chloroform-*d*) δ 214.7, 142.8, 128.5 (2 C), 128.4 (2 C), 125.7, 48.9, 48.2, 36.9, 36.0, 31.7, 28.8, 26.8, 25.9, 20.0, 15.9, 11.8.

***Mixture of diastereoisomers*:**

IR υ_{max} (film): 2930, 2857, 1709, 1455, 1376.

HRMS (APCI^{+}) *m/z* calcd for C_{18} H_{29} O $[M+H]^{+}$: 261.2213, found 261.2212.

$[\boldsymbol{\alpha}]^{25}_{589}$ = +6.5 (*c* 1.0, $CHCl_3$) for 96% ee and 91% ee.

Diastereomeric ratio Experiment (quantitative ^{1}H NMR)

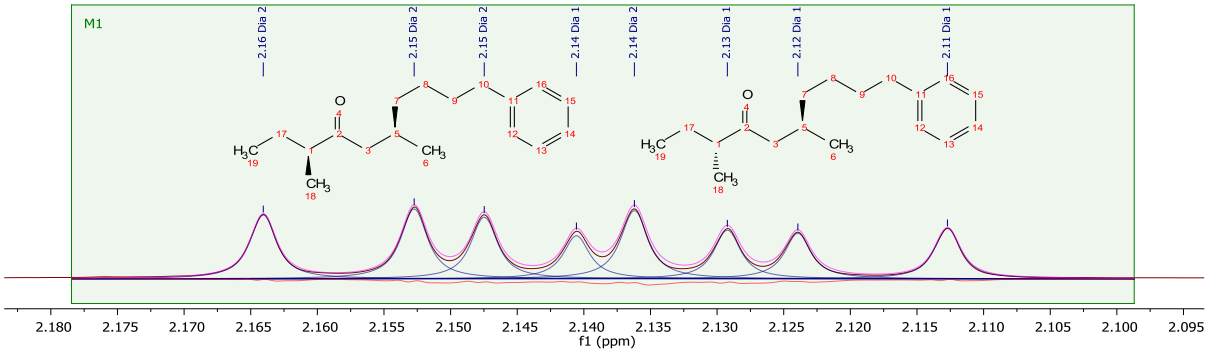

	ppm	Hz	Intensity	Width	Area	Compound
1	2.16	1514.8	302.4	1.66	14234.07	Dia 2
2	2.15	1506.9	330.9	1.66	15683.46	Dia 2
3	2.15	1503.2	291.9	1.66	13720.93	Dia 2
4	2.14	1498.4	204.3	1.64	9751.01	Dia 1
5	2.14	1495.3	323.3	1.70	15752.65	Dia 2
6	2.13	1490.4	230.4	1.66	10899.97	Dia 1
7	2.12	1486.7	216	1.66	10377.72	Dia 1
8	2.11	1478.9	238.3	1.66	11162.19	Dia 1

Total AUC Dia 2	59391.11	% Dia 2	**58%**	
Total AUC Dia 1	42190.89	% Dia 1	**42%**	
	Dia 1	**:**	**Dia 2**	
Ratio	**1**	**:**	**1.4**	

Enantiomeric excess calculation

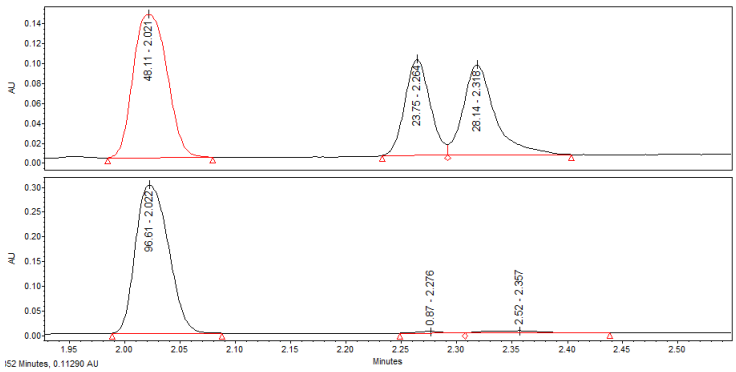

Thus, solving this system of equations:

$$R_1 + R_2 = 96.61\%$$

$$1.4 \times (R_1 + S_1) = (R_2 + S_2)$$

$$S_1 = 0.87\%$$

$$S_2 = 2.52\%$$

Leads to

S_1	0.9%
R_1	40.8%
S_2	2.5%
R_2	55.8%

Corresponding to 96% *ee* for “Dia 1” and 91% *ee* for “Dia 2”.

(R)-10-chloro-4-phenyldecan-2-one

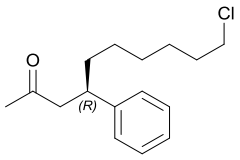

General Procedure B: CuCl (4.0 mg, 0.040 mmol, 0.1 eq.), (*R, R*) Ligand **L17** (23.3 mg, 0.040 mmol, 0.1 eq.), Et_2O (2.0 mL), Cp_2ZrHCl (208 mg, 0.807 mmol, 2.0 eq.), CH_2Cl_2 (0.5 mL), 6-chlorohex-1-ene (0.13 mL, 1.009 mmol, 2.5 eq.), AgOTf (15.6 mg, 0.061 mmol, 0.15 eq.), (*E*)-4-phenylbut-3-en-2-one (59 mg, 0.404 mmol, 1.0 eq.), TMSCl (0.26 mL, 2.018 mmol, 5.0 eq.).

The crude mixture was treated as described above and was purified by flash column chromatography (EtOAc/Hexane 5:100, SiO_2) to afford (*R*)-10-chloro-4-phenyldecan-2-one (94.8 mg, 0.355 mmol, 88%) as a slightly yellow oil.

HPLC analysis indicated an enantiomeric excess of 92% [Chiralpak® IB; flow: 0.8 mL/min; hexane/*i*-PrOH: 99:1; λ = 210 nm; major enantiomer, t_R = 9.8 min; minor enantiomer, t_R = 10.6 min]. Racemic product was realised using *General Procedure A*.

Absolute configuration was assigned by comparison to literature data.[8]

^{1}H NMR (400 MHz, Chloroform-*d*) δ 7.26 – 7.16 (m, 2H, 2 × Ar-H), 7.16 – 7.06 (m, 3H, 3 × Ar-H), 3.41 (t, *J* = 6.7 Hz, 2H, CH_2), 3.03 (dtd, *J* = 9.5, 7.2, 5.3 Hz, 1H, CH), 2.72 – 2.56 (m, 2H, CH_2), 1.95 (s, 3H, CH_3), 1.68 – 1.42 (m, 4H, 2 × CH_2), 1.34 – 0.97 (m, 6H, 3 × CH_2).

^{13}C NMR (101 MHz, Chloroform-*d*) δ 207.9, 144.4, 128.5 (2 C), 127.4 (2 C), 126.4, 50.9, 45.1, 41.2, 36.3, 32.5, 30.7, 28.7, 27.2, 26.7.

IR υ_{max} (film): 2980, 2930, 1715, 1494, 1453, 1357, 1159.

HRMS (APCI$^+$) *m/z* calcd for $C_{16}H_{24}OCl$ $[M+H]^+$: 267.1510, found 267.1510.

$[\alpha]^{25}_{589}$ = +9.5 (*c* 1.0, $CHCl_3$) for 92% ee.

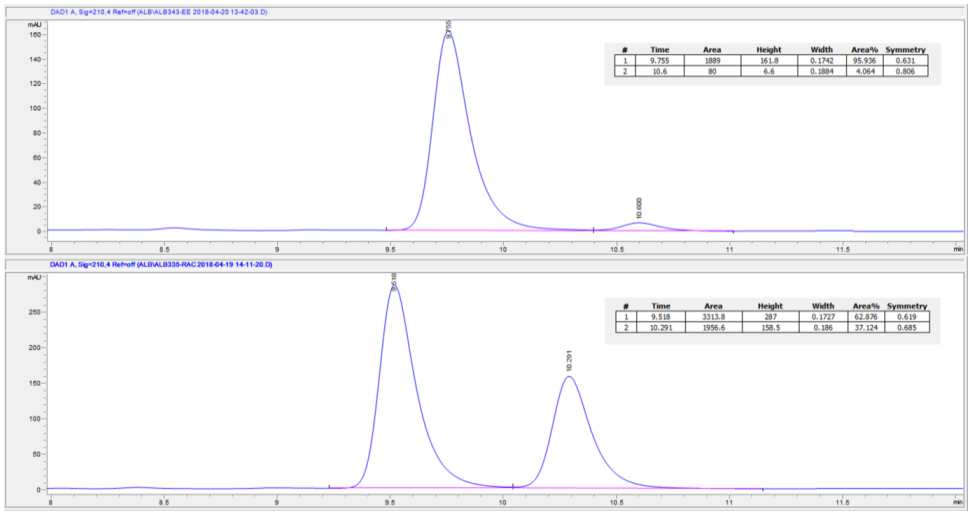

***(R)*-6-(2-bromophenyl)-4-phenylhexan-2-one**

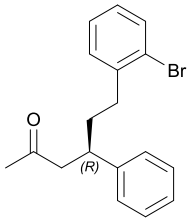

General Procedure B: CuCl (4.0 mg, 0.040 mmol, 0.1 eq.), (R,R) Ligand **L17** (23.5 mg, 0.040 mmol, 0.1 eq.), Et_2O (2.0 mL), Cp_2ZrHCl (208 mg, 0.807 mmol, 2.0 eq.), CH_2Cl_2 (0.5 mL), 1-bromo-2-vinylbenzene (0.13 mL, 1.009 mmol, 2.5 eq.), AgOTf (15.6 mg, 0.061 mmol, 0.15 eq.), (*E*)-4-phenylbut-3-en-2-one (59 mg, 0.404 mmol, 1.0 eq.), TMSCl (0.26 mL, 2.018 mmol, 5.0 eq.).

The crude mixture was treated as described above and was purified by flash column chromatography (EtOAc/Hexane 5:100, SiO_2) to afford (*R*)-6-(2-bromophenyl)-4-phenylhexan-2-one (120.4 mg, 0.364 mmol, 90%) as a slightly brown oil.

HPLC analysis indicated an enantiomeric excess of 93% [Chiralpak® IB; flow: 0.8 mL/min; hexane/*i*-PrOH: 99:1; λ = 210 nm; major enantiomer, t_R = 12.3 min;

minor enantiomer, t_R = 13.0 min]. Racemic product was realised using *General Procedure A*.

Absolute configuration was assigned by comparison to literature data.[8]

^{1}H NMR (400 MHz, Chloroform-*d*) δ 7.41 (dd, *J* = 8.0, 1.3 Hz, 1H, Ar-H), 7.30 – 7.07 (m, 6H, 6 × Ar-H), 7.07 – 7.00 (m, 1H, Ar-H), 6.99 – 6.90 (m, 1H, Ar-H), 3.15 (dtd, *J* = 9.5, 7.1, 5.2 Hz, 1H, CH), 2.77 – 2.62 (m, 2H, CH_2), 2.58 – 2.39 (m, 2H, CH_2), 1.94 (s, 3H, CH_3), 1.92 – 1.72 (m, 2H, CH_2).

^{13}C NMR (101 MHz, Chloroform-*d*) δ 207.7, 143.8, 141.4, 132.8, 130.3, 128.6 (2 C), 127.6 (2 C), 127.6, 127.4, 126.6, 124.3, 50.8, 41.2, 36.4, 34.3, 30.7.

IR υ_{max} (film): 2980, 1715, 1493, 1358, 1250, 1157, 1022.

HRMS (APCI$^+$) *m/z* calcd for C_{18} H_{20} O Br $[M+H]^+$: 331.0692, found 331.0692.

$[\alpha]^{25}_{589}$ = -6.6 (*c* 1.0, $CHCl_3$) for 93% ee.

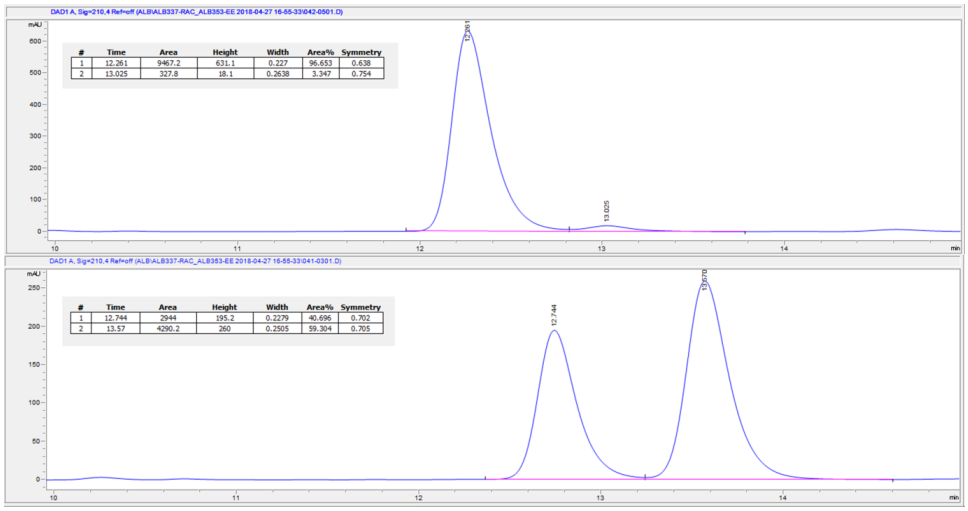

(*R*)-8-((tert-butyldimethylsilyl)oxy)-4-phenyloctan-2-one

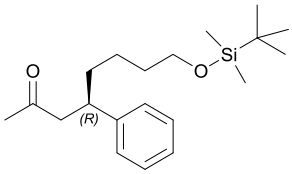

General Procedure B: CuCl (4.0 mg, 0.040 mmol, 0.1 eq.), (*R, R*) Ligand **L17** (23.5 mg, 0.040 mmol, 0.1 eq.), Et_2O (2.0 mL), Cp_2ZrHCl (208 mg, 0.807 mmol, 2.0 eq.), CH_2Cl_2 (0.5 mL), (but-3-en-1-yloxy)(tert-butyl)dimethylsilane (188.0 mg, 1.01 mmol, 2.5 eq.), AgOTf (15.6 mg, 0.061 mmol, 0.15 eq.), (*E*)-4-phenylbut-3-en-2-one (59 mg, 0.404 mmol, 1.0 eq.), TMSCl (0.26 mL, 2.02 mmol, 5.0 eq.).

Note: In order to prevent unwanted deprotection of sillyl ether, freshly distilled TMSCl stored in a Schlenk flask with CaH_2 under an argon atmosphere should be used. Performing below described work up is also beneficial.

The reaction was quenched by the addition of sat. aq. NH_4Cl (*ca* 0.5 ml) and diluted with Et_2O (2 mL). The reaction mixture was partitioned between the aqueous and organic phases, and the aqueous layer extracted by Et_2O. The combined organic materials were dried (Na_2SO_4), filtered, concentrated, and the resulting yellow oil was purified by flash column chromatography (EtOAc/Hexane 5:100, SiO_2) to afford (*R*)-8-((tert-butyldimethylsilyl)oxy)-4-phenyloctan-2-one (83.8 mg, 0.250 mmol, 62%) as a colourless clear oil.

HPLC analysis indicated an enantiomeric excess of 93% [Chiralpak® IB; flow: 0.8 mL/min; hexane/*i*-PrOH: 99:1; λ = 210 nm; minor enantiomer, t_R = 7.2 min; major enantiomer, t_R = 7.6 min]. Racemic product was realised using *General Procedure A*.

Absolute configuration was assigned by comparison to literature data.[8]

^{1}H NMR (400 MHz, Chloroform-*d*) δ 7.33 – 7.24 (m, 2H, 2 × Ar-H), 7.23 – 7.13 (m, 3H, 3 × Ar-H), 3.52 (t, *J* = 6.6 Hz, 2H, CH_2), 3.12 (dtd, *J* = 9.4, 7.2, 5.4 Hz, 1H, CH), 2.80 – 2.64 (m, 2H, CH_2), 2.02 (s, 3H, CH_3), 1.71 – 1.35 (m, 4H, 2 × CH_2), 1.29 – 1.08 (m, 2H, CH_2), 0.85 (s, 9H, 3 × CH_3), 0.00 (s, 6H, 2 × CH_3).

^{13}C NMR (101 MHz, Chloroform-*d*) δ 207.9, 144.4, 128.5 (2 C), 127.5 (2 C), 126.3, 63.0, 50.9, 41.3, 36.3, 32.7, 30.7, 25.9 (3 C), 23.7, 18.3, -5.3 (2 C).

IR υ_{max} (film): 2980, 1719, 1472, 1383, 1253, 1155, 1093.

HRMS ($APCI^+$) *m/z* calcd for $C_{20}H_{35}O_2Si$ $[M+H]^+$: 335.2401, 335.2401.

$[\alpha]^{25}_{589}$ = -5.8 (*c* 1.0, $CHCl_3$) for 93% ee.

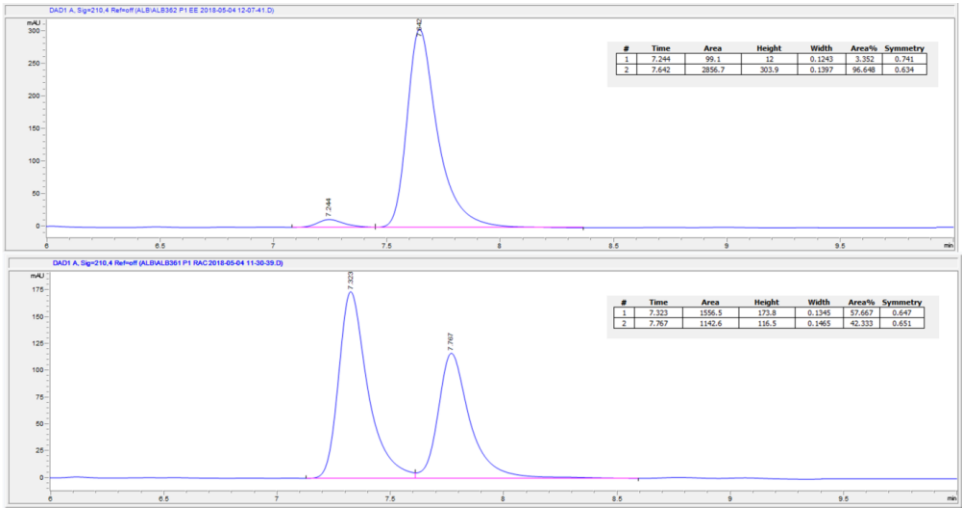

***(R)*-4-(tert-butyl)-8-phenyloctan-2-one**

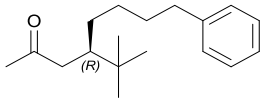

General Procedure B: CuCl (4.0 mg, 0.040 mmol, 0.1 eq.), Ligand **L17** (23.2 mg, 0.040 mmol, 0.1 eq.), Et_2O (2.0 mL), Cp_2ZrHCl (208 mg, 0.807 mmol, 2.0 eq.), CH_2Cl_2 (0.5 mL), 4-phenyl-1-butene (0.15 mL, 1.010 mmol, 2.5 eq.), AgOTf (15.6 mg, 0.061 mmol, 0.15 eq.), (*E*)-5,5-dimethylhex-3-en-2-one (51 mg, 0.404 mmol, 1.0 eq.), TMSCl (0.26 mL, 2.018 mmol, 5.0 eq.).

The crude mixture was treated as described above and was purified by flash column chromatography (EtOAc/Hexane 5:100, SiO_2) to afford (*R*)-4-(tert-butyl)-8-phenyloctan-2-one (74.2 mg, 0.287 mmol, 71%) as a slightly yellow oil.

SFC analysis indicated an enantiomeric excess of 83% [Chiralpak® IF-3; 1500 psi, 30 °C, flow: 1.5 mL/min; 1.0% to 30.0% MeOH in 5 min; λ = 218 nm; major enantiomer, t_R = 1.76 min; minor enantiomer, t_R = 1.84 min]. Racemic product was realised using *General Procedure A*.

Absolute configuration was assigned by comparison to literature data.[8]

^{1}H NMR (400 MHz, Chloroform-*d*) δ 7.24 – 7.15 (m, 2H, 2 × Ar-H), 7.14 – 7.05 (m, 3H, 3 × Ar-H), 2.51 (t, *J* = 7.7 Hz, 2H, CH_2), 2.48 – 2.38 (m, 1H, ½ × CH_2), 2.13 – 2.01 (m, 1H, ½ × CH_2), 2.05 (s, 3H, CH_3), 1.73 (dddd, *J* = 9.1, 6.0, 4.8, 2.9 Hz, 1H, CH), 1.64 – 1.39 (m, 3H, CH_2 & ½ × CH_2), 1.27 – 1.05 (m, 2H, CH_2), 0.98 – 0.83 (m, 1H, ½ × CH_2), 0.76 (s, 9H, 3 × CH_3).

^{13}C NMR (101 MHz, Chloroform-*d*) δ 209.1, 142.7, 128.4 (2 C), 128.2 (2 C), 125.6, 46.0, 42.9, 35.9, 33.4, 31.8, 31.2, 30.2, 28.4, 27.5 (3 C).

IR υ_{max} (film): 2980, 2889, 1717, 1472, 1382, 1251, 1156, 1073.

HRMS (APCI$^+$) *m/z* calcd for $C_{18}H_{29}O$ $[M+H]^+$: 261.2213, found 261.2215.

$[\alpha]^{25}_{589}$ = -12.0 (*c* 1.0, $CHCl_3$) for 83% ee.

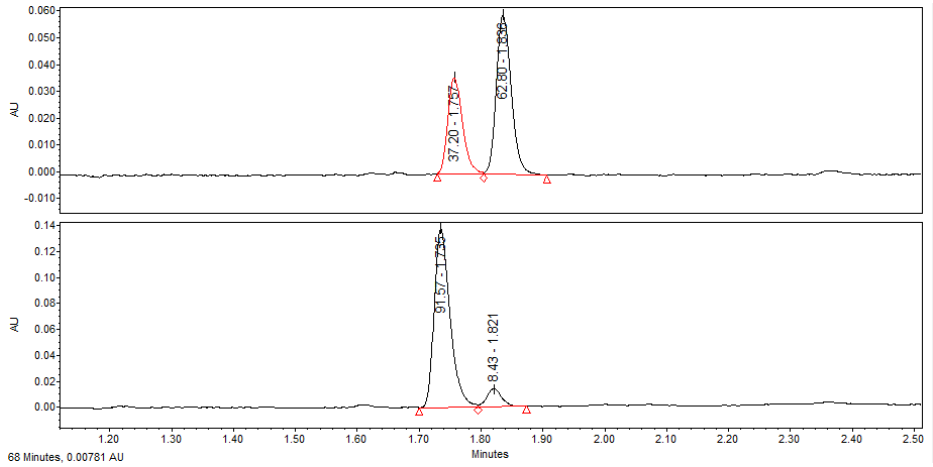

***(R)*-4-cyclohexyl-8-phenyloctan-2-one**

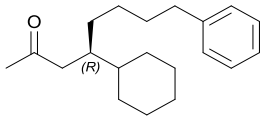

General Procedure B: CuCl (4.0 mg, 0.040 mmol, 0.1 eq.), Ligand **L17** (23.2 mg, 0.040 mmol, 0.1 eq.), Et_2O (2.0 mL), Cp_2ZrHCl (208 mg, 0.807 mmol, 2.0 eq.), CH_2Cl_2 (0.5 mL), 4-phenyl-1-butene (0.15 mL, 1.010 mmol, 2.5 eq.), AgOTf (15.6 mg, 0.061 mmol, 0.15 eq.), (*E*)-4-cyclohexylbut-3-en-2-one (61 mg, 0.401 mmol, 1.0 eq.), TMSCl (0.26 mL, 2.018 mmol, 5.0 eq.).

The crude mixture was treated as described above and was purified by flash column chromatography (EtOAc/Hexane 5:100, SiO_2) to afford (*R*)-4-cyclohexyl-8-phenyloctan-2-one (80.5 mg, 0.283 mmol, 70%) as a slightly yellow oil.

SFC analysis indicated an enantiomeric excess of 89% [Chiralpak® IG-3; 1500 psi, 30 °C, flow: 1.5 mL/min; 1.0% to 30.0% MeOH in 5 min; λ = 218 nm; minor

enantiomer, t_R = 3.34 min; major enantiomer, t_R = 3.50 min]. Racemic product was realised using *General Procedure A*.

Absolute configuration was assigned by comparison to literature data.[8]

^{1}H NMR (400 MHz, Chloroform-*d*) δ 7.24 – 7.15 (m, 2H, 2 × Ar-H), 7.14 – 7.05 (m, 3H, 3 × Ar-H), 2.56 – 2.48 (m, 2H, CH_2), 2.39 – 2.26 (m, 1H, ½ × CH_2), 2.20 – 2.07 (m, 1H, ½ × CH_2), 2.04 (s, 3H, CH_3), 1.78 – 1.71 (m, 1H, CH), 1.70 – 1.44 (m, 6H, 3 × CH_2), 1.33 – 0.98 (m, 9H, 4 × CH_2 & CH), 0.96 – 0.80 (m, 2H, CH_2).

^{13}C NMR (101 MHz, Chloroform-*d*) δ 209.6, 142.7, 128.4 (2 C), 128.2 (2 C), 125.6, 46.0, 39.0, 40.5, 35.8, 31.7, 31.2, 30.3, 30.2, 29.2, 27.0, 26.8, 26.7 (2 C).

IR υ_{max} (film): 2980, 2927, 1716, 1461, 1382, 1251, 1153, 1073.

HRMS (APCI$^+$) *m/z* calcd for $C_{20}H_{31}O$ $[M+H]^+$: 287.2369, found 287.2370.

$[\alpha]^{25}_{589}$ = -0.8 (*c* 1.0, $CHCl_3$) for 89% ee.

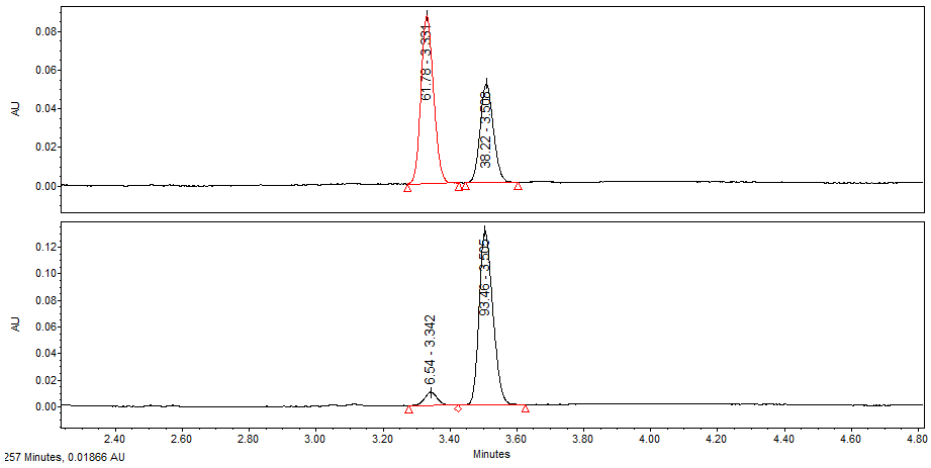

***(4R)*-4-(sec-butyl)-8-phenyloctan-2-one**

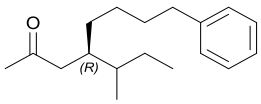

General Procedure B: CuCl (4.0 mg, 0.040 mmol, 0.1 eq.), Ligand **L17** (23.2 mg, 0.040 mmol, 0.1 eq.), Et_2O (2.0 mL), Cp_2ZrHCl (208 mg, 0.807 mmol, 2.0 eq.), CH_2Cl_2 (0.5 mL), 4-phenyl-1-butene (0.15 mL, 1.010 mmol, 2.5 eq.), AgOTf (15.6 mg, 0.061 mmol, 0.15 eq.), (*E*)-5-methylhept-3-en-2-one (51 mg, 0.404 mmol, 1.0 eq.), TMSCl (0.26 mL, 2.018 mmol, 5.0 eq.).

The crude mixture was treated as described above and was purified by flash column chromatography (EtOAc/Hexane 5:100, SiO_2) to afford (4*R*)-4-(sec-butyl)-8-phenyloctan-2-one (74.7 mg, 0.287 mmol, 71%) as a slightly yellow oil.

Quantitative ^{1}H NMR experiment analysis indicated a diastereomeric ratio of 1:1.2.

Diastereoisomer 1: **HPLC and SFC analysis** indicated an enantiomeric excess of 89% [SFC: Chiralpak® IG-3; 1500 psi, 30 °C, flow: 1.5 mL/min; 1.0% to 30.0% MeOH in 5 min; λ = 218 nm; minor enantiomer, t_R = 2.05 min; major enantiomer, t_R = 2.12 min. HPLC: Chiralpak® AY-H; flow: 1.0 mL/min; hexane/*i*-PrOH: 99.2:0.8; λ = 210 nm; major enantiomer, t_R = 7.4 min; minor enantiomer, t_R = 9.6 min].

Diastereoisomer 2: **HPLC and SFC analysis** indicated an enantiomeric excess of 92% [SFC: Chiralpak® IG-3; 1500 psi, 30 °C, flow: 1.5 mL/min; 1.0% to 30.0% MeOH in 5 min; λ = 218 nm; minor enantiomer, t_R = 2.05 min; major enantiomer, t_R = 2.12 min. HPLC: Chiralpak® AY-H; flow: 1.0 mL/min; hexane/*i*-PrOH: 99.2:0.8; λ = 210 nm; major enantiomer, t_R = 7.8 min; minor enantiomer, t_R = 7.8 min].

Absolute configuration was assigned by comparison to literature data.[8]

Mixture of Diastereoisomers:

^{1}H NMR (400 MHz, Chloroform-*d*) δ 7.34 – 7.25 (m, 2H, 2 × Ar-H), 7.24 – 7.15 (m, 3H, 3 × Ar-H), 2.62 (td, *J* = 7.5, 2.1 Hz, 2H, CH_2), 2.44 – 2.16 (m, 2H, CH_2), 2.17 – 2.11 (m, 3H, CH_3), 2.03 – 1.93 (m, 1H, CH), 1.69 – 1.56 (m, 2H, CH_2), 1.53 – 1.00 (m, 7H, CH & 3 × CH_2), 0.95 – 0.86 (m, 3H, CH_3), 0.86 – 0.76 (m, 3H, CH_3).

^{13}C NMR (101 MHz, Chloroform-*d*) δ 209.5 (2 C), 142.7 (2 C), 128.4 (4 C), 128.2 (4 C), 125.6 (2 C), 46.3, 44.9, 38.3, 37.6, 37.0, 36.3, 35.9 (2 C), 31.9, 31.7, 31.6, 30.4, 30.3, 30.0, 27.3, 27.1, 27.0, 26.1, 15.4, 14.6, 12.3, 12.2.

IR υ_{max} (film): 2980, 1716, 1461, 1381, 1251, 1154, 1073.

HRMS (APCI^{+}) *m/z* calcd for $C_{18}H_{29}O$ $[M+H]^{+}$: 261.2213, found 261.2215.

$[\alpha]^{25}_{589}$ = -0.8 (*c* 1.0, $CHCl_3$) for 89% ee and 92% ee.

Diastereomeric ratio Experiment (quantitative ^{1}H NMR)

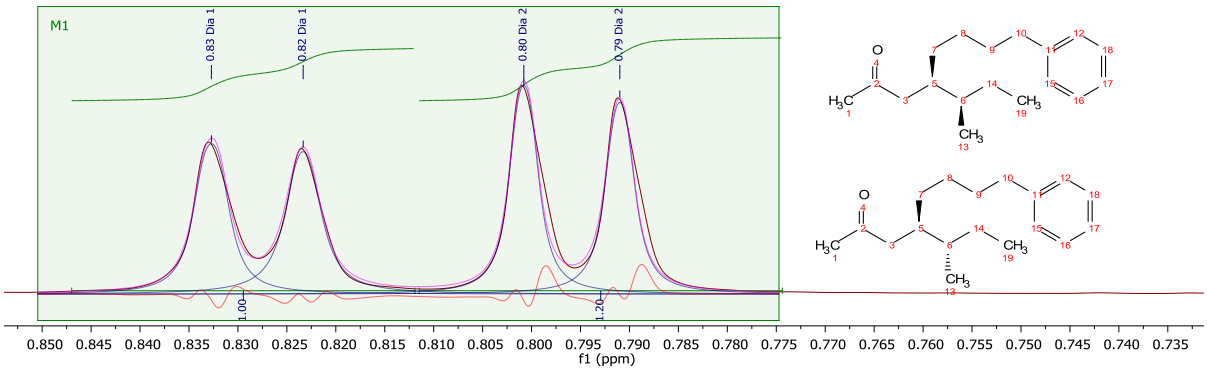

Enantiomeric excess calculation

HPLC analysis:

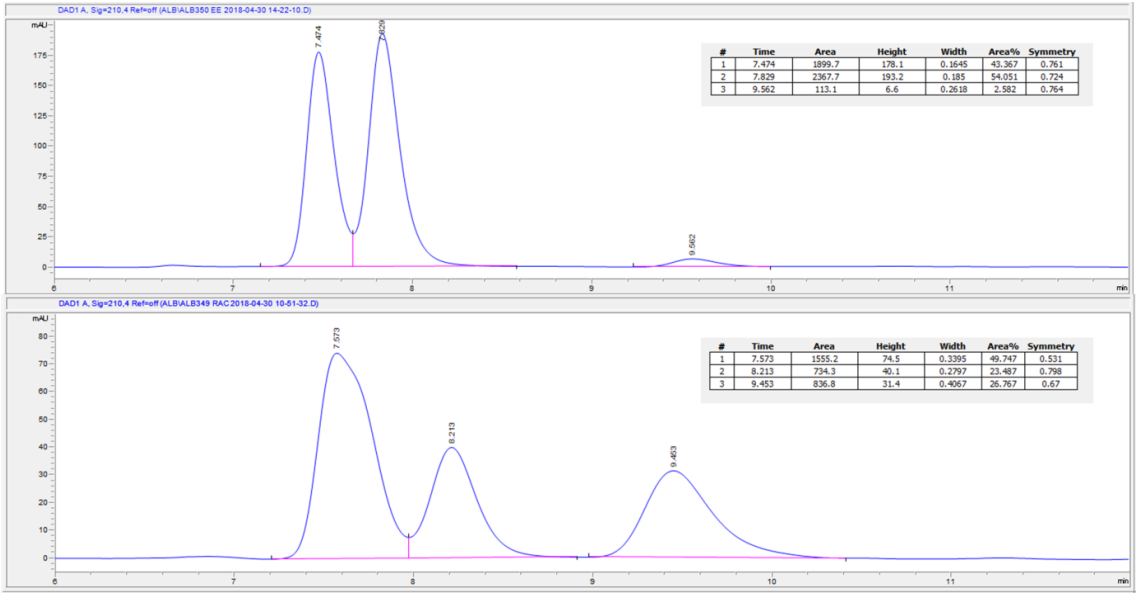

It was found that results of diasteremeric ratio analysis by HPLC closely correlate with the results of NMR analysis when peaks at 7.474 min and 9.562 min are assigned to one diastereomer ("Dia 1"), and peak 7.829 min is assigned to the other diastereomer ("Dia 2").

Ret time (min)	7.474	7.829	9.562
AUC	43.367%	54.051%	2.582%
	Dia 1	***Dia 2***	***Dia 1***

Dia 1	45.949%	**1**
Dia 2	54.051%	**1.18**

Leading to an enantiomeric excess of 89% ee for the minor diastereoisomer "Dia 1". Enantiomeric excess of "Dia 2" could not be determined via HPLC.

SFC analysis:

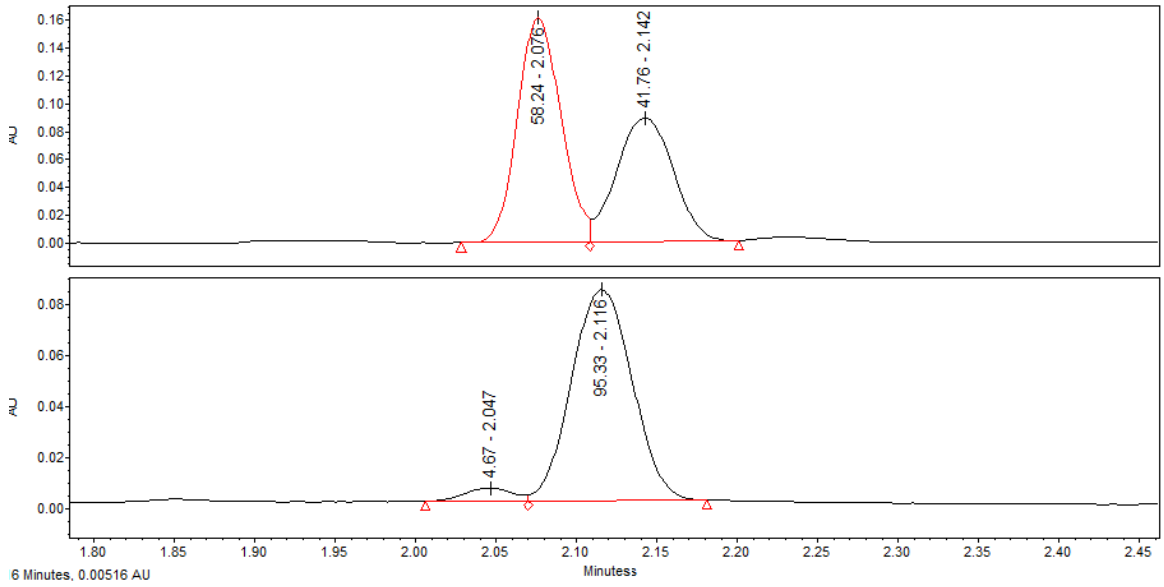

While separation of enantiomers was successful, diastereomeric ratio could not be determined by SFC. Thus to solve this problem, the following equations were used:

$$R_1 + R_2 = 95.33\%$$

$$S_1 + S_2 = 4.67\%$$

$$1.2 \times (R_1 + S_1) = (R_2 + S_2)$$

$$(R_1 - S_1) / (R_1 + S_1) = 89\%$$

Leads to

S_1	2.50%
R_1	42.95%
S_2	2.17%
R_2	52.38%

Corresponding to 89% *ee* for "Dia 1" and 92% *ee* for "Dia 2".

4.2 Cyclic copper-catalysed ACA products

(*S*)-3-hexyl-4,4-diphenylcyclohexan-1-one

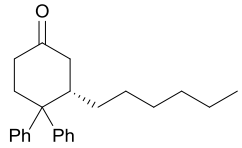

In a flamed dried round bottom flask was added CuCl (4.0 mg, 0.040 mmol, 0.10 eq.) and Ligand (23.0 mg, 0.044 mmol, 0.11 eq.). The flask was purged (3 × vacuum/argon), covered with aluminium foil to protect it from the light and dry Et_2O (2.0 mL) was then added under an argon atmosphere. The resulting colourless clear solution was stirred for 1 h at rt. In the meantime, Cp_2ZrHCl (208 mg, 0.81 mmol, 2.0 eq.) was added to a second flame dried round bottom flask, purged (3 × vacuum/argon), and covered with aluminium foil to protect it from light. Addition of dry CH_2Cl_2 (0.5 mL) under an argon atmosphere forms a milky solution. Schwartz reagent being unstable under these conditions after about 10 min, 1-hexene (0.12 mL, 1.01 mmol, 2.5 eq.) was rapidly added. After stirring for 15 min, the resulting yellow clear solution was manually swirled in order to remove the traces of Schwartz reagent on the inside walls of the flask and stirring was continued. After stirring for 1 h the foiled flask containing copper chloride, AgOTf (15.6 mg, 0.061 mmol, 0.15 eq.) was added and the grey-brown cloudy solution was stirred for 15 min precisely. The mixture was then transferred over about 30 sec via syringe using a syringe filter to the yellow clear solution. The resulting black mixture was then cooled with an ice bath and stirred for a further 5 min before 2',3'-dihydro-4'*H*-[1,1':1',1''-terphenyl]-4'-one (100 mg, 0.404 mmol, 1.0 eq.) and then TMSCl (0.26 mL, 2.02 mmol, 5.0 eq.) were added dropwise via syringe. Stirring at 0 °C was continued overnight for about 15 h. The reaction was then quenched by the addition of aqueous NH_4Cl (1 M, *ca* 0.1 mL) and stirring was continued for 30 min. The

mixture was concentrated under reduced pressure to remove polar solvents then diluted with hexane (*ca* 1 mL). After flash column chromatography (EtOAc/Hexane 5:100, SiO_2), the desired product (132 mg, 0.39 mmol, 98%) was obtained as a colourless oil.

Racemic product was realised using a 1:1 mixture of the *(R)* and *(S)* ligands.

HPLC analysis indicated an enantiomeric excess of 36% [Chiralpak® IB; flow: 0.8 mL/min; hexane/*i*-PrOH: 99:1; λ = 210 nm; major enantiomer, t_R = 9.1 min; minor enantiomer, t_R = 9.9 min].

^{1}H NMR (400 MHz, Chloroform-d) δ 7.56 – 7.48 (m, 2H, 2 × Ar-H), 7.40 – 7.31 (m, 2H, 2 × Ar-H), 7.30 – 7.08 (m, 6H, 6 × Ar-H), 3.07 – 2.92 (m, 2H, CH & ½ × CH_2), 2.80 (dd, *J* = 14.8, 5.1 Hz, 1H, ½ × CH_2), 2.61 (td, *J* = 13.5, 4.7 Hz, 1H, ½ × CH_2), 2.53 – 2.23 (m, 3H, CH_2 & ½ × CH_2), 1.46 – 1.34 (m, 1H, ½ × CH_2), 1.30 – 1.03 (m, 9H, 4 × CH_2 & ½ × CH_2), 0.82 (t, *J* = 7.1 Hz, 3H, CH_3).

^{13}C NMR (101 MHz, Chloroform-d) δ 211.6, 146.6, 145.1, 128.9 (2 C), 128.4 (2 C), 126.7 (2 C), 126.4 (2 C), 126.2, 125.8, 48.7, 43.1, 42.3, 38.4, 31.6, 30.1, 29.5, 29.0, 28.1, 22.5, 14.1.

IR υ_{max} (film): 2926, 1713, 1495, 1446, 1231, 746, 701.

HRMS (APCI$^+$) *m/z* calcd for $C_{24}H_{31}O$ $[M+H]^+$: 335.2369, found 335.2368.

Analytical data are in agreement with the literature.[9]

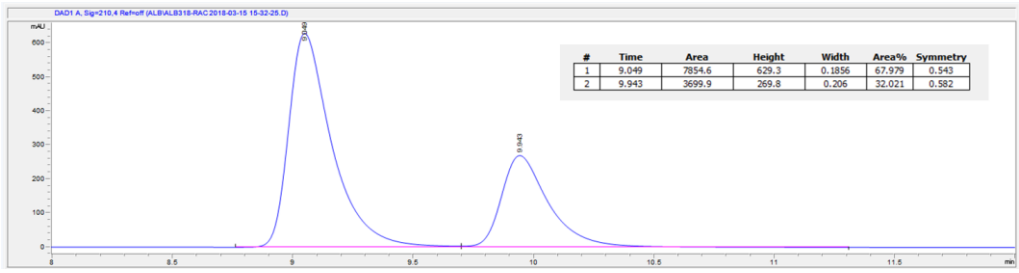

4.3 Exocyclic copper-catalysed ACA products

1-((2*S*)-2-(4-phenylbutyl)cyclohexyl)ethan-1-one

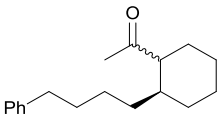

In a flame-dried round bottom flask was added CuCl (4.0 mg, 0.040 mmol, 0.10 eq.) and *(S)* **L46** (25.9 mg, 0.044 mmol, 0.11 eq.). The flask was purged (3 × argon/vacuum), covered with aluminium foil to protect it from the light and dry Et_2O (2.0 mL) was then added under an argon atmosphere. The resulting colourless clear solution was stirred for 1 h at room temperature. In the meantime, Cp_2ZrHCl (208 mg, 0.80 mmol, 2.0 eq.) was added to a second flame dried round bottom flask, purged (3 × argon/vacuum), and covered with aluminium foil to protect it from the light. Addition of dry CH_2Cl_2 (0.5 mL) under an argon atmosphere forms a milky solution. 4-phenylbutene (0.15 mL, 1.00 mmol, 2.5 eq.) was immidiately added as the Schwartz reagent is unstable with CH_2Cl_2 after about 10 min. After stirring for 15 min, the resulting yellow clear solution was manually swirled in order to remove the traces of Schwartz reagent on the inside walls of the flask and stirring was continued. After stirring the foiled flask containing CuCl for 1 h, AgOTf (15.5 mg, 0.060 mmol, 0.15 eq.) was added, and the grey-brown cloudy solution was stirred for precisely 15 min. The mixture was then transferred over about 30 sec via syringe using a syringe filter to the yellow clear solution. The resulting black mixture was then cooled with an ice bath and stirred for a further 5 min before the 1-(cyclohex-1-

en-1-yl)ethan-1-one (50 mg, 0.40 mmol, 1.0 eq.) and then TMSCl (0.51 mL, 4.03 mmol, 10.0 eq.) were added dropwise via syringe. Stirring at 0 °C was continued overnight for about 15 h. The reaction was then quenched by the addition of aqueous NH_4Cl (1 M, *ca* 0.1 mL) and stirring was continued for 5 h. The mixture was concentrated under reduced pressure then diluted with hexane (*ca* 10 mL), filtered and concentrated again under reduced pressure. After flash column chromatography (Hexane:EtOAc, 97:3, SiO_2), 1-((2*S*)-2-(4-phenylbutyl)cyclohexyl)-ethan-1-one (73 mg, 0.29 mmol, 72%) was obtained as a pale yellow oil.

Racemic product was realised using a 1:1 mixture of the *(R)* and *(S)* ligand **L28**.

Major diastereoisomer (*trans*)

SFC analysis indicated an enantiomeric excess of 93% [Chiralpak® IG-3; 1500 psi, 30 °C, flow: 1.5 mL/min; 1.0% to 30.0% MeOH in 5 min; λ = 218 nm; major enantiomer, t_R = 3.34 min; minor enantiomer, t_R = 4.80 min].

^{1}H NMR (400 MHz, Chloroform-d) δ 7.22 – 7.15 (m, 2H, 2 × Ar-H), 7.12 – 7.05 (m, 3H, 3 × Ar-H), 2.50 (ddd, *J* = 8.3, 6.9, 3.5 Hz, 2H, CH_2), 2.15 – 2.05 (m, 1H, CH), 2.04 (s, 3H, CH_3), 1.83 – 1.09 (m, 13H, CH & ½ × CH_2 & ½ × CH_2 & 5 × CH_2), 1.05 – 0.92 (m, 1H, ½ × CH_2), 0.87 – 0.72 (m, 1H, ½ × CH_2).

^{13}C NMR (101 MHz, Chloroform-d) δ 213.3, 142.7, 128.4 (2 C), 128.2 (2 C), 125.6, 57.9, 38.3, 35.8, 34.6, 31.6, 30.8, 29.8, 29.0, 26.1, 25.8 (2 C).

Minor Diastereoisomer (*cis*)

SFC analysis indicated an enantiomeric excess of 93% [Chiralpak® IG-3; 1500 psi, 30 °C, flow: 1.5 mL/min; 1.0% to 30.0% MeOH in 5 min; λ = 218 nm; major enantiomer, t_R = 2.99 min; minor enantiomer, t_R = 3.80 min].

^{1}H NMR (400 MHz, Chloroform-d) δ 7.23 – 7.16 (m, 2H, 2 × Ar-H), 7.14 – 7.06 (m, 3H, 3 × Ar-H), 2.56 – 2.43 (m, 3H, CH & CH_2), 2.02 (s, 3H, CH_3), 1.94 – 1.84 (m, 1H, CH), 1.79 – 1.07 (m, 13H, 6 × CH_2 & ½ × CH_2), 1.04 – 0.91 (m, 1H, ½ × CH_2).

^{13}C NMR (101 MHz, Chloroform-d) δ 211.8, 142.6, 128.4 (2 C), 128.2 (2 C), 125.6, 53.9, 36.5, 35.8, 31.5, 28.9, 28.6, 28.1, 27.4, 24.5, 23.6, 21.6.

Mixture of diastereoisomers (*trans*:*cis* 15:1)

IR υ_{max} (film): 2980, 2927, 1708, 1448, 1381, 1246, 1153, 1073.

HRMS (APCI) *m/z* calcd for $C_{18}H_{25}O$ $[M+H]^+$: 257.1911, found 257.1910.

$[\alpha]^{25}_{589}$ = -8.8 (*c* 1.0, $CHCl_3$) for 93% ee (*trans*) and 93% ee (*cis*).

Absolute configuration was assigned by comparison to literature data.[10]

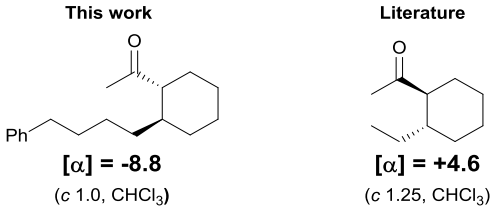

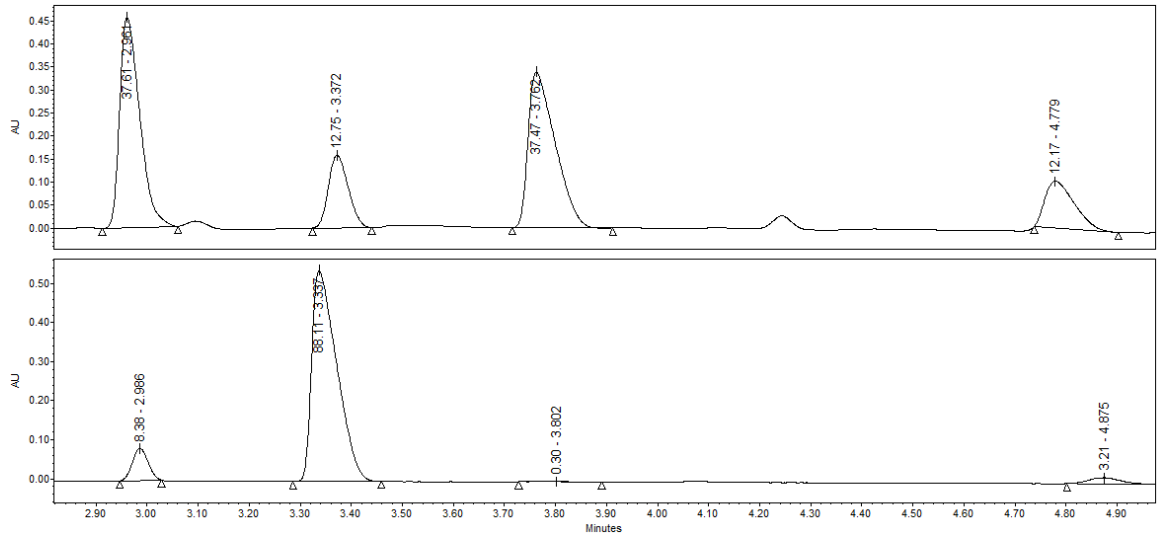
AU
37.61 - 2.561
12.75 - 3.372
37.47 - 3.762
12.17 - 4.779
88.11 - 3.337
8.38 - 2.986
0.30 - 3.802
3.21 - 4.875
Minutes

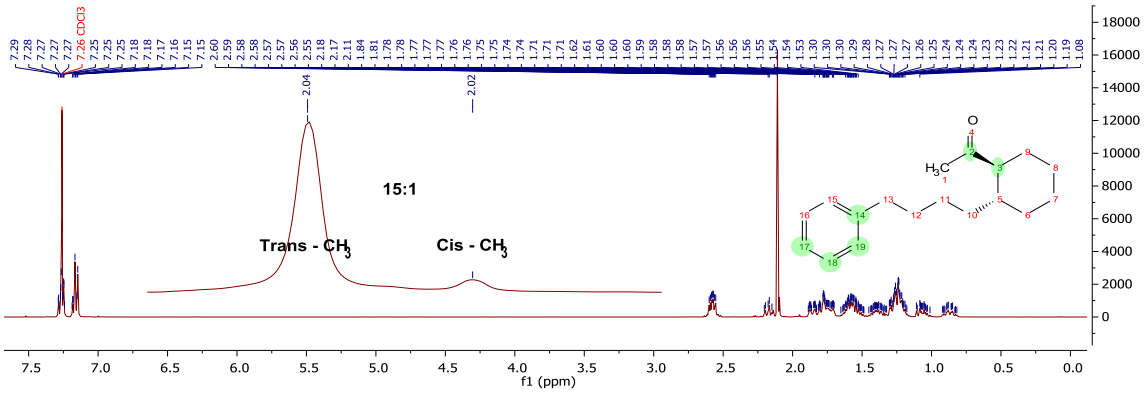
15:1
Trans - CH3
Cis - CH3
f1 (ppm)

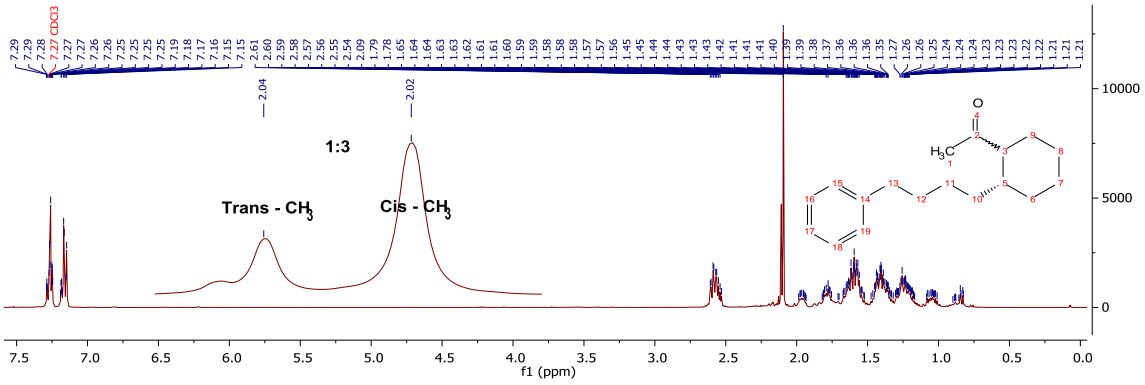
1:3
Trans - CH3
Cis - CH3
f1 (ppm)

4.4 Enones

(E)-4-(3-bromophenyl)but-3-en-2-one

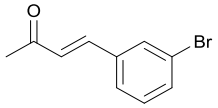

General Procedure C: Lithium hydroxide (68.8 mg, 2.789 mmol, 1.2 eq.), diethyl (2-oxopropyl)phosphonate (0.47 mL, 2.440 mmol, 1.05 eq.), 3-bromobenzaldehyde (430 mg, 2.324 mmol, 1.0 eq.), THF (10 mL).

The crude mixture was treated as described above and was purified by flash column chromatography (Hexane:EtOAc, 90:10, SiO_2) to afford (*E*)-4-(3-bromophenyl)but-3-en-2-one (394 mg, 1.748 mmol, 75%) as a pale yellow oil.

^{1}H NMR (500 MHz, Chloroform-*d*) δ 7.71 (t, *J* = 1.8 Hz, 1H, Ar-H), 7.58 – 7.40 (m, 3H, 2 × Ar-H & C=CH), 7.29 (t, *J* = 7.9 Hz, 1H, Ar-H), 6.72 (d, *J* = 16.3 Hz, 1H, C=CH), 2.40 (s, 3H, CH_3).

^{13}C NMR (126 MHz, Chloroform-*d*) δ 197.9, 141.5, 136.6, 133.2, 130.9, 130.5, 128.2, 126.8, 123.1, 27.8.

IR υ_{max} (film): 3059, 1692, 1670, 1611, 1359, 1257, 1179.

HRMS (APCI) *m/z* calcd for C_{10} H_{10} O Br $[M+H]^+$: 224.9909, found 224.9912.

Analytical data are in agreement with the literature.[11]

(E)-4-(4-chlorophenyl)but-3-en-2-one

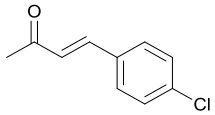

General Procedure C: Lithium hydroxide (57.5 mg, 2.399 mmol, 1.2 eq.), diethyl (2-oxopropyl)phosphonate (0.40 mL, 2.099 mmol, 1.05 eq.), 4-chlorobenzaldehyde (281 mg, 1.999 mmol, 1.0 eq.), THF (10 mL).

The crude mixture was treated as described above and was purified by flash column chromatography (Hexane:EtOAc, 90:10, SiO_2) to afford (*E*)-4-(4-chlorophenyl)but-3-en-2-one (319 mg, 1.759 mmol, 88%) as a pale yellow solid.

^{1}H NMR (500 MHz, Chloroform-*d*) δ 7.50 – 7.40 (m, 3H, 2 × Ar-H & C=CH), 7.40 – 7.33 (m, 2H, 2 × Ar-H), 6.68 (d, *J* = 16.3 Hz, 1H, C=CH), 2.37 (s, 3H, CH_3).

^{13}C NMR (126 MHz, Chloroform-*d*) δ 198.1, 142.0, 136.5, 133.0, 129.5 (2 C), 129.4 (2 C), 127.6, 27.8.

IR υ_{max} (film): 2981, 2361, 1691, 1669, 1610, 1491, 1359, 1256, 1090.

HRMS (APCI) *m/z* calcd for C_{10} H_{10} O Cl $[M+H]^+$: 181.0415, found 181.0416.

MP: 56.8 °C.

Analytical data are in agreement with the literature.[12]

***(E)*-4-(4-methoxyphenyl)but-3-en-2-one**

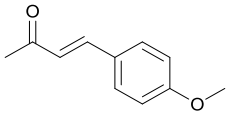

General Procedure C: Lithium hydroxide (89.9 mg, 3.755 mmol, 1.2 eq.), diethyl (2-oxopropyl)phosphonate (0.63 mL, 3.285 mmol, 1.05 eq.), 4-methoxybenzaldehyde (426 mg, 3.129 mmol, 1.0 eq.), THF (20 mL).

The crude mixture was treated as described above and was purified by flash column chromatography (Hexane:EtOAc, 90:10, SiO_2) to afford (*E*)-4-(4-methoxyphenyl)but-3-en-2-one (257 mg, 1.471 mmol, 47%) as a pale yellow solid.

^{1}H NMR (500 MHz, Chloroform-*d*) δ 7.53 – 7.43 (m, 3H, 2 × Ar-H & C=CH), 6.95 – 6.88 (m, 2H, 2 × Ar-H), 6.61 (d, *J* = 16.2 Hz, 1H, C=CH), 3.84 (s, 3H, CH_3), 2.36 (s, 3H, CH_3).

^{13}C NMR (126 MHz, Chloroform-*d*) δ 198.5, 161.7, 143.4, 130.1 (2 C), 127.2, 125.2, 114.6 (2 C), 55.5, 27.5.

IR υ_{max} (film): 2979, 2360, 1681, 1600, 1513, 1359, 1264, 1176, 1021.

HRMS (APCI) *m/z* calcd for $C_{11}H_{13}O_2$ $[M+H]^+$: 177.0910, found 177.0912.

MP: 67 °C.

Analytical data are in agreement with the literature.[12]

(E)-4-(4-nitrophenyl)but-3-en-2-one

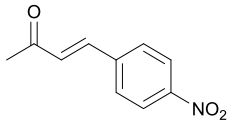

General Procedure C: Lithium hydroxide (26.6 mg, 1.112 mmol, 1.2 eq.), diethyl (2-oxopropyl)phosphonate (0.19 mL, 0.973 mmol, 1.05 eq.), 4-nitrobenzaldehyde (140 mg, 0.926 mmol, 1.0 eq.), THF (5 mL).

The crude mixture was treated as described above and was purified by flash column chromatography (Hexane:EtOAc, 90:10, SiO_2) to (*E*)-4-(4-nitrophenyl)but-3-en-2-one (139 mg, 0.731 mmol, 79%) as a pale yellow solid.

^{1}H NMR (500 MHz, Chloroform-*d*) δ 8.30 – 8.21 (m, 2H, 2 × Ar-H), 7.74 – 7.65 (m, 2H, 2 × Ar-H), 7.53 (d, *J* = 16.3 Hz, 1H, C=CH), 6.81 (d, *J* = 16.3 Hz, 1H, C=CH), 2.42 (s, 3H, CH_3).

^{13}C NMR (126 MHz, Chloroform-*d*) δ 197.6, 148.7, 140.8, 140.2, 130.5, 128.9 (2 C), 124.3 (2 C), 28.2.

IR υ_{max} (film): 3112, 2360, 1692, 1668, 1614, 1593, 1510, 1337, 1187.

HRMS (APCI) *m/z* calcd for C_{10} H_{10} O_3 N $[M+H]^+$: 192.0655, found 192.0658.

MP: 105 °C.

Analytical data are in agreement with the literature.[12]

(E)-4-(thiophen-3-yl)but-3-en-2-one

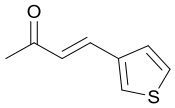

General Procedure C: Lithium hydroxide (164.0 mg, 6.848 mmol, 1.2 eq.), diethyl (2-oxopropyl)phosphonate (1.15 mL, 5.992 mmol, 1.05 eq.), thiophene-3-carbaldehyde (0.50 mL, 5.707 mmol, 1.0 eq.), THF (25 mL).

The crude mixture was treated as described above and was purified by flash column chromatography (Hexane:EtOAc, 90:10, SiO_2) to afford (*E*)-4-(thiophen-3-yl)but-3-en-2-one (352 mg, 2.311 mmol, 40%) as a pale yellow oil.

^{1}H NMR (400 MHz, Chloroform-*d*) δ 7.65 (ddd, *J* = 16.0, 1.8, 0.9 Hz, 1H, C=CH), 7.46 – 7.39 (m, 1H, Ar-H), 7.33 – 7.29 (m, 1H, Ar-H), 7.13 – 7.05 (m, 1H, Ar-H), 6.55 (dd, *J* = 16.0, 2.0 Hz, 1H, C=CH), 2.36 (s, 3H, CH_3).

^{13}C NMR (126 MHz, Chloroform-*d*) δ 197.7, 139.7, 135.7, 131.5, 128.9, 128.3, 125.8, 27.7.

IR υ_{max} (film): 3104, 1663, 1594, 1423, 1358, 1254, 1200.

HRMS (APCI) *m/z* calcd for C_8 H_9 O S $[M+H]^+$: 153.0369, found 153.0369.

(E)-4-(2-bromophenyl)but-3-en-2-one

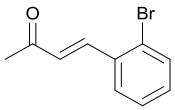

General Procedure C: Lithium hydroxide (41.0 mg, 1.713 mmol, 1.2 eq.), diethyl (2-oxopropyl)phosphonate (0.35 mL, 1.799 mmol, 1.05 eq.), 2-bromobenzaldehyde (0.20 mL, 1.713 mmol, 1.0 eq.), THF (10 mL).

The crude mixture was treated as described above and was purified by flash column chromatography (Hexane:EtOAc, 90:10, SiO_2) to afford (*E*)-4-(2-bromophenyl)but-3-en-2-one (222.1 mg, 0.993 mmol, 58%) as a pale brown oil.

^{1}H NMR (500 MHz, Chloroform-*d*) δ 7.89 (d, *J* = 16.3 Hz, 1H, C=CH), 7.62 (dt, *J* = 7.8, 1.7 Hz, 2H, 2 × Ar-H), 7.39 – 7.29 (m, 1H, Ar-H), 7.29 – 7.20 (m, 1H, Ar-H), 6.62 (d, *J* = 16.3 Hz, 1H, C=CH), 2.42 (s, 3H, CH_3).

^{13}C NMR (126 MHz, Chloroform-*d*) δ 198.3, 141.9, 134.5, 133.5, 131.4, 129.9, 127.8, 127.8, 125.6, 27.2.

IR υ_{max} (film): 2980, 1671, 1607, 1437, 1358, 1257, 1026.

HRMS (APCI$^+$) *m/z* calcd for C_{10} H_{10} O Br $[M+H]^+$: 224.9909, found 224.9912.

Analytical data are in agreement with the literature.[13]

(E)-5,5-dimethylhex-3-en-2-one

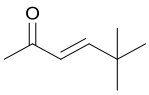

General Procedure C: Lithium hydroxide (185.2 mg, 7.734 mmol, 1.2 eq.), diethyl (2-oxopropyl)phosphonate (1.30 mL, 6.767 mmol, 1.05 eq.), pivalaldehyde (0.70 mL, 6.445 mmol, 1.0 eq.), THF (30 mL).

The crude mixture was treated as described above and was purified by flash column chromatography (Hexane:EtOAc, 90:10, SiO_2) to afford (*E*)-5,5-dimethylhex-3-en-2-one (356.2 mg, 2.836 mmol, 44%) as a colourless oil.

^{1}H NMR (400 MHz, Chloroform-*d*) δ 6.78 (dd, *J* = 16.3, 0.7 Hz, 1H, C=CH), 5.99 (dd, *J* = 16.3, 0.7 Hz, 1H, C=CH), 2.25 (s, 3H, CH_3), 1.08 (s, 9H, 3 × CH_3).

^{13}C NMR (101 MHz, Chloroform-*d*) δ 199.3, 158.1, 126.4, 33.8, 28.7 (3 C), 27.0.

IR υ_{max} (film):3659, 2980, 1472, 1461, 1251, 1152, 1073.

HRMS (APCI$^+$) *m/z* calcd for C_8 H_{15} O $[M+H]^+$: 127.1117, found 127.1116.

Analytical data are in agreement with the literature.[10]

(E)-4-cyclohexylbut-3-en-2-one

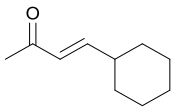

General Procedure C: Lithium hydroxide (177.9 mg, 7.430 mmol, 1.2 eq.), diethyl (2-oxopropyl)phosphonate (1.25 mL, 6.501 mmol, 1.05 eq.), cyclohexanecarbaldehyde (0.75 mL, 6.191 mmol, 1.0 eq.), THF (30 mL).

The crude mixture was treated as described above and was purified by flash column chromatography (Hexane:EtOAc, 90:10, SiO_2) to afford (*E*)-4-cyclohexylbut-3-en-2-one (399 mg, 2.600 mmol, 42%) as a pale yellow oil.

^{1}H NMR (400 MHz, Chloroform-*d*) δ 6.72 (dd, *J* = 16.1, 6.8 Hz, 1H, C=CH), 6.01 (dt, *J* = 16.1, 1.0 Hz, 1H, C=CH), 2.23 (s, 3H, CH_3), 2.20 – 2.07 (m, 1H, CH), 1.82 – 1.61 (m, 5H, 2 × CH_2 & ½ × CH_2), 1.37 – 1.06 (m, 5H, 2 × CH_2 & ½ × CH_2).

^{13}C NMR (101 MHz, Chloroform-*d*) δ 199.2, 153.4, 128.8, 40.6, 31.8 (2 C), 26.9, 25.9, 25.7 (2 C).

IR υ_{max} (film): 2924, 2852, 1673, 1623, 1448, 1357, 1252.

HRMS (APCI) *m/z* calcd for C_{10} H_{17} O $[M+H]^+$: 153.1274, found 153.1273.

Analytical data are in agreement with the literature.[10]

(E)-5-methylhept-3-en-2-one

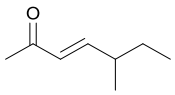

General Procedure C: Lithium hydroxide (201.2 mg, 8.402 mmol, 1.2 eq.), diethyl (2-oxopropyl)phosphonate (1.41 mL, 7.351 mmol, 1.05 eq.), methylbutyraldehyde (0.75 mL, 7.001 mmol, 1.0 eq.), THF (25 mL).

The crude mixture was treated as described above and was purified by flash column chromatography (Hexane:EtOAc, 90:10, SiO_2) to afford (*E*)-5-methylhept-3-en-2-one (514.3 mg, 4.075 mmol, 58%) as a pale yellow oil.

^{1}H NMR (400 MHz, Chloroform-*d*) δ 6.70 (dd, *J* = 16.0, 7.7 Hz, 1H, C=CH), 6.06 (dt, *J* = 16.0, 0.9 Hz, 1H, C=CH), 2.27 (s, 3H, CH_3), 2.31 – 2.18 (m, 1H, CH), 1.44 (p, *J* = 7.3 Hz, 2H, CH_2), 1.08 (dd, *J* = 6.7, 0.6 Hz, 3H, CH_3), 0.91 (t, *J* = 7.4 Hz, 3H, CH_3).

^{13}C NMR (101 MHz, Chloroform-*d*) δ 199.0, 153.6, 129.7, 38.3, 28.9, 26.9, 19.0, 11.7.

IR υ_{max} (film): 2980, 1548, 1462, 1381, 1251, 1151, 1074.

HRMS (APCI) *m/z* calcd for $C_8H_{15}O$ $[M+H]^+$: 127.1117, found 127.1117.

1-(cyclohex-1-en-1-yl)ethan-1-one

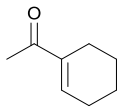

According to a modified procedure,[14] *N*-methoxy-*N*-methylcyclohex-1-ene-1-carboxamide (332 mg, 1.96 mmol, 1.0 eq.) was dissolved in Et_2O (15 mL) and the solution was cooled to –78 °C. MeLi, 1.6M in Et_2O (2.06 mL, 3.30 mmol, 1.5 eq.) was added dropwise via syringe. The reaction was quenched at –78 °C after stirring for 1 h by the dropwise addition of aqueous HCl (1 M, 10 mL). The organic and aqueous layers were partitioned and the aqueous phase was extracted with Et_2O (3 × 20 mL). The combined organic phases were dried over $MgSO_4$, filtered and concentrated under reduced pressure. After column chromatography (Hexane:EtOAc, 97:3, SiO_2), 1-(cyclohex-1-en-1-yl)ethan-1-one (84 mg, 0.68 mmol, 34%) was obtained as a pale yellow oil.

^{1}H NMR (400 MHz, Chloroform-d) δ 6.87 – 6.79 (m, 1H, C=CH), 2.21 (s, 3H, CH_3), 2.20 – 2.11 (m, 4H, 2 × CH_2), 1.61 – 1.49 (m, 4H, 2 × CH_2).

^{13}C NMR (101 MHz, Chloroform-d) δ 199.4, 140.9, 139.7, 26.1, 25.2, 23.0, 21.9, 21.5.

IR υ_{max} (film): 1933, 1664, 1384, 1235.

HRMS (ESI^+) *m/z* calcd for $C_8H_{13}O$ $[M+H]^+$: 125.0961, found 125.0960.

4.5 Amines

Note: Although all the amines were kept under high-vacuum for at least 5 h, residual solvent impurities were observed in products with high viscosity.

(*R*)-*N*-cyclopentyl-2,3-dihydro-1*H*-inden-1-amine

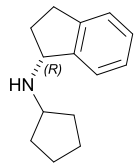

General Procedure D: Cyclopentanone (0.10 mL, 1.091 mmol, 1.4 eq.), (*R*)-2,3-dihydro-1*H*-inden-1-amine (0.1 mL, 0.779 mmol, 1.0 eq.), dry THF (10 mL), $NaB(OAc)_3H$ (264.3 mg, 1.247 mmol, 1.6 eq.).

The crude mixture was treated as described above and was purified by flash column chromatography (CH_2Cl_2:Hexane, 70:30, SiO_2) to afford (*R*)-*N*-cyclopentyl-2,3-dihydro-1*H*-inden-1-amine (46.8 mg, 0.234 mmol, 30%) as a pale yellow oil.

^{1}H NMR (500 MHz, Chloroform-*d*) δ 7.38 – 7.31 (m, 1H, Ar-H), 7.25 – 7.15 (m, 3H, 3 × Ar-H), 4.25 (t, *J* = 6.6 Hz, 1H, CH), 3.30 (p, *J* = 6.9 Hz, 1H, CH), 3.00 (ddd, *J* = 15.9, 8.5, 4.7 Hz, 1H, ½ × CH_2), 2.80 (dt, *J* = 15.9, 7.8 Hz, 1H, ½ × CH_2), 2.43 (dddd, *J* = 12.8, 8.5, 6.6, 4.7 Hz, 1H, ½ × CH_2), 1.96 – 1.86 (m, 2H, ½ × CH_2 & ½ × CH_2), 1.86 – 1.78 (m, 1H, ½ × CH_2), 1.78 – 1.69 (m, 2H, ½ × CH_2 & ½ × CH_2), 1.63 – 1.50 (m, 2H, ½ × CH_2 & ½ × CH_2), 1.46 – 1.34 (m, 2H, ½ × CH_2 & ½ × CH_2).

^{13}C NMR (126 MHz, Chloroform-*d*) δ 146.0, 143.5, 127.2, 126.2, 124.7, 124.0, 61.9, 57.8, 34.6, 34.0, 33.4, 30.4, 24.1, 24.0.

IR υ_{max} (film): 2950, 2860, 1456, 1354, 1153, 1126.

HRMS (EI^+) *m/z* calcd for $C_{14}H_{20}N$ $[M+H]^+$: 202.1590, found 202.1591.

$[\alpha]^{25}_{589}$= -19.1 (*c* 1.2, $CHCl_3$) for 99% ee.

(R)-N-((2,6,6-trimethylcyclohex-1-en-1-yl)methyl)-2,3-dihydro-1*H*-inden-1-amine

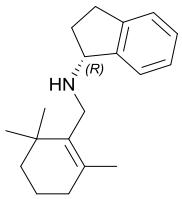

General Procedure D: 2,6,6-trimethylcyclohex-1-ene-1-carbaldehyde (0.15 mL, 0.935 mmol, 1.2 eq.), (*R*)-2,3-dihydro-1*H*-inden-1-amine (0.1 mL, 0.779 mmol, 1.0 eq.), THF (10 mL), $NaB(OAc)_3H$ (264.3 mg, 1.247 mmol, 1.6 eq.)

The crude mixture was treated as described above and was purified by flash column chromatography (CH_2Cl_2:Hexane, 70:30, SiO_2) then filtered through a strong cation exchange column ISOLUTE® SCX-2 with MeOH to wash off non-basic component followed by ammonia solution in MeOH (2 M) to afford (*R*)-N-((2,6,6-trimethylcyclohex-1-en-1-yl)methyl)-2,3-dihydro-1*H*-inden-1-amine (203 mg, 0.748 mmol, 96%) as a pale yellow oil.

^{1}H NMR (400 MHz, Chloroform-*d*) δ 7.32 – 7.19 (m, 1H, Ar-H), 7.17 – 7.04 (m, 3H, 3 × Ar-H), 4.14 (t, *J* = 6.4 Hz, 1H, CH), 3.18 (d, *J* = 11.4 Hz, 1H, ½ × CH_2), 3.12 (d, *J* = 11.4 Hz, 1H, ½ × CH_2), 2.93 (ddd, *J* = 15.9, 8.5, 5.1 Hz, 1H, ½ × CH_2), 2.73 (dt, *J* = 15.9, 8.5, 6.8 Hz, 1H, ½ × CH_2), 2.31 (dddd, *J* = 12.3, 8.5, 6.8, 5.1 Hz, 1H, ½ × CH_2), 1.88 – 1.80 (m, 3H, CH_2 & ½ × CH_2), 1.60 (s, 3H, CH_3), 1.54 – 1.46 (m, 2H, CH_2), 1.38 – 1.32 (m, 2H, CH_2), 0.96 (s, 3H, CH_3), 0.95 (s, 3H, CH_3).

^{13}C NMR (101 MHz, Chloroform-*d*) δ 145.6, 143.7, 136.4, 130.8, 127.3, 126.2, 124.7, 124.2, 64.0, 45.1, 39.6, 34.5, 33.2, 32.7, 30.6, 28.7, 28.6, 19.8, 19.5.

IR υ_{max} (film): 3021, 2926, 2846, 1477, 1457, 1358.

HRMS (EI$^+$) *m/z* calcd for $C_{19}H_{28}N$ [M+H]$^+$: 270.2216, found 270.2214.

$[\alpha]^{25}_{589}$= -1.4 (*c* 1.0, $CHCl_3$) for 99% ee.

(R)-N-benzyl-2,3-dihydro-1*H*-inden-1-amine

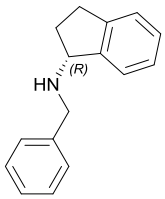

General Procedure D: Benzaldehyde (0.40 mL, 3.897 mmol, 1.0 eq.), (*R*)-2,3-dihydro-1*H*-inden-1-amine (0.5 mL, 3.897 mmol, 1.0 eq.), THF (20 mL), $NaB(OAc)_3H$ (991 mg, 4.676 mmol, 1.2 eq.).

The crude mixture was treated as described above and was purified by flash column chromatography (CH_2Cl_2:Hexane, 70:30, SiO_2) to afford (*R*)-*N*-benzyl-2,3-dihydro-1*H*-inden-1-amine (740 mg, 3.31 mmol, 85%) as a pale yellow oil.

^{1}H NMR (400 MHz, Chloroform-*d*) δ 7.52 – 7.33 (m, 5H, 5 × Ar-H), 7.32 – 7.17 (m, 4H, 4 × Ar-H), 4.33 (t, *J* = 6.7 Hz, 1H, CH), 4.04 – 3.87 (m, 2H, CH_2), 3.05 (ddd, *J* = 15.9, 8.5, 4.6 Hz, 1H, ½ × CH_2), 2.85 (dt, *J* = 15.9, 7.8 Hz, 1H, ½ × CH_2), 2.47 (dddd, *J* = 12.7, 8.2, 7.0, 4.6 Hz, 1H, ½ × CH_2), 1.91 (dddd, *J* = 12.7, 8.2, 7.3, 6.2 Hz, 1H, ½ × CH_2), 1.55 (br s, 1H, NH).

^{13}C NMR (101 MHz, Chloroform-*d*) δ 145.4, 143.7, 140.8, 128.4 (2 C), 128.1 (2 C), 127.4, 126.9, 126.2, 124.8, 124.1, 62.8, 51.4, 33.7, 30.4.

IR υ_{max} (film): 3024, 2938, 2846, 1453.

HRMS (EI$^+$) *m/z* calcd for $C_{16}H_{18}N$ [M+H]$^+$: 224.1439, found 224.1433.

$[\alpha]^{25}_{589}$= -1.7 (*c* 1.7, $CHCl_3$) for 99% ee.

Analytical data are in agreement with the literature.[15]

(R)-N-(4-methylcyclohexyl)-2,3-dihydro-1*H*-inden-1-amine

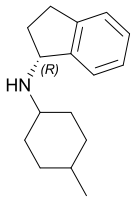

General Procedure D: 4-methylcyclohexan-1-one (0.48 mL, 3.897 mmol, 1.0 eq.), (*R*)-2,3-dihydro-1*H*-inden-1-amine (0.5 mL, 3.897 mmol, 1.0 eq.), dry THF (15 mL), $NaB(OAc)_3H$ (908 mg, 4.286 mmol, 1.1 eq.).

The crude mixture was treated as described above and was purified by flash column chromatography (CH_2Cl_2:Hexane, 70:30, SiO_2) to afford (*R*)-*N*-(4-methylcyclohexyl)-2,3-dihydro-1*H*-inden-1-amine (104 mg, 0.4676 mmol, 12%) as a pale yellow oil.

^{1}H NMR (400 MHz, Chloroform-*d*) δ 7.44 – 7.37 (m, 1H, Ar-H), 7.31 – 7.19 (m, 3H, 3 × Ar-H), 4.35 (t, *J* = 6.7 Hz, 1H, CH), 3.05 (ddd, *J* = 15.8, 8.6, 4.4 Hz, 1H, ½ × CH_2), 3.01 – 2.93 (m, 1H, CH), 2.84 (dt, *J* = 15.8, 7.9 Hz, 1H, ½ × CH_2), 2.53 – 2.40 (m, 1H, ½ × CH_2), 1.89 – 1.40 (m, 10H, ½ × CH_2 & CH & 4 × CH_2), 1.00 (d, *J* = 6.7 Hz, 3H, CH_3).

^{13}C NMR (101 MHz, Chloroform-*d*) δ 146.2, 143.5, 127.2, 126.2, 124.7, 124.1, 60.4, 52.0, 34.7, 30.7 (br s), 30.5 (br s), 30.4, 29.9, 29.8, 29.1, 20.7.

IR υ_{max} (film): 2948, 2847, 2360, 2326, 1455.

HRMS (EI^+) *m/z* calcd for $C_{16}H_{24}N$ $[M+H]^+$: 230.1903, found 230.1902.

$[\alpha]^{25}_{589}$ = -10.2 (*c* 1.5, $CHCl_3$) for 99% ee.

(R)-N-(pentan-3-yl)-2,3-dihydro-1*H*-inden-1-amine

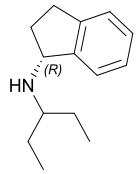

General Procedure D: Pentan-3-one (0.62 mL, 5.845 mmol, 1.5 eq.), (*R*)-2,3-dihydro-1*H*-inden-1-amine (0.5 mL, 3.897 mmol, 1.0 eq.), THF (15 mL), $NaB(OAc)_3H$ (991 mg, 4.676 mmol, 1.2 eq.).

The crude mixture was treated as described above and was purified by flash column chromatography (CH_2Cl_2:Hexane, 70:30, SiO_2) to afford (*R*)-*N*-(pentan-3-yl)-2,3-dihydro-1*H*-inden-1-amine (639 mg, 3.156 mmol, 81%) as a pale yellow oil.

^{1}H NMR (400 MHz, Chloroform-*d*) δ 7.34 – 7.26 (m, 1H, Ar-H), 7.19 – 7.07 (m, 3H, 3 × Ar-H), 4.20 (t, *J* = 6.9 Hz, 1H, CH), 2.92 (ddd, *J* = 15.8, 8.5, 4.4 Hz, 1H, ½ × CH_2), 2.71 (dt, *J* = 15.8, 7.7 Hz, 1H, ½ × CH_2), 2.57 (p, *J* = 5.8 Hz, 1H, CH), 2.35 (dddd, *J* = 12.4, 8.5, 6.9, 4.4 Hz, 1H, ½ × CH_2), 1.77 – 1.63 (m, 1H, ½ × CH_2), 1.52 – 1.29 (m, 4H, 2 × CH_2), 0.86 (t, *J* = 7.5 Hz, 3H, CH_3), 0.84 (t, *J* = 7.5 Hz, 3H, CH_3).

^{13}C NMR (101 MHz, Chloroform-*d*) δ 146.2, 143.5, 127.2, 126.3, 124.7, 124.1, 60.8, 58.4, 34.9 (br s), 30.3, 26.7, 26.0, 10.3, 9.7.

IR υ_{max} (film): 2960, 2934, 2360, 2340, 1459.

HRMS (EI^+) *m/z* calcd for $C_{14}H_{22}N$ $[M+H]^+$: 204.1747, found 204.1748.

$[\alpha]^{25}_{589}$ = -35.4 (*c* 1.0, $CHCl_3$) for 99% ee.

(1R)-N-(decan-3-yl)-2,3-dihydro-1*H*-inden-1-amine

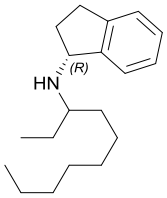

General Procedure D: *(R)*-2,3-dihydro-1*H*-inden-1-aminium chloride (300 mg, 1.768 mmol, 1.0 eq.), decan-3-one (0.40 mL, 2.122 mmol, 1.2 eq.), dry THF (15 mL), $NaB(OAc)_3H$ (599 mg, 2.829 mmol, 1.6 eq.)

The crude mixture was treated as described above and was purified by flash column chromatography (CH_2Cl_2:Hexane, 70:30, SiO_2) to afford the mixture of diastereoisomers (1*R*)-*N*-(decan-3-yl)-2,3-dihydro-1*H*-inden-1-amine (350 mg, 1.273 mmol, 72%) as a pale yellow oil.

Mixture of diastereoisomers (1:1)

^{1}H NMR (500 MHz, Chloroform-*d*) δ 7.43 – 7.35 (m, 1H, Ar-H), 7.28 – 7.18 (m, 3H, 3 × Ar-H), 4.34 – 4.26 (m, 1H, CH), 3.01 (dddd, *J* = 15.7, 8.6, 4.3, 1.4 Hz, 1H, ½ × CH_2), 2.82 (dt, *J* = 15.8, 7.9 Hz, 1H, ½ × CH_2), 2.71 (h, *J* = 5.8 Hz, 1H, CH), 2.50 – 2.40 (m, 1H, ½ × CH_2), 1.85 – 1.72 (m, 1H, ½ × CH_2), 1.61 – 1.25 (m, 14H, 7 × CH_2), 0.99 – 0.88 (m, 6H, 2 × CH_3).

^{13}C NMR (126 MHz, Chloroform-*d*) δ 146.4 (2 C), 143.4 (2 C), 127.2 (2 C), 126.3, 126.2, 124.7, 124.6, 124.0 (2 C), 60.8, 60.7, 57.2, 56.8, 35.1, 34.9, 34.4, 33.9, 31.9 (2 C), 30.3 (2 C), 30.0, 29.9, 29.4 (2 C), 27.3, 26.5, 26.1, 25.6, 22.7 (2 C), 14.1 (2 C), 10.3, 9.7.

IR υ_{max} (film): 2924, 2359, 1434, 1320, 1020.

HRMS (EI^+) *m/z* calcd for $C_{19}H_{32}N$ $[M+H]^+$: 274.2529, found 274.2528.

$[\alpha]^{25}_{589}$ = -15.4 (*c* 1.6, $CHCl_3$) for 99% ee.

(1R)-N-(2-methylpentan-3-yl)-2,3-dihydro-1*H*-inden-1-amine

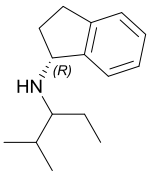

General Procedure D: (*R*)-2,3-dihydro-1*H*-inden-1-aminium chloride (300 mg, 1.768 mmol, 1.0 eq.), 2-methylpentan-3-one (0.26 mL, 2.122 mmol, 1.2 eq.), dry THF (15 mL), $NaB(OAc)_3H$ (599 mg, 2.829 mmol, 1.6 eq.).

The crude mixture was treated as described above and was purified by flash column chromatography (CH_2Cl_2:Hexane, 70:30, SiO_2) to afford the mixture of diastereoisomers (1*R*)-*N*-(2-methylpentan-3-yl)-2,3-dihydro-1*H*-inden-1-amine (234 mg, 1.078 mmol, 61%) as a pale yellow oil.

Mixture of diastereoisomers (1:1)

^{1}H NMR (500 MHz, Chloroform-*d*) δ 7.44 – 7.37 (m, 1H, Ar-H), 7.27 – 7.17 (m, 3H, 3 × Ar-H), 4.31 – 4.23 (m, 1H, CH), 3.06 – 2.96 (m, 1H, ½ × CH_2), 2.80 (dt, *J* = 15.8, 7.9 Hz, 1H, ½ × CH_2), 2.52 – 2.37 (m, 2H, CH & ½ × CH_2), 1.97 – 1.71 (m, 2H, CH & ½ × CH_2), 1.63 – 1.43 (m, 1H, ½ × CH_2), 1.41 – 1.20 (m, 1H, ½ × CH_2), 1.01 – 0.90 (m, 9H, 3 × CH_3).

^{13}C NMR (126 MHz, Chloroform-*d*) δ 146.6 (2 C), 143.6, 143.4, 127.2, 127.1, 126.2 (2 C), 124.6 (2 C), 124.1, 124.0, 63.0, 62.8, 61.8, 61.5, 35.2, 35.0, 30.3 (2 C), 30.1 (2 C), 23.6, 23.5, 18.8, 18.7, 18.3, 17.8, 11.2, 10.5.

IR υ_{max} (film): 2924, 2359, 1476, 1301, 1020.

HRMS (EI^+) *m/z* calcd for $C_{15}H_{24}N$ $[M+H]^+$: 218.1903, found 218.1904.

$[\alpha]^{25}_{589}$ = -18.3 (*c* 1.4, $CHCl_3$) for 99% ee.

(1R)-N-(heptan-3-yl)-2,3-dihydro-1*H*-inden-1-amine

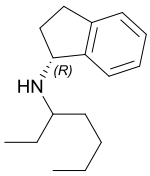

General Procedure D: *(R)*-2,3-dihydro-1*H*-inden-1-aminium chloride (400 mg, 2.358 mmol, 1.0 eq.), heptan-3-one (0.39 mL, 2.829 mmol, 1.2 eq.), dry THF (15 mL), $NaB(OAc)_3H$ (799 mg, 3.772 mmol, 1.6 eq.).

The crude mixture was treated as described above and was purified by flash column chromatography (CH_2Cl_2:Hexane, 70:30, SiO_2) to afford the mixture of diastereoisomers (1*R*)-*N*-(heptan-3-yl)-2,3-dihydro-1*H*-inden-1-amine (470 mg, 2.0279 mmol, 86%) as a pale yellow oil.

Mixture of diastereoisomers (1:1)

^{1}H NMR (400 MHz, Chloroform-*d*) δ 7.43 – 7.34 (m, 1H, Ar-H), 7.28 – 7.17 (m, 3H, 3 × Ar-H), 4.30 (td, *J* = 6.8, 1.9 Hz, 1H, CH), 3.01 (ddd, *J* = 15.8, 8.5, 4.3 Hz, 1H, ½ × CH_2), 2.88 – 2.75 (m, 1H, ½ × CH_2), 2.77 – 2.65 (m, 1H, CH), 2.52 – 2.39 (m, 1H, ½ × CH_2), 1.85 – 1.70 (m, 1H, ½ × CH_2), 1.63 – 1.27 (m, 8H, 4 × CH_2), 1.00 – 0.89 (m, 6H, 2 × CH_3).

^{13}C NMR (101 MHz, Chloroform-*d*) δ 146.5 (2 C), 143.4 (2 C), 127.2 (2 C), 126.2 (2 C), 124.7, 124.6, 124.0 (2 C), 60.9, 60.7, 57.2, 56.8, 35.2, 35.0, 34.1, 33.6, 30.3 (2 C), 28.3, 27.8, 27.4, 26.5, 23.1, 23.0, 14.2 (2 C), 10.2, 9.6.

IR υ_{max} (film): 2928, 2856, 2360, 1434.

HRMS (EI^+) *m/z* calcd for C_{16} H_{26} N $[M+H]^+$: 232.2060, found 232.2060.

$[\alpha]^{25}_{589}$ = -37.3 (*c* 1.0, $CHCl_3$) for 99% ee.

(R)-N-(2,8-dimethylnonan-5-yl)-2,3-dihydro-1*H*-inden-1-amine

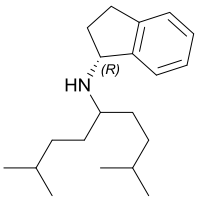

General Procedure D: *(R)*-2,3-dihydro-1*H*-inden-1-aminium chloride (500 mg, 2.947 mmol, 1.0 eq.), 2,8-dimethyl-5-oxononan-1-ylium (602 mg, 3.537 mmol, 1.2 eq.), dry THF (15 mL), $NaB(OAc)_3H$ (999 mg, 4.716 mmol, 1.6 eq.).

The crude mixture was treated as described above and was purified by flash column chromatography (CH_2Cl_2:Hexane, 70:30, SiO_2) to afford (*R*)-N-(2,8-dimethylnonan-5-yl)-2,3-dihydro-1*H*-inden-1-amine (557mg, 1.945 mmol, 66%) as a pale yellow oil.

^{1}H NMR (400 MHz, Chloroform-*d*) δ 7.41 – 7.36 (m, 1H, Ar-H), 7.27 – 7.19 (m, 3H, 3 × Ar-H), 4.30 (t, *J* = 6.8 Hz, 1H, CH), 3.00 (ddd, *J* = 15.8, 8.5, 4.1 Hz, 1H, ½ × CH_2), 2.82 (dt, *J* = 15.9, 8.0 Hz, 1H, ½ × CH_2), 2.73 (p, *J* = 5.8 Hz, 1H, CH), 2.46 (dddd, *J* = 12.3, 8.0, 6.8, 4.1 Hz, 1H, ½ × CH_2), 1.84 – 1.70 (m, 1H, ½ × CH_2), 1.64 – 1.35 (m, 6H, 2 × CH & 2 × CH_2), 1.34 – 1.16 (m, 4H, 2 × CH_2), 1.12 (br s, 1H, NH), 0.97 – 0.88 (m, 12H, 4 × CH_3).

^{13}C NMR (101 MHz, Chloroform-*d*) δ 146.5, 143.4, 127.2, 126.2, 124.6, 124.0, 60.8, 56.2, 35.2, 35.1, 34.6, 32.6, 32.0, 30.3, 28.5, 28.4, 22.8 (2 C), 22.7 (2 C).

IR υ_{max} (film): 2952, 2927, 2868, 1465.

HRMS (EI^+) *m/z* calcd for $C_{20}H_{34}N$ $[M+H]^+$: 288.2686, found 288.2685.

$[\alpha]^{25}_{589}$ = -12.4 (*c* 2.3, $CHCl_3$) for 99% ee.

***(R)*-*N*-(2,3-dihydro-1*H*-inden-1-yl)adamantan-2-amine**

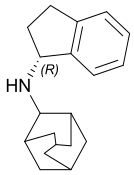

General Procedure D: *(R)*-2,3-dihydro-1*H*-inden-1-aminium chloride (500 mg, 2.947 mmol, 1.0 eq.), adamantan-2-one (531 mg, 3.537 mmol, 1.2 eq.), dry THF (15 mL), $NaB(OAc)_3H$ (999 mg, 4.716 mmol, 1.6 eq.).

The crude mixture was treated as described above and was purified by flash column chromatography (CH_2Cl_2:Hexane, 70:30, SiO_2) then filtered through a strong cation exchange column ISOLUTE® SCX-2 with MeOH to wash off non-basic component followed by ammonia solution in MeOH (2 M), then purified by flash column chromatography (CH_2Cl_2:Hexane, 70:30, SiO_2) to afford (*R*)-*N*-(2,3-dihydro-1*H*-inden-1-yl)adamantan-2-amine (464 mg, 1.739 mmol, 59%) as a pale yellow oil.

^{1}H NMR (400 MHz, Chloroform-*d*) δ 7.42 – 7.36 (m, 1H, Ar-H), 7.27 – 7.18 (m, 3H, 3 × Ar-H), 4.32 (t, *J* = 6.8 Hz, 1H, CH), 3.08 – 2.96 (m, 2H, CH & ½ × CH_2), 2.88 – 2.75 (m, 1H, ½ × CH_2), 2.52 – 2.39 (m, 1H, ½ × CH_2), 2.23 – 1.72 (m, 13H, ½ × CH_2 & 4 × CH & 4 × CH_2), 1.58 – 1.49 (m, 2H, CH_2), 1.24 (br s, 1H, NH).

^{13}C NMR (101 MHz, Chloroform-*d*) δ 146.7, 143.4, 127.1, 126.2, 124.6, 124.0, 60.4, 59.8, 38.1, 37.8, 37.5, 34.8, 33.9, 31.6, 31.5, 31.3, 30.4, 27.9 (2 C).

IR υ_{max} (film): 2900, 2847, 1458, 1083.

HRMS (EI^+) *m/z* calcd for $C_{19}H_{26}N$ $[M+H]^+$: 268.2060, found 268.2059.

$[\alpha]^{25}_{589}$ = -13.6 (*c* 2.5, $CHCl_3$) for 99% ee.

***(R)*-*N*-(1,7-diphenylheptan-4-yl)-2,3-dihydro-1*H*-inden-1-amine**

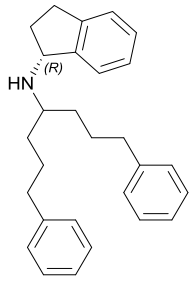

General Procedure D: (*R*)-2,3-dihydro-1*H*-inden-1-aminium chloride (650 mg, 3.843 mmol, 1.0 eq.), 1,7-diphenylheptan-4-one (1024 mg, 3.843 mmol, 1.0 eq.), dry THF (15 mL), $NaB(OAc)_3H$ (1303 mg, 6.148 mmol, 1.6 eq.).

The crude mixture was treated as described above and was purified by flash column chromatography (Hexane:EtOAc, 90:10, SiO_2) to afford (*R*)-*N*-(1,7-diphenylheptan-4-yl)-2,3-dihydro-1*H*-inden-1-amine (683 mg, 1.768 mmol, 46%) as a pale yellow oil.

^{1}H NMR (500 MHz, Chloroform-*d*) δ 7.36 – 7.26 (m, 5H, 5 × Ar-H), 7.27 – 7.17 (m, 9H, 9 × Ar-H), 4.25 (t, *J* = 6.7 Hz, 1H, CH), 2.99 (ddd, *J* = 15.8, 8.4, 4.4 Hz, 1H, ½ × CH_2), 2.86 – 2.75 (m, 2H, CH & ½ × CH_2), 2.69 – 2.59 (m, 4H, 2 × CH_2), 2.46 – 2.36 (m, 1H, ½ × CH_2), 1.79 – 1.61 (m, 5H, ½ × CH_2 & 2 × CH_2), 1.61 – 1.37 (m, 5H, 2 × CH_2 & NH).

^{13}C NMR (126 MHz, Chloroform-*d*) δ 146.3, 143.4, 142.6, 142.5, 128.4 (4 C), 128.3 (4 C), 127.2, 126.3, 125.7 (2 C), 124.7, 124.0, 60.7, 55.3, 36.2 (2 C), 35.0, 34.5, 33.9, 30.3, 27.9, 27.3.

IR υ_{max} (film): 2932, 2854, 1453.

HRMS (EI^+) *m/z* calcd for $C_{28}H_{34}N$ $[M+H]^+$: 384.2686, found 384.2683.

$[\alpha]^{25}_{589}$ = -20.1 (*c* 1.0, $CHCl_3$) for 99% ee.

***(R)-N*-(1,3-diphenylpropan-2-yl)-2,3-dihydro-1*H*-inden-1-amine**

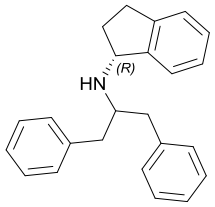

General Procedure D: (*R*)-2,3-dihydro-1*H*-inden-1-aminium chloride (700 mg, 4.138 mmol, 1.0 eq.), 1,3-diphenylpropan-2-one (870 mg, 4.138 mmol, 1.0 eq.), dry THF (15 mL), $NaB(OAc)_3H$ (1403 mg, 6.621 mmol, 1.6 eq.).

The crude mixture was treated as described above and was purified by flash column chromatography (CH_2Cl_2:Hexane, 70:30, SiO_2) then filtered through a strong cation exchange column ISOLUTE® SCX-2 with MeOH to wash off non-basic component followed by ammonia solution in MeOH (2 M) to afford (*R*)-*N*-(1,3-diphenylpropan-2-yl)-2,3-dihydro-1*H*-inden-1-amine (774 mg, 2.359 mmol, 57%) as a pale yellow oil.

^{1}H NMR (500 MHz, Chloroform-*d*) δ 7.39 – 7.11 (m, 14H, 14 × Ar-H), 4.26 (t, *J* = 6.9 Hz, 1H, CH), 3.36 – 3.27 (m, 1H, CH), 2.96 – 2.64 (m, 6H, 3 × CH_2), 2.41 – 2.31 (m, 1H, ½ × CH_2), 1.56 (br s, 1H, NH), 1.50 – 1.39 (m, 1H, ½ × CH_2).

^{13}C NMR (126 MHz, Chloroform-*d*) δ 145.8, 143.2, 139.5, 139.4, 129.5 (2 C), 129.3 (2 C), 128.4 (4 C), 127.2, 126.2 (3 C), 124.5, 123.9, 61.3, 59.6, 41.6, 41.3, 34.7, 30.0.

IR υ_{max} (film): 3025, 2924, 1495, 1453.

HRMS (EI^+) *m/z* calcd for C_{24} H_{26} N $[M+H]^+$: 328.2060, found 328.2058.

$[\alpha]^{25}_{589}$ = -35.1 (*c* 2.1, $CHCl_3$) for 99% ee.

_(R)-N_-isobutyl-2,3-dihydro-1_H_-inden-1-amine

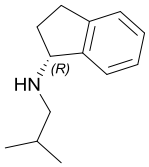

General Procedure D: *(R)*-2,3-dihydro-1*H*-inden-1-aminium chloride (700 mg, 4.138 mmol, 1.0 eq.), isobutyraldehyde (1.06 mL, 4.138 mmol, 1.0 eq.), dry THF (15 mL), $NaB(OAc)_3H$ (1403 mg, 6.621 mmol, 1.6 eq.).

The crude mixture was treated as described above and was purified by flash column chromatography (Hexane:EtOAc, 90:10, SiO_2) to afford (*R*)-*N*-isobutyl-2,3-dihydro-1*H*-inden-1-amine (520 mg, 2.731 mmol, 66%) as a pale yellow oil.

^{1}H NMR (500 MHz, Chloroform-*d*) δ 7.40 – 7.35 (m, 1H, Ar-H), 7.31 – 7.19 (m, 3H, 3 × Ar-H), 4.26 (t, *J* = 6.7 Hz, 1H, CH), 3.02 (ddd, *J* = 15.8, 8.6, 4.5 Hz, 1H, ½ × CH_2), 2.84 (dt, *J* = 15.8, 7.9 Hz, 1H, ½ × CH_2), 2.61 – 2.50 (m, 2H, CH_2), 2.43 (dddd, *J* = 12.6, 7.9, 7.0, 4.5 Hz, 1H, ½ × CH_2), 1.90 – 1.74 (m, 2H, CH & ½ × CH_2), 0.97 (d, *J* = 6.6 Hz, 6H, 2 × CH_3).

^{13}C NMR (126 MHz, Chloroform-*d*) δ 145.6, 143.6, 127.3, 126.2, 124.7, 124.1, 63.4, 55.4, 33.6, 30.4, 28.9, 20.9, 20.8.

IR υ_{max} (film): 3025, 2924, 1495, 1453.

HRMS (EI^+) *m/z* calcd for C_{24} H_{26} N $[M+H]^+$: 328.2060, found 328.2058.

$[\boldsymbol{\alpha}]^{25}_{589}$ = -35.1 (*c* 2.1, $CHCl_3$) for 99% ee.

***(R)-N*-(2,6-dimethylheptan-4-yl)-2,3-dihydro-1*H*-inden-1-amine**

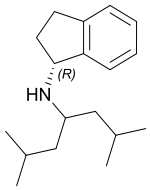

General Procedure D: (*R*)-2,3-dihydro-1*H*-inden-1-aminium chloride (200 mg, 1.182 mmol, 1.0 eq.), 2,6-dimethylheptan-4-one (0.21 mL, 1.182 mmol, 1.0 eq.), $NaB(OAc)_3H$ (401 mg, 1.892 mmol, 1.6 eq.).

The crude mixture was treated as described above and was purified by flash column chromatography (Hexane:EtOAc, 80:20, SiO_2) to afford (*R*)-*N*-(2,6-dimethylheptan-4-yl)-2,3-dihydro-1*H*-inden-1-amine (85 mg, 0.331 mmol, 28%) as a pale yellow oil.

^{1}H NMR (400 MHz, Chloroform-*d*) δ 7.32 – 7.25 (m, 1H, Ar-H), 7.17 – 7.08 (m, 3H, 3 × Ar-H), 4.21 (t, *J* = 6.7 Hz, 1H, CH), 2.91 (ddd, *J* = 15.8, 8.4, 4.3 Hz, 1H, ½ × CH_2), 2.73 (dt, *J* = 16.0, 7.6 Hz, 2H, CH & ½ × CH_2), 2.36 (dddd, *J* = 12.4, 8.0, 6.8, 4.3 Hz, 1H, ½ × CH_2), 1.74 – 1.55 (m, 3H, 2 × CH & ½ × CH_2), 1.37 – 1.10 (m, 4H, 2 × CH_2), 0.88 – 0.79 (m, 12H, 4 × CH_3).

^{13}C NMR (101 MHz, Chloroform-*d*) δ 146.3, 143.4, 127.2, 126.3, 124.7, 124.1, 60.6, 51.7, 45.3, 45.0, 35.3, 30.3, 24.9, 24.7, 23.4, 23.3, 22.9, 22.6.

IR υ_{max} (film): 3659, 2980, 2361, 1462, 1382, 1251, 1154, 1082.

HRMS (EI^+) *m/z* calcd for C_{18} H_{30} N $[M+H]^+$: 260.2373, found 260.2370.

$[\boldsymbol{\alpha}]^{25}_{589}$ = -25.0 (*c* 1.0, $CHCl_3$) for 99% ee.

***(R)-N*-(dicyclohexylmethyl)-2,3-dihydro-1*H*-inden-1-amine**

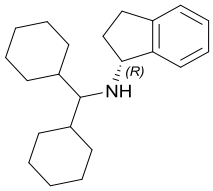

(R)-2,3-dihydro-1*H*-inden-1-aminium chloride (500 mg, 2.956 mmol, 1.0 eq.), was mixed with aq. NaOH (2M, 10mL) and CH_2Cl_2 (20 mL). The aqueous phase was extracted with CH_2Cl_2 (3 × 20 mL). The combined organic phases were dried over $MgSO_4$, filtered and concentrated under reduced pressure. 4-(cyclohexanecarbonyl)-cyclohexan-1-ylium (0.58 mL, 2.956 mmol, 1.0 eq.) was then added to a stirring solution of the freshly concentrated (*R*)-2,3-dihydro-1*H*-inden-1-amine in dry toluene (15 mL) at rt. After 5min, 25 g of activated 4 Å sieves were added. The mixture was then strongly stirred and refluxed for 5 days. When an acceptable ratio of the imine/amine was obtained according to ^{1}H NMR, the mixture was filtered through a pad of celite, rinsed with toluene and concentrated to remove the solvent. After keeping it under high vacuum for 30 min, dry ethanol (35 mL) was added followed by $NaBH_4$ (167.7 mg, 4.434 mmol, 1.5 eq.) and the suspension was stirred overnight (in practice, the reaction is done after about 2 hours). The solvent is then removed before diluting the mixture with CH_2Cl_2 (20 mL) and NaOH (2 M, *ca* 10 mL). The organic and aqueous layers were partitioned and the aqueous phase was extracted with CH_2Cl_2 (3 × 20 mL). The combined organic phases were dried over $MgSO_4$, filtered and concentrated under reduced pressure.

The crude mixture was treated as described above and was purified by flash column chromatography (Hexane, SiO_2), then filtered through a strong cation exchange column ISOLUTE® SCX-2 with MeOH to wash off non-basic component followed by

ammonia solution in MeOH (2 M) to afford (*R*)-*N*-(dicyclohexylmethyl)-2,3-dihydro-1*H*-inden-1-amine (171 mg, 0.709 mmol, 24%) as a brown oil.

^{1}H NMR (500 MHz, Chloroform-*d*) δ 7.48 – 7.42 (m, 1H, Ar-H), 7.28 – 7.17 (m, 3H, 3 × Ar-H), 4.27 (t, *J* = 6.6 Hz, 1H, CH), 3.04 – 2.95 (m, 1H, ½ × CH_2), 2.76 (dt, *J* = 15.6, 7.7 Hz, 1H, ½ × CH_2), 2.42 – 2.32 (m, 1H, ½ × CH_2), 2.30 – 2.24 (m, 1H, CH), 1.88 – 1.73 (m, 7H, ½ × CH_2 & 3 × CH_2), 1.73 – 1.62 (m, 4H, 2 × CH_2), 1.59 – 1.52 (m, 1H, CH), 1.48 – 1.38 (m, 1H, CH), 1.33 – 1.10 (m, 9H, 4 × CH_2 & ½ × CH_2), 1.08 – 0.98 (m, 1H, ½ × CH_2).

^{13}C NMR (126 MHz, Chloroform-*d*) δ 146.7, 143.6, 127.1, 126.1, 124.6, 123.9, 65.7, 64.0, 41.8, 40.4, 35.4, 31.6, 31.5, 30.2, 29.0, 28.8, 27.1, 26.9 (2 C), 26.8, 26.7 (2 C).

IR υ_{max} (film): 3021, 2849, 1448, 1260, 1126.

HRMS (EI$^+$) *m/z* calcd for C_{22} H_{34} N $[M+H]^+$: 312.2686, found 312.2685.

$[\boldsymbol{\alpha}]^{25}_{589}$ = -12.6 (*c* 1.0, $CHCl_3$) for 99% ee.

(R)-N-(2,4-dimethylpentan-3-yl)-2,3-dihydro-1*H*-inden-1-amine

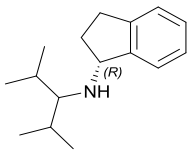

(R)-2,3-dihydro-1*H*-inden-1-aminium chloride (500 mg, 2.956 mmol, 1.0 eq.) was mixed with aq. NaOH (2M, 10mL) and CH_2Cl_2 (20 mL). The aqueous phase was extracted with CH_2Cl_2 (3 × 20 mL). The combined organic phases were dried over $MgSO_4$, filtered and concentrated under reduced pressure. 2,4-dimethylpentan-3-one (0.42 mL, 2.956 mmol, 1.0 eq.) was then added to a stirring solution of the freshly concentrated (*R*)-2,3-dihydro-1*H*-inden-1-amine in dry toluene (15 mL) at rt. After 5 min, 25 g of sieves were added. The mixture was then strongly stirred and

refluxed for 5 days. When an acceptable ratio of the imine/amine was obtained, the mixture was filtered through a pad of celite, rinsed with toluene and concentrated to remove the solvent. After keeping it under high vacuum for 30 min, dry ethanol (35 mL) was added followed by $NaBH_4$ (167.7 mg, 4.434 mmol, 1.5 eq.) and the suspension was stirred overnight (In practice, the reaction is done after 2 hours). The solvent is then removed before diluting the mixture with CH_2Cl_2 (20 mL) and NaOH (2 M, *ca* 10 mL). The organic and aqueous layers were partitioned and the aqueous phase was extracted with CH_2Cl_2 (3 × 20 mL). The combined organic phases were dried over $MgSO_4$, filtered and concentrated under reduced pressure.

The crude mixture was treated as described above and was purified by flash column chromatography (Hexane, SiO_2), then filtered through a strong cation exchange column ISOLUTE® SCX-2 with MeOH to wash off non-basic component followed by ammonia solution in MeOH (2 M) to afford (*S*)-*N*-(2,4-dimethylpentan-3-yl)-2,3-dihydro-1*H*-inden-1-amine (211 mg, 0.798 mmol, 27%) as a brown oil.

^{1}H NMR (500 MHz, Chloroform-*d*) δ 7.49 – 7.44 (m, 1H, Ar-H), 7.27 – 7.18 (m, 3H, 3 × Ar-H), 4.28 (t, *J* = 6.5 Hz, 1H, CH), 3.00 (ddd, *J* = 15.6, 8.2, 4.4 Hz, 1H, ½ × CH_2), 2.76 (dt, *J* = 15.6, 7.7 Hz, 1H, ½ × CH_2), 2.45 – 2.35 (m, 1H, ½ × CH_2), 2.27 (t, *J* = 5.4 Hz, 1H, CH), 1.94 – 1.85 (m, 1H, ½ × CH_2), 1.85 – 1.73 (m, 2H, 2 × CH), 1.02 – 0.92 (m, 12H, 4 × CH_3).

^{13}C NMR (126 MHz, Chloroform-*d*) δ 146.8, 143.6, 127.1, 126.1, 124.6, 124.0, 66.7, 63.9, 35.5, 31.5, 30.2 (2 C), 21.3, 21.0, 18.6, 18.4.

IR υ_{max} (film): 3069, 2956, 2870, 2360, 1472, 1381, 1081.

HRMS (EI^+) *m/z* calcd for $C_{16}H_{26}N$ $[M+H]^+$: 232.2060, found 232.2061.

$[\alpha]^{25}_{589}$ = -18.4 (*c* 1.0, $CHCl_3$) for 99% ee.

(1*R*)-*N*-(2,2,4-trimethylpentan-3-yl)-2,3-dihydro-1*H*-inden-1-amine

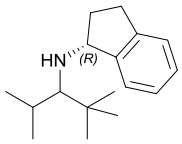

(*R*)-2,3-dihydro-1*H*-inden-1-aminium chloride (1.00 g, 5.89 mmol, 1.0 eq.) was mixed with aq. NaOH (2 M, 10 mL) and CH_2Cl_2 (20 mL). The aqueous phase was extracted with CH_2Cl_2 (3 × 20 mL). The combined organic phases were dried over $MgSO_4$, filtered and concentrated under reduced pressure. Isobutyraldehyde (0.59 mL, 6.48 mmol, 1.1 eq.) was then added to a stirring solution of the freshly concentrated (*R*)-2,3-dihydro-1*H*-inden-1-amine in dry Et_2O (15 mL) at rt. Molecular sieves were then added and the mixture was let to stir for 1 h. The reaction mixture was then cooled down at -78 °C and *t*-BuLi (1.7 M solution in pentane, 6.93 mL, 11.8 mmol, 2.0 eq.) was added dropwise. The reaction was allowed to slowly warm up to room temperature overnight. NH_4Cl (aq. sat., *ca* 20 mL) was added to quench the reaction. The organic and aqueous layers were partitioned and the aqueous phase was extracted with Et_2O (3 × 20 mL). The combined organic phases were dried over $MgSO_4$, filtered and concentrated under reduced pressure. After column chromatography (Hexane:EtOAc, 90:10, SiO_2), the amine was obtained as a pale yellow oil (650 mg, 2.65 mmol, 45%).

^{1}H NMR (400 MHz, Chloroform-d) δ 7.46 – 7.41 (m, 1H, Ar-H), 7.25 – 7.17 (m, 3H, 3 × Ar-H), 4.33 (t, *J* = 6.2 Hz, 1H, CH), 3.05 – 2.93 (m, 1H, ½ × CH_2), 2.80 – 2.65 (m, 1H, ½ × CH_2), 2.40 – 2.26 (m, 2H, CH & ½ × CH_2), 2.04 (hd, *J* = 6.9, 1.8 Hz, 1H, CH), 1.88 – 1.74 (m, 1H, ½ × CH_2), 1.09 (d, *J* = 7.2 Hz, 3H, CH_3), 1.05 (d, *J* = 7.2 Hz, 3H, CH_3), 0.92 (s, 9H, 3 × CH_3).

^{13}C NMR (101 MHz, Chloroform-d) δ 146.8, 143.9, 127.2, 126.1, 124.7, 123.8, 68.8, 63.7, 35.9, 34.5, 30.2, 29.0, 27.7 (3 C), 26.1, 18.2.

IR υ_{max} (film): 2955, 2868, 2360, 1476, 1367, 1080.

HRMS (EI$^+$) *m/z* calcd for $C_{17}H_{28}N$ $[M+H]^+$: 246.2216, found 246.2215.

$[\alpha]^{25}_{589}$ = -32.0 (*c* 1.0, $CHCl_3$) for 99% ee.

N-phenyl-2-vinylaniline

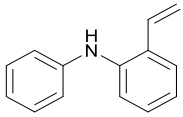

General Procedure F: $Pd_2(dba)_3$ (22 mg, 0.024 mmol, 0.8 mol %), XPhos (33 mg, 0.069 mmol, 2.3 mol %), sodium *tert*-butoxide (345 mg, 3.59 mmol, 1.2 eq.), 1,4-dioxane (3.0 mL), aniline (0.33 mL, 3.59 mmol, 1.2 eq.), 2-bromostyrene (0.40 mL, 2.99 mmol, 1.0 eq.).

The crude mixture was treated as described above and was purified by flash column chromatography (Hexane, SiO_2) to afford *N*-phenyl-2-vinylaniline (576 mg, 2.96 mmol, 99%) as a slightly yellow oil.

^{1}H NMR (400 MHz, Chloroform-d) δ 7.54 – 7.47 (m, 1H, Ar-H), 7.33 – 7.19 (m, 4H, 4 × Ar-H), 7.09 – 6.86 (m, 5H, 4 × Ar-H & C=CH), 5.72 (ddd, *J* = 17.5, 2.2, 1.4 Hz, 1H, C=CH), 5.56 (br s, 1H, NH), 5.35 (dt, *J* = 10.9, 1.7 Hz, 1H, C=CH).

^{13}C NMR (101 MHz, Chloroform-d) δ 144.1, 140.1, 132.8, 130.0, 129.3 (2 C), 128.6, 127.2, 122.5, 120.5, 120.0, 117.2 (2 C), 116.3.

IR υ_{max} (film): 3397, 3047, 1595, 1498, 1454, 1309.

HRMS (ESI$^+$) *m/z* calcd for $C_{14}H_{14}N$ $[M+H]^+$: 196.1121, found 196.1121.

2-methyl-5*H*-dibenzo[*b*,*f*]azepine

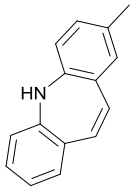

General Procedure E: $Pd_2(dba)_3$ (7.1 mg, 0.008 mmol, 0.8 mol %), DavePhos (9.2 mg, 0.023 mmol, 2.3 mol %), sodium *tert*-butoxide (299 mg, 3.11 mmol, 3.0 eq.), 1,4-Dioxane (1.0 mL), 2-chloro-4-methylaniline (0.15 mL, 1.24 mmol, 1.2 eq.), 2-bromostyrene (0.13 mL, 1.04 mmol, 1.0 eq.).

The crude mixture was treated as described above and was purified by flash column chromatography (Hexane:EtOAc, 99:1, SiO_2) to afford 2-methyl-5*H*-dibenzo[*b*,*f*]azepine (157 mg, 0.76 mmol, 73%) as a yellow solid.

^{1}H NMR (400 MHz, Chloroform-d) δ 6.99 – 6.90 (m, 1H, Ar-H), 6.83 – 6.70 (m, 3H, 3 × Ar-H), 6.61 (d, *J* = 2.0 Hz, 1H, Ar-H), 6.42 (dd, *J* = 7.8, 1.1 Hz, 1H, C=CH), 6.34 (d, *J* = 7.9 Hz, 1H, C=CH), 6.30 – 6.18 (m, 2H, Ar-H), 4.81 (br s, 1H, NH), 2.11 (s, 3H, CH_3).

^{13}C NMR (101 MHz, Chloroform-d) δ 148.7, 145.8, 132.3, 132.1 (2 C), 131.0, 130.5, 129.9, 129.7, 129.6, 129.4, 122.9, 119.2 (2 C), 20.3.

IR υ_{max} (film): 2918, 1471, 1258, 1123.

HRMS (ESI$^+$) *m/z* calcd for $C_{15}H_{14}N$ $[M+H]^+$: 208.1121, found 208.1120.

MP: 173 °C.

4-methyl-5*H*-dibenzo[*b*,*f*]azepine

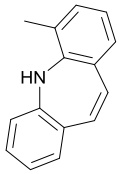

General Procedure E: $Pd_2(dba)_3$ (13.7 mg, 0.015 mmol, 0.75 mol %), DavePhos (17.7 mg, 0.045 mmol, 2.3 mol %), sodium *tert*-butoxide (575 mg, 5.98 mmol, 3.0 eq.), 1,4-dioxane (2.0 mL), 2-chloro-6-methylaniline (0.29 mL, 2.39 mmol, 1.2 eq.), 2-bromostyrene (0.25 mL, 1.99 mmol, 1.0 eq.).

The crude mixture was treated as described above and was purified by flash column chromatography (Hexane:EtOAc, 99:1, SiO_2) to afford 4-methyl-5*H*-dibenzo[*b*,*f*]azepine (267 mg, 1.29 mmol, 65%) as a dark yellow solid.

^{1}H NMR (400 MHz, Chloroform-d) δ 7.07 (ddd, *J* = 7.8, 7.1, 1.8 Hz, 1H, Ar-H), 7.02 – 6.98 (m, 1H, Ar-H), 6.95 – 6.85 (m, 2H, 2 × Ar-H), 6.82 – 6.75 (m, 2H, Ar-H & C=CH), 6.62 (dd, *J* = 7.8, 1.1 Hz, 1H, C=CH), 6.42 (d, *J* = 2.6 Hz, 2H, 2 × Ar-H), 5.15 (br s, 1H, NH), 2.31 (s, 3H, CH_3).

^{13}C NMR (101 MHz, Chloroform-d) δ 148.3, 146.6, 132.7, 131.8, 131.1, 130.6, 130.3, 130.2, 129.2, 128.7, 126.2, 123.2, 122.6, 120.4, 17.8.

IR υ_{max} (film): 3393, 3017, 2972, 1463, 1244, 1112.

HRMS (ESI$^+$) *m/z* calcd for $C_{15}H_{14}N$ $[M+H]^+$: 208.1121, found 208.1121.

MP: 77 °C.

3-methoxy-5*H*-dibenzo[*b*,*f*]azepine

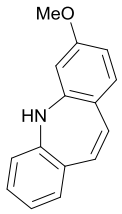

General Procedure E: $Pd_2(dba)_3$ (13.7 mg, 0.015 mmol, 0.75 mol %), DavePhos (17.7 mg, 0.045 mmol, 2.3 mol %), sodium *tert*-butoxide (575 mg, 5.98 mmol, 3.0 eq.), 1,4-dioxane (2.0 mL), 2-chloro-5-methoxyaniline (0.30 mL, 2.39 mmol, 1.2 eq.), 2-bromostyrene (0.25 mL, 1.99 mmol, 1.0 eq.).

The crude mixture was treated as described above and was purified by flash column chromatography (Hexane:EtOAc, 99:1 to 95:5, SiO_2) to afford 3-methoxy-5*H*-dibenzo[*b*,*f*]azepine (82 mg, 0.36 mmol, 18%) as a yellow solid.

^{1}H NMR (400 MHz, Chloroform-d) δ 7.03 – 6.96 (m, 1H, Ar-H), 6.85 – 6.73 (m, 3H, 3 × Ar-H), 6.49 – 6.44 (m, 1H, Ar-H), 6.36 (dd, *J* = 8.3, 2.4 Hz, 1H, C=CH), 6.23 (d, *J* = 11.7 Hz, 1H, Ar-H), 6.16 (d, *J* = 11.7 Hz, 1H, Ar-H), 6.06 (d, *J* = 2.4 Hz, 1H, C=CH), 4.90 (br s, 1H, NH), 3.75 (s, 3H, CH_3).

^{13}C NMR (101 MHz, Chloroform-d) δ 161.2, 149.6, 147.5, 131.7 (2 C), 130.4, 129.9, 129.6, 129.1, 123.1, 122.6, 119.2, 107.4, 105.6, 55.3.

IR υ_{max} (film): 3331, 2972, 1616, 1597, 1575, 1523, 1473, 1331, 1268, 1030.

HRMS (ESI^+) *m/z* calcd for C_{15} H_{14} O N $[M+H]^+$: 224.1070, found 224.1069.

MP: 185 °C.

3-methyl-5*H*-dibenzo[*b*,*f*]azepine

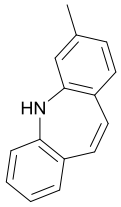

General Procedure E: $Pd_2(dba)_3$ (13.7 mg, 0.015 mmol, 0.75 mol %), DavePhos (17.7 mg, 0.045 mmol, 2.3 mol %), sodium *tert*-butoxide (575 mg, 5.98 mmol, 3.0 eq.), 1,4-dioxane (2.0 mL), 2-chloro-5-methylaniline (339 mg, 2.39 mmol, 1.2 eq.), 2-bromostyrene (0.25 mL, 1.99 mmol, 1.0 eq.).

The crude mixture was treated as described above and was purified by flash column chromatography (Hexane:EtOAc, 99:1, SiO_2) to afford 3-methyl-5*H*-dibenzo[*b*,*f*]azepine (66 mg, 0.32 mmol, 16%) as a yellow solid.

^{1}H NMR (400 MHz, Chloroform-d) δ 7.01 (ddd, *J* = 7.9, 6.9, 2.1 Hz, 1H, Ar-H), 6.87 – 6.79 (m, 2H, 2 × Ar-H), 6.75 (d, *J* = 7.6 Hz, 1H, Ar-H), 6.64 (ddd, *J* = 7.7, 1.7, 0.8 Hz, 1H, Ar-H), 6.47 (dd, *J* = 7.8, 1.1 Hz, 1H, C=CH), 6.34 – 6.22 (m, 3H, C=CH & 2 × Ar-H), 4.89 (br s, 1H, NH), 2.21 (s, 3H, CH_3).

^{13}C NMR (101 MHz, Chloroform-d) δ 148.2 (2 C), 139.7, 132.0, 131.1, 130.5, 130.4, 129.8, 129.3, 126.9, 123.7, 122.9, 120.1, 119.2, 20.9.

IR υ_{max} (film): 3344, 3028, 2915, 1476, 1314, 1244.

HRMS (ESI$^+$) *m/z* calcd for C_{15} H_{14} N $[M+H]^+$: 208.1121, found 208.1121.

MP: 220 °C.

(*S*)-*N*-phenyl-2,3-dihydro-1*H*-inden-1-amine

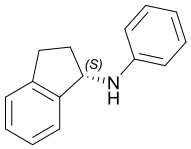

General Procedure F: $Pd_2(dba)_3$ (21 mg, 0.023 mmol, 0.8 mol %), XPhos (31 mg, 0.066 mmol, 2.3 mol %), sodium *tert*-butoxide (328 mg, 3.42 mmol, 1.2 eq.), 1,4-dioxane (3.0 mL), (*S*)-2,3-dihydro-1*H*-inden-1-amine hydrochloride (580 mg, 3.42 mmol, 1.2 eq.), bromobenzene (0.3 mL, 2.85 mmol, 1.0 eq.).

Note: (S)-2,3-dihydro-1H-inden-1-amine hydrochloride was deprotonated by adding an aqueous solution of NaOH (2 M, ca 10 mL) until pH = 14. The aqueous layer was extracted with CH_2Cl_2 (3 × 20 mL) and the combined organic phases were dried over $MgSO_4$, filtered and concentrated under reduced pressure.

The crude mixture was treated as described above and was purified by flash column chromatography (Hexane:EtOAc, 99:1, SiO_2) to afford (*S*)-*N*-phenyl-2,3-dihydro-1*H*-inden-1-amine (434 mg, 2.08 mmol, 73%) as a yellow oil.

^{1}H NMR (400 MHz, Chloroform-d) δ 7.32 – 7.24 (m, 1H, Ar-H), 7.22 – 7.06 (m, 5H, 5 × Ar-H), 6.68 – 6.57 (m, 3H, 3 × Ar-H), 4.92 (t, *J* = 6.7 Hz, 1H, CH), 3.79 (br s, 1H, NH), 2.98 – 2.88 (m, 1H, ½ × CH_2), 2.85 – 2.75 (m, 1H, ½ × CH_2), 2.56 – 2.43 (m, 1H, ½ × CH_2), 1.88 – 1.74 (m, 1H, ½ × CH_2).

^{13}C NMR (101 MHz, Chloroform-d) δ 147.8, 144.6, 143.7, 129.4 (2 C), 128.0, 126.7, 124.9, 124.3, 117.4, 113.2 (2 C), 58.6, 34.0, 30.3.

IR υ_{max} (film): 3398, 3021, 2936, 1601, 1502, 1311, 1248.

HRMS (ESI^+) *m/z* calcd for $C_{15}H_{16}N$ $[M+H]^+$: 210.1277, found 210.1281.

$[\alpha]^{25}_{589}$= +55.1 (*c* 1.0, $CHCl_3$) for 99% ee.

(*S*)-*N*-mesityl-2,3-dihydro-1*H*-inden-1-amine

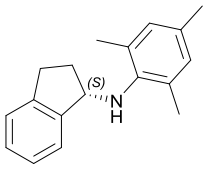

General Procedure F: $Pd_2(dba)_3$ (21 mg, 0.022 mmol, 0.8 mol %), ±BINAP (40 mg, 0.066 mmol, 2.3 mol %), sodium *tert*-butoxide (648 mg, 6.75 mmol, 2.4 eq.), 1,4-dioxane (3.0 mL), (*S*)-2,3-dihydro-1*H*-inden-1-amine hydrochloride (572 mg, 3.37 mmol, 1.2 eq.), 2-bromo-1,3,5-trimethylbenzene (0.43 mL, 2.81 mmol, 1.0 eq.).

Note: (S)-2,3-dihydro-1H-inden-1-amine hydrochloride was deprotonated by adding an aqueous solution of NaOH (2 M, ca 10 mL) until pH = 14. The aqueous layer was extracted with CH_2Cl_2 (3 × 20 mL) and the combined organic phases were dried over $MgSO_4$, filtered and concentrated under reduced pressure.

Note: Due to the steric hindrance of 2-bromo-1,3,5-trimethylbenzene, XPhos was replaced by ±BINAP and 2.4 eq. of sodium tert-butoxide was used instead of 1.2 eq.

The crude mixture was treated as described above and was purified by flash column chromatography (Hexane:EtOAc, 99:1, SiO_2) to afford (*S*)-*N*-mesityl-2,3-dihydro-1*H*-inden-1-amine (352 mg, 1.40 mmol, 50%) as a yellow oil.

^{1}H NMR (400 MHz, Chloroform-d) δ 7.26 – 7.05 (m, 4H, 4 × Ar-H), 6.78 – 6.73 (m, 2H, 2 × Ar-H), 4.66 (t, *J* = 6.8 Hz, 1H, CH), 3.09 (br s, 1H, NH), 3.00 – 2.88 (m, 1H, ½ × CH_2), 2.79 – 2.66 (m, 1H, ½ × CH_2), 2.40 – 2.27 (m, 1H, ½ × CH_2), 2.17 (s, 3H, CH_3), 2.16 (s, 6H, 2 × CH_3), 1.86 – 1.72 (m, 1H, ½ × CH_2).

^{13}C NMR (101 MHz, Chloroform-d) δ 145.7, 143.1, 142.6, 130.8, 129.6 (2 C), 129.1 (2 C), 127.6, 126.4, 124.8, 124.4, 62.7, 35.0, 30.1, 20.6, 18.9 (2 C).

IR υ_{max} (film): 2941, 2853, 1713, 1482, 1448, 1232, 1157, 1104.

HRMS (ESI$^+$) *m/z* calcd for $C_{18}H_{22}N$ $[M+H]^+$: 252.1747, found 252.1747.

$[\alpha]^{25}_{589}$= -88.9 (*c* 1.0, $CHCl_3$) for 99% ee.

(*S*)-*N*-(2,4,6-triisopropylphenyl)-2,3-dihydro-1*H*-inden-1-amine

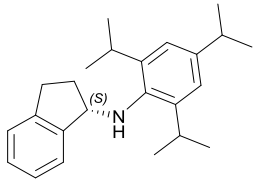

General Procedure F: $Pd_2(dba)_3$ (81 mg, 0.088 mmol, 5.0 mol %), ±BINAP (66 mg, 0.11 mmol, 6.0 mol %), sodium *tert*-butoxide (510 mg, 5.30 mmol, 3.0 eq.), toluene (4.0 mL), (*S*)-2,3-dihydro-1*H*-inden-1-amine hydrochloride (300 mg, 1.77 mmol, 1.0 eq.), 2-bromo-1,3,5-triisopropylbenzene (0.54 mL, 2.12 mmol, 1.2 eq.).

Note: (S)-2,3-dihydro-1H-inden-1-amine hydrochloride was deprotonated by adding an aqueous solution of NaOH (2 M, ca 10 mL) until pH = 14. The aqueous layer was extracted with CH_2Cl_2 (3 × 20 mL) and the combined organic phases were dried over $MgSO_4$, filtered and concentrated under reduced pressure.

Note: Due to the steric hindrance of 2-bromo-1,3,5-triisopropylbenzene, several changes had to be realised such as equivalents and solvent.

The crude mixture was treated as described above and was purified by flash column chromatography (Hexane:EtOAc, 99:1, SiO_2) to afford (*S*)-*N*-(2,4,6-triisopropylphenyl)-2,3-dihydro-1*H*-inden-1-amine (158 mg, 0.48 mmol, 27%) as a yellow oil.

^{1}H NMR (400 MHz, Chloroform-d) δ 7.32 – 7.15 (m, 4H, 4 × Ar-H), 6.97 (s, 2H, 2 × Ar-H), 4.60 (t, *J* = 6.7 Hz, 1H, CH), 3.28 (hept, *J* = 6.9 Hz, 2H, 2 × CH), 3.19 (br s, 1H, NH), 3.05 (ddd, *J* = 15.9, 8.3, 4.8 Hz, 1H, ½ × CH_2), 2.96 – 2.68 (m, 2H, CH & ½ × CH_2), 2.52 – 2.35 (m, 1H, ½ × CH_2), 2.06 – 1.86 (m, 1H, ½ × CH_2), 1.28 (t, *J* = 7.2 Hz, 12H, 4 × CH_3), 1.17 (d, *J* = 6.9 Hz, 6H, 2 × CH_3).

^{13}C NMR (101 MHz, Chloroform-d) δ 145.5, 143.2, 143.1, 141.5 (2 C), 139.5, 127.5, 126.2, 124.7, 124.5, 121.3 (2 C), 65.5, 34.6, 33.9, 30.2, 27.8 (2 C), 24.3 (2 C), 24.2 (2 C), 24.1 (2 C).

IR υ_{max} (film): 2959, 2867, 1467.

HRMS (ESI^{+}) *m/z* calcd for C_{24} H_{34} N $[M+H]^{+}$: 336.2686, found 336.2686.

$[\alpha]^{25}_{589}$= -11.5 (*c* 1.0, $CHCl_3$) for 99% ee.

(*S*)-*N*-(2,3-dihydro-1*H*-inden-1-yl)naphthalen-1-amine

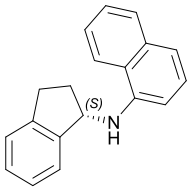

General Procedure F: $Pd_2(dba)_3$ (135 mg, 0.147 mmol, 5.0 mol %), ±BINAP (110 mg, 0.18 mmol, 6.0 mol %), sodium *tert*-butoxide (850 mg, 8.84 mmol, 3.0 eq.), toluene (3.5 mL), (*S*)-2,3-dihydro-1*H*-inden-1-amine hydrochloride (500 mg, 2.95 mmol, 1.0 eq.), 1-bromonaphthalene (0.50 mL, 3.54 mmol, 1.2 eq.).

Note: (S)-2,3-dihydro-1H-inden-1-amine hydrochloride was deprotonated by adding an aqueous solution of NaOH (2 M, ca 10 mL) until pH = 14. The aqueous layer was extracted with CH_2Cl_2 (3 × 20 mL) and the combined organic phases were dried over $MgSO_4$, filtered and concentrated under reduced pressure.

The crude mixture was treated as described above and was purified by flash column chromatography (Hexane:EtOAc, 99:1, SiO_2) to afford (*S*)-N-(2,3-dihydro-1*H*-inden-1-yl)naphthalen-1-amine (706 mg, 2.71 mmol, 92%) as a yellow oil.

^{1}H NMR (400 MHz, Chloroform-d) δ 7.85 – 7.74 (m, 2H, 2 × Ar-H), 7.51 – 7.23 (m, 8H, 8 × Ar-H), 6.88 (dt, *J* = 7.5, 0.9 Hz, 1H, Ar-H), 5.23 (q, *J* = 6.5 Hz, 1H, CH), 4.64 (br s, 1H, NH), 3.17 – 3.07 (m, 1H, ½ × CH_2), 3.06 – 2.94 (m, 1H, ½ × CH_2), 2.80 – 2.69 (m, 1H, ½ × CH_2), 2.12 – 2.01 (m, 1H, ½ × CH_2).

^{13}C NMR (101 MHz, Chloroform-d) δ 144.5, 143.9, 142.9, 134.5, 128.7, 128.1, 126.8, 126.6, 125.8, 125.0, 124.7, 124.5, 123.4, 120.0, 117.3, 105.0, 58.8, 33.8, 30.5.

IR υ_{max} (film): 3424, 3047, 2938, 1580, 1524, 1477, 1407, 1369.

HRMS (ESI$^+$) *m/z* calcd for C_{19} H_{18} N $[M+H]^+$: 260.1434, found 260.1436.

$[\boldsymbol{\alpha}]^{25}_{589}$= +118.1 (*c* 1.0, $CHCl_3$) for 99% ee.

(*E*)-2-styrylaniline

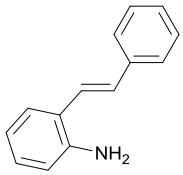

According to a modified procedure,[16] $Pd(OAc)_2$ (8 mg, 0.035 mmol, 1.0 mol %), P(*o*-Tol)$_3$ (86 mg, 0.284 mmol, 8.0 mol %) and 2-bromoaniline (610 mg, 3.55 mmol, 1.0 eq.) were added into a flame dried Biotage© microwave vial and purged (3 × argon/vacuum). Et_3N (3.5 mL) and styrene (0.49 mL, 4.25 mmol, 1.2 eq.) were added then the microwave vial was sealed using a microwave cap. The resulting mixture was stirred overnight at 125 °C using a oil bath. After completion, the reaction was diluted in CH_2Cl_2 (*ca* 15 mL) and poured into water (*ca* 15 mL). The

organic and aqueous layers were partitioned and the aqueous phase was extracted with CH_2Cl_2 (3 × 20 mL). The combined organic phases were dried over $MgSO_4$, filtered and concentrated under reduced pressure. After flash column chromatography (Hexane:EtOAc, 95:5, SiO_2), (*E*)-2-styrylaniline (294 mg, 1.17 mmol, 33%) was obtained as a pale yellow solid.

^{1}H NMR (400 MHz, Chloroform-d) δ 7.58 – 7.50 (m, 2H, 2 × Ar-H), 7.47 – 7.34 (m, 3H, 3 × Ar-H), 7.34 – 7.25 (m, 1H, Ar-H), 7.20 (d, *J* = 16.1 Hz, 1H, Ar-H), 7.16 – 7.11 (m, 1H, Ar-H), 7.02 (d, *J* = 16.1 Hz, 1H, Ar-H), 6.89 – 6.81 (m, 1H, C=CH), 6.75 (dd, *J* = 8.0, 1.2 Hz, 1H, C=CH), 3.84 (br s, 2H, NH_2).

^{13}C NMR (101 MHz, Chloroform-d) δ 144.0, 137.6, 130.4, 128.7 (3 C), 127.6, 127.3, 126.4 (2 C), 124.3, 123.9, 119.2, 116.3.

IR υ_{max} (film): 3358, 3031, 1489, 1456, 1342, 1255, 967.

HRMS (ESI$^+$) *m/z* calcd for $C_{14}H_{14}N$ $[M+H]^+$: 196.1121, found 196.1122.

MP: 101 °C.

(*E*)-*N*-phenyl-2-styrylaniline

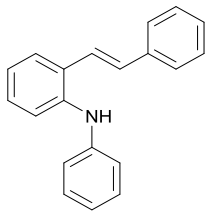

General Procedure F: $Pd_2(dba)_3$ (12 mg, 0.013 mmol, 0.8 mol %), XPhos (18 mg, 0.037 mmol, 2.3 mol %), sodium *tert*-butoxide (186 mg, 1.94 mmol, 1.2 eq.), 1,4-dioxane (1.6 mL), (*E*)-2-styrylaniline (284 mg, 1.45 mmol, 0.9 eq.), bromobenzene (0.17 mL, 1.61 mmol, 1.0 eq.).

The crude mixture was treated as described above and was purified by flash column chromatography (Hexane:EtOAc, 99:1, SiO_2) to afford (*E*)-*N*-phenyl-2-styrylaniline (355 mg, 1.31 mmol, 90%) as a yellow oil.

^{1}H NMR (400 MHz, Chloroform-d) δ 7.55 – 7.48 (m, 1H, Ar-H), 7.45 – 7.37 (m, 2H, 2 × Ar-H), 7.31 – 7.08 (m, 8H, 8 × Ar-H), 7.01 – 6.89 (m, 4H, 2 × Ar-H & 2 × C=CH), 6.84 (tt, *J* = 7.4, 1.1 Hz, 1H, Ar-H), 5.50 (br s, 1H, NH).

^{13}C NMR (126 MHz, Chloroform-d) δ 144.0, 140.5, 137.5, 131.0, 129.6, 129.4 (2 C), 128.7 (2 C), 128.5, 127.7, 127.2, 126.6 (2 C), 124.4, 122.6, 120.6, 119.9, 117.4 (2 C).

IR υ_{max} (film): 3026, 1593, 1496, 1310, 955.

HRMS (ESI$^+$) *m/z* calcd for $C_{20}H_{18}N$ $[M+H]^+$: 272.1434, found 272.1435.

(*E*)-2,4,6-trimethyl-*N*-(2-styrylphenyl)aniline

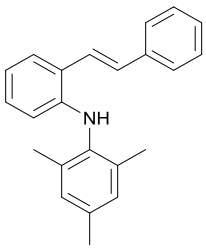

General Procedure F: $Pd_2(dba)_3$ (19 mg, 0.021 mmol, 0.8 mol %), BINAP (37 mg, 0.060 mmol, 2.3 mol %), sodium *tert*-butoxide (603 mg, 6.28 mmol, 2.4 eq.), 1,4-dioxane (2.6 mL), (*E*)-2-styrylaniline (562 mg, 2.88 mmol, 1.1 eq.), 2-bromo-1,3,5-trimethylbenzene (0.40 mL, 2.61 mmol, 1.0 eq.).

The crude mixture was treated as described above and was purified by flash column chromatography (Hexane:EtOAc, 99:1, SiO_2) to afford (*E*)-2,4,6-trimethyl-*N*-(2-styrylphenyl)aniline (808 mg, 2.58 mmol, 99%) as a yellow oil.

^{1}H NMR (400 MHz, Chloroform-d) δ 7.61 – 7.55 (m, 2H, 2 × Ar-H), 7.49 (dd, *J* = 7.6, 1.6 Hz, 1H, Ar-H), 7.44 – 7.37 (m, 3H, 3 × Ar-H), 7.33 – 7.27 (m, 1H, Ar-H), 7.15 – 7.03 (m, 2H, 2 × Ar-H), 6.99 – 6.95 (m, 2H, 2 × Ar-H), 6.83 (td, *J* = 7.5, 1.2 Hz, 1H, C=CH), 6.26 (dd, *J* = 8.2, 1.2 Hz, 1H, C=CH), 5.20 (br s, 1H, NH), 2.34 (s, 3H, CH_3), 2.19 (s, 6H, 2 × CH_3).

^{13}C NMR (101 MHz, Chloroform-d) δ 143.9, 137.7, 135.8, 135.1 (2 C), 130.7, 129.3 (2 C), 128.8 (3 C), 127.6, 127.3, 126.5 (2 C), 124.4, 124.3 (2 C), 118.6, 113.1, 20.9, 18.3 (2 C).

IR υ_{max} (film): 3042, 3024, 2916, 1597, 1490, 1455, 1312, 963.

HRMS (ESI^{+}) *m/z* calcd for C_{23} H_{24} N $[M+H]^{+}$: 314.1903, found 314.1902.

2-(2,2-diphenylvinyl)-*N*-phenylaniline

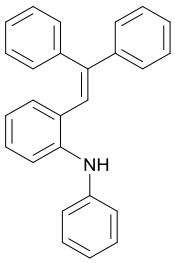

General Procedure F: $Pd_2(dba)_3$ (7.3 mg, 0.008 mmol, 0.8 mol %), XPhos (10.9 mg, 0.023 mmol, 2.3 mol %), sodium *tert*-butoxide (115 mg, 1.20 mmol, 2.4 eq.), 1,4-dioxane (1.0 mL), 2-(2,2-diphenylvinyl)aniline (243 mg, 0.90 mmol, 0.9 eq.), bromobenzene (0.10 mL, 1.00 mmol, 1.0 eq.).

The crude mixture was treated as described above and was purified by flash column chromatography (Hexane:EtOAc, 99:1, SiO_2) to 2-(2,2-diphenylvinyl)-*N*-phenylaniline (191 mg, 0.55 mmol, 61%) as an orange viscous oil.

^{1}H NMR (400 MHz, Chloroform-d) δ 7.39 – 7.13 (m, 13H, 13 × Ar-H), 7.10 – 7.04 (m, 1H, Ar-H), 6.99 – 6.88 (m, 5H, 5 × Ar-H), 6.72 – 6.65 (m, 1H, C=CH), 5.65 (br s, 1H, NH).

^{13}C NMR (101 MHz, Chloroform-d) δ 144.7, 143.2, 143.2, 141.2, 139.8, 130.8, 130.4 (2 C), 129.2 (2 C), 128.3 (2 C), 128.2 (2 C), 128.1 (2 C), 127.8, 127.8, 127.7, 127.6, 124.2, 120.9, 120.7, 118.1 (2 C), 117.4.

IR υ_{max} (film): 3402, 3053, 2980, 1593, 1496, 1305.

HRMS (ESI$^+$) *m/z* calcd for $C_{26}H_{22}N$ $[M+H]^+$: 348.1747, found 348.1748.

Diphenylamine

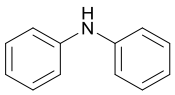

Bromobenzene (0.20 mL, 1.88 mmol, 1.0 eq.), aniline (0.19 mL, 2.06 mmol, 1.1 eq.), $Pd(dba)_2$ (2.2 mg, 4 μmol, 0.2 mol %), P(*t*-Bu)$_3$ (1.4 μL, 6 μmol, 0.3 mol %) and sodium *tert*-butoxide (541 mg, 5.63 mmol, 3.0 eq.) were added to toluene (2 mL) under argon atmosphere, and the mixture was refluxed for about 8 hours. After completion of the reaction, the mixture was cooled to rt and the reaction mixture was poured into water (10 mL). The organic and aqueous layers were partitioned and the aqueous phase was extracted with EtOAc (3 × 10 mL). The combined organic phases were dried over $MgSO_4$, filtered and concentrated under reduced pressure. After column chromatography (Hexane:EtOAc, 97:3, SiO_2), diphenylamine (116 mg, 0.70 mmol, 37%) was obtained as a white solid.

^{1}H NMR (400 MHz, Chloroform-d) δ 7.23 – 7.14 (m, 4H, 4 × Ar-H), 7.04 – 6.95 (m, 4H, 4 × Ar-H), 6.90 – 6.81 (m, 2H, 2 × Ar-H), 5.61 (br s, 1H, NH).

^{13}C NMR (101 MHz, Chloroform-d) δ 143.1 (2 C), 129.4 (4 C), 121.0 (2 C), 117.8 (4 C).

Analytical data are in agreement with the literature. [17]

4.6 Phosphoramidite ligands

Note: All the phosphoramidite ligands were put under high-vacuum for at least 5 h, however some ligands retained residual solvent due to their foamy nature.

_N_-cyclopentyl-_N_-((_R_)-2,3-dihydro-1_H_-inden-1-yl)dinaphtho[2,1-d:1',2'-_f_][1,3,2]dioxaphosphepin-4-amine

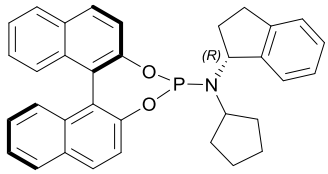

General Procedure G: Triethylamine (1.77 mL, 12.722 mmol, 5.0 eq.), PCl_3 (0.27 mL, 3.053 mmol, 1.2 eq.), CH_2Cl_2 (20 mL), (*R*)-*N*-cyclopentyl-2,3-dihydro-1*H*-inden-1-amine (512 mg, 2.544 mmol, 1.0 eq.), (*R*)-binaphthol (316 mg, 1.1 mmol, 1.0 eq.).

The crude mixture was treated as described above and was purified by flash column chromatography (Hexane:CH_2Cl_2, 80:20, SiO_2) to afford *N*-cyclopentyl-*N*-((*R*)-2,3-dihydro-1*H*-inden-1-yl)dinaphtho[2,1-d:1',2'-*f*][1,3,2]dioxaphosphepin-4-amine (250 mg, 0.4834 mmol, 19%) as a foamy white solid.

^{1}H NMR (400 MHz, Chloroform-*d*) δ 7.84 (dd, *J* = 22.1, 8.5 Hz, 2H, 2 × Ar-H), 7.72 (dd, *J* = 16.3, 8.4 Hz, 2H, 2 × Ar-H), 7.50 (d, *J* = 7.5 Hz, 1H, Ar-H), 7.43 (dd, *J* = 8.8, 3.7 Hz, 2H, 2 × Ar-H), 7.36 – 7.04 (m, 9H, 9 × Ar-H), 4.60 (q, *J* = 8.9 Hz, 1H, CH), 3.32 – 3.16 (m, 1H, CH), 2.83 – 2.72 (m, 1H, ½ × CH_2), 2.59 – 2.44 (m, 1H, ½ × CH_2), 2.34 – 2.22

(m, 1H, ½ × CH_2), 2.03 – 1.75 (m, 4H, ½ × CH_2 & CH_2 & ½ × CH_2), 1.67 – 1.51 (m, 3H, ½ × CH_2 & CH_2), 1.32 – 1.16 (m, 2H, CH_2).

^{13}C NMR (101 MHz, Chloroform-*d*) δ 150.2, 150.1, 150.0, 144.2 (2 C), 143.3, 132.8, 132.7, 131.3, 130.5, 130.2, 129.5, 128.3, 128.2, 127.2, 127.1, 126.3, 125.9, 125.8, 124.8, 124.7, 124.4, 124.3, 124.2, 124.1, 122.4 (2 C), 121.6 (2 C), 60.9, 60.8, 56.5, 56.3, 35.5 – 35.1 (m, 2C), 34.2 – 34.0 (m), 29.9, 24.3, 24.1.

^{31}P NMR (162 MHz, Chloroform-*d*) δ 151.4.

IR υ_{max} (film): 2954, 1589, 1461, 1230, 1125.

HRMS (EI^+) *m/z* calcd for C_{34} H_{31} O_2 N P $[M+H]^+$: 516.2087, found 516.2085.

$[\boldsymbol{\alpha}]^{25}_{589}$= -109.2 (*c* 0.5, $CHCl_3$) for 99% ee.

N-((*R*)-2,3-dihydro-1*H*-inden-1-yl)-*N*-((2,6,6-trimethylcyclohex-1-en-1-yl)methyl)dinaphtho[2,1-d:1',2'-*f*][1,3,2]dioxaphosphepin-4-amine

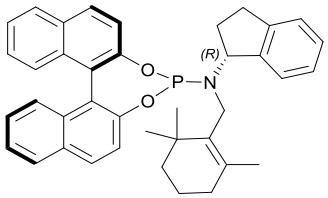

General Procedure G: Triethylamine (2.95mL, 21.193 mmol, 5.0 eq.), PCl_3 (0.37 mL, 4.239 mmol, 1.0 eq.), CH_2Cl_2 (40 mL), (*R*)-*N*-((2,6,6-trimethylcyclohex-1-en-1-yl)methyl)-2,3-dihydro-1*H*-inden-1-amine (1142 mg, 4.239 mmol, 1.0 eq.), (*R*)-binaphthol (1213 mg, 4.239 mmol, 1.0 eq.).

The crude mixture was treated as described above and was purified by flash column chromatography (Hexane:CH_2Cl_2, 80:20, SiO_2) to afford *N*-((*R*)-2,3-dihydro-1H-inden-1-yl)-*N*-((2,6,6-trimethylcyclohex-1-en-1-yl)methyl)dinaphtho[2,1-d:1',2'-

f][1,3,2]dioxaphosphepin-4-amine (216 mg, 0.3815 mmol, 9%) as a foamy white solid.

^{1}H NMR (400 MHz, Chloroform-*d*) δ 7.88 (d, *J* = 8.7 Hz, 1H, Ar-H), 7.82 (dd, *J* = 8.3, 1.4 Hz, 1H, Ar-H), 7.74 – 7.63 (m, 2H, 2 × Ar-H), 7.53 (d, *J* = 7.5 Hz, 1H, Ar-H), 7.45 (d, *J* = 8.8 Hz, 1H, Ar-H), 7.39 (dd, *J* = 8.8, 0.9 Hz, 1H, Ar-H), 7.35 – 7.04 (m, 9H, 9 × Ar-H), 4.77 (td, *J* = 7.9, 2.5 Hz, 1H, CH), 3.34 – 3.18 (m, 2H, CH_2), 2.78 (dt, *J* = 16.0, 6.6 Hz, 1H, ½ × CH_2), 2.51 (dt, *J* = 16.4, 8.4 Hz, 1H, ½ × CH_2), 2.12 – 2.01 (m, 2H, CH_2), 1.90 – 1.82 (m, 2H, CH_2), 1.74 (s, 3H, CH_3), 1.54 – 1.45 (m, 2H, CH_2), 1.43 – 1.34 (m, 2H, CH_2), 1.03 (s, 6H, 2 × CH_3).

^{13}C NMR (126 MHz, Chloroform-*d*) δ 150.7, 150.6, 150.2, 143.9, 141.8, 135.24, 135.18, 132.90, 132.7, 131.3, 131.2, 130.3, 130.2, 129.6, 128.24, 128.19, 127.3, 127.2, 127.1, 126.0, 125.9, 125.7, 125.0, 124.9, 124.6, 124.34, 124.28, 124.1, 122.5, 122.4, 121.4, 121.3, 61.1, 61.0, 41.6, 41.3, 39.3, 34.8, 32.6, 30.5, 30.2, 28.9, 28.9, 28.3, 28.3, 20.7, 20.6, 19.2.

^{31}P NMR (162 MHz, Chloroform-*d*) δ 147.1.

IR υ_{max} (film): 2360, 2340, 1230, 1069.

HRMS (EI^{+}) *m/z* calcd for C_{39} H_{39} O_2 N P $[M+H]^{+}$: 584.2713, found 584.2708.

$[\boldsymbol{\alpha}]^{25}_{589}$= -15.0 (*c* 0.5, $CHCl_3$) for 99% ee.

_N_-benzyl-_N_-((_R_)-2,3-dihydro-1_H_-inden-1-yl)dinaphtho[2,1-d:1',2'-_f_][1,3,2]dioxaphosphepin-4-amine

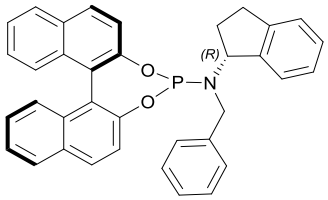

General Procedure G: Triethylamine (1.56 mL, 11.195 mmol, 5.0 eq.), PCl_3 (0.20 mL, 2.239 mmol, 1.0 eq.), CH_2Cl_2 (20 mL), (*R*)-*N*-benzyl-2,3-dihydro-1*H*-inden-1-amine (500 mg, 2.239 mmol, 1.0 eq.), (*R*)-binaphthol (641 mg, 2.239 mmol, 1.0 eq.).

The crude mixture was treated as described above and was purified by flash column chromatography (Hexane:CH_2Cl_2, 80:20, SiO_2) to afford *N*-benzyl-*N*-((*R*)-2,3-dihydro-1*H*-inden-1-yl)dinaphtho[2,1-d:1',2'-*f*][1,3,2]dioxaphosphepin-4-amine (396 mg, 0.739 mmol, 33%) as a foamy white solid.

^{1}H NMR (400 MHz, Chloroform-*d*) δ 7.90 (d, *J* = 8.8 Hz, 1H, Ar-H), 7.87 – 7.79 (m, 1H, Ar-H), 7.78 – 7.66 (m, 2H, 2 × Ar-H), 7.52 (dd, *J* = 8.7, 0.9 Hz, 1H, Ar-H), 7.41 – 7.19 (m, 6H, 6 × Ar-H), 7.19 – 7.02 (m, 10H, 10 × Ar-H), 4.80 (dt, *J* = 11.7, 7.4 Hz, 1H, CH), 3.98 (dd, *J* = 15.8, 8.6 Hz, 1H, ½ × CH_2), 3.87 (dd, *J* = 15.8, 7.2 Hz, 1H, ½ × CH_2), 2.79 – 2.66 (m, 1H, ½ × CH_2), 2.62 – 2.49 (m, 1H, ½ × CH_2), 2.17 – 2.02 (m, 1H, ½ × CH_2), 2.00 – 1.86 (m, 1H, ½ × CH_2).

^{13}C NMR (101 MHz, Chloroform-*d*) δ 150.0, 149.9, 149.5, 143.7, 142.7, 142.6, 140.22, 140.20, 132.9, 132.6, 131.4, 130.6, 130.3, 129.8, 128.3, 128.2, 128.0, 127.9, 127.6, 127.1, 127.0, 126.7, 126.15, 126.06, 125.9, 125.1, 124.83, 124.81, 124.5, 124.2, 124.1, 122.2, 122.0, 121.9, 62.7, 62.5, 48.2, 48.1, 33.11, 33.06, 30.5.

^{31}P NMR (162 MHz, Chloroform-*d*) δ 147.5.

IR υ_{max} (film): 2360, 2340, 1230.

HRMS (EI^+) *m/z* calcd for $C_{36}H_{29}O_2NP$ $[M+H]^+$: 538.1930, found 538.1931.

$[\alpha]^{25}_{589}$= -111.5 (*c* 0.5, $CHCl_3$) for 99% ee.

_N_-((_R_)-2,3-dihydro-1_H_-inden-1-yl)-_N_-(4-methylcyclohexyl)dinaphtho[2,1-d:1',2'-_f_][1,3,2]dioxaphosphepin-4-amine

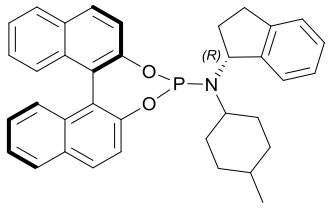

General Procedure G: Triethylamine (1.10 mL, 7.869 mmol, 5.0 eq.), PCl_3 (0.14 mL, 1.574 mmol, 1.0 eq.), CH_2Cl_2 (20 mL), (*R*)-*N*-(4-methylcyclohexyl)-2,3-dihydro-1*H*-inden-1-amine (361 mg, 1.574 mmol, 1.0 eq.), (*R*)-binaphthol (451 mg, 1.574 mmol, 1.0 eq.).

The crude mixture was treated as described above and was purified by flash column chromatography (Hexane:CH_2Cl_2, 80:20, SiO_2) to afford *N*-((*R*)-2,3-dihydro-1*H*-inden-1-yl)-*N*-(4-methylcyclohexyl)dinaphtho[2,1-d:1',2'-*f*][1,3,2]dioxaphosphepin-4-amine (97.3 mg, 0.173 mmol, 11%) as a foamy white solid.

^{1}H NMR (400 MHz, Chloroform-*d*) δ 7.90 – 7.67 (m, 4H, 4 × Ar-H), 7.55 – 7.47 (m, 1H, Ar-H), 7.49 – 7.37 (m, 2H, 2 × Ar-H), 7.34 – 7.05 (m, 9H, 9 × Ar-H), 4.66 (dt, *J* = 12.2, 8.0 Hz, 1H, CH), 2.80 (ddt, *J* = 14.2, 7.4, 3.5 Hz, 1H, ½ × CH_2), 2.65 – 2.47 (m, 2H, CH & ½ × CH_2), 2.36 – 2.21 (m, 1H, ½ × CH_2), 2.04 – 1.26 (m, 8H, CH & ½ × CH_2 & 3 × CH_2), 1.20 – 0.95 (m, 2H, CH_2), 0.83 (d, *J* = 7.1 Hz, 3H, CH_3).

^{13}C NMR (101 MHz, Chloroform-*d*) δ 150.4, 150.3, 150.0, 144.6 – 144.0 (m), 143.2, 132.8, 132.7, 131.3, 130.5, 130.2, 129.5, 128.3, 128.2, 127.2, 127.1, 126.4, 126.3,

125.9, 125.8, 124.8, 124.6, 124.5, 124.3, 124.14, 124.08, 122.42, 122.40, 122.2, 121.61, 121.58, 60.6, 60.5, 55.0, 54.9, 54.5, 54.4, 36.4 – 35.7 (m), 34.9, 31.8, 31.62, 31.58, 30.5 – 30.2 (m), 29.9, 29.2 – 28.6 (m), 25.9, 22.1, 17.3.

^{31}P NMR (162 MHz, Chloroform-*d*) δ 151.4.

IR υ_{max} (film): 2360, 2341, 1212.

HRMS (EI^+) *m/z* calcd for C_{36} H_{35} O_2 N P $[M+H]^+$: 544.2400, found 544.2399.

$[\alpha]^{25}_{589}$= -95.8 (*c* 1.3, $CHCl_3$) for 99% ee.

N-((*R*)-2,3-dihydro-1*H*-inden-1-yl)-*N*-(pentan-3-yl)dinaphtho[2,1-d:1',2'-*f*][1,3,2]dioxaphosphepin-4-amine

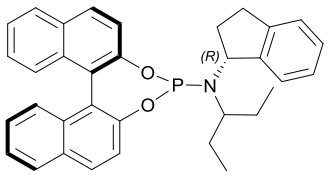

General Procedure G: Triethylamine (2.18 mL, 15.615 mmol, 5.0 eq.), PCl_3 (0.27 mL, 3.123 mmol, 1.0 eq.), CH_2Cl_2 (20 mL), (*R*)-*N*-(pentan-3-yl)-2,3-dihydro-1*H*-inden-1-amine (635 mg, 3.123 mmol, 1.0 eq.), (*R*)-binaphthol (894 mg, 3.123 mmol, 1.0 eq.).

The crude mixture was treated as described above and was purified by flash column chromatography (Hexane:CH_2Cl_2, 80:20, SiO_2) to afford *N*-((*R*)-2,3-dihydro-1*H*-inden-1-yl)-*N*-(pentan-3-yl)dinaphtho[2,1-d:1',2'-*f*][1,3,2]dioxaphosphepin-4-amine (894 mg, 1.718 mmol, 55%) as a foamy white solid.

^{1}H NMR (400 MHz, Chloroform-*d*) δ 8.00 – 7.86 (m, 4H, 4 × Ar-H), 7.73 (d, *J* = 7.6 Hz, 1H, Ar-H), 7.63 (d, *J* = 8.7 Hz, 1H, Ar-H), 7.51 (d, *J* = 8.7 Hz, 1H, Ar-H), 7.46 – 7.18 (m, 9H, 9 × Ar-H), 4.77 (dt, *J* = 14.9, 7.8 Hz, 1H, CH), 3.06 – 2.94 (m, 1H, ½ × CH_2), 2.85 –

2.66 (m, 2H, CH & ½ × CH_2), 2.51 – 2.37 (m, 1H, ½ × CH_2), 2.28 – 2.13 (m, 1H, ½ × CH_2), 1.98 – 1.83 (m, 1H, ½ × CH_2), 1.80 – 1.67 (m, 1H, ½ × CH_2), 1.68 – 1.44 (m, 2H, CH_2), 0.98 (t, *J* = 7.4 Hz, 3H, CH_3), 0.76 (t, *J* = 7.4 Hz, 3H, CH_3).

^{13}C NMR (101 MHz, Chloroform-*d*) δ 150.35, 150.26, 149.9, 144.4, 143.4, 132.82, 132.79, 131.3, 130.4, 130.2, 129.6, 128.3, 128.2, 127.4, 127.2, 127.1, 126.4, 126.0, 125.9, 125.2, 124.8, 124.7, 124.3, 124.1, 124.0, 122.40, 122.38, 122.3, 59.9, 59.8, 58.0, 57.9, 36.7 – 36.2 (m), 30.4, 29.52, 29.46, 27.3 – 27.1 (m), 11.6, 11.5.

^{31}P NMR (162 MHz, Chloroform-*d*) δ 149.3.

IR υ_{max} (film): 2360, 1212.

HRMS (EI^+) *m/z* calcd for C_{34} H_{33} O_2 N P $[M+H]^+$: 518.2243, found 518.2244.

$[\alpha]^{25}_{589}$= -124.8 (*c* 1.2, $CHCl_3$) for 99% ee.

N-((*R*)-2,3-dihydro-1*H*-inden-1-yl)-*N*-(heptan-3-yl)dinaphtho[2,1-d:1',2'-*f*][1,3,2]dioxaphosphepin-4-amine

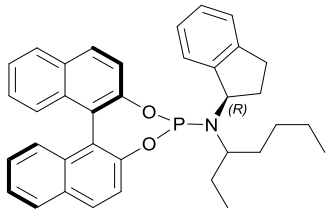

<u>General Procedure G:</u> Triethylamine (1.19 mL, 8.566 mmol, 5.0 eq.), PCl_3 (0.15 mL, 1.713 mmol, 1.0 eq.), CH_2Cl_2 (20 mL), (1*R*)-*N*-(heptan-3-yl)-2,3-dihydro-1*H*-inden-1-amine (396 mg, 1.713 mmol, 1.0 eq.), (*R*)-binaphthol (490 mg, 1.713 mmol, 1.0 eq.).

The crude mixture was treated as described above and was purified by flash column chromatography (Hexane:CH_2Cl_2, 80:20, SiO_2) to afford *N*-((*R*)-2,3-dihydro-1*H*-inden-1-yl)-*N*-(heptan-3-yl)dinaphtho[2,1-d:1',2'-*f*][1,3,2]dioxaphosphepin-4-amine (40 mg, 0.068 mmol, 4%) as a foamy white solid.

Mixture of diastereoisomers (1:1)

^{1}H NMR (400 MHz, Chloroform-*d*) δ 7.88 – 7.75 (m, 4H, 4 × Ar-H), 7.64 – 7.57 (m, 1H, Ar-H), 7.50 (d, *J* = 8.8 Hz, 1H, Ar-H), 7.38 (d, *J* = 8.7 Hz, 1H, Ar-H), 7.34 – 7.27 (m, 3H, 3 × Ar-H), 7.27 – 7.07 (m, 6H, 6 × Ar-H), 4.65 (dt, *J* = 14.7, 7.5 Hz, 1H, CH), 2.95 – 2.83 (m, 1H, ½ × CH_2), 2.81 – 2.70 (m, 1H, CH), 2.69 – 2.56 (m, 1H, ½ × CH_2), 2.40 – 2.25 (m, 1H, ½ × CH_2), 2.16 – 2.01 (m, 1H, ½ × CH_2), 1.81 – 1.64 (m, 1H, ½ × CH_2), 1.63 – 1.51 (m, 1H, ½ × CH_2), 1.50 – 0.96 (m, 6H, 3 × CH_2), 0.90 – 0.59 (m, 6H, 2 × CH_3).

^{13}C NMR (126 MHz, Chloroform-*d*) δ 150.28, 150.26, 150.21, 150.19, 149.94, 149.90, 144.5, 143.4, 143.3, 132.8, 132.7, 131.3, 130.39, 130.37, 130.2, 129.53, 129.49, 128.2, 128.1, 127.4, 127.3, 127.15, 127.13, 127.06, 126.39, 126.37, 125.9, 125.8, 125.2, 125.1, 124.8, 124.6, 124.31, 124.29, 124.0, 123.9, 122.34, 122.32, 122.30, 122.2, 121.8, 121.75, 121.72, 121.70, 59.8, 59.6, 56.7, 56.6, 56.4, 56.3, 36.82, 36.77, 37.0 – 35.9 (m), 34.7 – 33.9 (m), 30.4, 29.52, 29.48, 29.4, 28.7, 28.0 – 27.1 (m), 23.1, 22.8, 14.2, 14.1, 11.5, 11.4.

^{31}P NMR (162 MHz, Chloroform-*d*) δ 149.6, 149.5.

IR υ_{max} (film): 2956, 2932, 2360, 1430, 1212.

HRMS (EI^+) *m/z* calcd for C_{36} H_{37} O_2 N P $[M+H]^+$: 546.2556, found 546.2555.

$[\alpha]^{25}_{589}$= -106.9 (*c* 1.5, $CHCl_3$) for a mixture of diastereoisomers at 99% ee.

_N_-((_R_)-2,3-dihydro-1_H_-inden-1-yl)-_N_-(2-methylpentan-3-yl)dinaphtho[2,1-d:1',2'-_f_][1,3,2]dioxaphosphepin-4-amine

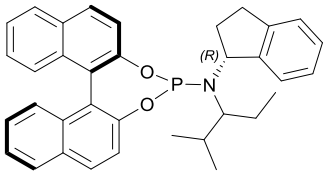

General Procedure G: Triethylamine (1.84 mL, 13.227 mmol, 5.0 eq.), PCl_3 (0.23 mL, 2.645 mmol, 1.0 eq.), CH_2Cl_2 (20 mL), (1*R*)-*N*-(2-methylpentan-3-yl)-2,3-dihydro-1*H*-inden-1-amine (575 mg, 2.645 mmol, 1.0 eq.), (*R*)-binaphthol (757 mg, 2.645 mmol, 1.0 eq.).

The crude mixture was treated as described above and was purified by flash column chromatography (Hexane:CH_2Cl_2, 80:20, SiO_2) to afford *N*-((*R*)-2,3-dihydro-1*H*-inden-1-yl)-*N*-(2-methylpentan-3-yl)dinaphtho[2,1-d:1',2'-*f*][1,3,2]dioxaphosphepin-4-amine (577 mg, 1.084 mmol, 41%) as a foamy white solid.

Mixture of diastereoisomers (1:1)

^{1}H NMR (500 MHz, Chloroform-*d*) δ 8.05 – 7.81 (m, 4H, 4 × Ar-H), 7.70 (d, *J* = 7.5 Hz, 1H, Ar-H), 7.66 – 7.62 (m, 1H, Ar-H), 7.58 (d, *J* = 8.7 Hz, 1H, Ar-H), 7.55 – 7.50 (m, 1H, Ar-H), 7.48 – 7.07 (m, 8H, 8 × Ar-H), 4.89 – 4.77 (m, 1H, CH), 3.00 – 2.86 (m, 1H, ½ × CH_2), 2.70 – 2.54 (m, 2H, CH & ½ × CH_2), 2.33 – 2.03 (m, 3H, CH_2 & CH), 1.93 – 1.78 (m, 1H, ½ × CH_2), 1.72 – 1.50 (m, 1H, ½ × CH_2), 1.11 (t, *J* = 7.3 Hz, 2H, ⅔ × CH_3), 1.06 – 0.93 (m, 6H, CH_3 & ⅓ × CH_3 & ⅔ × CH_3), 0.71 (d, *J* = 7.0 Hz, 1H, ⅓ × CH_3).

^{13}C NMR (126 MHz, Chloroform-*d*) δ 150.7, 150.6, 150.34, 150.27, 150.0, 149.9, 144.5, 144.2, 143.2, 142.8, 132.9, 132.8, 131.3, 130.4, 130.31, 130.28, 130.2, 129.6, 128.3, 128.2, 128.1, 127.49, 127.47, 127.2, 127.1, 126.14, 126.09, 125.95, 125.93, 125.82, 125.79, 124.74, 124.67, 124.3, 124.2, 122.7, 122.4, 122.35, 122.33, 121.50,

121.48, 121.23, 121.21, 62.3, 62.1, 60.9, 60.8, 34.7 – 33.8 (m), 33.7, 33.6, 32.6, 32.5, 30.6, 30.3, 24.8 – 24.4 (m), 22.7, 22.5, 21.5, 20.9, 18.64, 18.60, 17.71, 17.67, 11.3.

^{31}P NMR (202 MHz, Chloroform-*d*) δ 148.6, 147.9.

IR υ_{max} (film): 2958, 2870, 1431, 1231.

HRMS (EI^+) *m/z* calcd for C_{35} H_{35} O_2 N P $[M+H]^+$: 532.2400, found 532.2408.

$[\alpha]^{25}_{589}$= -129.0 (*c* 1.0, $CHCl_3$) for a mixture of diastereoisomers at 99% ee.

N-(decan-3-yl)-*N*-((*R*)-2,3-dihydro-1H-inden-1-yl)dinaphtho[2,1-d:1',2'-*f*][1,3,2]dioxaphosphepin-4-amine

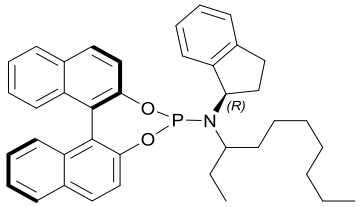

General Procedure G: Triethylamine (0.88 mL, 6.281 mmol, 5.0 eq.), PCl_3 (0.11 mL, 1.256 mmol, 1.0 eq.), CH_2Cl_2 (20 mL), (1*R*)-*N*-(decan-3-yl)-2,3-dihydro-1*H*-inden-1-amine (343 mg, 1.256 mmol, 1.0 eq.), (*R*)-binaphthol (360 mg, 1.256 mmol, 1.0 eq.).

The crude mixture was treated as described above and was purified by flash column chromatography (Hexane:CH_2Cl_2, 80:20, SiO_2) to afford *N*-(decan-3-yl)-*N*-((*R*)-2,3-dihydro-1*H*-inden-1-yl)dinaphtho[2,1-d:1',2'-*f*][1,3,2]dioxaphosphepin-4-amine (21 mg, 0.038 mmol, 3%) as a foamy white solid.

Mixture of diastereoisomers (1:1)

^{1}H NMR (500 MHz, Chloroform-*d*) δ 7.98 – 7.87 (m, 4H, 4 × Ar-H), 7.75 – 7.67 (m, 1H, Ar-H), 7.61 (d, *J* = 8.8 Hz, 1H, Ar-H), 7.48 (dd, *J* = 8.8, 3.1 Hz, 1H, Ar-H), 7.44 – 7.37 (m, 3H, 3 × Ar-H), 7.36 – 7.19 (m, 6H, 6 × Ar-H), 4.81 – 4.70 (m, 1H, CH), 3.05 – 2.95 (m, 1H, ½ × CH_2), 2.92 – 2.81 (m, 1H, CH), 2.80 – 2.68 (m, 1H, ½ × CH_2), 2.50 –

2.37 (m, 1H, ½ × CH_2), 2.23 – 2.15 (m, 1H, ½ × CH_2), 1.92 – 1.05 (m, 11H, 5 × CH_2 & ½ × CH_2), 1.00 – 0.69 (m, 9H, 2 × CH_3 & CH_2 & ½ × CH_2).

^{13}C NMR (126 MHz, Chloroform-*d*) δ 150.3, 150.25, 150.20 150.19, 149.94, 149.89, 144.5, 143.35, 143.27, 132.8, 131.3, 130.4, 130.2, 129.53, 129.48, 128.2, 128.1, 127.4, 127.3, 127.15, 127.13, 127.06, 126.40, 126.37, 125.9, 125.8, 125.2, 125.1, 124.8, 124.6, 124.3, 124.0, 123.9, 122.34, 122.32, 122.28, 122.2, 121.8, 121.8, 121.71, 121.70, 60.3 – 59.4 (m), 56.7, 56.6, 56.34, 56.30, 37.12, 37.07, 36.9 – 36.2 (m), 34.7 – 34.0 (m), 31.93, 31.89, 30.4, 30.0, 29.7, 29.5, 29.4, 29.3, 27.7 – 27.4 (m), 27.2, 26.5, 22.8, 22.6, 14.2, 14.1, 11.5, 11.4.

^{31}P NMR (162 MHz, Chloroform-*d*) δ 149.6, 149.4.

IR υ_{max} (film): 2955, 2854, 1431, 1231.

HRMS (EI^+) *m/z* calcd for $C_{39}H_{43}O_2NP$ $[M+H]^+$: 588.3026, found 588.3024.

$[\alpha]^{25}_{589}$= -50.8 (*c* 2.5, $CHCl_3$) for a mixture of diastereoisomers at 99% ee.

N-((*R*)-2,3-dihydro-1*H*-inden-1-yl)-*N*-(2,8-dimethylnonan-5-yl)dinaphtho[2,1-d:1',2'-*f*][1,3,2]dioxaphosphepin-4-amine

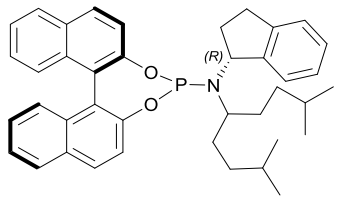

<u>General Procedure G:</u> Triethylamine (0.83 mL, 5.927 mmol, 5.0 eq.), PCl_3 (0.10 mL, 1.185 mmol, 1.0 eq.), CH_2Cl_2 (20 mL), (*R*)-*N*-(2,8-dimethylnonan-5-yl)-2,3-dihydro-1*H*-inden-1-amine (341 mg, 1.185 mmol, 1.0 eq.), (*R*)-binaphthol (339 mg, 1.185 mmol, 1.0 eq.).

The crude mixture was treated as described above and was purified by flash column chromatography (Hexane:CH_2Cl_2, 80:20, SiO_2) to afford *N*-((*R*)-2,3-dihydro-1*H*-inden-1-yl) -*N*- (2,8-dimethylnonan-5-yl)dinaphtho[2,1-d:1',2'-*f*][1,3,2]dioxaphosphepin-4-amine (153 mg, 0.261 mmol, 22%) as a foamy white solid.

^{1}H NMR (400 MHz, Chloroform-*d*) δ 7.88 – 7.75 (m, 4H, 4 × Ar-H), 7.61 (d, *J* = 7.5 Hz, 1H, Ar-H), 7.49 (d, *J* = 8.7 Hz, 1H, Ar-H), 7.37 (d, *J* = 8.8 Hz, 1H, Ar-H), 7.34 – 7.26 (m, 3H, 3 × Ar-H), 7.26 – 7.08 (m, 6H, 6 × Ar-H), 4.73 – 4.60 (m, 1H, CH), 2.95 – 2.83 (m, 1H, ½ × CH_2), 2.79 – 2.74 (m, 1H, CH), 2.70 – 2.56 (m, 1H, ½ × CH_2), 2.40 – 2.24 (m, 1H, ½ × CH_2), 2.14 – 2.02 (m, 1H, ½ × CH_2), 1.74 – 1.49 (m, 2H, CH_2), 1.48 – 1.16 (m, 5H, 2 × CH & CH_2 & ½ × CH_2), 1.16 – 1.03 (m, 1H, ½ × CH_2), 0.92 – 0.68 (m, 14H, 4 × CH_3 & CH_2).

^{13}C NMR (126 MHz, Chloroform-*d*) δ 150.3, 150.2, 149.9, 144.5, 143.3, 132.8, 131.3, 130.3, 130.2, 129.6, 128.2, 128.1, 127.4, 127.15, 127.06, 126.4, 125.9, 125.8, 125.2, 124.8, 124.6, 124.3, 124.0, 123.9, 122.30, 122.28, 121.75, 121.73, 59.8, 59.8 – 59.6 (m), 55.64, 55.60, 37.0 – 36.0 (m), 36.2, 35.7, 35.1, 33.3 – 32.3 (m), 30.4, 28.7, 28.1, 23.0, 22.8, 22.6, 22.5.

^{31}P NMR (162 MHz, Chloroform-*d*) δ 149.6.

IR υ_{max} (film): 2952, 2360, 1431, 1231, 1067.

HRMS (EI^+) *m/z* calcd for C_{35} H_{35} O_2 N P $[M+H]^+$: 532.2400, found 532.2398.

$[\alpha]^{25}_{589}$= -108.8 (*c* 1.1, $CHCl_3$) for 99% ee.

_N_-(adamantan-2-yl)-_N_-((_R_)-2,3-dihydro-1H-inden-1-yl)dinaphtho[2,1-d:1',2'-_f_][1,3,2]dioxaphosphepin-4-amine

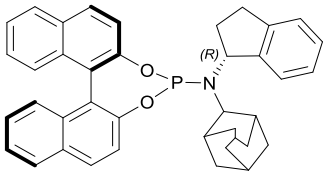

General Procedure G: Triethylamine (1.13 mL, 8.130 mmol, 5.0 eq.), PCl_3 (0.14 mL, 1.626 mmol, 1.0 eq.), CH_2Cl_2 (20 mL), (*R*)-*N*-(2,3-dihydro-1*H*-inden-1-yl)adamantan-2-amine (435 mg, 1.626 mmol, 1.0 eq.), (*R*)-binaphthol (465 mg, 1.626 mmol, 1.0 eq.).

The crude mixture was treated as described above and was purified by flash column chromatography (Hexane:CH_2Cl_2, 80:20, SiO_2) to afford *N*-(adamantan-2-yl)-*N*-((*R*)-2,3-dihydro-1*H*-inden-1-yl)dinaphtho[2,1-d:1',2'-*f*][1,3,2]dioxaphosphepin-4-amine (60 mg, 0.098 mmol, 6%) as a foamy white solid.

^{1}H NMR (500 MHz, Chloroform-*d*) δ 7.99 (d, *J* = 8.8 Hz, 1H, Ar-H), 7.92 (dd, *J* = 8.3, 1.2 Hz, 1H, Ar-H), 7.76 (dd, *J* = 8.2, 1.2 Hz, 1H, Ar-H), 7.66 (d, *J* = 8.8 Hz, 1H, Ar-H), 7.62 – 7.53 (m, 2H, 2 × Ar-H), 7.46 – 7.16 (m, 9H, 9 × Ar-H), 7.13 (d, *J* = 7.4 Hz, 1H, Ar-H), 4.99 – 4.91 (m, 1H, CH), 3.15 (d, *J* = 20.4 Hz, 1H, CH), 2.81 – 2.67 (m, 2H, CH & ½ × CH_2), 2.65 – 2.57 (m, 1H, CH), 2.52 – 2.41 (m, 1H, ½ × CH_2), 2.19 – 2.12 (m, 2H, ½ × CH_2 & CH), 1.98 – 1.93 (m, 2H, CH_2), 1.93 – 1.82 (m, 1H, ½ × CH_2), 1.79 – 1.51 (m, 8H, CH & 3 × CH_2 & ½ × CH_2), 1.44 – 1.37 (m, 1H, ½ × CH_2).

^{13}C NMR (126 MHz, Chloroform-*d*) δ 151.0, 150.9, 149.9, 143.5, 142.9, 132.93, 132.91, 132.7, 131.3, 130.33, 130.28, 129.6, 128.3, 128.1, 127.3, 127.2, 127.1, 125.9, 125.9, 125.7, 124.8, 124.7, 124.5, 124.3, 124.1, 122.60, 122.58, 122.4, 120.9, 120.8, 62.34, 62.32, 61.5, 61.4, 39.7, 39.10, 39.08, 38.55, 38.52, 35.55, 35.53, 35.0, 34.9, 33.0, 32.2, 32.1, 31.6, 31.5, 29.8, 27.6.

^{31}P NMR (202 MHz, Chloroform-*d*) δ 144.7.

IR υ_{max} (film): 2907, 2850, 2359, 1507, 1214.

HRMS (EI^+) *m/z* calcd for C_{39} H_{37} O_2 N P $[M+H]^+$: 582.2556, found 582.2556.

$[\alpha]^{25}_{589}$= -21.0 (*c* 1.5, $CHCl_3$) for 99% ee.

N-((*R*)-2,3-dihydro-1*H*-inden-1-yl)-*N*-(1,7-diphenylheptan-4-yl)dinaphtho[2,1-d:1',2'-*f*][1,3,2]dioxaphosphepin-4-amine

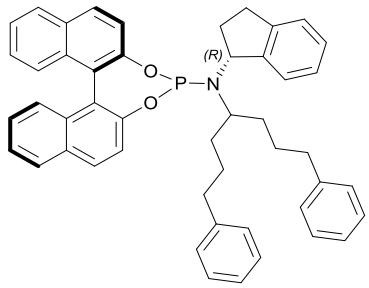

General Procedure G: Triethylamine (1.24 mL, 8.903 mmol, 5.0 eq.), PCl_3 (0.16 mL, 1.781 mmol, 1.0 eq.), CH_2Cl_2 (20 mL), (*R*)-*N*-(1,7-diphenylheptan-4-yl)-2,3-dihydro-1*H*-inden-1-amine (683 mg, 1.781 mmol, 1.0 eq.), (*R*)-binaphthol (509 mg, 1.781 mmol, 1.0 eq.).

The crude mixture was treated as described above and was purified by flash column chromatography (Hexane:CH_2Cl_2, 80:20, SiO_2) to afford *N*-((*R*)-2,3-dihydro-1*H*-inden-1-yl) -*N*- (1,7-diphenylheptan-4-yl)dinaphtho[2,1-d:1',2'-*f*][1,3,2]dioxaphosphepin-4-amine (142 mg, 0.214 mmol, 12%) as a foamy white solid.

^{1}H NMR (500 MHz, Chloroform-*d*) δ 7.94 (d, *J* = 8.8 Hz, 1H, Ar-H), 7.92 – 7.84 (m, 3H, 3 × Ar-H), 7.65 (d, *J* = 7.6 Hz, 1H, Ar-H), 7.49 (d, *J* = 8.7 Hz, 1H, Ar-H), 7.46 – 7.12 (m, 18H, 18 × Ar-H), 7.05 (d, *J* = 7.4 Hz, 2H, 2 × Ar-H), 4.71 (dt, *J* = 16.0, 7.8 Hz, 1H, CH), 3.09 – 2.94 (m, 2H, ½ × CH_2 & CH), 2.78 – 2.67 (m, 1H, ½ × CH_2), 2.65 – 2.50 (m, 3H, CH_2 & ½ × CH_2), 2.48 – 2.30 (m, 2H, ½ × CH_2 & ½ × CH_2), 2.20 – 2.08 (m, 1H, ½ ×

CH_2), 1.91 – 1.63 (m, 5H, 2 × CH_2 & ½ × CH_2), 1.43 (d, *J* = 34.1 Hz, 3H, CH_2 & ½ × CH_2).

^{13}C NMR (126 MHz, Chloroform-*d*) δ 150.1, 150.0, 149.8, 144.8 – 144.3 (m), 143.4 – 142.9 (m), 142.4, 142.3, 132.8, 132.74, 132.73, 131.3, 130.3, 130.2, 129.5, 128.5, 128.4, 128.3, 128.25, 128.16, 128.1, 127.4, 127.1, 127.0, 126.5, 126.0, 125.9, 125.8, 125.6, 125.0, 124.9, 124.7, 124.4, 123.95, 123.91, 122.29, 122.27, 122.1, 121.9, 121.8, 59.6, 59.4, 54.5, 37.6 – 36.5 (m), 36.8, 36.2, 35.7, 34.2 – 33.3 (m), 30.4, 28.6, 27.9.

^{31}P NMR (202 MHz, Chloroform-*d*) δ 149.2.

IR υ_{max} (film): 2940, 2855, 1590, 1360, 1154.

HRMS (EI$^+$) *m/z* calcd for $C_{48}H_{45}O_2NP$ $[M+H]^+$: 698.3182, found 698.3181.

$[\alpha]^{25}_{589}$= -85.5 (*c* 1.0, $CHCl_3$) for 99% ee.

N-((*R*)-2,3-dihydro-1*H*-inden-1-yl)-*N*-(1,3-diphenylpropan-2-yl)dinaphtho[2,1-d:1',2'-*f*][1,3,2]dioxaphosphepin-4-amine

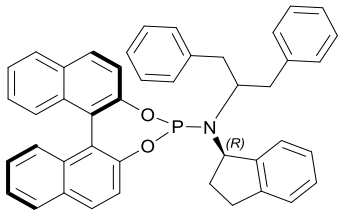

General Procedure G: Triethylamine (1.64 mL, 11.757 mmol, 5.0 eq.), PCl_3 (0.21 mL, 2.351 mmol, 1.0 eq.), CH_2Cl_2 (10 mL), (*R*)-*N*-(1,3-diphenylpropan-2-yl)-2,3-dihydro-1*H*-inden-1-amine (770 mg, 2.351 mmol, 1.0 eq.), (*R*)-binaphthol (673.3 mg, 2.351 mmol, 1.0 eq.).

The crude mixture was treated as described above and was purified by flash column chromatography (Hexane:CH_2Cl_2, 80:20, SiO_2) to afford *N*-((*R*)-2,3-dihydro-1*H*-

inden-1-yl) -*N*- (1,3-diphenylpropan-2-yl)dinaphtho[2,1-d:1',2'-*f*][1,3,2]dioxaphosphepin-4-amine (110.2 mg, 0.172 mmol, 7%) as a foamy white solid.

^{1}H NMR (500 MHz, Chloroform-*d*) δ 8.04 (d, *J* = 8.7 Hz, 1H, Ar-H), 7.99 – 7.93 (m, 1H, Ar-H), 7.86 – 7.78 (m, 2H, 2 × Ar-H), 7.63 – 7.01 (m, 20H, 20 × Ar-H), 6.74 (d, *J* = 6.6 Hz, 2H, 2 × Ar-H), 4.83 – 4.67 (m, 1H, CH), 3.41 – 3.10 (m, 3H, CH & ½ × CH_2 & ½ × CH_2), 2.96 – 2.87 (m, 1H, ½ × CH_2), 2.88 – 2.79 (m, 1H, ½ × CH_2), 2.78 – 2.61 (m, 1H, ½ × CH_2), 2.56 – 2.35 (m, 1H, ½ × CH_2), 2.06 – 1.76 (m, 1H, ½ × CH_2), 1.43 – 1.21 (m, 1H, ½ × CH_2).

^{13}C NMR (126 MHz, Chloroform-*d*) δ 150.2, 150.1, 149.9, 144.9 – 144.4 (m), 142.4 – 141.9 (m), 139.7, 139.4, 132.8, 132.76, 131.4, 130.5, 130.4, 129.8, 129.6, 129.5, 128.34, 128.27, 128.2, 128.1, 127.6, 127.2, 127.1, 126.3, 126.2, 126.1, 125.9, 125.8, 124.8, 124.4, 124.1, 124.0, 122.3, 122.2, 122.1, 121.6, 121.5, 60.9, 60.4 – 59.6 (m), 45.2 – 43.6 (m), 42.4 – 41.6 (m), 34.3 – 32.2 (m), 30.5.

^{31}P NMR (202 MHz, Chloroform-*d*) δ 149.4.

IR υ_{max} (film): 2980, 1462, 1230, 1154, 1030.

HRMS (EI^{+}) *m/z* calcd for C_{44} H_{37} O_2 N P $[M+H]^{+}$: 642.2556, found 642.2554.

$[\boldsymbol{\alpha}]^{25}_{589}$ = -50.9 (*c* 1.0, $CHCl_3$) for 99% ee.

_N_-((_R_)-2,3-dihydro-1_H_-inden-1-yl)-_N_-isobutyldinaphtho[2,1-d:1',2'-_f_][1,3,2]dioxaphosphepin-4-amine

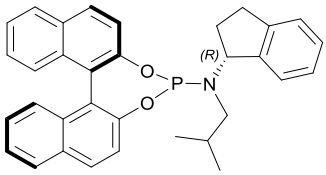

General Procedure G: Triethylamine (1.84 mL, 13.207 mmol, 5.0 eq.), PCl_3 (0.23 mL, 2.641 mmol, 1.0 eq.), CH_2Cl_2 (20 mL), (*R*)-*N*-isobutyl-2,3-dihydro-1*H*-inden-1-amine (500 mg, 2.641 mmol, 1.0 eq.), (*R*)-binaphthol (756.3 mg, 2.641 mmol, 1.0 eq.).

The crude mixture was treated as described above and was purified by flash column chromatography (Hexane:CH_2Cl_2, 80:20, SiO_2) to afford *N*-((*R*)-2,3-dihydro-1*H*-inden-1-yl) -*N*- isobutyldinaphtho[2,1-d:1',2'-*f*][1,3,2]dioxaphosphepin-4-amine (110.2 mg, 0.211 mmol, 8%) as a foamy white solid.

^{1}H NMR (500 MHz, Chloroform-*d*) δ 8.01 (d, *J* = 8.8 Hz, 1H, Ar-H), 7.98 – 7.92 (m, 1H, Ar-H), 7.90 – 7.81 (m, 2H, 2 × Ar-H), 7.61 – 7.54 (m, 2H, 2 × Ar-H), 7.49 (d, *J* = 8.8 Hz, 1H, Ar-H), 7.46 – 7.18 (m, 9H, 9 × Ar-H), 4.89 (q, *J* = 7.5 Hz, 1H, CH), 3.01 – 2.91 (m, 1H, ½ × CH_2), 2.82 – 2.65 (m, 3H, ½ × CH_2 & CH_2), 2.38 – 2.28 (m, 1H, ½ × CH_2), 2.18 – 2.06 (m, 1H, ½ × CH_2), 1.62 – 1.49 (m, 1H, CH), 0.81 (d, *J* = 6.6 Hz, 3H, CH_3), 0.78 (d, *J* = 6.6 Hz, 3H, CH_3).

^{13}C NMR (126 MHz, Chloroform-d) δ 150.3, 150.2, 149.6, 143.6, 142.83, 142.80, 132.88, 132.6, 132.7, 131.4, 130.5, 130.3, 129.7, 128.3, 128.2, 127.5, 127.2, 127.1, 126.1, 126.0, 125.9, 125.2, 124.9, 124.7, 124.3, 124.2, 124.1, 122.29, 122.27, 122.2, 121.79, 121.77, 61.8, 61.7, 52.5, 52.4, 32.33, 32.31, 30.5, 28.30, 28.26, 20.4, 20.3.

^{31}P NMR (202 MHz, Chloroform-*d*) δ 149.7.

IR υ_{max} (film): 3659, 2980, 1462, 1382, 1231, 1155.

HRMS (EI^+) *m/z* calcd for $C_{33}\ H_{31}\ O_2\ N\ P\ [M+H]^+$: 504.2087, found 504.2086.

$[\boldsymbol{\alpha}]^{25}_{589}$ = -109.4 (*c* 1.0, $CHCl_3$) for 99% ee.

N-((*R*)-2,3-dihydro-1*H*-inden-1-yl)-*N*-(2,6-dimethylheptan-4-yl)dinaphtho [2,1-d:1',2'-*f*][1,3,2]dioxaphosphepin-4-amine

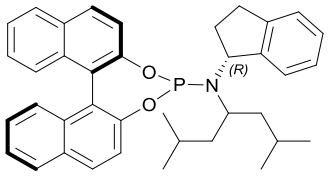

General Procedure G: Triethylamine (2.36 mL, 16.935 mmol, 5.0 eq.), PCl_3 (0.30 mL, 3.387 mmol, 1.0 eq.), CH_2Cl_2 (25 mL), (*R*)-*N*-(2,6-dimethylheptan-4-yl)-2,3-dihydro-1*H*-inden-1-amine (878 mg, 3.387 mmol, 1.0 eq.), (*R*)-binaphthol (969.8 mg, 3.387 mmol, 1.0 eq.).

The crude mixture was treated as described above and was purified by flash column chromatography (Hexane:CH_2Cl_2, 80:20, SiO_2) to afford *N*-((*R*)-2,3-dihydro-1*H*-inden-1-yl) -*N*- (2,6-dimethylheptan-4-yl)dinaphtho[2,1-d:1',2'-*f*][1,3,2]dioxaphosphepin-4-amine (406.2 mg, 0.711 mmol, 21%) as a foamy white solid.

^{1}H NMR (500 MHz, Chloroform-*d*) δ 7.97 – 7.83 (m, 4H, 4 × Ar-H), 7.66 (d, *J* = 7.5 Hz, 1H, Ar-H), 7.59 (d, *J* = 8.7 Hz, 1H, Ar-H), 7.50 – 7.44 (m, 1H, Ar-H), 7.41 – 7.28 (m, 4H, 4 × Ar-H), 7.26 – 7.14 (m, 5H, 5 × Ar-H), 4.82 – 4.72 (m, 1H, CH), 3.27 – 3.09 (m, 1H, CH), 3.05 – 2.95 (m, 1H, ½ × CH_2), 2.77 – 2.67 (m, 1H, ½ × CH_2), 2.39 – 2.27 (m, 1H, ½ × CH_2), 2.21 – 2.10 (m, 1H, ½ × CH_2), 1.91 – 1.79 (m, 1H, CH), 1.61 – 1.45 (m, 4H, CH & CH_2 & ½ × CH_2), 1.39 – 1.23 (m, 1H, ½ × CH_2), 0.87 (d, *J* = 6.7 Hz, 3H, CH_3), 0.80 (d, *J* = 6.7 Hz, 3H, CH_3), 0.73 (d, *J* = 5.9 Hz, 3H, CH_3), 0.39 – 0.24 (m, 3H, CH_3).

^{13}C NMR (126 MHz, Chloroform-*d*) δ 150.2, 150.1, 149.9, 144.4 – 143.9 (m), 143.7, 132.9, 132.8, 131.3, 130.5, 130.2, 129.7, 129.0, 128.2, 128.1, 127.5, 127.09, 127.06, 126.3, 125.9, 125.8, 125.7, 125.3, 124.7, 124.6, 124.3, 124.0, 123.9, 122.5, 122.2, 121.71, 121.69, 59.7, 51.1, 45.9 – 45.0 (m), 36.4 – 34.3 (m), 30.6, 24.9, 24.5, 23.8, 23.3, 22.6, 20.7.

^{31}P NMR (243 MHz, Chloroform-*d*) δ 151.0.

IR υ_{max} (film): 3064, 2954, 2866, 2360, 1590, 1506, 1232, 1064.

HRMS (EI$^+$) *m/z* calcd for $C_{38}H_{41}O_2NP$ $[M+H]^+$: 574.2869, found 574.2869.

$[\alpha]^{25}_{589}$ = -86.8 (*c* 1.0, $CHCl_3$) for 99% ee.

(11b*S*)-*N*-((*S*)-2,3-dihydro-1*H*-inden-1-yl)-*N*-(nonan-5-yl)dinaphtho [2,1-d:1',2'-*f*][1,3,2]dioxaphosphepin-4-amine

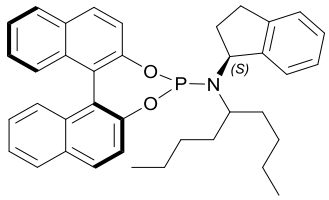

This ligand was part of a shared ligand library and was not synthesized by the author even though it was used in this work. It can be found in previously reported procedures, similar to the General Procedure G.[6]

^{1}H NMR (400 MHz, Chloroform-*d*) δ 8.00 – 7.88 (m, 4H, 4 × Ar-H), 7.74 (d, *J* = 7.6 Hz, 1H, Ar-H), 7.63 (d, *J* = 8.7 Hz, 1H, Ar-H), 7.51 (dd, *J* = 8.8, 0.9 Hz, 1H, Ar-H), 7.46 – 7.19 (m, 9H, 9 × Ar-H), 4.85 – 4.72 (m, 1H, CH), 3.09 – 2.89 (m, 2H, CH & ½ × CH_2), 2.83 – 2.70 (m, 1H, ½ × CH_2), 2.53 – 2.38 (m, 1H, ½ × CH_2), 2.29 – 2.14 (m, 1H, ½ × CH_2), 1.87 – 1.74 (m, 1H, ½ × CH_2), 1.76 – 1.61 (m, 1H, ½ × CH_2), 1.56 – 1.41 (m, 3H,

CH_2 & ½ × CH_2), 1.38 – 1.06 (m, 6H, ½ × CH_2 & 2 × CH_2 & ½ × CH_2), 0.99 – 0.85 (m, 7H, ½ × CH_2 & 2 × CH_3).

^{13}C NMR (101 MHz, Chloroform-*d*) δ 150.3, 150.2, 149.9, 144.6, 143.3, 132.8, 131.3, 130.4, 130.2, 129.5, 128.3, 128.1, 127.4, 127.2, 127.1, 126.4, 125.92, 125.86, 125.2, 124.8, 124.6, 124.3, 124.0, 123.9, 122.33, 122.31, 122.27, 121.83, 121.81, 59.8, 59.6, 55.2, 55.1, 36.95, 36.89, 36.7 (br m), 34.8 (br m), 30.4, 29.4, 28.8, 23.2, 22.9, 14.2, 14.1.

^{31}P NMR (162 MHz, Chloroform-*d*) δ 149.8.

Analytical data are in agreement with the literature.[6]

(11b*S*)-*N*-cyclohexyl-*N*-((*S*)-2,3-dihydro-1H-inden-1-yl)dinaphtho [2,1-d:1',2'-*f*][1,3,2]dioxaphosphepin-4-amine

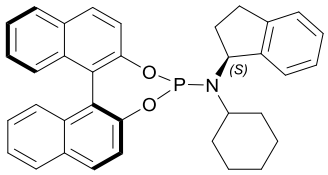

This ligand was part of a shared ligand library and was not synthesized by the author even though it was used in this work. It can be found in previously reported procedures, similar to the General Procedure G.[6]

^{1}H NMR (400 MHz, Chloroform-*d*) δ 8.00 – 7.80 (m, 4H, 4 × Ar-H), 7.63 (d, *J* = 7.5 Hz, 1H, Ar-H), 7.60 – 7.48 (m, 2H, 2 × Ar-H), 7.46 – 7.36 (m, 3H, 3 × Ar-H), 7.36 – 7.16 (m, 6H, 6 × Ar-H), 4.77 (dt, *J* = 12.6, 8.2 Hz, 1H, CH), 2.98 – 2.87 (m, 1H, ½ × CH_2), 2.81 – 2.60 (m, 2H, ½ × CH_2 & CH), 2.47 – 2.34 (m, 1H, ½ × CH_2), 2.16 – 2.01 (m, 2H, ½ × CH_2 & ½ × CH_2), 1.97 – 1.89 (m, 1H, ½ × CH_2), 1.83 – 1.54 (m, 3H, CH_2 & ½ × CH_2), 1.51 – 1.42 (m, 1H, ½ × CH_2), 1.41 – 0.73 (m, 4H, 2 × CH_2).

^{13}C NMR (101 MHz, Chloroform-*d*) δ 150.4, 150.3, 150.0, 144.4, 143.2, 132.8, 132.7, 131.3, 130.4, 130.2, 129.5, 128.3, 128.2, 127.2, 127.1 (2 C), 126.4, 125.9, 125.8, 124.8, 124.6, 124.5, 124.3, 124.13, 124.07, 122.39, 122.37, 122.1, 121.60, 121.58, 60.5, 60.3, 54.7, 54.6, 36.5 – 36.1 (br m, 2 C), 34.9 (br m), 30.0, 26.4, 26.3, 25.4.

^{31}P NMR (162 MHz, Chloroform-*d*) δ 151.5.

Analytical data are in agreement with the literature.[6]

(11b*S*)-*N*-cycloheptyl-*N*-((*S*)-2,3-dihydro-1H-inden-1-yl)dinaphtho [2,1-d:1',2'-*f*][1,3,2]dioxaphosphepin-4-amine

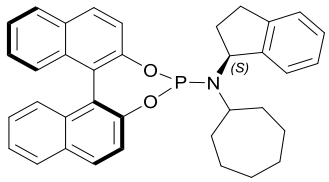

This ligand was part of a shared ligand library and was not synthesized by the author even though it was used in this work. It can be found in previously reported procedures, similar to the General Procedure G.[6]

^{1}H NMR (400 MHz, Chloroform-*d*) δ 7.99 – 7.82 (m, 4H, 4 × Ar-H), 7.64 (d, *J* = 7.5 Hz, 1H, Ar-H), 7.58 – 7.48 (m, 2H, 2× Ar-H), 7.44 – 7.37 (m, 3H, 3 × Ar-H), 7.36 – 7.17 (m, 6H, 6 × Ar-H), 4.76 (dt, *J* = 13.2, 8.2 Hz, 1H, CH), 2.99 – 2.88 (m, 2H, CH & ½ × CH_2), 2.75 – 2.61 (m, 1H, ½ × CH_2), 2.49 – 2.38 (m, 1H, ½ × CH_2), 2.18 – 2.05 (m, 2H, ½ × CH_2 & ½ × CH_2), 2.05 – 1.91 (m, 2H, ½ × CH_2 & ½ × CH_2), 1.86 – 1.71 (m, 1H, ½ × CH_2), 1.67 – 1.52 (m, 2H, CH_2), 1.46 – 1.22 (m, 4H, 2 × CH_2), 1.15 – 0.98 (m, 2H, CH_2).

^{13}C NMR (101 MHz, Chloroform-*d*) δ 150.3, 150.2, 150.1, 143.1, 132.8, 132.7, 131.3, 130.5, 130.2, 129.6, 128.2, 128.2, 127.2, 127.1, 126.4, 125.9, 125.8, 124.8, 124.62, 124.58, 124.3, 124.1, 124.0, 122.38, 122.36, 122.2, 121.7, 121.6, 60.7, 56.6, 56.5, 38.4 (m), 36.9 (m), 30.1, 27.3, 27.1, 25.2, 25.1.

^{31}P NMR (162 MHz, Chloroform-*d*) δ 151.2.

Analytical data are in agreement with the literature.[6]

(11b*S*)-*N*-((*S*)-2,3-dihydro-1*H*-inden-1-yl)-*N*-isopropyldinaphtho [2,1-d:1',2'-*f*][1,3,2]dioxaphosphepin-4-amine

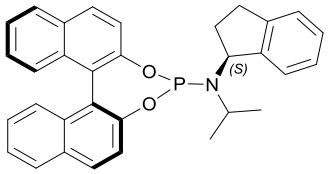

This ligand was part of a shared ligand library and was not synthesized by the author even though it was used in this work. It can be found in previously reported procedures, similar to the General Procedure G.[6]

^{1}H NMR (400 MHz, Chloroform-*d*) δ 7.89 – 7.74 (m, 4H, 4 × Ar-H), 7.55 – 7.45 (m, 2H, 2 × Ar-H), 7.40 (dd, *J* = 8.8, 0.9 Hz, 1H, Ar-H), 7.34 – 7.27 (m, 3H, 3 × Ar-H), 7.25 – 7.08 (m, 6H, 6 × Ar-H), 4.66 (dt, *J* = 15.4, 8.1 Hz, 1H, CH), 3.32 – 3.18 (m, 1H, CH), 2.93 – 2.81 (m, 1H, ½ × CH_2), 2.69 – 2.55 (m, 1H, ½ × CH_2), 2.44 – 2.31 (m, 1H, ½ × CH_2), 2.13 – 1.97 (m, 1H, ½ × CH_2), 1.21 (d, *J* = 6.7 Hz, 3H, CH_3), 1.11 (d, *J* = 6.7 Hz, 3H, CH_3).

^{13}C NMR (101 MHz, Chloroform-*d*) δ 150.3, 150.2, 150.0, 144.6, 144.5, 143.1, 132.8, 132.7, 131.3, 130.5, 130.2, 129.5, 128.3, 128.2, 127.3, 127.2, 127.1, 126.5, 125.9, 125.8, 124.8, 124.7, 124.6, 124.3, 124.1, 124.0, 122.4, 122.3, 121.69, 121.67, 59.5, 59.3, 46.0, 45.9, 36.8 – 36.4 (m), 30.2, 25.14, 25.08, 23.92, 23.86.

^{31}P NMR (162 MHz, Chloroform-*d*) δ 151.4.

Analytical data are in agreement with the literature.[6]

(11b*S*)-*N*-cyclooctyl-*N*-((*S*)-2,3-dihydro-1*H*-inden-1-yl)dinaphtho [2,1-d:1',2'-*f*][1,3,2]dioxaphosphepin-4-amine

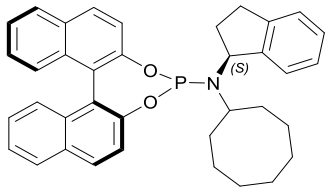

This ligand was part of a shared ligand library and was not synthesized by the author even though it was used in this work. It can be found in previously reported procedures, similar to the General Procedure G.[6]

^{1}H NMR (400 MHz, Chloroform-*d*) δ 8.01 – 7.84 (m, 4H, 4 × Ar-H), 7.67 – 7.49 (m, 3H, 3 × Ar-H), 7.46 – 7.17 (m, 9H, 9 × Ar-H), 4.76 (dt, *J* = 13.4, 8.1 Hz, 1H, CH), 3.18 – 3.04 (m, 1H, CH), 3.02 – 2.90 (m, 1H, ½ × CH_2), 2.76 – 2.63 (m, 1H, ½ × CH_2), 2.51 – 2.35 (m, 1H, ½ × CH_2), 2.25 – 1.78 (m, 5H, ½ × CH_2 & 2 × CH_2), 1.68 – 1.53 (m, 2H, CH_2), 1.39 – 1.06 (m, 7H, 3 × CH_2 & ½ × CH_2), 0.91 – 0.74 (m, 1H, ½ × CH_2).

^{13}C NMR (101 MHz, Chloroform-*d*) δ 150.3, 150.2, 150.1, 143.1, 132.84, 132.79, 131.3, 130.5, 130.2, 129.7, 128.3, 128.1, 127.3, 127.09, 127.06, 126.4, 125.9, 125.8, 124.75, 124.71, 124.6, 124.3, 123.9, 122.4, 122.3, 121.7, 60.7, 60.6, 54.8, 54.7, 37.5 – 36.6 (m, 2 C), 36.5 – 35.6 (m), 30.2, 26.3, 25.8, 25.6, 24.5.

^{31}P NMR (162 MHz, Chloroform-*d*) δ 151.7.

Analytical data are in agreement with the literature.[6]

(11b*S*)-*N*-benzhydryl-*N*-((*S*)-2,3-dihydro-1*H*-inden-1-yl)dinaphtho[2,1-d:1',2'-*f*][1,3,2]dioxaphosphepin-4-amine

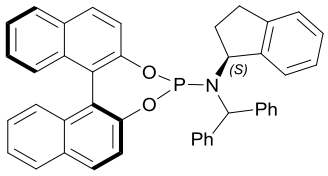

This ligand was part of a shared ligand library and was not synthesized by the author even though it was used in this work. It can be found in previously reported procedures, similar to the General Procedure G.[6]

^{1}H NMR (400 MHz, Chloroform-*d*) δ 7.87 (d, *J* = 8.8 Hz, 1H, Ar-H), 7.81 (dd, *J* = 7.9, 1.1 Hz, 1H, Ar-H), 7.74 – 7.65 (m, 2H, 2 × Ar-H), 7.46 (dd, *J* = 8.8, 1.0 Hz, 2H, 2 × Ar-H), 7.35 – 7.05 (m, 20H, 20 × Ar-H), 5.50 – 5.42 (m, 1H, CH), 4.97 – 4.86 (m, 1H, CH), 2.58 – 2.47 (m, 1H, ½ × CH_2), 2.43 – 2.30 (m, 1H, ½ × CH_2), 1.71 – 1.58 (m, 2H, CH_2).

^{13}C NMR (126 MHz, Chloroform-*d*) δ 150.0, 149.9, 149.7, 144.1, 143.4, 143.4, 142.8, 142.62, 142.59, 132.8, 132.6, 131.4, 130.4, 130.3, 129.4, 129.3, 128.89, 128.86, 128.3, 128.22, 128.19, 128.1, 127.7, 127.14, 127.11, 127.09, 126.9, 126.3, 126.0, 125.8, 125.50, 125.48, 125.0, 124.8, 124.3, 124.2, 124.1, 122.3, 122.3, 122.2, 121.4, 121.4, 62.6, 62.5, 61.7, 61.6, 35.0 – 34.3 (m), 30.1.

^{31}P NMR (162 MHz, Chloroform-*d*) δ 146.5.

Analytical data are in agreement with the literature.[6]

(11b*S*)-*N*,*N*-diphenyldinaphtho[2,1-d:1',2'-*f*][1,3,2]dioxaphosphepin-4-amine

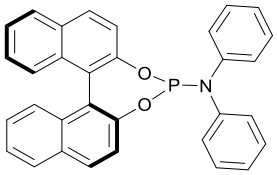

General Procedure G: Triethylamine (0.41 mL, 2.95 mmol, 5.0 eq.), PCl_3 (0.05 mL, 0.59 mmol, 1.0 eq.), CH_2Cl_2 (6 mL), diphenylamine (100 mg, 0.59 mmol, 1.0 eq.), (*S*)-binaphthol (169 mg, 0.59 mmol, 1.0 eq.).

The crude mixture was treated as described above and was purified by flash column chromatography (Hexane:CH_2Cl_2, 80:20, SiO_2) to afford (11b*S*)-*N*,*N*-diphenyldinaphtho[2,1-d:1',2'-*f*][1,3,2]dioxaphosphepin-4-amine (176 mg, 0.36 mmol, 61%) as a foamy white solid.

^{1}H NMR (400 MHz, Chloroform-*d*) δ 7.93 – 7.80 (m, 2H, 2 × Ar-H), 7.71 – 7.65 (m, 1H, Ar-H), 7.50 – 7.40 (m, 2H, 2 × Ar-H), 7.31 (m, 2H, 2 × Ar-H), 7.22 – 7.10 (m, 4H, 4 × Ar-H), 7.04 – 6.84 (m, 11H, 11 × Ar-H).

^{13}C NMR (126 MHz, Chloroform-*d*) δ 149.8, 149.7, 148.6, 144.9, 144.8, 143.1, 132.8, 132.3, 131.5, 130.4, 129.3, 129.2, 128.7, 128.3, 127.9, 127.1, 126.7, 126.5, 126.4, 126.1, 125.8, 124.9, 124.6, 124.4, 124.34, 124.30, 121.90, 121.87, 121.69, 121.67, 121.0, 117.8.

^{31}P NMR (162 MHz, Chloroform-*d*) δ 139.1.

IR υ_{max} (film): 3058, 1590, 1487, 1231, 1189, 946.

HRMS (ESI^+) *m/z* calcd for $C_{32}H_{23}O_2NP$ $[M+H]^+$: 484.1461, found 484.1461.

$[\alpha]^{25}_{589}$ = +133.1 (*c* 1.0, $CHCl_3$) for 99% ee.

5-((11b*S*)-dinaphtho[2,1-d:1',2'-*f*][1,3,2]dioxaphosphepin-4-yl)-5*H*-dibenzo[*b*,*f*]azepine

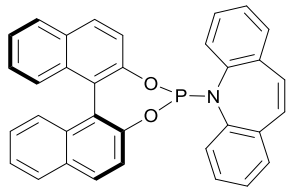

General Procedure G: Triethylamine (1.08 mL, 7.76 mmol, 5.0 eq.), PCl_3 (0.14 mL, 1.55 mmol, 1.0 eq.), CH_2Cl_2 (16 mL), 5*H*-dibenzo[*b*,*f*]azepine (300 mg, 1.55 mmol, 1.0 eq.), (*S*)-binaphthol (444 mg, 1.55 mmol, 1.0 eq.).

The crude mixture was treated as described above and was purified by flash column chromatography (Hexane:CH_2Cl_2, 80:20, SiO_2) to afford 5-((11b*S*)-dinaphtho[2,1-d:1',2'-*f*][1,3,2]dioxaphosphepin-4-yl)-5*H*-dibenzo[*b*,*f*]azepine (567 mg, 1.12 mmol, 72%) as a foamy white solid.

^{1}H NMR (400 MHz, Chloroform-*d*) δ 7.90 (d, *J* = 8.8 Hz, 1H, Ar-H), 7.86 – 7.78 (m, 1H, Ar-H), 7.71 – 7.63 (m, 1H, Ar-H), 7.53 (dd, *J* = 8.8, 0.8 Hz, 1H, Ar-H), 7.34 (d, *J* = 8.8 Hz, 1H, Ar-H), 7.33 – 7.24 (m, 2H, 2 × Ar-H), 7.22 – 7.05 (m, 9H, 9 × Ar-H), 7.04 – 7.00 (m, 1H, Ar-H), 6.93 – 6.80 (m, 3H, 3 × Ar-H), 6.76 (dd, *J* = 8.8, 0.8 Hz, 1H, Ar-H), 6.44 (ddd, *J* = 8.2, 7.4, 1.6 Hz, 1H, Ar-H).

^{13}C NMR (101 MHz, Chloroform-*d*) δ 150.0, 149.9, 148.7, 143.1, 142.8, 142.5, 136.5, 136.4, 135.2, 132.9, 132.2, 131.5, 131.4, 131.35, 130.33, 130.2, 129.2, 129.09, 129.06, 129.02, 128.98, 128.9, 128.6, 128.4, 128.3, 127.9, 127.1, 126.8, 126.7, 126.2, 126.1, 125.7, 124.9, 124.32, 124.28, 124.2, 122.2, 122.1, 121.5, 121.15, 121.12.

^{31}P NMR (162 MHz, Chloroform-d) δ 137.9.

Analytical data are in agreement with the literature.[18]

5-((11b*S*)-dinaphtho[2,1-d:1',2'-*f*][1,3,2]dioxaphosphepin-4-yl)-10,11-dihydro-5*H*-dibenzo[*b*,*f*]azepine

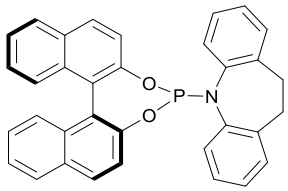

*Note: General Procedure G do not afford ligands containing azepine derivatives, with the ligand **L28** being the sole exception.*

General Procedure H: PCl_3 (0.15 mL, 1.69 mmol, 1.1 eq.), THF (4.0 mL), triethylamine (0.43 mL, 3.07 mmol, 2.0 eq.), THF (2.0 mL), (*S*)-binaphthol (440 mg, 1.54 mmol, 1.0 eq.), THF (2.0 mL), 10,11-dihydro-5*H*-dibenzo[*b*,*f*]azepine (300 mg, 1.54 mmol, 1.0 eq.), THF (3.0 mL), *n*-BuLi (2.5 M in hexane, 0.65 mL, 1.61 mmol, 1.05 eq.).

The crude mixture was treated as described above and was purified by flash column chromatography (Hexane:CH_2Cl_2, 80:20, SiO_2) to afford 5-((11b*S*)-dinaphtho[2,1-d:1',2'-*f*] [1,3,2]dioxaphosphepin-4-yl) -10,11- dihydro-5H-dibenzo[*b*,*f*]azepine (236 mg, 0.46 mmol, 30%) as a foamy white solid.

^{1}H NMR (400 MHz, Chloroform-d) δ 7.92 (d, *J* = 8.8 Hz, 1H, Ar-H), 7.84 (d, *J* = 8.4 Hz, 1H, Ar-H), 7.67 (d, *J* = 8.2 Hz, 1H, Ar-H), 7.56 (dd, *J* = 8.8, 1.0 Hz, 1H, Ar-H), 7.37 – 6.90 (m, 13H, 13 × Ar-H), 6.85 (td, *J* = 7.5, 1.3 Hz, 1H, Ar-H), 6.64 (dd, *J* = 8.8, 0.9 Hz, 1H, Ar-H), 6.34 (td, *J* = 7.7, 1.6 Hz, 1H, Ar-H), 3.83 – 3.71 (m, 1H, ½ × CH_2), 3.58 – 3.46 (m, 1H, ½ × CH_2), 2.93 – 2.80 (m, 2H, CH_2).

^{13}C NMR (126 MHz, Chloroform-d) δ 149.9, 149.8, 148.6, 143.1, 142.4, 142.2, 137.5, 136.2, 136.2, 132.9, 132.2, 131.5, 130.6, 130.4, 130.1, 129.0, 128.9, 128.59, 128.57,

128.3, 127.9, 127.6, 127.5, 127.1, 126.9, 126.5, 126.45, 126.38, 126.2, 126.1, 125.6, 124.9, 124.4, 124.35, 124.30, 122.2, 121.2, 120.88, 120.85, 31.9, 31.3.

^{31}P NMR (162 MHz, Chloroform-d) δ 136.3.

Analytical data are in agreement with the literature.[18]

(11b*S*)-*N*-phenyl-*N*-(2-vinylphenyl)dinaphtho[2,1-d:1',2'-*f*][1,3,2]dioxaphosphepin-4-amine

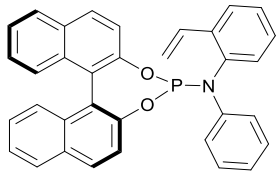

General Procedure H: PCl_3 (0.15 mL, 1.69 mmol, 1.1 eq.), THF (4.0 mL), triethylamine (0.43 mL, 3.07 mmol, 2.0 eq.), THF (2.0 mL), (*S*)-binaphthol (440 mg, 1.54 mmol, 1.0 eq.), THF (2.0 mL), *N*-phenyl-2-vinylaniline (300 mg, 1.54 mmol, 1.0 eq.), THF (3.0 mL), *n*-BuLi (2.5 M in hexane, 0.65 mL, 1.61 mmol, 1.05 eq.).

The crude mixture was treated as described above and was purified by flash column chromatography (Hexane:CH_2Cl_2, 80:20, SiO_2) to afford (11b*S*)-*N*-phenyl-*N*-(2-vinylphenyl)dinaphtho[2,1-d:1',2'-*f*] [1,3,2]dioxaphosphepin-4-amine (100 mg, 0.20 mmol, 13%) as a foamy white solid.

^{1}H NMR (400 MHz, Chloroform-*d*) δ 7.92 – 7.79 (m, 2H, 2 × Ar-H), 7.74 – 7.67 (m, 1H, Ar-H), 7.53 – 7.39 (m, 3H, 3 × Ar-H), 7.36 – 7.26 (m, 2H, 2 × Ar-H), 7.22 – 7.08 (m, 4H, 4 × Ar-H), 7.06 – 6.85 (m, 8H, 7 × Ar-H & C=CH), 6.85 – 6.79 (m, 1H, Ar-H), 6.78 – 6.72 (m, 1H, Ar-H), 5.64 (dd, *J* = 17.5, 1.3 Hz, 1H, C=CH), 5.19 (dd, *J* = 11.0, 1.2 Hz, 1H, C=CH).

^{13}C NMR (126 MHz, Chloroform-*d*) δ 149.9, 149.8, 148.5, 145.7, 145.6, 140.2, 140.1, 136.9, 136.8, 133.3, 132.9, 132.8, 132.3, 131.6, 131.55, 131.51, 130.5, 130.4, 129.2,

128.7, 128.3, 128.0, 127.2, 127.1, 126.8, 126.2, 126.0, 125.8, 125.0, 124.5, 124.4, 124.3, 122.9, 122.0 – 121.8 (m), 121.7 – 121.6 (m), 115.6.

^{31}P NMR (162 MHz, Chloroform-*d*) δ 139.7.

IR υ_{max} (film): 3061, 1590, 1491, 1231, 1203, 948.

HRMS (ESI$^+$) *m/z* calcd for $C_{34}H_{25}O_2NP$ $[M+H]^+$: 510.1617, found 510.1619.

$[\alpha]^{25}_{589}$ = +93.0 (*c* 1.0, $CHCl_3$) for 99% ee.

5-((11b*S*)-dinaphtho[2,1-d:1',2'-*f*][1,3,2]dioxaphosphepin-4-yl)-2-methyl-5*H*-dibenzo[*b*,*f*]azepine

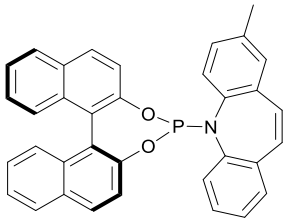

General Procedure H: PCl_3 (0.07 mL, 0.82 mmol, 1.1 eq.), THF (2.0 mL), triethylamine (0.21 mL, 1.50 mmol, 2.0 eq.), THF (1.0 mL), (*S*)-binaphthol (214 mg, 0.75 mmol, 1.0 eq.), THF (1.0 mL), 2-methyl-5*H*-dibenzo[*b*,*f*]azepine (155mg, 0.75 mmol, 1.0 eq.), THF (2.0 mL), *n*-BuLi (2.5 M in hexane, 0.31 mL, 0.785 mmol, 1.05 eq.).

The crude mixture was treated as described above and was purified by flash column chromatography (Hexane:CH_2Cl_2, 80:20, SiO_2) to afford 5-((11b*S*)-dinaphtho[2,1-d:1',2'-*f*][1,3,2]dioxaphosphepin-4-yl)-2-methyl-5*H*-dibenzo[*b*,*f*]azepine (214 mg, 0.41 mmol, 55%) as a foamy white solid.

Mixture of diastereoisomers (1:1)

^{1}H NMR (400 MHz, Chloroform-*d*) δ 7.89 (d, *J* = 8.8 Hz, 2H, 2 × Ar-H), 7.81 (dt, *J* = 8.2, 1.0 Hz, 2H, 2 × Ar-H), 7.72 – 7.63 (m, 2H, 2 × Ar-H), 7.53 (dt, *J* = 8.8, 0.9 Hz, 2H, 2 × Ar-H), 7.37 – 6.71 (m, 32H, 32 × Ar-H), 6.47 – 6.38 (m, 1H, Ar-H), 6.20 – 6.12 (m, 1H, Ar-H), 2.20 (s, 3H, CH_3), 2.05 (s, 3H, CH_3).

^{13}C NMR (126 MHz, Chloroform-*d*) δ 150.1, 150.0, 149.9, 148.8, 143.1, 142.9, 142.7, 140.6, 140.4, 140.0, 136.44, 136.41, 136.2, 136.1, 135.9, 135.2, 134.92, 132.88, 132.2, 131.6, 131.5, 131.43, 131.38, 131.3, 130.3, 130.2, 129.7, 129.3, 129.2, 129.0 – 128.9 (m), 128.8, 128.5, 128.3, 128.24, 128.17, 128.1, 127.9, 127.7, 127.13, 127.07, 126.8, 126.6, 126.1, 126.0, 125.7, 125.6, 124.8, 124.4 – 124.1 (m), 122.3 – 122.1 (m), 121.6, 121.5, 121.2 – 121.0 (m), 20.9, 20.7.

^{31}P NMR (162 MHz, Chloroform-*d*) δ 139.3, 137.8.

IR υ_{max} (film): 3019, 1485, 1208, 948.

HRMS (ESI^{+}) *m/z* calcd for $C_{35}H_{25}O_2NP$ $[M+H]^{+}$: 522.1617, found 522.1619.

$[\alpha]^{25}_{589}$ = +237.3 (*c* 1.0, $CHCl_3$) for 99% ee.

EXSY: *To prove that two diasteroisomers are formed, an EXSY experiment was carried out. Since no chemical-exchange exist between the two methyl signals, they are not interconverting (like rotamers) but are two distinct compounds (diastereoisomers).*

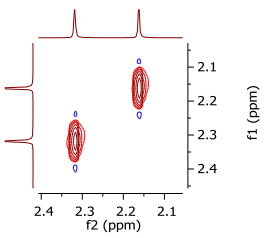

(11b*S*)-*N*-phenyl-*N*-(2-((*E*)-styryl)phenyl)dinaphtho[2,1-d:1',2'-*f*][1,3,2]dioxaphosphepin-4-amine

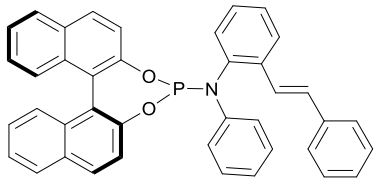

General Procedure H: PCl_3 (0.12 mL, 1.42 mmol, 1.1 eq.), THF (3.0 mL), triethylamine (0.36 mL, 2.58 mmol, 2.0 eq.), THF (1.5 mL), (*S*)-binaphthol (369 mg, 1.29 mmol, 1.0 eq.), THF (1.5 mL), (*E*)-*N*-phenyl-2-styrylaniline (350 mg, 1.29 mmol, 1.0 eq.), THF (3.0 mL), *n*-BuLi (2.5 M in hexane, 0.54 mL, 1.35 mmol, 1.05 eq.).

The crude mixture was treated as described above and was purified by flash column chromatography (Hexane:CH_2Cl_2, 80:20, SiO_2) to afford (11b*S*)-*N*-phenyl-*N*-(2-((*E*)-styryl)phenyl) dinaphtho[2,1-d:1',2'-*f*] [1,3,2]dioxaphosphepin-4-amine (102 mg, 0.18 mmol, 14%) as a foamy white solid.

^{1}H NMR (400 MHz, Chloroform-*d*) δ 8.00 – 7.88 (m, 2H, 2 × Ar-H), 7.84 – 7.69 (m, 2H, 2 × Ar-H), 7.60 – 6.85 (m, 24H, 24 × Ar-H).

^{13}C NMR (126 MHz, Chloroform-*d*) δ 150.04, 149.99, 148.7, 148.1, 145.9, 145.8, 144.9, 144.1, 141.0, 140.9, 137.6, 136.57, 136.55, 135.6, 133.0, 132.4, 131.9, 131.8, 131.6, 131.1, 130.6, 130.31, 130.29, 129.6, 129.5, 129.4, 129.3, 129.1, 128.9, 128.8, 128.8, 128.6, 128.5, 128.2, 128.1, 127.9, 127.8, 127.6, 127.34, 127.30, 127.2, 126.9, 126.8, 126.74, 126.68, 126.6, 126.3, 126.3, 126.1, 125.9, 125.24, 125.21, 125.1, 124.6, 124.5, 124.4, 123.3, 122.7, 122.6, 122.1, 122.0, 121.8, 121.75, 121.73, 120.7, 120.1, 117.5.

^{31}P NMR (162 MHz, Chloroform-*d*) δ 139.8.

IR υ_{max} (film): 3056, 2360, 1592, 1491, 1230, 1199, 947.

HRMS (ESI$^+$) *m/z* calcd for C_{40} H_{29} O_2 N P $[M+H]^+$: 586.1930, found 586.1930.

$[\alpha]^{25}_{589}$ = +48.1 (*c* 1.0, $CHCl_3$) for 99% ee.

(11b*S*)-*N*-((*S*)-2,3-dihydro-1*H*-inden-1-yl)-*N*-phenyldinaphtho [2,1-d:1',2'-*f*][1,3,2]dioxaphosphepin-4-amine

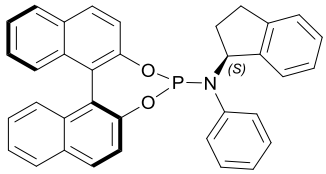

General Procedure H: PCl_3 (0.20 mL, 2.26 mmol, 1.1 eq.), THF (5.0 mL), triethylamine (0.57 mL, 4.1 mmol, 2.0 eq.), THF (2.5 mL), (*S*)-binaphthol (588 mg, 2.06 mmol, 1.0 eq.), THF (2.5 mL), (*S*)-*N*-phenyl-2,3-dihydro-1*H*-inden-1-amine (430 mg, 2.06 mmol, 1.0 eq.), THF (5.0 mL), *n*-BuLi (2.5 M in hexane, 0.86 mL, 2.16 mmol, 1.05 eq.).

The crude mixture was treated as described above and was purified by flash column chromatography (Hexane:CH_2Cl_2, 80:20, SiO_2) to afford (11b*S*)-*N*-((*S*)-2,3-dihydro-1*H*-inden-1-yl) -*N*- phenyldinaphtho [2,1-d:1',2'-*f*] [1,3,2]dioxaphosphepin-4-amine (540 mg, 1.03 mmol, 50%) as a foamy white solid.

^{1}H NMR (400 MHz, Chloroform-*d*) δ 8.24 (d, *J* = 8.8 Hz, 1H, Ar-H), 8.20 – 8.14 (m, 1H, Ar-H), 8.09 – 8.03 (m, 1H, Ar-H), 8.01 – 7.94 (m, 1H, Ar-H), 7.90 – 7.81 (m, 2H, 2 × Ar-H), 7.71 – 7.44 (m, 9H, 9 × Ar-H), 7.43 – 7.37 (m, 1H, Ar-H), 7.33 – 7.21 (m, 5H, 5 × Ar-H), 5.43 (q, *J* = 6.5 Hz, 1H, CH), 2.90 – 2.75 (m, 2H, CH_2), 2.62 – 2.52 (m, 1H, ½ × CH_2), 2.49 – 2.36 (m, 1H, ½ × CH_2).

^{13}C NMR (126 MHz, Chloroform-*d*) δ 149.93, 149.87, 149.3, 144.0, 142.7, 141.0, 140.8, 133.0, 132.7, 131.6, 130.6, 130.5, 129.8, 129.72, 129.66, 128.5, 128.4, 128.3,

127.6, 127.3, 127.2, 126.3, 126.2, 126.0, 125.8, 125.6, 125.0, 124.8, 124.5, 124.4, 124.3, 122.4, 122.3, 121.7, 121.6, 63.8 (d, *J* = 12.8 Hz), 32.6 (d, *J* = 2.8 Hz), 30.2.

^{31}P NMR (162 MHz, Chloroform-*d*) δ 141.2.

IR υ_{max} (film): 3059, 2945, 2358, 1590, 1462, 1327, 1226, 1065, 947.

HRMS (ESI$^+$) *m/z* calcd for C_{35} H_{27} O_2 N P $[M+H]^+$: 524.1774, found 524.1775.

$[\boldsymbol{\alpha}]^{25}_{589}$ = +99.0 (*c* 1.0, $CHCl_3$) for 99% ee.

(11b*S*)-*N*-((*S*)-2,3-dihydro-1*H*-inden-1-yl)-*N*-mesityldinaphtho[2,1-d:1',2'-*f*][1,3,2]dioxaphosphepin-4-amine

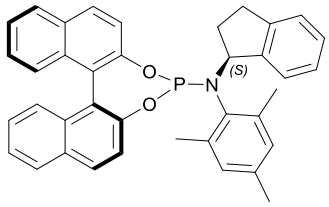

General Procedure H: PCl_3 (0.13 mL, 1.53 mmol, 1.1 eq.), THF (3.5 mL), triethylamine (0.39 mL, 2.78 mmol, 2.0 eq.), THF (2.0 mL), (*S*)-binaphthol (399 mg, 1.39 mmol, 1.0 eq.), THF (2.0 mL), (*S*)-*N*-mesityl-2,3-dihydro-1*H*-inden-1-amine (350 mg, 1.39 mmol, 1.0 eq.), THF (3.5 mL), *n*-BuLi (2.5 M in hexane, 0.58 mL, 1.46 mmol, 1.05 eq.).

The crude mixture was treated as described above and was purified by flash column chromatography (Hexane:CH_2Cl_2, 80:20, SiO_2) to afford (11b*S*)-*N*-((*S*)-2,3-dihydro-1H-inden-1-yl) -*N*- mesityldinaphtho [2,1-d:1',2'-f] [1,3,2] dioxaphosphepin-4-amine (345 mg, 0.61 mmol, 44%) as a foamy white solid.

^{1}H NMR (400 MHz, Chloroform-*d*) δ 7.95 (d, *J* = 8.8 Hz, 1H, Ar-H), 7.92 – 7.88 (m, 1H, Ar-H), 7.86 – 7.80 (m, 1H, Ar-H), 7.69 – 7.64 (m, 1H, Ar-H), 7.45 (dd, *J* = 8.7, 0.9 Hz, 1H, Ar-H), 7.42 – 7.26 (m, 5H, 5 × Ar-H), 7.25 – 7.10 (m, 4H, 4 × Ar-H), 7.09 – 6.99 (m,

2H, 2 × Ar-H), 6.91 – 6.86 (m, 1H, Ar-H), 6.72 – 6.66 (m, 1H, Ar-H), 5.18 – 5.08 (m, 1H, CH), 2.95 – 2.83 (m, 1H, ½ × CH_2), 2.61 – 2.49 (m, 1H, ½ × CH_2), 2.36 (s, 3H, CH_3), 2.35 – 2.27 (m, 1H, ½ × CH_2), 2.26 (s, 3H, CH_3), 2.17 (s, 3H, CH_3), 1.99 – 1.85 (m, 1H, ½ × CH_2).

^{13}C NMR (126 MHz, Chloroform-*d*) δ 150.7, 150.6, 148.8, 145.0, 142.31, 142.29, 139.4, 139.3, 139.10, 139.06, 138.0, 137.9, 136.59, 136.57, 132.9, 132.5, 131.4, 130.3, 130.2, 129.6, 129.2, 129.1, 128.3, 128.0, 127.8, 127.1, 127.0, 126.9, 126.0, 125.7, 125.5, 124.7, 124.6, 124.5, 124.4, 124.3, 122.3, 122.1, 121.44, 121.42, 65.2 (d, *J* = 14.2 Hz), 32.8 (d, *J* = 3.3 Hz), 30.7, 20.9, 20.0, 19.9 (d, *J* = 2.3 Hz).

^{31}P NMR (162 MHz, Chloroform-*d*) δ 147.2.

IR υ_{max} (film): 2922, 2851, 2359, 1591, 1431, 1327, 1230, 1208, 1067, 946.

HRMS (ESI$^+$) *m/z* calcd for C_{38} H_{33} O_2 N P $[M+H]^+$: 566.2243, found 566.2240.

$[\alpha]^{25}_{589}$ = +166.7 (*c* 1.0, $CHCl_3$) for 99% ee.

(11b*S*)-*N*-mesityl-*N*-(2-((*E*)-styryl)phenyl)dinaphtho [2,1-d:1',2'-*f*][1,3,2]dioxaphosphepin-4-amine

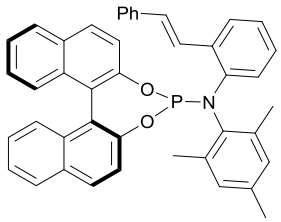

General Procedure H: PCl_3 (0.29 mL, 3.33 mmol, 1.1 eq.), THF (7.0 mL), triethylamine (0.84 mL, 6.06 mmol, 2.0 eq.), THF (3.5 mL), (*S*)-binaphthol (868 mg, 3.03 mmol, 1.0 eq.), THF (3.5 mL), (*E*)-2,4,6-trimethyl-*N*-(2-styrylphenyl)aniline (950 mg, 3.03 mmol, 1.0 eq.), THF (7.0 mL), *n*-BuLi (2.5 M in hexane, 1.27 mL, 3.18 mmol, 1.05 eq.).

The crude mixture was treated as described above and was purified by flash column chromatography (Hexane:CH_2Cl_2, 80:20, SiO_2) to afford (11b*S*)-*N*-mesityl-*N*-(2-((*E*)-styryl)phenyl)dinaphtho[2,1-d:1',2'-*f*][1,3,2]dioxaphosphepin-4-amine (232 mg, 0.36 mmol, 12%) as a foamy white solid.

^{1}H NMR (400 MHz, Chloroform-*d*) δ 7.97 – 7.88 (m, 2H, 2 × Ar-H), 7.82 – 7.76 (m, 1H, Ar-H), 7.50 (dd, *J* = 8.8, 0.9 Hz, 1H, C=CH), 7.45 – 7.12 (m, 15H, 15 × Ar-H), 7.00 – 6.87 (m, 3H, 3 × Ar-H), 6.71 (dd, *J* = 8.8, 0.9 Hz, 1H, C=CH), 6.57 – 6.50 (m, 1H, Ar-H), 6.47 (d, *J* = 16.0 Hz, 1H, Ar-H), 2.66 (s, 3H, CH_3), 2.30 (s, 3H, CH_3), 2.19 (s, 3H, CH_3).

^{13}C NMR (126 MHz, Chloroform-*d*) δ 150.6, 150.5, 148.5, 142.0, 139.2, 139.0, 138.14, 138.10, 137.6, 136.6, 136.5, 133.8, 132.9, 132.3, 131.4, 130.5, 130.3, 130.2, 129.99, 129.97, 129.3, 128.8, 128.4 (2 C), 128.3, 127.8, 127.7, 127.4, 127.3, 127.2, 127.1, 126.9, 126.5 (2 C), 126.0, 125.6, 124.9, 124.7, 124.62, 124.57, 124.3, 122.0, 121.4, 121.0, 120.9, 21.0, 20.9, 20.5.

^{31}P NMR (162 MHz, Chloroform-*d*) δ 142.0.

IR υ_{max} (film): 3058, 3023, 2918, 1495, 1477, 1228, 945.

HRMS (ESI^+) *m/z* calcd for $C_{43}\ H_{35}\ O_2\ N\ P$ $[M+H]^+$: 628.2400, found 628.2396.

$[\boldsymbol{\alpha}]^{25}_{589}$ = -27.0 (*c* 1.0, $CHCl_3$) for 99% ee.

1-(dinaphtho[2,1-d:1',2'-*f*][1,3,2]dioxaphosphepin-4-yl)-2-methylindoline

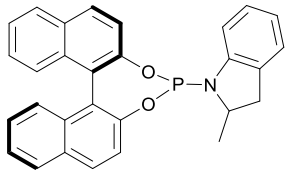

General Procedure G: Triethylamine (1.57 mL, 11.26 mmol, 5.0 eq.), PCl_3 (0.20 mL, 2.25 mmol, 1.0 eq.), CH_2Cl_2 (22 mL), 2-methylindoline (300 mg, 2.25 mmol, 1.0 eq.), (*S*)-binaphthol (677 mg, 2.36 mmol, 1.0 eq.).

The crude mixture was treated as described above and was purified by flash column chromatography (Hexane:CH_2Cl_2, 80:20, SiO_2) to afford 1-(dinaphtho[2,1-d:1',2'-*f*][1,3,2]dioxaphosphepin-4-yl)-2-methylindoline (576 mg, 1.34 mmol, 57%) as a foamy white solid.

Mixture of diastereoisomers (1:1)

^{1}H NMR (400 MHz, Chloroform-d) δ 7.95 – 7.70 (m, 7H, 7 × Ar-H), 7.60 – 7.55 (m, 1H, Ar-H), 7.48 (ddd, *J* = 8.8, 6.5, 1.0 Hz, 2H, 2 × Ar-H), 7.41 – 7.13 (m, 13H, 13 × Ar-H), 7.08 – 6.97 (m, 3H, 3 × Ar-H), 6.85 – 6.79 (m, 1H, Ar-H), 6.78 – 6.63 (m, 4H, 4 × Ar-H), 6.55 – 6.48 (m, 1H, Ar-H), 4.46 – 4.24 (m, 1H, CH), 3.75 – 3.52 (m, 1H, CH), 3.25 (ddt, *J* = 15.5, 9.0, 1.2 Hz, 1H, ½ × CH_2), 3.04 (dd, *J* = 15.5, 9.0 Hz, 1H, ½ × CH_2), 2.44 (dt, *J* = 15.5, 2.2 Hz, 1H, ½ × CH_2), 2.30 (d, *J* = 15.5 Hz, 1H, ½ × CH_2), 0.98 (d, *J* = 6.4 Hz, 3H, CH_3), 0.74 (d, *J* = 6.5 Hz, 3H, CH_3).

^{13}C NMR (126 MHz, Chloroform-d) δ 150.21, 150.17, 149.94, 149.90, 149.6, 149.2, 145.9, 145.8, 145.3, 145.2, 133.0, 132.9, 132.8, 132.7, 131.7, 131.3, 131.2, 131.1, 131.0, 130.79, 130.76, 130.63, 130.60, 130.2, 129.8, 128.52, 128.50, 128.3, 127.22, 127.18, 127.1, 127.0, 126.9, 126.4, 126.3, 126.1, 125.7, 125.1, 125.0, 124.9, 124.7, 124.4, 124.3, 122.9, 122.54, 122.52, 122.3, 121.93, 121.90, 121.7, 121.3, 121.2,

113.7, 113.6, 112.8, 112.7, 56.0 (d, *J* = 4.7 Hz), 55.6 (d, *J* = 13.8 Hz), 37.9, 37.7, 23.4 (d, *J* = 1.9 Hz), 23.3 (d, *J* = 2.7 Hz).

^{31}P NMR (162 MHz, Chloroform-d) δ 148.3, 146.0.

IR υ_{max} (film): 3055, 1590, 1479, 1460, 1221, 1070, 948.

HRMS (ESI$^+$) *m/z* calcd for $C_{29}H_{23}O_2NP$ $[M+H]^+$: 448.1461, found 448.1460.

$[\boldsymbol{\alpha}]^{25}_{589}$ = +185.7 (*c* 1.0, $CHCl_3$) for 99% ee.

(11b*S*)-*N*-((*S*)-2,3-dihydro-1*H*-inden-1-yl)-*N*-(2,4,6-triisopropylphenyl)dinaphtho[2,1-d:1',2'-*f*][1,3,2]dioxaphosphepin-4-amine

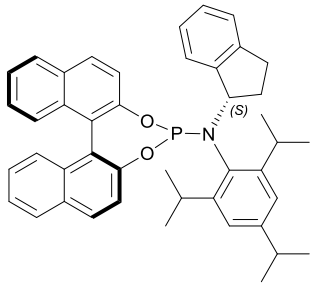

General Procedure H: PCl_3 (0.04 mL, 0.49 mmol, 1.1 eq.), THF (1.0 mL), triethylamine (0.12 mL, 0.89 mmol, 2.0 eq.), THF (0.5 mL), (*S*)-binaphthol (128 mg, 0.45 mmol, 1.0 eq.), THF (0.5 mL), (*S*)-N-(2,4,6-triisopropylphenyl)-2,3-dihydro-1*H*-inden-1-amine (150 mg, 0.45 mmol, 1.0 eq.), THF (1.0 mL), *n*-BuLi (2.5 M in hexane, 0.19 mL, 0.47 mmol, 1.05 eq.).

The crude mixture was treated as described above and was purified by flash column chromatography (Hexane:CH_2Cl_2, 80:20, SiO_2) to afford (11b*S*)-*N*-((*S*)-2,3-dihydro-1*H*-inden-1-yl) -*N*- (2,4,6-triisopropylphenyl) dinaphtho [2,1-d:1',2'-*f*] [1,3,2] dioxaphosphepin-4-amine (95 mg, 0.15 mmol, 33%) as a foamy white solid.

Diastereoisomer 1 (major):

^{1}H NMR (400 MHz, Chloroform-*d*) δ 7.97 – 7.75 (m, 3H, 3 × Ar-H), 7.70 (d, *J* = 8.8 Hz, 1H, Ar-H), 7.57 – 7.47 (m, 1H, Ar-H), 7.41 – 7.08 (m, 8H, 8 × Ar-H), 7.03 – 6.90 (m, 2H, 2 × Ar-H), 6.87 – 6.66 (m, 3H, 3 × Ar-H), 4.99 (p, *J* = 3.5 Hz, 1H, CH), 3.71 (p, *J* = 6.8 Hz, 1H, CH), 3.18 (p, *J* = 6.8 Hz, 1H, CH), 2.89 – 2.70 (m, 2H, CH & ½ × CH_2), 2.43 – 2.23 (m, 2H, CH_2), 1.60 – 1.42 (m, 1H, ½ × CH_2), 1.25 – 1.09 (m, 12H, 4 × CH_3), 0.85 (d, *J* = 6.7 Hz, 3H, CH_3), 0.69 (d, *J* = 6.8 Hz, 3H, CH_3).

^{31}P NMR (162 MHz, Chloroform-*d*) δ 145.0.

Diastereoisomer 2 (minor):

^{1}H NMR (400 MHz, Chloroform-d) δ 7.97 – 7.74 (m, 4H, 4 × Ar-H), 7.57 – 7.47 (m, 1H, Ar-H), 7.41 – 7.08 (m, 8H, 8 × Ar-H), 7.03 – 6.90 (m, 2H, 2 × Ar-H), 6.87 – 6.66 (m, 3H, 3 × Ar-H), 4.88 (dt, *J* = 8.6, 2.4 Hz, 1H, CH), 3.97 (p, *J* = 6.8 Hz, 1H, CH), 3.00 (p, *J* = 6.8 Hz, 1H, CH), 2.89 – 2.70 (m, 1H, CH), 2.22 – 2.12 (m, 1H, ½ × CH_2), 2.10 – 2.01 (m, 1H, ½ × CH_2), 1.88 – 1.69 (m, 2H, CH_2), 1.49 (d, *J* = 6.9 Hz, 3H, CH_3), 1.25 – 1.09 (m, 9H, 3 × CH_3), 0.97 (d, *J* = 6.9 Hz, 3H, CH_3), 0.17 (d, *J* = 6.8 Hz, 3H, CH_3).

^{31}P NMR (162 MHz, Chloroform-d) δ 138.7.

Mixture of diastereoisomers (2:1)

^{13}C NMR (126 MHz, Chloroform-*d*) δ 151.4, 151.3, 150.6, 150.5, 150.4, 150.3, 149.64, 149.61, 149.5, 149.15, 149.11, 149.0, 148.6, 148.45, 148.42, 145.4, 145.0, 142.4, 142.0, 134.8, 134.7, 132.91, 132.89, 132.86, 132.8, 132.7, 131.5, 131.4, 131.3, 130.5, 130.4, 130.3, 129.9, 129.8, 128.4, 128.3, 128.2, 128.1, 127.6, 127.5, 127.2, 127.13, 127.11, 127.02, 127.00, 126.2, 126.13, 126.07, 125.9, 125.2, 124.9, 124.8, 124.6,

124.4, 124.3, 124.3, 124.1, 122.4, 122.3, 122.2, 122.02, 121.98, 121.9, 121.84, 121.76, 121.7, 121.5, 121.4, 66.15, 66.12, 62.3, 62.2, 34.2, 34.1, 32.3, 31.0, 30.8, 29.5, 29.2, 29.1, 28.7, 28.4, 27.6, 27.5, 26.5, 26.4, 25.93, 25.90, 25.3, 24.3, 24.21, 24.16, 24.0, 22.72, 22.69, 21.7.

IR υ_{max} (film): 3657, 2980, 2888, 1462, 1382, 1230, 1153, 1071, 947.

HRMS (ESI$^+$) *m/z* calcd for C_{44} H_{45} O_2 N P $[M+H]^+$: 650,3182, found 650,3177.

$[\alpha]^{25}_{589}$ = +85.5 (*c* 1.0, $CHCl_3$) for 99% ee.

EXSY: *To prove that two diasteroisomers are formed, an EXSY experiment was carried out. Since no chemical-exchange exist between the two signals, they are not interconverting (like rotamers) but are two distinct compounds (diastereoisomers).*

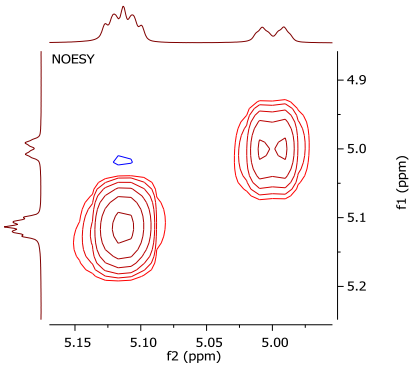

5-(dinaphtho[2,1-d:1',2'-*f*][1,3,2]dioxaphosphepin-4-yl)-4-methyl-5*H*-dibenzo[*b*,*f*]azepine

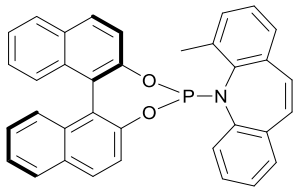

General Procedure H: PCl_3 (0.11 mL, 1.22 mmol, 1.1 eq.), THF (2.5 mL), triethylamine (0.31 mL, 2.22 mmol, 2.0 eq.), THF (1.2 mL), (*R*)-binaphthol (318 mg, 1.11 mmol, 1.0 eq.), THF (1.2 mL), 4-methyl-5*H*-dibenzo[*b*,*f*]azepine (230 mg, 1.11 mmol, 1.0 eq.), THF (2.5 mL), *n*-BuLi (2.5 M in hexane, 0.47 mL, 1.16 mmol, 1.05 eq.).

The crude mixture was treated as described above and was purified by flash column chromatography (Hexane:CH_2Cl_2, 80:20, SiO_2) to afford 5-(dinaphtho[2,1-d:1',2'-*f*][1,3,2] dioxaphosphepin-4-yl) -4- methyl -5*H*- dibenzo [*b*,*f*] azepine (373 mg, 0.72 mmol, 65%) as a foamy white solid.

Diastereoisomer 1 (major):

^{1}H NMR (400 MHz, Chloroform-d) δ 7.99 (d, *J* = 8.8 Hz, 1H, Ar-H), 7.93 – 7.84 (m, 3H, 3 × Ar-H), 7.70 (dt, *J* = 8.2, 0.9 Hz, 1H, Ar-H), 7.60 (dd, *J* = 8.7, 0.9 Hz, 1H, Ar-H), 7.48 – 6.77 (m, 14H, 14 × Ar-H), 6.57 – 6.51 (m, 1H, Ar-H), 2.74 (s, 3H, CH_3).

^{31}P NMR (162 MHz, Chloroform-d) δ 137.5.

Diastereoisomer 2 (minor):

^{1}H NMR (400 MHz, Chloroform-d) δ 7.93 – 7.84 (m, 1H, Ar-H), 7.48 – 6.77 (m, 20H, 20 × Ar-H), 2.66 (s, 3H, CH_3).

^{31}P NMR (162 MHz, Chloroform-d) δ 142.5.

Mixture of diastereoisomers (2:1)

^{13}C NMR (126 MHz, Chloroform-d) δ 150.0, 149.9, 149.1, 149.0, 148.8, 148.6, 142.5, 142.4, 142.1, 142.0, 140.1, 140.0, 139.9, 138.20, 138.16, 138.0, 137.9, 137.64, 137.61, 137.54, 137.49, 136.60, 136.58, 135.4, 132.8, 132.7, 132.5, 131.9, 131.7, 131.44, 131.36, 131.3, 131.23, 131.19, 131.0, 130.4, 130.3, 130.2, 130.1, 129.6, 129.0, 128.9, 128.82, 128.80, 128.7, 128.6, 128.30, 128.27, 128.1, 127.9, 127.8, 127.2, 127.04, 127.02, 126.9, 126.8, 126.75, 126.69, 126.6, 126.4, 126.03, 126.01, 125.7, 125.5, 124.8, 124.7, 124.4, 124.3, 124.1, 124.0, 122.4, 122.03, 122.01, 121.9, 121.6, 120.68, 120.66, 19.6, 19.4, 19.3.

IR υ_{max} (film): 3055, 2360, 1507, 1462, 1219, 1202.

HRMS (ESI$^+$) *m/z* calcd for C_{35} H_{25} O_2 N P $[M+H]^+$: 522.1617, found 522.1614.

$[\boldsymbol{\alpha}]^{25}_{589}$ = -205.4 (*c* 1.0, $CHCl_3$) for 99% ee.

EXSY: *To prove that two diasteroisomers are formed, an EXSY experiment was carried out. Since no chemical-exchange exist between the two methyl signals, they are not interconverting (like rotamers) but are two distinct compounds (diastereoisomers).*

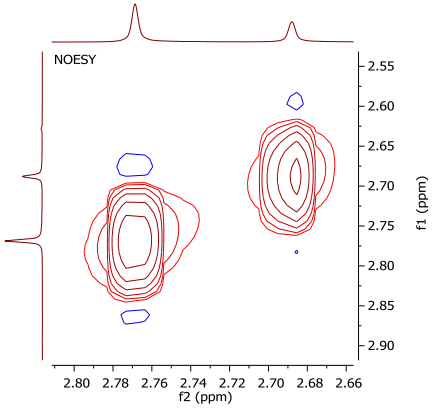

(11b*S*)-*N*-((*S*)-2,3-dihydro-1*H*-inden-1-yl)-*N*-(naphthalen-1-yl)dinaphtho[2,1-d:1',2'-*f*][1,3,2]dioxaphosphepin-4-amine

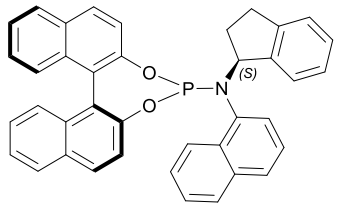

General Procedure H: PCl_3 (0.37 mL, 4.24 mmol, 1.1 eq.), THF (9.0 mL), triethylamine (1.07 mL, 7.71 mmol, 2.0 eq.), THF (4.5 mL), (*S*)-binaphthol (1104 mg, 3.86 mmol, 1.0 eq.), THF (4.5 mL), (*S*)-*N*-(2,3-dihydro-1*H*-inden-1-yl)naphthalen-1-amine (1000 mg, 3.86 mmol, 1.0 eq.), THF (9.0 mL), *n*-BuLi (2.5 M in hexane, 1.62 mL, 4.05 mmol, 1.05 eq.).

The crude mixture was treated as described above and was purified by flash column chromatography (Hexane:CH_2Cl_2, 80:20, SiO_2) to afford (11b*S*)-*N*-((*S*)-2,3-dihydro-1*H*-inden-1-yl)-*N*-(naphthalen-1-yl)dinaphtho[2,1-d:1',2'-*f*][1,3,2]dioxaphosphepin-4-amine (234 mg, 0.42 mmol, 11%) as a foamy white-off solid.

^{1}H NMR (400 MHz, Chloroform-*d*) δ 8.68 (d, *J* = 8.5 Hz, 1H, Ar-H), 8.10 (d, *J* = 7.6 Hz, 1H, Ar-H), 8.02 – 7.82 (m, 3H, 3 × Ar-H), 7.77 – 7.50 (m, 5H, 5 × Ar-H), 7.43 – 6.78 (m, 12H, 12 × Ar-H), 6.17 (d, *J* = 8.9 Hz, 1H, Ar-H), 5.47 (q, *J* = 7.7 Hz, 1H, CH), 2.62 – 2.42 (m, 2H, CH_2), 2.34 – 2.20 (m, 1H, ½ × CH_2), 2.02 – 1.88 (m, 1H, ½ × CH_2).

^{13}C NMR (126 MHz, Chloroform-*d*) δ 150.1, 150.0, 148.7, 143.8, 142.7, 136.2, 134.5, 134.2, 132.9, 132.2, 131.4, 130.8, 130.4, 130.0, 128.5, 128.3, 128.2, 127.8, 127.7, 127.3, 127.2, 127.0, 126.9, 126.3, 126.2, 126.0, 125.84, 125.79, 125.5, 125.2, 124.84, 124.81, 124.78, 124.7, 124.44, 124.40, 124.1, 122.3, 121.3, 120.4, 65.8, 65.6, 31.92, 31.87, 29.9.

^{31}P NMR (162 MHz, Chloroform-*d*) δ 140.8.

IR υ_{max} (film): 3055, 2927, 2851, 1591, 1506, 1462, 1227.

HRMS (ESI$^+$) *m/z* calcd for $C_{39}H_{29}O_2NP$ $[M+H]^+$: 574.1930, found 574.1928.

$[\alpha]^{25}_{589}$ = +15.1 (*c* 1.0, $CHCl_3$) for 99% ee.

(11b*S*)-*N*-(2-(2,2-diphenylvinyl)phenyl)-*N*-phenyldinaphtho [2,1-d:1',2'-*f*][1,3,2]dioxaphosphepin-4-amine

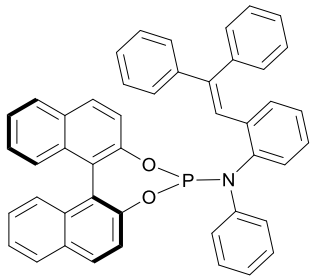

General Procedure H: PCl_3 (0.05 mL, 0.57 mmol, 1.1 eq.), THF (1.2 mL), triethylamine (0.15 mL, 1.04 mmol, 2.0 eq.), THF (0.6 mL), (*S*)-binaphthol (149 mg, 0.52 mmol, 1.0 eq.), THF (0.6 mL), 2-(2,2-diphenylvinyl)-*N*-phenylaniline (181 mg, 0.52 mmol, 1.0 eq.), THF (1.2 mL), *n*-BuLi (2.5 M in hexane, 0.22 mL, 0.55 mmol, 1.05 eq.).

The crude mixture was treated as described above and was purified by flash column chromatography (Hexane:CH_2Cl_2, 80:20, SiO_2) to afford (11b*S*)-*N*-(2-(2,2-diphenylvinyl)phenyl) -*N*- phenyldinaphtho[2,1-d:1',2'-*f*] [1,3,2]dioxaphosphepin-4-amine (203 mg, 0.31 mmol, 59%) as a foamy white solid.

^{1}H NMR (400 MHz, Chloroform-d) δ 7.96 – 7.87 (m, 2H, 2 × Ar-H), 7.79 – 7.74 (m, 1H, Ar-H), 7.49 – 7.07 (m, 17H, 17 × Ar-H), 7.03 – 6.73 (m, 12H, 12 × Ar-H).

^{13}C NMR (126 MHz, Chloroform-d) δ 150.0, 149.9, 148.7, 145.2, 145.1, 143.4, 142.7, 142.6, 140.1, 137.09, 137.06, 132.9, 132.3, 131.5, 130.9, 130.8, 130.7, 130.5 – 130.3 (m), 129.3, 128.5, 128.3, 128.2, 128.1, 128.0, 127.9, 127.5, 127.4, 127.2, 127.1, 126.8,

126.1, 126.0, 125.8, 125.6, 125.0, 124.44, 124.37, 124.3, 123.7, 123.6, 123.3, 122.0, 121.9, 121.7, 118.1.

^{31}P NMR (162 MHz, Chloroform-d) δ 139.5.

IR υ_{max} (film): 3057, 2360, 1590, 1489, 1253, 1231, 1071, 947.

HRMS (ESI$^+$) *m/z* calcd for $C_{46}H_{33}O_2NP$ $[M+H]^+$: 662.2243, found 662.2242.

$[\alpha]^{25}_{589}$ = -86.0 (*c* 1.0, $CHCl_3$) for 99% ee.

5-(dinaphtho[2,1-d:1',2'-*f*][1,3,2]dioxaphosphepin-4-yl)-3-methoxy-5*H*-dibenzo[*b*,*f*]azepine

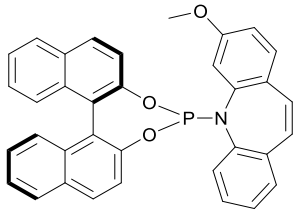

General Procedure H: PCl_3 (0.03 mL, 0.34 mmol, 1.1 eq.), THF (0.6 mL), triethylamine (0.09 mL, 0.63 mmol, 2.0 eq.), THF (0.3 mL), (*R*)-binaphthol (90 mg, 0.31 mmol, 1.0 eq.), THF (0.3 mL), 3-methoxy-5H-dibenzo[*b*,*f*]azepine (70 mg, 0.31 mmol, 1.0 eq.), THF (0.6 mL), *n*-BuLi (2.5 M in hexane, 0.13 mL, 0.33 mmol, 1.05 eq.).

The crude mixture was treated as described above and was purified by flash column chromatography (Hexane:CH_2Cl_2, 80:20, SiO_2) to afford 5-(dinaphtho[2,1-d:1',2'-*f*][1,3,2] dioxaphosphepin-4-yl) -3- methoxy -5*H*- dibenzo[*b*,*f*]azepine (18 mg, 0.03 mmol, 11%) as a foamy white solid.

Mixture of diastereoisomers (1:1)

^{1}H NMR (400 MHz, Chloroform-*d*) δ 8.03 – 7.88 (m, 5H, 5 × Ar-H), 7.77 (dd, *J* = 8.0, 1.0 Hz, 2H, 2 × Ar-H), 7.65 (dd, *J* = 8.8, 0.9 Hz, 1H, Ar-H), 7.61 – 7.51 (m, 2H, 2 × Ar-H), 7.45 – 7.06 (m, 20H, 20 × Ar-H), 7.02 – 6.80 (m, 6H, 6 × Ar-H), 6.73 – 6.60 (m, 4H, 4 × Ar-H), 6.52 – 6.47 (m, 2H, 2 × Ar-H), 3.51 (s, 3H, CH_3), 2.73 (s, 3H, CH_3).

^{13}C NMR (126 MHz, Chloroform-*d*) δ 160.7, 160.3, 150.4, 150.3, 149.8, 149.7, 148.7, 148.6, 144.0, 142.6, 142.3, 141.7, 136.9, 136.0, 132.9, 132.8, 132.3, 132.1, 131.5, 131.2, 131.1, 130.4, 130.3, 130.2, 129.9, 129.7, 129.3, 129.2, 129.15, 129.12, 129.08, 129.0, 128.9, 128.8, 128.7, 128.33, 128.31, 128.26, 128.2, 128.0, 127.9, 127.5, 127.1, 126.93, 126.90, 126.6, 126.4, 126.2, 126.1, 125.8, 125.7, 124.90, 124.86, 124.4, 124.3, 124.3, 124.22, 124.18, 122.1, 121.5, 121.4, 121.2, 120.7, 113.9, 113.8, 113.5, 112.7, 112.6, 55.3, 54.3.

^{31}P NMR (162 MHz, Chloroform-*d*) δ 138.5, 138.1.

IR υ_{max} (film): 3055, 2929, 1603, 1503, 1326, 1226, 947.

HRMS (ESI^{+}) *m/z* calcd for C_{35} H_{25} O_3 N P $[M+H]^{+}$: 538.1567, found 538.1564.

$[\boldsymbol{\alpha}]^{25}_{589}$ = -179.0 (*c* 1.0, $CHCl_3$) for 99% ee.

EXSY: *To prove that two diasteroisomers are formed, an EXSY experiment was carried out. Since no interactions exist between the two signals, they are not interconverting (like rotamers) but are two distinct compounds (diastereoisomers).*

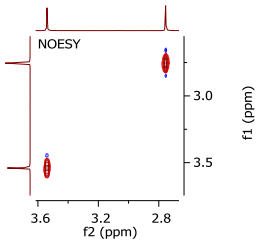

5-(dinaphtho[2,1-d:1',2'-*f*][1,3,2]dioxaphosphepin-4-yl)-3-methyl-5*H*-dibenzo[*b*,*f*]azepine

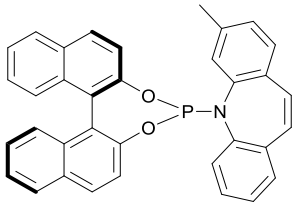

General Procedure H: PCl_3 (0.06 mL, 0.64 mmol, 1.1 eq.), THF (1.4 mL), triethylamine (0.16 mL, 1.16 mmol, 2.0 eq.), THF (0.7 mL), (*R*)-binaphthol (166 mg, 0.58 mmol, 1.0 eq.), THF (0.7 mL), 3-methyl-5*H*-dibenzo[*b*,*f*]azepine (120 mg, 0.58 mmol, 1.0 eq.), THF (1.4 mL), *n*-BuLi (2.5 M in hexane, 0.24 mL, 0.61 mmol, 1.05 eq.).

The crude mixture was treated as described above and was purified by flash column chromatography (Hexane:CH_2Cl_2, 80:20, SiO_2) to afford 5-(dinaphtho[2,1-d:1',2'-*f*][1,3,2] dioxaphosphepin-4-yl)-3-methyl -5*H*- dibenzo [*b*,*f*] azepine (162 mg, 0.31 mmol, 54%) as a foamy white solid.

Mixture of diastereoisomers (1:1)

^{1}H NMR (400 MHz, Chloroform-*d*) δ 8.05 – 7.74 (m, 6H, 6 × Ar-H), 7.70 – 7.56 (m, 3H, 3 × Ar-H), 7.45 – 7.17 (m, 19H, 19 × Ar-H), 7.15 – 6.85 (m, 10H, 10 × Ar-H), 6.79 – 6.66 (m, 3H, 3 × Ar-H), 6.54 – 6.50 (m, 1H, Ar-H), 1.95 (s, 3H, CH_3), 1.27 (s, 3H, CH_3).

^{13}C NMR (126 MHz, Chloroform-*d*) δ 150.32, 150.26, 149.7, 149.6, 148.9, 148.75, 148.73, 143.1, 142.92, 142.90, 142.8, 142.6, 142.5, 142.32, 142.27, 139.4, 139.2, 136.70, 136.67, 136.0, 133.2, 132.92, 132.86, 132.4, 132.2, 132.0, 131.53, 131.51, 131.46, 131.4, 130.4, 130.34, 130.29, 130.2, 129.31, 129.28, 129.2, 129.15, 129.07, 129.0, 128.93, 128.87, 128.8, 128.7, 128.5, 128.34, 128.32, 128.2, 128.1, 128.0, 127.8, 127.3, 127.1, 127.0, 126.9, 126.8, 126.4, 126.12, 126.08, 125.8, 125.7, 124.8, 124.5, 124.4, 124.3, 124.2, 124.12, 124.08, 122.1, 121.82, 121.80, 121.7, 121.0, 120.83, 120.81, 20.5, 19.8.

^{31}P NMR (162 MHz, Chloroform-*d*) δ 139.0, 138.5.

IR υ_{max} (film): 3054, 1590, 1501, 1220, 948.

HRMS (ESI^{+}) *m/z* calcd for C_{35} H_{25} O_2 N P $[M+H]^{+}$: 522.1617, found 522.1616.

$[\boldsymbol{\alpha}]^{25}_{589}$ = -422.7 (*c* 1.0, $CHCl_3$) for 99% ee.

EXSY: *To prove that two diasteroisomers are formed, an EXSY experiment was carried out. Since no chemical-exchange exist between the two signals, they are not interconverting (like rotamers) but are two distinct compounds (diastereoisomers).*

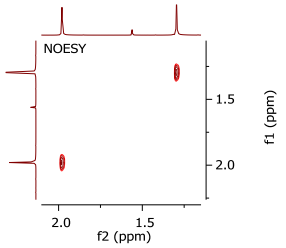

5-((11b*S*)-2,6-diphenyldinaphtho[2,1-*d*:1',2'-*f*][1,3,2]dioxaphosphepin-4-yl)-5*H*-dibenzo[*b*,*f*]azepine

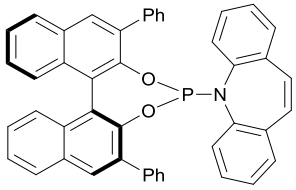

General Procedure H: PCl_3 (0.08 mL, 0.87 mmol, 1.1 eq.), THF (2.0 mL), triethylamine (0.22 mL, 1.58 mmol, 2.0 eq.), THF (1.0 mL), (*S*)-3,3'-diphenyl-[1,1'-binaphthalene]-2,2'-diol (347 mg, 0.79 mmol, 1.0 eq.), THF (1.0 mL), 5*H*-dibenzo[*b*,*f*]azepine (153 mg, 0.79 mmol, 1.0 eq.), THF (2.0 mL), *n*-BuLi (2.5 M in hexane, 0.33 mL, 0.83 mmol, 1.05 eq.).

The crude mixture was treated as described above and was purified by flash column chromatography (Hexane:CH_2Cl_2, 80:20, SiO_2) to afford 5-((11b*S*)-2,6-diphenyl-dinaphtho [2,1-d:1',2'-*f*] [1,3,2]dioxaphosphepin-4-yl) -5*H*- dibenzo[*b*,*f*]-azepine (410 mg, 0.62 mmol, 78%) as a foamy white solid.

^{1}H NMR (400 MHz, Chloroform-*d*) δ 8.13 (s, 1H, Ar-H), 8.06 – 7.86 (m, 5H, 5 × Ar-H), 7.63 – 7.36 (m, 10H, 10 × Ar-H), 7.33 – 7.23 (m, 4H, 4 × Ar-H), 7.08 – 6.97 (m, 3H, 3 × Ar-H), 6.90 – 6.82 (m, 1H, Ar-H), 6.73 – 6.66 (m, 1H, Ar-H), 6.60 (d, *J* = 11.6 Hz, 1H,

Ar-H), 6.46 – 6.36 (m, 2H, 2 × Ar-H), 5.95 (d, *J* = 7.9 Hz, 1H, Ar-H), 5.81 – 5.72 (m, 1H, Ar-H).

^{13}C NMR (126 MHz, Chloroform-*d*) δ 146.7, 142.5, 142.4, 142.2, 138.3, 137.4, 136.2, 135.28, 135.26, 134.5, 132.7, 132.6, 131.3, 130.8, 130.7, 130.4, 130.21, 130.19, 130.1, 129.0, 128.60, 128.56, 128.5, 128.44, 128.41, 128.3, 128.2, 128.1, 128.00, 127.97, 127.9, 127.5, 127.3, 127.0, 126.9, 126.4, 126.09, 126.07, 125.8, 125.2, 125.0, 125.0, 124.2.

^{31}P NMR (162 MHz, Chloroform-*d*) δ 136.0.

IR υ_{max} (film): 3053, 1486, 1455, 1407, 1195, 961.

HRMS (ESI$^+$) *m/z* calcd for $C_{46}H_{31}O_2NP$ $[M+H]^+$: 660.2082, found 660.2087.

$[\alpha]^{25}_{589}$ = +237.2 (*c* 1.0, $CHCl_3$) for 99% ee.

5-((11*cS*)-2-phenyldinaphtho[2,1-*d*:1',2'-*f*][1,3,2]dioxaphosphepin-4-yl)-5*H*-dibenzo[*b,f*]azepine

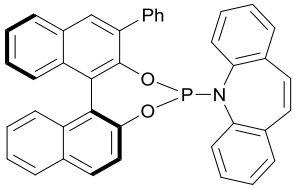

General Procedure H: PCl_3 (0.08 mL, 0.92 mmol, 1.1 eq.), THF (2.0 mL), triethylamine (0.23 mL, 1.68 mmol, 2.0 eq.), THF (1.0 mL), (*S*)-3-phenyl-[1,1'-binaphthalene]-2,2'-diol (304 mg, 0.84 mmol, 1.0 eq.), THF (1.0 mL), 5*H*-dibenzo[*b,f*]azepine (162 mg, 0.84 mmol, 1.0 eq.), THF (2.0 mL), *n*-BuLi (2.5 M in hexane, 0.35 mL, 0.88 mmol, 1.05 eq.).

The crude mixture was treated as described above and was purified by flash column chromatography (Hexane:CH_2Cl_2, 80:20, SiO_2) to afford 5-((11*cS*)-2-

phenyldinaphtho[2,1-*d*:1',2'-*f*][1,3,2]dioxaphosphepin-4-yl)-5*H*-dibenzo[*b*,*f*]azepine (346 mg, 0.59 mmol, 71%) as a foamy white solid.

Mixture of diastereoisomers (1:1)

^{1}H NMR (400 MHz, Chloroform-*d*) δ 8.18 (s, 1H, Ar-H), 8.07 – 8.00 (m, 2H, 2 × Ar-H), 7.98 – 7.75 (m, 8H, 8 × Ar-H), 7.63 – 6.91 (m, 29H, 29 × Ar-H), 6.88 – 6.74 (m, 5H, 5 × Ar-H), 6.71 – 6.62 (m, 2H, 2 × Ar-H), 6.53 – 6.34 (m, 3H, 3 × Ar-H), 5.98 (d, J = 8.0 Hz, 1H, Ar-H), 5.70 (d, J = 8.0 Hz, 1H, Ar-H).

^{13}C NMR (126 MHz, Chloroform-*d*) δ 150.5, 150.5, 149.2, 146.7, 146.6, 146.5, 143.3, 143.1, 142.6, 142.6, 142.5, 142.3, 142.2, 142.1, 138.5, 138.3, 136.5, 136.5, 136.3, 136.3, 135.3, 135.3, 135.1, 135.1, 134.8, 133.1, 132.7, 132.6, 132.4, 131.7, 131.5, 131.5, 131.4, 131.0, 130.8, 130.6, 130.6, 130.4, 130.4, 130.3, 130.2, 129.1, 129.1, 129.0 – 128.8 (m), 128.8, 128.7, 128.5, 128.5, 128.4, 128.2, 128.2, 128.1, 128.1, 127.9, 127.9, 127.7, 127.6, 127.2, 127.1, 127.0, 127.0, 126.7, 126.7, 126.3, 126.2, 126.1, 125.8, 125.8, 125.4, 125.2, 124.9, 124.4, 124.2, 124.2, 122.1, 121.4, 121.2, 121.2.

^{31}P NMR (162 MHz, Chloroform-*d*) δ 137.2, 135.7.

IR υ_{max} (film): 3054, 1486, 1458, 1411, 1205, 956.

HRMS (ESI^{+}) *m/z* calcd for $C_{40}H_{27}O_2NP$ $[M+H]^{+}$: 584.1774, found 584.1772.

$[\alpha]^{25}_{589}$ = +312.7 (*c* 1.0, $CHCl_3$) for 99% ee.

4.7 Zirconocene hydrochloride

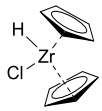

Commercially available Schwartz reagent (or zirconocene hydrochloride) was not examined due to its high per mol price. Moreover, it has previously been reported that more consistent results are obtained when freshly prepared reagent is used.[19] **Our studies also showed that the quality of Schwartz reagent is critical for consistent experimental results.**

Schwartz reagent was prepared according to a literature procedure from Cp_2ZrCl_2.[20] Zirconocene dichloride (30.0 g, 103 mmol, 1.0 eq.) was added to a flame-dry 250 mL Schlenk flask wrapped with aluminium foil under argon. Dry THF (140 mL) was added and the suspension was stirred at 35 °C for 30 min. $LiAlH_4$ (2 M in Et_2O, 28.2 mmol, 0.3 eq.) was added dropwise to the mixture over about 30 min with vigorous (magnetic stirring bar) stirring. The resulting suspension was stirred at 35 °C for 3 hours. The red mixture was then Schlenk-filtered under argon and washed with THF (300 mL in total), CH_2Cl_2 (250 mL in total), and Et_2O (250 mL in total). The precipitate was dried under high vacuum for 2 h to give a white powder (22.6 g, 87.6 mmol, 85%) that was then stored under argon in a small flame-dried aluminium foiled Schlenk flask.

Note: The lithium aluminum hydride ($LiAlH_4$) reduction of zirconocene dichloride (Cp_2ZrCl_2) leads to over-reduction and give zirconocene dihydride (Cp_2ZrH_2). Treatment of Cp_2ZrH_2 with CH_2Cl_2 converts the dihydride back into the Schwartz's reagent.

Material obtained this way has an average purity of >95% (zirconocene dihydride being the impurity). The average % purity of prepared Schwartz reagent was determined through the following procedure: a known amount of Schwartz reagent was mixed with a known amount of excess acetone, and then diluted in an NMR tube in C_6D_6. The relative areas of the signal for the mono and diisopropoxides were determined by ^1H NMR corresponding to Cp_2ZrHCl and Cp_2ZrH_2, respectively.

The Schwartz reagent can be kept and remain pure for months under these storage conditions if flushed (3 × vacuum/argon) after each use.

4.8 Zirconocene chlorotriflate

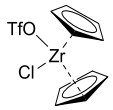

Zirconocene chlorotriflate was prepared according to a modified procedure from a patent.[21] Zirconocene dichloride (500 mg, 1.71 mmol, 1.0 eq.) was added to a flame-dry 500 mL two-neck round-bottom flask (or ideally a Schlenk flask) wrapped with aluminium foil and purged (3 × vacuum/argon). Dry toluene (140 mL) was added and the reaction was stirred until homogeneous (~5 min). A solution of AgOTf (527 mg, 2.05 mmol, 1.2 eq.) in toluene (70 mL) was added dropwise at rt for 30 min using a dropping funnel. The resulting cloudy mixture was further stirred at rt for 1 h, then at 60 °C for 4 h, to finally be Schlenk-filtered under argon to remove the AgCl precipitate. The yellow filtrate was concentrated under reduced pressure. The resulting solid was further dried under high vacuum overnight to afford a pale yellow-ish powder (526 mg, 1.30 mmol, 76%) that was then stored under argon in a small flame-dried aluminium foiled Schlenk flask.

^{1}H NMR (400 MHz, Chloroform-d) δ 6.63 (s, 5H, 5 × Ar-H), 6.52 (s, 5H, 5 × Ar-H).

^{19}F NMR (376 MHz, Chloroform-d) δ -77.5 (CF_3).

MP: 105 °C ± 1 °C.

Analytical data are in agreement with the literature.[21]

4.9 Complexes

CuOTf-L17 complex

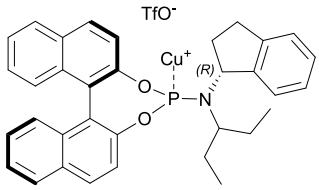

In a flamed dried round bottom flask was added CuCl (6.0 mg, 0.06 mmol, 1.0 eq.) and (*R,R*) ligand **L17** (31.4 mg, 0.06 mmol, 1.0 eq.). The flask was purged (3 × argon/vacuum), covered with aluminium foil to protect it from the light and dry $CDCl_3$ (0.7 mL) was then added under an argon atmosphere. The resulting colourless clear solution was stirred for 1 h at rt. AgOTf (23.4 mg, 0.09 mmol, 0.15 eq.) was then added, and the grey-brown cloudy solution was stirred for precisely 15 min. In the meantime, a NMR tube was fitted with a NMR septum and parafilmed. The tube was purged (3 × argon/vacuum), flamed dried and covered with aluminium foil to protect it from the light, to which the catalyst mixture was finally transferred over about 30 sec via syringe using a syringe filter. The NMR tube was then brought to the NMR instrument, at which point the foil protection was removed just before introduction of the tube.

^{1}H NMR (500 MHz, Chloroform-*d*) δ 8.09 – 7.96 (m, 3H, 3 × Ar-H), 7.88 (d, *J* = 8.2 Hz, 1H, Ar-H), 7.67 – 7.50 (m, 4H, 4 × Ar-H), 7.49 – 7.40 (m, 3H, 3 × Ar-H), 7.39 – 7.21 (m, 5H, 5 × Ar-H), 4.91 – 4.79 (m, 1H, CH), 3.35 (dd, *J* = 16.1, 9.1 Hz, 1H, ½ × CH_2), 2.98 – 2.75 (m, 3H, ½ × CH_2 & CH & ½ × CH_2), 2.55 – 2.40 (m, 1H, ½ × CH_2), 1.98 – 1.77 (m,

2H, CH_2), 1.64 – 1.50 (m, 1H, ½ × CH_2), 1.47 – 1.33 (m, 1H, ½ × CH_2), 0.87 (q, *J* = 8.2, 7.7 Hz, 6H, 2 × CH_3).

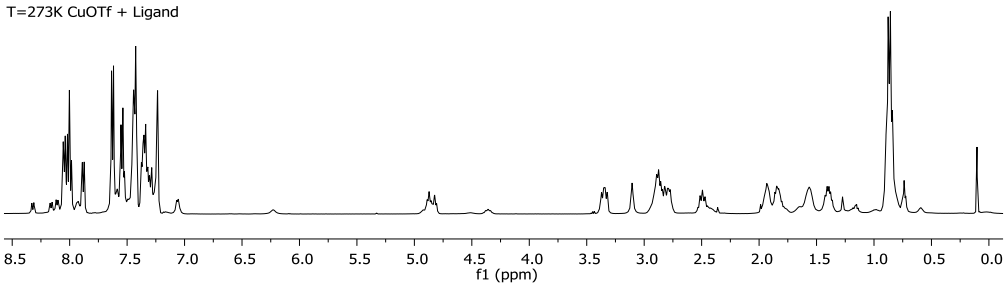

^{19}F NMR (376 MHz, Chloroform-*d*) δ -77.7 (s, CF_3).

^{31}P NMR (202 MHz, Chloroform-*d*) δ 126.0 (d, *J* = 876.2 Hz, ^{109}Ag-P), 126.0 (d, *J* = 758.6 Hz, ^{107}Ag-P), 119.3 (br s, Cu-P).

4.10 Others

(but-3-en-1-yloxy)(*tert*-butyl)dimethylsilane

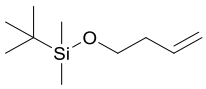

In a flame dried flask was added but-3-en-1-ol (0.3 mL, 3.486 mmol, 1.0 eq.) and imidazole (474.7 mg, 6.973 mmol, 2.0 eq.) in 5 mL CH_2Cl_2, followed by TBSCl (536.0 mg, 3.556 mmol, 1.02 eq.) under an Ar atmosphere with a strong stirring. The reaction was stirred at room temperature for 48 h before water (5 mL) was added. The aqueous layer was extracted with pentanes (2 × 10 mL). The combined organic layers were dried on anhydrous sodium sulfate, filtered and concentrated in vacuum. *(Note: product is volatile. Use an ice bath during removal of solvents if required).* The crude product was passed through a short column of silica gel with pentanes to afford a clear oil (510 mg, 2.719 mmol, 78%).

^{1}H NMR (400 MHz, Chloroform-*d*) δ 5.76 (ddt, *J* = 17.1, 10.2, 6.8 Hz, 1H, C=CH), 5.07 – 4.92 (m, 2H, C=CH_2), 3.60 (t, *J* = 6.8 Hz, 2H, CH_2), 2.22 (qt, *J* = 6.8, 1.3 Hz, 2H, CH_2), 0.84 (s, 9H, 3 × CH_3), 0.00 (s, 6H, 2 × CH_3).

^{13}C NMR (101 MHz, Chloroform-*d*) δ 135.4, 116.3, 62.8, 37.5, 25.9 (3 C), 18.4, -5.2 (2 C).

Analytical data are in agreement with the literature.[22]

3,7-diethylnonan-5-one

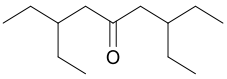

Turning Mg (352 mg, 14.479 mmol, 1.45 eq.) was added into a flask and flame dried. THF (15 mL) was charged into the flask to immerse magnesium and small amount of I_2 (one granule) was added to activate it. The solution turned brown, and then became colourless again after a while. A solution of 3-(bromomethyl)pentane (1.68 mL, 11.982 mmol, 1.2 eq.) dissolved in THF (15 mL) was added and the mixture was heated at reflux for at least 3 h. Meanwhile, 3-ethylpentanoic acid (1300 mg, 9.985 mmol, 1.0 eq.) was diluted in CH_2Cl_2 (2 mL) and oxalyl chloride (0.84 mL, 9.985 mmol, 1.0 eq.) was added dropwise at rt. The reaction was stirred for 2 h and monitored. After cooling down to room temperature and then to 0 °C, the Grignard reagent solution was added dropwise to a solution of CuI (2282 mg, 11.982 mmol, 1.2 eq.) in THF (10 mL) at 0 °C. The mixture was stirred for 30 min then cooled down to -78 °C. Freshly prepared acyl chloride was added dropwise. The reaction was then stirred for at least 2 h. Upon completion, the reaction was quenched with aq. HCl (1M, 10 mL). After stirring for 30 min, the organic and aqueous layers were partitioned and the aqueous phase was extracted with CH_2Cl_2 (3 × 10 mL). The combined organic phases were dried over $MgSO_4$, filtered and

concentrated under reduced pressure. After column chromatography (Hexane, SiO_2), 3,7-diethylnonan-5-one was obtained as a pale yellow oil (402 mg, 1.997 mmol, 20%).

^{1}H NMR (400 MHz, Chloroform-*d*) δ 2.23 (d, *J* = 6.7 Hz, 4H, 2 × CH_2), 1.74 (hept, *J* = 6.4 Hz, 2H, 2 × CH), 1.33 – 1.11 (m, 8H, 4 × CH_2), 0.78 (t, *J* = 7.5 Hz, 12H, 4 × CH_3).

^{13}C NMR (101 MHz, Chloroform-*d*) δ 211.6, 47.5 (2 C), 36.5 (2 C), 25.8 (4 C), 10.8 (4 C).

IR υ_{max} (film): 2962, 2931, 1712, 1460, 1380, 1152, 1056.

HRMS (EI) *m/z* calcd for $C_{13}H_{27}O$ $[M+H]^+$: 199.2056, found 199.2058.

3-ethylpentanoic acid

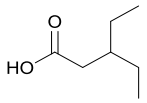

Methyl 3-ethylpentanoate (100 mg, 0.693, 1.0 eq.) was added to a solution of MeOH (10 mL) followed with aq. NaOH 2M (10 mL). The mixture was stirred overnight at rt then quenched with NH_4Cl (aq. sat., *ca* 20 mL). The organic and aqueous layers were partitioned and the aqueous phase was extracted with Et_2O (3 × 10 mL). The combined organic phases were dried over $MgSO_4$, filtered and concentrated under reduced pressure to afford a colorless oil (90 mg, 0.686 mmol, 99%). No further purification was needed.

^{1}H NMR (400 MHz, Chloroform-*d*) δ 11.57 (br s, 1H, CO_2H), 2.21 (d, *J* = 7.0 Hz, 2H, CH_2), 1.68 (p, *J* = 6.6 Hz, 1H, CH), 1.40 – 1.20 (m, 4H, 2 × CH_2), 0.82 (t, *J* = 7.4 Hz, 6H, 2 × CH_3).

^{13}C NMR (101 MHz, Chloroform-*d*) δ 180.4, 38.2, 37.7, 25.8 (2 C), 10.8 (2 C).

IR υ_{max} (film): 2963, 1704, 1460, 1285.

HRMS (EI) *m/z* calcd for $C_7 H_{13} O_2$ $[M+H]^+$: 129.0921, not found.

methyl 3-ethylpentanoate

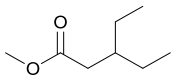

According to a modified procedure reported by Sanford et al.,[23] ethyl magnesium bromide (3 M in Et_2O, 0.73 mL, 2.19 mmol, 2.5 eq.) was added to a stirring solution of $CuBr{\cdot}SMe_2$ (18 mg, 0.09 mmol, 0.1 eq.) in dry TBME (1.5 mL) at -78 °C. Methyl (*E*)-pent-2-enoate (100 mg, 0.87 mmol, 1.0 eq.) was then added dropwise and stirred for 4 h at -78 °C. NH_4Cl (aq. sat., *ca* 10 mL) was poured into the reaction mixture to quench it and stirred 30 min. The organic and aqueous layers were partitioned and the aqueous phase was extracted with Et_2O (3 × 10 mL). The combined organic phases were dried over $MgSO_4$, filtered and concentrated under reduced pressure to afford the desired product (125 mg, 0.87 mmol, 99%) as a colorless oil. No further purification was needed.

^{1}H NMR (500 MHz, Chloroform-d) δ 3.69 (s, 3H, CH_3), 2.26 (d, *J* = 7.0 Hz, 2H, CH_2), 1.83 – 1.69 (m, 1H, CH), 1.45 – 1.24 (m, 4H, 2 × CH_2), 0.89 (t, *J* = 7.5 Hz, 6H, 2 × CH_3).

^{13}C NMR (126 MHz, Chloroform-d) δ 174.2, 51.4, 38.3, 37.9, 25.8 (2 C), 10.8 (2 C).

IR υ_{max} (film): 2980, 2916, 1736, 1382, 1251, 1152, 1072, 954.

HRMS (GCMS Methane Cl) *m/z* calcd for $C_8 H_{17} O_2$ $[M+H]^+$: 145.1223, found 145.1227.

1,7-diphenylheptan-4-one

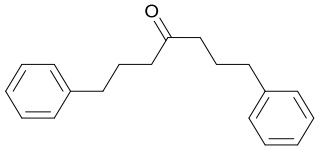

Turning Mg (21.1 mg, 0.868 mmol, 1.8 eq.) was added into a flask and flame dried. THF (5 mL) was charged into the flask to immerse magnesium and small amount of I_2 (one granule) was added to activate it. The solution turned brown, and then became colourless again after a while. A solution of (3-bromopropyl)benzene (0.11 mL, 0.724 mmol, 1.5 eq.) dissolved in THF (3 mL) was added and the mixture was heated at reflux for at least 3 h. After cooling down at rt then -78 °C, the Grignard reagent solution was added dropwise to a solution of *N*-methoxy-*N*-methyl-4-phenylbutanamide (100 mg, 0.482 mmol, 1.0 eq.) in THF (10 mL) at -78 °C. The mixture was stirred for 6 h and finally quenched with aq. NaOH 2 M (10 mL). After 30 min, the organic and aqueous layers were partitioned and the aqueous phase was extracted with CH_2Cl_2 (3 × 10 mL). The combined organic phases were dried over $MgSO_4$, filtered and concentrated under reduced pressure. After column chromatography (Hexane, SiO_2), 1,7-diphenylheptan-4-one was obtained as a pale yellow oil (63 mg mg, 0.236 mmol, 49%).

^{1}H NMR (500 MHz, Chloroform-*d*) δ 7.30 (dd, *J* = 8.2, 6.8 Hz, 4H, 4 × Ar-H), 7.24 – 7.10 (m, 6H, 6 × Ar-H), 2.63 (t, *J* = 7.6 Hz, 4H, 2 × CH_2), 2.41 (t, *J* = 7.4 Hz, 4H, 2 × CH_2), 1.92 (p, *J* = 7.5 Hz, 4H, 2 × CH_2).

^{13}C NMR (126 MHz, Chloroform-*d*) δ 210.7, 141.6 (2 C), 128.5 (4 C), 128.4 (4 C), 125.9 (2 C), 42.0 (2 C), 35.1 (2 C), 25.2 (2 C).

IR υ_{max} (film): 3026, 1712, 1453, 1372, 1154.

HRMS (GCMS Methane Cl) *m/z* calcd for C_{19} H_{23} O $[M+H]^+$: 267.1743, found 267.1743.

Analytical data are in agreement with the literature.[24]

cyclohex-1-en-1-ylmethanol

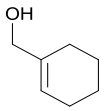

In a flame dried round bottom flask was added methyl cyclohex-1-ene-1-carboxylate (0.30 mL, 2.20 mmol, 1.0 eq.) in anhydrous CH_2Cl_2 (20 mL) at -78 °C followed by the addition of DIBAL-H, 1M in CH_2Cl_2 (6.60 mL, 6.60 mmol, 3.0 eq.) dropwise. The reaction was stirred for 2 h at -78 °C. After completion, the reaction was quenched with MeOH (0.5 mL) at -78 °C, then water (0.5 mL). The mixture was allowed to slowly warm up at rt, filtered through a pad of Celite, and concentrated under reduced pressure. Cyclohex-1-en-1-ylmethanol (242 mg, 2.16 mmol, 98%) was obtained without further purification as a colorless oil.

^{1}H NMR (400 MHz, Chloroform-d) δ 5.64 – 5.59 (m, 1H, C=CH), 3.91 (s, 2H, CH_2), 1.95 (ddd, *J* = 7.4, 5.9, 3.9 Hz, 4H, 2 × CH_2), 1.64 – 1.46 (m, 4H, 2 × CH_2), 1.23 (br s, 1H, OH).

^{13}C NMR (101 MHz, Chloroform-d) δ 137.6, 123.0, 67.7, 25.6, 24.9, 22.5, 22.4.

IR υ_{max} (film): 3319, 2925, 1437, 1007.

HRMS (EI^+) *m/z* calcd for C_7 H_{12} O $[M+H]^+$: 112.0888, not found.

cyclohex-1-ene-1-carbaldehyde

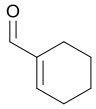

According to a modified procedure,[25] MnO_2 (5.53 g, 63.6 mmol, 20 eq.) was added to a solution of cyclohex-1-en-1-ylmethanol (357 mg, 3.18 mmol, 1.0 eq.) in CH_2Cl_2 (17.5 mL) at rt and stirred overnight. The reaction mixture was filtered using a pad of SiO_2, rinsed with CH_2Cl_2, and the filtrate solution was concentrated under reduced pressure at 20 °C. *Note: Decomposition was observed with a bath at 40 °C*. Cyclohex-1-ene-1-carbaldehyde (70 mg, 0.64 mmol, 20%) was obtained without further purification as a pale yellow oil.

^{1}H NMR (400 MHz, Chloroform-d) δ 9.34 (s, 1H, O=CH), 6.73 (tt, *J* = 3.7, 1.9 Hz, 1H, C=CH), 2.27 (qd, *J* = 4.6, 3.7, 2.2 Hz, 2H, CH_2), 2.13 (ddq, *J* = 5.9, 3.7, 1.9 Hz, 2H, CH_2), 1.61 (tt, *J* = 8.9, 4.6 Hz, 4H, 2 × CH_2).

^{13}C NMR (101 MHz, Chloroform-d) δ 194.4, 151.5, 141.6, 26.5, 22.0, 21.32, 21.27.

IR υ_{max} (film): 2852, 1687, 1260.

HRMS (ESI$^+$) *m/z* calcd for $C_7H_{11}O$ $[M+H]^+$: 111.0804, found 111.0805.

***S*-ethyl cyclohex-1-ene-1-carbothioate**

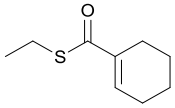

According to a modified procedure,[26] Me_3SiSEt (0.71 mL, 4.40 mmol, 2.0 eq.) was added to a solution of methyl cyclohex-1-ene-1-carboxylate (0.30 mL, 2.20 mmol, 1.0 eq.) in THF (5 mL), followed by the portionwise addition of $AlCl_3$ (352 mg, 2.64 mmol, 1.2 eq.). The resulting mixture was stirred at reflux for 3 h and then quenched at rt by addition of aqueous phosphate buffer solution (pH 7). The

reaction mixture was partitioned between the aqueous and organic phases, and the aqueous layer was extracted with Et_2O (3 × 10 mL). The combined organic phases were dried over $MgSO_4$, filtered and concentrated under reduced pressure. After column chromatography (Hexane:EtOAc, 97:3, SiO_2), *S*-ethyl cyclohex-1-ene-1-carbothioate (373 mg, 2.18 mmol, 99%) was obtained as a pale yellow oil.

^{1}H NMR (500 MHz, Chloroform-*d*) δ 6.99 (tt, *J* = 3.9, 1.7 Hz, 1H, C=CH), 2.93 (q, *J* = 7.4 Hz, 2H, CH_2), 2.33 (tq, *J* = 5.9, 2.1 Hz, 2H, CH_2), 2.24 (tdd, *J* = 5.9, 3.9, 2.7 Hz, 2H, CH_2), 1.73 – 1.60 (m, 4H, 2 × CH_2), 1.29 (t, *J* = 7.4 Hz, 3H, CH_3).

^{13}C NMR (126 MHz, Chloroform-*d*) δ 193.1, 138.5, 138.0, 25.8, 24.0, 22.9, 22.0, 21.6, 14.9.

IR υ_{max} (film): 2930, 1657, 1449, 1165.

HRMS (ESI$^+$) *m/z* calcd for $C_9H_{15}OS$ $[M+H]^+$: 171.0838, found 171.0840.

cyclohex-1-ene-1-carboxylic acid

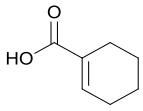

According to a modified procedure,[14] methyl cyclohex-1-ene-1-carboxylate (0.30 mL, 2.20 mmol, 1.0 eq.), MeOH (4 mL) and NaOH, 2M in water (2.20 mL, 4.40 mmol, 2.0 eq.) were added in a flask and stirred for 48 h at rt. After full conversion, the reaction mixture was quenched with HCl (1M) up to pH 1. The biphasic mixture was concentrated under reduced pressure to remove MeOH, diluted in Et_2O (5 mL) and the aqueous phase was extracted with Et_2O (3 × 10 mL). The combined organic phases were dried over $MgSO_4$, filtered and concentrated under reduced pressure. Cyclohex-1-ene-1-carboxylic acid (247 mg, 1.98 mmol, 90%) was obtained without further purification as a pale yellow oil.

^{1}H NMR (400 MHz, Chloroform-*d*) δ 11.93 (s, 1H, CO_2H), 7.07 (dq, *J* = 3.9, 1.9 Hz, 1H, C=CH), 2.24 – 2.11 (m, 4H, 2 × CH_2), 1.65 – 1.49 (m, 4H, 2 × CH_2).

^{13}C NMR (101 MHz, Chloroform-*d*) δ 173.1, 142.5, 129.7, 26.0, 23.7, 22.0, 21.3.

IR υ_{max} (film): 2934, 1682, 1423, 1306.

HRMS (ESI^+) *m/z* calcd for $C_7 H_9 O_2$ $[M+H]^+$: 125.0608, found 125.0607.

N-methoxy-*N*-methylcyclohex-1-ene-1-carboxamide

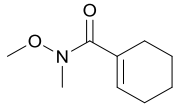

According to a modified procedure,[14] *N*,*O*-Dimethylhydroxylamine hydrochloride (1.72 g, 17.6 mmol, 8.0 eq.) was dissolved in CH_2Cl_2 (50 mL) and the reaction was cooled down to 0 °C. Dimethylaluminum chloride, 1M in hexane (17.6 mL, 17.6 mmol, 8.0 eq.) was then added dropwise and the reaction was stirred for 1 h and allowed to slowly warm up to rt with the ice bath. Methyl cyclohex-1-ene-1-carboxylate (0.30 mL, 2.20 mmol, 1.0 eq.) in CH_2Cl_2 (50 mL) was added and the reaction was further stirred at rt for 48 h. The resulting cloudy solution was quenched with water (50 mL). The organic and aqueous layers were partitioned and the aqueous phase was extracted with Et_2O (3 × 30 mL). The combined organic phases were dried over $MgSO_4$, filtered and concentrated under reduced pressure. After column chromatography (Hexane:EtOAc, 95:5, SiO_2), *N*-methoxy-*N*-methylcyclohex-1-ene-1-carboxamide (332 mg, 1.96 mmol, 89%) was obtained as a pale yellow oil.

^{1}H NMR (400 MHz, Chloroform-*d*) δ 6.10 (tt, *J* = 3.8, 1.8 Hz, 1H, C=CH), 3.58 (s, 3H, CH_3), 3.16 (s, 3H, CH_3), 2.25 – 2.15 (m, 2H, CH_2), 2.12 – 2.02 (m, 2H, CH_2), 1.67 – 1.51 (m, 4H, 2 × CH_2).

^{13}C NMR (101 MHz, Chloroform-*d*) δ 172.0, 133.9, 131.1, 61.0, 33.8, 25.6, 25.0, 22.2, 21.7.

IR υ_{max} (film): 2931, 2858, 1631, 1437, 1377, 989.

HRMS (ESI^+) *m/z* calcd for $C_9 H_{16} O_2 N$ $[M+H]^+$: 170.1176, found 170.1175.

ethene-1,1-diyldibenzene

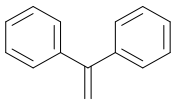

The product was synthesized following a previously published procedure and analytical data are in agreement with the literature.[27]

^{1}H NMR (400 MHz, Chloroform-*d*) δ 7.40 – 7.32 (m, 10H, 10 × Ar-H), 5.49 (s, 2H, $C=CH_2$).

^{13}C NMR (101 MHz, Chloroform-*d*) δ 150.1, 141.5, 128.3 (2 C), 128.2 (2 C), 127.7, 114.3.

1-(2,2-dibromovinyl)-2-nitrobenzene

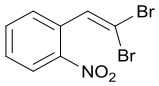

According to a modified procedure,[28] 2-nitrobenzaldehyde (100 mg, 0.66 mmol, 1.0 eq.) and CBr_4 (230 mg, 0.69 mmol, 1.05 eq.) were dissolved in CH_2Cl_2 (3.5 mL) and cooled at 0 °C. Triphenylphosphine (366 mg, 1.39 mmol, 2.1 eq.) was then added portionwise (3 × 122 mg). The reaction mixture was further stirred at 0 °C for 1 h until completion. Hexane (*ca* 5 mL) was added to precipitate the triphenylphosphine oxide. The resulting mixture was filtered through a pad of silica, rinsed with 10:90 EtOAc:Hexane and concentrated under reduced pressure to afford 1-(2,2-

dibromovinyl)-2-nitrobenzene (81 mg, 0.26 mmol, 40%) as a brownish solid without further purification.

^{1}H NMR (400 MHz, Chloroform-*d*) δ 8.13 (dd, *J* = 8.2, 1.3 Hz, 1H, Ar-H), 7.78 (s, 1H, C=CH), 7.72 – 7.49 (m, 3H, 3 × Ar-H).

^{13}C NMR (101 MHz, Chloroform-*d*) δ 146.8, 134.0, 133.5, 131.7, 131.4, 129.4, 124.8, 93.2.

Analytical data are in agreement with the literature.[29]

(2-(2-nitrophenyl)ethene-1,1-diyl)dibenzene

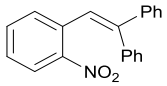

According to a modified procedure,[30] $PhB(OH)_2$ (36 mg, 0.30 mmol, 2.3 eq.), $Pd(OAc)_2$ (2.9 mg, 0.013 mmol, 10 mol %) and XPhos (6.2 mg, 0.013 mmol, 10 mol %) were dissolved in acetonitrile (0.3 mL). 1-(2,2-dibromovinyl)-2-nitrobenzene (40 mg, 0.13 mmol, 1.0 eq.) and a solution of K_3PO_4 (2 M, 0.2 mL, 0.39 mmol, 3.0 eq.) were finally added and the reaction was stirred at 40 °C until completion. The reaction was diluted with water (*ca* 5 mL) then the organic and aqueous layers were partitioned and the aqueous phase was extracted with EtOAc (3 × 10 mL). The combined organic phases were dried over $MgSO_4$, filtered and concentrated under reduced pressure. After column chromatography (Hexane:EtOAc, 99:1, SiO_2), (2-(2-nitrophenyl)ethene-1,1-diyl)dibenzene (15 mg, 0.05 mmol, 38%) was obtained as a yellow solid.

^{1}H NMR (400 MHz, Chloroform-d) δ 7.90 – 7.84 (m, 1H, Ar-H), 7.30 – 7.23 (m, 5H, 5 × Ar-H), 7.21 – 7.10 (m, 6H, C=CH & 5 × Ar-H), 7.05 – 6.99 (m, 2H, 2 × Ar-H), 6.96 – 6.90 (m, 1H, Ar-H).

^{13}C NMR (101 MHz, Chloroform-d) δ 149.1, 145.7, 142.4, 139.4, 133.9, 132.8, 132.5, 130.9 (2 C), 128.4 (4 C), 128.3 (3 C), 127.8, 127.5, 124.4, 123.9.

Analytical data are in agreement with the literature.[31]

2-(2,2-diphenylvinyl)aniline

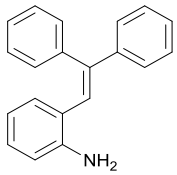

(2-(2-nitrophenyl)ethene-1,1-diyl)dibenzene (644 mg, 2.14 mmol, 1.0 eq.) and iron powder (716 mg, 12.83 mmol, 6.0 eq.) were dissolved in acetic acid (11.0 mL) and stirred at 85 °C until completion. The reaction was filtered through a pad of celite, rinsed with EtOAc (*ca* 40 mL), and basified with the slow addition of a saturated solution of $NaHCO_3$. The organic and aqueous layers were partitioned and the aqueous phase was extracted with EtOAc (3 × 20 mL). The combined organic phases were dried over $MgSO_4$, filtered and concentrated under reduced pressure. After column chromatography (Hexane:EtOAc, 95:5, SiO_2), 2-(2,2-diphenylvinyl)aniline (241 mg, 0.88 mmol, 41%) was obtained as an pale yellow oil.

^{1}H NMR (400 MHz, Chloroform-*d*) δ 7.39 – 7.30 (m, 5H, 5 × Ar-H), 7.28 – 7.21 (m, 3H, 3 × Ar-H), 7.19 – 7.15 (m, 2H, 2 × Ar-H), 7.01 – 6.95 (m, 1H, Ar-H), 6.83 – 6.81 (m, 1H, C=CH), 6.77 (ddt, *J* = 7.7, 1.3, 0.6 Hz, 1H, Ar-H), 6.65 (dd, *J* = 8.1, 1.2 Hz, 1H, Ar-H), 6.53 – 6.47 (m, 1H, Ar-H), 3.74 (br s, 2H, NH_2).

^{13}C NMR (101 MHz, Chloroform-*d*) δ 144.6, 144.1, 143.4, 140.0, 130.5 (2 C), 130.4, 128.2 (4 C), 128.1 (2 C), 128.0, 127.6, 127.4, 124.4, 123.6, 118.2, 115.4.

IR υ_{max} (film): 3465, 3376, 3055, 3023, 2917, 1618, 1492, 1454, 1444, 1311, 1275.

HRMS (ESI$^+$) *m/z* calcd for $C_{20}H_{18}N$ $[M+H]^+$: 272.1434, found 272.1432.

Analytical data are in agreement with the literature.[32]

(*S*)-2,2'-bis(methoxymethoxy)-1,1'-binaphthalene

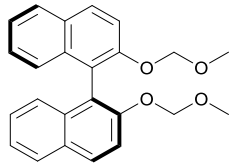

NaH (60% in mineral oil, 2.8 g, 69.4 mmol, 4.0 eq.) was dissolved in THF (50 mL) and stirred at 0 °C for 10 min. *(S)*-binaphthol (5.0 g, 17.3 mmol, 1.0 eq.) in THF (30 mL) was then added dropwise at 0 °C. The reaction was stirred for 1 h at 0 °C before the dropwise addition of chloromethyl methyl ether (2.8 mL, 36.4 mmol, 2.1 eq.). The resulting mixture was further stirred overnight at rt. The reaction was diluted in Et_2O (130 mL) and the organic layer was washed with water (2 × 40 mL), dried over $MgSO_4$, filtered and concentrated under reduced pressure. After column chromatography (Hexane:EtOAc, 80:20, SiO_2), (*S*)-2,2'-bis(methoxymethoxy)-1,1'-binaphthalene (6.2 g, 16.5 mmol, 95%) was obtained as a white solid.

^{1}H NMR (400 MHz, Chloroform-d) δ 7.80 – 7.76 (m, 2H, 2 × Ar-H), 7.72 – 7.67 (m, 2H, 2 × Ar-H), 7.41 (d, *J* = 9.0 Hz, 2H, 2 × Ar-H), 7.21 – 7.12 (m, 2H, 2 × Ar-H), 7.08 – 6.97 (m, 4H, 4 × Ar-H), 4.91 (d, *J* = 6.8 Hz, 2H, 2 × ½ × CH_2), 4.80 (d, *J* = 6.8 Hz, 2H, 2 × ½ × CH_2), 2.97 (s, 6H, 2 × CH_3).

^{13}C NMR (101 MHz, Chloroform-d) δ 152.7 (2 C), 134.0 (2 C), 129.9 (2 C), 129.4 (2 C), 127.9 (2 C), 126.3 (2 C), 125.6 (2 C), 124.1 (2 C), 121.3 (2 C), 117.3 (2 C), 95.3 (2 C), 55.8 (2 C).

Analytical data are in agreement with the literature.[33]

(*S*)-3,3'-dibromo-2,2'-bis(methoxymethoxy)-1,1'-binaphthalene

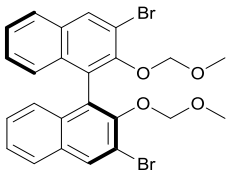

(*S*)-2,2'-bis(methoxymethoxy)-1,1'-binaphthalene (6.2 g, 16.6 mmol, 1.0 eq.) was dissolved in THF (80 mL) and the reaction was cooled at -78 °C before the dropwise addition of *n*-BuLi (2.5 M in hexane, 15.9 mL, 39.7 mmol, 2.4 eq.). The pale yellow solution turned brown. The reaction was then allowed to warm up at 0 °C and stirred for 1 h. Bromine (2.6 mL, 49.7 mmol, 3.0 eq.) in pentane (20 mL) was added dropwise at -78 °C over 20 min and the reaction was further stirred overnight at rt. After completion, the reaction was poured in a saturated solution of Na_2SO_3 (150 mL). The organic and aqueous layers were partitioned and the aqueous phase was extracted with EtOAc (3 × 40 mL). The combined organic phases were dried over $MgSO_4$, filtered and concentrated under reduced pressure. After column chromatography (Hexane:EtOAc, 90:10, SiO_2), (*S*)-3,3'-dibromo-2,2'-bis(methoxymethoxy)-1,1'-binaphthalene (4.1 g, 7.6 mmol, 46%) was obtained as a yellow soft solid.

^{1}H NMR (400 MHz, Chloroform-*d*) δ 8.31 (s, 2H, 2 × Ar-H), 7.86 – 7.80 (m, 2H, 2 × Ar-H), 7.50 – 7.44 (m, 2H, 2 × Ar-H), 7.36 – 7.20 (m, 4H, 4 × Ar-H), 4.87 (d, *J* = 5.8 Hz, 2H, 2 × ½ × CH_2), 4.86 (d, *J* = 5.8 Hz, 2H, 2 × ½ × CH_2), 2.61 (s, 6H, 2 × CH_3).

^{13}C NMR (101 MHz, Chloroform-*d*) δ 150.2 (2 C), 133.1 (2 C), 133.0 (2 C), 131.5 (2 C), 127.4 (2 C), 126.9 (4 C), 126.6 (2 C), 126.1 (2 C), 117.4 (2 C), 99.2 (2 C), 56.3 (2 C).

Analytical data are in agreement with the literature.[33]

(*S*)-3-bromo-2,2'-bis(methoxymethoxy)-1,1'-binaphthalene

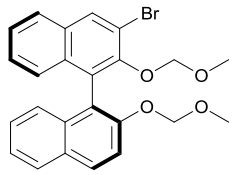

The desired product was obtained as a side-product from the synthesis of (*S*)-3,3'-dibromo-2,2'-bis(methoxymethoxy)-1,1'-binaphthalene. After column chromatography (Hexane:EtOAc, 90:10, SiO_2), (*S*)-3-bromo-2,2'-bis(methoxymethoxy)-1,1'-binaphthalene (2.3 g, 5.1 mmol, 31%) was obtained as a yellow soft solid.

^{1}H NMR (400 MHz, Chloroform-*d*) δ 8.26 – 8.24 (m, 1H, Ar-H), 7.99 – 7.95 (m, 1H, Ar-H), 7.89 – 7.79 (m, 2H, 2 × Ar-H), 7.59 (d, *J* = 9.1 Hz, 1H, Ar-H), 7.44 – 7.34 (m, 2H, 2 × Ar-H), 7.31 – 7.14 (m, 4H, 2 × Ar-H), 5.15 (d, *J* = 6.9 Hz, 1H, ½ × CH_2), 5.04 (d, *J* = 6.9 Hz, 1H, ½ × CH_2), 4.78 (d, *J* = 5.4 Hz, 1H, ½ × CH_2), 4.74 (d, *J* = 5.4 Hz, 1H, ½ × CH_2), 3.19 (s, 3H, CH_3), 2.70 (s, 3H, CH_3).

^{13}C NMR (101 MHz, Chloroform-*d*) δ 152.9, 149.6, 133.9, 133.1, 132.4, 131.7, 130.1, 129.6, 127.8 (2 C), 127.0, 126.8, 126.5, 126.2, 125.8, 125.5, 124.2, 120.0, 117.7, 116.3, 99.0, 94.9, 56.6, 56.0.

Analytical data are in agreement with the literature.[34]

(*S*)-3,3'-diphenyl-[1,1'-binaphthalene]-2,2'-diol

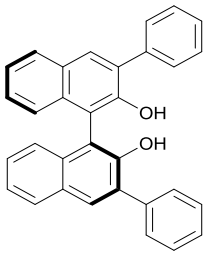

According to a modified procedure,[30] (*S*)-3,3'-dibromo-2,2'-bis(methoxymethoxy)-1,1'-binaphthalene (787 mg, 1.48 mmol, 1.0 eq.), $PhB(OH)_2$ (901 mg, 4.44 mmol, 3.0 eq.), $Pd(OAc)_2$ (16.6 mg, 0.074 mmol, 5 mol %), PPh_3 (42.7 mg, 0.163 mmol,

11 mol %) and K_3PO_4 (942 mg, 4.44 mmol, 3.0 eq.) were dissolved in degassed THF (15 mL). The reaction was stirred at reflux overnight until completion and was then poured in a saturated solution of NH_4Cl (*ca* 10 mL). The organic and aqueous layers were partitioned and the aqueous phase was extracted with Et_2O (3 × 20 mL). The combined organic phases were dried over $MgSO_4$, filtered and concentrated under reduced pressure. The crude was then diluted in 1,4-dioxane (8 mL) and a solution of HCl (4 M in 1,4-dioxane, 3.0 mL, 11.8 mmol, 8.0 eq.) was added. The reaction was then stirred at 50 °C overnight until completion and the resulting mixture was concentrated under reduced pressure. After column chromatography (Hexane:EtOAc, 90:10, SiO_2), (*S*)-3,3'-diphenyl-[1,1'-binaphthalene]-2,2'-diol (344 mg, 0.78 mmol, 53%) was obtained as a white solid.

^{1}H NMR (400 MHz, Chloroform-*d*) δ 8.17 (s, 2H, 2 × Ar-H), 8.09 – 8.02 (m, 2H, 2 × Ar-H), 7.92 – 7.87 (m, 4H, 4 × Ar-H), 7.67 – 7.35 (m, 12H, 12 × Ar-H), 5.54 (br s, 2H, 2 × OH).

^{13}C NMR (101 MHz, Chloroform-*d*) δ 150.4 (2 C), 137.7 (2 C), 133.2 (2 C), 131.6 (2 C), 130.9 (2 C), 129.8 (4 C), 129.6 (2 C), 128.6 (4 C), 127.9 (2 C), 127.5 (2 C), 124.5 (4 C), 112.7 (2 C).

Analytical data are in agreement with the literature.[35]

(*S*)-3-phenyl-[1,1'-binaphthalene]-2,2'-diol

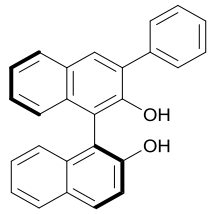

According to a modified procedure,[30] (*S*)-3-bromo-2,2'-bis(methoxymethoxy)-1,1'-binaphthalene (903 mg, 1.99 mmol, 1.0 eq.), $PhB(OH)_2$ (1.21 g, 5.98 mmol, 3.0 eq.), $Pd(OAc)_2$ (22.4 mg, 0.10 mmol, 5 mol %), PPh_3 (57.5 mg, 0.219 mmol, 11 mol %) and K_3PO_4 (1.27 g, 5.98 mmol, 3.0 eq.) were dissolved in degassed THF (20 mL). The reaction was stirred at reflux overnight until completion and was then poured in a saturated solution of NH_4Cl (*ca* 15 mL). The organic and aqueous layers were partitioned and the aqueous phase was extracted with Et_2O (3 × 20 mL). The combined organic phases were dried over $MgSO_4$, filtered and concentrated under reduced pressure. The crude was then diluted in 1,4-dioxane (8 mL) and a solution of HCl (4 M in 1,4-dioxane, 4.0 mL, 15.9 mmol, 8.0 eq.) was added. The reaction was then stirred at 50 °C overnight until completion and the resulting mixture was concentrated under reduced pressure. After column chromatography (Hexane:EtOAc, 90:10, SiO_2), (*S*)-3-phenyl-[1,1'-binaphthalene]-2,2'-diol (309 mg, 0.86 mmol, 43%) was obtained as a white foamy solid.

^{1}H NMR (400 MHz, Chloroform-*d*) δ 8.06 – 7.87 (m, 4H, 4 × Ar-H), 7.76 – 7.71 (m, 2H, 2 × Ar-H), 7.54 – 7.29 (m, 8H, 8 × Ar-H), 7.26 – 7.22 (m, 1H, Ar-H), 7.19 – 7.14 (m, 1H, Ar-H), 5.29 (br s, 1H, OH), 5.11 (br s, 1H, OH).

^{13}C NMR (101 MHz, Chloroform-*d*) δ 152.7, 150.3, 137.4, 133.4, 133.0, 131.5, 131.4, 130.7, 129.6 (2 C), 129.5 (2 C), 128.5 (2 C), 128.46, 128.42, 127.8, 127.4 (2 C), 124.4, 124.3, 124.2, 124.0, 117.8, 111.8, 111.5.

Analytical data are in agreement with the literature.[36]

5 Experimental workflows

5.1 Yield estimation by NMR

When clearly stated, the yield of reactions was estimated using NMR spectroscopy which proved particularly useful during condition optimisation. This section describes the experimental workflow used to compute NMR yields. It is of crucial importance to calibrate at least once an external standard with a NMR signal of the compound of interest as the integration using non-quantitative NMR leads to yield error up to 20% (observed empirically). Errors in NMR yield compared to isolated material are usually due to poor calibration. **According to control experiments, the calibrated NMR yields were always within ±3% error compared to isolated yields.**

Any compound can be used as an external standard as long as it is unreactive, stable and completely soluble. Preferably, the ^{1}H NMR chemical shift of interest should be in a region empty of other signals to avoid overlap that would deteriorate the measurement. A list of external standards commonly used is provided (**Table 6.1**).

Table 6.1. List of external standards commonly used. Chemical shifts (δ) were obtained in Chloroform-*d*.

Compounds	proton	multiplicity	^{1}H NMR δ (ppm)
NO_2Me	CH_3	s	4.33
CH_2Br_2	CH_2	s	4.94
Toluene	CH_3	s	2.36

An example of calibration and NMR yield measurement is provided below for the ACA to exocyclic enone. An identical experimental workflow was used throughout the different projects treated in this work.

5.1.1 Calibration

To a 5 mL round bottom flask was added pure compound **6.1** (36.1 mg, 0.140 mmol) followed by a solution of NO_2Me in $CDCl_3$ (0.7 mL, 7.6 µL/mL, 0.098 mmol). The resulting flask was gently stirred by hand to obtain a homogeneous solution. Using a glass Pasteur pipette, the solution was then transferred into a NMR tube and the ^1H NMR data was acquired (**Figure 6.1**).

*Note: Enough material of compound **6.1** was isolated by combining the crude of ten screening experiments that yielded traces of product. The equivalents are irrelevant as long as a known precise amount of the compound of interest is added. The material quantity (mmol) was arbitrarily decided due to the lack of more material, and corresponds to approximately 25% yield on the screening scale. The stock solution of NO_2Me in $CDCl_3$ was prepared using a 10 mL volumetric flask for accurate concentration.*

Using Mestrenova software for processing, the signals of interest (mostly singlets) were manually peak peaked (**Figure 6.1**). In this example, the external standard NO_2Me (4.23 ppm), diastereoisomer 1 and diastereoisomer 2 of **6.1** (2.03 & 2.02 ppm, respectively) were taken. Interestingly, Mestrenova automatically provides the area under the curve used to calculate the integration (View > Tables > Peaks under "Area"). "Line Fitting Region" can also be used to visualize the signal fitting and this is particularly useful when working with overlapping signals in crude NMR spectra. The tabulated area values can then be copy-pasted in a spreadsheet

(*e.g.* Excel) and used to quickly estimate the amount of product by NMR (called "mmol NMR" in **Figure 6.1**). This value will differ from the actual amount of product added into the NMR tube such that their ratio provides a correction factor, also called a calibration ratio. **The calibration should be repeated at least twice to identify reproducibility issues.**

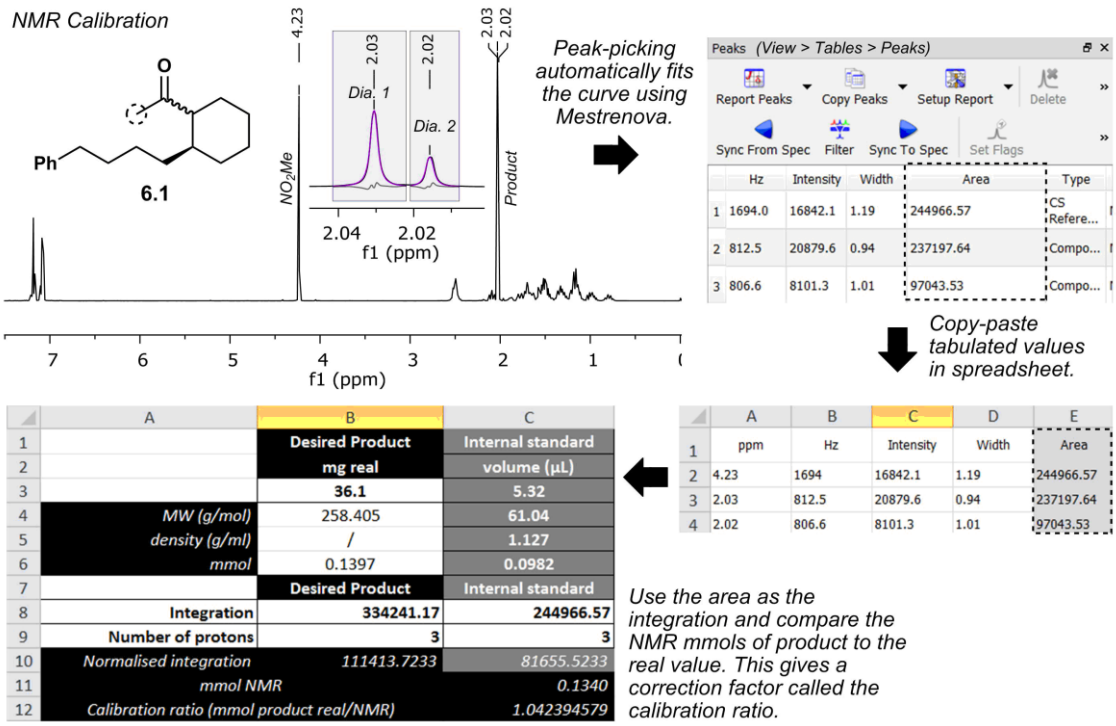

Figure 6.1. Workflow to realise the ^{1}H NMR calibration of the NO_2Me external standard (4.23 ppm) to compound **6.1** diastereoisomers (2.03 & 2.02 ppm).

5.1.2 Measurement

After workup or filtration, the crude mixture was concentrated under reduced pressure in a 5 mL round bottom flask to avoid droplets on the side of the flask. A solution of NO_2Me in $CDCl_3$ (0.7 mL, 7.6 µL/mL, 0.098 mmol) was then added to solubilise the crude mixture and the resulting solution was then gently stirred by hand to obtain a homogeneous solution. Using a glass Pasteur pipette, the solution was finally transferred into a NMR tube and the ^{1}H NMR data was acquired.

Note: The solvent volume must always be identical to the calibration as the concentration affects the acquisition, hence the correction factor. Also, the same NMR machine used for the calibration must be utilized. Overall, the measurement must be realised in identical settings to the calibration.

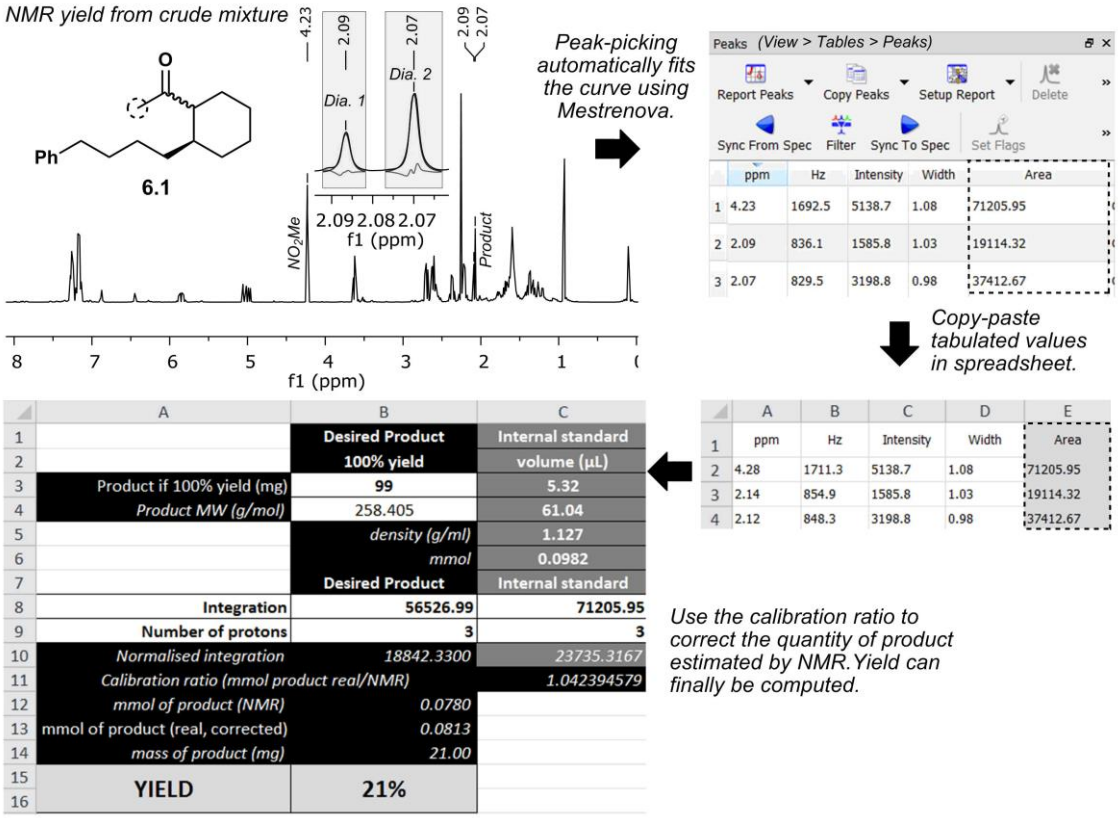

	A	B	C
1		Desired Product	Internal standard
2		100% yield	volume (µL)
3	Product if 100% yield (mg)	99	5.32
4	Product MW (g/mol)	258.405	61.04
5		density (g/ml)	1.127
6		mmol	0.0982
7		Desired Product	Internal standard
8	Integration	56526.99	71205.95
9	Number of protons	3	3
10	Normalised integration	18842.3300	23735.3167
11	Calibration ratio (mmol product real/NMR)		1.042394579
12	mmol of product (NMR)	0.0780	
13	mmol of product (real, corrected)	0.0813	
14	mass of product (mg)	21.00	
15	YIELD	21%	
16			

Figure 6.2. Workflow to compute ^{1}H NMR yield of compound **6.1** diastereoisomers (2.09 & 2.07 ppm) using NO_2Me external standard (4.23 ppm).

The reverse process used during calibration is then utilized (**Figure 6.2**). Using Mestrenova software, the signals of interest were manually peak peaked (external standard NO_2Me, diastereoisomer 1 and diastereoisomer 2 of **6.1**). Mestrenova then automatically provides the area under the curve used to calculate the integration (View > Tables > Peaks under "Area"). "Line Fitting Region" can also be used to visualize and adjust the signal fitting and this is particularly useful when working

with overlapping signals in NMR spectra of crude mixture. The tabulated area values can then be copy-pasted in a spreadsheet (*e.g.* Excel) and used to estimate the amount of product by NMR (called "mmol of product (NMR)" in **Figure 6.2**). Correction of the value with the calibration ratio affords the real amount of product present in the NMR tube, from which the yield can automatically be deduced.

5.2 Yield and *ee* measurement by HPLC

This section describes the workflow used to acquire the conversion and *ee* values by HPLC on a chiral colum. It was utilized during the kinetic studies of the ACAs to acyclic and cyclic enones. Such approach is illustrated here with the acyclic enones.

5.2.1 Calibration

Using HPLC or SFC instruments, conditions that separate the product enantiomers **6.2b**, the starting material **6.2a** and an external standard **6.3** were identified (**Figure 6.3**).

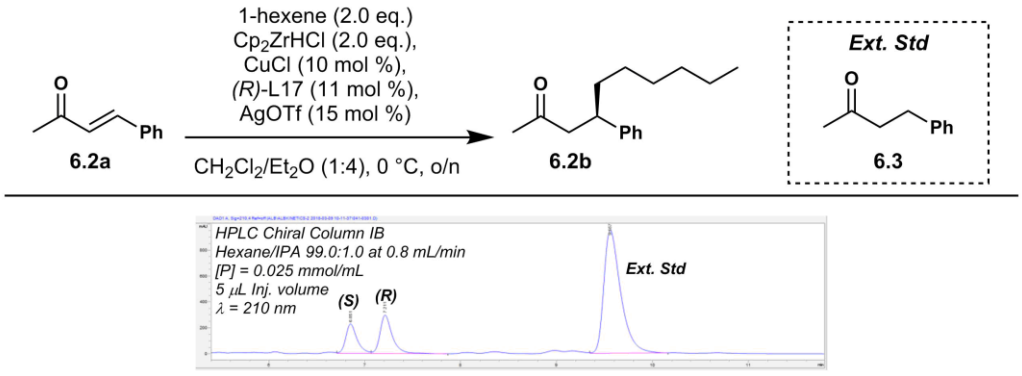

Figure 6.3. ACAs to acyclic enone **6.2a** affording product **6.2b** with the external standard **6.3** used to follow reaction conversion and *ee* over time by HPLC on a chiral column.

The external standard was chosen based on its retention time, optimal absorption wavelength and solubility (here, in hexane). A list of external standards is provided in **Table 6.2**. In our case, we chose compound **6.3** to be our external standard using HPLC instrument due to better separation. At this stage, it is crucial to analyse a crude reaction mixture in order to confirm that there is no overlap with impurities under the optimum separation conditions and that *ee's* of the crude mixture and isolated material are identical. Otherwise, *ee* and yield measurements might be incorrectly estimated due to the presence of impurities.

At the screening reaction scale, quantitative formation of the product (94 mg, 0.404 mmol) in a total volume of 2.8 mL represented a concentration of 0.15 mmol/mL in the flask. Taking an aliquot with the tip of a 1 mL syringe (87 ± 3 μL) diluted in hexane (1 mL) gave a concentration of 12 μmol/mL in the analytical vial when the yield was quantitative. *Note: Microsyringes are prohibited due to the presence of precipitates in the reaction mixture.* Ideally, we want the same concentration of external standard in the analytical samples, representing a stock solution of the external standard **6.3** in hexane at 1.85 mg/mL. The volume injection was then adjusted to ensure that the peak heights in corresponding analytical samples did not exceed 1.0 AU (saturation of the UV probe is observed above 1.5 AU). Absorption at 0.5 AU is advised to allow higher injection volumes at low yield (*i.e.* <10% yield).

Table 6.2. Commonly used external standards

Structures	Names	λ_{max} (nm)
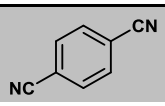	1,4-Dicyanobenzene	235
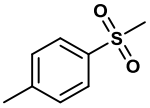	Methyl *p*tolylsulphone (for aqueous systems)	225
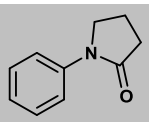	*N*-Phenyl pyrrolidinone	245
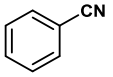	Benzonitrile	215
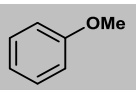	Anisole	225
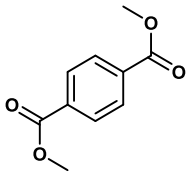	Dimethyl terephthalate	245
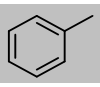	Toluene	210
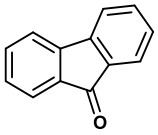	9-Fluorenone	257
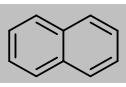	Naphtalene	220
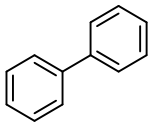	Biphenyl	250
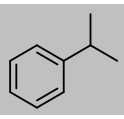	Cumene	210
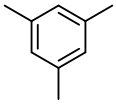	Mesitylene	220
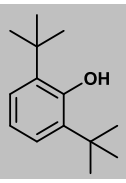	BHT	205
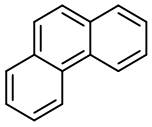	Phenanthrene	210, 257

If the absorption coefficient of the product and the external standard were too dissimilar (*i.e.* 0.4 and 0.8 AU respectively as shown in **Figure 6.3**), then the concentration of the external standard and the injection volume were modified empirically to reach similar levels of peak heights (*i.e.* 0.4 and 0.5 AU). Finally, seven solutions of the product at different concentrations were prepared as presented in **Table 6.3**. Aliquots (87 µL) of each sample were taken and diluted in a solution of the external standard in hexane (1 mL, 1.85 mg/mL, 12 µmol/mL).

Table 6.3. Calibration datapoints spanning different ranges of concentration to confirm linearity of the correlation at different levels of yields.

Theo. yield	[P] in flask (mmol/mL)	[ES] in vial (µmol/mL)	Aliquot
133%	0.20	12.0	87 µL in 1 mL
100%	0.15	12.0	87 µL in 1 mL
67%	0.10	12.0	87 µL in 1 mL
33%	0.05	12.0	87 µL in 1 mL
17%	0.025	12.0	87 µL in 1 mL
7%	0.010	12.0	87 µL in 1 mL
3%	0.005	12.0	87 µL in 1 mL

A calibration curve was depicted to correlate the area of the peak of interest over the area of the external standard (area under the curve, AUC) with the actual experimental concentration (**Figure 6.4**). A linear fit was obtained in the region of 0–20 mmol/mL for 2 µL injection volume and 0–15 mmol/mL for 5 µL injection volume. There is a break in linearity over 15 mmol/mL in the case of 5 µL injection due to saturation of the UV probe with the external standard.

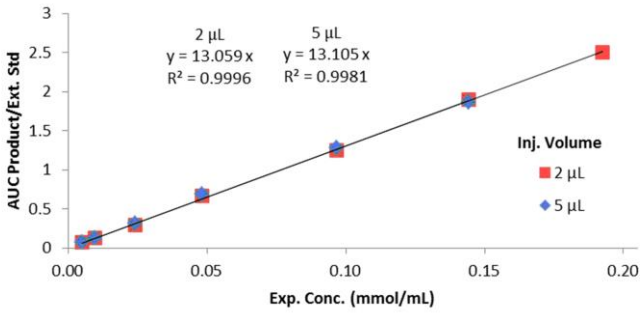

Figure 6.4. Calibration curve for the ACA to acyclic enone to monitor reaction conversion over time by HPLC on a chiral column at different injection volumes.

5.2.2 Measurement

To monitor the reactions, a small volume of the reaction mixture was withdrawn at specified time points by syringe. All the timings were carefully and accurately followed using a timer (± 30 sec), which was started upon addition of the TMSCl additive. As the reaction is heterogeneous (appearance of precipitate over time), the use of microsyringes is prohibited and ineffective (immediate blockage of the needle). Instead, an aliquot was withdrawn with the tip of a 1 mL syringe (87 ± 3 µL) and placed into an MS vial loaded with a small stirring bar. Each aliquot (87 µL) was then quenched with a sat. solution of NH_4Cl (2 drops) and stirred for 30 min in order to remove any metal traces. Solvents (CH_2Cl_2 & Et_2O) were removed under reduced pressure before adding hexane (0.5 mL). The vial mixture was stirred overnight to allow the slow precipitation of all the organometallics in hexane. *Note: At least 6 h of stirring are necessary for the full precipitation of aggregates and avoid blockage of the HPLC injection needle!* The sample was then filtered over cotton/MgSO4 and the vial was rinsed with hexane. The sample mixture was concentrated under reduced pressure, and finally diluted in a solution of external standard in hexane (1 mL, 1.85 mg/mL, 12 µmol/mL). Two chromatograms of each sample were recorded by

HPLC by 2 µL and 5 µL injection volumes following the conditions shown in **Figure 6.3**. Peak areas were integrated at a wavelength of 210 nm. 2 µL injection volume was used to follow the reaction kinetics in its entirety and 5 µL injection was realised to "zoom" in the region below 10% yield and accurately follow the first minutes of the reaction. Using the calibration curve (**Figure 6.4**), the area of the peak of interest over the area of the external standard peak allowed for measuring the concentration of product in the flask over time. For every experiment, the total concentration of known UV active components was also monitored to ensure it remained constant, indicating no unexpected side reactivity.

5.3 Design of experiment

Condition screening was realised using design of experiment theory in order to efficiently identify the optimal conditions in terms of yield for the ACAs to acyclic and exocyclic enones. Many reviews describe the theory behind this optimisation method and it will not be discussed here.[37] This section illustrates the DoE workflow used in this work with the condition screening of exocyclic enone but does not elaborate on the other screening campaign by concision. The design of experiment was realised using the opensource R package (R version 3.5.1, 2018-07-02)[38] with *DoE.base* library installed via the CRAN project (*https://cran.r-project.org/).* Commercial softwares also exist such as *Stat-Ease Design Expert* or *JMP*.

5.3.1 Scoping

A design of experiment is only effective if a response is quantifiable to unearth trends (*i.e.* yields > traces). Two experiments at low and high condition levels are realised to analyse the boundaries of the design of experiment within which reactivity should always be obtained. Low level represents all the factors at

minimum values (or maximum in the specific case of dilution) while high level is the opposite. In this condition optimisation, we studied five factors listed in **Table 6.4**.

Table 6.4. Scoping of the design of experiment of the ACA to exocyclic enone. Yield determined by NMR.

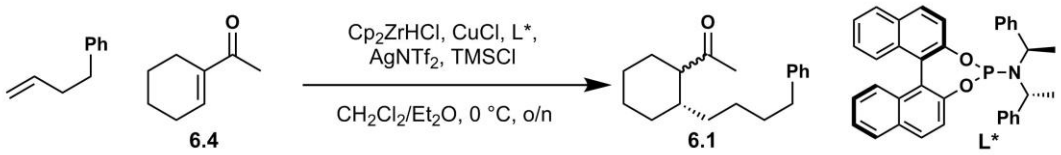

Factors	Low	High
Schwartz eq.	1.1	2.2
Alkene/Schwartz ratio	1.25	2
Cu eq.	0.1	0.2
$AgNTf_2$/Cu ratio	1.4	2.2
TMSCl eq.	2.5	10
Yield	61%	48%

Both extreme conditions provided quantifiable yields, which allowed for directly realising the screening. If no reactivity was observed at this stage whether at low or high levels, the range of conditions explored in the design of experiment should have been adjusted until quantifiable yields were obtained.

5.3.2 Screening

The amount of runs to carry out depends on the number of factors being studied. As we examine five factors in this example, the optimum number of runs is sixteen according to a two-level fractional factorial design (**Table 6.5**). Here, fractional factorial means that each factor is examined at both a low and a high level. Note that in the case of numerous factors to examine (>6 factors in total), it is advised to realise a quicker screening (yellow tile in **Table 6.5**) and to first identify the main contributing factors to the response variable. A second screening is finally realised on only the most important factors for thorough examination (<6 factors).

Table 6.5. Regular two-level fractional factorial design. White is the normal amount of experiments to explore all variables in a full factorial design. Green is the optimum for characterisation. Yellow is statistically less robust but good enough for quicker screening. Red should be avoided and is used for ruggedness testing of the factors. The numbers within the tiles represent the amount of center points to carry out.

		Number of factors							
		2	**3**	**4**	**5**	**6**	**7**	**8**	**9**
Runs	**4**	/	2						
	8		/	2	2	2	2		
	16			/	4	4	4	4	4
	32				/	4	4	4	4
	64					/	8	8	8
	128						/	16	16
	256							/	32
	512								/

To our sixteen runs must be added centre points in order to estimate the experimental noise within the system. The amount of required centre points is subjective but we suggest four for sixteen runs with five factors (**Table 6.5**). We therefore have a total of twenty runs to carry out with the design of experiment instead of thirty-two for a full two-level factorial design. The reaction runs were randomised to avoid biases in the data and distributed in four blocks (one per centre point) and ideally one block of runs was carried out per day. The results are shown in **Table 6.6**. Several responses were monitored such as the yield, the amount of remaining starting material, *dr*, and *ee's* of product diastereoisomers. The tabulated values can then be processed to identify the most important factors and the optimum conditions.

Table 6.6. Runs carried out for the design of experiments of the ACA to exocyclic enone. Yield determined by calibrated ^{1}H NMR.

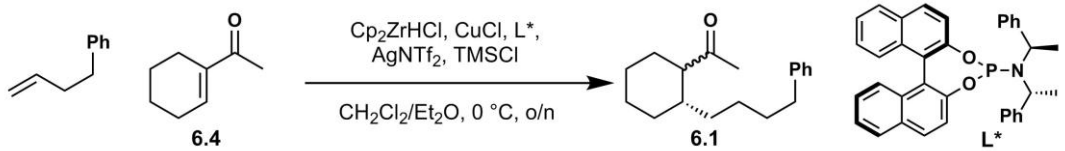

Block	Schwartz eq.	Alkene/Schwartz ratio	Cu eq.	$AgNTf_2$/Cu ratio	TMSCl eq.	Yield	SM	dr	$ee_{dia\ 1}$	$ee_{dia\ 2}$
#1	1.65	1.625	0.15	1.8	6.25	66%	0%	0.5	11%	11%
	1.1	1.25	0.1	1.4	2.5	52%	18%	1.1	10%	24%
	2.2	2	0.2	1.4	10	60%	0%	0.8	2%	1%
	1.1	2	0.2	2.2	2.5	29%	0%	1	3%	3%
	2.2	1.25	0.2	1.4	2.5	53%	6%	1.2	6%	1%
#2	1.65	1.625	0.15	1.8	6.25	53%	0%	0.6	9%	28%
	2.2	1.25	0.1	1.4	10	78%	0%	1.3	3%	10%
	1.1	1.25	0.2	2.2	10	22%	0%	0.1	4%	3%
	2.2	2	0.1	2.2	2.5	54%	10%	1.2	15%	3%
	1.1	2	0.2	1.4	2.5	56%	0%	0.9	3%	1%
#3	1.65	1.625	0.15	1.8	6.25	76%	0%	0.5	2%	2%
	1.1	2	0.1	2.2	10	41%	7%	0.9	1%	2%
	2.2	2	0.1	1.4	2.5	19%	0%	2.5	3%	15%
	1.1	1.25	0.1	2.2	2.5	66%	4%	0.9	5%	0%
	1.1	1.25	0.2	1.4	10	58%	1%	0.6	2%	2%
#4	1.1	2	0.1	1.4	10	56%	4%	0.7	25%	2%
	2.2	1.25	0.1	2.2	10	75%	0%	0.4	17%	11%
	2.2	1.25	0.2	2.2	2.5	68%	0%	0.6	6%	8%
	2.2	2	0.2	2.2	10	52%	0%	0.4	18%	12%
	1.65	1.625	0.15	1.8	6.25	66%	0%	0.6	4%	8%

5.3.3 Processing

First, the experimental error can easily be calculated from the tabulated values by analysing the standard error of the centre points. In this example, the centre points affords 65 ± 9% yield on average. Such results immediately demonstrate the presence of reproducibility issues that will have to be dealt with before ligand optimisation. The use of dedicated stirring bars and round-botom flasks to avoid cross-contamination of metals while avoiding screening apparatus proved successful.

Second, a visual way to identify the factors that are important to improve the yield is to depict the half-normal probability plot (**Figure 6.5-A**). Put simply, the most (statistically) significant factors will be on the right side of the graph while those within the noise will be on the left side. In this example, the alkene/Schwartz ratio and the Schwartz equivalent are the most significant factors to improve the yield. It is common to realise an ANOVA test on these identified factors to confirm their significance ($p < 0.05$). Unfortunately, these factors were not significant ($p \simeq 0.1$) due to the noise present in the data (reproducibility issues).

Finally, the interaction plot is informative about the effect of each factor on the yield (**Figure 6.5-B**). It is common to add the center points in the interaction plots to quantify the curvature of the interaction as it is not necessarily linear such that the optimum might be within the boundaries (omitted in this example as mostly linear). The Schwartz and TMSCl equivalents afforded better yields at a high level while the alkene/Schwartz ratio, copper equivalent and $AgNTf_2$/copper ratio were preferred at a low level. The same analysis can then be realised for each response variable, such as the amount of remaining starting material, *dr* and *ee's* of product

diastereoisomers. Overall, the analysis afforded the optimum conditions as shown in **Figure 6.5-C**.

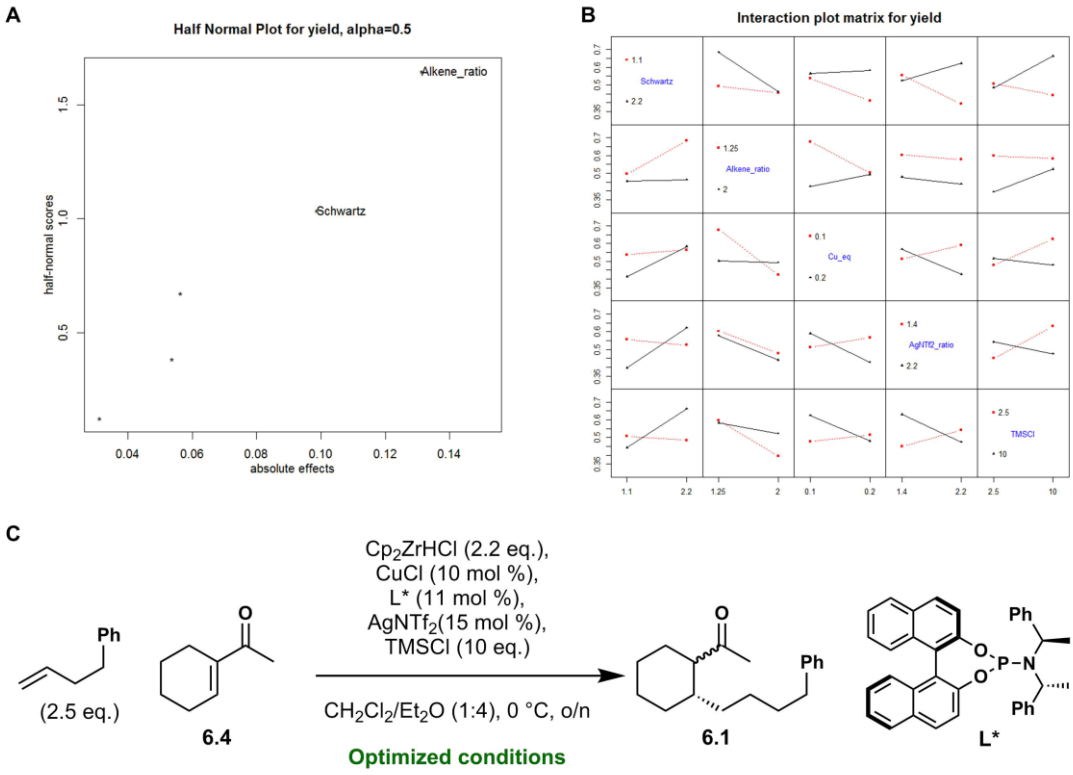

Figure 6.5. Processing of the tabulated values of the ACA to exocyclic enone. **A)** Half-normal probability plot. Labels are for factors with $p < 0.5$. **B)** Interaction plot matrix for yield.

6 References

1 B. Huber and B. Roling, *Electrochim. Acta*, 2011, **56**, 6569–6572.

2 M. S. Taylor, D. N. Zalatan, A. M. Lerchner and E. N. Jacobsen, *J. Am. Chem. Soc.*, 2005, **127**, 1313–1317.

3 A. F. Abdel-Magid and S. J. Mehrman, *Org. Process Res.*, 2006, **10**, 971–1031.

4 D. Tsvelikhovsky and S. L. Buchwald, *J. Am. Chem. Soc.*, 2010, **132**, 14048–14051.

5 S. Maity and N. Zheng, *Angew. Chem. Int. Ed.*, 2012, **51**, 9562–9566.

6 Z. Gao and S. P. Fletcher, *Chem. Sci.*, 2017, **8**, 641–646.

7 T. M. Beck and B. Breit, *Angew. Chem. Int. Ed.*, 2017, **56**, 1903–1907.

8 P. M. C. Roth and S. P. Fletcher, *Org. Lett.*, 2015, **17**, 912–915.

9 R. M. Maksymowicz, P. M. C. Roth and S. P. Fletcher, *Nat. Chem.*, 2012, **4**, 649–654.

10 S. Biswas, J. P. Page, K. R. Dewese and T. V. RajanBabu, *J. Am. Chem. Soc.*, 2015, **137**, 14268–14271.

11 F. Chen, Y. Zhang, L. Yu and S. Zhu, *Angew. Chem. Int. Ed.*, 2017, **56**, 2022–2025.

12 V. Bethi and R. A. Fernandes, *J. Org. Chem.*, 2016, **81**, 8577–8584.

13 L. Minuti, F. Piazzolla and A. Temperini, *Euro. J. Org. Chem.*, 2017, **2017**, 5370–5377.

14 T. N. Grant and F. G. West, *Org. Lett.*, 2007, **9**, 3789–3792.

15 M. R. Adams, C. H. Tien, R. McDonald and A. W. H. Speed, *Angew. Chem. Int. Ed.*, 2017, **56**, 16660–16663.

16 Y. H. Jang and S. W. Youn, *Org. Lett.*, 2014, **16**, 3720–3723.

17 S. Suárez-Pantiga, R. Hernández-Ruiz, C. Virumbrales, M. R. Pedrosa and R. Sanz, *Angew. Chem. Int. Ed.*, 2019, **58**, 2129–2133.

18 S. Panda and J. M. Ready, *J. Am. Chem. Soc.*, 2018, **140**, 13242–13252.

19 I. Némethová, Z. Sorádová and R. Šebesta, *Synthesis*, 2017, **49**, 2461–2469.

20 S. L. Buchwald, S. J. LaMaire, R. B. Nielsen, B. T. Watson and S. M. King, *Org. Synth.*, 1993, **71**, 77.

21 J. Imuta, J. Saito, T. Ueda and T. Mukaiyama, *Catalyst for olefin polymerization, process for the polymerization of olefin, and transition metal compound employable for the catalyst*, European Patent Office, EP0519746A1, 1992.

22 A. K. Ghosh and J. Li, *Org. Lett.*, 2009, **11**, 4164–4167.

23 K. J. Stowers, K. C. Fortner and M. S. Sanford, *J. Am. Chem. Soc.*, 2011, **133**, 6541–6544.

24 C.-D. Chen, J.-W. Huang, M. Leung and H. Li, *Tetrahedron*, 1998, **54**, 9067–9078.

25 J. Ito, D. Sakuma and Y. Nishii, *Chem. Lett.*, 2015, **44**, 297–299.

26 Z. Gao and S. P. Fletcher, *Chem. Commun.*, 2017, **53**, 10216–10219.

27 T. W. Liwosz and S. R. Chemler, *Chem. - A Eur. J.*, 2013, **19**, 12771–12777.

28 A. R. Kunzer and M. D. Wendt, *Tetrahedron Lett.*, 2011, **52**, 1815–1818.

29 A. K. Morri, Y. Thummala and V. R. Doddi, *Org. Lett.*, 2015, **17**, 4640–4643.

30 J. Y. J. Wang, T. Palacin and S. P. Fletcher, *Org. Lett.*, 2019, **21**, 378–381.

31 B. Song, T. Knauber and L. J. Gooßen, *Angew. Chem. Int. Ed.*, 2013, **52**, 2954–2958.

32 M. Shen, B. E. Leslie and T. G. Driver, *Angew. Chem. Int. Ed.*, 2008, **47**, 5056–5059.

33 Y. Xu, G. C. Clarkson, G. Docherty, C. L. North, G. Woodward and M. Wills, *J. Org.*

Chem., 2005, **70**, 8079–8087.

34 Y. Li and Q. Li, *Org. Lett.*, 2012, **14**, 4362–4365.

35 T. Ooi, M. Kameda and K. Maruoka, *J. Am. Chem. Soc.*, 2003, **125**, 5139–5151.

36 B. Li and P. Chiu, *Euro. J. Org. Chem.*, 2011, **2011**, 3932–3937.

37 S. A. Weissman and N. G. Anderson, *Org. Process Res. Dev.*, 2015, **19**, 1605–1633.

38 R Core Team, *R: A Language and Environment for Statistical Computing*, R Foundation for Statistical Computing, Vienna, Austria, 2013.

7

Computational section

1 Multivariate modelling

1.1 General information

Multivariate modelling was performed using R, version 3.5.1 software package.[1] Several libraries were installed via the CRAN project (*https://cran.r-project.org/)* to realise statistical modelling with preimplemented functions. The *caret* library was used for cross-validation and prediction of the external validation set while the graphs were produced with *ggplot2* and *ggrepel* libraries. The descriptor values were normalised automatically using pre-implemented scaling functions. Likewise, statistical measures (*e.g.* coefficient of determination, standard deviation, *etc.*) were computed from premade functions in the R package. Correlation plots for the Pearson colinearity evaluation of descriptors was realised with the *corrplot* library.

If containing flexible substituents, conformation sampling of molecular geometries was performed with wSterimol Python script[2] or Spartan, Version 16 software package.[3] Optimisation of each conformation was carried out at the PM6-DH2 or PM7 semi-empirical level of theory using Mopac, Version 2016 software package,[4] from which Cartesian coordinates within 20 kJ/mol (~5 kcal/mol) were reoptimized at the density functional theory (DFT) level of theory. DFT geometry optimizations and frequency analyses were performed using the Gaussian 09, Revision D.01 software package.[5] Molecular geometries were fully optimized at the level of density functional theory, using the M06-2X[6–8] or ωB97xD[9] functionals as clearly stated, without any symmetry constraints. The effective core potentials (ECPs) of Hay and Wadt with a double-ζ basis set (LanL2DZ)[10,11] was used for Cu and Zr transition metals if modelling the entire catalyst and the 6-31G(d) basis set was used for H, C,

N, O, P and Cl elements. All stationary points were checked as ground state by the absence of imaginary vibrational frequency. Thermochemistry was evaluated at the solution standard state of 1 mol·dm^{-3} and temperature of 298.15 K. Gas phase species were evaluated at standard pressure of 1 bar. 3D molecular graphics were generated by Open source Pymol Version 1.8.6.0.[12] All energetic terms were reported in kJ/mol and are relative energy values.

The molecular descriptors were computed from geometries optimized at the DFT level of theory, unless otherwise stated. Likewise, Boltzmann ensembles of molecular descriptors were computed from energies obtained at the DFT level of theory, unless otherwise stated. Sterimol parameters were computed from wSterimol Python script[2] and AlogPS values from the Virtual Computational Chemistry Laboratory (*http://www.vcclab.org/lab/alogps/*).[13] Spartan, Version 16 software package[3] generated several parameters at the PM7 semi-empirical level of theory or ωB97xD/6-31G(d) DFT level of theory, as clearly stated. In a non-exhaustive list, there was the CPK molecular model area, CPK volume, CPK ovality, polarizability, E^{HOMO}, E^{LUMO}, dipole moment and polar area. Frequencies, NBO values and magnetic shielding tensors were collected using the Gaussian 09, Revision D.01 software package.[5] Distances, angles and dihedrals were generated semi-automatically within open source Pymol Version 1.8.6.0[12] with the help of in-house python scripts.

1.2 Appendix – Chapter 2

Twelve models were realised in total in an iterative way as presented in **Chapter 2**. However, only the two most important models -the initial **Model I** and final

Model II- are presented below due to the repetitive nature of the process. The code is freely available and disclosed for all the models in *ACS Catalysis*.[14]

1.2.1 Model I

Using the initial dataset presented in **Table 7.1** and **Scheme 7.1**, Model I involves the lipophilicity parameter logP (calculated from the amine subgroup and not the entire ligand) with a positive coefficient and passed all the statistical tests: the training set possesses a satisfactory 6:1 ratio between the amount of datapoints (6 ligands) and descriptors (logP only), which produced a good fit (R^2) of 89% and a RMSE of 0.66 kJ/mol. Internal validation with leave-one-out cross validation (LOOCV) also proved the model to be fairly robust, particularly in consideration of the limited amount of data in the training set (R^2_{CV} = 78% & RMSE = 0.96 kJ/mol). ANOVA test confirmed the statistical significance of the only parameter (p < 0.05) and external validation formed from a hold-out subset of three ligands also afforded a good R^2 (87%) and an RMSE of 1.93 kJ/mol. The final figure was depicted as shown in **Chapter 2**.

Table 7.1. Dataset employed to construct Model I. Values are in kJ/mol except for AlogPS (no dimension).

Ligands	ddG	AlogPS	fit	lwr	upr	|ddG–fit|
Training						
L2	4.16	1.30	3.34	2.27	4.41	0.82
L5	4.91	2.03	4.77	3.84	5.70	0.13
L9	1.30	0.90	2.55	1.25	3.85	1.25
L11	5.71	2.63	5.95	4.79	7.11	0.24
L6	7.75	3.55	7.76	5.94	9.58	0.01
L10	3.01	0.85	2.45	1.12	3.79	0.55
Validation						
L4	4.00	-0.05	0.69	-1.34	2.71	3.31
L7	4.63	1.86	4.44	3.52	5.36	0.19
L8	5.64	2.67	6.03	4.85	7.22	0.39
Predicted						
T5	*NA*	1.86	4.44	3.52	5.36	*NA*
T1	*NA*	5.09	10.79	7.63	13.95	*NA*
T2	*NA*	4.59	9.80	7.09	12.52	*NA*
T3	*NA*	1.47	3.67	2.68	4.67	*NA*
T12	*NA*	0.79	2.34	0.96	3.71	*NA*
T4	*NA*	1.86	4.44	3.52	5.36	*NA*
T6	*NA*	1.61	3.95	2.99	4.90	*NA*
T7	*NA*	0.31	1.39	-0.34	3.13	*NA*
T8	*NA*	0.85	2.45	1.12	3.79	*NA*
T9	*NA*	2.94	6.56	5.20	7.92	*NA*
T10	*NA*	0.58	1.92	0.40	3.45	*NA*
T11	*NA*	0.81	2.37	1.02	3.74	*NA*
L14	*NA*	5.28	11.16	7.83	14.49	*NA*
L13	*NA*	4.07	8.78	6.52	11.04	*NA*
L12	*NA*	2.99	6.66	5.27	8.05	*NA*
T20	*NA*	6.98	14.50	9.62	19.39	*NA*
T19	*NA*	5.40	11.39	7.96	14.83	*NA*
L15	*NA*	2.71	6.11	4.90	7.32	*NA*
L17	*NA*	1.45	3.63	2.63	4.64	*NA*
L18	*NA*	1.54	3.81	2.84	4.78	*NA*
L19	*NA*	2.33	5.36	4.35	6.38	*NA*
L22	*NA*	5.14	10.88	7.68	14.09	*NA*
L16	*NA*	2.44	5.58	4.52	6.64	*NA*
L8	*NA*	2.67	6.03	4.85	7.22	*NA*
L21	*NA*	0.54	1.85	0.29	3.40	*NA*

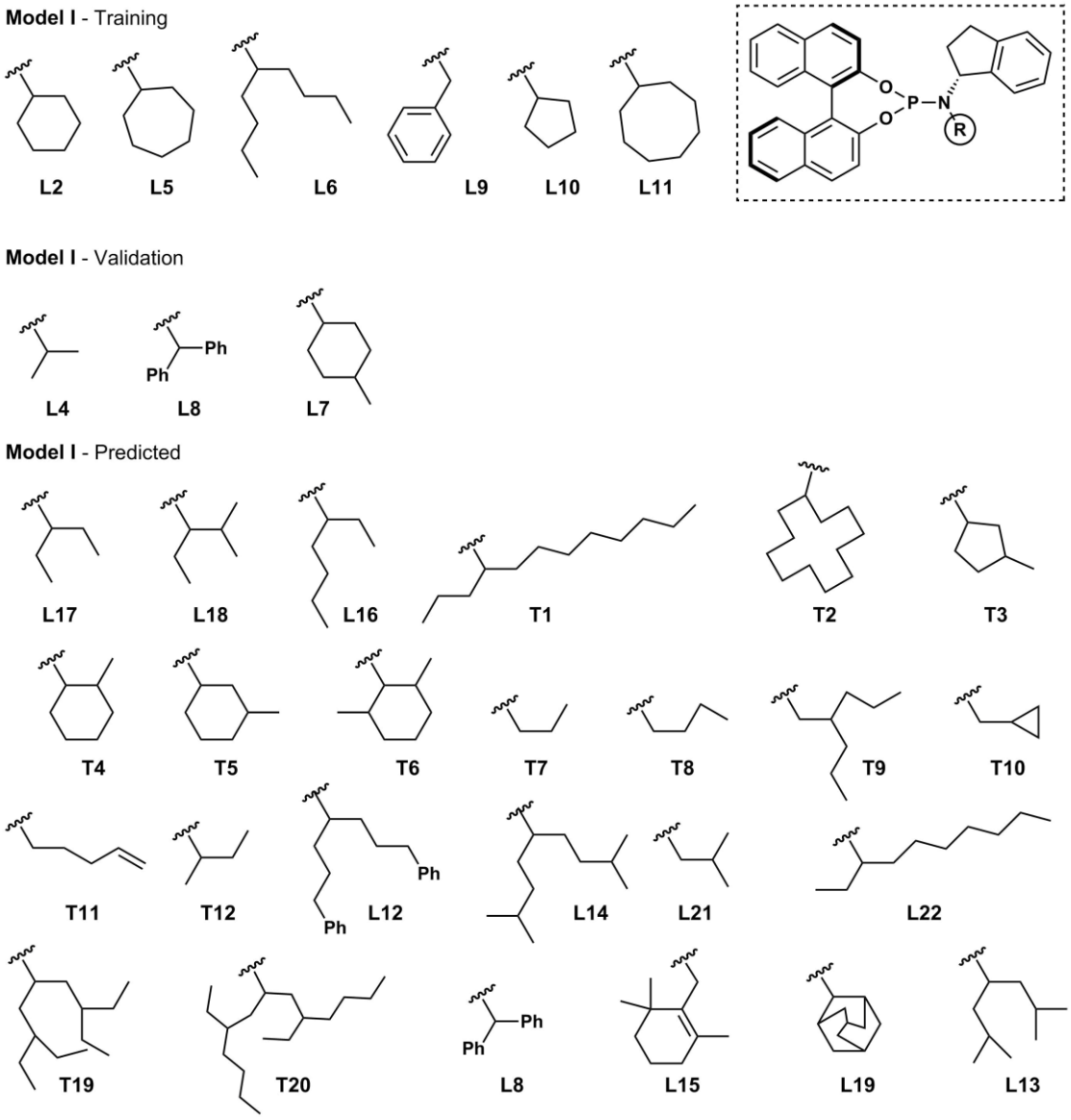

Scheme 7.1. List of ligands in the dataset employed to construct **Model I**.

1.2.2 Model II

Using the final dataset presented in **Table 7.2**, the final model called **Model II** possessed fourteen ligands in the training set for only two descriptors in the model equation, which produced a good fit (R^2 = 84%, RMSE = 0.91 kJ/mol). The HOMO energy and dipole moment were calculated using Spartan, Version 16 software package[3] at the PM7 semi-empirical level of theory. Additionally, LOOCV (R^2_{CV} = 75%, RMSE = 1.16 kJ/mol) and the external test set (six ligands, R^2_{ext} = 86%, RMSE = 0.93 kJ/mol)) remained satisfactory. Finally, the ANOVA test confirmed the statistical significance of the descriptors ($p < 0.05$). The resulting figure was depicted as shown in **Chapter 2**.

Table 7.2. Dataset employed to construct Model II. Values are in kJ/mol except for HOMO energy in eV and dipole moment in Debye.

Ligand	ddG	HOMO	Dipole	fit	lwr	upr	|ddG–fit|
Training							
L2	4.16	-8.25	2.27	4.88	3.99	5.77	0.72
L5	4.91	-8.26	2.27	4.03	3.07	4.98	0.88
L9	1.30	-8.32	1.76	1.57	0.16	2.98	0.27
L11	5.71	-8.26	2.17	4.55	3.80	5.30	1.15
L22	7.75	-8.24	2.03	7.04	6.24	7.83	0.71
L14	8.47	-8.21	2.03	9.59	8.19	10.99	1.12
L20	4.78	-8.31	1.41	4.28	2.59	5.98	0.50
L21	1.21	-8.28	2.16	2.89	1.89	3.88	1.68
L10	3.01	-8.27	2.08	4.17	3.47	4.88	1.16
L7	4.63	-8.26	2.32	3.76	2.68	4.84	0.87
L8	5.64	-8.27	1.73	6.02	5.04	7.00	0.38
L6	7.75	-8.25	1.98	6.42	5.72	7.12	1.33
L13	7.75	-8.23	2.00	8.03	7.02	9.04	0.28
L18	7.01	-8.24	2.07	6.83	6.06	7.59	0.18
Validation							
L4	4.00	-8.26	2.26	4.08	3.14	5.01	0.08
L15	4.74	-8.25	2.55	3.40	1.82	4.99	1.34
L19	4.74	-8.25	2.30	4.73	3.77	5.68	0.01
L17	7.45	-8.25	2.09	5.84	5.18	6.49	1.61
L12	8.47	-8.24	1.91	7.65	6.69	8.61	0.82
L16	7.59	-8.24	1.98	7.28	6.43	8.12	0.31

Ligand	ddG	HOMO	Dipole	fit	lwr	upr	|ddG–fit|
Predicted							
T1	*NA*	-8.25	2.06	5.99	5.35	6.64	*NA*
T2	*NA*	-8.24	2.02	7.07	6.27	7.86	*NA*
T3	*NA*	-8.26	2.21	4.34	3.52	5.17	*NA*
T4	*NA*	-8.26	2.19	4.45	3.66	5.24	*NA*
T5	*NA*	-8.25	2.34	4.51	3.47	5.56	*NA*
T6	*NA*	-8.22	2.29	7.35	6.25	8.45	*NA*
T7	*NA*	-8.25	2.11	5.73	5.07	6.39	*NA*
T8	*NA*	-8.28	2.18	2.78	1.75	3.82	*NA*
T9	*NA*	-8.28	2.06	3.42	2.59	4.24	*NA*
T10	*NA*	-8.30	1.92	2.44	1.38	3.50	*NA*
T11	*NA*	-8.28	2.06	3.42	2.59	4.24	*NA*
T12	*NA*	-8.25	2.17	5.41	4.69	6.13	*NA*
T13	*NA*	-8.27	1.77	5.81	4.92	6.70	*NA*
T14	*NA*	-8.28	1.85	4.53	3.75	5.31	*NA*
T15	*NA*	-8.25	2.14	5.57	4.89	6.26	*NA*
T16	*NA*	-8.24	2.15	6.38	5.62	7.14	*NA*
T17	*NA*	-8.25	1.90	6.84	6.02	7.66	*NA*
T18	*NA*	-8.25	1.73	7.74	6.54	8.94	*NA*
T19	*NA*	-8.26	2.05	5.19	4.58	5.80	*NA*
T20	*NA*	-8.25	1.95	6.58	5.84	7.31	*NA*
T21	*NA*	-8.28	2.16	2.89	1.89	3.89	*NA*
T22	*NA*	-8.26	2.29	3.92	2.92	4.92	*NA*
T23	*NA*	-8.25	2.04	6.10	5.45	6.75	*NA*
T24	*NA*	-8.25	2.21	5.20	4.42	5.98	*NA*

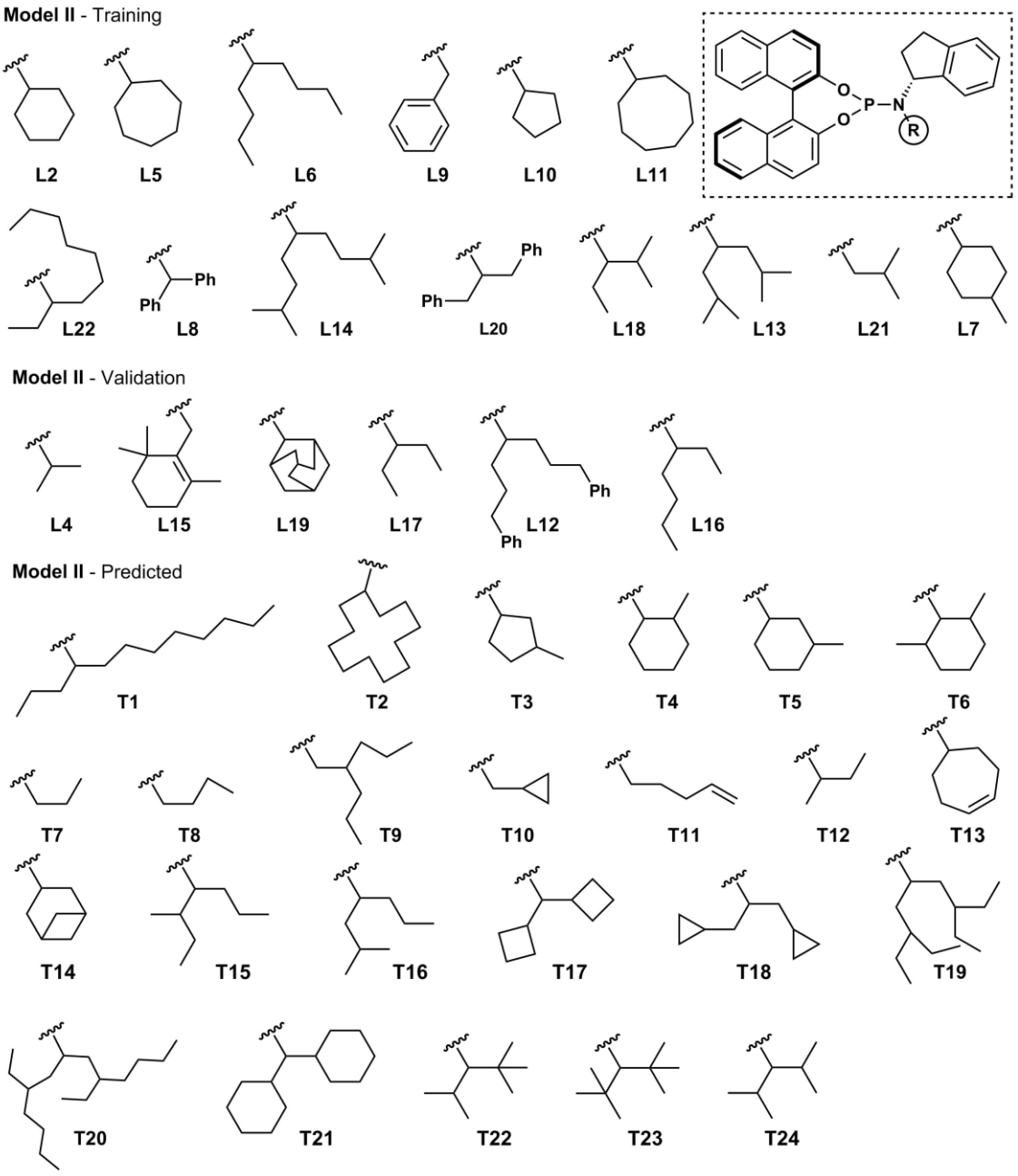

Scheme 7.2. List of ligands in the dataset employed to construct Model II.

1.3 Appendix – Chapter 3

1.3.1 Case study 1

The work by the Sigman laboratory about multidimensional steric parameters possesses two interesting statistical models that only uses Sterimol parameters: the desymmetrization of bisphenol and the Nozaki-Hiyama-Kishi (NHK) coupling allylation.[15] Both projects are explored below.

1.3.1.1 The desymmetrization of bisphenol

Reproducibility of Sterimol parameters. The Sterimol values were repeated as the Cartesian coordinates were not provided in the supporting information. Such task is not trivial as the Sterimol steric values highly depend on the software package and the input geometry. Likewise, the molecular geometry depends on the conformational sampling (if any) and the optimisation level of theory. The substituent geometries were modelled with the anchored atom represented with hydrogen (Hyd) or methyl (Me). Those were fed to the wSterimol Pyton script to generate and optimize the conformers of each substituent at the semi-empirical PM6-DH2 level of theory. All the conformers within 3 kcal/mol were further optimized at the M06-2X/6-311+g(d,p)//M06-2X/6-31g(d) level of theory. Sterimol values of the minimum-energy conformer at both levels of theory were computed and compared with the tabulated values (**Table 7.3**). No improvement was observed with a quantum mechanical level of theory so it was decided to continue with PM6-DH2 (Hyd) substituents instead. The use of methyl as the anchored atom gave slightly different results.

Table 7.3. Reproducibility attempts of the Sterimol values in the seminal work. The Sterimol values were generated at the semi-empirical PM6-DH2 and M06-2X/6-311+g(d,p)//M06-2X/6-31g(d) level of theory. The anchored atom for the calculation of Sterimol parameters was modelled as either hydrogen (Hyd) or methyl (Me).

	Paper			**PM6-DH2 (Hyd)**			**M06-2X (Hyd)**			**PM6-DH2 (Me)**			**M06-2X (Me)**		
Groups	L	B_1	B_5	L	B_1	B_5	L	B_1	B_5	L	B_1	B_5	L	B_1	B_5
Me	2.87	1.52	2.04	2.98	1.51	2.02	2.99	1.51	2.03	3.42	1.88	2.02	3.43	1.88	2.02
Et	4.11	1.52	3.17	4.15	1.56	3.16	4.14	1.55	3.16	4.60	1.88	3.17	4.59	1.88	3.16
Ph	6.28	1.71	3.11	6.37	1.70	3.15	6.36	1.70	3.15	6.79	1.70	3.16	6.80	1.70	3.15
Bn	4.62	1.52	6.02	4.84	1.57	6.03	4.69	1.55	6.07	5.18	1.90	6.04	5.12	1.90	6.07
***i*Pr**	4.11	1.90	3.17	4.12	1.92	3.18	4.10	1.91	3.18	4.57	1.92	3.18	4.56	1.91	3.17
***t*Bu**	4.11	2.60	3.17	4.09	2.76	3.18	4.07	2.76	3.18	4.55	2.76	3.19	4.54	2.76	3.17
Cy	6.17	1.91	3.49	6.19	1.93	3.53	6.19	1.92	3.49	6.66	1.92	3.50	6.65	1.92	3.48
CH_2*t*Bu	4.89	1.52	4.18	5.10	1.56	4.45	5.07	1.55	4.44	5.62	1.88	4.44	5.65	1.90	4.39
$CHEt_2$	4.72	2.13	4.01	4.14	2.07	4.47	4.10	2.06	4.48	5.57	2.04	4.41	5.48	1.92	4.45
CH_2*i*Pr	4.92	1.52	4.45	5.09	1.56	4.46	4.13	1.55	4.44	5.55	1.88	4.43	5.58	1.87	4.42
$CHPh_2$	5.15	2.01	6.02	6.01	1.94	6.10	5.90	1.90	6.11	6.43	2.01	6.14	6.64	1.90	6.15
Ad	6.17	3.16	3.49	6.19	3.17	3.51	6.16	3.16	3.49	6.63	3.17	3.51	6.61	3.15	3.49
			R^2	0.96	0.99	0.99	0.94	0.99	0.99	0.97	0.94	0.99	0.96	0.91	0.99

Multivariate modelling. The two $\Delta\Delta G^{\ddagger}$ values of each substituent were averaged instead of using duplicates as shown in the original paper. The recalculated Sterimol values were used to retrain the original statistical model while wSterimol Python script generated wB_1, wB_5 and wL parameters for another model containing parameters derived from Boltzmann ensemble (**Table 7.4**). The maximum and minimum values were obtained in the 3.0 kcal/mol energy window.

The model with Sterimol parameters involves B_1 and L with a positive and negative coefficients, respectively. The coefficient of determination and RMSE of the model are excellent (R^2 = 97%, RMSE = 0.080 kcal/mol). LOOCV gave satisfactory results (R^2 = 92%, RMSE = 0.13 kcal/mol) and the ANOVA test was passed for both descriptors (B_1 = 6.9×10^{-8}, L = 7.3×10^{-3}). Using identical settings, a model was trained based on the wSterimol parameters. The equation correlating $\Delta\Delta G^{\ddagger}$ free energies employs wB_1 and wL parameters with positive and negative coefficients, respectively. The coefficient of determination and RMSE of the wSterimol model are excellent (R^2 = 96%, RMSE = 0.090 kcal/mol). LOOCV gave satisfactory results (R^2 = 91%, RMSE = 0.13 kcal/mol) and the ANOVA test was passed for both descriptors (wB_1 = 2.1×10^{-7}, $_wL$ = 1.4×10^{-2}). Using the minimum and maximum Sterimol values of conformers that are tabulated, the potential impact of conformational sampling on the wSterimol model was estimated. The final figure was depicted as shown in **Chapter 3**.

Table 7.4. Dataset employed in the desymmetrization of bisphenol. The parameters were generated at the semi-empirical PM6-DH2 level of theory. The substituent geometries were modelled with the anchored atom represented with hydrogen (Hyd).

Groups	L	B_1	B_5	ddG	wB_1	wB_5	wL	$^{min}B_1$	$^{min}B_5$	^{min}L	$^{max}B_1$	$^{max}B_5$	^{max}L	fit	|ddG–fit|
Me	2.98	1.51	2.02	0.5430	1.51	2.02	2.98	1.51	2.02	2.98	1.51	2.02	2.98	0.6428	0.0998
Et	4.15	1.56	3.16	0.6030	1.56	3.16	4.15	1.56	3.16	4.15	1.56	3.16	4.15	0.5770	0.0260
Ph	6.37	1.70	3.15	0.5110	1.70	3.15	6.37	1.70	3.15	6.37	1.70	3.15	6.37	0.4923	0.0187
Bn	4.84	1.57	6.03	0.4385	1.57	6.00	5.43	1.57	5.96	4.84	1.57	6.03	6.10	0.4652	0.0267
***i*Pr**	4.12	1.92	3.18	0.8845	1.92	3.18	4.12	1.92	3.18	4.12	1.92	3.18	4.12	0.9005	0.0160
***t*Bu**	4.09	2.76	3.18	1.7240	2.76	3.18	4.09	2.76	3.18	4.09	2.76	3.18	4.09	1.6517	0.0723
Cy	6.19	1.93	3.53	0.7220	1.93	3.53	6.19	1.93	3.53	6.19	1.93	3.53	6.19	0.7142	0.0078
CH_2*t*Bu	5.10	1.56	4.45	0.5820	1.56	4.45	5.09	1.56	4.45	4.79	1.57	4.49	5.10	0.4883	0.0937
$CHEt_2$	4.14	2.07	4.47	1.1195	2.01	4.45	4.54	1.93	3.69	3.77	2.07	4.51	5.13	0.9411	0.1784
CH_2*i*Pr	5.09	1.56	4.46	0.3495	1.56	4.44	4.79	1.56	4.02	4.18	1.57	4.46	5.09	0.5166	0.1671
$CHPh_2$	6.01	1.94	6.10	0.8170	1.98	6.12	5.85	1.92	6.05	5.56	2.04	6.17	6.02	0.7908	0.0262
Ad	6.19	3.17	3.51	1.7055	3.17	3.51	6.19	3.17	3.51	6.19	3.17	3.51	6.19	1.8189	0.1134

1.3.1.2 The Nozaki-Hiyama-Kishi (NHK) coupling allylation

Reproducibility of Sterimol parameters. The Sterimol values were repeated as the Cartesian coordinates were not provided in the supporting information. The substituent geometries were modelled with the anchored atom represented with hydrogen (Hyd) or methyl (Me). Those were fed to the wSterimol Pyton script to generate and optimize the conformers of each substituent at the semi-empirical PM6-DH2 level of theory. Sterimol values of the minimum-energy conformer were computed and compared with the tabulated values (**Table 7.5**). In this case, the use of methyl as the anchored atom gave the more reproducible results such that modelling was carried out at the PM6-DH2 level of theory with a methyl group at the terminal atom.

Table 7.5. Reproducibility attempts of the Sterimol values in the seminal work. The Sterimol values were computed at the semi-empirical PM6-DH2 level of theory. The anchored atom for the calculation of Sterimol parameters was modelled as either hydrogen (Hyd) or methyl (Me).

	Paper			**PM6-DH2 (Hyd)**			**PM6-DH2 (Me)**		
Groups	L	B_1	B_5	L	B_1	B5	L	B_1	B_5
Me	2.87	1.52	2.04	2.98	1.51	2.02	3.42	1.88	2.02
Et	4.11	1.52	3.17	4.15	1.56	3.16	4.6	1.88	3.17
***i*Pr**	4.11	1.90	3.17	4.12	1.92	3.18	4.57	1.92	3.18
***t*Bu**	4.11	2.60	3.17	4.09	2.76	3.18	4.55	2.76	3.19
$CHPr_2$	6.17	1.90	4.54	4.15	2.07	5.71	6.5	2.04	5.67
CEt_3	4.92	2.94	4.18	4.10	3.18	4.51	5.43	2.80	4.51
$CHiPr_2$	4.12	2.08	4.19	5.09	2.06	4.49	5.53	2.12	4.49
Ad	6.17	3.16	3.49	6.19	3.17	3.51	6.63	3.17	3.51
			R^2	0.66	0.99	0.97	0.95	0.97	0.97

Multivariate modelling. The two $\Delta\Delta G^{\ddagger}$ values of each substituent were averaged instead of using duplicates as shown in the original paper. The recalculated Sterimol

values were used to retrain the original statistical model while wSterimol Python script generated wB_1, wB_5 and wL parameters for another model containing parameters derived from Boltzmann ensemble (**Table 7.6**). The maximum and minimum values were obtained in the 3.0 kcal/mol energy window.

The model with Sterimol parameters only involves the B_1 descriptor with a positive coefficient. The coefficient of determination is satisfactory (R^2 = 83%). Using identical settings, a model was trained based on the wSterimol parameters. The equation correlating $\Delta\Delta G^{\ddagger}$ free energies employs wB_1 parameter with a positive coefficients. The coefficient of determination of the wSterimol model is excellent (R^2 = 83%). LOOCV gave satisfactory results (R^2 = 81%) and the ANOVA test was passed ($wB_1 = 1.8\times10^{-5}$). Using the minimum and maximum Sterimol values of conformers that are tabulated, the potential impact of conformational sampling on the wSterimol model was estimated and showed a similar behaviour than the one observed with the desymmetrization of bisphenol project. It was therefore not further investigated.

Table 7.6. Dataset employed in the Nozaki-Hiyama-Kishi (NHK) coupling allylation. The parameters were generated at the semi-empirical PM6-DH2 level of theory. The substituent geometries were modelled with the anchored atom represented with methyl (Me).

Groups	L	B_1	B_5	ddG	wL	wB_1	wB_5	^{min}L	^{max}L	$^{min}B_1$	$^{max}B_1$	$^{min}B_5$	$^{max}B_5$	fit	|ddG–fit|
Me	2.87	1.52	2.04	-0.65	3.42	1.88	2.02	3.42	3.42	1.88	1.88	2.02	2.02	-0.47	0.18
Et	4.11	1.52	3.17	-0.68	4.60	1.88	3.17	4.60	4.60	1.88	1.88	3.17	3.17	-0.47	0.21
***i*Pr**	4.11	1.90	3.17	-0.30	4.57	1.92	3.18	4.57	4.57	1.92	1.92	3.18	3.18	-0.44	0.14
***t*Bu**	4.11	2.60	3.17	0.47	4.55	2.76	3.19	4.55	4.55	2.76	2.76	3.19	3.19	0.30	0.17
$CHPr_2$	6.17	1.90	4.54	-0.30	6.12	2.16	5.42	4.56	6.98	1.92	2.79	4.49	5.75	-0.22	0.08
CEt_3	4.92	2.94	4.18	0.28	5.29	2.86	4.51	4.55	5.52	2.79	3.18	4.49	4.56	0.39	0.11
$CHiPr_2$	4.12	2.08	4.19	0.12	5.40	2.14	4.50	4.64	5.60	2.03	2.28	4.49	4.55	-0.24	0.36
Ad	6.17	3.16	3.49	0.57	6.63	3.17	3.51	6.63	6.63	3.17	3.17	3.51	3.51	0.66	0.09

1.3.2 Case study 2

The work by the Song laboratory about a quantitative correlation between *N*-substituent sizes of chiral ligands and enantioselectivities possesses two interesting statistical models that only uses Sterimol parameters.[16] The first model attempts to use the full amine structure in the ligand while the second more successful model describes the amine moiety in the ligands with alkyl subgroups. These projects are explored below.

1.3.2.1 Full amine model

Reproducibility of Sterimol parameters. The Sterimol values were repeated as the Cartesian coordinates were not provided in the supporting information. The substituent geometries were modelled with the anchored atom represented with hydrogen (Hyd) or methyl (Me). Those were fed to the wSterimol Python script to generate and optimize the conformers of each substituent at the semi-empirical PM6-DH2 level of theory. Sterimol values of the minimum-energy conformer were computed and compared with the tabulated values (**Table 7.7**). To our dismay, the values were not reproducible probably due to a lack of conformational sampling. We therefore decided to take the best fit, such that the wSterimol parameters were computed at the PM6-DH2 level of theory with a hydrogen group at the terminal atom.

Table 7.7. Reproducibility attempts of the Sterimol values in the seminal work. The Sterimol values were computed at the semi-empirical PM6-DH2 level of theory. The anchored atom for the calculation of Sterimol parameters was modelled as either hydrogen (Hyd) or methyl (Me).

	Paper			PM6-DH2 (Hyd)			PM6-DH2 (Me)		
Groups	L	B_1	B_5	L	B_1	B_5	L	B_1	B_5
NH_2	2.78	1.35	1.97	2.91	0.95	1.96	3.39	1.55	2.04
NHMe	3.53	1.35	3.08	4.03	0.96	3.19	4.54	1.55	3.19
NHEt	4.83	1.35	3.42	4.05	0.96	4.44	4.55	1.55	4.37
NHBu	6.88	1.35	4.87	4.16	0.96	6.97	5.50	1.62	4.39
$NHCH_2$*i*Pr	6.07	1.35	4.47	4.05	0.96	5.72	5.01	1.55	5.69
$NHCH_2$Bu	8.13	1.35	5.89	4.20	0.96	8.23	5.58	1.55	8.11
NH*i*Pr	4.83	1.35	4.13	4.98	0.96	4.46	5.50	1.62	4.39
NH*s*Bu	6.07	1.35	4.47	4.51	1.40	5.04	6.66	1.64	4.38
NMe_2	3.53	1.35	2.56	4.01	1.35	3.19	4.51	1.55	3.19
NEt_2	4.83	1.35	4.39	4.03	1.34	4.48	4.57	1.55	4.44
N(-C_4H_8-)	4.90	1.90	4.09	4.16	1.50	4.15	4.81	1.55	4.12
N(-C_5H_{10}-)	6.17	1.91	3.49	6.09	1.50	3.50	6.61	1.55	3.46
			R^2	0.44	0.68	0.94	0.72	-0.26	0.89

Multivariate modelling. The two $\Delta\Delta G^{\ddagger}$ values of each substituent were averaged instead of using duplicates as shown in the original paper. The recalculated Sterimol values were used to retrain the original statistical model while wSterimol Python script generated wB_1, wB_5 and wL parameters for another model containing parameters derived from Boltzmann ensemble (**Table 7.8**). The maximum and minimum values were obtained in the 3.0 kcal/mol energy window.

The best model with Sterimol parameters involves B_5 parameter with a positive coefficient. The coefficient of determination is extremely low (R^2 = 27%), suggesting that there is no correlation between the Sterimol steric parameters and the enantioselectivity as clearly explained by the authors of the seminal study. Using identical settings, a model was however trained based on the wSterimol parameters.

The equation correlating $\Delta\Delta G^{\ddagger}$ free energies employs wB_5 and also led to a low coefficient of determination (R^2 = 32%). Drawing the corresponding model, two datapoints seem to be off track. Investigation on these two tabulated values with the outlierTest() function and the boxplot visualization technique strongly suggested the presence of two outliers in the dataset. Accordingly, the NH*s*Bu and NH*i*Pr substituents were removed. The final model involves wB_5 and wB_1 parameters with positive and negative coefficients, respectively. The coefficient of determination and RMSE of the wSterimol model are satisfactory (R^2 = 84%, RMSE = 0.145 kcal/mol). LOOCV gave satisfactory results (R^2 = 71%, RMSE = 0.204 kcal/mol) and the ANOVA test was passed for both descriptors ($wB_5 = 7.6\times10^{-4}$, $wB_1 = 5.1\times10^{-2}$). Using the minimum and maximum Sterimol values of conformers that are tabulated, the potential impact of conformational sampling on the wSterimol model was estimated. The final figure was depicted as shown in **Chapter 3**.

Table 7.8. Dataset employed to describe the *N*-substituent sizes of the full amine of chiral ligands. The parameters were generated at the semi-empirical PM6-DH2 level of theory. The substituent geometries were modelled with the anchored atom represented with hydrogen (Hyd). NH*i*Pr and NH*s*Bu were identified as outliers.

Groups	L	B_1	B_5	ddG	wL	wB_1	wB_5	^{min}L	^{max}L	$^{min}B_1$	$^{max}B_1$	$^{min}B_5$	$^{max}B_5$	fit	|ddG–fit|
NH_2	2.91	0.95	1.96	0.57	2.91	0.95	1.96	2.91	2.91	0.95	0.95	1.96	1.96	0.55	0.02
NHMe	4.03	0.96	3.19	0.83	4.03	0.96	3.19	4.03	4.03	0.96	0.96	3.19	3.19	0.81	0.01
NHEt	4.05	0.96	4.44	1.16	4.06	0.96	4.43	4.03	1.97	0.96	0.96	3.65	4.44	1.08	0.08
NHBu	4.16	0.96	6.97	1.32	4.31	1.05	5.96	3.92	7.48	0.96	1.50	3.79	6.97	1.36	0.04
$NHCH_2$*i*Pr	4.05	0.96	5.72	1.32	4.23	1.09	5.53	4.05	6.16	0.96	1.50	4.57	5.72	1.24	0.07
$NHCH_2$Bu	4.20	0.96	8.23	1.47	4.55	1.07	6.73	3.95	8.38	0.96	1.50	4.85	8.23	1.52	0.05
NH*i*Pr	4.98	0.96	4.46	2.09	4.54	1.18	4.44	4.07	4.98	0.96	1.40	4.38	4.46	*NA*	*NA*
NH*s*Bu	4.51	1.40	5.04	2.27	5.33	1.21	4.80	4.06	6.27	0.92	1.50	4.45	5.61	*NA*	*NA*
NMe_2	4.01	1.35	3.19	0.42	4.01	1.35	3.19	4.01	4.01	1.35	1.35	3.19	3.19	0.58	0.16
NEt_2	4.03	1.34	4.48	0.64	4.06	1.37	4.48	4.03	5.06	1.34	1.68	4.47	4.48	0.85	0.20
N(-C_4H_8-)	4.16	1.50	4.15	1.04	4.16	1.50	4.15	4.16	4.16	1.50	1.50	4.15	4.15	0.69	0.35
N(-C_5H_{10}-)	6.09	1.50	3.50	0.47	6.06	1.50	3.50	6.09	6.09	1.50	1.50	3.50	3.50	0.55	0.08

1.3.2.2 Alkyl sub-groups model

Reproducibility of Sterimol parameters. The Sterimol values were repeated as the Cartesian coordinates were not provided in the supporting information. The substituent geometries were modelled with the anchored atom represented with hydrogen (Hyd) or methyl (Me). Those were fed to the wSterimol Python script to generate and optimize the conformers of each substituent at the semi-empirical PM6-DH2 level of theory. Sterimol values of the minimum-energy conformer were computed and compared with the tabulated values (**Table 7.9**). The values were fairly reproducible, even though there is probablya a lack of conformational sampling for the flexible substituents. We therefore computed the wSterimol parameters at the PM6-DH2 level of theory with a hydrogen group at the terminal atom.

Table 7.9. Reproducibility attempts of the Sterimol values in the seminal work. The Sterimol values were computed at the semi-empirical PM6-DH2 level of theory. The anchored atom for the calculation of Sterimol parameters was modelled as hydrogen (Hyd).

	Paper			**PM6-DH2 (Hyd)**		
Groups	L	B_1	B_5	L	B_1	B_5
H	2.06	1.00	1.00	2.00	1.00	1.00
Me	2.87	1.52	2.04	2.98	1.51	2.02
Et	4.11	1.52	3.17	4.15	1.56	3.17
Bu	6.17	1.52	4.54	6.23	1.56	4.55
CH_2*i*Pr	4.92	1.52	4.45	4.18	1.56	4.44
CH_2Bu	6.97	1.52	4.94	4.27	1.56	6.97
***i*Pr**	4.11	1.90	3.17	4.12	1.92	3.18
***s*Bu**	4.92	1.90	3.49	4.13	1.92	4.47
			R^2	0.81	1.00	0.93

Multivariate modelling. The two $\Delta\Delta G^{\ddagger}$ values of each substituent were averaged instead of using duplicates as shown in the original paper. The recalculated Sterimol values were used to retrain the original statistical model while wSterimol Python script generated wB_1, wB_5 and wL parameters for another model containing parameters derived from Boltzmann ensemble (**Table 7.10**). The maximum and minimum values were obtained in the 3.0 kcal/mol energy window. The two alkyl chains are called "X" and "Y". *Note: For an unknown reason, only eleven entries were disclosed in the original paper, although twelve datapoints should have been reported to match the full amine dataset.* Directly using the outlierTest() function and the boxplot visualization technique, we identified again two outliers, namely "NH*s*Bu" and "NH*i*Pr" which was consistent with the previous observations. The best model with Sterimol parameters involves $^{X}B_1$ and $^{Y}B_1$ parameters with negative and positive coefficients, respectively. The coefficient of determination and RMSE are satisfactory (R^2 = 80%, RMSE = 0.182 kcal/mol). However, LOOCV gave poor results (R^2 = 46%, RMSE = 0.321 kcal/mol) and the ANOVA test was passed for both descriptors ($^{X}B_1 = 5.7\times10^{-3}$, $^{Y}B_1 = 3.8\times10^{-2}$). Using identical settings, a model was trained based on the wSterimol parameters. The same outliers were identified with the outlierTest() function and were removed. The equation correlating $\Delta\Delta G^{\ddagger}$ free energies employs ^{X}wL and ^{Y}wL with negative and positive coefficients, respectively. The coefficient of determination and RMSE of the wSterimol model are satisfactory (R^2 = 96%, RMSE = 0.08 kcal/mol). LOOCV gave satisfactory results (R^2 = 87%, RMSE = 0.151 kcal/mol) and the ANOVA test was passed for both descriptors ($^{X}wL = 1.4\times10^{-4}$, $^{Y}wL = 1.7\times10^{-4}$). The final figure was depicted as shown in **Chapter 3**.

Table 7.10. Dataset employed to describe the *N*-substituent sizes of chiral ligands with the alkyl subgroups. The parameters were generated at the semi-empirical PM6-DH2 level of theory. The substituent geometries were modelled with the anchored atom represented with hydrogen (Hyd). H-*i*Pr and H-*s*Bu were identified as outliers.

Groups	$^{X}B_1$	$^{X}B_5$	^{X}L	$^{Y}B_1$	$^{Y}B_5$	^{Y}L	ddG	$^{X}wB_1$	$^{X}wB_5$	^{X}wL	$^{X}B_1^{min}$	$^{X}B_5^{min}$	$^{X}L^{min}$	$^{X}B_1^{max}$	$^{X}B_5^{max}$	$^{X}L^{max}$
H-H	1.00	1.00	2.06	1.00	1.00	2.06	0.57	1.00	1.00	2.00	1.00	1.00	2.00	1.00	1.00	2.00
H-Me	1.00	1.00	2.06	1.52	2.04	2.87	0.83	1.00	1.00	2.00	1.00	1.00	2.00	1.00	1.00	2.00
H-Et	1.00	1.00	2.06	1.52	3.17	4.11	1.16	1.00	1.00	2.00	1.00	1.00	2.00	1.00	1.00	2.00
H-Bu	1.00	1.00	2.06	1.52	4.54	6.17	1.32	1.00	1.00	2.00	1.00	1.00	2.00	1.00	1.00	2.00
H-CH$_2$*i*Pr	1.00	1.00	2.06	1.52	4.45	4.92	1.32	1.00	1.00	2.00	1.00	1.00	2.00	1.00	1.00	2.00
H-CH$_2$Bu	1.00	1.00	2.06	1.52	4.94	6.97	1.47	1.00	1.00	2.00	1.00	1.00	2.00	1.00	1.00	2.00
H-*i*Pr	1.00	1.00	2.06	1.90	3.17	4.11	2.09	1.00	1.00	2.00	1.00	1.00	2.00	1.00	1.00	2.00
H-*s*Bu	1.00	1.00	2.06	1.90	3.49	4.92	2.27	1.00	1.00	2.00	1.00	1.00	2.00	1.00	1.00	2.00
Me-Me	1.52	2.04	2.87	1.52	2.04	2.87	0.42	1.51	2.02	2.98	1.51	2.02	2.98	1.51	2.02	2.98
Et-Et	1.52	3.17	4.11	1.52	3.17	4.11	0.64	1.56	3.17	4.15	1.56	3.17	4.15	1.56	3.17	4.15
Bu-Bu	1.52	4.54	6.17	1.52	4.54	6.17	0.29	1.56	5.05	4.89	1.56	3.54	3.76	1.56	5.70	6.41

Table 7.10. Continued.

Groups	$^{Y}wB_1$	$^{Y}wB_5$	^{Y}wL	$^{Y}B_1^{min}$	$^{Y}B_5^{min}$	$^{Y}L^{min}$	$^{Y}B_1^{max}$	$^{Y}B_5^{max}$	$^{Y}L^{max}$	fit	|ddG–fit|
H-H	1.00	1.00	2.00	1.00	1.00	2.00	1.00	1.00	2.00	0.56	0.01
H-Me	1.51	2.02	2.98	1.51	2.02	2.98	1.51	2.02	2.98	0.83	0.00
H-Et	1.56	3.17	4.15	1.56	3.17	4.15	1.56	3.17	4.15	1.15	0.02
H-Bu	1.56	5.05	4.89	1.56	3.54	3.76	1.56	5.70	6.41	1.35	0.04
H-CH_2*i*Pr	1.56	4.44	4.78	1.56	4.03	4.18	1.57	4.46	5.09	1.32	0.01
H-CH_2Bu	1.56	5.83	5.21	1.56	3.73	3.77	1.56	6.97	7.25	1.44	0.03
H-*i*Pr	1.92	3.18	4.12	1.92	3.18	4.12	1.92	3.18	4.12	*NA*	*NA*
H-*s*Bu	1.92	4.34	4.29	1.92	3.65	4.10	1.93	4.50	5.10	*NA*	*NA*
Me-Me	1.51	2.02	2.98	1.51	2.02	2.98	1.51	2.02	2.98	0.51	0.09
Et-Et	1.56	3.17	4.15	1.56	3.17	4.15	1.56	3.17	4.15	0.45	0.20
Bu-Bu	1.56	5.05	4.89	1.56	3.54	3.76	1.56	5.70	6.41	0.41	0.12

1.3.3 Case study 3

The work by the Song laboratory about a quantitative correlation between *N*-substituent sizes of chiral 1,2-amino phosphinamide ligands and enantioselectivities possesses an interesting statistical model that only uses Sterimol parameters.[17] This project is explored below.

Reproducibility of Sterimol parameters. The Sterimol values were repeated as the Cartesian coordinates were not provided in the supporting information. The substituent geometries were modelled with the anchored atom represented with hydrogen (Hyd). Those were fed to the wSterimol Python script to generate and optimize the conformers of each substituent at the semi-empirical PM6-DH2 level of theory. Sterimol values of the minimum-energy conformer were computed and compared with the tabulated values (**Table 7.11**). The values were fairly reproducible. We therefore computed the wSterimol parameters at the PM6-DH2 level of theory with a hydrogen group at the terminal atom.

Multivariate modelling. The recalculated Sterimol values were used to retrain the original statistical model while wSterimol Python script generated wB_1, wB_5 and wL parameters for another model containing parameters derived from Boltzmann ensemble (**Table 7.12**). The maximum and minimum values were obtained in the 3.0 kcal/mol energy window. The two alkyl chains are called “X” and ”Y”. The best model with Sterimol parameters involves $^{X}B_1$ and $^{Y}B_5$ parameters with negative and positive coefficients, respectively. The coefficient of determination and RMSE are satisfactory (R^2 = 95%, RMSE = 0.129 kcal/mol). Additionally, LOOCV gave however good results (R^2 = 90%, RMSE = 0.18 kcal/mol) and the ANOVA test was passed for both descriptors ($^{X}B_1 = 1.2\times10^{-6}$, $^{Y}B_5 = 2.9\times10^{-4}$).

Table 7.11. Reproducibility attempts of the Sterimol values in the seminal work. The Sterimol values were computed at the semi-empirical PM6-DH2 level of theory. The anchored atom for the calculation of Sterimol parameters was modelled as hydrogen (Hyd).

	Paper			PM6-DH2 (Hyd)		
Groups	L	B_1	B_5	L	B_1	B_5
H	2.20	1.17	1.17	2.00	1.00	1.00
Et	4.33	1.71	3.38	4.15	1.56	3.17
Bu	6.39	1.71	4.89	6.23	1.56	4.55
CH_2Bu	7.26	1.71	5.13	4.27	1.56	6.97
***i*Pr**	4.27	2.10	3.38	4.12	1.92	3.18
Me	3.04	1.70	2.22	2.98	1.51	2.02
***c*Hex**	5.46	2.08	4.59	6.19	1.93	3.53
$CHEt_2$	5.41	2.26	4.13	4.14	2.07	4.47
Bn	5.44	1.70	6.20	4.84	1.57	6.03
CH_2(*p*$CH_3C_6H_4$)	5.73	1.70	7.48	5.60	1.57	7.13
1-NapCH_2	4.23	1.70	7.35	4.81	1.57	7.26
			R^2	0.74	1.00	0.94

Finally, external validation with unseen values afforded excellent coefficient of determination and standard error (R^2 = 98%, RMSE = 0.115 kcal/mol). Using identical settings, a model was trained based on the wSterimol parameters. The equation correlating $\Delta\Delta G^{\ddagger}$ free energies employs ${}^{X}wB_1$ and ${}^{Y}wB_5$ with negative and positive coefficients, respectively. The coefficient of determination and RMSE of the wSterimol model are satisfactory (R^2 = 94%, RMSE = 0.146 kcal/mol). LOOCV gave satisfactory results (R^2 = 88%, RMSE = 0.196 kcal/mol) and the ANOVA test was passed for both descriptors (${}^{X}wB_1 = 3.5\times10^{-6}$, ${}^{Y}wB_5 = 8.2\times10^{-4}$). Using the minimum and maximum Sterimol values of conformers that are tabulated, the potential impact of conformational sampling on the wSterimol model was estimated. The final figure was depicted as shown in **Chapter 3**.

Table 7.12. Dataset employed to describe the *N*-substituent sizes of chiral 1,2-amino phosphinamide ligands with two alkyl subgroups. The parameters were generated at the semi-empirical PM6-DH2 level of theory. The substituent geometries were modelled with the anchored atom represented with hydrogen (Hyd).

Groups	$^{x}B_{1}^{min}$	$^{x}B_{5}^{min}$	$^{x}L^{min}$	$^{x}wB_{1}$	$^{x}wB_{5}$	^{x}wL	$^{x}B_{1}^{max}$	$^{x}B_{5}^{max}$	$^{x}L^{max}$
Training									
H-H	1.00	1.00	2.00	1.00	1.00	2.00	1.00	1.00	2.00
H-Et	1.00	1.00	2.00	1.00	1.00	2.00	1.00	1.00	2.00
H-Bu	1.00	1.00	2.00	1.00	1.00	2.00	1.00	1.00	2.00
H-CH_2Bu	1.00	1.00	2.00	1.00	1.00	2.00	1.00	1.00	2.00
H-*i*Pr	1.00	1.00	2.00	1.00	1.00	2.00	1.00	1.00	2.00
Me-Me	1.51	2.02	2.98	1.51	2.02	2.98	1.51	2.02	2.98
Et-Et	1.56	3.17	4.15	1.56	3.17	4.15	1.56	3.17	4.15
H-*c*Hex	1.00	1.00	2.00	1.00	1.00	2.00	1.00	1.00	2.00
H-$CHEt_2$	1.00	1.00	2.00	1.00	1.00	2.00	1.00	1.00	2.00
H-Bn	1.00	1.00	2.00	1.00	1.00	2.00	1.00	1.00	2.00
H-CH_2(*p*CH_3Ph)	1.00	1.00	2.00	1.00	1.00	2.00	1.00	1.00	2.00
H-CH_2Nap	1.00	1.00	2.00	1.00	1.00	2.00	1.00	1.00	2.00
Test									
Et-Me	1.56	3.17	4.15	1.56	3.17	4.15	1.56	3.17	4.15
H-CH_2*i*Pr	1.00	1.00	2.00	1.00	1.00	2.00	1.00	1.00	2.00
H-*s*Bu	1.00	1.00	2.00	1.00	1.00	2.00	1.00	1.00	2.00
H-CH_2(*p*ClPh)	1.00	1.00	2.00	1.00	1.00	2.00	1.00	1.00	2.00
H-CH_2(*p*CF_3Ph)	1.00	1.00	2.00	1.00	1.00	2.00	1.00	1.00	2.00
H-CH_2(*p*MeOPh)	1.00	1.00	2.00	1.00	1.00	2.00	1.00	1.00	2.00
CH_2Bu-Me	1.56	3.73	3.77	1.56	5.83	5.21	1.66	6.97	7.25

Table 7.12. Continued.

Groups	$^{Y}B_1^{min}$	$^{Y}B_5^{min}$	$^{Y}L^{min}$	$^{Y}wB_1$	$^{Y}wB_5$	^{Y}wL	$^{Y}B_1^{max}$	$^{Y}B_5^{max}$	$^{Y}L^{max}$	ddG	fit	|ddG–fit|
Training												
H-H	1.00	1.00	2.00	1.00	1.00	2.00	1.00	1.00	2.00	0.426	0.634	0.208
H-Et	1.56	3.17	4.15	1.56	3.17	4.15	1.56	3.17	4.15	1.071	0.944	0.127
H-Bu	1.56	3.54	3.76	1.56	5.05	4.89	1.56	5.70	6.41	1.016	1.212	0.196
H-CH_2Bu	1.56	3.73	3.77	1.56	5.83	5.21	1.66	6.97	7.25	1.188	1.323	0.135
H-*i*Pr	1.92	3.18	4.12	1.92	3.18	4.12	1.92	3.18	4.12	1.163	0.945	0.218
Me-Me	1.51	2.02	2.98	1.51	2.02	2.98	1.51	2.02	2.98	-0.218	-0.196	0.022
Et-Et	1.56	3.17	4.15	1.56	3.17	4.15	1.56	3.17	4.15	-0.107	-0.127	0.020
H-*c*Hex	1.93	3.53	6.19	1.93	3.53	6.19	1.93	3.53	6.19	1.156	0.995	0.161
H-$CHEt_2$	1.94	3.69	4.12	2.02	4.46	4.52	2.07	4.51	5.14	1.045	1.128	0.083
H-Bn	1.57	5.96	4.84	1.57	6.00	5.43	1.57	6.03	6.10	1.535	1.347	0.188
H-CH_2(*p*CH_3Ph)	1.57	7.02	5.41	1.57	7.11	5.71	1.57	7.15	6.09	1.571	1.505	0.066
H-CH_2Nap	1.57	6.04	4.84	1.57	6.79	6.00	1.57	7.26	7.59	1.323	1.460	0.137
Test												
Et-Me	1.51	2.02	2.98	1.51	2.02	2.98	1.51	2.02	2.98	-0.332	-0.291	0.041
H-CH_2*i*Pr	1.56	4.02	4.17	1.56	4.44	4.79	1.57	4.46	5.09	1.066	1.125	0.059
H-*s*Bu	1.92	3.64	4.10	1.92	4.32	4.31	1.93	4.50	5.11	1.234	1.108	0.126
H-CH_2(*p*ClPh)	1.50	7.42	5.25	1.50	7.42	5.48	1.50	7.42	5.90	1.512	1.550	0.038
H-CH_2(*p*CF_3Ph)	1.57	7.52	5.91	1.57	7.67	6.16	1.57	7.72	6.38	1.490	1.585	0.095
H-CH_2(*p*MeOPh)	1.57	7.65	5.09	1.57	7.98	5.95	1.57	8.14	6.49	1.584	1.629	0.045
CH_2Bu-Me	1.51	2.02	2.98	1.51	2.02	2.98	1.51	2.02	2.98	-0.311	-0.291	0.020

Table 7.12. Continued.

Groups	$^{X}B_1$	$^{X}B_5$	^{X}L	$^{Y}B_1$	$^{Y}B_5$	^{Y}L	ddG
Training							
H-H	1.17	1.17	2.20	1.17	1.17	2.20	0.426
Me-Me	1.70	2.22	3.04	1.70	2.22	3.04	-0.218
Et-Et	1.71	3.38	4.33	1.71	3.38	4.33	-0.107
H-Et	1.17	1.17	2.20	1.71	3.38	4.33	1.071
H-*i*Pr	1.17	1.17	2.20	2.10	3.38	4.27	1.163
H-Bu	1.17	1.17	2.20	1.71	4.89	6.39	1.016
H-CH_2Bu	1.17	1.17	2.20	1.71	5.13	7.26	1.188
H-*c*Hex	1.17	1.17	2.20	2.08	4.59	5.46	1.156
H-$CHEt_2$	1.17	1.17	2.20	2.26	4.13	5.41	1.045
H-Bn	1.17	1.17	2.20	1.70	6.20	5.44	1.535
H-CH_2(*p*CH_3Ph)	1.17	1.17	2.20	1.70	7.48	5.73	1.571
H-CH_2Nap	1.17	1.17	2.20	1.70	7.35	4.23	1.323
Test							
Et-Me	1.71	3.38	4.33	1.70	2.22	3.04	-0.332
H-CH_2*i*Pr	1.17	1.17	2.20	1.71	4.65	5.21	1.066
H-*s*Bu	1.17	1.17	2.20	2.12	3.91	5.30	1.234
H-CH_2(*p*ClPh)	1.17	1.17	2.20	1.72	7.52	5.07	1.512
H-CH_2(*p*CF_3Ph)	1.17	1.17	2.20	1.71	8.01	5.74	1.490
H-CH_2(*p*MeOPh)	1.17	1.17	2.20	1.70	8.65	4.90	1.584
CH_2Bu-Me	1.71	5.13	7.26	1.70	2.22	3.04	-0.311

2 Density functional theory

2.1 General information

Density functional theory (DFT) geometry optimizations and frequency analyses were performed using the Gaussian 09, Revision D.01 software package.[5] Molecular geometries were fully optimized at the level of density functional theory, using the B3LYP,[18–21] M06-2X,[6–8] ωB97xD[9] or B97D[22,23] functionals as clearly stated without any symmetry constraints. B97D pure functional was used to accelerate the calculations with density fitting. The effective core potentials (ECPs) of Hay and Wadt with a double-ζ basis set (LanL2DZ)[10,11] was sometimes used for Cu and Zr transition metals and the 6-31G(d) or def2SVP basis set was used for H, C, N, O, P and Cl. The energies were further refined using a larger basis set (def2tzvpp) by single-point calculations, in implicit solvent treated with the Solvation Model based on Density (SMD)[24] universal solvation model when clearly stated. In the case of a combination of solvents in the experimental conditions, only the major solvent was used such that the dieletric constant of Et_2O was utilized in the 4:1 Et_2O/CH_2Cl_2 solvent combination. Vibrational frequencies were used to classify stationary points. All stationary points were checked as either ground state or transition structures by the presence of zero or a single imaginary vibrational frequency, respectively. Thermochemistry was evaluated at the solution standard state of 1 mol·dm^{-3} and temperature of 298.15 K. Gas phase species were evaluated at standard pressure of 1 bar. Gibbs free energies were calculated using vibrational frequencies with *GoodVibes* python script[25] employing a quasi-harmonic approximation for entropy

calculation with a free-rotor description below 100 cm^{-1}, as proposed by Grimme.[26] 3D molecular graphics were generated by Open source Pymol Version 1.8.6.0.[12] wSterimol[2] and Mopac version 2016[4] for semi-empirical calculations were used to realise conformational samplings on substituents when required. Transition structures were connected to ground states structures using intrinsic reaction coordinate (IRC) calculations or chemical expertise.

2.2 Appendix – Chapter 2

A DFT mechanistic study of the ACA to linear enones was carried out at the B97D level of theory with density fitting to accelerate the calculations (**Table 7.13**). Several modelling simplifications were considered to obtain a workable system. Thus, the alkylzirconocene was truncated to only two alkyl carbons while **L17** ligand (isopentyl) was replaced by **L2** (cyclohexyl) to reduce the amount of conformers to examine. The counterion of TMS was also considered in the outer shell of the catalyst and was computed at an infinite distance from copper. There were in total height different transition states, from which different conformations were explored. *(S, S)*-**TS-1** is the most favoured pathway to form the *(S)* product while *(S, R)*-**TS-2** is the most favoured pathway to form the *(R)* product. Note that *(S, S)*-**TS-3** is still lower than *(S, R)*-**TS-2** by 4.0 kJ/mol.

3D coordinates of *(S, S)*-**TS-1** and *(S, R)*-**TS-2** discussed in **Chapter 2** are disclosed (**Table 7.14** and **Table 7.15**). Note that the geometries are positively charged.

Table 7.13. Transition structures of the ACA to linear enones computed at the B97D/def2tzvpp//B97D/def2SVP/def2SVP level of theory.

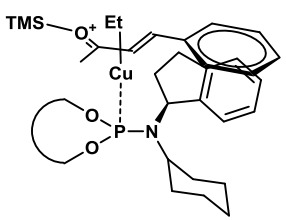

(S, S)-**TS-1**
s-cis "up"
0 kJ/mol

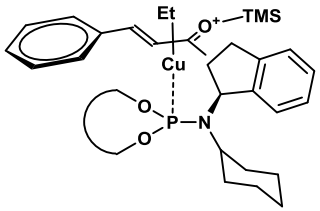

(S,R)-**TS-2**
s-cis "up"
6.0 kJ/mol

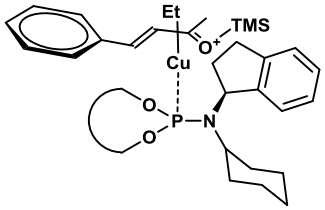

(S, S)-**TS-3**
s-cis "down"
2.0 kJ/mol

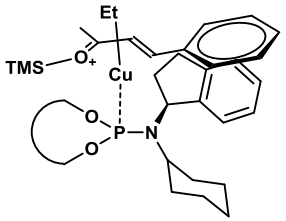

(S,R)-**TS-4**
s-cis "down"
16.1 kJ/mol

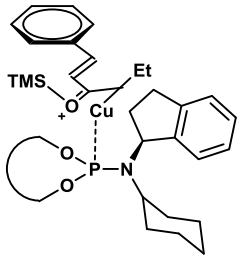

(S,R)-**TS-5**
s-trans "down"
12.6 kJ/mol

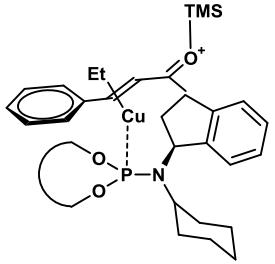

(S, S)-**TS-6**
s-trans "up"
13.1 kJ/mol

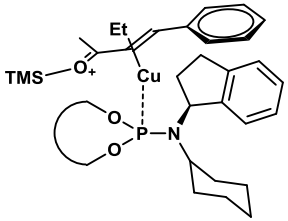

(S, S)-**TS-7**
s-trans "down"
13.4 kJ/mol

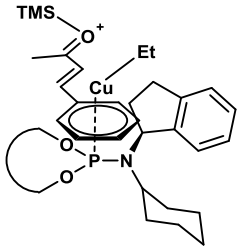

(S,R)-**TS-8**
s-trans "up"
19.9 kJ/mol

Table 7.14. 3D coordinates of the transition structures *(S,S)*-**TS-1** of the ACA to linear enones presented in **Chapter 2**.

Cu	-1.91530900	-0.29532200	-0.30367100	C	3.20453100	-4.57906600	-2.12022300
C	-2.48496300	-1.64774200	-1.92693200	C	4.10476200	-2.88452500	-0.05131700
H	-1.41296300	-1.92489900	-1.88911100	C	4.58484900	-4.18279100	-0.15867200
H	-3.05382700	-2.56943500	-2.09960100	H	5.31424600	-4.55299000	0.57257800
C	-3.52834000	-1.73590900	-0.04955000	C	4.14246400	-5.03687700	-1.20717200
C	-1.54756300	-1.10749300	3.26488700	H	4.53882500	-6.05664900	-1.28589700
C	-3.07463500	-1.12118300	1.23148400	C	5.48169100	-0.11717900	-0.79404200
H	-0.54799800	-0.64484200	3.15773500	C	6.34397300	1.59938700	1.27399300
H	-1.46313800	-1.93367700	3.99676500	C	7.25283000	1.12795100	0.33828600
H	-3.65163400	-0.31173800	1.69540100	H	8.30803300	1.42184800	0.39606300
C	-1.99303500	-1.63859800	1.93442700	C	6.81176900	0.27184600	-0.70831900
O	-1.30761300	-2.64475700	1.38536500	H	7.52878500	-0.08050700	-1.46018700
C	-2.84979600	-0.59259300	-2.96216100	H	2.84158500	-5.23254800	-2.92366200
H	-2.10828100	0.22698000	-3.01499500	H	4.45288800	-2.24032600	0.76145500
H	-2.91674600	-1.05204900	-3.97099300	H	5.15709200	-0.76947600	-1.61033900
H	-3.84381500	-0.15093600	-2.75046100	H	6.66731400	2.27355200	2.07749500
O	0.87265900	0.32259400	0.90068900	H	1.93102300	1.82775900	2.72845300
P	-0.05242100	0.86070200	-0.39778600	H	0.31733500	-1.18051500	-3.45050700
O	1.00270000	0.58264800	-1.66651700	N	-0.10604400	2.52085700	-0.42310300
C	3.12728700	-0.04261600	0.09747700	Si	-0.00302900	-3.70184000	1.87681900
C	2.24186900	0.57419100	0.98745400	C	-0.67877400	-4.81682600	3.23936100
C	1.58192900	-0.68133500	-1.76111300	H	-1.60955300	-5.32373700	2.91723700
C	2.62043700	-1.03290200	-0.89426300	H	0.06366300	-5.60215400	3.48762000
C	2.67667200	-3.25591700	-2.02780700	H	-0.89415200	-4.25938300	4.17188900
C	3.15076000	-2.37330900	-0.98343100	C	0.35381100	-4.62792200	0.28352500
C	1.66291300	-2.80341900	-2.92435600	H	0.57919900	-3.91823300	-0.53427100
C	1.10501000	-1.54422800	-2.78169300	H	1.23584700	-5.28733300	0.39983700
H	1.31795400	-3.47620000	-3.71932900	H	-0.50821900	-5.25241700	-0.02205900
C	4.52098600	0.33207900	0.16291200	C	1.47374600	-2.68460500	2.44906000
C	4.01912700	1.74079500	2.14472400	H	1.27419500	-2.13078500	3.38552600
C	2.67552800	1.43069300	2.03075100	H	2.33010500	-3.36406300	2.63100800
H	4.36934700	2.40061100	2.94821800	H	1.77909100	-1.96263200	1.67213100
C	4.96643000	1.22963200	1.20776900	C	-2.41991100	3.00782300	-1.45210500

H	-2.38377600	1.95146700	-1.78005100
H	-2.18333700	3.63971600	-2.32586800
C	-2.22964500	2.79959500	0.93296700
C	-3.60333000	2.88716200	0.63471900
C	-4.55617700	2.63425000	1.63362300
C	-4.11555400	2.29693200	2.92784500
C	-2.73910800	2.21985900	3.21989600
C	-1.78282700	2.46776700	2.21873500
H	-5.62948400	2.69289500	1.41293300
H	-4.85077800	2.09794900	3.71756700
H	-2.41348800	1.97049300	4.23739100
H	-0.70917600	2.39757200	2.42957700
C	1.12046300	3.34613300	-0.60111600
C	1.10478700	4.11108800	-1.93650900
C	1.37209300	4.29248300	0.58692300
H	1.97040200	2.64237100	-0.64069100
C	2.42946600	4.87559800	-2.12952900
H	0.25850900	4.82862200	-1.93311200
H	0.93488600	3.39366100	-2.76073100
C	2.70786600	5.03488600	0.39262900
H	0.55262200	5.03561300	0.65797100
H	1.37460700	3.71390700	1.52749400
C	2.72079200	5.80862600	-0.93940300
H	2.40059500	5.44796400	-3.07601100
H	3.25364100	4.13856300	-2.22403800
H	2.88563700	5.71999100	1.24334200
H	3.53127600	4.29105500	0.39654700
H	3.69470300	6.31480900	-1.07973700
H	1.94748700	6.60411100	-0.90211800
C	-3.80212300	3.29691600	-0.81406300
H	-4.63137200	2.76177800	-1.31313900
H	-4.03771500	4.38014800	-0.86892700
C	-1.41000300	3.19384800	-0.28543800
H	-1.18058900	4.27265100	-0.19880700
H	-2.25257700	-0.35199400	3.64383800
H	-3.30915900	-2.81003100	-0.05249500
C	-4.88691800	-1.38814700	-0.53974500
C	-5.72535100	-2.38721100	-1.07896200
C	-5.34100300	-0.05187000	-0.52844200
C	-6.99593100	-2.05890900	-1.57743900
H	-5.37946300	-3.42926100	-1.09717500
C	-6.60956300	0.27884000	-1.02707500
H	-4.68958500	0.72761100	-0.12193200
C	-7.44250600	-0.72529000	-1.55279700
H	-7.64202100	-2.84661800	-1.98452800
H	-6.95025000	1.32205000	-1.00773000
H	-8.43547500	-0.47015300	-1.94299000

Table 7.15. 3D coordinates of the transition structures *(S,R)*-**TS-2** of the ACA to linear enones presented in **Chapter 2**.

Cu	-1.87048200	0.20607300	-0.18086700
C	-3.91991700	0.65635700	-0.48486900
H	-4.88799200	0.38220400	-0.04864300
H	-3.54141100	1.51641600	0.10687800
C	-3.37979900	-1.33173800	0.10696300
C	-0.17342300	-2.47177300	2.03420900
C	-2.01983600	-1.85195400	0.42329600
H	-0.34785400	-3.16033000	2.88286100
H	0.59896200	-1.74229900	2.34199500
H	-1.49633700	-2.47065100	-0.31305400
C	-1.44864800	-1.76533800	1.68068500
O	-2.07035400	-1.03836300	2.62051700
C	-4.02577900	0.92297300	-1.97632000
H	-3.07857100	1.28903300	-2.41349900
H	-4.33458100	0.01618800	-2.52789800
H	-4.79719900	1.69984700	-2.16044000
O	1.02374200	0.38961500	0.83616500
P	0.18378900	0.96044700	-0.49832400
O	1.03773400	0.21845400	-1.73706300
C	2.93275200	-0.88401300	0.04878400
C	2.39234300	0.12927400	0.84874900
C	1.13013700	-1.16918000	-1.65893900
C	2.03824800	-1.75100300	-0.77097200
C	1.15424200	-3.97223900	-1.49320800
C	2.03293000	-3.19033600	-0.64792800
C	0.30522800	-3.31025000	-2.43057000
C	0.27982300	-1.92842400	-2.50304000
H	-0.34180400	-3.91414400	-3.07879100
C	4.36970000	-1.03752700	0.03486600
C	4.54852500	0.71794000	1.78125500
C	3.17936800	0.91058900	1.73375400
H	5.16833300	1.31165600	2.46462100
C	5.18013200	-0.23227700	0.92422800
C	1.13212200	-5.39364500	-1.35665800
C	2.81681900	-3.88027000	0.32695800
C	2.76074900	-5.26267500	0.44306300
H	3.36960400	-5.76750500	1.20340100
C	1.92094100	-6.03065600	-0.41045800
H	1.89283700	-7.12270400	-0.31206600
C	5.03557600	-1.93400100	-0.85579400
C	6.59907000	-0.39021500	0.91546100
C	7.20994600	-1.28632900	0.05095500
H	8.30127200	-1.39660100	0.04962600
C	6.41884300	-2.05423400	-0.84767600
H	6.90667700	-2.74520600	-1.54637600
H	0.46919200	-5.97229900	-2.01245100
H	3.46189400	-3.30399300	0.99662500
H	4.44159300	-2.52577900	-1.55892300
H	7.19831400	0.22108000	1.60229100
H	2.67880400	1.65560700	2.36037900
H	-0.37407300	-1.39454000	-3.20214200
N	0.59839900	2.55310500	-0.73153800
Si	-1.63532800	-0.49370300	4.21617400
C	-3.18255600	0.43108400	4.75419500
H	-4.04049200	-0.25996300	4.86894000
H	-3.02000100	0.93515200	5.72751700
H	-3.46125500	1.20017900	4.00832100
C	-1.27412000	-1.97487300	5.32482500
H	-0.31165000	-2.45963300	5.07504700
H	-1.21660300	-1.64286500	6.38132400
H	-2.07679900	-2.73544500	5.25727900
C	-0.13967500	0.64515100	4.04428700
H	-0.32076200	1.41475200	3.27154800
H	0.06069900	1.15847600	5.00625200
H	0.77340200	0.09096900	3.75699900
C	2.02186500	2.94643800	-0.91797900

C	2.31356500	3.44608100	-2.34476500
C	2.48098800	3.96288200	0.14289700
H	2.62579300	2.03339500	-0.77666400
C	3.81738200	3.74305500	-2.50386700
H	1.73248200	4.37128400	-2.53436300
H	1.97816600	2.68312200	-3.07133100
C	3.98426200	4.25840100	-0.02067000
H	1.90800500	4.90571300	0.02985400
H	2.26261900	3.56344000	1.15061200
C	4.30468900	4.74940500	-1.44475500
H	4.02123000	4.12076200	-3.52366400
H	4.38197400	2.79418400	-2.39274100
H	4.30564100	5.00433400	0.73097900
H	4.55124000	3.32665800	0.18263900
H	5.39191900	4.92395000	-1.55380100
H	3.80396100	5.72560300	-1.61372100
C	-0.44775200	3.55385400	-1.00073900
C	-1.12994000	3.48083200	-2.39703900
H	0.05206600	4.53687100	-0.89931900
C	-2.49895700	4.17860800	-2.19749500
H	-1.28051700	2.41175800	-2.64569000
H	-0.51376100	3.92640300	-3.19608200
H	-2.41150700	5.26779000	-2.39215200
H	-3.28787100	3.79471300	-2.87004900
C	-1.63243100	3.54626900	-0.04771200
C	-1.64976500	3.27608600	1.32736400
C	-2.86544800	3.40062200	2.02558500
C	-4.03547700	3.80277000	1.35056200
C	-4.00765300	4.07908400	-0.03055500
C	-2.79880300	3.94077800	-0.72954900
H	-0.72821800	2.98143500	1.84431400
H	-2.90018600	3.19684700	3.10265300
H	-4.97686300	3.89796900	1.90587000
H	-4.92305400	4.38613100	-0.55247000
H	0.21322200	-3.04697300	1.17958500
H	-3.96356100	-1.20078500	1.02693400
C	-4.11642500	-2.04781000	-0.97142100
C	-5.50069100	-2.28496800	-0.83039000
C	-3.47396000	-2.46601900	-2.15807900
C	-6.22370600	-2.93510000	-1.84253800
H	-6.01013700	-1.96181500	0.08725600
C	-4.19582200	-3.11283400	-3.17250000
H	-2.40212700	-2.27916800	-2.28734200
C	-5.57343800	-3.35082400	-3.01801700
H	-7.29720900	-3.12066600	-1.71285700
H	-3.68306000	-3.43118200	-4.08911000
H	-6.13783400	-3.85793400	-3.81025100

3 References

1 R Core Team, *R: A Language and Environment for Statistical Computing*, R Foundation for Statistical Computing, Vienna, Austria, 2013.

2 A. V. Brethomé, S. P. Fletcher and R. S. Paton, *ACS Catal.*, 2019, **9**, 2313–2323.

3 *Spartan'16*, Wavefunction, Inc., Irvine, CA, 2016.

4 J. J. P. Stewart, *MOPAC2016*, Stewart Computational Chemistry, Colorado Springs, 2016.

5 M. J. Frisch, G. W. Trucks, H. B. Schlegel, G. E. Scuseria, M. A. Robb, J. R. Cheeseman, G. Scalmani, V. Barone, B. Mennucci, G. A. Petersson, H. Nakatsuji, M. Caricato, X. Li, H. P. Hratchian, A. F. Izmaylov, J. Bloino, G. Zheng, J. L. Sonnenberg, M. Hada, M. Ehara, K. Toyota, R. Fukuda, J. Hasegawa, M. Ishida, T. Nakajima, Y. Honda, O. Kitao, H. Nakai, T. Vreven, J. Montgomery, J. A., J. E. Peralta, F. Ogliaro, M. Bearpark, J. J. Heyd, E. Brothers, K. N. Kudin, V. N. Staroverov, R. Kobayashi, J. Normand, K. Raghavachari, A. Rendell, J. C. Burant, S. S. Iyengar, J. Tomasi, M. Cossi, N. Rega, J. M. Millam, M. Klene, J. E. Knox, J. B. Cross, V. Bakken, C. Adamo, J. Jaramillo, R. Gomperts, R. E. Stratmann, O. Yazyev, A. J. Austin, R. Cammi, C. Pomelli, J. W. Ochterski, R. L. Martin, K. Morokuma, V. G. Zakrzewski, G. A. Voth, P. Salvador, J. J. Dannenberg, S. Dapprich, A. D. Daniels, Ö. Farkas, J. B. Foresman, J. V. Ortiz, J. Cioslowski and D. J. Fox, *Gaussian 09, Revision D.01*, Gaussian Inc., Wallingford, 2009.

6 Y. Zhao and D. G. Truhlar, *Theor. Chem. Acc.*, 2008, **120**, 215–241.

7 N. Mardirossian and M. Head-Gordon, *J. Chem. Theory Comput.*, 2016, **12**, 4303–4325.

8 S. E. Wheeler and K. N. Houk, *J. Chem. Theory Comput.*, 2010, **6**, 395–404.

9 Y. S. Lin, G. De Li, S. P. Mao and J. Da Chai, *J. Chem. Theory Comput.*, 2013, **9**, 263–272.

10 W. R. Wadt and P. J. Hay, *J. Chem. Phys.*, 1985, **82**, 284–298.

11 P. J. Hay and W. R. Wadt, *J. Chem. Phys.*, 1985, **82**, 270–283.

12 *The PyMOL Molecular Graphics System, Version 1.8*, Schrödinger LLC, 2015.

13 I. V. Tetko and V. Y. Tanchuk, *J. Chem. Inf. Comput. Sci.*, 2002, **42**, 1136–1145.

14 A. V Brethomé, R. S. Paton and S. P. Fletcher, *ACS Catal.*, 2019, **9**, 7179–7187.

15 K. C. Harper, E. N. Bess and M. S. Sigman, *Nat. Chem.*, 2012, **4**, 366–374.

16 H. Huang, H. Zong, G. Bian and L. Song, *J. Org. Chem.*, 2012, **77**, 10427–10434.

17 H. Huang, H. Zong, G. Bian, H. Yue and L. Song, *J. Org. Chem.*, 2014, **79**, 9455–9464.

18 C. Lee, W. Yang and R. G. Parr, *Phys. Rev. B*, 1988, **37**, 785–789.

19 A. D. Becke, *J. Chem. Phys.*, 1993, **98**, 5648–5652.

20 P. J. Stephens, F. J. Devlin, C. F. Chabalowski and M. J. Frisch, *J. Phys. Chem.*, 1994, **98**, 11623–11627.

21 S. H. Vosko, L. Wilk and M. Nusair, *Can. J. Phys.*, 1980, **58**, 1200–1211.

22 S. Grimme, *J. Comput. Chem.*, 2006, **27**, 1787–1799.

23 S. Grimme, S. Ehrlich and L. Goerigk, *J. Comput. Chem.*, 2011, **32**, 1456–1465.

24 A. V. Marenich, C. J. Cramer and D. G. Truhlar, *J. Phys. Chem. B*, 2009, **113**, 6378–6396.

25 I. Funes-Ardoiz and R. S. Paton, *GoodVibes, Version 2.0.3*, 2018.

26 S. Grimme, *Chem. Eur. J.*, 2012, **18**, 9955–9964.